PB2003-104175

Wind and Seismic Effects

Proceedings of the 34th Joint Panel Meeting

NIST Special Publication 987

Stephen A. Cauffman, Editor

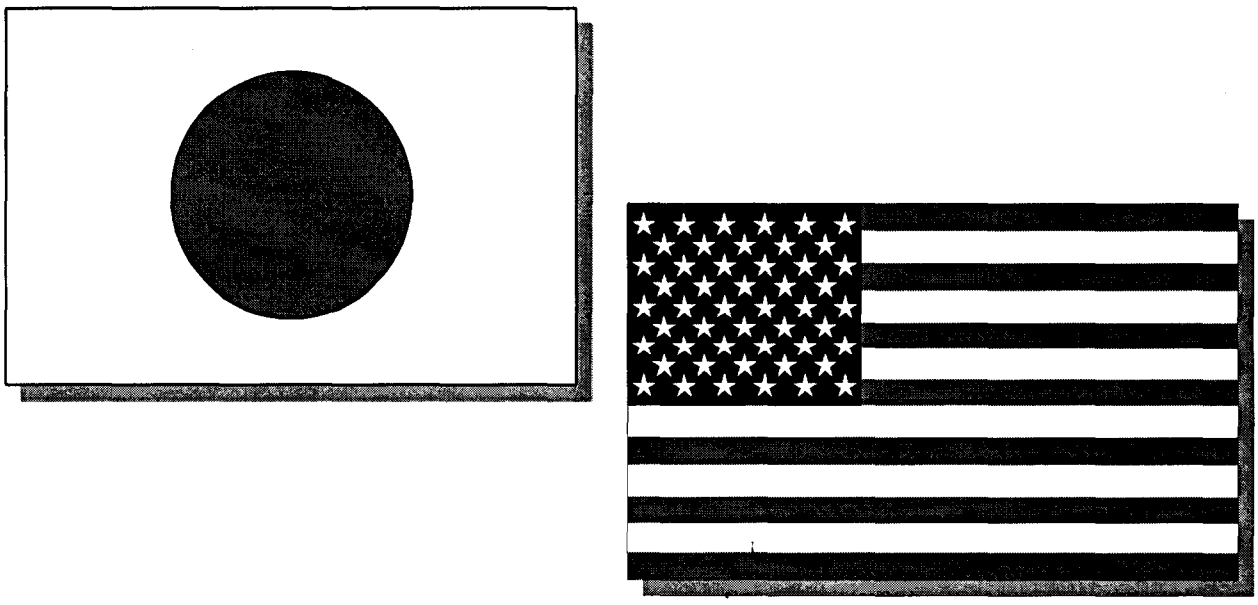

NIST National Institute of Standards and Technology • Technology Administration • U.S. Department of Commerce

The National Institute of Standards and Technology was established in 1988 by Congress to "assist industry in the development of technology . . . needed to improve product quality, to modernize manufacturing processes, to ensure product reliability . . . and to facilitate rapid commercialization . . . of products based on new scientific discoveries."

NIST, originally founded as the National Bureau of Standards in 1901, works to strengthen U.S. industry's competitiveness; advance science and engineering; and improve public health, safety, and the environment. One of the agency's basic functions is to develop, maintain, and retain custody of the national standards of measurement, and provide the means and methods for comparing standards used in science, engineering, manufacturing, commerce, industry, and education with the standards adopted or recognized by the Federal Government.

As an agency of the U.S. Commerce Department's Technology Administration, NIST conducts basic and applied research in the physical sciences and engineering, and develops measurement techniques, test methods, standards, and related services. The Institute does generic and precompetitive work on new and advanced technologies. NIST's research facilities are located at Gaithersburg, MD 20899, and at Boulder, CO 80303. Major technical operating units and their principal activities are listed below. For more information contact the Publications and Program Inquiries Desk, 301-975-3058.

Office of the Director
- National Quality Program
- International and Academic Affairs

Technology Services
- Standards Services
- Technology Partnerships
- Measurement Services
- Information Services

Advanced Technology Program
- Economic Assessment
- Information Technology and Applications
- Chemistry and Life Sciences
- Electronics and Photonics Technology

Manufacturing Extension Partnership Program
- Regional Programs
- National Programs
- Program Development

Electronics and Electrical Engineering Laboratory
- Microelectronics
- Law Enforcement Standards
- Electricity
- Semiconductor Electronics
- Radio-Frequency Technology[1]
- Electromagnetic Technology[1]
- Optoelectronics[1]
- Magnetic Technology[1]

Materials Science and Engineering Laboratory
- Intelligent Processing of Materials
- Ceramics
- Materials Reliability[1]
- Polymers
- Metallurgy
- NIST Center for Neutron Research

Chemical Science and Technology Laboratory
- Biotechnology
- Physical and Chemical Properties[2]
- Analytical Chemistry
- Process Measurements
- Surface and Microanalysis Science

Physics Laboratory
- Electron and Optical Physics
- Atomic Physics
- Optical Technology
- Ionizing Radiation
- Time and Frequency[1]
- Quantum Physics[1]

Manufacturing Engineering Laboratory
- Precision Engineering
- Manufacturing Metrology
- Intelligent Systems
- Fabrication Technology
- Manufacturing Systems Integration

Building and Fire Research Laboratory
- Applied Economics
- Structures
- Building Materials
- Building Environment
- Fire Research

Information Technology Laboratory
- Mathematical and Computational Sciences[2]
- Advanced Network Technologies
- Computer Security
- Information Access
- Convergent Information Systems
- Information Services and Computing
- Software Diagnostics and Conformance Testing
- Statistical Engineering

[1] At Boulder, CO 80303.
[2] Some elements at Boulder, CO.

NIST Special Publication 987

Wind and Seismic Effects

Proceedings of the 34th Joint Panel Meeting

Stephen A. Cauffman, Editor

Materials and Construction Research Division,
Building and Fire Research Laboratory,
National Institute of Standards and Technology,
Gaithersburg, MD 20899-8611

September 2002

U.S. Department of Commerce
Donald L. Evans, Secretary

Technology Administration
Phillip J. Bond, Under Secretary for Technology

National Institute of Standards and Technology
Arden L. Bement, Jr., Director

National Institute of Standards and Technology Special Publication 987
Natl. Inst. Stand. Technol. Spec. Publ. 987, 382 pages (September 2002)
CODEN: NSPUE2

U.S. GOVERNMENT PRINTING OFFICE
WASHINGTON: 2002

For sale by the Superintendent of Documents, U.S. Government Printing Office
Internet: bookstore.gpo.gov — Phone: (202) 512-1800 — Fax: (202) 512-2250
Mail Stop SSOP, Washington, DC 20402-0001

PREFACE

This publication contains the Proceedings of the 34th Joint Meeting of the U.S.-Japan Panel on Wind and Seismic Effects. The technical meetings were held at the National Institute of Standards and Technology in Gaithersburg, Maryland during 13-15 May 2002 followed by three-day technical site visits. Thirty papers were written, 15 by each side. Twenty-eight papers were presented orally; 15 by the U.S.-side and 13 by the Japan-side. The papers were organized into five Sessions: Geotechnical Engineering and Ground Motion; Next-Generation Building and Infrastructure Systems; Wind; Dams; and Transportation Systems and three Technical Themes: Terrorism -- Collapse of the WTC and Pentagon Wedge A; Disaster Information; and Management of Infrastructure Systems.

BACKGROUND

Responding to the need for improved engineering and scientific practices through exchange of technical data and information, research personnel, and research equipment, the United States and Japan in 1961 created the U.S.-Japan Cooperative Science Program. Three collateral programs comprise the Cooperative Science Program. The U.S.-Japan Cooperative Program in Natural Resources (UJNR), one of the three, was created in January 1964. The objective of UJNR is to exchange information on research results and exchange scientists and engineers in the area of natural resources for the benefit of both countries. UJNR is composed of 16 Panels each responsible for specific technical subjects.

The Panel on Wind and Seismic Effects was established in 1969. Eighteen U.S. and 14 Japanese organizations participate with representatives of private sector organizations to develop and exchange technologies aimed at reducing damages from high winds, earthquakes, storm surge, and tsunamis. This work is produced through collaboration between U.S. and Japanese member researchers working in five Task Committees. Each committee focuses on specific technical issues, e.g., earthquake strong motion data. The Panel provides the vehicle to exchange technical data and information on design and construction of civil engineering lifelines, buildings, and water front structures, and to exchange high wind and seismic measurement records. Annual meetings alternate between Japan and the United States (odd numbered years in Japan; even numbered years in the United States). These one-week technical meetings including technical site visits that follow the meetings provide the forum to discuss ongoing research and research results. The National Institute of Standards and Technology (NIST) provides the U.S.-side chair and secretariat. The Public Works Research Institute (PWRI), Japan, provides the Japan-side chair and secretariat.

Task Committee meetings, exchanges of data and information through technical presentations at annual Panel meetings, exchanges of guest researchers, visits to respective research laboratories and informal interactions between Panel meetings, joint workshops and seminars, and joint cooperative research programs all contribute to the development and effective delivery of knowledge that has influenced design and construction practices in both countries. Guest research exchanges have advanced the state of technology in areas of steel, concrete, and masonry structures under seismic forces; developed techniques to analyze risks from liquefaction; modeled water seepage in dam foundations; performed comparative analyses of seismic design of U.S. and Japanese bridges.

Direct communication between counterpart country organizations is the cornerstone of the Panel. Effective information exchanges and exchanges of personnel and equipment have strengthened domestic programs of both countries. There are opportunities for experts in various technical fields to get to know their foreign counterparts, conduct informal exchanges, bring their respective views to the frontiers of

knowledge, and advance knowledge of their specialties.

The Panel's activities resulted in improved building and bridge standards and codes and design and construction practices in hydraulic structures in both countries, for example:

- created and exchanged digitized earthquake records used as the basis of design and research in Japan and the United States;
- transferred earthquake engineering information and strong-motion measurement techniques for use by seismically active countries, e.g., Australia, Canada, Italy, Mexico, Peru, Taiwan, Turkey, and North Africa;
- produced data that advanced retrofit techniques for bridge structures;
- developed field test data for use in aerodynamic retrofit of bridge structures;
- produced full-scale test data that advanced seismic design standards for buildings;
- advanced technology for repairing and strengthening reinforced concrete, steel, and masonry structures;
- improved *in-situ* measurement methods for soil liquefaction and stability under seismic loads;
- created a database comparing Japanese and U.S. standard penetration tests to improve prediction of soil liquefaction;
- created a database on storm surge and tsunamis and verified mathematical models of tsunami and storm surge warning systems;
- established a library resource of current research on wind and earthquake engineering and on storm surge and tsunamis;
- published proceedings of Panel meetings, Task Committee Workshops, and special publications such as List of Panel Publications and translated from Japanese to English a two-volume series on earthquake resistant construction using base isolation systems;
- gained better knowledge of both countries' research, design, and construction capabilities from in-depth visits to the host country's laboratories and building and public work projects. Results of such visits contribute to creation of new Task Committees, agendas for Joint Panel meetings and task committee workshops, special visits of U.S.-Japan researchers, and joint collaborative research.

HIGHLIGHTS OF THE TECHNICAL SITE VISITS

Four technical sites visits occurred during 16-18 May 2002 at three locations.

New York City

1. World Trade Center

On 16 May 2002, the Panel delegation visited the engineering firm of LZA Technologies, a division of the Thornton Tomasetti Group, New York, NY to discuss the structural engineers response to the World Trade Center emergency, reconstruction plans, recommendations for risk management, and other lessons learned from the disaster. Mr. Donald Freeman, Director of Preservation and Senior Associate welcomed the delegation and discussed the work that was performed to clean up the wreckage from the collapse of the WTC towers One and Two, and other related damaged structures. Key points from the briefing include:

- Subsequent to the September 11th attacks, 450 buildings were investigated for safety concerns,
- The towers were constructed on reclaimed land from a 200-year-old landfill, mostly garbage. This area includes lower Manhattan Island West of Green Street.

- There were three subways crossing the site, of great concern for flooding of these tunnels, which would have shut down most subway operations in New York City.
- The core columns were 1 m by 2 m by 15 cm thick. They were not designed for lateral loads or for seismic activities.
- All of the structural steel in the buildings was fire proofed with spray on material. The WTC Buildings One and Two had asbestos spray on fireproofing up to floor 39 and non-asbestos fireproofing beyond the 39th floor.
- At the time of the building design, there were no seismic concerns; the outer tubes were designed to resist all lateral loads.
- Initial assessment from the debris pile shortly after the collapse revealed no fire proofing on any of the metal. This may be due to the aircraft impact, extremely hot temperatures from burning aviation fuels, and impact after collapsing; but the cause is uncertain.
- To a large extent the framing was pushed outward away from the direction of each wall.
- Several sections of the outer walls remained intact and survived the collapse.
- Failure to other buildings in the area and damage was caused by falling debris and fire.
- The office responsible for emergency management and actions during a crisis such as this, the Port Authority of New York and New Jersey, recent former owners of the WTC and designer, and other organizations had their offices located in the WTC. The collapse severely hampered their ability to function and caused a long delay in the commencement of rescue operations.
- LZA was contracted by NY City to manage all structural engineering components of the clean up operations.
- The US Occupational Safety and Health Administration and the Environmental Protection Agency provided a perimeter for respiratory control due to all the materials and chemicals present in the debris pile. This perimeter was established two months after the collapse.
- Four engineering/construction firms were sub-contracted to perform the actual clean up activities under the general control of LZA. The work was subdivided between the four companies. BOVIS and AMEC shared the responsibility for towers one and two, Turner had responsibility for Tower 7, and Tully Construction Company the responsibility for the rest of the buildings in the 6.4 ha (16 ac) site. SEAoNY (Structural Engineers Association of New York) Teams were operating as subcontractors to LZA Technologies.
- LZA Technologies staff performed structural assessments of 450 buildings; identified unstable structures; developed demolition and stabilization procedures when taking down collapsed and damaged buildings; identified safe locations for placing heavy equipment; developed and coordinated survey monitoring programs; inspected over 400 buildings; performed detailed investigations of damaged structures.
- Approximately 200 engineers working in 12-hour shifts inspected buildings and investigated the site during the first week; many were volunteers.
- The buildings that were damaged and removed from the WTC site are 1, 2, 3, 4, 5, 6, and 7. Building 7 is the one that burned uncontrollably for several hours.
- There is one building, the Bankers Trust Building, which may not be salvageable.
- There is one very old building, 90 West Building, that did extremely well from fire damage due to the presence of terra-cotta protection.
- The slurry walls were unbraced and very dangerous. The wall at Liberty Street did experience several centimeters of movement. All of the walls were braced and are stable.

Following the presentation at LZA Technologies, the group was taken to the WTC site to view the ongoing clean up activities. The tour began in the American Express Building, which is immediately adjacent to

the site. From the 26th floor, an excellent view was afforded of the site and all activities. After this, a walking tour of the site was provided, essentially along the west slurry wall of the 160 m (510 ft) by 30 m (98 ft) by 27 m (98 ft) deep pit where more than 764,555 m^3 (1 million yd^3)of rubble was removed. Explanations of the ongoing activities were provided.

San-Francisco

2. San Francisco-Oakland Bay Bridge and Golden Gate Bridge
http://www.mtc.ca.gov/projects/bay_bridge/bbmain.htm

The delegation was hosted by Mr. Robert Tanaka, California Department of Transportation (CALTRANS) who provided the delegation a briefing on the East Span Replacement of the Oakland-San Francisco Bay Bridge, followed by site visits to the San Raphael Bridge and the Golden Gate Bridge. CALTRANS maintains, operates, and administers seven State-owned toll bridges on San Francisco Bay and one bridge each in Los Angeles and San Diego.

The West Span Crossing of San Francisco-Oakland Bay Bridge is part of Interstate 80 connecting the city of San Francisco and Yerba Buena Island. It is 2,870 m (9,260 ft) long and consists of two suspension bridges. This structure was opened to traffic in 1936 and has an average daily traffic volume of 270,000 vehicles. It is currently undergoing substructure and superstructure seismic retrofitting. The estimate for seismic retrofit is $250 million. Work began in July 1999; it is scheduled to be completed in April 2003.

Richard Heringer, CALTRANS summarized the work for stiffening the west side of the San Francisco-Oakland Bay Bridge superstructure by replacing all bearings with unidirectional isolator bearings that permitted sliding in the longitudinal direction. Significant retrofit was performed at the base of the towers and improved the connection of tower to pier. The superstructure retrofit included installing perforated plates and replacing the 500,000 rivets with round head bolts. Installation of 96 dampers is a major component of the retrofit.

Following the 1989 Loma Prieta earthquake that collapsed a section of the east span of the San Francisco-Oakland Bay Bridge, CALTRANS started work to replace the East Span to meet current seismic standards. CALTRANS undertook an extensive design and public review process. Running from Yerba Buena Island to Oakland, the new structure will feature a self-anchored, single-tower suspension span across the shipping channel transitioning to a skyway. The current bridge is double-decked; the replacement will feature side-by-side decks. A 5 m (16 ft) wide bicycle and pedestrian path will run along the eastbound deck of the 3.2 km (2 mi) long structure. Its tower is 162 m (525 ft) above the water. This new structure will be on Interstate 80 and connect Yerba Buena Island and the city of Oakland. It will consist of a self-anchored suspension bridge section and post-tensioned concrete box-girder skyway section. This structure will accommodate an average daily traffic volume of 270,000 vehicles. The present estimate for the construction of this structure is $2.6 billion. Work began in February 2002 and is scheduled for completion in 2007.

The delegation visited the San Raphael Bridge $400 million dollar seismic retrofit project where its substructure was extensively modified. This structure is on Interstate 580 and connects the cities of Richmond and San Rafael. It is 5.5 miles long and consists of two steel cantilever bridge sections and many steel truss sections. This structure was opened to traffic in 1956 and has an average daily traffic volume of 60,000 vehicles. It is currently undergoing substructure and superstructure seismic retrofitting. The present estimate for seismic retrofit contract is $484 million. Work began in August 2000 and is scheduled to be completed in December 2004.

Lastly, the delegation visited the Golden Gate Bridge where they discussed its seismic retrofit project. Mr. Dennis Mulligan, chief engineer of the seismic retrofit project welcomed the delegation. Following the 1989 Loma Prieta earthquake the Golden Gate Authority began a study to retrofit the bridge. It was divided into three phases: north viaduct; south structure; and the suspension bridge itself. Dampers were installed at the towers and bridge truss and at the arch pylon/bridge trusses. The towers were stiffened, the saddle/cable connection was strengthened, and isolators were installed on the viaduct. The cables were inspected in 1991 and 2000 and were assessed to be in good condition.

Golden Gate Bridge

The Golden Gate Bridge is internationally known as one of the greatest suspension bridges ever built. Since opening in 1937, it has served as a critical link in California's highway system and as an engine of economic vitality, supporting the region's industry, commerce and tourism. The Golden Gate Bridge now carries 42 million vehicles a year and is visited by more than 10 million people annually. The Golden Gate Bridge remains vulnerable to earthquakes and could fail during an earthquake of magnitude 7.0 or greater on the nearby San Andreas or Hayward faults. The U.S. Geological Survey reports a 70 % probability of a magnitude 6.7 or greater earthquake striking the Bay Area prior to 2030. Under the leadership of Bay Area Congressional members the Golden Gate Bridge, Highway and Transportation District (District), the public agency that built, operates and maintains the Bridge, is seeking an additional $119 million in federal allocations. Once completed, the $388 million project will protect the Golden Gate Bridge from nearby earthquakes up to magnitude 8.3.

The Golden Gate Bridge seismic retrofit is separated into three construction phases. Phase 1 retrofitted the North Viaduct and was completed in December 2001. The second phase began in summer 2001 and will retrofit the South Viaduct, Anchorage, Fort Point arch, and South Pylons, while the third phase, once funded, will retrofit the North Anchorage, the Main Span and Main Towers. The retrofit design maintains the Golden Gate Bridge's aesthetic and historic integrity, while strengthening the Bridge to withstand a maximum credible earthquake.

CALTRANS is constructing a new Carquinez Bridge that the delegation did not visit. This new structure will be on Interstate 80 near Vallejo, CA. It will be a suspension bridge 1.3 km (0.8 mi) long. This structure will have an average daily traffic volume of 116,000 vehicles. The present estimate for the construction of this structure is $188 million. Work began in January, 2000 and is scheduled to be completed in December, 2003.

Reno, Nevada

3. University of Nevada-Reno

The delegation visited the University of Nevada-Reno (UNR) campus in the morning of May 18, 2002. Dr. Ian Buckle, Director, Center for Civil Engineering Earthquake Research, University of Nevada-Reno, NV http://bric.ce.unr.edu/cceer.htm hosted the delegation. Following a welcome by Dr. Maragakis, Dean of the Civil and Environmental Engineering Department, the delegation discussed recent research projects in earthquake engineering, participated in short presentations on recent research, and observed current upgrades to their new Multi-Shake Table Facility.

The delegation first visited the Mackay Building, which currently houses the engineering library and the museum of mining and geology. The Mackay building is an un-reinforced masonry building constructed in

1908. It is the second oldest building on campus. It is on the National Register of Historic Buildings. Since it is on the National Register, options for seismic retrofit were limited; thus base isolation was selected. Completed in 1993, the Mackay Building retrofit uses a combination of high-damping rubber isolators and friction dampers. The building rests on sixty high-damping rubber isolators at the edges of the building. Forty friction dampers were installed to support the floor and to reduce the floor span since the building live loads are relatively high. The stairs at the front of the building are now cantilevered from the building frame. The building is instrumented to record its response during seismic events.

UNR received a Network for Earthquake Engineering Simulation (NEES) award from the National Science Foundation (NSF) to invest in equipment to upgrade experimental earthquake simulators. $100 million was provided to 10 universities. UNR received $7 million for upgrades: $4.4 million from NSF; $1.6 million from the Department of Housing and Urban Development; and $1 million from the Department of Energy.

The delegation participated in presentations on some of the research being conducted at UNR. Hisham Nada presented research that is being conducted for CALTRANS to improve the seismic performance of flared bridge columns. During a seismic event, the plastic hinge shifts down and failure of the column occurs just below the flare. CALTRANS has issued new guidance for construction of flared columns that creates a gap between the beams and columns. UNR is investigating the efficiency of the new detail, the effect of lowering the confinement ratio at the top of the column, and the effect of column height on the shear level. Experimental work in support of this research is being conducted on 1/5-scale specimens.

Lyle Carden presented his research on improving the seismic performance of steel girder bridges through the application of ductile substructures and seismic isolation. The application of ductile substructure and seismic isolation is to assure that the bridge superstructure remains elastic during a seismic event. The objectives of this work are to investigate the load path and the behavior of components, demonstrate improved performance through the use of ductile members in the substructure and seismic isolation. Experimental work has been performed on 2/5-scale, two girder specimens, with static loads applied at the deck level. Dynamic testing will be performed on the shake facility at UNR.

Lyle Carden presented a second paper on research performed for CALTRANS related to the replacement of the East Span of the San Francisco-Oakland Bay Bridge. UNR is evaluating the shear link that will be used in the tower for self-supporting suspension span. UNR has conducted two tests on the shear link to date. UNR is also evaluating high performance steel A709 HPS70W for energy dissipation under earthquake loading for the East Span replacement program.

Fabio Sanchez-Camargo made the final presentation on his research into the seismic performance of bridge restrainers at intermediate hinges. In multi-span bridges, out-of-phase movement of adjacent frames can lead to excessive displacement. This research, focused on concrete bridges, will result in a model of typical hinge details for evaluation of restrainers under seismic loadings.

The visit to UNR concluded with a tour of the structures laboratory. The laboratory was constructed in 1992. The laboratory includes a dual shake table facility. The shake tables became operational in 1998. The existing shake table facility is being upgraded to add a third shake table. Additional upgrades are being made to give all three-shake tables biaxial loading capability. The upgrades are being funded through the National Science Foundation's Network for Earthquake Engineering Simulation (NEES) program.

4. **DIS Systems INC.**, Sparks, Nevada. www.dis-inc.com.

Mr. Konrad Erikesen, Vice President, Engineering and Marketing, Dr. Amarnath Kasalanati, and Mr. Danny Sommers hosted the delegation. Since DIS' creation in 1982, as a manufacture of base isolators and energy dissipators, the organization supplied isolators for more than 100-bridge projects and 80-buildings worldwide. About 50 % of these buildings are in Japan. Example projects include Oakland City Hall, San Francisco City Hall, several hospitals and emergency centers, the Asian Art Museum in San Francisco; several CALTRANS bridges and the Golden Gate Bridge, and the JFK Light Rail System in NY.

The delegation toured DIS' manufacturing plant and discussed its seismic isolator testing capability, with 1.8×10^6 kg (2,000 tons) of compression capacity and shear capacity of 4.1×10^5 kg (450 tons) with ± 70 cm stroke. DIS maintains an extensive database of tested isolator properties. These isolators absorb up to 40 MPa load and 400 percent shear strain. DIS' largest isolators are 1.5 m diameter, 0.75 m tall, weigh 2.7×10^3 kg (3 tons), and carry 300 tons. The vertical load carrying capacity of these isolators is about 100 kg/cm^2 or about 8,274 kPa (1200 psi) axial stress. These elastomeric isolators consist of a central lead core, energy dissipator, that is surrounded by horizontal layers of rubber and steel reinforcing plates capped with steel load plates top and bottom that are anchored to the column above and the floor below.

DIS monitors many of their installed systems of the past 10 years. They perform 12 year and 6 year aging tests on their isolators. We were told the isolator stiffness has increased by 2% to 5%.

DIS performs quality control inspection for each isolator throughout its manufacturing process. Individual inspection records are kept for each inspection. The rejection rate was reported to be about 1 %. DIS has not registered for ISO 9000 compliance since accreditation is not required in the US market and at this point in their manufacturing, DIS management does not see a need to be ISO accredited. One of their largest customers, Japan has approved DIS' isolators through the Building Council of Japan. When the company increases in size, the Vice President for Engineering and Manufacturing said DIS will apply for ISO 9000 registration.

DIS is about a $10 million business employing 40 staff; 30 are on the shop floor. Their Headquarters is in Lafayette, CA. DIS' manufacturing factory is in Sparks, NV where they produce about 1000 isolators annually.

ABSTRACT

This publication is the Proceedings of the 34th Joint Meeting of the US-Japan Panel on Wind and Seismic Effects. The meeting was held at the National Institute of Standards and Technology, Gaithersburg, Maryland during 13-15 May 2002. The Proceedings include the technical program, list of members, Panel Resolutions, Task Committee Reports, and the 30 technical papers authored for this joint meeting.

The manuscripts were presented within five Sessions: Geotechnical Engineering and Ground Motion; Next-Generation Building and Infrastructure Systems; Wind; Dams; and Transportation Systems and three Technical Themes: Terrorism -- Collapse of the WTC and Pentagon Wedge A; Disaster Information; and Management of Infrastructure Systems.

KEYWORDS: Bridges; building performance; disaster information systems; disaster reduction; earthquakes; geotechnical engineering; ground failures; ground motion; infrastructure; liquefaction; masonry; measurements; risk assessment; seismic; standards; structural engineering; and wind loads.

CONTENTS

AGENDA
34th TECHNICAL PANEL MEETING on WIND AND SEISMIC EFFECTS
13-15 May 2002

Monday 13 May

1000 **OPENING CEREMONIES**
(Lecture Room B, Administration Building)

Call to order by Mr. Stephen CAUFFMAN, Secretary-General US-side Panel

Opening remarks by Dr. Arden L. BEMENT, Jr. Director, National Institute of Standards and Technology

Remarks by Mr. Koichi MORIMOTO, Counsellor for Science and Technology, Embassy of Japan

Remarks by Dr. Shyam SUNDER, Chairman US-side, Panel on Wind and Seismic Effects, Chief, Structures Division, Building and Fire Research Laboratory

Remarks by Dr. Tadahiko SAKAMOTO, Chairman Japan-Side, Panel on Wind and Seismic Effects, Chief Executive, Public Works Research Institute

Introduction of U.S. Members by U.S. Panel Chairman

Introduction of Japan Members by Japan Panel Chairman

Elect Joint Meeting Chairman

Adopt Agenda

Adjourn

1115 **Group Photograph**

TECHNICAL SESSION 1

1130-1250 **Technical Session 1** – GEOTECHNICAL ENGINEERING AND GROUND MOTION

Chairman: Dr. Tadahiko SAKAMOTO

1130 *Seismic Performance of Urban, Reclaimed, and Port Areas - Full Scale Experiment Using Blast Technique*, Takahiro SUGANO* and Eiji KOHAMA, PARI

1145 *A Review of Empirical Evidence For Site Coefficients in Building-Code Provisions,*

Roger BORCHERDT, USGS (Presentation by Mehmet CELEBI)

1200 *A Practical Procedure for Formulating Level 2 Earthquake Motions Based on Scenario Earthquakes*, Shojiro KATAOKA*, NILIM, Jun MURAKOSHI, PWRI, and Keiichi TAMURA, PWRI

1215 *Identifying Site Frequencies from Building Response Records*, Mehmet CELEBI, USGS

1230 *Evaluation of Earth Pressure Acting on Embedded Pile-cap Based on Liquefaction Test Using Large-scale Shaking Table*, Shuji TAMURA*, Shinshu University, Chikahiro MINOWA, NRIESDP, Kohji TOKIMATSU, TIT, Shunji FUJII, Kajima Tech. Res. Inst., Kaeko YAHATA, Taisei Corp., and Tomio TSUCHIYA, Takenaka Research & Dev. Inst.

1245 Discussion

1305 **Lunch**

TASK COMMITTEE MEETINGS

1415-1700 **Task Committee Meetings**

T/C A: **Geotechnical Engineering and Ground Motion.** Dr. Osamu MATUO, NILIM and Dr. Takahiro SUGANO, PARI (Japan-side Co-Chairs) and Dr. Mehmet CELEBI, USGS and Dr. Michael SHARP, Corps of Engineers (U.S.-side Co-Chairs)
Admin. Bldg. Room CR-111

T/C B: **Next-generation Building and Infrastructure Systems.** Dr. Masaomi TESHIGAWARA, BRI and Mr. Keiichi OHTANI, NIED (Japan-side Co-Chairs) and Dr. George LEE, MCEER and Dr. Peter CHANG, NSF (U.S.-side Co-Chairs)
Admin. Bldg. Room CR-113

T/C C: **Dams.** Dr. Yoshikazu YAMAGUCHI, PWRI (Japan-side Chair) and Dr. Robert HALL, Corps of Engineers (U.S.-side Chair)
BFRL Conf. Room B-221 (Bldg 226)

T/C D: **Wind.** Dr. Hisashi OKADA, BRI and Dr. Nobuyuki HIRAHARA, PWRI (Japan-side Co-Chairs) Dr. Peter CHANG, NSF (U.S.-side Chair)
Structures Conference Room B-139 (Bldg 226)

T/C G: **Transportation Systems.** Dr. Hiroshi SATO, PWRI (Japan-side Chair) and Dr. Phillip YEN, FHWA (U.S.-side Chair)
Admin. Bldg. Lecture Room B

1700 **Conclusion of Day 1**

Tuesday 14 May

TECHNICAL SESSION 2

0815-0935 **Technical Session 2 – NEXT-GENERATION BUILDING AND INFRASTRUCTURE SYSTEMS**

Chairman: Dr. Shyam SUNDER

0815 *Project on 3-D Full Scale Earthquake Testing Facility*, Keiichi OHTANI*, Tsuneo KATAYAMA, Heki SHIBATA and Nobuyuki OGAWA, NIED

0830 *Smart Damping Technologies for Dynamic Hazard Mitigation*, B. F. Spencer Jr., University of Notre Dame

0845 *Research and Development Programs on Timber Structures in Japan*, Hiroshi ISODA, BRI, Hisashi OKADA, BRI, Naohito KAWAI, NILIM, and Nobuyoshi YAMAGUCHI, PWRI Presented by Masaomi TESHIGAWARA, BRI

0900 *Modeling Regional Economic Resilience to Earthquakes: A Computable general Equilibrium Analysis of Lifeline Disruptions*, Adam ROSE*, The Pennsylvania State University and Shu-Yi LIAO, California Energy Commission

0915 Discussion

0935 **Break**

TECHNICAL SESSION 3

0955-1115 **Technical Session 3 - WIND ENGINEERING**

Chairman: Dr. Shyam SUNDER

0955 *Aerodynamic Stability of a Super Long-Span Bridge with Slotted Box Girder*, Hiroshi SATO*, PWRI, Nobuyuki HIRAHARA, HSBA, Koichiro FUMOTO, HSBA, Shigeru HIRANO, HSBA, and Shigeki KUSUHARA, HSBA

1010 *Wind Effects on Long Span Cable Stayed Bridges: Assessment and Validation*, Nicholas JONES* and Ender OZKAN, Johns Hopkins University

1025 *Strategy on Wind Engineering Research in BRI and NILIM*, Hisashi OKADA, BRI, Yasuo OKUDA* BRI, Hitomitsu KIKITSU, BRI and Masamiki OHASHI, NILIM

1040 *Next Generation Wind Tunnels for Simulation of Straight-Line, Thunderstorm- and Tornado-Like Winds*, Partha SARKAR*, and Fred L. HAAN, Jr., Iowa State University

1055 Discussion

1115 Adjourn For Lunch

1130 **Lunch**

TECHNICAL SESSION 4

1230-1335 **Technical Session 4 – DAMS**

Chairman: Dr. Shyam SUNDER

1230 *Seismic Performance Evaluation of Intake Towers*, Richard C. DOVE*, US Army Corps of Engineers and Enrique E. MATHEU, Louisiana State University

1245 *Present State of Measurement of Earthquake Motion and Nation-Wide Networking of Seismographs at Dam Sites in Japan,* Shuji TAKASU, PWRI, Hitoshi YOSHIDA, NILIM, Yoshikazu YAMAGUCHI*, PWRI, Takashi SASAKI, PWRI, and Kenji INAGAKI, NILIM

1300 *Deformation Analysis and Remediation for Small Earth Dams*, Michael K. SHARP*, US Army CORPS and Scott STEEDMAN, Whitby Byrd and Associates, London, UK

1315 Discussion

1335 **Break**

TECHNICAL SESSION *5*

1355 - 1630 **Technical Session *5* – TRANSPORTATION SYSTEMS**

Chairman: Dr. Shyam SUNDER

1355 *An Evaluation of the Force Reduction Factor in the Force-Based Seismic Design,* Gakuho WATANABE and Kazuhiko KAWASHIMA*, Tokyo Institute of Technology

1410 *Bolu Viaduct-1 Subjected to Near-Fault Ground Motion,* Sunwoo PARK, Lendis Corporation, Hamid GHASEMI*, FHWA, Jerry SHEN, Lendis Corporation, and Phillip YEN, FHWA

1425 *2002 Seismic Design Specifications for Highway Bridges*, Shigeki UNJOH*, PWRI, Shoichi NAKATANI, NILIM, Keiichi TAMURA, PWRI, Jiro FUKUI, PWRI, and Jun-ichi HOSHIKUMA, PWRI

1440 *Development of National Guidelines for Seismic Performance Testing,* W. Phillip YEN*, Jerry J. SHEN, and John O'FALLON, FHWA

1455 Discussion

STRATEGIC PLANNING SESSION

1530-1700 **Strategic Planning Session (Panel Chairs and Secretariat)**

1700 **Conclusion of Day 2**

Wednesday 15 May

SPECIAL THEME 1 - TERRORISM: COLLAPSE of the WTC and PENTAGON WEDGE A

Chairman: Dr. Tadahiko SAKAMOTO

0845-0950

0845 *Standards, Technologies, and Practices for Cost-Effective Safety and Security of Buildings and Critical Facilities,* Shyam SUNDER, NIST

0900 *FEMA/ASCE Building Performance Assessment Team Study of the World Trade Center Events,* Michael MAHONEY, FEMA

0915 *Terrorist Threats Against the Pentagon*, Robert L. HALL*, James T. BAYLOT, Robert J. DINAN, Richard DOVE, John HAYES, John HAYS, W. Matthew HOSSLEY, James L. O'DANIEL, Thomas R. SLAWSON, and Stanley C. WOODSON, US Army Corps of Engineers
0930 Discussion
0950 Break

SPECIAL THEME 2 - DISASTER INFORMATION

Chairman: Dr. Tadahiko SAKAMOTO

1005-1050

1005 *Natural-Technologic Events: The Frequency And Severity of Toxic Releases During and After Natural Disasters With Emphasis on Wind and Seismic Events*, Stacy YOUNG, National Center for Environmental Health, CDC
1020 *Disaster Information Systems and Seismic Countermeasure for Field Facilities in NTT*, Kazuhiko FUJIHASHI, NTT
1035 Discussion
1050 Break

SPECIAL THEME 3- MANAGEMENT OF INFRASTRUCTURE SYSTEMS

Chairman: Dr. Tadahiko SAKAMOTO

1105 - 1210

1105 *Management of Infrastructure Facilities to Ensure the Function as Disaster Protection*, Tadayuki TAZAKI, Takeo NAKAJIMA, and Kazuhiro NISHIKAWA*, NILIM
1120 *Information Systems for Infrastructure Management and Emergency Response*, William ROPER, George Washington University
1135 *Risk Assessment on Storm Surge Flood*, Ken-ichi TORII* and Fuminori KATO, NILIM
1150 Discussion
1210 Adjourn for lunch

1215 Lunch

TASK COMMITTEE REPORTS AND RESOLUTIONS

1330-1430 Report of Task Committees

Chairman: Dr. Tadahiko SAKAMOTO

T/C A: Geotechnical Engineering and Ground Motion
T/C B: Next-generation Building and Infrastructure Systems
T/C C: Dams

T/C D. Wind Engineering
T/C G: Transportation Systems and summary of 17th US-Japan Bridge Workshop, November 2001

1430-1530 **Adoption of Final Resolutions**

1530 **Break**

CLOSING CEREMONIES

1545 Call to Order by Mr. Stephen CAUFFMAN, Secretary-General, U.S.-Side Panel

Closing Remarks by Dr. Tadahiko SAKAMOTO, Chairman Japan-Side Panel

Closing Remarks by Dr. Shyam SUNDER, Chairman U.S.-Side Panel

1615 **Conclusion of 34th Joint Panel Technical Sessions**

LIST OF PANEL MEMBERS

UNITED STATES-SIDE PANEL ON WIND AND SEISMIC EFFECTS
MEMBERSHIP LIST

30 April 2002

Dr. S. Shyam Sunder
Chairman, U.S.-side Panel
Chief, Structures Division
Building and Fire Research Laboratory
National Institute of Standards and Technology
100 Bureau Drive, Stop 8611
Gaithersburg, MD 20899-8611
301-975-6061 FAX:301-869-6275
sunder@nist.gov

Mr. Stephen A. Cauffman
Secretary-General, U.S.-side Panel
Research Engineer
National Institute of Standards and Technology
Building and Fire Research Laboratory,
Structures Division
100 Bureau Drive, Stop 8611
Gaithersburg, MD 20899-8611
301-975-6051 FAX: 301-869-6275
stephen.cauffman@nist.gov

Dr. Daniel P. Abrams
Director, Mid-America Earthquake Center
Hanson Engineers Professor of Civil Engineering
University of Illinois
1241 Newmark Laboratory
205 North Mathews Avenue
Urbana, IL 61801
217-244-6302 FAX:217-333-3821
d-abrams@uiuc.edu

Dr. Kharaiti L. Abrol
Principal Structural Engineering Consultant
Room 475
Department of Veterans Affairs
810 Vermont Avenue, NW
Washington, DC 20420
202-565-5579 FAX:202-565-5478
abrkha@hq.med.va.gov

Dr. Jon Ake
Geophysicist
Seismotectonics and Geophysics Section
Code D-8330
P.O. Box 25007
Bureau of Reclamation
U.S. Department of the Interior
Denver, CO 80225
303-445-3169 FAX:303-236-9127
jake@do.usbr.gov

Dr. Clifford J. Astill
Program Director
Division of Biological and Critical Systems
National Science Foundation
4201 Wilson Boulevard - Room 545
Arlington, VA 22230
703-306-1361 FAX:703-306-0291
castill@nsf.gov

Mr. John Baals
Seismic Safety Coordinator
P.O. Box 25007 (D-8110)
Bureau of Reclamation
U.S. Department of the Interior
Denver, CO 80225
303-236-3999 x534 FAX:303-236-9099
jbaals@do.usbr.gov

Dr. Celso S. Barrientos
Supervisory Physical Scientist
National Environmental Satellite Data Information Service - Code E/RA28
National Oceanic and Atmospheric Administration
U.S. Department of Commerce
5200 Auth Road

Camp Springs, MD 20746
301-713-9384 x109 FAX: 301-713-4598
Celso.S.Barrientos@noaa.gov

Dr. Eddie N. Bernard
Director, Pacific Marine Environmental Laboratory
National Oceanic and Atmospheric Administration
U.S. Department of Commerce
7600 Sand Point Way, NE
BIN C15700/Building 3
Seattle, WA 98115-0070
206-526-6800 FAX:206-526-4576
Eddie.N.Bernard@noaa.gov

Dr. David M. Boore
U.S. Geological Survey
345 Middlefield Road MS 977
Menlo Park, CA 94025
650-329-5616 FAX:650-329-5163
boore@usgs.gov

Dr. Roger D. Borcherdt
U.S. Geological Survey
U.S. Department of the Interior
345 Middlefield Road, MS 977
Menlo Park, CA 94025
650-329-5619 FAX:650-329-5163
borcherdt@usgs.gov

Dr. Mehmet K. Celebi
Research Civil Engineer
U.S. Geological Survey
U.S. Department of the Interior
345 Middlefield Road, MS 977
Menlo Park, CA 94025
650-329-5623 FAX: 650-329-5163
celebi@usgs.gov

Mr. Harish Chander
U.S. Dept. of Energy (EH-31),
CXXI, Room 2016 (GTN)
19901 Germantown Road
Germantown, MD 20874-1290
301-903-6681 FAX:301-903-8693
harish.chander@hq.doe.gov

Dr. Peter Chang
National Science Foundation
4201 Wilson Boulevard – Room 545
Arlington, VA 22230
703-292-8360
pchang@nsf.gov

Dr. C.Y. Chen
Senior Civil/Geotechnical Engineer
Office of Foreign Buildings
Department of State
Code SA-6, Rm. 347
Washington, DC 20520
703-875-6207 FAX:703-875-6204
chency@state.gov

Dr. Ken Chong
(Serving as Guest Researcher NIST's Building Materials Division during FY 2002)
Program Director
Mechanics and Materials
Engineering Directorate
National Science Foundation
4201 Wilson Boulevard - Room 545
Arlington, VA 22230
703-292-7008 FAX:703-292-9053
kchong@nsf.gov

Mr. James D. Cooper
Director, Office of Bridge Technology
Federal Highway Administration
U.S. Department of Transportation
400 7th Street SW
Washington, DC
202-366-4589 FAX 703-285-2766
Jim.Cooper@igate.fhwa.dot.gov

Dr. James F. Costello
Senior Structural Engineer
Structural and Geological Engineering Branch

Office of Nuclear Regulatory Research
US Nuclear Regulatory Commission
Mail Stop T10-L1
Washington, DC 20555
301-415-6009
jfc@nrc.gov

Mr. William Freeborne
Housing and Urban Development
Room 8132
451 Seventh Street, SW
Washington, DC 20410
202-708-4370 x5725 FAX:202-708-5873
william_e._freeborne@hud.gov

Dr. Joseph Golden
Forecast Systems Laboratory
National Oceanic and Atmospheric Administration
Rm. DSRC-2B133
325 Broadway Street
Boulder, CO 80302
303-497-6098
jgolden@fsl.noaa.gov

Dr. John Gross
Leader, Structural Systems and Design Group
Building and Fire Research Laboratory
National Institute of Standards and Technology
100 Bureau Drive, Stop 8611
Gaithersburg, MD 20899-8611
301-975-6068 FAX:301-869-6275
john.gross@nist.gov

Dr. Robert L. Hall
Chief, Structural Analysis Group
US Army Engineer Research and Development Center
Waterways Experiment Station
Office Address: CEERD-GS
3909 Halls Ferry Road
Vicksburg, MS 39180-6199
601-634-2567 FAX:601-634-3412
Robert.L.Hall@erdc.usace.army.mil

Dr. Allen M. Hittelman
Chief, Solid Earth Geophysics Division
E/GC1, National Geophysical Data Center
NOAA, NESDIS
325 Broadway
Boulder, CO 80303-3328
303-497-6591 FAX:303-497-6513
allen.m.hittelman@noaa.gov

Dr. Mary Ellen Hynes
Chief, Earthquake Engineering and Geophysics Branch
Geotechnical Laboratory
Office Address: CEERD-GS-R
US Army Engineer Research and Development Center
Waterways Experiment Station
3909 Halls Ferry Road
Vicksburg, MS 39180
601-634-2280 FAX:601-634-3453
mary.e.hynes@erdc.usace.army.mil

Mr. Roger M. Kenneally
Structural Engineer
Structural and Seismic Engineering Branch
Mail Stop T10-L1
US Nuclear Regulatory Commission
Washington, DC 20555
301-415-6303
rmk@nrc.gov

Mr. James Lander
Geophysicist
Cooperative Institute for Research in Environmental Sciences
University of Colorado
Campus Box 449, Room 152 RL3
3100 Marine Street

Boulder, CO 80309
303-497-6446 FAX: 303-497-6513
jlander@ngdc.noaa.gov

Dr. George Lee
Director, Multidisciplinary Center for Earthquake Engineering Research (MCEER)
State University of New York at Buffalo
Red Jacket Quadrangle
Buffalo, NY 14261
716-645-3391 x111 FAX:716-645-3399
gclee@mceermail.buffalo.edu

Dr. H.S. Lew
Structures Division
Building and Fire Research Laboratory
National Institute of Standards and Technology
100 Bureau Drive Stop 8611
Gaithersburg, MD 20899-861
301-975-6060 FAX:301-869-6275
hai.lew@nist.gov

Mr. Michael Mahoney
Physical Scientist
Federal Emergency Management Agency
500 C Street, SW
Washington, DC 20472
202-646-2794 FAX:202-646-4387
mike.mahoney@fema.gov

Dr. Josephine Malilay
Disaster Assessment and Epidemiology Section
National Center for Environmental Health
F-46 Center for Disease Control and Prevention
4770 Buford Highway, NE
Atlanta, GA 30341
404-489-1359 FAX: 404-498-1355
jmalilay@cdc.gov

Dr. Francis G. McLean
Value Engineering Program Manager
Code D-8170
P.O. Box 25007
Bureau of Reclamation
U.S. Department of the Interior
Denver, CO 80225
303-445-3091 FAX:303-6475
FMCLEAN@do.usbr.gov

Dr. Raymond E. Meyer
Department of State
SA14/Room 1705
USAID/Washington, DC 20523-1443
202-712-1078 FAX: 202-216-3707
Rmeyer@usaid.gov

Dr. Martin C. Miller
Chief, Coastal Oceanography Branch
USAE, Waterways Experiment Station
Coastal and Hydraulics Laboratory
(CEWES-CR-O)
3909 Halls Ferry Road
Vicksburg, MS 39180
601-634-3999 FAX:601-634-4314
martin.c.miller@erdc.usace.army.mil

Dr. Jack Moehle
Director, Pacific Earthquake Engineering Research Center (PEER)
1301 South 46th Street
Richmond, CA 94804-4698
510-231-9554 FAX: 510-231-9471
moehle@eerc.berkeley.edu

Mr. Ugo Morelli
Policy Manager
Federal Emergency Management Agency
500 C Street, SW
Washington, DC 20472
202-646-2810 FAX:202-646-2577
ugo.morelli@fema.gov

Dr. William Roper
Professor and Chairman

Civil and Environmental
Engineering Department
George Washington University
Phillips Hall, Room 643
The Academic Center
801 22nd St., N.W.
Washington, DC 20052
202-994-4901 FAX: 202 994-0127
wroper@seas.gwu.edu

Dr. Erdal Safak
Research Structural Engineer
U.S. Geological Survey
Box 25046, MS 966
Denver Federal Center
Denver, CO 80225
303-273-8593 FAX:303-273-8600
safak@usgs.gov

Dr. Michael Sharp
Director, Centrifuge Research Center
Geotechnical and Structures Laboratory
US Army Engineer Research and
Development Center
Waterways Experiment Station
3909 Halls Ferry Road
Vicksburg, MS 39180-6199
601-634-4127 FAX: 601-634-4894
michael.k.sharp@erdc.usace.army.mil

Dr. Charles E. Smith
Senior Technical Advisor
Engineering and Research Branch
U. S. Minerals Management Service
381 Elden Street, MS 4021
Herndon, VA 20170-4817
703-787-1561 Fax 703-787-1549
smithc@mms.gov or
Charles.E.Smith@mms.gov

Dr. W. Phillip Yen
Seismic Hazard Mitigation
Office of Infrastructure, R&D
Federal Highway Administration
6300 Georgetown Pike
McLean, VA 22101
202-493-3056 FAX: 202-493-3442
Wen-huei.Yen@fhwa.dot.gov

Mr. Ray Zelinski
Chief, Earthquake Engineering Office
California Department of Transportation
Division of Engineering Services, MS9-2/7J
P.O. Box 168041
Sacramento, CA 95816
916-227-8806 FAX: 916-227-8242
ray.j.zelinski@dot.ca.gov

TEMPORARY US-SIDE MEMBERS

Dr. Richard C. Dove
US Army Engineer Research and Development Center
Waterways Experiment Station
3909 Halls Ferry Road
Vicksburg. MS 39180-6199
601-634-2883
richard.c.dove@erdc.usace.army.mil

Dr. Hamid Ghasemi
Turner-Fairbank Highway Research Center
Federal Highway Administration
6300 Georgetown Pike
McLean, VA 22101
703-285-2447
hamid.ghasemi@fhwa.dot.gov

Dr. Nicholas P. Jones
Professor and Chair
Department of Civil Engineering
Johns Hopkins University
3400 N. Charles Street
Baltimore, MD 21218-2686
410-516-7874; (F) 410-516-7473
nick@jhu.edu

Dr. Enrique E. Matheu
Department of Civil and Environmental Engineering
Louisiana State University
Office address:
U.S. Army Engineer Research and Development Center
3909 Halls Ferry Road, ATTN: CEERD-GS-M
Vicksburg, MS 39180
Tel: 601-634-3235, Fax: 601-634-3412
Enrique.E.Matheu@erdc.usace.army.mil

Professor Adam Rose
Department Head, Energy, Environmental, & Mineral Economics
The Pennsylvania State University
221 Eric A. Walker Building
University Park, PA 16802-5010
(T) 814-863-0179
azr1@psu.edu

Dr. Partha P. Sarkar
Associate Professor and Wilson Chair
Director, Wind Simulation and Testing Laboratory
Department of Aerospace Engineering and Engineering Mechanics
2271 Howe Hall, Room 1200
Iowa State University
Ames, IA 50011-2271
515-294-0719 515-294-3262
ppsarkar@iastate.edu

Dr. B.F. Spencer, Jr.
Leo E. and Patti Ruth Linbeck Professor of Engineering
Department of Civil Engineering and Geological Sciences
156 Fitzpatrick Hall
University of Notre Dame
Notre Dame, IN 46556-0767
(T) 219-631-6247, (F) 443-646-0675
219-315-0738 (Mobile)
spencer@nd.edu

Stacy Young, MS MPH
Fellow, Association of Schools of Public Health
Centers for Disease Control and Prevention
National Center for Environmental Health
1600 Clifton Rd., NE (Mailstop E-23)
Atlanta, GA 30333
404-498-1877; 404-498-1355
say5@cdc.gov

JAPAN-SIDE PANEL ON WIND AND SEISMIC EFFECTS
MEMBERSHIP LIST

STEERING COMMITTEE MEMBERS

Dr. Tadahiko Sakamoto
Chairman, Japan-side Panel on Wind and Seismic Effects
Chief Executive, Independent Administrative Institution
Public Works Research Institute
1-6 Minamihara, Tsukuba-shi, Ibaraki-ken 305-8516
Tel: 0298-79-6700
Fax: 0298-79-6741
E-mail: sakamoto@pwri.go.jp

Dr. Michio Okahara
Secretary-General, Japan-side Panel on Wind and Seismic Effects
Executive Director, Independent Administrative Institution
Public Works Research Institute
1-6, Minamihara, Tsukuba-shi, Ibaraki-ken 305-8516
Tel: 0298-79-6700
Fax: 0298-79-6702
E-mail: okahara@pwri.go.jp

Mr. Minoru Akiyama
Director, Geographic Department
Geographical Survey Institute
Ministry of Land, Infrastructure and Transport
1, Kitasato, Tsukuba-shi, Ibaraki-ken 305-0811
Tel:0298-64-1111
Fax:0298-64-1804
E-mail: m-akiyoama@gsi.go.jp

Mr. Ippei Eguchi
Senior Assistant for Disaster Prevention
Planning Division
Administration Department
Japan Meteorological Agency
1-3-4, Ohte-machi, Chiyoda-ku, Tokyo 100-8918
Tel: 03-3212-8341
Fax: 03-3211-2032

Mr. Tadayuki Gotou
Director, Building Disaster Prevention Office
Housing Bureau
Ministry of Land, Infrastructure and Transport
2-1-3, Kasumigaseki, Chiyoda-ku, Tokyo 100-8918
Tel: 03-5253-8514
Fax: 03-5253-1630
E-mail: gotou-t2gr@mlit.go.jp

Dr. Nobuo Hamada
Director, Seismological Volcano logicale
Research Department
Meteorological Research Institute
Japan Meteorological Agency
1-1, Nagamine, Tsukuba-shi, Ibaraki-ken 305-0052
Tel: 0298-53-8675
Fax: 0298-53-3730
E-mail: nhamada@mri-jma.go.jp

Dr. Susumu Iai
Director, Earthquake Disaster Prevention Laboratory
Independent Administrative Institution
Port and Airport Research Institute
3-1-1, Nagase, Yokosuka-shi, Kanagawa-ken 239-0826
Tel: 0468-44-5030
Fax: 0468-44-0839
E-mail: iai@ipc.pari.go.jp

Mr. Masanori Iiba
Chief Research Engineer
Department of Structural Engineering
Independent Administrative Institution
Building Research Institute
1, Tatehara, Tsukuba-shi, Ibaraki-ken 305-8020
Tel:0298-64-6637
Fax:0298-64-6770
E-mail: iiba@kenken.go.jp

Mr. Takashi Kaminosono
Research Coordinator for Disaster Mitigation of Buildings
Research Center for Disaster Risk Management
Institute for Land and Infrastructure Management
Ministry of Land, Infrastructure and Transport
1, Asahi, Tsukuba-shi, Ibaraki-ken 305-0804
Tel:0298-64-4963
Fax:0298-64-0598
E-mail: kaminosono-t92rx@nilim.go.jp

Prof. Kazuhiko Kawashima
Professor, Department of Civil Engineering
Tokyo Institute of Technology
2-12-1, O-okayama, Meguro-ku, Tokyo 152-0033
Tel: 03-5734-2922
Fax: 03-3729-0728
E-mail: kawasima@cv.titech.ac.jp

Mr. Seiya Kinoshita
Director, International Division for Infrastructure
Policy Bureau
Ministry of Land Infrastructure and Transport
2-1-3, Kasumigaseki, Chiyoda-ku, Tokyo 100-8918
Tel: 03-5253-8315
Fax: 03-5253-1562
E-mail: kinoshita-s2jg@mlit.go.jp

Mr. Satoru Kondo
Director, River Division
Institute for Land and Infrastructure Management
Ministry of Land, Infrastructure and Transport
1, Asahi, Tsukuba-shi, Ibaraki-ken 305-0804
Tel:0298-64-2211
Fax:0298-64-1168
E-mail: kondou-s86uj@nilim.go.jp

Mr. Norishige Kubo
Deputy Director, International Division for Infrastructure
Policy Bureau
Ministry of Land Infrastructure and Transport
2-1-3, Kasumigaseki, Chiyoda-ku, Tokyo 100-8918
Tel:03-5253-8315
Fax:03-5253-1562

Mr. Takaaki Kusakabe
Head, Earthquake Disaster Prevention Division
Research Center for Disaster Risk Management
Institute for Land and Infrastructure and Management
Ministry of Land, Infrastructure and Transport
1, Asahi, Tsukuba-shi, Ibaraki-ken 305-0804
0298-64-2211
0298-64-0598
E-mail: ksakabe-t88d8@nilim.go.jp

Mr. Osamu Matsuo
Research Coordinator for Earthquake Disaster Prevention
Research Center for Disaster Risk Management
Institute for Land and Infrastructure Management
Ministry of Land, Infrastructure and Transport
1, Asahi, Tsukuba-shi, Ibaraki-ken 305-0804
Tel: 0298-64-2926
Fax: 0298-64-0598
E-mail: matsuo-o92rm@nilim.go.jp

16 Mr. Kiyoshi Minami
Director, Division of Road Management
Road Bureau
Ministry of Land, Infrastructure and Transport
2-1-3, Kasumigaseki, Chiyoda-ku, Tokyo 100-8918
Tel: 03-5253-8111
Fax: 03-5253-1618
E-mail: minami-k2z4@mlit.go.jp

Mr. Chikahiro Minowa
Scientific Research Advisor
Independent Administrative Institution
Research Institute for Earth Science and Disaster Prevention
3-1, Tennodai, Tsukuba-shi, Ibaraki-ken 305-0006
Tel: 0298-51-1611
Fax: 0298-51-1674
E-mail: minowa@bosai.go.jp

Mr. Masayuki Mori
International Cooperation Coordinator,
International Science and Technology Affairs Division,
Science and Technology Policy Bureau
Ministry of Education, Culture, Sports, Science and Technology
2-2-1, Kasumigaseki, Chiyoda-ku, Tokyo 100-8918
Tel: 03-5253-4055
Fax: 03-3581-5909
E-mail: m5mori@mext.go.jp

Mr. Akiyoshi Mukai
Chief Research Engineer, Department of Structural Engineering
Independent Administrative Institution
Building Research Institute
1, Tatehara, Tsukuba-shi, Ibaraki-ken 305-0802
Tel:0298-64-6662
Fax:0298-64-6773
E-mail: mukai@kenken.go.jp

Mr. Jun Murakoshi
Team Leader, Bridge Structure Team,
Structures Research Group
Independent Administrative Institution
Public Works Research Institute
1-6, Minamihara, Tsukuba-shi, Ibaraki-ken 305-8516
Tel:0298-79-6793
Tel:0298-79-6739
E-mail: murakosi@pwri.go.jp

Dr. Isao Nishiyama
Advanced Research Engineer
Production Engineering Department
Independent Administrative Institution
Building Research Institute
1, Tatehara, Tsukuba-shi, Ibaraki-ken 305-0802
Tel: 0298-64-6681
Fax: 0298-64-6772
E-mail: isao@kenken.go.jp

Mr. Akihiko Nunomura
Counselor .Prime Ministers' Secretarist
Cabinet Office
1-2-2, Kasumigaseki, Chiyoda-ku, Tokyo 100-8918
Tel: 03-3501-5693
Fax: 03-3501-5199

Dr. Hisashi Okada
Director, Structural Engineering Department
Independent Administrative Institution
Building Research Institute
1, Tatehara, Tsukuba-shi, Ibaraki-ken 305-0802
Tel: 0298-64-2151
Fax: 0298-64-2989
E-mail: okada@kenken.go.jp

Mr. Kazunori Oodaira
Director, Disaster Risk Management Division
River Bureau
Ministry of Land, Infrastructure and Transport
2-1-3, Kasumigaseki, Chiyoda-ku, Tokyo 100-8918
Tel: 03-3580-8111
Fax: 03-5253-1608
E-mail: oodaira-k2rb@mlit.go.jp

Dr. Izuru Ohkawa
Head, Construction Techniques Division
Production Department
Building Research Institute
Independent Administrative Institution
1, Tatehara, Tsukuba-shi, Ibaraki-ken 305-0802
Tel: 0298-64-6627
Fax: 0298-64-6773
E-mail: okawa@kenken.go.jp

Mr. Keiichi Ohtani
Project-Director, Project of 3-D Full-Scale Earthquake Testing Facility
National Research Institute for Earth Science and Disaster Prevention
3-1, Tennodai, Tsukuba-shi, Ibaraki-ken 305-0006
Tel: 0298-51-1611
Fax: 0298-52-8512
E-mail: ohtani@bosai.go.jp

Mr. Takuaki Ohyama
Head, Infections Diseases Division
Institute of Infections Diseases
Ministry of Health, Labor and Welfare
1-23-1, Toyama, Shinjyuku-ku, Tokyo 162-8640
Tel: 03-5285-1268
Fax: 03-5285-1129
E-mail: Ohyamat@nih.go.jp

Dr. Hiroshi Sato
Director, Structures Research Group
Independent Administrative Institution
Public Works Research Institute
1-6, Minamihara, Tsukuba-shi, Ibaraki-ken 305-8516
Tel: 0298-79-6726
Fax: 0298-79-6739
E-mail: hsato@pwri.go.jp

Dr. Takahiro Sugano
Chief, Structural Dynamics Laboratory
Structural Engineering Division
Independent Administrative Institution
Port and Airport Research Institute
3-1-1, Nagase, Yokosuka-shi, Kanagawa-ken 239-0826
Tel: 0468-44-5058
Fax: 0468-44-0839
E-mail: macsuga@ipc.pari.go.jp

Mr. Tetsuya Suzuki
Director, Structure Department
Independent Administrative Institution
Civil Engineering Research Institute of Hokkaido
1-3, Hiragishi, Toyohira-ku, Sapporo-shi
Hokkaido 062-8601
Tel: 011-841-5175
Fax: 011-820-2714
E-mail: 73302@ceri.go.jp

Mr. Yasushi Taguchi
Director, Research and Development Policy Division
Research and Development Bureau
Ministry of Education, Culture, Sports ,Science and Technology
1-3-2,Kasumigaseki,Chiyoda-ku,Tokyo 100-8966
Tel: 03-5253-4134
Fax: 03-5253-4139
E-mail: ytaguchi@mext.go.jp

Dr. Shigeo Takahashi
Director, Hydraulic Engineering Division
Independent Administrative Institution
Port and Harbor Research Institute
3-1-1, Nagase, Yokosuka-shi, Kanagawa-ken 239-0826
Tel: 0468-44-5036
Fax: 0468-44-1274
E-mail: takahashi_s@cc.pari.go.jp

Mr. Shuji Takasu
Director, Hydraulic Engineering Research Group
Independent Administrative Institution
Public Works Research Institute
1-6, Minamihara, Tsukuba-shi, Ibaraki-ken 305-8516
Tel: 0298-79-6723
Fax: 0298-79-6737
E-mail: takasu@pwri.go.jp

Mr. Yukio Takemura
Director, Typhoon Research Division
Meteorological Research Institute
Japan Meteorological Agency
Ministry of Land, Infrastructure and Transport
1-1, Nagamine, Tsukuba-shi, Ibaraki-ken 305-0052
Tel: 0298-53-8663
Fax: 0298-53-8735
E-mail: ytakemur@mri-jma.go.jp

Dr. Keiichi Tamura
Team Leader, Ground Vibration Research Team
Earthquake Disaster Prevention Research Group
Independent Administrative Institution
Public Works Research Institute
1-6, Minamihara, Tsukuba-shi, Ibaraki-ken 305-8516
Tel: 0298-79-6770
Fax: 0298-79-6735
E-mail: tamura@pwri.go.jp

Mr. Tadayuki Tazaki
Director-General, Institute for Land and Infrastructure Management
Ministry of Land, Infrastructure and Transport
1, Asahi, Tsukuba-shi, Ibaraki-ken 305-0804
Tel:0298-64-2211
Fax:0298-64-2148
E-mail tazaki-t82aa@nilim.go.jp

Dr. Masaomi Teshigawara
Chief Research Engineer
Department of Structural Engineering, Research Coodinator
Independent Administrative Institution
Building Research Institute
1, Tatehara, Tsukuba-shi, Ibaraki-ken 305-0802
Tel: 0298-64-6753
Fax: 0298-64-6773
E-mail: teshi@kenken.go.jp

Mr. Ken-ichi Tokida
Director, Earthquake Disaster Prevention Research Group
Independent Administrative Institution
Public Works Research Institute
1-6, Minamihara, Tsukuba-shi, Ibaraki-ken 305-8516
Tel: 0298-79-6700
Fax:0298-79-6736
E-mail: tokida@pwri.go.jp

Mr. Ken-ichi Torii
Head, Coastal Division
Institute for Land and Infrastructure Management
Ministry of Land, Infrastructure and Transport
1, Asahi, Tsukuba-shi, Ibaraki-ken 305-0804
Tel: 0298-64-2327
Fax: 0298-64-1168
E-mail: torii-k92fr@nilim.go.jp

Mr. Shinichiro Ueno
Director, Disaster Prevention Office
Coast Administration and Disaster Prevention Division
Ports and Harbors Bureau
Ministry of Land, Infrastructure and Transport
2-1-3, Kasumigaseki, Chiyoda-ku, Tokyo 100-8918
Tel: 03-5253-8689
Fax: 03-5253-1654
E-mail: ueno-s2sk@milt.go.jp

Dr. Shigeki Unjoh
Team Leader, Earthquake Engineering Research Team
Earthquake Disaster Prevention Research Group
Independent Administrative Institution
Public Works Research Institute
Minamihara1-6, Tsukuba-shi, Ibaraki-ken 305-8516
Tel: 0298-79-6773
Fax: 0298-79-6736
E-mail: unjoh@pwri.go.jp

Dr. Yoshikazu Yamaguchi
Team Leader, Dam Structure Research Team
Hydraulic Engineering Research Group
Independent Administrative Institution
Public Works Research Institute
1-6, Minamihara, Tsukuba-shi, Ibaraki-ken 305-8516
Tel: 0298-79-6780
Fax: 0298-79-6737
E-mail: yamaguti@pwri.go.jp

Dr. Hiroyuki Yamanouchi
Chief Executive
Independent Administrative Institution
Building Research Institute
1, Takehara, Tsukuba-shi, Ibaraki-ken 305-0802
Tel: 0298-64-2151
Fax: 0298-64-2989
E-mail: yamanoch@kenken.go.jp

TEMPORARY COMMITTEE MEMBERS

Mr. Kazuhiko Fujihashi
Senior Research Engineer, Supervisor
Disaster Prevention and Environmental Protection Group,
Civil Engineering Project
Access Network Service Systems Laboratories
Nippon Telegraph and Telephone Corporation (NTT)
1-7-1, Hanabatake, Tsukuba-shi, Ibaraki-ken 305-0805
Tel: 0298-68-6241
Fax: 0298-68-6259
E-mail: fujihasi@ansl.ntt.co.jp

Mr. Koichiro Fumoto
Senior Researcher, Structures Research Group
Independent Administrative Institution
Public Works Research Institute
1-6, Minamihara, Tsukuba-shi, Ibaraki-ken 305-8516
Tel: 0298-79-6726
Fax: 0298-79-6739
E-mail: fumoto@pwri.go.jp

Mr. Masahiro Ishida
Senior Researcher, Research Administration and International Cooperation Division
Planning and Research Administration Department
Institute for Land and Infrastructure Management
Ministry of Land, Infrastructure and Transport
1, Asahi, Tsukuba-shi, Ibaraki-ken 305-0804
Tel: 0298-64-2211
E-mail: ishida-m92bs@nilim.go.jp

Mr. Shojiro Kataoka
Senior Researcher
Earthquake Disaster Prevention Division
National Institute for Land and Infrastructure Management
Ministry of Land, Infrastructure and Transport
1, Asahi, Tsukuba-shi, Ibaraki-ken 305-0804
Tel: 0298-64-3245
Fax: 0298-64-0598
E-mail: kataoka-s92rc@nilim.go.jp

Mr. Takeo Nakajima
Director, Planning and Research Administration Department
Institute for Land and Infrastructure Management
Ministry of Land, Infrastructure and Transport
1, Asahi, Tsukuba-shi, Ibaraki-ken 305-0804
Tel: 0298-64-2826
Fax: 0298-64-1527
E-mail: nakajima-t92b4@nilim.go.jp

Mr. Kazuhiko Nishikawa
Research Coordinator for evaluation
Planning and Research Administration Department
Institute for Land and Infrastructure Management
Ministry of Land, Infrastructure and Transport
1, Asahi, Tsukuba-shi, Ibaraki-ken 305-0804
Tel: 0298-64-3725
Fax: 0298-64-1527
E-mail: nishikawa-k92br@nilim.go.jp

Dr. Shuji Tamura
Associate Professor, Architecture and Civil Engineering
Faculty of Engineering
Shinshu University
4-17-1, Wakasato, Nagano-shi 380-8553
Tel: 026-269-5362
E-mail: tamura@gipwc.shinshu-u.ac.jp

SECRETARIES COMMITTEE MEMBERS

Dr. Michio Okahara
Secretary-General, Japan-side Panel on Wind and Seismic Effects
Executive Director, Independent Administrative Institution
Public Works Research Institute
1-6, Minamihara, Tsukuba-shi, Ibaraki-ken 305-8516
Tel: 0298-79-6700
Fax: 0298-79-6702
E-mail: okahara@pwri.go.jp

Mr. Jiro Fukui
TeamLeader, Foundation Engineering Team
Structure Research Group
Independent Administrative Institution
Public Works Research Institute
1-6, Minamihara, Tsukuba-shi, Ibaraki-ken 305-8516
Tel: 0298-79-6794
Fax: 0298-79-6739
E-mail: fukui@pwri.go.jp

Mr. Kenji Ikeda
Director, Structures Division
Structures Department
Independent Administrative Institution
Civil Engineering Research Institute of Hokkaido
1-3, Hiragishi, Toyohira-ku, Sapporo-shi
Hokkaido 062-8602
Tel: 011-841-1115
Fax: 011-820-2714
E-mail: ikedak@ceri.go.jp

Mr. Naohito Kawai
Head, Structural Standard Division
Building Department
Institute for Land and Infrastructure Management
Ministry of Land, Infrastructure and Transport
1, Tachihara, Tsukuba-shi, Ibaraki-ken 305-0802
Tel: 0298-64-4299
Fax: 0298-64-6774
E-mail:kawai-n92hp@nilim.go.jp

Mr. Takaaki Kusakabe
Head, Earthquake Disaster Prevention Division
Research Center for Disaster Risk Management
Institute for Land and Infrastructure Management
Ministry of Land, Infrastructure and Transport
1, Asahi, Tsukuba-shi, Ibaraki-ken 305-0804
Tel: 0298-64-2211
Fax: 0298-64-0598
E-mail:ksakabe-t88d8@nilim.go.jp

Mr. Osamu Matsuo
Research Coordinator for Earthquake Disaster Prevention
Research Center for Disaster Risk Management
Institute for Land and Infrastructure Management
Ministry of Land, Infrastructure and Transport
1, Asahi, Tsukuba-shi, Ibaraki-ken 305-0804
Tel: 0298-64-2926
Fax: 0298-64-0598
E-mail: matsuo-o92rm@nilim.go.jp

Mr. Chikahiro Minowa
Scientific Research Advisor
Independent Administrative Institution
Research Institute for Earth Science and Disaster Prevention
3-1, Tennodai, Tsukuba-shi, Ibaraki-ken 305-0006
Tel: 0298-51-1611
Fax: 0298-51-1674
E-mail: minowa@bosai.go.jp

Mr. Jun Murakoshi
TeamLeader, Bridge Structure Team
Structures Research Group
Independent Administrative Institution
Public Works Research Institute
1-6, Minamihara, Tsukuba-shi, Ibaraki-ken, 305-8516
Tel: 0298-79-6793
Fax: 0298-79-6739
E-mail: murakosi@pwri.go.jp

Mr. Shoichi Nakatani
Head, Bridge Division
Road Department
Institute for Land and Infrastructure Management
Ministry of Land, Infrastructure and Transport
1, Asahi, Tsukuba-shi, Ibaraki-ken 305-0804
Tel: 0298-64-2905
Fax: 0298-64-0178
E-mail: nakatani-s92gw@nilim.go.jp

Dr. Tetsuo Nakazawa
Head, The Second Research Laboratory
Typhoon Research Department
Meteorological Research Institute
Japan Meteorological Agency
Ministry of Land, Infrastructure and Transport
1-1, Nagamine, Tsukuba-shi, Ibaraki-ken 305-0052
Tel: 0298-53-8671
Fax: 0298-53-8735
E-mail : nakazawa@mri-jra.go.jp

Dr. Nobuyuki Ogawa
Deputy Project Director,
Special Project on the 3-D Full-Scale
Earthquake Testing Facility
Disaster Prevention Research Group
National Research Institute for Earth Science and Disaster Prevention
3-1, Tennodai, Tsukuba-shi, Ibaraki-ken 305-0006
Tel: 0298-51-1611
Fax: 0298-52-8512
E-mail: ogawa@bosai.go.jp

Dr. Hisashi Okada
Director, Structural Engineering Department
Independent Administrative Institution
Building Research Institute
1, Tatehara, Tsukuba-shi, Ibaraki-ken 305-0802
Tel: 0298-64-2151
Fax: 0298-64-2989
E-mail: okada@kenken.go.jp

Dr. Yasuo Okuda
Chief Research Engineer, Department of Structural Engineering
Independent Administrative Institution
Building Research Institute
1, Tatehara, Tsukuba-shi, Ibaraki-ken 305-0802
Tel: 0298-64-6618
Fax: 0298-64-6773
E-mail: y_okuda@kenken.go.jp

Mr. Keiichi Ohtani
Project-Director, Project of 3-D Full-Scale Earthquake Testing Facility
Independent Administrative Institution
National Research Institute for Earth Science and Disaster Prevention
3-1, Tennodai, Tsukuba-shi, Ibaraki-ken, 305-0006
Tel: 0298-51-1611 Ext. 321
Fax: 0298-52-8512
E-mail: ohtani@bosai.go.jp

Mr. Yoshiyuki Saito
General Projector for Research
Independent Administrative Institution
Civil Engineering Research Institute of Hokkaido
1-3, Hiragishi, Toyohira-ku, Sapporo-shi
Hokkaido 062-0931
Tel: 011-841-1119
Fax: 011-824-1226
E-mail: 90117@ceri.go.jp

Dr. Hiroshi Sato
Director, Structures Research Group
Independent Administrative Institution
Public Works Research Institute
1-6, Minamihara, Tsukuba-shi, Ibaraki-ken 305-8516
Tel: 0298-79-6726
Fax: 0298-79-6739
E-mail: hsato@pwri.go.jp

Dr. Takahiro Sugano
Head, Structural Dynamics Division
Geotechnical and Structural Engineering Department
Independent Administrative Institution
Port and Airport Research Institute
3-1-1, Nagase, Yokosuka-shi, Kanagawa-ken 239-0826
Tel: 0468-44-5058
Fax: 0468-44-0839
E-mail: macsuga@ipc.pari.go.jp

Dr. Keiichi Tamura
TeamLeader, Ground Vibration Research Team
Earthquake Disaster Prevention Research Group
Independent Administrative Institution
Public Works Research Institute
1-6, Minamihara, Tsukuba-shi, Ibaraki-ken 305-8516
Tel: 0298-79-6770
Fax: 0298-79-6735
E-mail: tamura@pwri.go.jp

Dr. Masaomi Teshigawara
Chief Research Engineer
Structural Engineering Department
Independent Administrative Institution
Building Research Institute
1, Tatehara, Tsukuba-shi, Ibaraki-ken 305-0802
Tel: 0298-64-6753
Fax: 0298-64-6773
E-mail: teshi@kenken.go.jp

Mr. Ken-ichi Tokida
Director, Earthquake Disaster Prevention Research Group
Independent Administrative Institution
Public Works Research Institute
1-6, Minamihara, Tsukuba-shi, Ibaraki-ken 305-8516
Tel: 0298-79-6700 (ext.4211)
Fax: 0298-79-6736
E-mail: tokida@pwri.go.jp

Mr. Ken-ichi Torii
Head, Coastal Division
River Department
Institute for Land and Infrastructure Management
Ministry of Land, Infrastructure and Transport
1, Asahi, Tsukuba-shi, Ibaraki-ken 305-0804
Tel: 0298-64-2327
Fax: 0298-64-1168
E-mail: torii-k92fr@nilim.go.jp

Mr. Masaharu Tsuzawa
Head, Planning Division
Geographic Department
Geographical Survey Institute
Ministry of Land, Infrastructure and Transport
1, Kitasato, Tsukuba-shi, Ibaraki-ken 305-0811
Tel: 0298-64-5917
Fax: 0298-64-1804
E-mail: tsuzawa@gsi.go.jp

Dr. Shigeki Unjoh
TeamLeader, Earthquake Engineering Research Team
Earthquake Disaster Prevention Research Group
Independent Administrative Institution
Public Works Research Institute
1-6, Minamihara, Tsukuba-shi, Ibaraki-ken 305-8516
Tel: 0298-79-6773
Fax: 0298-79-6736
E-mail: unjoh@pwri.go.jp

Dr. Yoshikazu Yamaguchi
TeamLeader, Dam Structure Research Team
Hydraulic Engineering Research Group
Independent Administrative Institution
Public Works Research Institute
1-6, Minamihara, Tsukuba-shi, Ibaraki-ken 305-8516
Tel: 0298-79-6780
Fax: 0298-79-6737
E-mail: yamaguti@pwri.go.jp

RESOLUTIONS

May 15, 2002

RESOLUTIONS OF THE THIRTY-FOURTH JOINT MEETING U.S.-JAPAN PANEL ON WIND AND SEISMIC EFFECTS (UJNR)

National Institute of Standards and Technology, Gaithersburg, Maryland, USA
13-15 May 2002

The following resolutions are hereby adopted:

1. The Thirty-fourth Joint Panel Meeting provided the forum to exchange valuable technical information that is beneficial to both countries. In view of the importance of cooperative programs on the subject of wind and seismic effects, the continuation of Joint Panel Meetings is considered essential. Both sides agreed to explore new ideas and areas to strengthen cooperative activities in support of the Panel's mission.

2. The following activities have been conducted since the Thirty-third Joint Meeting:

   a. Technology Exchanges. Technical experts, technical documents, and applications of the electronic media have been exchanged. These exchanges have contributed to the development of new research programs and enhanced ongoing research in both countries.

   b. Task Committee Workshops and meetings. The Panel held one workshop and one meeting:
      1. Task Committee (B), U.S.-Japan grantee's meeting for Composite and Hybrid Structures, June 24-27, 2001, Berkeley CA, USA.
      2. Task Committee (G), 17th U.S.- Japan Bridge Engineering Workshop, 12-14 November 2001, Tsukuba, Japan.

3. The Panel approved the Task Committee reports presented during the 34th Joint Panel Meeting. Each report included objectives, scope of work, accomplishments and future plans.

4. The Panel's Strategic Plan was approved at its 33rd Joint Panel Meeting. Implementation of the Strategic Plan has started. The following are the highlights of the 34th Joint Meeting.

a. The full Panel Meetings were conducted within the new assembly format: three-day technical meetings followed by three-days of technical site visits rather than the former 12-day full Panel Meetings.
b. The Strategic Plan encourages greater private sector involvement as was demonstrated from papers and presentations from Universities and Government/private sector partner experts. In addition, two of the three technical site visits were hosted by private sector organizations.
c. A Steering Committee, consisting of the Chair and Secretary-General of both sides and the T/C Chairs from both sides reviewed the Strategic Plan and its progress in implementing the recommendations. The Panel has implemented many of the recommendations of the Strategic Plan and will work toward more complete implementation of the plan's recommendations.

5. The Panel approved the new Task Committee D (Wind Engineering) whose operating charter was submitted at the 34th Joint Panel Meeting and met the criteria described in the Strategic Plan.

6. The Panel endorses the following five proposed Task Committee Workshops or Coordinating Committee Meetings during the coming year:

a. Task Committee (A), 5th U.S.-Japan Workshop on Geotechnical Earthquake Engineering, Early 2003, San Diego, CA, USA.
b. Task Committee (B), 3rd U.S.-Japan Technical Coordinating Committee Meeting on Auto-Adaptive Media (Smart Structural Systems), October 2002, Tsukuba, Japan.
c. Task Committee (C), 3rd U.S.-Japan Workshop on Advanced Research on Earthquake Engineering for Dams, June 2002, San Diego, CA, USA.
d. Task Committee (D), 3rd U.S.-Japan Workshop on Design for Wind and Wind Hazard Mitigation, Fall 2002, Seattle, WA, USA.
e. Task Committee (G), 18th U.S.-Japan Bridge Engineering Workshop, October 2002, USA.

In the event that T/C co-chairs consider it essential to conduct a joint meeting or workshop that is not included in this Resolution, the T/C co-chairs will make such a request through their respective Secretary-General for approval by the U.S. and Japan Joint Panel Chairmen.

The U.S. and Japan-side Task Committee Chairs, with concurrence of the Joint Panel

Chairmen, will develop and schedule their Workshops. Both sides' Secretaries-General will be kept informed of the planning, conduct, and results of workshops or committee meetings including resolutions and reports. Results of each activity conducted before the 35th Joint Panel Meeting will be presented at the 35th Joint Panel Meeting.

7. The Panel focused attention to the topic terrorism -- the collapse of the World Trade Center (WTC) and the Pentagon Wedge A by featuring a special Panel Meeting theme to discuss this topic. Following the Panel Meeting, a technical site visit was scheduled to visit the WTC site in New York City to discuss the structural collapses in greater detail.

8. The Panel recognizes the importance of continuing its joint research programs on Soil Liquefaction and Countermeasures and on Auto-Adaptive Media (Smart Structural Systems), and developing a U.S.-Japan coordinated research plan utilizing the NEES facilities in the USA and diverse laboratories in Japan, including E-Defense.

9. The Panel resolved to explore collaboration on research in the area of progressive collapse of buildings.

10. The Panel resolved to explore formation of a new Task Committee on Disaster Information Technology to include information technology, public health, and security aspects of development of next-generation building systems.

11. The U.S.- and Japan-sides will encourage the conduct of joint investigations following earthquake and wind disasters in the U.S. and Japan.

12. The results of the Panel's work should be disseminated to improve the quality of life globally. The Panel will make use of the internet to the extent possible to disseminate information.

13. The Thirty-fifth Joint Panel Meeting of the UJNR Panel on Wind and Seismic Effects will be held by the Japan-side Panel, in Japan in May 2003. The Japan-side Secretariat at PWRI will propose dates, program, location, and itinerary with the concurrence of the U.S.-side Panel.

MANUSCRIPTS

SESSION 1

GEOTECHNICAL ENGINEERING AND GROUND MOTION

Seismic Performance of Urban, Reclaimed and Port Areas -Full Scale Experiment Using Blast Technique

by

Takahiro Sugano[1] and Eiji Kohama[2]

ABSTRACT

A full scale lateral spreading experiment was carried out on November 13th, 2001 at Tokachi port in Hokkaido island, Japan. The primary objective of the experiment was to assess the performance of steel sheet pile quay walls subjected to liquefaction/lateral spreading. Two 5.5 m deep quay walls were designed and constructed, to investigate the damage mechanism of steel sheet pile quay walls. They were constructed with seismic design coefficients of k=0.15 and k=0 separately. The test site was reclaimed with dredged fine sand about 18 months before the test. The depth of the reclaimed sand layer was about 8 m and the test field area was around 4800 m^2 (50 m by 96 m).

Controlled blast technique was used to induce liquefaction/lateral spreading, and 127 blast holes each consisting 4 kg explosive material for lower part and 3 kg for upper part were charged. The total weight of explosive material was 840 kg.

Various structures such as group pipe piles, gas pipes and buried structures were installed with measuring instruments. Two liquefaction remediation methods and several new measurement techniques were adopted. Forteen organizations were participated in this project.

KEYWORDS: Full scale field experiment, Liquefaction, Lateral spreading, Reclaimed land

1. INTRODUCTION

The 1995 Hyogoken-Nambu earthquake caused severe soil liquefaction in extensive areas of reclaimed land in Kobe. The soil liquefaction induced large ground displacements in the horizontal direction, which resulted in damage to buried structure such as lifeline pipes and foundations. Also, many caisson type quay walls were damaged in Kobe Port during the earthquake.

Generally, three sets of data can be used to investigate the mechanism of damages;

1) Strong motion record nearby the damaged facility,
2) Geotechecnical data, design conditions and damage data (i.e. deformation). and,
3) Numerical simulation or model test results

However, an important piece of information as 'behavior of structures during earthquake' is not available. In this project, we focused on the behavior of full scale structures during liquefaction state and 14 organizations were jointed in the project as shown in Table 1.

[1] Head, Structural Dynamics Division, Geotechnical and Structural Engineering Department, Port and Airport Research Institute, 3-1-1 Nagase, Yokosuka, Kanagawa 239-0826, JAPAN

[2] Research Engineer, ditto

2. OUTLINES OF THE EXPERIMENT

The test site was located in Pier No.4 at Tokachi Port in Hokkaido. The Pier No.4 filling construction was completed in June 2000 with use of dredged fine sands. The experimental yard area was around 4800 m^2 (50 m by 96 m) and it was separated into two parts. In one part, steel sheet pile quay wall which was designed with seismic coefficient of k=0.15 was installed the other part the one designed with k=0 was employed. In this paper, the k=0.15 part is refered as region (A), and k=0 part as region (B). In region (B), 4% slope (25 m width, 50 m long) were constructed to induce lateral spreading.

The typical soil profile is shown in Fig.1. The particle size distribution of the soils are shown in Fig.2, as can be sheen most of the soil samples are in 'possibility of liquefaction' zone.

2.1 Blast sequence

The blast hole is indicated in Fig.3 from A1 to A54 , from B1 to B48 and from C1 to C25. The first ignitions were A1 and B1 at the same time. Then, ignite next holes in order with 500 ms time interval which showed snake walking in plan view. Each hole consisting 4 kg explosive material for lower part and 3 kg for upper part were charged with 200 ms time interval, the ignite order was from lower part to top part.

2.2 Lift up mechanism (Fig.3)

In region (A), The Japanese Geotechinical Society installed eight buried structures such as sewage water pipes to investigate the lift up mechanism during liquefaction and the countermeasures. The dimensions of the installed cylindrical structures were 1 m in diameter and 3.8 m in length.

2.3 Performance of Cement deep mixing soil improvement/Permeable grouting improvement during liquefaction

UC Berkeley and Japan Cement Deep Mixing Association installed four cement deep mixed specimens in region (A) as a 3.4 m by 3.4 m foot print cement deep mixing improvement to depth of 8 m (full improvement of reclaimed layer), 5.5 m , 3.5 m and no treatment.

Permeable Grouting Method Association and Port and Airport Research Institute tried to injected 8 hrs gel time chemical grout in between sheet pile quay wall and the anchor pile to investigate the efficiency of permeable grouting method as shown left bottom zone of region (A) in Fig.3.

2.4 Performance of steel sheet pile quay walls

Port and Airport Research Institute, Japan Dredging and Reclamation Engineering Association and Japan Steel Pipe Pile Association constructed two steel sheet pile quay walls with different design seismic coefficients including strain gauges and load cells. In region (A), the quay wall with seismic coefficient of k=0.15 ,and in region (B), the quay wall with k=0 were constructed.

At the tie rod connectors just behind the sheet piles in region (B), special explosives were used so as to cut the tie rod to induce lateral spreading during liquefaction.

2.5 Performance of lifelines subjected to lateral spreading

UC San Diego and Waseda University carried out the pile experiment. The three sets of pile foundations were installed behind the k=0 quay walls to determine the effect of pile groups on the pile response.

300 mm diameter steel pipe piles in pile groups having 900 mm spacing and a concrete pile cap (three single piles, 4-pile group, and 9-pile group) were constructed.

Two pipes were installed to intersect the lateral spreading direction at 90 degree angle, and one pipe was installed in the lateral spreading direction as shown in the right bottom part of Fig.3.

Ten wireless transmition dynamic GPS devices (10 Hz time interval) were installed and attached to the structures to measure the deformation of structures during lateral spreading.

2.6 Investigation on the mechanism of lateral spreading

Waseda university installed 11 GPS devices on the surface of slope with 1 Hz measurement interval, and installed vertical optical fiber modules to measure the deformation inside the slope.

2.7 Evaluation of impervious sheet properties when large deformations occur during and after earthquake

National Institute for Land and Infrastructure Management Yokosuka, installed the impervious sheet used for garbage dumping ground. Many of Japanese garbage dumping grounds are located in coastal area. To keep the garbage material and polluting matter inside the designated area, the performance of impervious sheet is important.

2.8 Survey and Sounding techniques

Port and Airport Research Institute conducted several sounding tests as follows: SPT-blow count, seismic cone penetration test, portable cone penetration test, automatic Swedish weight sounding, and dilatometer test. These tests were conducted about a couple of months before, the day before and after the blast. It is also planed to perform them in June 2002.

National Institute of Advanced Industrial Science and Technology research team used the resistivity method to measure the density profile of the liquefied soil.

Earthquake Research Institute, Tokyo Univ. and Port and Airport Research Institute compared the data obtained from the dynamic GPS installed in region (A) and conventional laser survey data.

Chuo Univ. used the radio controlled helicopter to take photos of the experimental site before and after the blast and automatic computer processing technique to measure the deformation. Chuo Univ. also installed CCD camera into the vertical transparent cylinder to visualize the soil profile during the test.

Waseda Univ. team tried to detect the liquefied soil layer profile during liquefaction by using acoustic tomography with pseudo random binary sequence code technique.

UC Berkely and Port and Airport Research Institute installed both conventional strain gauge type accelerometers and wireless accelerometers which using the micro electro mechanical systems and bluetooth transmission. In this project around 800 sensors were installed and total length of signal cable between sensor and amplifier was about 40 km. The data obtained from wireless accelerometers showed good agreement with the data obtained from conventional accelerometers.

2.9 Re-liquefaction phenomena

Civil Engineering Research Institute of Hokkaido is interested in the re-liquefaction phenomena and curried out the post experiment on Dec. 14th , 2002 with UC San Diego and Port and Airport Research Institute. In region (B), the

controlled blast were applied with the group pile foundations as its center.

3. SUMMARY OF RESULTS

The overall deformation of the test field is shown in Fig.4. The maximum horizontal displacement of quay wall in region (A) was about 30 cm, region (B) was about 130 cm respectively. Due to the horizontal movement of quay walls, lateral spreading was occurred in region (B). However, three sets of group piles played a role in control works against lateral spreading as shown in Fig.5.

In this experiment, acceleration caused by controlled blasting could not simulate actual earthquake acceleration as shown in Fig.5. Fig.5 shows an acceleration time history recorded at region (A) quay wall, the maximum acceleration was over 10 g. On the other hand, excess pore water pressure was built up overburden pressure as shown in Fig.6.

The bending moment distribution of initial condition, maximum displacement condition and residual condition are shown in Fig.7. The failure of sheet pile quay walls occurred due to the reduction of resistance of anchor pile during liquefaction, then sand water mixture fluid push the quay walls.

Many kinds of challenges to investigate seismic performance of urban, reclaimed and port were conducted in collaboration with 14 organizations. The reports in this paper include wide filed subjects related to liquefaction/lateral spreading phenomena. The analysis works is presently continuing by individual organization participated in this experiment. The results will be presented in the future.

Table 1 Organizations of the research project

Organization	Research content	Role
Port and Airport Research Institute (PARI)	1. Investigation on the dynamic characteristics of ground before and after liquefaction 2. Investigation on seismic behavior of sheet piles, anchor piles and tie rods/wires	supervision of entire experiment, measurement of behavior of sheet piles and analysis
National Institute for Land and Infrastructure Management (NILIM)	1. Evaluation of impervious sheet properties when large deformations occur during and after earthquake 2. Investigation on characteristic of microtremor before and after earthquake	analysis of experimental results
Japan Dredging and Reclamation Engineering Association (JDREA)	Investigation on seismic behavior of sheet piles, anchor piles, tie rods and surrounding ground	execution management and analysis
Japanese Association for Steel Pipe Piles (JASPP)	Investigation on seismic behavior of sheet piles, anchor piles, tie rods and surrounding ground	measurement of sheet piles displacement and analysis
University of California, San Diego (UCSD)	Investigation on behavior of pile groups and buried pipes	Measurement and analysis about interaction between structure and ground during lateral flow
Cement Deep Mixing Association (CDM Association)	Investigation on properties of ground improved by cement deep mixing method	cement mix design, execution management and analysis
University of California, Berkrey (UCB)	Investigation on properties of ground improved by cement deep mixing method	measurement of improved ground behavior and analysis
The Japanese Geotechnical Society (JGS)	Investigation on behavior of buried pipes imposed to up-lift pressure of liquefaction	measurement of underground pipe behavior and analysis
Waseda University (Waseda Univ.)	1. Investigation on ground movement during and after lateral flow and behavior of buried single pile 2. Investigation on elastic wave velocity in liquefied ground 3. Measurement of vibration at adjacent buildings 4. Measurement of underground displacements	acoustic tomography, measurement of underground displacement by using optical fiber, GPS, etc.
Permeable Grouting Method Association (PGM Association)	Confirmation of efficiency of permeable grouting method	execution management and analysis
Tokyo University, Earthquake Research Institute (Tokyo Univ.)	Measurement of 3D dynamic displacements by GPS	measurement by dynamic GPS
Chuo University (Chuo Univ.)	1. Investigation on water film phenomenon occurred by liquefaction 2. Measurement of ground displacements	measurement by borehole-camera and radio-control helicopter
National Institute of Advanced Industrial Science and Technology (NIAIST)	Investigation on underground density profile of liquefied soil	measurement by resistivity method
Civil Engineering Research Institute of Hokkaido (CERI)	Investigation on behavior of re-liquefied ground	analysis of experimental results

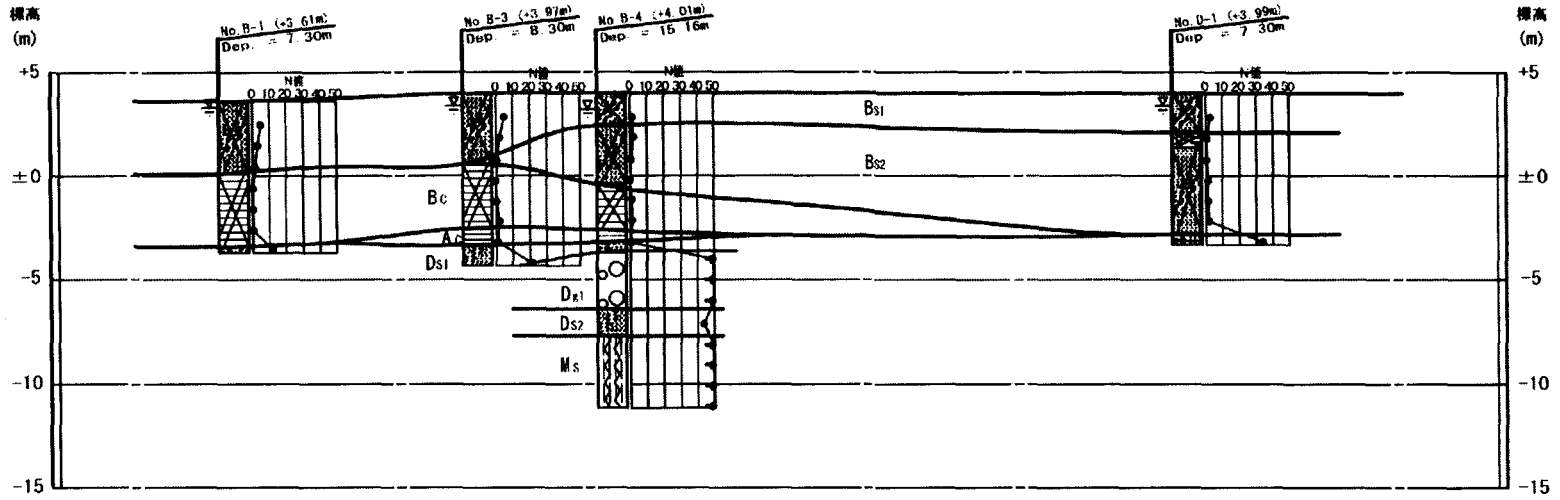

Fig.1 Typical soil profile

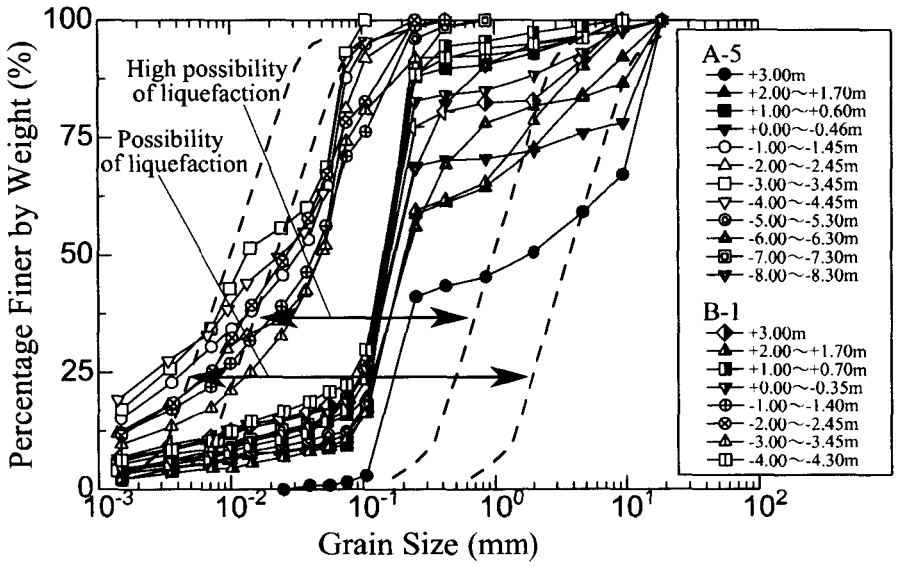

Fig.2 Particle size distribution

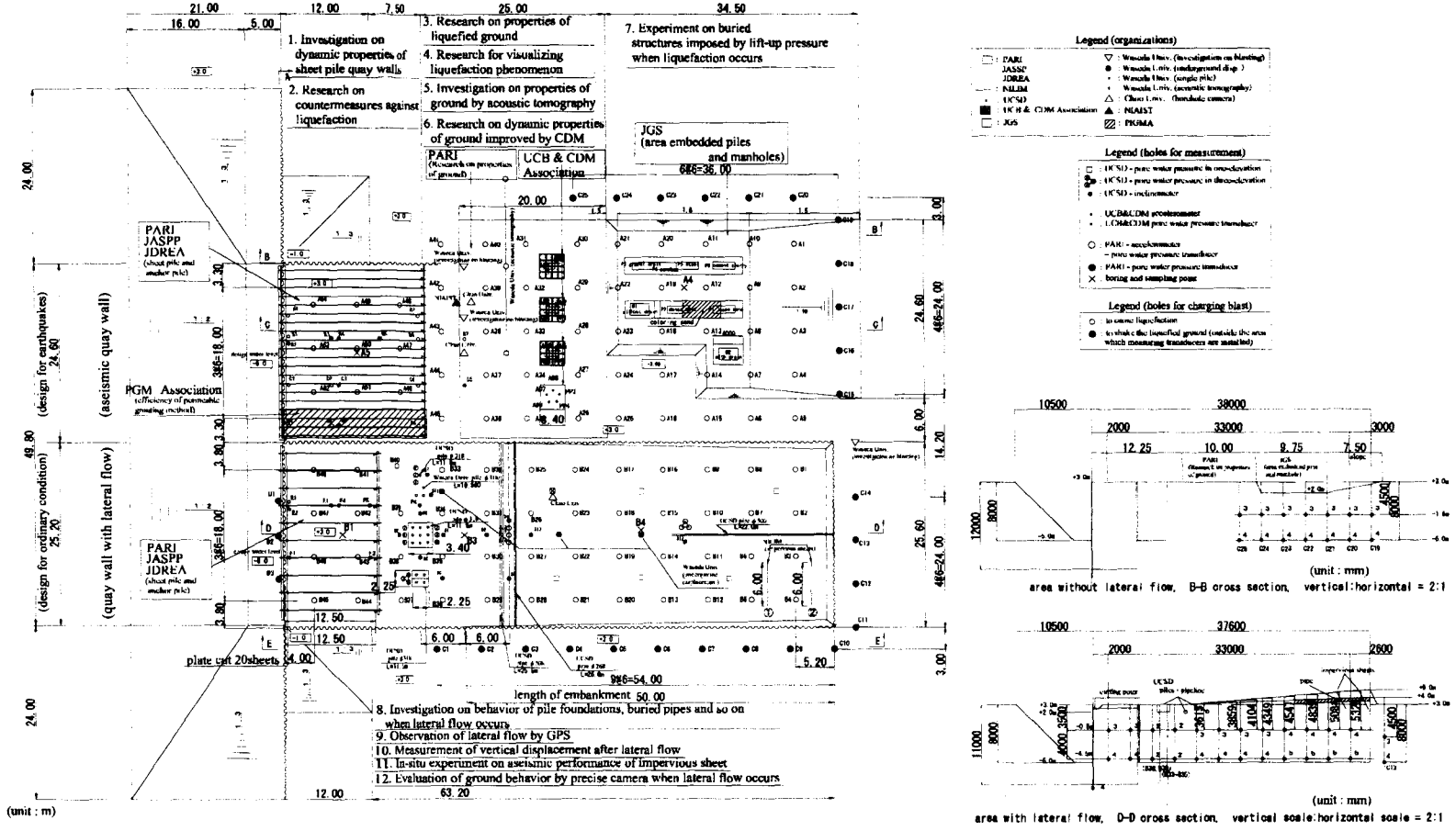

Fig. 3 Plan view of the test site

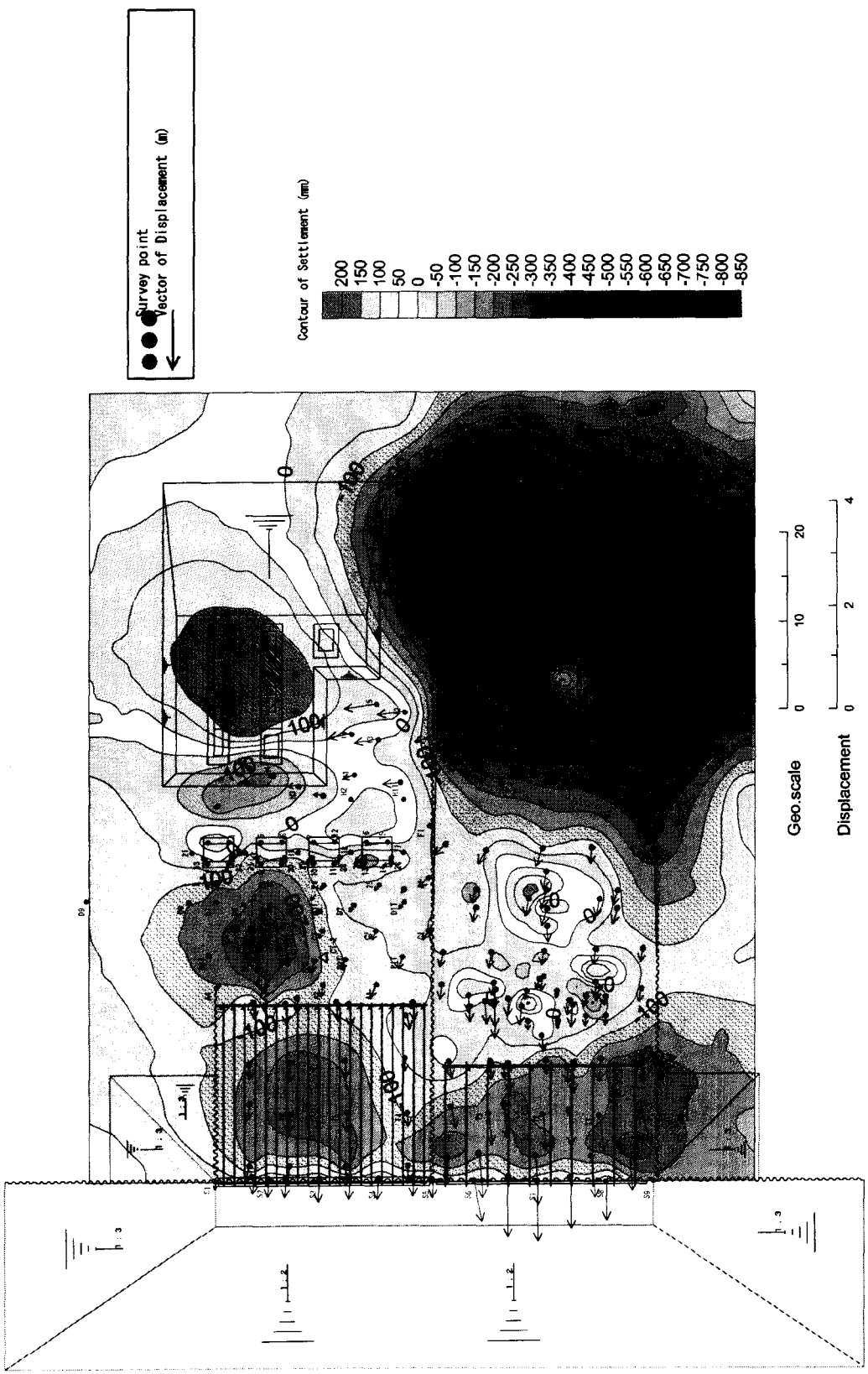

Fig.4 Deformation of test fields

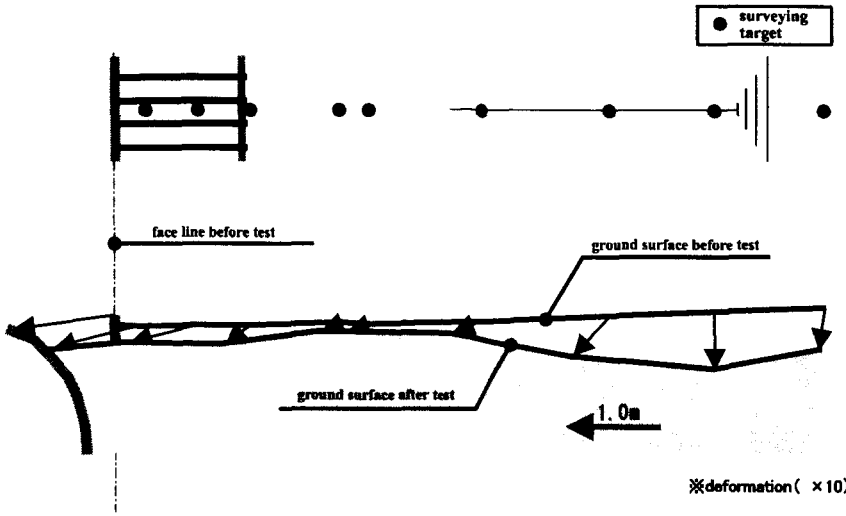

Fig.5 Lateral spreading deformation

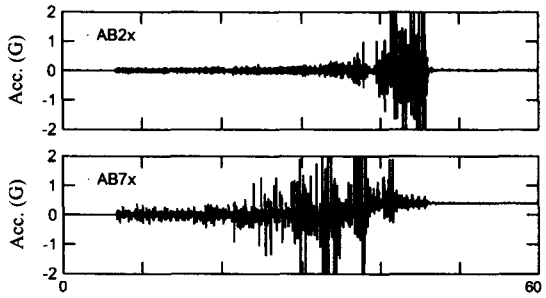

Fig.6 Acc. caused by blast

Fig.7 Excess pore water pressure

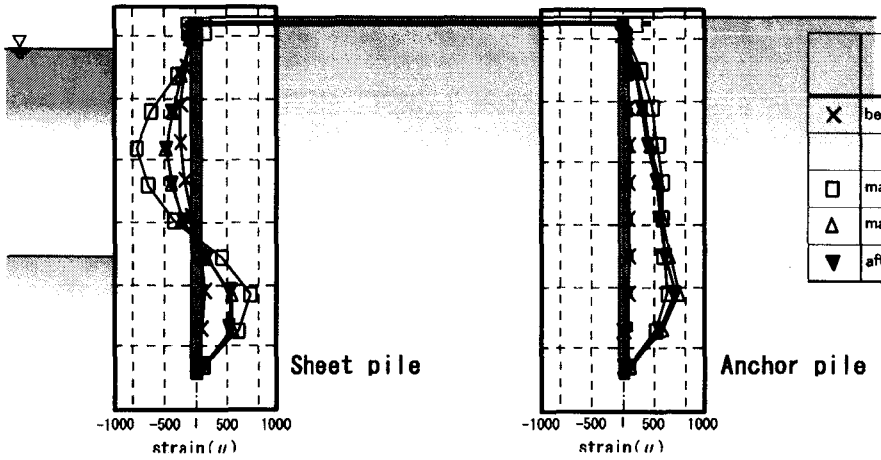

	イベント	Time (sec)	Tension in tie rod (kN/m)
×	before test	0.000	52.2
		45.725	184.4
□	max strain in sheet pile	45.760	150.2
△	max strain in anchor pile	46.575	99.4
▼	after test	90.000	90.2

Fig.8 Strain distribution of sheet and anchor pile

Photograph Test site : before experiment

Photograph Tokachi port from window of airplane

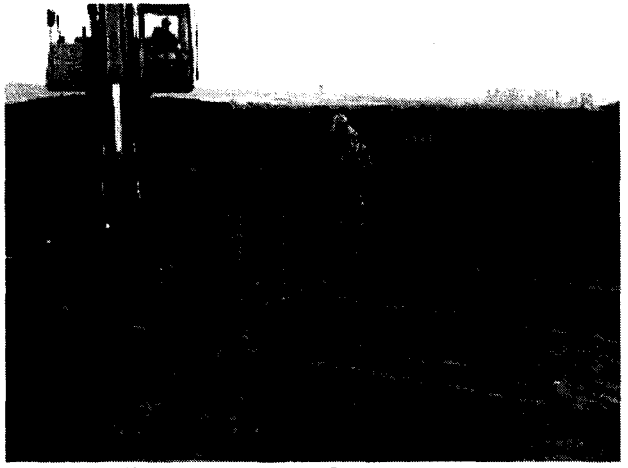

Photograph Under construction

Photograph Installing blast

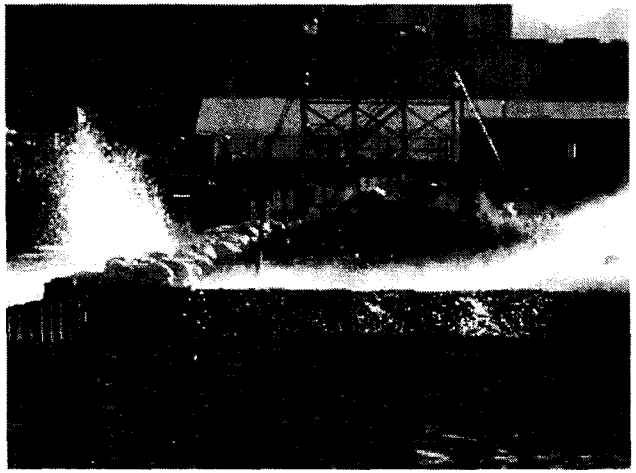

Photograph During blast

Photograph Visitors during blast

Photograph Boiling sand caused by liquefaction

Photograph After sand boil

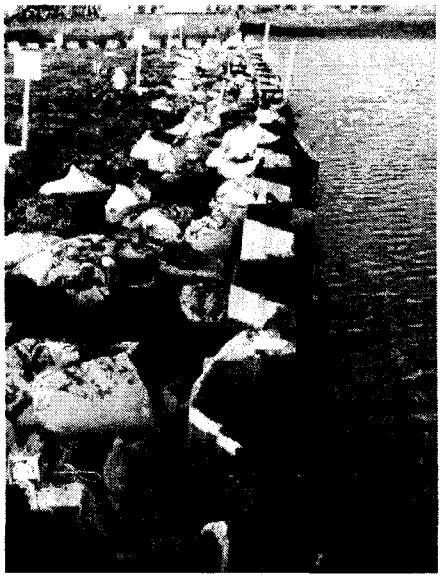

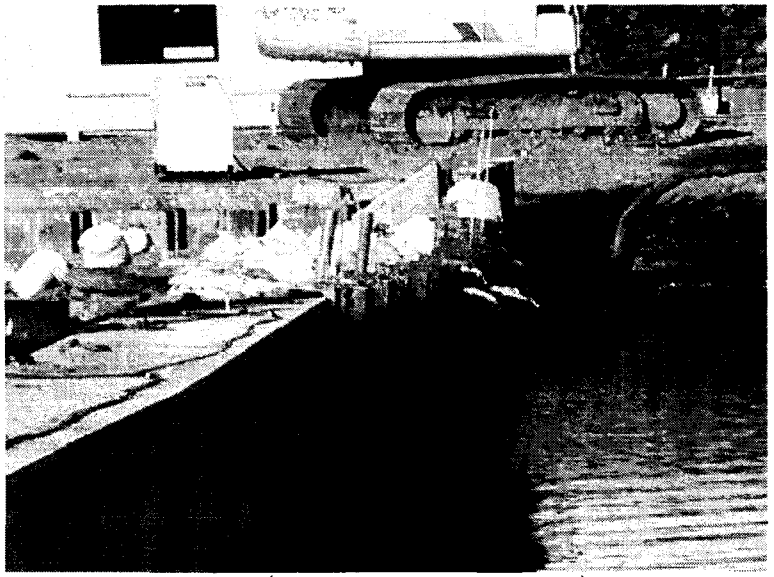

Photograph Sheet pile quay wall after blast (PARI, JDREA & JASPP)

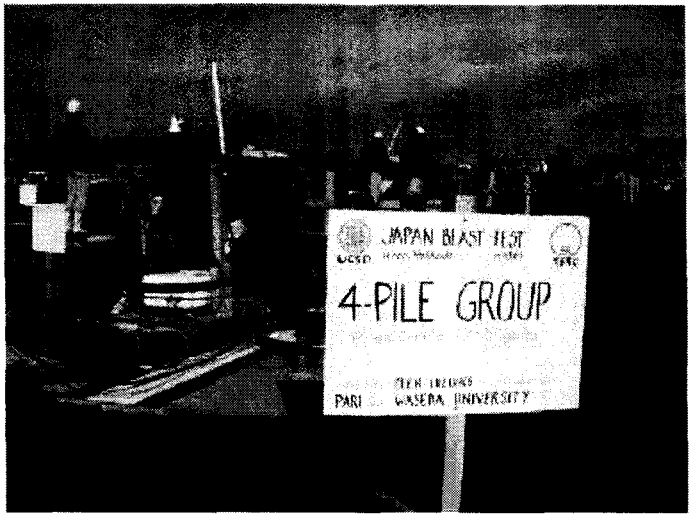

Photograph Pile groups (UCSD)

Photograph Pile groups (UCSD)

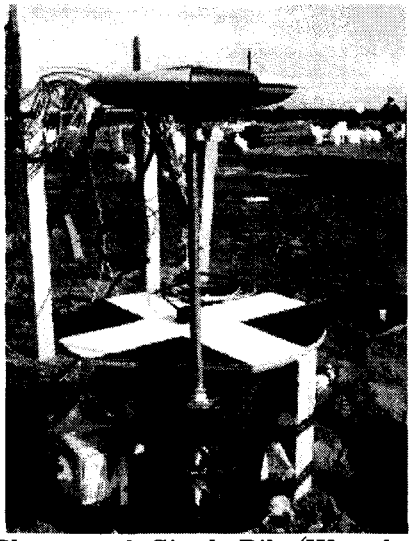

Photograph Single Pile (Waseda Univ.)

Photograph Impervious sheet (NILIM)

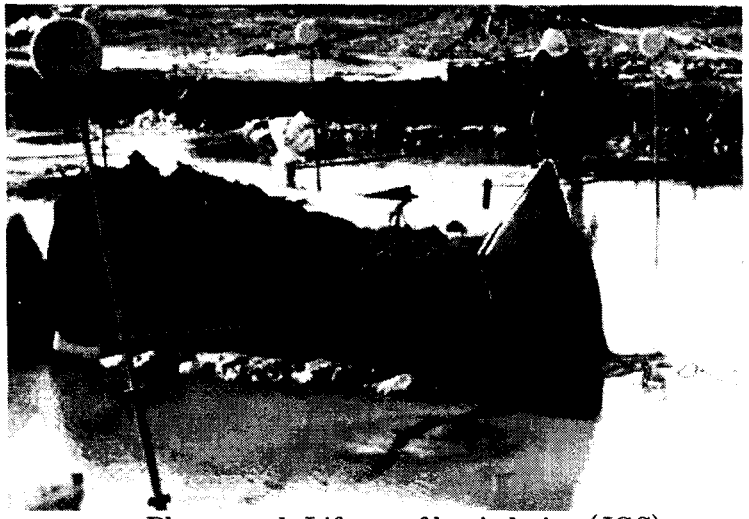

Photograph Lift-up of buried pipe (JGS)

Photograph Improved ground by CDM (UCB & CDM Association)

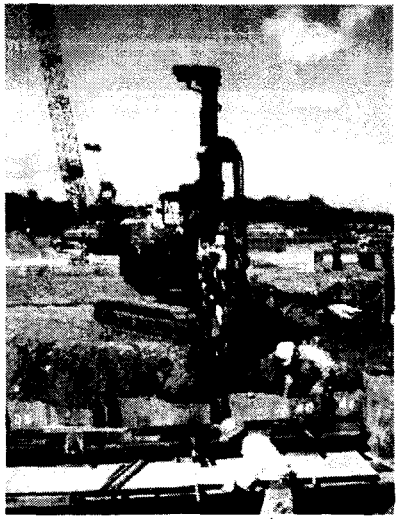

Photograph Execution of PGM (PGM Association)

Photograph Radio control helicopter (Chuo Univ.)

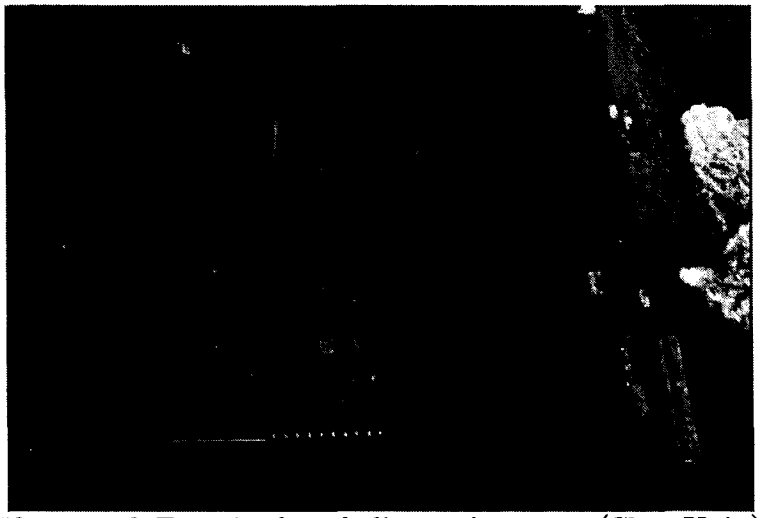

Photograph Test site from helicopter's camera (Chuo Univ.)

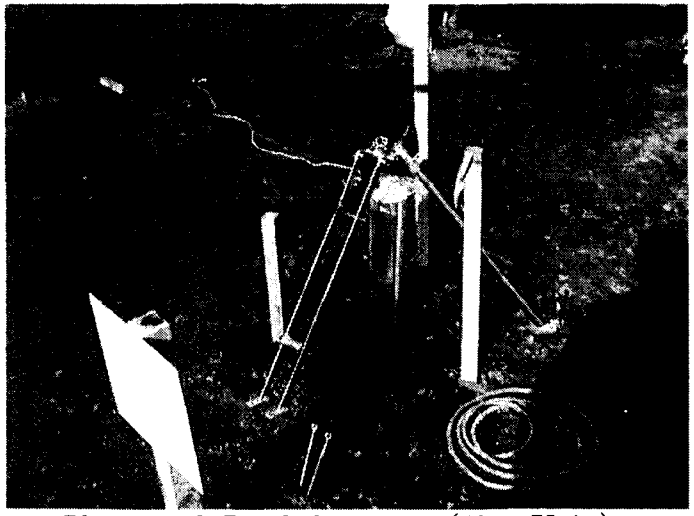

Photograph Borehole camera (Chuo Univ.)

Photograph Re-liquefaction test during heavy storm on Dec 14th, 2002

A Review of Empirical Evidence For Site Coefficients in Building-Code Provisions

by

Roger D. Borcherdt [a)]

ABSTRACT

Site-response coefficients, F_a and F_v, used in U.S. building code provisions are based on empirical data for motions up to 0.1g. For larger motions they are based on theoretical and laboratory results. The Northridge earthquake of 17 January 1994 and other recent earthquakes have provided significant new sets of empirical data up to 0.5g. These data together with recent site characterizations based on shear-wave velocity measurements provide empirical estimates of the site coefficients at base accelerations up to 0.5g for Site Classes C and D. These empirical estimates of F_a and F_v as well as their decrease with increasing base acceleration level are consistent at the 95 percent confidence level with those in present building code provisions, with the exception of estimates for F_a at levels of 0.1 and 0.2 g, which are less than the than the lower confidence bound by amounts up to 13 percent. The site-coefficient estimates are consistent at the 95 percent confidence level with those of several other investigators for base accelerations greater than 0.3 g. These consistencies and present code procedures indicate that changes in the site coefficients are not warranted.

KEYWORDS: Amplification, Building Codes, Design Spectra, Ground-motion, International Building Code, NEHRP Provisions, Northridge Earthquake, Shear-Wave Velocity, Site Coefficients, Site Classes, Uniform Building Code

1.0 INTRODUCTION

Present US building codes are based on empirical estimates of site coefficients, F_a and F_v, derived from recordings of the Loma Prieta earthquake at the 0.1g level (Borcherdt 1993, 1994) and derived at higher levels using numerical modeling and laboratory results (Seed, et al., 1994). The Northridge earthquake of 17 January 1994 and other recent earthquakes have provided sets of ground-motion recordings with peak ground accelerations at levels up to 0.5g. These new data provide an opportunity to further evaluate site coefficients as currently specified in US building codes.

This paper provides a review of the empirical evidence for site coefficients as derived by analyses of Northridge earthquake recordings (Borcherdt, 2002) and those derived by a number of other investigators using other databases and procedures.

2.0 COMPARISON OF SITE COEFFICIENTS DERIVED USING VARIOUS METHODS

Estimates of the short-period F_a and mid-period F_v site coefficients have been derived relatively recently by a number of investigators using a variety of databases and procedures. Results of these investigations are compared herein with those derived from Northridge by Borcherdt (2002). Estimates of F_a and F_v together with corresponding 95 percent confidence intervals for each site class as derived by Borcherdt (2002) are plotted in Figures 1 and 2. Corresponding code values ($F_{a\ code\ Table}$, $F_{v\ code\ Table}$) and results derived by Crouse and McGuire (1996), Dobry et al. (1999), Joyner and Boore (2000), Rodriguez-Marek et al. (1999), Silva et al. (2000), and Stewart et al. (2001, 2002) are provided for comparison.

Crouse and McGuire (1996) derived estimates of site coefficients using a set of empirically based attenuation curves based on strong-motion recordings from a select group of 16 U.S. earthquakes, which included the Landers earthquake, but was completed before the Northridge data could be incorporated. Site

[a)] United States Geological Survey
Menlo Park, CA 94025

classifications were based on a separately compiled database. The site coefficients were derived from empirical predictions at various magnitude and acceleration levels. Ratios of spectral levels at specific periods were computed from averages for the magnitude acceleration pairs, from which averages for the short and mid period band were computed.

Dobry et al. (1999) derived amplification ratios using the Northridge strong-motion data from ratios of response spectral ordinates for nearby soil-rock pairs. Their database is a subset of that used by Borcherdt (2002). They derived estimates from ratios computed using a hypocentral distance norm (method 1) and from ratios computed by normalizing the response spectra for various soil sites to the corresponding value predicted by Silva using the Abrahamson and Silva (1997) attenuation relation for rock (method 2). Estimates of the short and mid-period site coefficients were derived from averages of the response spectral ratios over the short- (0.1 - 0.5 s) and mid- (0.4 – 2.0 s) period bands. Estimates of the mean and standard deviation were derived for Site Classes C and D from a subset of sites for which the ratios were considered most reliable. Averages of their ratios for base acceleration intervals of 0.04 - 0.14 g, 0.15 - 0.24 g, and 0.25 - 0.35 g are plotted (Figures 1 and 2).

Joyner and Boore (2000) derived estimates of F_a and F_v by adding a new term to their regression relation of the form

$$(a_6 + a_7 PSV_{ref}) \log(V / V_{ref}), \tag{3}$$

where V is the average V_{30} for the site class, V_{ref} is the average V_{30} for the reference site condition, PSV_{ref} is the predicted pseudo spectral velocity for the reference site condition, a_6 and a_7 are coefficients determined by regression, and distance is measured as closest distance to projected rupture surface. Their estimates are based on a database, which does not include the Northridge, Landers, or Loma Prieta data sets. Their estimates are not averaged over a period band, but correspond to spectral ratios at 0.2 and 1.0 seconds. Their estimates of F_a and F_v as derived with respect to a reference site velocity of 1068 m/s are plotted (Figures 1 and 2).

Rodriguez-Marek et al. (1999) used the strong-motion recordings from the Loma Prieta and Northridge earthquakes. They classified the sites based on general geologic and geotechnical information, but did not consider shear-velocity measurements essential to their classification scheme. They developed attenuation relations for each earthquake and site class from which they developed amplification factors with respect to an attenuation relation for site class B.

Silva et al. (2000) developed generic shear-wave velocity profiles for the surficial geologic units in California. Silva used these profiles and a random vibration theory equivalent linear model to estimate amplification factors as a function of frequency. He developed estimates based on both Peninsular Ranges and EPRI models of randomized material profiles. He also developed curves for conditions considered most appropriate for both the western and eastern U.S. Estimates inferred from figures in Silva et al. (2000) for the Peninsular Ranges model are plotted (Figures 1 and 2).

Stewart et al. (2001) used a large database recently compiled by Silva (PEER, http://peer.berkeley.edu/smcat/). It includes recordings from the Northridge, and other earthquakes that have occurred up until 1999. Recording sites were classified using mapped surface geology. Their estimates of F_a and F_v were derived from ratios of response spectral acceleration as computed from the recordings at the site and a reference peak acceleration as predicted by the attenuation functions of Abrahamson and Silva, 1997. Their estimates of F_a and F_v are derived from averages over the appropriate period band. They used linear regressions of the logarithm of estimates for F_a and F_v on the logarithm of predicted reference peak ground acceleration to derive the estimates of the amplification factors as a function of input acceleration level.

The procedures and database used by Borcherdt (2002) differs in two important respects from those of other investigators. The amplification factors are computed with respect to that for a nearby reference site to minimize effects of variations in source radiation pattern and crustal

propagation path. The estimates are based only on the data recorded from the Northridge earthquake. The sites are classified using shear velocity as either measured or estimated for each recording site. Classification of the sites using shear velocity is preferred because seismic response correlates better with shear velocity than with geologic age. In addition, shear velocity is preferred because the actual site characteristics at several recording sites were found to differ from those shown on the geologic maps. The reason for this difference is that several of the sites are located near a geologic boundary that may have been generalized or the geology mapped at the surface is not the same as that within a few feet of the surface.

The estimates of site coefficients by various investigators (Figures 1 and 2) vary depending on the database, the reference ground motion, the site-classification method, and the procedure used to infer the resultant site factors. In addition to previously stated differences in procedures to develop reference motions and resultant estimates of the site coefficients, the site classification method is thought to be a significant contributor to uncertainty in the various estimates. Limited shear-wave velocity data at most of the strong-motion recording sites necessitates the use of mapped geology to classify the sites. Unfortunately, units on most geologic maps have been mapped for purposes of inferring geologic history and not seismic response. For example, in the San Francisco Bay region (Borcherdt, 1994) soil units mapped as quaternary alluvium (Qal) excluding the Holocene units may contain deposits ranging from fine-grained clays and sands with $v_{s_{30}}$ near 250 m/s to over consolidated, very dense course-grained sandy gravels with $v_{s_{30}}$ near 600 m/s. Similarly, rock units mapped as Tertiary in age may vary from firm to soft sandstones and siltstones with $v_{s_{30}}$ near 300 m/s to hard to firm rhyolites with little or no weathering and $v_{s_{30}}$ near 1000 m/s. Without shear-velocity information, sites with rocks of Tertiary and Mesozoic age tend to be classified as class B sites resulting in higher average reference motions and hence lower estimates for the site coefficients than would be obtained were sites correctly classified using shear-velocity information. The uncertainties induced by geologic classifications are expected to be a significant contributor to the differences in the estimates derived by the various investigators using the different databases from different geologic and tectonic regions. As a further explanation of some of the uncertainties in estimates derived by various investigators, results not based on Northridge strong-motion data are necessarily derived from data sets with fewer data with base acceleration levels above 0.2g, and hence, would not be expected to show as large a dependencies on peak acceleration. In addition, estimates derived at individual periods of 0.2 and 1.0 seconds are expected to be less and greater than those, respectively, computed as averages over the short (0.1-0.5 s) and mid-period (0.4-2.0 s) bands.

Results derived by Stewart et al. (2001) are consistently less than those derived by other investigators and only within the 95 percent confidence band for peak accelerations greater than about 0.35 g to 0.42 g depending on site class. Stewart et al. (2001) attributes this difference to the fact that their estimates are referenced to "soft rock" as opposed to "firm to hard" rock used for the code, however uncertainties caused by the necessity to classify sites using geologic age may also be a contributor. Results of Stewart (2002) referenced to a velocity of 1050 m/s are also shown. These estimates compare better with those in the code. Further discussion will be limited to the estimates derived from averages by Crouse and McGuire (1996), Dobry et al. (1999), Rodriguez-Marek et al. (1999), Silva et al. (2000) for the Peninsular Ranges, and Stewart (2002).

Comparison of the short-period F_a estimates

derived from averages for Site Classes C and D shows that the estimates of Silva et al. (2000) for the Peninsular Ranges and Rodriguez-Marek et al. (1999) are near or within the 95 percent confidence band for the sample estimates of the ordinates to the true population regression line derived by Borcherdt (2002) for each base acceleration level. Their estimates and those of Crouse and McGuire (1996) and Borcherdt (2002) exceed the code values for each base acceleration level. Estimates by Crouse and McGuire (1996) and Stewart (2002) are below the 95 percent confidence bound for base

acceleration levels near 0.2 g and less. The value of Dobry et al. (1999) for Site Class D at the 0.1 g is significantly less than the code value. Their values for Site Class C at 0.1g and 0.3 g are within the 95 percent confidence band, but their value at 0.2 g is not. With the exception of the estimates by Crouse and McGuire (1996) for Site Class C estimates derived by each investigator decrease with increasing base acceleration.

Comparison of the mid-period F_v estimates for Site Class C shows that the estimates of Crouse and McGuire (1996) and Silva et al. (2000) exceed the code values and are within the confidence band derived by Borcherdt (2002) for each base acceleration level. The estimates of Rodriguez-Marek et al. (1999) are significantly less than the code values and outside the 95 percent confidence band except for base acceleration of 0.4g. The Dobry et al. (1999) values do not show a well-defined dependence on peak acceleration and are within the confidence band only at 0.3 g. Estimates derived for Site Class C by Crouse and McGuire (1996) and Silva et al. (2000) do not show a dependence on base acceleration.

Comparison of the mid-period F_v estimates for Site Class D shows that the estimates of Silva et al. (2000) exceed the code values and are within the confidence band for each base acceleration level. Estimates derived by Crouse and McGuire (1996) and Rodriguez-Marek et al. (1999) are within the confidence band for base accelerations 0.3 g and greater, but below the band for accelerations 0.2g and less. Each of these estimates shows a dependence on base acceleration.

3.0 CONCLUSIONS

Recent estimates of site coefficients derived by various investigators vary depending on the database, the reference ground motion, the site-classification method, and the procedure used to infer the resultant site factors. These variations tend to suggest the lack of a consensus for modifying the code factors. However, the consistent tendency for the estimates of F_a derived by Crouse and McGuire (1996), and Rodriguez-Marek (1999), Silva et al. (2000), and those herein to exceed the code values at each base acceleration suggests that some increase in the F_a factors might be appropriate for Site Classes C and D. Similarly, the tendency for the estimates of F_v by Crouse and McGuire (1996), Silva et al. (2000), and Borcherdt (2002) to exceed those of the code for Site Class C might be used to argue that some increase in F_v for Site Class C is appropriate. An increase in estimates of F_v for Site Class D can be argued on the basis of the consistency between the Silva et al. (2000) results, the results of Borcherdt (2002), and the Joyner and Boore result at 1 second, but not the results of the other investigators. In summary, variation in the estimates derived by various investigators and the uncertainty associated with the various estimates does not support a significant change in the site coefficients F_a and F_v as currently specified in US building codes.

4.0 ACKNOWLEDGMENTS

Discussions during the initial research with two special colleagues, the late W. B. Joyner and the late H.P. Liu, were helpful.

5.0 REFERENCES

Borcherdt, R. D., 1994, Estimates of site-dependent response spectra for design (Methodology and Justification), *Earthquake Spectra*, **10**, 617-653.

Borcherdt, R. D., 2002, Empirical evidence for site coefficients in building-code provisions, *Earthquake Spectra*, accepted.

Crouse, C. B., and McGuire, J. W., 1996, Site response studies for purpose of revising NEHRP seismic provisions, *Earthquake Spectra*, **12**, 407-439.

Dobry, R., Martin, G. M., Parra, E., and Bhattacharya, A., 1994, Development of site-dependent ratios of elastic response spectra (RRS) and site categories for building seismic codes, Proceedings NCEER, SEAOC, BSSC workshop on site response during earthquakes and seismic code provisions, University of Southern California, Los Angeles, California, November 18 - 20, 1992.

Dobry, R., Ramos, R., and Power, M. S., 1999, Site factors and site categories in seismic codes, *Technical Report MCEER-99-0010*, 81 pp.

International Council of Building Officials (ICBO), 2000, *2000 International. Building Code*, http://www.icbo.org/.

NEHRP (National Earthquake Hazards Reduction Program) Recommended Provisions for Seismic Regulations for New Buildings, 1994 Edition, 1995, Federal Emergency Management Agency Reports *FEMA 222A, FEMA 223A.*

NEHRP (National Earthquake Hazards Reduction Program) Recommended Provisions for Seismic Regulations for New Buildings, 1997 Edition, 1998, Federal Emergency Management Agency, Washington, D. C., *FEMA 302, FEMA 303.*

Rodriguez-Marek, A., Bray, J. D., and Abrahamson, N., 1999, Characterization of site response general categories, PEER Report 1999/03, Pacific Earthquake Engineering Research Center, Berkeley, Ca.

Seed, R. B., Dickenson, S. E., and Mok, C. M., 1994, Site effects on strong shaking and seismic risk; recent developments for seismic design codes and practice, *American Society Civil Engineering Structures Congress*, **12**, 573-578.

Silva, W., Darragh, R., Gregor, N., Martin, G., Abrahamson, N., and Kircher, C., 2000, Reassessment of site coefficients and near-fault factors for building code provisions, *USGS EHRP program report 98-HQ-GR-1010.*

Stewart, J. P., Liu, A. H., and Baturay, M. B., 2001, Amplification factors for spectral acceleration and duration in active regions, California Strong-motion Instrumentation Program Report 2001- , *in press.*

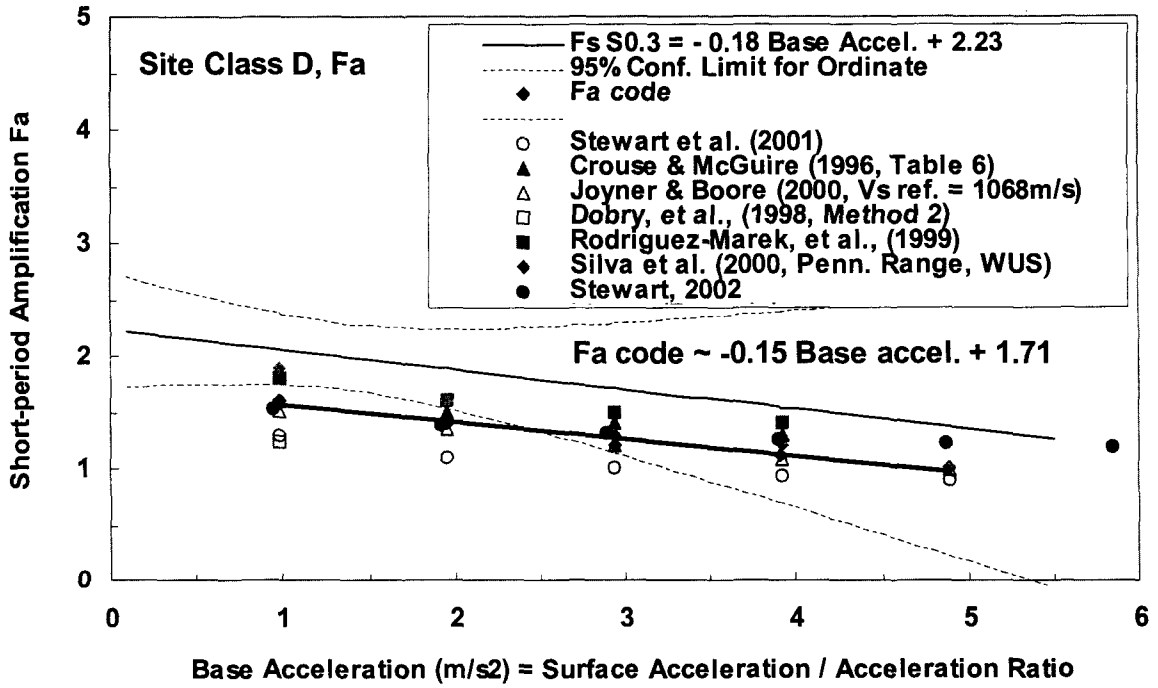

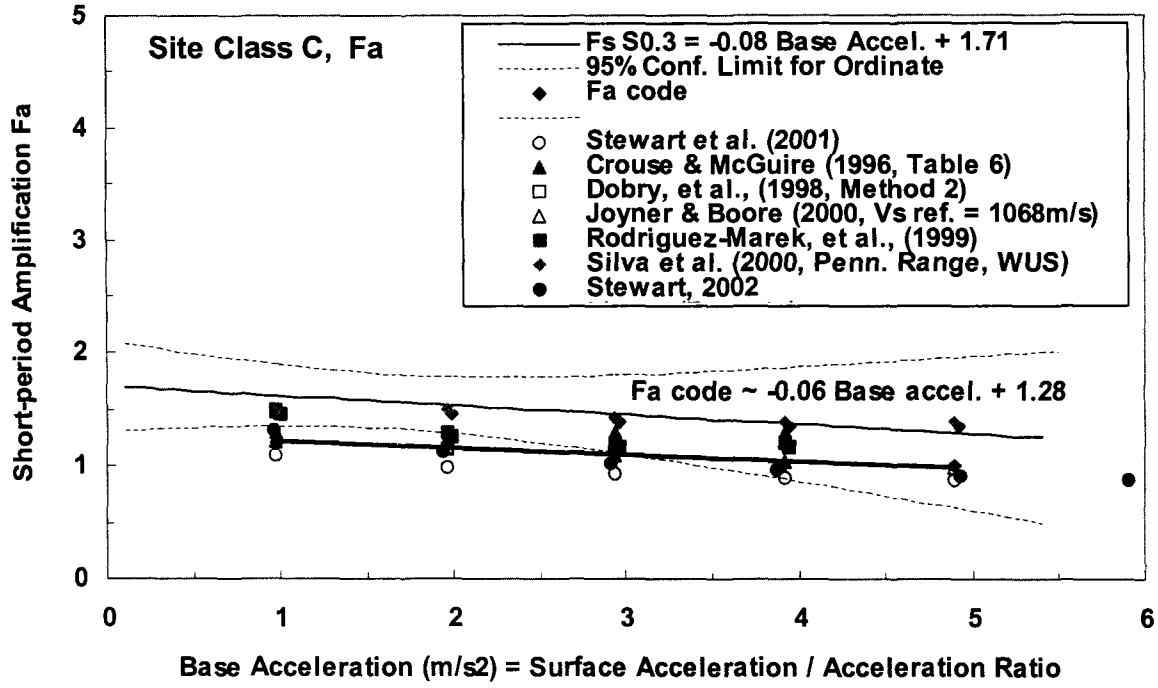

Figure 1. Empirical estimates of the short-period site coefficient F_a for site classes D and C as derived by several investigators.

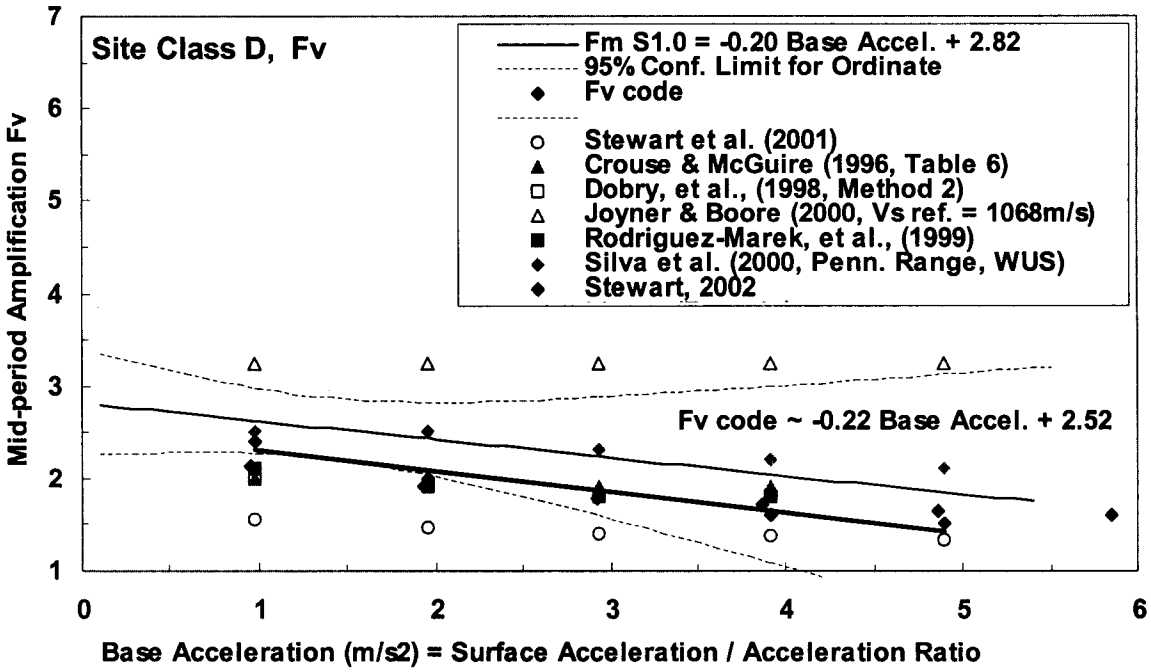

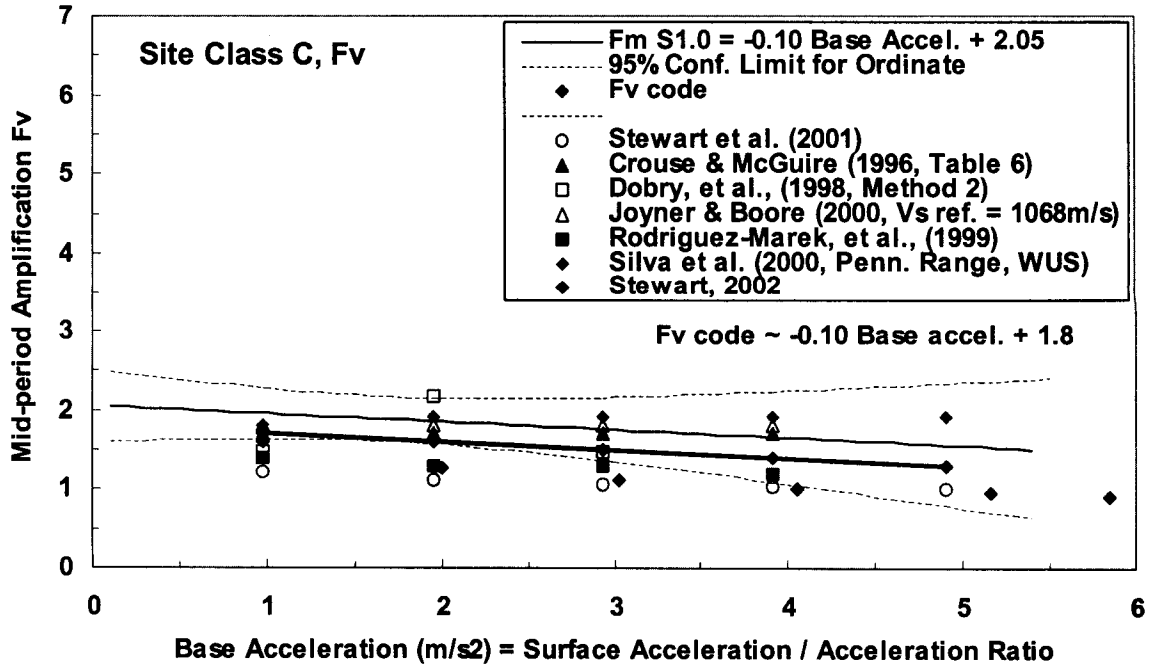

Figure 2. Empirical estimates of the mid-period site coefficient F_v for site classes D and C as derived by several investigators.

A Practical Procedure for Formulating Level 2 Earthquake Motions Based on Scenario Earthquakes

by

Shojiro Kataoka[1], Jun Murakoshi[2] and Keiichi Tamura[3]

ABSTRACT

A procedure for formulating Level 2 earthquake motion (L2 motion) is presented. Tokyo Bay mouth area is given as an example of target site. The most influential earthquake out of possible events around the area is selected as a scenario earthquake; its location and size are assumed the same as those of the 1923 Kanto earthquake. The L2 motion is evaluated following numerous strong motion simulations assuming various source fault models for the scenario earthquake. A stochastic Green's function method is proposed and applied to the simulations. The L2 motion is compared with probabilistic seismic hazard and the input motions specified in the current design specification for highway bridges.

KEY WORDS: Level 2 Earthquake Motion
Scenario Earthquake
Strong Motion Simulation
Stochastic Green's Function

1. INTRODUCTION

The design specifications for highway bridges, railroad bridges, port facilities, and so on, were revised in Japan following the 1995 Hyogo-ken Nanbu earthquake, which caused great damage to infrastructure including those structures. As for highway bridges, the main features of the revision regarding seismic design force is that Type II ground motion, i.e. ground motion from inland direct strike type earthquake like the Hyogo-ken Nanbu earthquake, is to be taken into account besides Type I ground motion, i.e. ground motion from plate boundary type large-scale earthquake.

These two types of ground motions are both classified as those with high intensity and low probability to occur during the service period of the bridge. They are applied to seismic design based on ductility design and dynamic analysis methods. The target seismic performances of bridge for them are set to prevent fatal damage for bridge of standard importance and to limit damage for bridge of high importance. These design ground motions with high intensity are called "Level 2 earthquake motions" in the current design specification for highway bridges, which has been newly revised in 2002. On the other hand, design ground motions that cover ground motion highly probable to occur during service period of bridge are called "Level 1 ground motions". The target seismic performance of bridge for Level 1 earthquake motions is usually

[1] Senior Researcher, Earthquake Disaster Prevention Division, Research Center for Disaster Risk Management, National Institute for Land and Infrastructure Management, Ministry of Land, Infrastructure and Transport, 1 Asahi, Tsukuba 305-0804, Japan

[2] Team Leader, Bridge Structure Research Team, Structure Research Group, Independent Administrative Institution Public Works Research Institute, 1-6 Minamihara, Tsukuba 305-8516, Japan

[3] Team Leader, Ground Vibration Research Team, Earthquake Disaster Prevention Research Group, ditto.

set to have no damage.

The new design specification for highway bridges (Japan Road Association, 2002), DS02 from now on, describes Level 1 and 2 earthquake motions as the standard acceleration response spectra, as well as the previous edition published in 1996 (DS96). DS96 had requested designers to use these design ground motions without exception. DS02, however, doesn't. The designers need to set up Level 1 and 2 earthquake motions in case that they can do so appropriately with adequate consideration regarding seismicity, ground structure and soil condition around the target site in addition to strong motion records etc.

Attenuation relations, which are derived by regression analyses of strong motion records, have been used to estimate peak amplitude or response spectrum from earthquake magnitude and distance between source and site. Since those records are mostly moderate and naturally lacking in very high intensity, the attenuation relations may have insufficient accuracy to estimate earthquake motion with very high intensity. Thus, it is adequate to use them to set up Level 1 earthquake motions with consideration of regional difference. On the other hand, we need to utilize the other kind of methods to estimate high-intensity earthquake motion at the target site with sufficient accuracy in order to set up Level 2 earthquake motions.

We have been studying and developing a practical procedure to estimate strong ground motion and set up Level 2 earthquake motion. The procedure consists of selection of scenario earthquakes for the target site, simulation of strong ground motions caused by the scenario earthquakes with consideration of uncertainty of source parameters, and formulation of Level 2 earthquake motion. In this paper, the procedure is presented giving Tokyo Bay mouth area as an example of target site.

2. SELECTION OF SCENARIO EARTHQUAKES

Earthquake motion possible to be observed at a site is different from that at the other site. It is not only because of the difference of ground structure and soil condition but earthquakes possibly occur around each site. Therefore, it is desirable that Level 2 earthquake motions for each site are determined with consideration of a set of scenario earthquakes that are selected based on the tectonic setting of the region (Japan Society of Civil Engineers, 1996).

In this paper, Kannonzaki site (35.250N, 139.750E) in Tokyo Bay mouth area is given as an example of target site to evaluate Level 2 earthquake motion and a scenario earthquake is selected based on the occurrence of past earthquakes and distribution of active faults around the site. Figure 1 shows epicenters of the past earthquakes (JMA magnitude M_J >=6.5) occurred around the site and distribution of active faults. The 1923 Kanto earthquake (M_J = 7.9) has the largest magnitude among the past earthquakes and its fault plane spreads beneath the site (see Figure 3). The largest magnitude possibly caused by the active faults in Figure 1 is M_J = 7.3 (Matsuda, 1995). Thus, recurrence of the 1923 Kanto earthquake can be considered as the most influential one and is selected as the scenario earthquake for Level 2 earthquake motion for Kannonzaki site.

3. SIMULATION METHOD

A stochastic Green's function method is proposed here to simulate strong motion caused by scenario earthquakes. As shown in Figure 2, the fault

plane is divided into $N_l \times N_w$ subfaults to take the fault rupture process into account. Then the ground motions due to the subfaults are calculated and summed up to synthesize the ground motion due to the target source fault (Irikura, 1986).

The ground motion from each subfault is also the sum of ground motions from hypothetical element earthquakes of which location, length, and width are the same as the subfault but the slip is $1/N_d$. Then the seismic moment, which indicates the total energy released by an earthquake, of the element earthquakes should be set to $1/(N_l \times N_w \times N_d)$ of the scenario earthquake. The ground motion due to the element earthquakes can be produced to fit observed ground motions in a stochastic sense and used as Green's function (stochastic Green's function). In this paper, the Green's functions are generated by fitting their acceleration response spectra and envelopes to empirical models of those of ground motion on engineering bedrock of which S-wave velocity is 700[m/s] (Satoh et al., 2002). Thus, the resulting ground motion due to the target event is that on the engineering bedrock.

4. STRONG MOTION SIMULATION

4.1 Source fault models of the scenario earthquakes

The 1923 Kanto earthquake is considered recurrent but not with the same rupture process. Thus, it is necessary to consider uncertainty of source parameters to be prepared for future earthquakes. The locations of rupture starting point and asperities and rupture velocity are chosen here as uncertain parameters and their effects on strong motion are examined by changing them systematically, while the fault plane geometry is fixed.

Wald and Somerville (1995) proposed a variable-slip fault rupture model of the 1923 Kanto earthquake as shown in Figure 3. The fault model has the length of 130[km], width of 70[km], strike of 290[deg], dip of 25[deg]. The rupture starts from the hypocenter and propagates radially at rupture velocity of 3.0[km/s]. The epicenters of the 1923 Kanto earthquake in Figures 1 and 3 are located differently because the epicenter in Figure 3 was determined independently of JMA using local and teleseismic P-wave arrival times.

Kanamori (1991) proposed an average empirical relationship between seismic moment, Mo[N·m], and rupturearea, S[km^2], as $Mo = 1.23 \times 10^{15} S^{3/2}$ assuming stress drop is 3.0[MPa]. Substituting S=130 × 70=9100[km^2] into the equation yields $Mo = 1.06 \times 10^{21}$[N·m], which is more than 30% larger than that of the 1923 Kanto earthquake, 7.8×10^{20}[N·m], estimated by Wald and Somerville (1995). Here we set the seismic moment of the scenario earthquakes to 1.06×10^{21}[N·m] as it is more likely to occur in the future.

Somerville et al. (1999) proposed a procedure to identify rectangle asperities from a variable-slip model and applied it to 15 crustal earthquakes. Figure 3 shows the rectangle asperities identified from the variable-slip model of the 1923 Kanto earthquake by the procedure. Since two asperities have been identified here, we call the larger one "Asp#1" and the smaller "Asp#2". The average slip over Asp#1 and Asp#2 become 2.00 times and 2.09 times of the average slip over the entire fault. Those values are very close to the value 2.01, which Somerville et al. (1999) found as the average of asperities of the 15 crustal earthquakes. Asp#1 and Asp#2 cover 17% and 8.5% of the area of the entire fault, respectively.
Based on these characteristics of the source fault of the 1923 Kanto earthquake, we assume: the

source faults of the scenario earthquakes have one or two asperities; in case of one asperity, it covers about 25% of the area of the entire fault; in case of two asperities, the larger and the smaller cover about 17% and 8.5% of the area of the entire fault, respectively; the average slip over the asperities are just 2 times of the average slip over the entire fault, i.e. 3.03[m]. The background, the rest of the entire fault, is set to have uniform slip of 0.91[m] to maintain the average slip over the entire fault.

As shown in Figure 4, the locations of asperities and rupture starting point are changed to examine effects on strong motion. The rupture velocity is also set to have three different values: 2.6, 3.0, and 3.3[km/s]. Now the source fault models of the scenario earthquakes have 9 patterns of the locations of asperities, 5 locations of rupture starting point, and 3 rupture velocities so that we have total of $9 \times 5 \times 3 = 135$ source fault models for the following strong motion simulation.

4.2 Variation of ground motion due to uncertainty of source parameters

Strong motion simulations are carried out using the 135 source fault models by the stochastic Green's function method explained earlier in this paper. Figure 5 shows the acceleration response spectra of the 135 simulated strong motions. We can see and understand that the acceleration response varies about 5 times due to the variety of the source fault models and it is very important to conduct such simulations to set up design ground motion for prevention of unexpected damage. It is also shown that the simulated strong motions can be much stronger than the standard acceleration response spectrum of the Type I ground motion specified in DS02.

5. EXMAMPLE OF LEVEL 2 EARTHQUAKE MOTION

The acceleration response spectra of the 135 simulated strong motions are compared with those with 2, 5, and 10 % probability of exceedance in 100 years derived by probabilistic seismic hazard analyses (Nakao et al., 2002). An attenuation model of acceleration response spectrum (Takahashi et al., 2000) is employed for the analyses. These three curves are within the variation range of the 135 acceleration response spectra.

If, for example, the Level 2 earthquake motion is set to have the acceleration response spectrum consists of three straight lines shown in Figure 6, the waveforms of the Level 2 earthquake motion can be as shown in Figure 7. One of the simulated waves is chosen and its Fourier amplitude spectrum is modified so that its acceleration response spectrum fits to the target one to obtain the waveforms in Figure 7. The acceleration and velocity waveforms have large amplitude of about 1100[cm/s2] and 150[cm/s] and long duration of strong motion.

6. SUMMARY

A procedure for formulating Level 2 earthquake motion is discussed and presented. Kannonzaki site in Tokyo Bay mouth area is given as an example of target site. The Level 2 earthquake motion evaluated here is based on the most influential earthquake and strong motion simulations by the stochastic Green's function method including the effects of uncertainty of the source parameters. The source parameters, especially the locations of asperities, have great effects on the simulated strong motions. An example of Level 2 earthquake motion with large amplitude and long duration is presented.

ACKNOWLEDGEMENT

In order to promote the present study, "Technical Committee on Methodology for Formulating Level 2 Earthquake Motions (Chairman: Prof. Tatsuo Ohmachi, Tokyo Institute of Technology)" has been established at the National Institute for Land and Infrastructure Management. The authors would like to thank all members of the committee for the valuable discussion.

REFERENCES:

Irikura, K. (1986): Prediction of strong acceleration motions using empirical Green's function, *Proc. 7th Japan Earthq. Eng. Symp.*, pp. 151-156.

Japan Road Association (2002): *Design specifications for highway bridges, Part V. Seismic design* (in Japanese).

Japan Society of Civil Engineers (1996): *Proposal on earthquake resistance for civil engineering structures* (in Japanese).

Kanamori, H. (ed.) (1991): *Physics of earthquake* (in Japanese).

Matsuda, T. (1995): Seismic zoning map of Japanese islands, with maximum magnitudes derived from active fault data, *Bull. Earthq. Res. Inst., Univ. of Tokyo*, Vol. 65, pp.289-319 (in Japanese).

Nakao, Y. et al. (2002): Seismic hazard map for all Japan, *Proc. 11th Japan Earthq. Eng. Symp.* (submitting, in Japanese).

Satoh et al. (2002): Empirical models of acceleration response spectra and envelopes at engineering bedrock using K-NET strong motion records, *Proc. 11th Japan Earthq. Eng. Symp.* (submitting, in Japanese).

Somerville, P. et al. (1999): Characterizing crustal earthquake slip models for the prediction of strong ground motion, *Seism. Res. Letters*, Vol. 70, No. 1, pp. 59-80.

Takahashi, T. et al. (2000): A spectral attenuation model for Japan using strong motion data base, *Proc. 6th Int. Conf. on Seismic Zonation*, 6p. (CD-ROM)

The Research Group on Active Faults of Japan (1991): *Active faults in Japan*, Rev. Ed., Univ.of Tokyo Press (in Japanese).

Wald, D. J. and Somerville, P. G. (1995): Variable-slip model of the Great 1923 Kanto, Japan earthquake: Geodetic and body-waveform analysis, *Bull. Seism. Soc. Am.*, Vol. 85, No. 1, pp. 157-177.

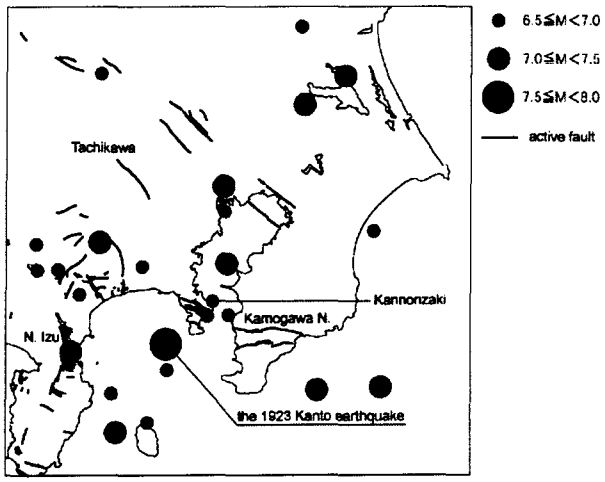

Figure 1. Epicenters of major earthquakes (M_J >=6.5) occurred around Kannonzaki site in the past and distribution of active faults (The Research Group on Active Faults of Japan, 1991). The locations of epicenters are determined by Japan Meteorological Agency (JMA).

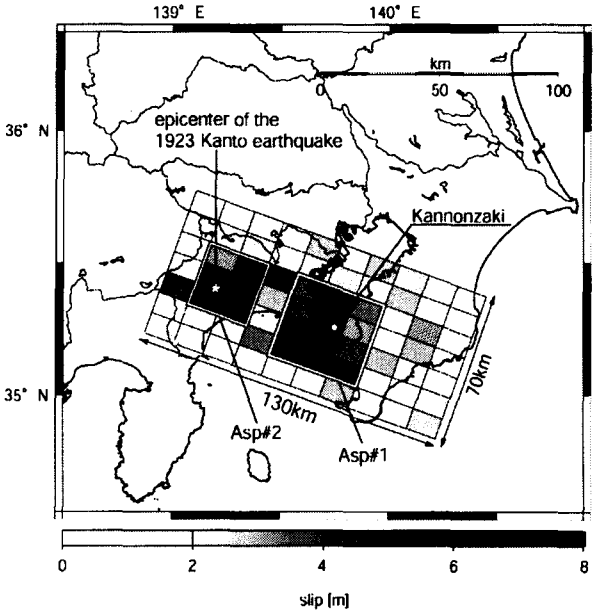

Figure 3. Map showing the rectangle asperities, Asp#1 and Asp#2, identified from the variable-slip model of the 1923 Kanto earthquake (Wald and Somerville, 1995) and the location of Kannonzaki site.

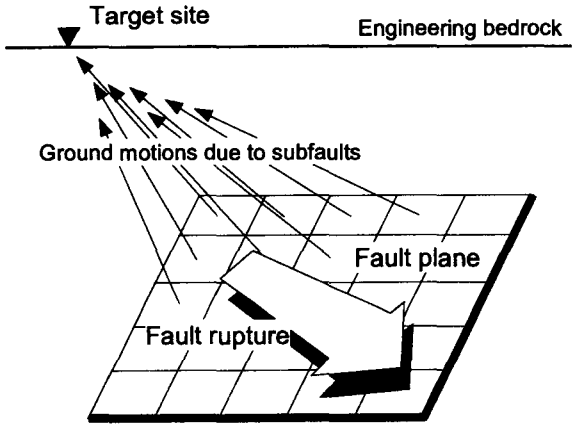

Figure 2. Schematic illustration of the synthesis of ground motions due to subfaults to produce the ground motion due to the target source fault model.

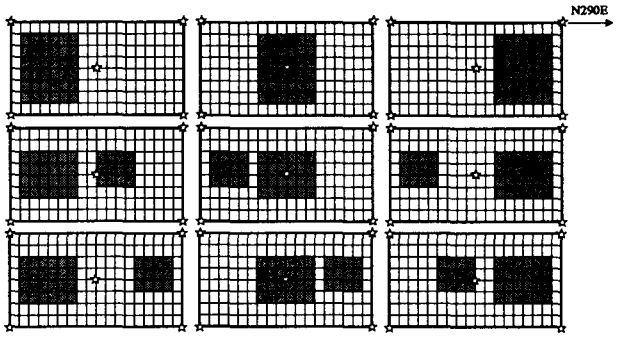

Figure 4. Source fault models used in the simulation with locations of asperities (shade) and rupture starting points (star).

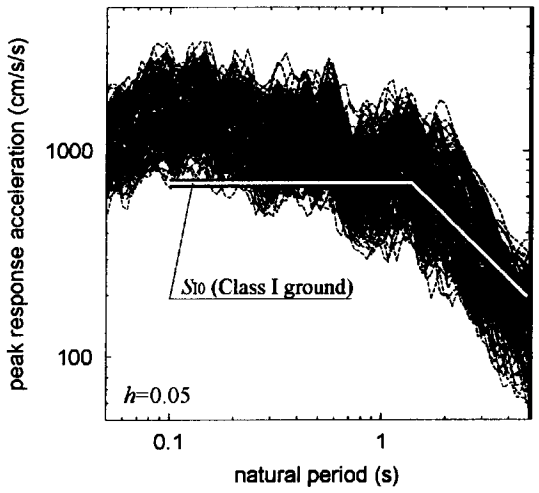

Figure 5. Acceleration response spectra of the 135 simulated waves on the engineering bedrock at Kannonzaki site compared with S_{I0} for Class 1 ground of DS02.

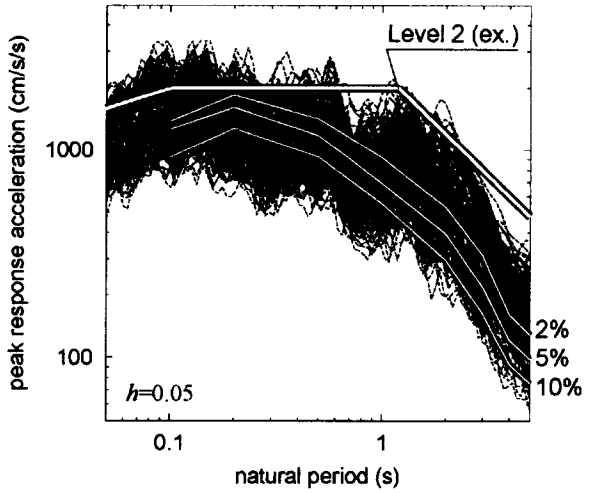

Figure 6. The same as Figure 5 but compared with acceleration response spectra with 2, 5, and 10% probability of exceedance in 100 years derived by probabilistic seismic hazard analyses (Nakao et al., 2002). An example of Level 2 earthquake motion formulated based on the simulated waves is also shown.

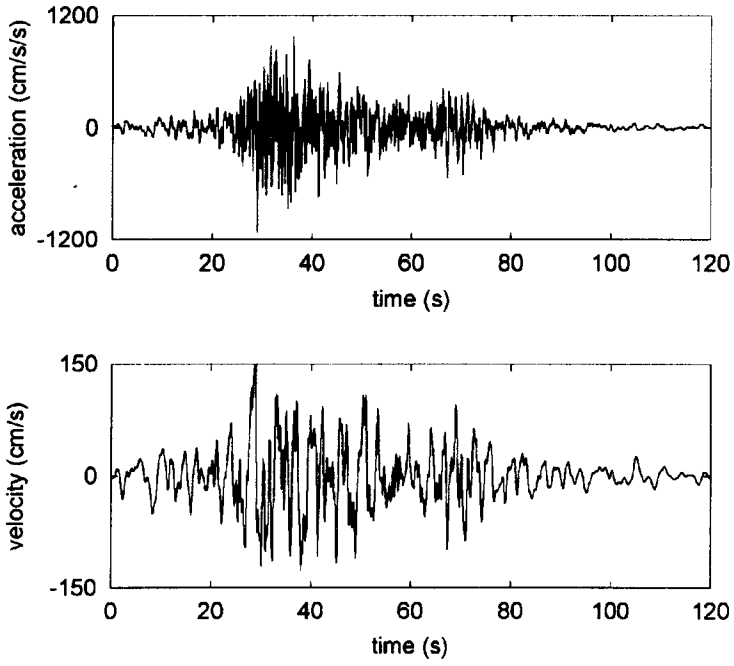

Figure 7. Acceleration and velocity waveforms of an example of Level 2 earthquake motion. One of the simulated waves is chosen and its Fourier amplitude spectrum is modified so that its acceleration response spectrum fits to the example of Level 2 earthquake motion shown in Figure 6.

Identification of Site Frequencies from Building Response Records

by

M. Çelebi[1]

ABSTRACT

A simple procedure to identify site frequencies using earthquake response records from roofs and basements of buildings is presented. For this purpose, data from five different buildings are analyzed using only spectral analyses techniques. Additional data such as free-field records in close proximity to the buildings and site characterization data are also used to estimate site frequencies and thereby to provide convincing evidence and confirmation of the site frequencies inferred from the building records. Furthermore, simple code-formula is used to calculate site frequencies and compare them with the identified site frequencies from records. Results show that the simple procedure is effective in identification of site frequencies and provides relatively reliable estimates of site frequencies when compared with other methods. Therefore the simple procedure for estimating site frequencies using earthquake records can be useful in adding to the data base of site frequencies. Such data bases can be used to better estimate site frequencies of those sites with similar geological structures.

KEYWORDS: site-frequency, structural frequency, structural response, spectral analysis, cross-spectrum, transfer function, coherence.

[1] Earthquake Hazards Team, USGS (MS977), 345 Middlefield Rd., Menlo Park, Ca, 94025

1.0 INTRODUCTION

Reliable calculations and/or estimates of the fundamental frequency of a building and its site are essential during analysis and design process. Various code formulas based on empirical data are generally used to estimate the fundamental frequency of a structure. Alternatively, if dynamic modal analysis is performed, fundamental frequencies and mode shapes are obtained. For existing structures, in addition to code formulas and available analytical tools such as modal analyses, various methods of testing including ambient and forced vibration testing procedures may be used to determine dynamic characteristics. Reliable strong-shaking dynamic characteristics are obtained, when and if the structures are instrumented and their on-scale responses are recorded during strong shaking events. Spectral procedures and system identification techniques applied to the recorded strong shaking response data yield very accurate assessments of the actual dynamic characteristics.

While structural frequencies can be calculated using mathematical models or determined from records, identification of site frequencies are not as straightforward; hence, often, the estimation of site frequencies are made using simple empirical relationships with rough parametric values and without mathematical modeling. Recent codes provide approximate estimates of site frequencies if geotechnical logs are available. Furthermore, there are always some uncertainties in prediction of site frequencies because of the assumptions made in establishing representative site characteristics. The frequently used simple formula, $T_s=4H/V_s$, requires minimal but reasonable characterization of depth to bedrock and representative average shear wave velocities of layered media (International Building Code, 2000).

In this paper, the objective is to show that, when and if structural response records are available from both the roof and ground floors or basements of building structures, simple spectral analyses procedures can be used to convincingly identify not only structural frequencies but also site frequencies.

The benefits of such an identification procedure is considerable. Identified site frequencies can be used in data bases that aim to classify site characteristics against dynamic characteristics, and, in assessing other techniques used to identifying site frequencies. Furthermore, the procedure can be applied to sets of data available from code-type instrumented buildings (three tri-axial accelerographs placed at the roof, mid-height and basement of buildings) as well as from buildings instrumented with multiple sets of sensors in different floors. A data base that results from such assessments can be used for similar sites when, otherwise, there is insufficient information to infer site frequencies.

The scope of this paper is limited to demonstration of the procedure with five sets of building response data, four obtained during the 1989 Loma Prieta earthquake and another obtained during the Whittier, California earthquake. The intent here is to identify structural frequencies and site frequencies from synchronized strong-shaking data recorded during strong-shaking events from instrumented structures. Low-amplitude test data is not used in this study.

For all of the five cases included in this study, detailed assessments of structural characteristics as well as assessments of site frequencies were included in previous studies with much wider scopes (Çelebi, 1992, 1993a,b,c, 1994, 1998). This study concentrates on primarily for identification of site frequencies using recorded building responses motions. It is envisioned that data bases of site frequencies extracted from building responses records may be developed for future use.

2.0 THE PROCEDURE

In order to identify site frequencies, the following steps are essential:

1. At least two pairs of horizontal components of recorded data, one pair from the roof and the other from the ground floor or basement are required. Either parallel and/or orthogonal pairs of data from roof or basement can be used.
2. The structural frequencies are identified first. The roof and/or upper floor records are naturally the best suited for this. The following well known methods are used to identify structural frequencies:
   a. spectral analyses (amplitude spectra and spectral ratios, cross-spectra and coherence and phase relationships) and
   b. system identification methods. In the event that system identification procedures are used, the roof and/or upper floor data constitute the output and basement and/or ground floor records are adopted as the input motion.
3. Once structural frequencies are confidently identified, then the site frequency distinguished:
   a. if one of the non-structural dominant peaks of cross-spectrum of ground-floor (or basement) motions is different than the structural frequency, than that frequency is likely the site frequency,
   b. if the spectral ratio cancels out a dominant frequency that clearly appears in amplitude and/or cross-spectrum, then that frequency is not a structural frequency but it most likely is the site frequency, and/or,
   c. cross-spectra or normalized cross-spectra $[S_{xy}/\max(S_{xy})]$ calculated from pairs of roof and basement (or ground floor) data exhibit site frequencies.
4. Availability of free-field records from a free-field station that is in the proximity of the building adds further confidence in confirming the identified site frequency. The amplitude spectra of the components of and/or cross-spectrum of orthogonal horizontal components of

free-field motions usually reveals the site frequency.

5. If, in addition, site characterization data (depth to bedrock, geological borehole data, shear-wave velocities of different layers of soil below the foundation) is available, transfer functions can be calculated to add further confidence.ions can be calculated to add further confidence.

2.1 Case 1: Pacific Park Plaza [PPP], Emeryville, California:

Detailed analyses of 1989 Loma Prieta earthquake (M_s=7.1) response recordings of the 30-story, reinforced concrete framed Pacific Park Plaza [PPP] in Emeryville, California, have been presented by Çelebi and Safak (1992), Anderson, Mirando and Bertero (1991) and Çelebi (1998). Recently compiled borehole and site characterization information is also available (Gibbs, Fumal and Powers, 1994). Figure 1 shows plan view, instrumentation scheme of the building and the location of the free-field stations associated with this building instrumentation. The available free-field strong motion recording is pertinent to the convincing identification of the site frequency. Figures 2a and b depict building accelerations recorded at the core of the top instrumented level, at the core of the ground floor and the associated south free-field of the three-winged building. Corresponding amplitude spectra are provided in Figures 2c and d. The first three modal structural frequencies (periods) clearly identified from the recordings are 0.38, 0.95 and 1.95 Hz (2.63, 1.05, 0.34 s). The peak at 0.7 Hz that appears in the amplitude spectra of the roof also appear as the dominant peak in the amplitude spectra of the ground floor and the south free-field (SFF). However, this peak at 0.7 Hz disappears in the spectral ratios calculated from the amplitude spectra of the roof and ground floor as depicted in Figures 2e and f. This indicates that 0.7 is the site frequency as, although it appears in the roof spectra, it cancels out when ratios are calculated.

In Figure 3, cross-spectra, calculated from pairs of orthogonal components of acceleration recorded at the (a) roof , (b) gound floor and (c) free-field are presented. The roof cross-spectrum clearly identifies the aforementioned frequencies of the first three modes. These modes are coupled torsional-translational modes (Çelebi, 1998). The peak at 0.7 Hz that appears in the cross-spectrum of the roof appears as the dominant peak in the cross-spectra of the ground floor and the south free-field (SFF). Next, when the normalized cross-spectra are calculated for the ground floor and free-field, the site frequency at 0.7 Hz is distinguishable from the structural frequencies in the normalized cross-spectrum of the roof (Figure 2d). This is further confirmed by the lowest frequency peak at 0.7 Hz of the transfer function (Figure 4) calculated by using Haskell's shear wave-propagation method (Haskell, 1953, 1960) using site characterization data related to variation of shear wave velocities with depth (Gibbs, Fumal and Powers, 1994). The depth to bedrock has been adopted from a map by Hensolt (1993) as 150 m. (~500 ft).

2.2 Case 2: Two-story Office Building [OAK], Oakland, California:

McClure (1991) provides detailed particulars of the two-story office building in Oakland, California. The instrumentation scheme of this building as well as accelerations recorded during the 1989 Loma Prieta earthquake from the roof, second and ground floors are provided in Figure 5. Ambient tests of the building performed in the 1965 yielded first mode frequency (period) as 2.13 Hz (0.47 sec) and 2.08 Hz (0.48 sec) for the NS and EW, respectively, and forced vibration tests, also performed in 1965, yielded 2.35 Hz (0.426 sec) (Bouwkamp and Blohm, 1966). These and other assessments of modal frequencies of the building are summarized in Table 1.

Figure 6 shows amplitude spectra of recorded accelerations in both the NS and EW directions and rotational accelerations (difference between parallel records) at the three structural levels (roof, second floor and ground floor). Figure 7 shows time-histories, amplitude spectra and spectral ratios for pairs of recorded accelerations at the roof and ground floor. From the spectra,

three distinctive frequencies (0.82-0.85, 1.65 and 1.95 HZ) are identified. The frequencies 1.65 Hz and 1.95 Hz are structural frequencies determined by the fact that they have a very high ratio amplitude as seen in the in the spectral ratio plots (Figure 6g-6i) calculated from the pairs of amplitude spectra of the roof and ground floor motions (Figure 6d-6f). These two frequencies are very close to one another. Therefore, given the structural irregularity created mainly by the north and east end walls, the structure responds in a closely-coupled translational-torsional mode with frequency between 1.65-2 Hz. The 0.82-0.85 Hz (NS) and 0.65-0.85 Hz (EW) frequencies that appear in the amplitude spectra do not appear in the spectral ratios because they cancel out. Therefore, it is safe to declare that the site frequency is between 0.65-0.85 Hz.

Figure 8 depicts coherence, phase angle and cross-spectrum of the pairs of parallel motions at the roof [CH2 and CH3] and ground floor [CH6 and CH7]. Because the 2-story building is very rigid, both the structural frequency and the site frequency appear in the cross-spectrum plots of the roof and ground floor motions, although the amplitude of the site frequency at the ground floor is much larger than that of the structural frequency.

There is no free-field station associated with the building; however, recently documented site characterization data in proximity to the building (Gibbs, Fumal and Powers, 1993) allows determination of site transfer function (Figure 9). Depth to bedrock (two cases) have been estimated from Hensolt map (1993). There is a good match between the lowest frequency (0.6-0.7 Hz) in Figure 9 and the site frequency (0.65-0.85) extracted from the building records (Figures 6-7).

2.3 Case 3: Santa Clara County Office Building [SCCOB], San Jose, Ca.

The building for Case 3, Santa Clara County Office Building (SCCOB) in San Jose, California is perhaps the most complex response cases caused by three close frequencies (0.38, 0.45, and 0.57 Hz) (Çelebi, 1998). Figure 10 depicts the instrumentation scheme and the relative location of the building and the epicentral locations of the three earthquakes that were recorded on and before October 17, 1989 Loma Prieta, Ca. earthquake.

Figure 11 shows the very unique responses of the roof of the building to the three different earthquakes. These are typical exhibitions of coupled torsional and translational responses with significant beating effect caused by closely spaced translational frequency (0.45 Hz) with the torsional frequency (0.57 Hz) and low critical damping of approximately 2 % of the structural system (Çelebi, 1994, 1998, Boroschek and Mahin, 1991). Due to this type of behavior, the building was retrofitted by adding viscous elastic dampers (Crosby, Kelly and Singh, 1994). Although strong shaking data has not been recorded since the retrofit in 1994, it is expected that in the future the response of this building will not resemble those in Figure 11 and due to expected shift in building frequency and increased damping, the beating effect will disappear.

Figures 12a-c shows pairs of parallel translational accelerations at the roof and their differences representing torsional accelerations (NS: CH6, CH7, and CH6-CH7) and (EW: CH4, CH5 and CH4-CH5) and translational accelerations (NS: CH22, EW: CH20 and CH21) at base of the SCCOB. Corresponding amplitude spectra of these motions are provided in Figure 12d-f. The fundamental frequency (period) of the building at 0.45 Hz (2.22 sec) belongs to the translational mode and the frequency (period) at 0.57 Hz (1.75 s) belongs to the torsional mode; hence, the closely coupled translational-torsional response of the building that causes the beating effect. Details of these effects are provided by Çelebi (1994, 1998) and Boroschek and Mahin (1991). The frequency at 0.38 Hz (2.63 sec) belongs to the site.

The attributions to structural and site frequencies are confirmed by the spectral ratios of roof motions with respect to base motions (Figures 13 a and b). The site frequency (0.38 Hz) cancels out in the spectral ratios of roof/base motions. This

frequency (0.38 Hz) also appears in the cross-spectra of orthogonal (CH21 and CH22) and parallel (CH20 and CH21) pairs of motions at the base; hence, indicating that it is site related and not structural related.

Limited geological logs (Earth Sciences, 1971) available allows approximate calculation of site transfer function using estimated shear wave-velocities and depth to bedrock estimated anywhere between 150-270 m. Figure 14 shows that the site, in the Santa Clara basin, is capable of generating motions with periods between 2-3 seconds, depending on the assumed depth to bedrock. The long-period site characterization is also confirmed by a study of the basin effect in the Santa Clara (CA) by Frankel and Vidale (1992) who concluded that 2-5 second long-period motions can be generated in this particular basin.

2.4 Case 4: Embarcadero Building [EMB], San Francisco, Ca.

Figure 15 shows a three-dimensional view and the instrumentation scheme of the Embarcadero Building (EMB) in San Francisco, Ca.

Figures 16a-b show the acceleration responses recorded at the roof and basement of EMB in the NS and EW directions, respectively. The normalized amplitude spectra of these motions are depicted in Figures 16c-d. The reason these spectra are normalized is to show the significant peaks of both the roof and basement in the same plot. Otherwise, since the building is tall, the basement spectra would not clearly be seen if they are plotted on an equal scale. The fundamental frequencies (periods) of the building are identified as 0.19 Hz (5.26s) in the NS and 0.16 Hz (6.25s) in the EW directions respectively. Detailed analyses of recorded data from this building is presented by Astaneh, Bonovitz and Chen (1991), and Çelebi (1993a). Figures 16e-f show the ratios of amplitude spectra of pairs of roof and basement motions. The site frequency (period) at 0.7-0.8 Hz (1.25-1.43 sec) clearly seen in the normalized amplitude spectra of basement motions cancels out in the spectral ratio plots. In the spectral ratio plots (Figure 17 e-f), the second (NS: 0.57Hz [1.75 s], EW: 0.46 Hz [1.02 s]) and third (NS; 0.98 Hz and EW: 0.77 Hz) modal frequencies are clearly identifiable. These periods, in general, follow the T, T/3, T/5 rule-of-thumb.

Figure 17 shows coherence, phase angle and cross-spectrum plots of the pairs of motions at the roof (NS: CH17 and CH18) and at the base (NS: CH4 and CH6). Cross-spectrum of the pair of roof motions, shown in Figure 17e clearly indicates the third modal frequency (0.98 Hz). The same for basement motions has a much wider frequency band that includes the 0.98 Hz frequency. This implies that the site frequency (~0.7-0.9 Hz) that appears in the amplitude spectrum of the basement motions is very close to the third modal frequency in the NS direction and possibly causes resonance.

The site frequency is 0.7-0.8 Hz (1.25-1.43 sec) and is identifiable in the cross-spectra. The site transfer function, presented in Figure 19, confirms this identification. Site characterization data has been adopted from Gibbs and others (1994).

2.5 Case 5: Norwalk Buildings, Norwalk, Ca. [NOR]

Figure 19 shows the extensive instrumentation for the two buildings and the site at 12400 block of Imperial Highway, Norwalk, Ca. In this study, only Building B (hereby called NOR) and the south free-field (SFF) is considered. Responses of both buildings and three of the four free-field stations were recorded during the 1987 Whittier, Ca. earthquake (M_s=5.8). Detailed studies of these records are reported elsewhere (Çelebi, 1993b and c).

Figure 20 shows (a,b) NS and EW accelerations at the roof and the basement of NOR and its south free-field. Figures 20c and d show the corresponding amplitude spectra calculated from these accelerations. Figures 20e anf f show the corresponding spectral ratios calculated from the amplitude spectra. The fundamental structural frequencies of Building B are identified as 0.76 Hz (NS) and 0.83 Hz (EW). The very small peak

at 0.3 Hz observed in the amplitude spectra as well as in the basement cross spectra is the site frequency. It is noted that this frequency cancels out in the spectral ratio plots (Figures 20e and f). Another possible larger mode site frequencies is detectable at approximately 1.7 Hz. This frequency also cancels out in the spectral ratio plots.

The depth to bedrock in the vicinity of the buildings is not well described; however, logs from existing nearby oil wells indicate that below 500 m depth, well-cemented sandstone and marine rock are prevalent. The site transfer function using estimated shear wave velocities is shown in Figure 21 and exhibits that the site is capable of generating motions with low frequencies (e.g. 0.3 Hz).

3.0 ESTIMATES OF SITE FREQUENCY USING CODE FORMULA:

In order to assess the reliability of the extracted site frequencies and to facilitate comparisons, the approximate site formula (T_s=4H/V_s) is used to calculate approximate periods of the sites using the site characterization data displayed in the site transfer function plots (Figures 4, 9, 14, 18 and 22). These calculations are summarized in Table 2 and compared with the site frequencies assessed from earthquake records and site transfer functions. It is noted herein that the above simple formula uses an average shear wave velocity, $V_s(ave)=H/(\Sigma (h_i/V_{si})$ and that while the Uniform Building Code (1997) does not state a limitation on the total depth for which this formula can be used, the new International Building Code (2000) limits the use of this relationship up to a depth of ~ 30m (100ft).

4. DISCUSSION AND CONCLUSIONS

A procedure that is used to identify site frequency from building responses recorded during earthquakes has been presented. The procedure distinguishes site frequency among several frequencies that appear in amplitude spectra and cross-spectra of horizontal records from roof and basements of buildings. These results are further substantiated by analyses of additional data from associated free-field records of each building and site transfer function calculated by using site characterization data. Furthermore, these results are compared with simple code formula computation even though the formula, T=4H/Vs, may be limited to layered media with depths to 30 meters (100ft) (International Building Code, 2000). All results presented for five cases are summarized in Table 2 and comparatively plotted in Figure 23. As noted both in Table 2 and Figure 23, the site frequencies identified from building records are higher than those estimated by transfer functions and the simple code formula.

The procedure can be used to process numerous sets of accumulated data from instrumented structures and promises to be an effective and simple technique to identify site frequencies from actual building responses recorded during earthquakes.

The only real difficulty in applying this procedure could arise when and if the site and structural frequencies are identical or if they are too close to one another; in which case, further examination of the data by other procedures can be applied or estimates of free-field data or site data can be used to clarify the situation.

5.0 REFERENCES

1. Anderson, J. C., Miranda, E., and Bertero, V. V., 1991, Evaluation of the seismic performance of a thirty-story RC building, University of California, Berkeley, California, Earthquake Engineering Research Center Report 91/16, December 1991.
2. Astaneh, A., Bonowitz, D., and Chen, C.,1991, Evaluating design provisions and actual performance of a modern high-rise steel structure. *SMIP91 Seminar on Seismological and Engrg. Implications of Recent Strong-Motion Data*, California Department of Conservation, Division of Mines and Geology, 5-1--5-10.

3. Boroschek, R. L., and Mahin, S. A.,1991, Investigation of the seismic response of a lightly-damped torsionally-coupled building, University of California, Berkeley, California, Earthquake Engineering Research Center Report 91/18, December 1991.
4. Bouwkamp, J. G., and Blohm, J. K., 1966, Dynamic response of a two story steel frame structure, Bull. Seismological Society of America, 56, 6.
5. Çelebi, M., and Safak, E., 1992, Seismic response of Pacific Park Plaza. I: Data and preliminary analysis, *J. Struct. Engrg.*, ASCE, 118(6), 1547-1565, June 1992.
6. Çelebi, M., 1993a, Seismic response of eccentrically braced tall building, *J. Struct. Engrg.*, ASCE, 119 (4), 1188-1205, April 1993.
7. Çelebi, M., 1993b, Seismic responses of two adjacent buildings. I. Data and analyses, *J. Struct. Engrg.*, ASCE, 119(8), 2461-2476, August 1993.
8. Çelebi, M., 1993c, Seismic responses of two adjacent buildings. II. Interaction, *J. Struct. Engrg.*, ASCE, 119 (8), 2477-2492, August 1993.
9. Çelebi, M., 1994, Response study of a flexible building using three earthquake records, ASCE, Structures Congress, Atlanta, Georgia, April 1994.
10. Çelebi, M., 1998, Performance of Building structures – A Summary, *in* The Loma Prieta, California, Earthquake of October 17, 1989 – Building Structures (M. Çelebi, *editor*), **USGS Prof. Paper 1552-C**,pp. c5-c76, January 1998.
11. Crosby, P., Kelly, J., and Singh, J. P., 1994, Utilizing visco-elastic dampers in the seismic retrofit of a thirteen story steel-framed building, *in* Structures Congress XII, Atlanta, Ga., v. 2: American Society of Civil Engineers, p. 1286-1291.
12. Earth Sciences Associates, 1971, Soil and foundation investigation for the proposed Santa Clara County Civic Center, Technical Report, Earth Sciences Associates, Palo Alto, Ca., November 1971.
13. Fumal. T. E., 1991, A compilation of the geology and measured and estimated shear-wave velocity profiles at strong-motion stations that recorded the Loma Prieta, California, earthquake, *U.S.G.S. Open-File Report 91-311,* Menlo Park, Ca.
14. Frankel, A., and Vidale, 1992, A three-dimensional simulation of seismic waves in the Santa Clara Valley, California from a Loma Prieta aftershock, *Bull. Seism.. Soc. of America*, 82, 5, pp. 2045-2074.
15. Tamura, Y., Matsui,M. Pagnin, L-C, and Yoshida, A., 2001, Measurement of Wind-induced Response of Buildings using RTK-GPS, Proceedings of the 5th Asia-Pacific Conference on Wind Engineering, Kyoto, October 21-24, 2001 (to be published).
16. Gibbs. J. F., Fumal, T. E., and Powers, T. J., 1993, Seismic velocities and geological logs from borehole measurements at eight strong-motion stations that recorded the 1989 Loma Prieta, California, earthquake, *U.S.G.S. Open-File Report 93-376,* Menlo Park, Ca.
17. Gibbs, J. F., Fumal, T. E., Borcherdt, D. M., Warrick, R., Liu, H-S, and Westerlund, R., 1994, Seismic velocities and geologic logs from borehole measurements at three downhole arrays in San Francisco, California, *U.S.G.S. Open-File Report 94-706,* Menlo Park, Ca.
18. Gibbs, J. F., Fumal, T. E., Boore, D. M., and Joyner, W. B., 1992, Seismic velocities and geologic logs from borehole measurements at seven strong-motion stations that recorded the Loma Prieta earthquake, *U.S.G.S. Open-File Report 92-287,* Menlo Park, Ca.
19. Gibbs, J. F., Fumal, T. E., and Powers, T. J., 1994, Seismic velocities and geologic logs from borehole measurements at seven strong-motion stations that recorded the 1989 Loma Prieta, California, earthquake, U.S. Geological Survey, Open-File Report 94-222, Menlo Park, Ca., 104 pages.
20. Hensolt, W. H., 1993, Central San Francisco Bay Region bedrock contour map, *in preparation*, personal communication.

21. Haskell, N. A., 1953, The dispersion of surface waves on multi-layered media, *Bull. Seismological Soc. Am.*, 43(1), 17-34.
22. Haskell, N. A., 1960, Crustal reflection of plane SH waves, *J. Geophysical Res.*, 65(12), 4147-4150.
23. McClure, F. E., 1991, Analysis of a two-story Oakland office building during the Loma Prieta earthquake, *SMIP91:Seminar on Seismological and Engineering Implications of Recent Strong-Motion Data,*California Department of Conservation, Division Mines and Geology, 13-1--13-13-11, May 1991.

Table 1. Modal Frequencies (Periods) of the 2-Story Oakland Building

Assessment Method	Modal Frequencies [Hz] (Periods [seconds])		Comments
	NS	EW	
1965 Ambient Test (McClure, 1991)	2.13 (1^{st}) (0.47)	2.08 (0.48)	Walls in, no plaster
1965 Forced Vibration Test (Bouwkamp & Blohm,1966)	(1^{st}) 2.35 (0.426), (2^{nd}) 7.70 (0.130)		Walls in with plaster
1988 UBC (McClure, 1991)	2.29 (0.437)		Code Formula
McClure Computer Model (1991)	(1^{st}) 1.59 (0.63), (2^{nd}) 5.0 (0.20)		w/o plaster
	(1^{st}) 2.16 (0.463), (2^{nd}) 7.69 (0.130)		With plaster
Spectral analyses (this study)	1.95(0.51) Translational, 1.65 (0.61) Torsional		Loma Prieta (1989) data

Table 2. Assessment of site period (frequency) using code formula [$V_s(ave)=H/(\Sigma (h_i/V_{si})]$, earthquake records and transfer functions.

Method	Parameter	PPP	OAK_2ST		SCCOB		EMB	NOR
			A	B	A	B		
	$H=\Sigma h_i$ [m]	150	152	169	270	500	64	500
Formula	$\Sigma (h_i/Vs_i)$	0.46	0.41	0.46	0.66	1.05	0.33	1.01
	Vs(Ave) [m/s]	329.5	366.5	369.6	407.8	478.3	195.8	493.7
	Site T=4H/Vs [s]	1.82	1.65	1.83	2.65	4.18	1.31	4.05
	Site f=1/t [Hz]	0.55	0.60	0.55	0.38	0.24	0.76	0.25
Records	Structural T(s)	2.63	0.51(trans.), 0.61 (tors.)		2.22(trans.), 1.75(tors.)		5.26(NS) 6.25(EW)	1.32(NS) 1.20(EW)
	Structural f(Hz)	0.38	1.95(trans.), 1.65(tors.)		0.45(trans.), 0.57(tors.)		0.19(NS) 0.16(EW)	0.76(NS) 0.83(EW)
	Site T (s)	1.33	1.18-1.25		2.63		1.11-1.42	3.3
	Site f (Hz)	0.7	0.8-0.85		0.38		0.7-0.9	0.3
Transfer Function	Site T (s)	1.18-1.54	1.43-1.54		2.0-4.0		1.25-1.42	3.3
	Site f(Hz)	0.65-0.85	0.65-0.70		0.25-0.5		0.7-0.8	0.3

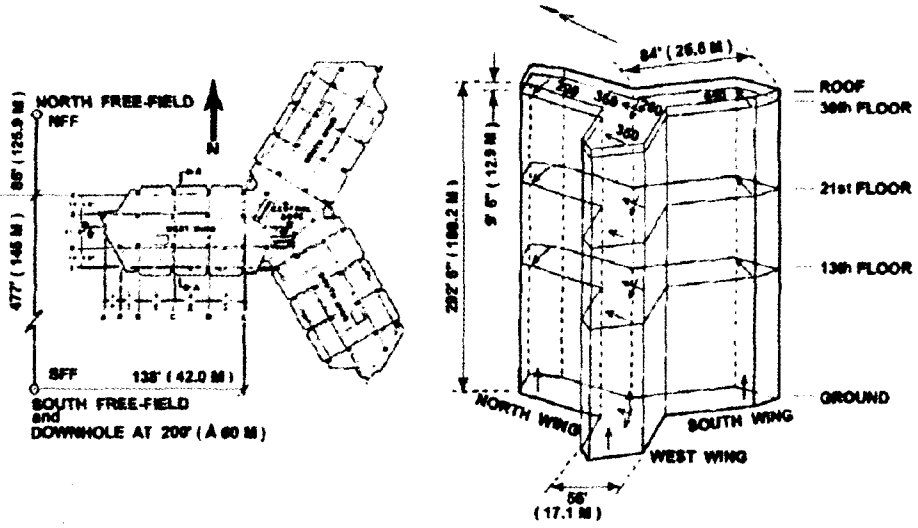

Figure 1. General Layout and Instrumentation Scheme of Pacific Park Plaza, Emeryville, Ca.

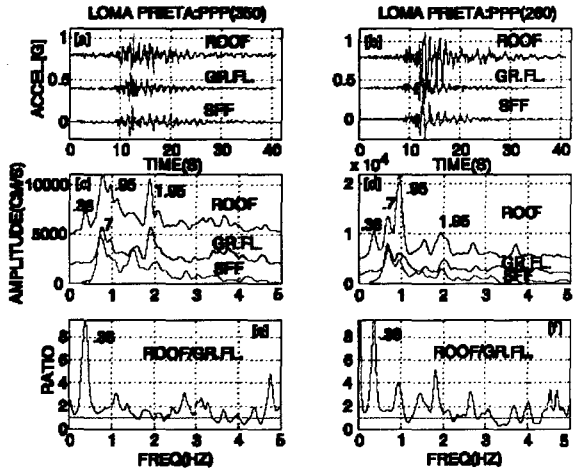

Figure 2. (a,b) Recorded orthogonal accelerations at the roof, ground floor and south free-field of Pacifica park Plaza, (c,d) corresponding amplitude spectra and (e,f) ratios of amplitude spectra.

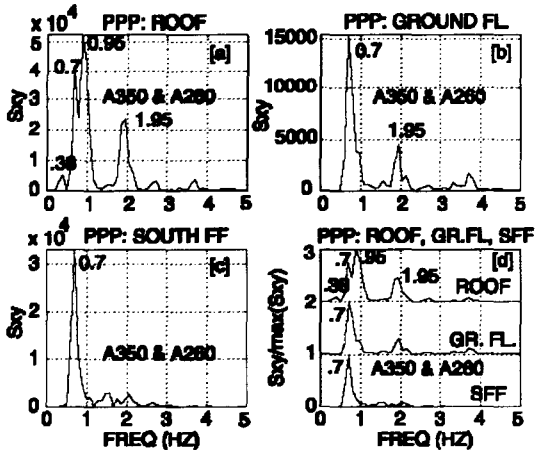

Figure 3. Cross-spectra of motions at the (a) roof, (b) ground floor, and (c) free-field of Pacific Park Plaza, Emeryville, California, and (d) normalized cross-spectra.

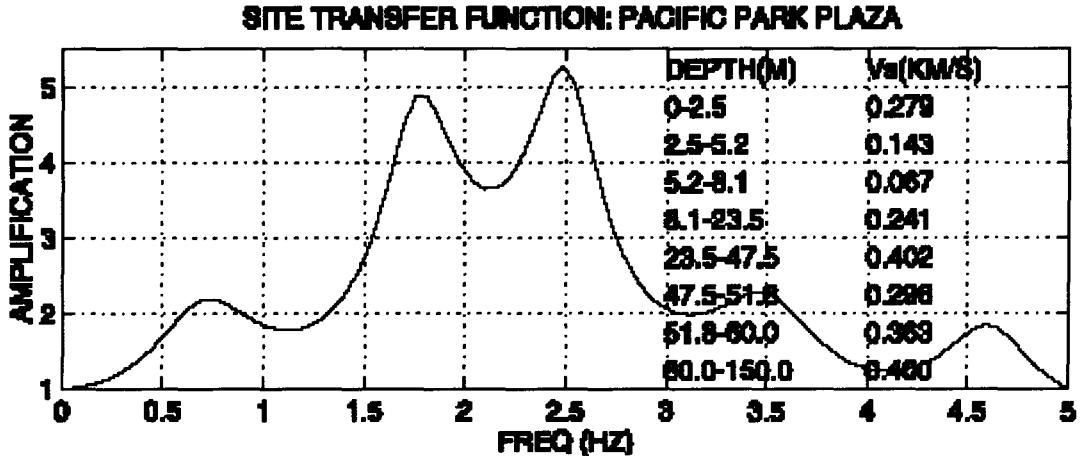

Figure 4. Site transfer function for described characterization at Pacific Park Plaza.

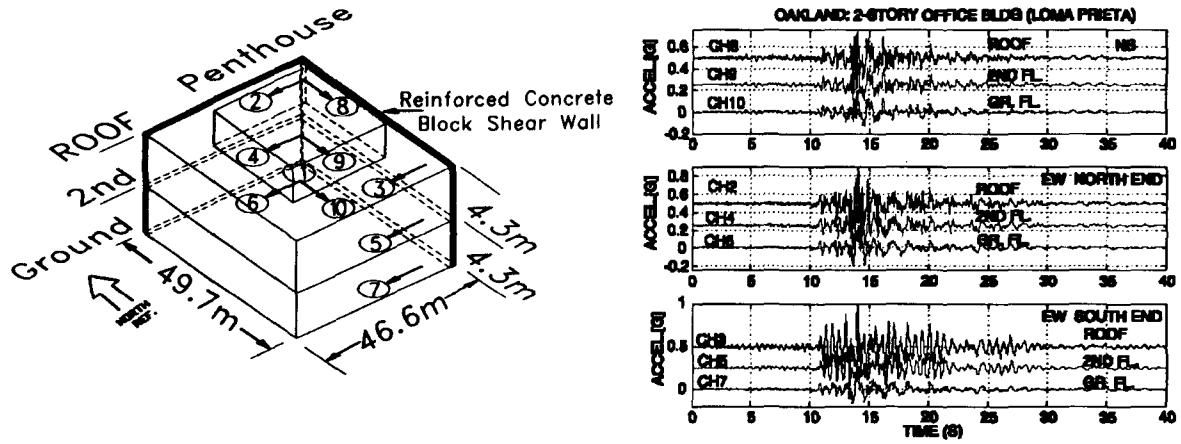

Figure 5. (Left) Instrumentation scheme of the torsionally eccentric 2-story building in Oakland, Ca. and (Right) Accelerations recorded at the roof, second and ground floors during the 1989 Loma Prieta, Ca. earthquake.

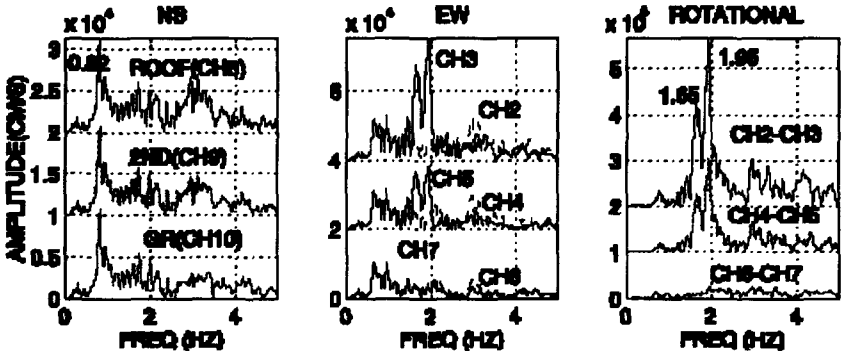

Figure 6. Amplitude spectra of translational and torsional accelerations recorded at Oakland (2-Story Building).

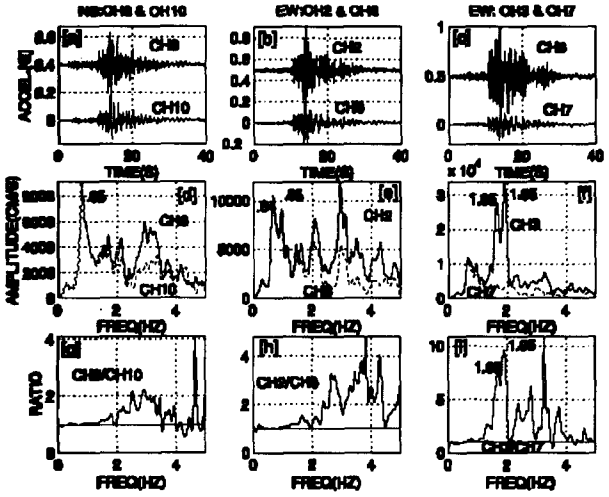

Figure 7. [a-c] Time-histories of roof and ground floor acceleration pairs, [d-f] corresponding amplitude spectra and [g-i] corresponding roof/ground floor spectral ratios.

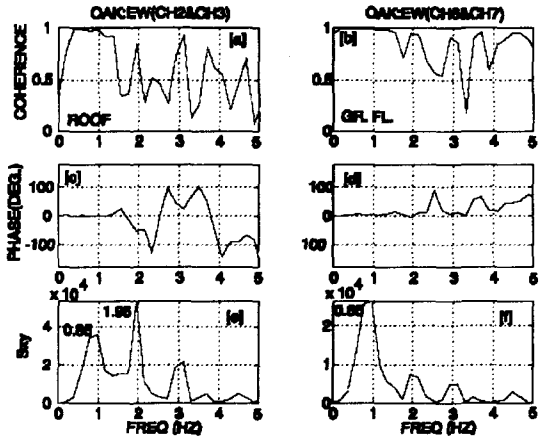

Figure 8. [a,b] Coherence, [c,d] phase and [e,f] cross-spectra plots of pairs of parallel motions at the roof (CH2 and CH3) and ground floor [CH6 and CH7].

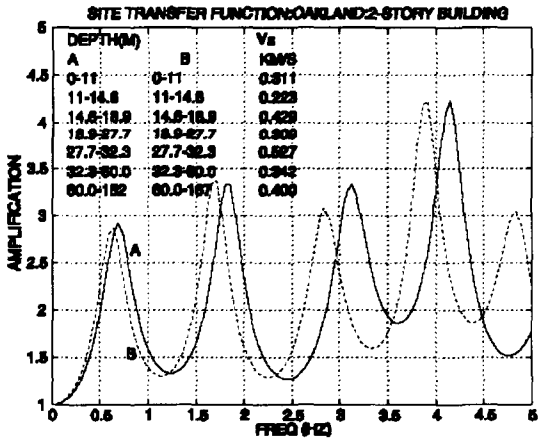

Figure 9. Computed site transfer function for described site characterization (see figure) of the site of the 2-story building, Oakland, California.

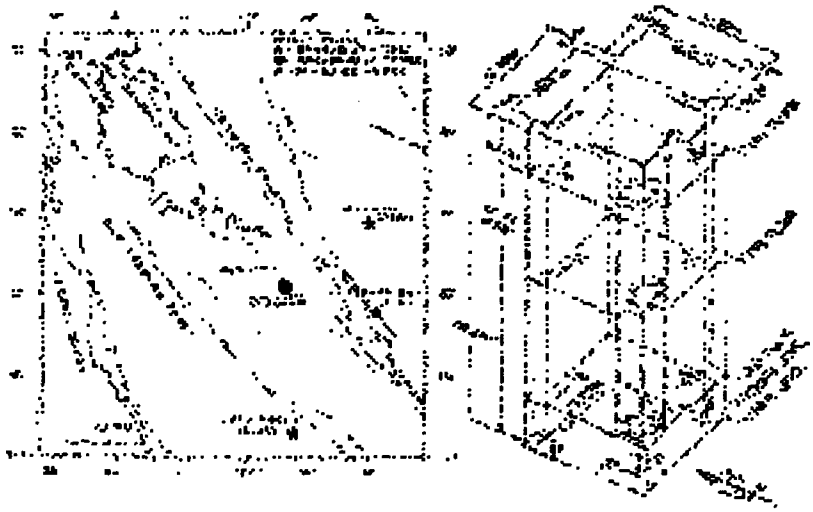

Figure 10. Location map of Santa Clara County Office Building in San Jose, Ca. and the epicenters of the three earthquakes that were recorded by the instrumentation array within the building.

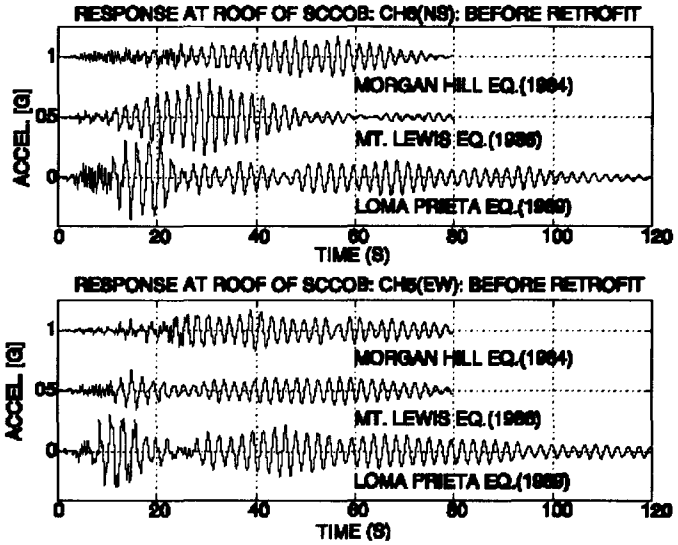

Figure 11. Time histories of accelerations recorded at the roof of the Santa Clara County Office Building during the 1989 Loma Prieta, 1996 Morgan Hill and 1994 Mt. Lewis earthquakes. The building was retrofitted in 1994. The responses exhibit beating effect caused by closely couple translational and torsional modes and low damping.

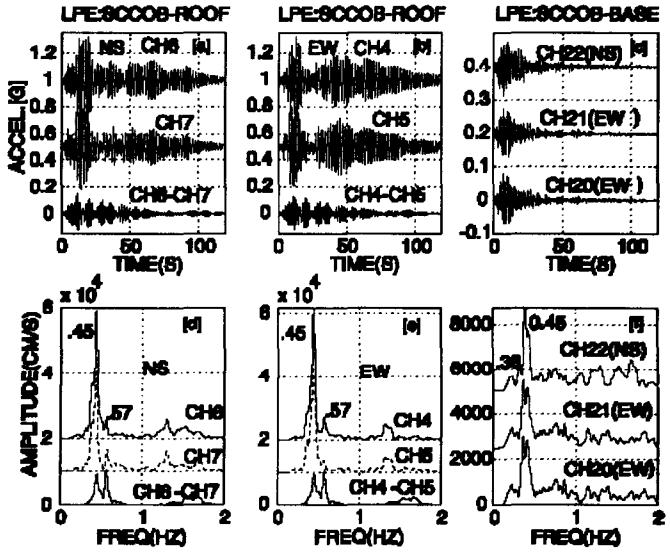

Figure 12. [a-c]Translational and torsional accelerations at the roof and translational accelerations at the basement and [d-f] their amplitude spectra.

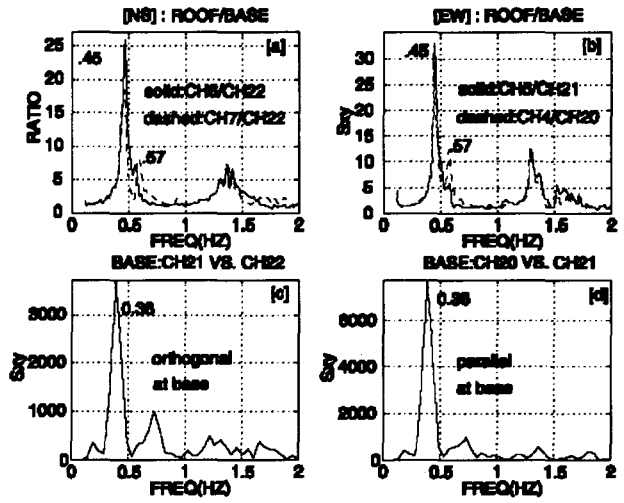

Figure 13. (a and b) Spectral ratios of roof/basement motions indicate structural frequencies (translational [0.45 Hz], and torsional [0.57 HZ]) and cross-spectrum of basement motions indicate site frequency (0.38 HZ).

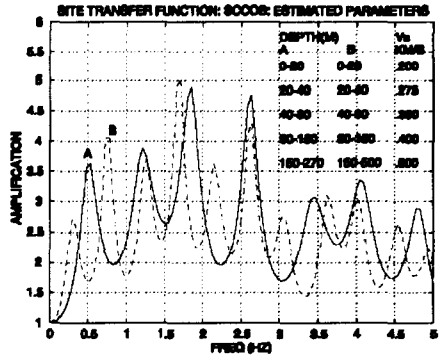

Figure 14. Site transfer functions for 2 postulated depths to bedrock (SCCOB) site.

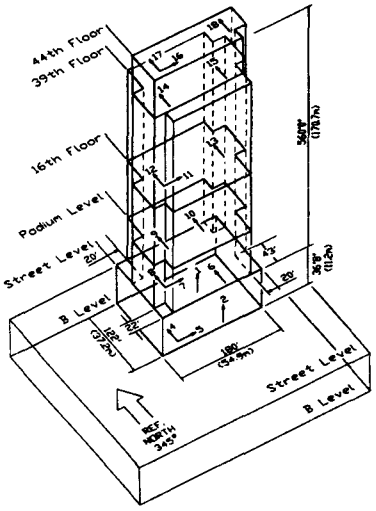

Figure 15. Three-dimensional schematic of Embarcadero Building [EMB] and its instrumentation scheme.

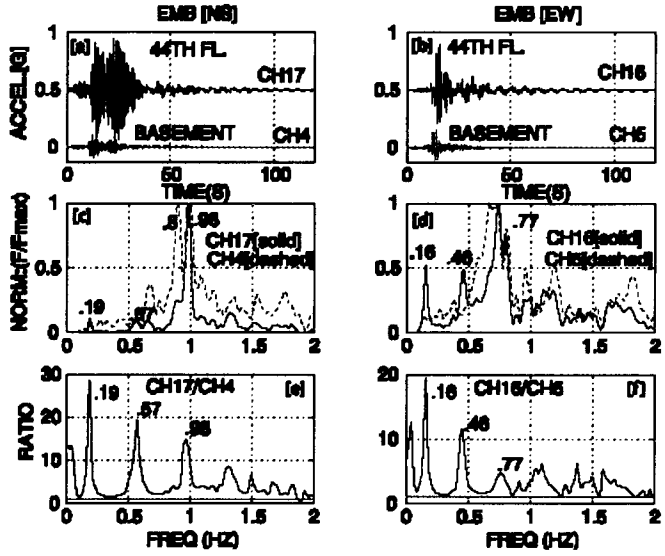

Figure 16. [a-c] Time-histories of roof and ground floor acceleration pairs of EMB in theNS and EW directions, [d-f] corresponding amplitude spectra and [g-i] corresponding roof/ground floor spectral ratios.

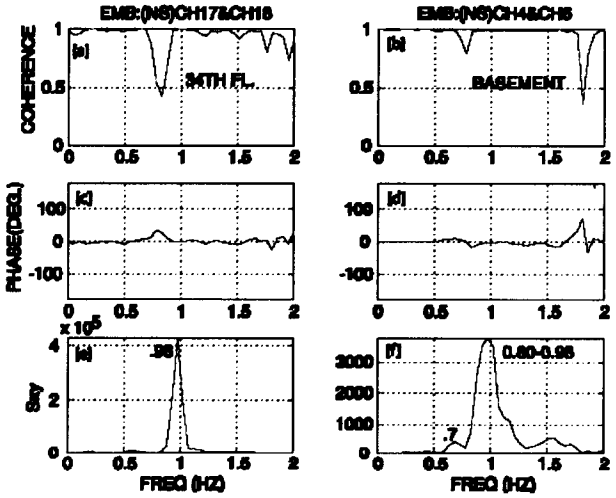

Figure 17. [a,b] Coherence, [c,d] phase angle and [e,f] cross-spectra plots of pairs of parallel motions at the roof (CH17 and CH18) and basement [CH4 and CH5].

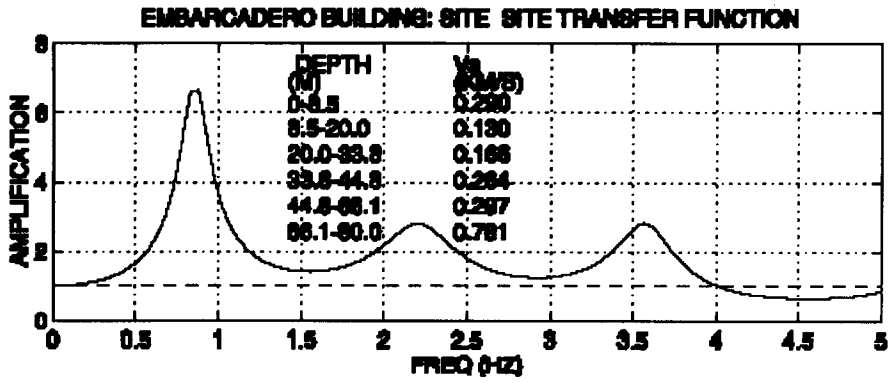

Figure 18. Site transfer function for EMB site.

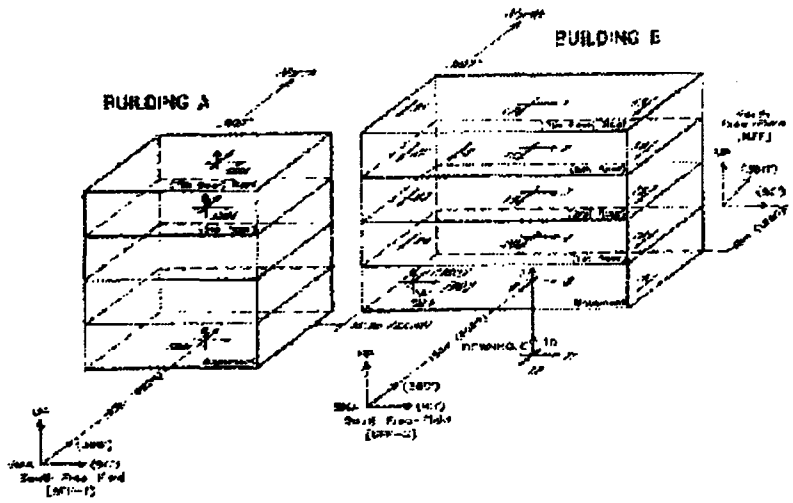

Figure 19. Instrumentation of the two buildings and the site at 12400 block of Imperil Highway, Norwalk, Ca. In this sudy, Building B (NOR) and the south free-field (SFF) is considered.

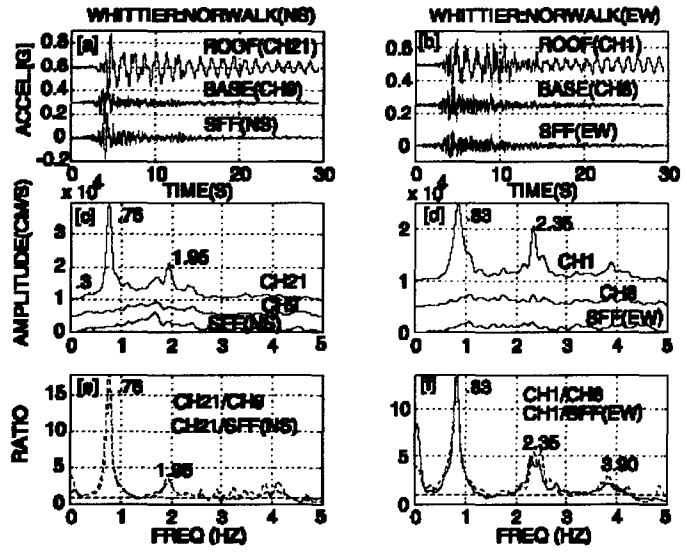

Figure 20. [a-c] NS and EW time-histories of roof, basement and SFF accelerations of NOR building, [c-d] corresponding amplitude spectra and [g-i] corresponding roof/ground and roof/free-field spectral ratios.

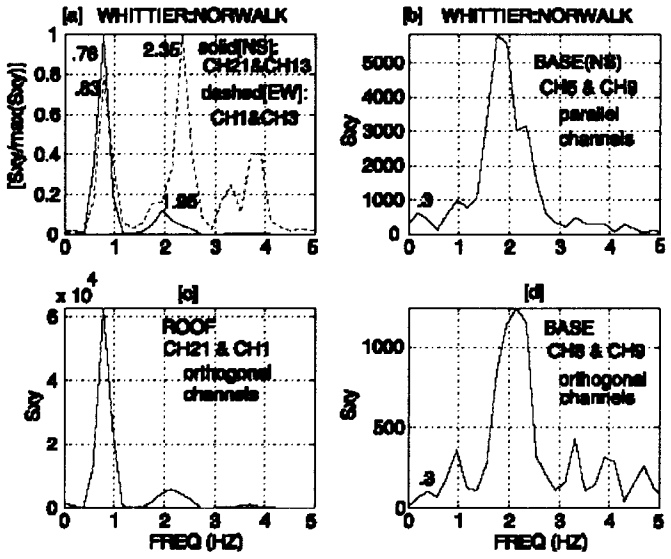

Figure 21. [a] Normalized cross-spectra of pairs of parallel NS accelerations [CH21 and CH13] at the roof and EW accelerations [CH1 and CH3] at the roof and second floor, and cross-spectrum of [b] parallel NS accelerations [CH5 and CH9] at the base, [c] orthogonal accelerations [CH 21 and CH1] at the roof and [d] orthogonal accelerations at the base [CH8 and CH9].

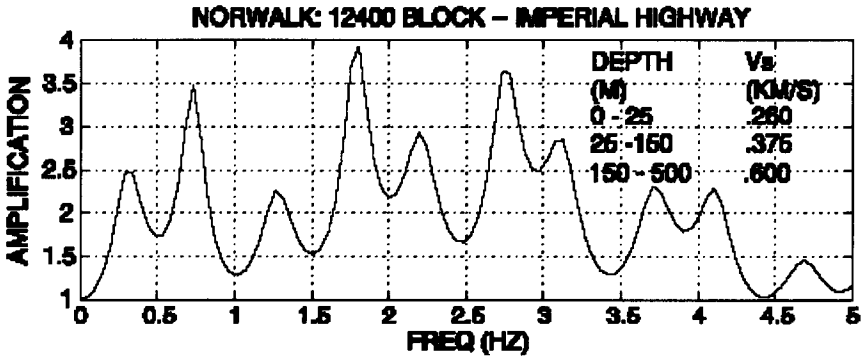

Figure 22. Site transfer function for NOR site.

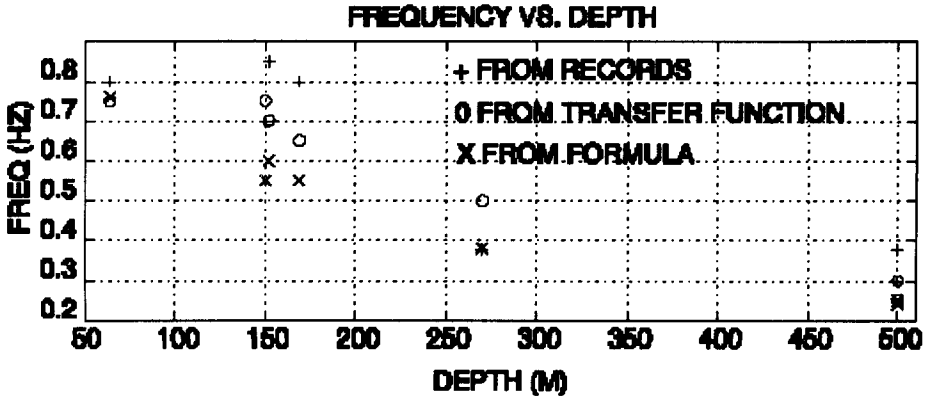

Figure 23. Variation of site frequency with depth using 3 methods.

Evaluation of Earth Pressure Acting on Embedded Pile-cap Based on Liquefaction Test Using Large-scale Shaking Table

by

Shuji Tamura[1], Chikahiro Minowa[2], Kohji Tokimatsu[3], Shunji Fujii[4], Kaeko Yahata[5] and Tomio Tsuchiya[6]

ABSTRACT

Shaking table tests are conducted using a large-scale laminar shear box to investigate the effects of non-liquefied crust overlying liquefied soils on an embedded footing. It is shown that (1) The total earth pressure before liquefaction is induced mainly by the inertial force of the building. The shear force at the pile heads corresponds to the difference between the total earth pressure and the inertial force; (2) The total earth pressure after liquefaction is induced mainly by the soil deformation. The shear force at the pile heads corresponds to the sum of the total earth pressure and the inertial force of the building; (3) The relation between the relative displacement and the total earth pressure is linear before liquefaction. It becomes nonlinear with the development of pore water pressure and the total earth pressure decreases with cyclic loading after liquefaction; (4) The peak value of the total earth pressure for the super-structure with a low natural frequency is larger than that with a high natural frequency. This is probably because the inertial force of the super-structure with a low natural frequency may interrupt the response of the footing that tends to move with the ground.

KEY WORDS: Seismic Earth Pressure
Liquefaction
Pile
Shaking Table Test

1. INTRODUCTION

During the 1995 Hyogoken-Nambu earthquake, extensive soil liquefaction occurred on the reclaimed land areas of Kobe. Many damaged piles in such liquefied soil have been reported. It indicates that the effects of liquefaction on piles should be taken into account in foundation design.

Soil-pile-structure interaction during liquefaction has been studied by field investigations (Oh-Oka et al, 1998), numerical analyses (Fujii et al., 1998, Tokimatsu et al., 1998), centrifuge tests (Sato et al., 1995) and large-scale shaking table tests (Tamura et al., 2000). Most research efforts of these studies have focused on the evaluation of soil-pile interaction including p-y relations during soil liquefaction. Thus, knowledge of the effects of non-liquefied crust overlying liquefied soil on an embedded footing remains limited. The evaluation of the kinematic force acting on an embedded footing is an important consideration in the seismic design method using p-y curve for pile foundations.

This paper investigated earth pressure acting on an embedded footing of a building during soil liquefaction, using a large-scale laminar shear box. The objects of this paper are; 1) to study major factor affecting earth pressure; 2) to study the relation between the relative displacement

[1] Associate Professor, Shinshu University, 4-17-1 Wasasato, Nagano-shi, Japan, 380-8553
[2] Scientific Research Advisor, National Research Institute for Earth Science and Disaster Prevention, 3-1 Ten-nodai, Tsukuba-shi, Japan, 305-0006
[3] Professor, Tokyo Institute of Technology, 2-12-1 O-okayama, Meguro-ku, Tokyo, Japan, 152-8552
[4] General Manager, Taisei Corporation, 344-1 Nase-cho, Totsuka-ku, Yokohama-shi, Japan, 245-0051
[5] Chief Research Engineer, Kajima Technical Research Institute, 2-19-1, Tobitakyu, Chofu-shi, Japan, 182-0036
[6] Chief Researcher, Takenaka Research & Development Institute, 1-5-1 Inzai-shi, Chiba, Japan, 270-1395

and earth pressure; 3) to study phase difference between the inertial force of the building and earth pressure, and 4) to study the effects of a natural frequency of the super-structure on earth pressure.

2. MODEL PREPARATION

Shaking table tests were performed at NIED (National Research Institute for Earth Science and Disaster Prevention) in Tsukuba, Japan. A large-scale laminar shear box 6 m high, 3.5 m wide and 12 m long (shaking direction) was mounted on the shaking table. A sketch of a large-scale laminar shear box including a soil-pile-structure system for Model B-S is presented in Fig. 1. Four steel piles with a diameter of 16.5 cm, a length of 5.3 m, a thickness of 3.7 mm and EI=1259 kNm^2 were installed in a three-layer soil profile with a thickness of 6m. This profile included a 4.5 m layer of Kasumigaura sand (e_{max}=0.96, e_{min}=0.57, D_{50}=0.31 mm, F_c=5.4%) with a shear wave velocity of 90 m/s, placed on top of a 1.5 m layer of gravel with V_S = 230 m/s. The water level was about GL-0.5 m, that is, 0.5 m dry sand overlying 4 m saturated sand. The predominant frequency of the ground was about 5 Hz. The super-structure model with a mass of 14200 kg was supported by 4 vibration isolation rubbers, 4 laminated rubber bearings and 2 viscous dampers fixed on a steel footing (2.5m long, 1.8m wide and 1.6m high). The footing with a mass of 2100 kg was embedded 0.5 m in the dry sand. A mass of the super-structure is about 6 times that of the footing. The super-structure had a natural frequency of about 5.4 Hz, which was larger than the predominant frequency of the ground. The pile heads were rigidly linked to the footing, while their tips were connected to the laminar shear box by hinges.

The test set up of Model B-L is similar to that of Model B-S, except that the super-structure was supported by 4 laminar rubber bearings and 2 viscous dampers only. The natural frequency of this super-structure was about 1.3 Hz, which was lower than the predominant frequency of the ground.

Both models, B-S and B-L, were excited by RINKAI92, which is a synthesized ground motion for the Tokyo Bay area expecting the re-occurrence of the 1923 Kanto earthquake. The amplitude of the motion was scaled as 240 cm/s^2. Acceleration, displacement, excess pore water pressure and strain of the piles were recorded during the tests.

3. TEST RESULTS AND DISCUSSION

3.1 Dynamic Response of Soil-Pile-Structure System

Figure 2 shows the acceleration time histories of the super-structure, the ground surface and the shaking table for Models B-S and B-L. Figure 3 shows the time histories of bending moment at the pile heads for both models. The bending moment begins to increase rapidly at 8 seconds in both models. The acceleration of the super-structure, in contrast, begins to increase at 2 seconds as shown in Fig. 2. Figure 4 shows the time histories and the vertical distribution of the excess pore water pressure. The excess pore water pressure begins to increase rapidly at 8 seconds in both models. This corresponds to the time when the bending moment at the pile heads begins to increase rapidly. This suggests that the bending moment is apparently influenced by soil liquefaction.

Soil liquefaction progressed from the upper layer to the bottom. The lower part of the saturated sand layer almost liquefied at about 20 seconds. The ground acceleration and the development of the excess pore water for Model B-S are roughly the same as that of Model B-L. This indicates that the soil response for Model B-S is similar to that of Model B-L. The acceleration of the super-structure, however, contains higher frequency components in Model B-S than in Model B-L until 8 seconds. The predominant frequency of Model B-S becomes smaller and is similar to that of Model B-L after 8 seconds.

Figure 5 shows the time histories of the footing and the ground surface displacements and Fig. 6 shows those of relative displacements between the footing and the ground surface for both models. The displacements were calculated by

the double integration of accelerometer recordings. The relative displacement, ΔD can be defined by

$$\Delta D = \Delta B - \Delta S \quad (1)$$

in which ΔB = displacement of the footing and ΔS = displacement of the ground surface. The footing displacement is almost the same as the ground surface displacement at first. A small phase difference occurs between the ground surface displacements and the footing after 8 seconds. This produces the relative displacement as shown in Fig. 6. The phase difference of Model B-L is larger than that of Model B-S. Thus, the relative displacement of Model B-L is larger than that of Model B-S as shown in Fig. 6.

3.2 Evaluation of Earth Pressure on Embedded Foundation

Figure 7 is a schematic figure showing the seismic earth pressure acting on an embedded footing. The total earth pressure acting on the footing, P can be expressed by

$$P = P_p - P_a = Q - F \quad (2)$$

in which P_p = earth pressure at passive side, P_a = earth pressure at active side, Q = the sum of shear forces at the pile heads and F = the inertial force of the building, that is, the sum of the inertial forces of the super-structure and the footing. Q can be calculated by the differentiation of the measured strain at the pile head.

In order to evaluate the accuracy of the shear force at the pile heads, the shear force and the inertial force of the building for Model A-L are compared in Fig. 8. The test set up of Model A-L is similar to that of Model B-L except that the footing was not embedded. The earth pressure therefore does not act on the footing in Model A-L. The shear force at the pile heads and the inertial force show a fairly good agreement, indicating that the total earth pressure can be evaluated by Eq. (2).

Figure 9 shows the time histories of the total earth pressure on the footing for both models. The total earth pressure recording contains higher frequency components in Model B-S than in Model B-L until 8 seconds. The tendency is similar to the acceleration of the super-structure as shown in Fig. 2(a). From 8 to 20 seconds when soil liquefaction is developing, the total earth pressure is large and contains low frequency components for both models despite the difference in the natural frequency of the super-structure. The total earth pressure gets small after 20 seconds when the saturated sand liquefies completely.

To examine the effects of the inertial force and the soil deformation on the total earth pressure, fourier spectra of the total earth pressure, the inertial force of the building and the ground displacement are shown in Fig. 10. The predominant frequencies of the total earth pressure are 3.6 Hz and 1.2 Hz for Models B-S and B-L, respectively until 8 seconds. The frequency agrees with the predominant frequency of the inertial force. This indicates that the total earth pressure is strongly correlated to the response of the super-structure before soil liquefaction. The predominant frequency of the total earth pressure for both models is 0.6 Hz, which corresponds to the predominant frequency of the soil displacement from 12 to 28 seconds. This suggests that the total earth pressure is induced mainly by the soil deformation after liquefaction.

3.3 Relation between Earth Pressure and Relative Displacement

To clarify the mechanism of the total earth pressure acting on the footing, the relation between the total earth pressure and the relative displacement (ΔD) for Models B-S and B-L is shown in Fig. 11. The relation between the relative displacement and the total earth pressure is linear for both models until about 8 seconds. It becomes nonlinear with the development of the pore water pressure from 8 to 20 seconds. The nonlinearity in behavior is significant in Model B-L. The total earth pressure is seen to degrade with cyclic loading from 20 to 30 seconds.

3.4 Relation between Earth Pressure and Inertial Force of Building

In general, the phase difference between inertial and kinematic forces can be classified into the following two types in which F_b and F_g are natural frequencies of the building and the ground, respectively (Nishimura et al, 1997):
1) If $F_b > F_g$, inertial and kinematic forces tend to be in phase.
2) If $F_b < F_g$, inertial and kinematic forces tend to be out of phase by 180 degrees.

The phase differences above are based on an assumption that the total earth pressure and the ground displacement should be in phase. The total earth pressure acting on the footing, however, depends on the relative displacement. Taking into account the displacement of the soil and the footing, the phase can be classified into four types as shown in Fig. 12.
(a) If $F_b > F_g$ and $\Delta S > \Delta B$, the total earth pressure tends to be in phase with the inertial force. Thus, the shear force at the pile heads corresponds to the sum of the total earth pressure and the inertial force of the building.
(b) If $F_b < F_g$ and $\Delta S > \Delta B$, the total earth pressure tends to be out of phase by 180 degrees with the inertial force. Thus, the shear force at the pile heads corresponds to the difference between the total earth pressure and the inertial force of the building.
(c) If $F_b > F_g$ and $\Delta S < \Delta B$, the total earth pressure tends to be out of phase by 180 degrees with the inertial force. Thus, the shear force at the pile heads corresponds to the difference between the total earth pressure and the inertial force of the building.
(d) If $F_b < F_g$ and $\Delta S < \Delta B$, the total earth pressure tends to be in phase with the inertial force. Thus, the shear force at the pile heads corresponds to the sum of the total earth pressure and the inertial force of the building.

To investigate the phase difference during soil liquefaction, the relation between the total earth pressure and the inertial force of the building for the two tests is shown in Fig. 13. The data fallen in the first and third quadrants show that the total earth pressure tends to be in phase with the inertial force, while those in the second and forth quadrants show that the total earth pressure tends to be out of phase by 180 degrees with the inertial force. A gray (blue) line in the figure shows that ΔS is smaller than ΔB, while a black line shows that ΔS is larger than ΔB.

Most of the data for both models fall in the second and forth quadrants until 8 seconds. This indicates that the total earth pressure tends to be out of phase by 180 degrees with the inertial force. In case of Model B-S, a gray (blue) line is dominant, indicating that ΔS is smaller than ΔB when the total earth pressure reaches its peak. Considering that F_b is higher than F_g in this period, the total earth pressure tends to be out of phase with the inertial force as shown in Fig. 12 (c). In case of Model B-L, on the contrary, a black line is dominant, indicating that ΔS tends to be larger than ΔB. F_b is smaller than F_g in this period. Thus, the inertial force and the total earth pressure tend to be out of phase as shown in Fig. 12(b). The value of the total earth pressure in this period is about 60-70 percent of the inertial force for both models. This indicates that the non-liquefied crust tends to counteract the inertial force transmitted from the building to the pile heads. Therefore, the bending moment at the pile heads is very small until 8 seconds as shown in Fig. 3.

Most data for both models fall in the first and third quadrants from 8 to 20 seconds, indicating that the total earth pressure tends to be in phase with the inertial force. A black line is dominant, indicating that ΔS tends to be larger than ΔB when the total earth pressure reaches its peak. Considering that F_b is higher than F_g due to liquefaction in both models, the total earth pressure tends to be in phase with the inertial force as shown in Fig. 12(a). This indicates that the shear force at the pile heads corresponds to the sum of the total earth pressure and the inertial force of the building. Therefore, the bending moment at the pile heads increase rapidly at 8 seconds as shown in Fig. 3. The tendency above is significant in Model B-L and is ambiguous in both models from 20 to 30 seconds.

3.5 Effects of Natural Frequency of Building on Earth Pressure

The peak value of the total earth pressure in

Model B-L is larger than that in Model B-S from 8 to 20 seconds as shown in Fig. 13. Taking into account the similar soil response for both models (Fig. 2,4), the difference may be caused by the natural frequency of the super-structure. To clarify the effects of the natural frequency of the super-structure on the total earth pressure, the relation between the acceleration of the footing and the super-structure for the two tests is shown in Fig. 14. The acceleration of the footing and the super-structure tend to be in phase in Model B-S. This indicates that the inertial force of the super-structure does not interrupt the response of the footing. The footing can move with the ground and the relative displacement tends to be small. In case of Model B-L, in contrast, the acceleration of the super-structure tends to be out of phase with that of the footing. This indicates that the inertial force of the building may interrupt the response of the footing that tends to move with the ground. As a result, the relative displacement is large. This is the reason that, the peak value of the total earth pressure for Model B-L is larger than that of Model B-S.

4. CONCLUSION

Shaking table tests are conducted using a large-scale laminar shear box to investigate the effects of non-liquefied crust overlying liquefied soil on an embedded footing. The following conclusions are drawn:

(1) The total earth pressure before liquefaction is induced mainly by the inertial force of the building, because the total earth pressure acting on the footing tends to be out of phase by 180 degrees with the inertial force of the building. The shear force at the pile heads corresponds to the difference between the total earth pressure and the inertial force.

(2) The total earth pressure after liquefaction is induced mainly by the soil deformation, because the total earth pressure acting on the footing tends to be in phase with the inertial force of the building. The shear force at the pile heads corresponds to the sum of the total earth pressure and the inertial force.

(3) The relation between the relative displacement and the total earth pressure is linear before liquefaction. It becomes nonlinear with the development of the pore water pressure and the total earth pressure decreases with cyclic loading after liquefaction.

(4) The peak value of the total earth pressure for the super-structure with a low natural frequency is larger than that with a high natural frequency. This is probably because that the inertial force of the super-structure with a low natural frequency may interrupt the response of the footing that tends to move with the ground.

ACKNOWLEDGMENTS

This test was jointly conducted by NIED, STA, Tokyo Institute of Technology, Kajima Corp., Taisei Corp., Takenaka Corp., Nippon Steel Corp. and Tokyo Soil Research Corp. The contribution and support of the members for this work are appreciated.

REFERENCES

Fujii, S., Isemoto, N., Satou, Y., Kaneko, O., Funahara, H., Arai, T. and Tokimatsu, K. [1998]. Investigation and analysis of a pile foundation damaged by liquefaction during the 1995 Hyogoken-Nambu earthquake, Soils and Foundations, Special Issue on Geotechnical Aspects of the 1995 Hyogoken Nambu Earthquake, No. 2, pp. 179-192.

Nishimura, A., Murono, Y. and Nagatsuma, S. [1997]. Experimental study on the seismic design method for pile foundation in the soft ground (Part 1-3), Pros., 32nd Japan National Conf. on Geotech. Engrg., Vol. 1, pp. 961-966, (in Japanese)

Oh-Oka, H., Fukui, M., Hatanaka, M., Ohara, J. and Honda, S. [1998]. Permanent deformation of steel pipe piles penetraiting compacted fill at wharf on port Island, Soils and Foundations, Special Issue on Geotechnical Aspects of the 1995 Hyogoken Nambu Earthquake, No. 2, pp. 147-162.

Sato, M., Shamoto, Y. and Zhang, J. -M. [1995].

Soil pile-structure during liquefaction on centrifuge, Proc., 3rd Inter. Conf. on Rec. Adv. in Geotech. Earthq. Engrg & Soil Dyn., 1, pp. 135-142.

Tamura, S., Suzuki Y., Tsuchiya T., Fujii S. and Kagawa T.[2000]. Dynamic response and failure mechanisms of a pile foundation during soil liquefaction by shaking table test with a large-scale laminar shear box, Proc., of 12th World Conf. on Earthq. Engrg., Reference No. 903.

Tokimatsu, K. and Asaka, Y. [1998]. Effects of liquefaction-induced ground displacements on pile performance in the 1995 Hyogoken-Nambu Earthquake, Soils and Foundations, Special Issue of Geotechnical Aspects on the 1995 Hyogoken Nambu Earthquake, No. 2, pp. 163-177.

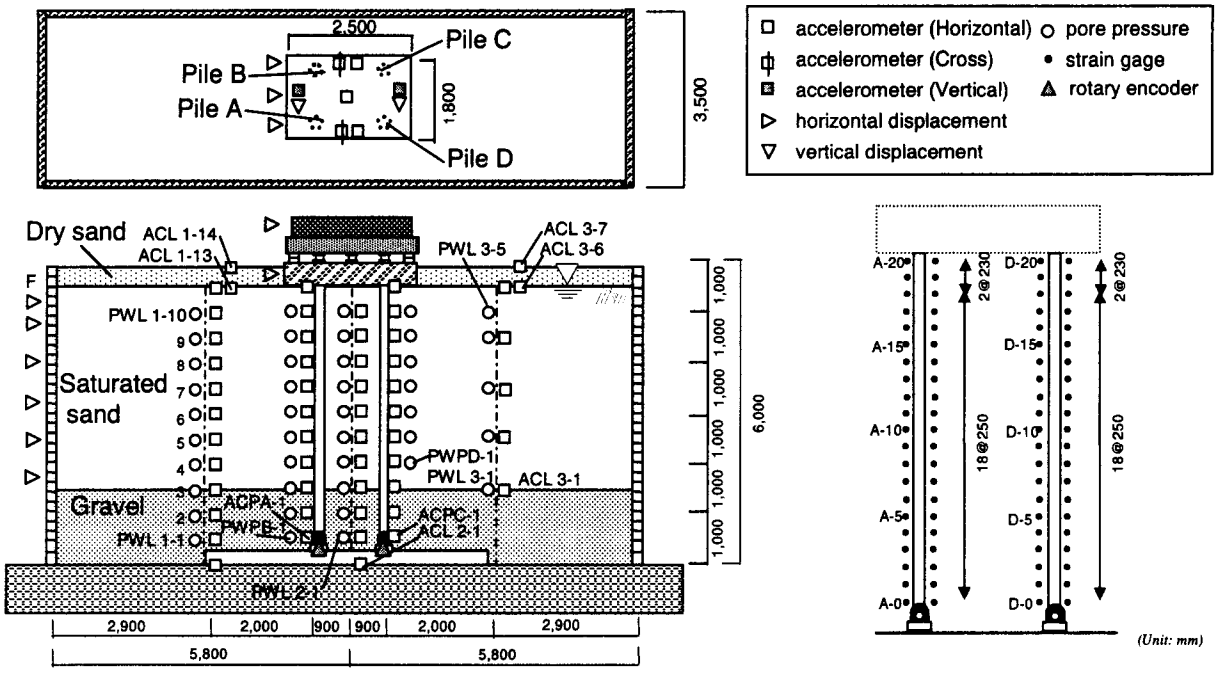

Fig. 1. Test setup(Model B-S)

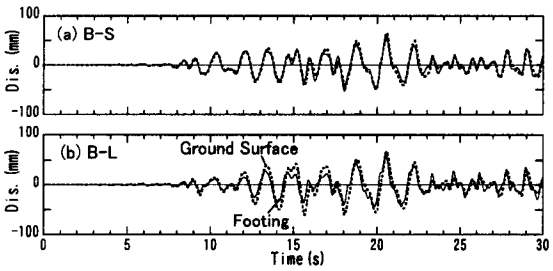

Fig. 5. Time histories of footing and ground displacement

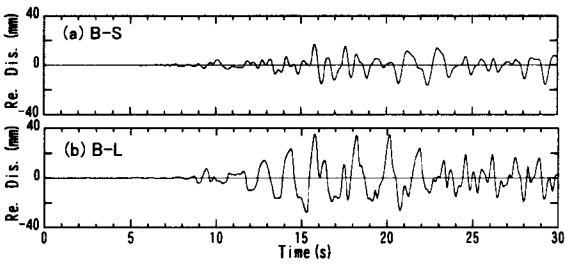

Fig. 6. Time histories of relative displacement between footing and ground surface

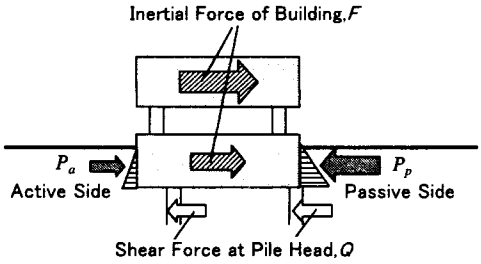

Fig. 7. Schematic figure showing seismic earth pressure acting on footing

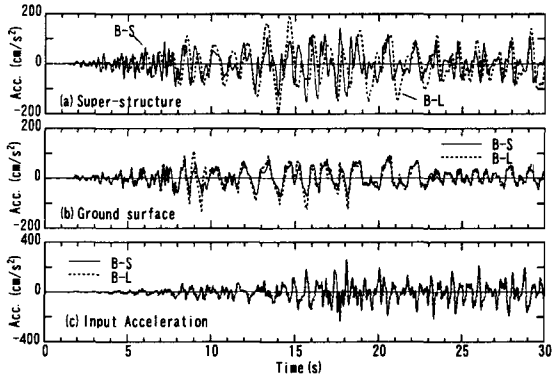

Fig. 2. Time histories of acceleration

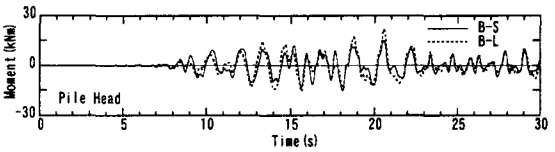

Fig. 3. Time history of bending moment at pile head

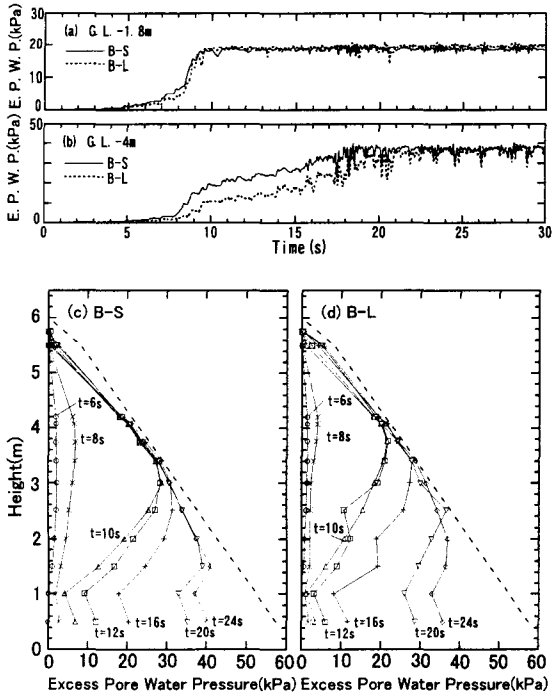

Fig.4.Time histories and vertical distribution of excess pore water pressure

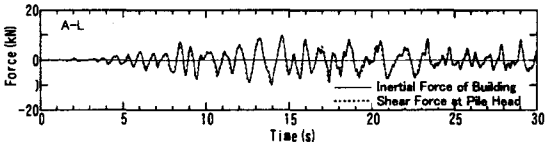

Fig.8. Time history of inertial force of building and shear force at pile head

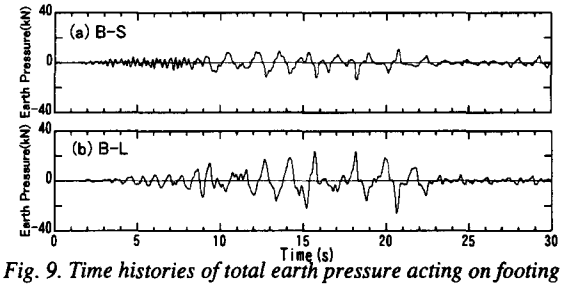

Fig. 9. Time histories of total earth pressure acting on footing

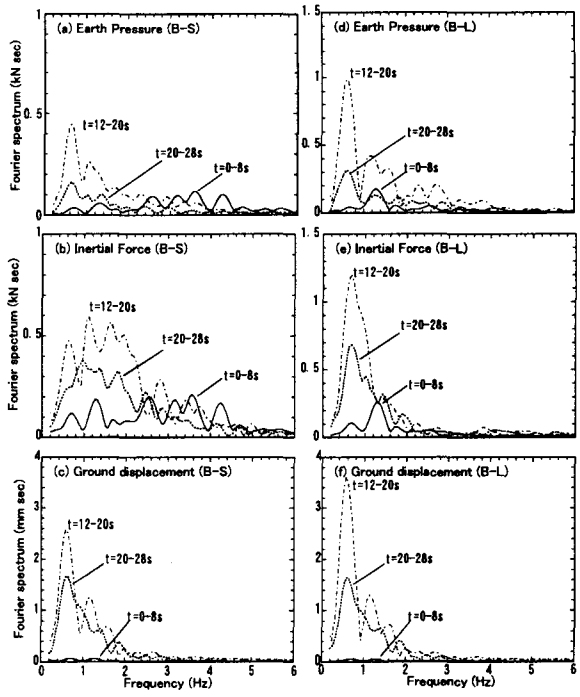

Fig. 10. Fourier spectra of earth pressure, inertial force and soil displacement

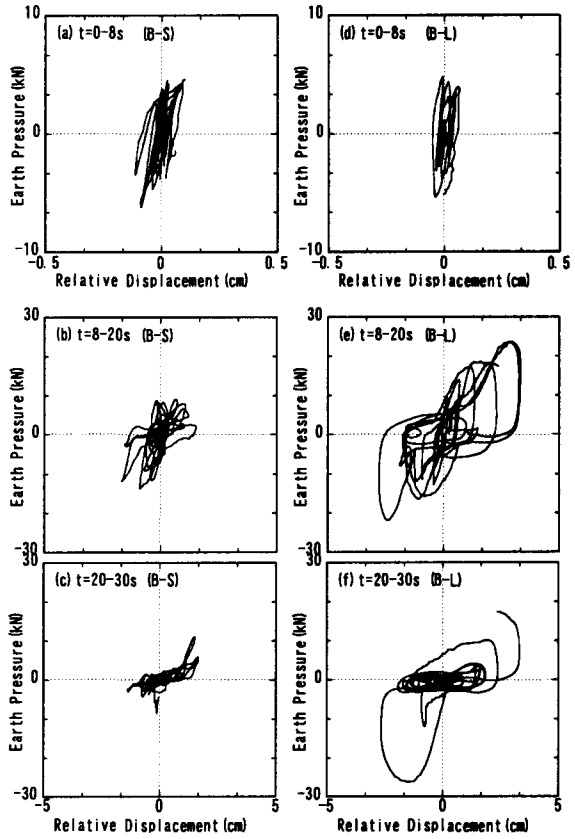

Fig. 11. Relation between relative displacement and total earth pressure

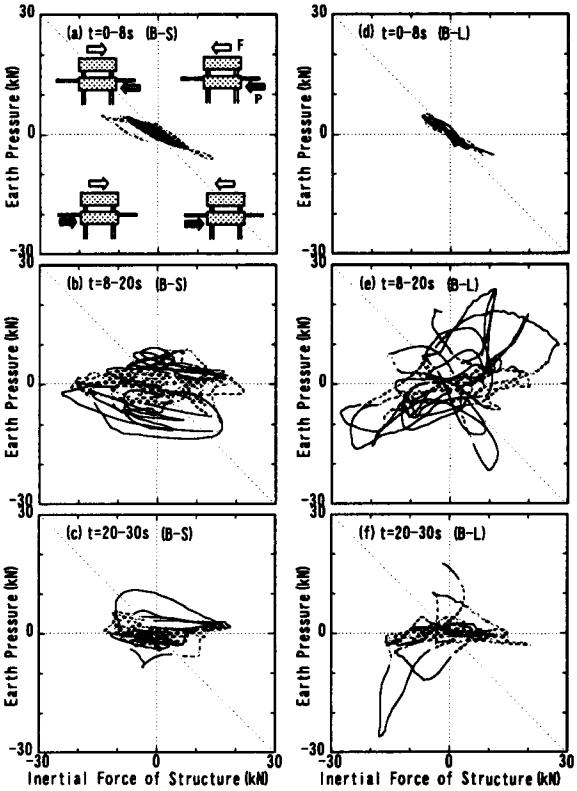

Fig. 13. Relation between inertial force and total earth pressure

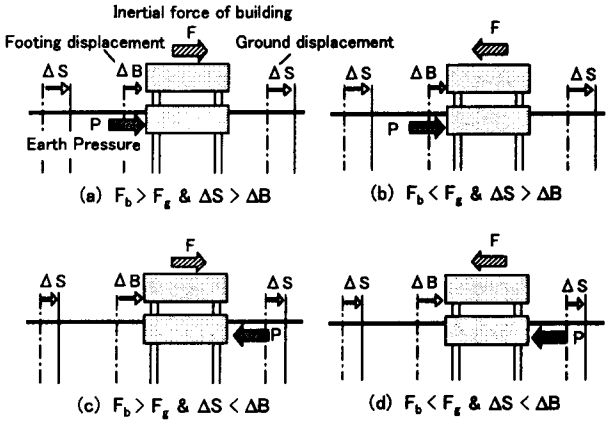

Fig. 12. Schematic figure showing relation between inertial force and total earth pressure

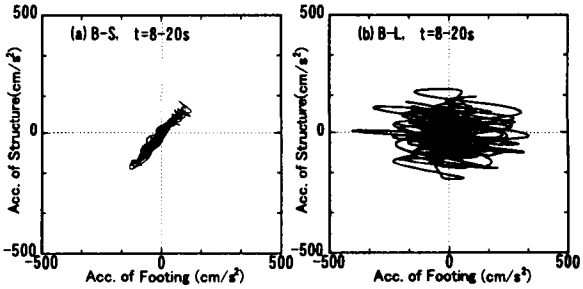

Fig. 14. Relation between acceleration of footing and super-structure

SESSION 2

NEXT-GENERATION BUILDING AND INFRASTRUCTURE SYSTEMS

Project on 3-D Full-Scale Earthquake Testing Facility (The Second Report)

by

Keiichi Ohtani[1], Nobuyuki Ogawa[2], Tsuneo Katayama[3], Heki Shibata[4]

ABSTRACT

The Hanshin-Awaji Earthquake (January 17, 1995) clearly demonstrated that the occurrence of very strong ground motion in the area near to the seismic fault is capable of causing severe structural damage beyond general estimation. It has emphasized the importance of earthquake engineering research into why and how structures collapse in real earthquake conditions. Considering the lessons learnt from recent earthquake disasters, NIED plan to construct a "3-D Full-Scale Earthquake Testing Facility ("E-Defense" is the nickname of this facility)", which will be able to simulate the processes of destruction of structures under the condition of real strong earthquake motions.

The basic performances of "E-Defense" are maximum lording capacity 1,200 tons, maximum velocity 200 cm/s and maximum displacement 2m p-p for horizontal excitation and maximum velocity 70 cm/s, maximum displacement 1m p-p for vertical excitation to realize destructive ground motion. The construction work of "E-Defense" has began at early 2000, five year after the Hanshin-Awaji Earthquake and will be completed at the beginning of 2005, ten years after that Earthquake. Now, we are conducting the construction works of the facility at the Miki-city, near Kobe-city, and the manufacturing of actuators, oil-pressure supply system and other major parts of shaking table at the Mitsubishi Heavy Industry Co.

"E-Defense" is the very large scale and high performance testing facility in the world. Therefore, many researchers, which are belonging not only Japanese but also worldwide organizations, can use this facility for their researches. "E-Defense" should be operated the international common use. For the international collaboration and the dissemination of research results (including test data), Earthquake Engineering Network ("EE-net") will also construct until the completion of "E-Defense". EE-net will connect, through a high performance Internet, distributed major earthquake engineering research organization.

We consider that the researchers together from worldwide and research projects will determine and evaluate by the International Committee. We hope that "E-Defense" and EE-net will be situated to one of the cooperative research organization for the earthquake disaster mitigation in the world.

KEY WORDS:

Failure mechanism of structures
Full Scale Testing
International Common Use
3-D Shaking Table
Network of Earthquake Research

[1] Project Director, 3-D Full-Scale Earthquake Testing Facility (E-Defense), National Research Institute for Earth Science and Disaster Prevention (NIED), Tsukuba, Japan

[2] Project Sub-Director, E-Defense, NIRD, Japan

[3] President, NIED, Japan

[4] Visiting Research Fellow, NIED, Japan

1. INTRODUCTION

The Hanshin-Awaji Earthquake (Hyogoken-Nanbu Earthquake, January 17, 1995) clearly demonstrated that the occurrence of very strong ground motion in the area near to the seismic fault is capable of causing severe structural damage beyond general estimation. The destructive earthquake occurred in the worldwide in the recent years, such as Northridge earthquake (1994), Umbria-Marche earthquake (1997), Kocaeli earthquake (1999), Ji-ji earthquake (1999), El Salvador earthquake (2000), Gujarat earthquake (2001) and so on.

In order to reduce the hazards associated with large earthquakes, it is essential to improve the reliability of earthquake resistance estimations and reinforcement methods in the construction of urban and major structures. For this purpose, failure mechanisms and collapse processes of various kinds of full-scale structures must be investigated. Many types of experimental apparatus have been used for such investigations, and some of them have as large a size as possible to alleviate any difficulties arising from limitation of the model>Considering the lessons learnt from recent earthquake disasters, the National Research Institute for Earth Science and Disaster Prevention (NIED) planned to build a new three-dimensional, full-scale, earthquake testing facility, which can carry large-size soil and structure models and reproduce the processes of structural failure. This facility is expected to become a powerful tool for international collaboration in earthquake engineering research. It also requires international cooperation to successfully complete the facility and to use it effectively for engineering purposes.

Following the technical developments and surveys in earthquake engineering and related fields, the NIED began the design and construction of this new facility in the Japanese fiscal year of 1998. This paper summarizes the construction plan and Earthquake Engineering Network (EE-Net), which is the tool for ensure of the international collaboration and the dissemination of research results.

2. E-DEFENSE (3-D FULL-SCALE EARTHQUAKE TESTING FACILITY)

Based on the lessons learnt from Hanshin-Awaji earthquake, the Minister of State for Science and Technology was inquired to the Council for Aeronautics, Electronics and Other Advanced Technology, which is the one inquire organization of the Minister, for the discussion of the effective arrangement of research bases for earthquake disaster mitigation at March 29,1996. The Council was reported to the Minister at September 3, 1997.

The report was clearly pointed out the arrangement of large-scale three-dimensional earthquake simulator facility as the core facility of research bases for earthquake disaster mitigation.

NIED initiated the project on the large-scale three-dimensional earthquake simulator facility just after the occurrence of Hanshin-Awaji earthquake. The research and development for core technology for this facility (E-Defense) was started on 1995. The fundamental concepts of this project based on the report by the council.

The E-Defense will construct as the core facility of the research bases for earthquake disaster mitigation. Therefore, we need to clear the positions of the E-Defense.

1) Position of earthquake simulator for the main element of development of the "Time-Space Domain Simulation System for Earthquake Disaster.)
2) Position of the clearly understanding of failure mechanism of structures.
3) Position of the response mechanism for the request from major subject of earthquake engineering.

The importance of promoting the strengthening

and rationalization of earthquake-proof structural design is just one of the lessons from Hanshin-Awaji earthquake. Because earthquake vibrations involve three-dimensional movement, it is necessary to set up a three-dimensional earthquake simulator facility to accurately reproduce earthquake motions. To perform tests on real-size objects or large-scale models of test structures and foundations, it is desirable to have the large-scale three-dimensional shaking table. If large-scale 3-dimensional shaking table is available, tests could be performed to shed new light on the mechanism of dynamic failure using real-size structures. If a stage reached whereby design based on such discovery can be performed, this will contribute immensely to reducing earthquake disaster.

The main specification of E-Defense is shown in Table 1. The actuator performance for horizontal and vertical axes is shown in Fig. 1.

3. CONSTRUCTION AND MANUFACTURING OF E-DEFENSE

NIED have commenced the development work of shaking mechanism with very large size of hydraulic actuators in fiscal year 1995 and completed performance tests successfully in 1998. Following the above technical development and surveys in earthquake engineering and related fields, NIED have began the design and construction of E-Defense in 1998.

Figure 2 shows the drawing bird eye view of E-Defense. We will construct several buildings, such as laboratory building, measurement and control building, hydraulic oil unit building, preparation building and so on. The 3-dimensional shaking table will be installed in the laboratory building. Hydraulic oil will be supplied to shaking table by pipelines via underground culvert. The reaction foundation (shaking table foundation) has weight of about 2GN (200,000 tonf) and set to the bedrock directly.

The construction work has been began in 1998 and will be completed at the beginning of 2005. The new facility will start to operate at the 10 years after the Hanshin-Awaji earthquake. The E-Defense is constructed in "Miki Earthquake Disaster memorial Park (tentative name)", which is being constructed in Miki city, on the north of Kobe city. The construction of shaking table foundation was started at the construction site in January 2000. Figure 3 shows the aerial photograph of the site before the construction work. Figure 4 shows the scene of the first concrete casting for the foundation. The D51 (diameter 51 mm) reinforcing bars used for the foundation, such as the foundation for Nuclear Power Plant. Figure 5 is the recent construction condition.

The manufacturing of testing equipments, such as actuators, 3-dimensional link joint, oil power pump unit, accumulator unit and so on, were started in 1998. By the construction of manufactured unit are limited some size by the condition of transportation. The setup working will be done at the site. Figure 6 shows the set-upped actuator in the preparation building.

4. EARTHQUAKE ENGINEERING NETWORK

The report by the Council was strongly suggested that E-Defense should be operated the international common use. It is important to arrange the utilizing structures, equipment and support section for outside users. To ensure the international common use and disseminate the test results, we will construct and install the Earthquake Engineering Network (EE-Net).

The EE-Net has tow major functions: The one is the connection tool between E-Defense in Miki and the Super Computer in Tsukuba. The other one is the connection tool between NIED and the other organization, such as research institute, university, private sector and so on. This function is not only limited to domestic, but also international manner.

We will install the tele-observation and tele-discussion capabilities, but not install the tele-operation function. Because, conducting of shaking table test, especially failure test, has very delicate and dangerous factors. Therefore, the operation of shaking table will limit by the shaking table administrator, who is the specialist of operation. Figure 7 shows the schematic image of EE-Net, and Table 2
Shows the security control system for different kind of users.

5. CONCLUDING REMARKS

Based on the lessons learnt from Hanshin-Awaji earthquake, we, NIED, need more research to understand the failure mechanism of different kind of structures during earthquake. For this research needs, we began the construction project of E-Defense (3-D Full-Scale Earthquake Testing Facility) and EE-Net (Earthquake Engineering Network). After completion, these tools will be perfectly opened to international use.

We strongly hope that these tools are contributed to the dramatic progress of the earthquake engineering research, especially the understanding of structural failure mechanism, the progress of the earthquake resistant design of structures and the evaluation/reevaluation of structural performance during earthquake, by the coordination and collaboration research works in the worldwide bases.

REFERNCES:

Ohtani, K, Katayama, T, Shibata, H. (1998) "Project on 3-D Full-Scale Earthquake Testing Facility – First Report-", *30UJNR*

Ogawa, N, Ohtani, K, Katayama, T, Shibata, H. (1999) "World's Largest Shaking Table Takes Shapes in Japan – A Summary of Construction Plan and Technical Development-", *SmiRT 16*

Ohtani. K, Ogawa, N, Katayama, T, Shibata, H, Nakagawa, O, Ohtomo, T. (2001) "World's Largest Shaking Table Takes Shapes in Japan (The 2nd Report)", *SmiRT 17*

Ohtani, K. (2001) "Tools for Seismic Safety Evaluation of Structures", *NEA/CSNI/R(2001)13/VOL3*

Ohtani, K, Ogawa, N, Katayama, T, Shibata, H. (2002) "3-D Full-Scale Earthquake Testing Facility and Earthquake Engineering Network", *3WCSC*

Payload	12MN(1200tonf)	
Size	20m × 15m	
Driving Type	Accumulator Charge Electro-Hydraulic Servo Control	
Shaking Direction	X·Y - Horizontal	Z-Vertical
Maximum Acceleration (at Maximum Loading)	>900cm/s²	>1,500cm/s²
Maximum Velocity	200cm/s	70cm/s
Maximum Displacement	±100cm	±50cm
Moment	verturning Momnt	Yawing Moment
	150MN·m	40MN·m

Table 1. Main Specification of E-Defense

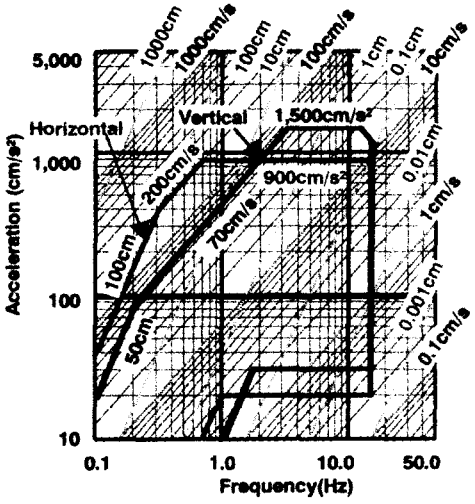

Fig. 1. Limit Performance of E-Defense

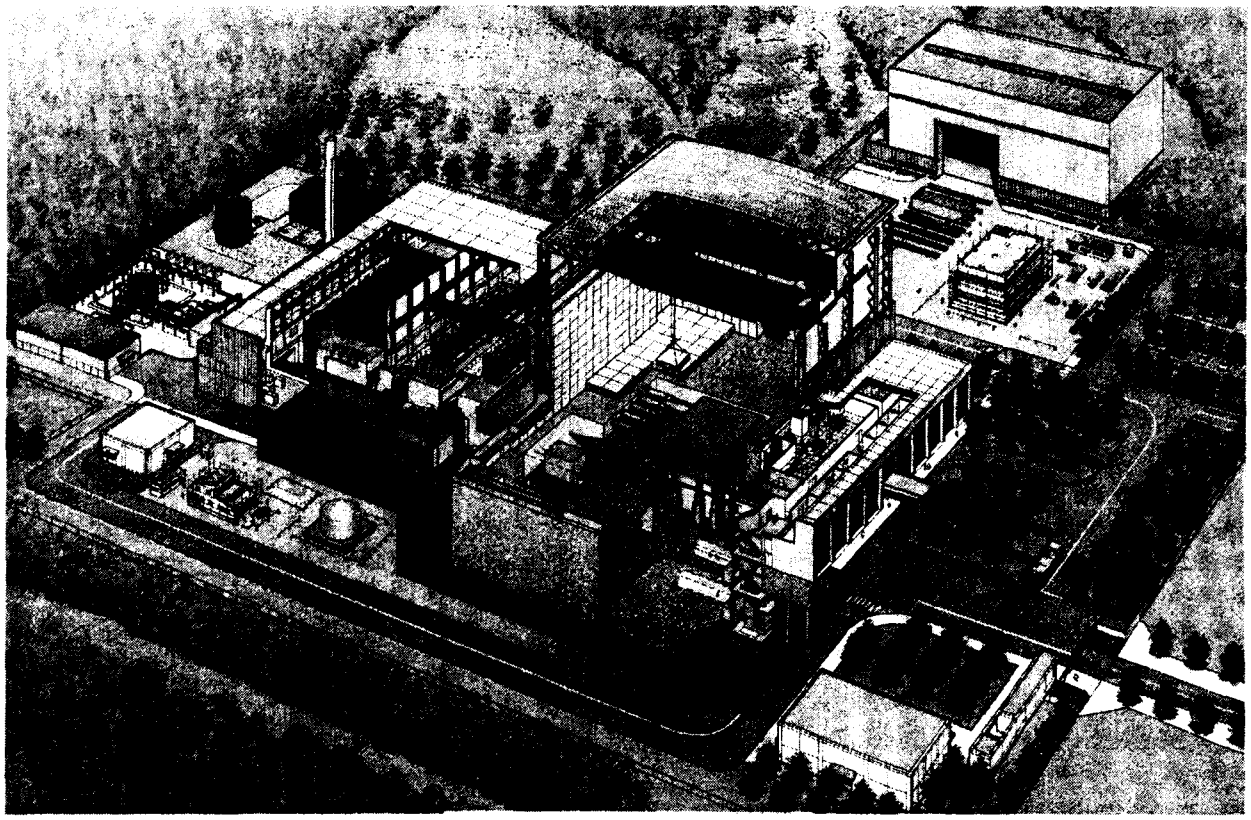

Fig. 2 Layout of E-Defense

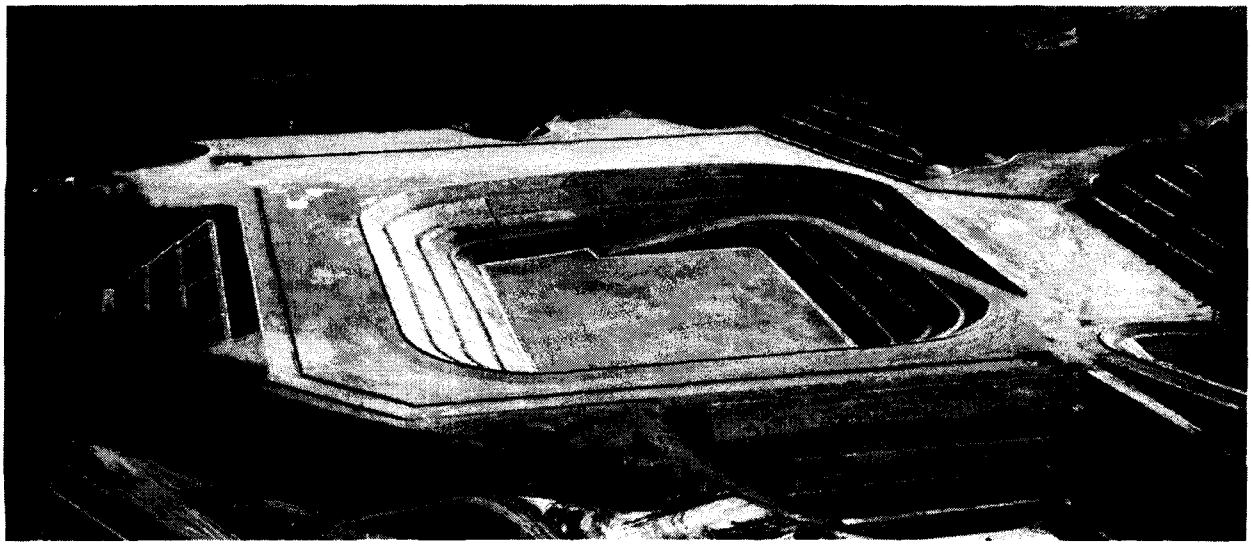

Fig. 3 Construction Site at Miki, near Kobe (January 17, 2000)

Fig. 4 First Concrete Casting for Shaking Table Foundation (June 20. 200)

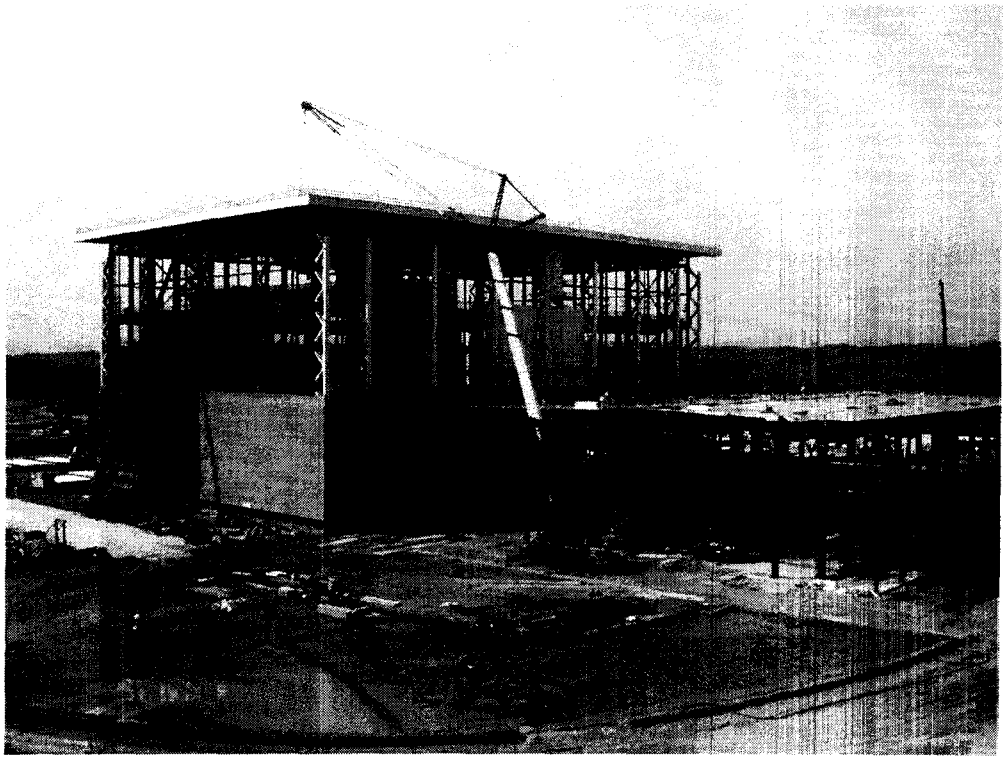

Fig. 5 Recent Construction Condition (April 18, 2002)

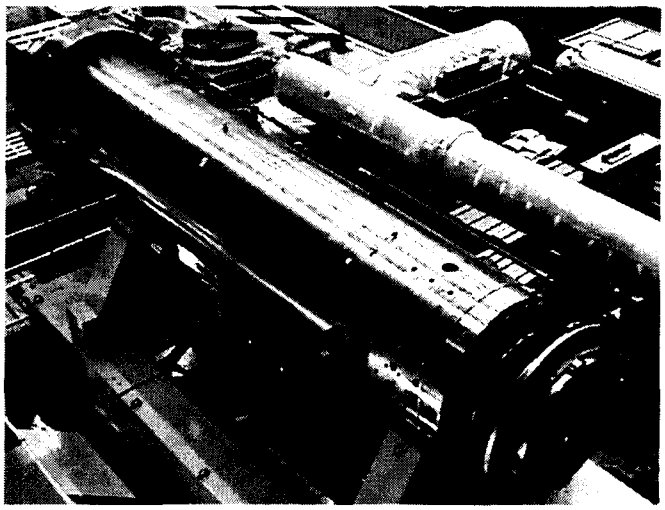

Fig. 6 Set-upped Horizontal Actuator

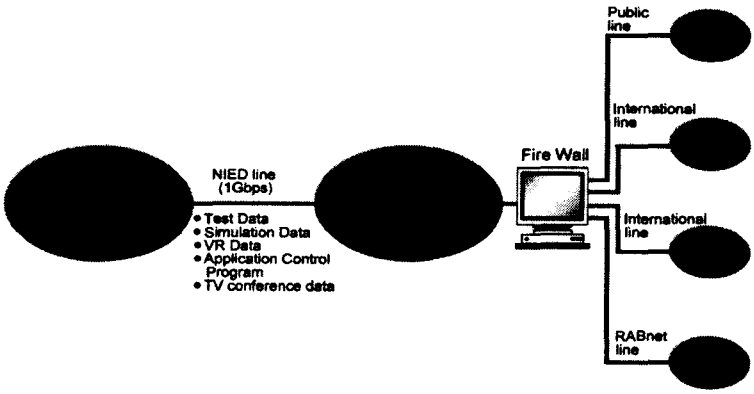

Fig. 7 Schematic Images of EE-Net

Table 2 Security Control for Users

Shaking table administrator	○	○	○	○	○
Shaking table User (at Miki)	×	○	○	○	○
Mathematical simulator administrator	×	○	○	○	○
Mathematical simulator user (at Miki)	×	○	○	○	○
Mathematical simulator user (at TSUKUBA)	×	○	○	○	○
Network administrator	×	—	—	○	○
Network User (at Miki)	×	—	—	○	○
Network User (at TSUKUBA)	×	—	—	○	○
RABnet User	×	○	○	○	○
US NEES User	×	○	○	○	○
EU JRC User	×	○	○	○	○
Internet User	×	×	×	×	○ (limited access)

○: Accessible ×: Inaccessible —: Accessible depending on user skill

Smart Damping Technologies for Dynamic Hazard Mitigation

by

B.F. Spencer Jr.[1]

ABSTRACT

In recent years, considerable attention has been paid to research and development of structural control devices, with particular emphasis on alleviation of wind and seismic response of buildings and bridges. In both areas, serious efforts have been undertaken to develop the structural control concept into a workable technology. To date, full-scale active and hybrid control systems have been designed and installed in approximately 40 commercial buildings and 15 bridges (during construction). Yet the engineering community is reluctant to fully embrace this new technology. Demonstrated cost-effectiveness and reliability are key considerations for acceptance and successful implementation of structural control. Because of their low power requirements and fail-safe character, smart damping strategies appear quite attractive in this regard. The focus of this paper will be to review a number of smart damping approaches that have been proposed and implemented in full-scale structures.

1.0 INTRODUCTION

Passive supplemental damping strategies, including base isolation systems, viscoelastic dampers and tuned mass dampers, are well understood and are accepted by the engineering community as a means for mitigating the effects of dynamic loadings such as strong earthquakes and high winds. However, these passive-device methods are unable to adapt to structural changes and to varying usage patterns and loading conditions.

For more than two decades, researchers have investigated the possibility of using active control methods to improve upon passive approaches to reduce structural responses (Soong 1990; Spencer and Sain 1997; Housner *et al.* 1997; Soong and Spencer 2002). The first full-scale application of active control to a building was accomplished by the Kajima Corporation in 1989 (Kobori 1994). The Kyobashi Seiwa building is an 11-story (33.1 m) building with a total floor area of 423 m^2. An active mass driver (AMD) system was installed, consisting of two AMDs — the primary AMD is used for transverse motion and has a mass of 4 tons, while the secondary AMD has a mass of 1 ton and is employed to reduce torsional motion. The role of the active system is to reduce building vibration under strong winds and moderate earthquake excitations and consequently to increase the comfort of occupants of the building. Since that time, active/hybrid structural control has been successfully applied in approximately 40 commercial buildings and 15 bridges (during construction).

Although extensive analytical and experimental structural control research has been conducted in both the U.S. and Japan in the last decade, with the exception of one experimental system installed on a bridge in Oklahoma (discussed later in this paper), none of these full-scale active control installations are located the U.S. Many possible reasons can be cited for this disparity. For example, the civil engineering profession and construction industry in the U.S. are conservative and generally reluctant to apply new technologies. The absence of verified and consensus-approved analysis, design and testing procedures represent additional impediments to the application of this technology. However, more notable is the lack of research and development expenditures by the U.S. construction industry. This situation is in sharp contrast to the Japanese construction industry, which invests heavily in the development and implementation of new

[1]Dept. of Civil Engineering and Geological Sciences, University of Notre Dame, 156 Fitzpatrick Hall, Notre Dame, IN 46556 USA.

technologies. Yet even in Japan, few new projects for implementation of active control systems are being initiated. This situation is partly due to the modest number of tall buildings and long-span bridges being planned for the near future and partly due to a number of serious challenges that remain before active control can gain general acceptance by the engineering and construction professions at large. These challenges include: (i) reducing capital cost and maintenance, (ii) eliminating reliance on external power, (iii) increasing system reliability and robustness, and (iv) gaining acceptance of non-traditional technology.

Despite the impediments that exist to wider application of control to civil engineering structures, the future appears quite bright. Smart damping (also known as semiactive control) strategies are particularly promising in addressing many of the challenges to this technology, offering the reliability of passive devices, yet maintaining the versatility and adaptability of fully active systems. The remainder of this paper discusses several smart damping strategies that have recently been proposed, both in the U.S. and in Japan, for control of civil engineering structures, as well as several applications of this technology. Such systems may facilitate near-term acceptance of control technology by practitioners as an important means for mitigating dynamic hazards.

2.0 SMART DAMPING DEVICES

Smart damping devices have received a great deal of attention in recent years because they offer the adaptability of active control devices without requiring the associated large power sources. In fact, many can operate on battery power, which is critical during seismic events when the main power source to the structure may fail. According to presently accepted definitions, a smart damping device is one which cannot inject mechanical energy into the controlled structural system (i.e., including the structure and the control device), but has properties that can be controlled to optimally reduce the responses of the system. Therefore, in contrast to active control devices, smart damping devices do not have the potential to destabilize (in the bounded input/ bounded output sense) the structural system. Studies have shown that appropriately implemented smart damping systems perform significantly better than passive devices and have the potential to achieve, or even surpass, the performance of fully active systems, thus allowing for the possibility of effective response reduction during a wide array of dynamic loading conditions (Dyke *et al.* 1998; Spencer *et al.* 2000). Examples of such devices include variable-orifice fluid dampers, controllable friction devices, variable stiffness devices, adjustable tuned liquid dampers, and controllable fluid dampers (Spencer and Sain 1997). Of these classes of smart dampers, two have already been implemented in full-scale structures and will be discussed in the subsequent sections.

2.1 variable-orifice Dampers

One means of achieving a smart damping device is to use a controllable, electromechanical, variable-orifice valve to alter the resistance to flow of a conventional hydraulic fluid damper. A schematic of such a device is given in Fig. 1, which typically operates on approximately 50 watts of power.

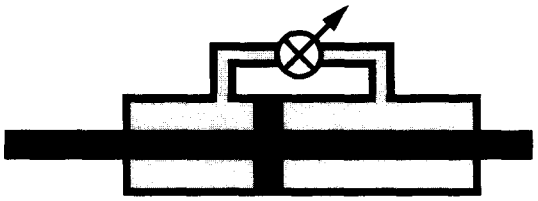

Figure 1. Schematic of Variable-Orifice Damper.

Sack and Patten (1993) conducted experiments in which a hydraulic actuator with a controllable orifice was implemented in a single-lane model bridge to dissipate the energy induced by vehicle traffic. These studies were followed by a full-scale experiment conducted on a bridge on interstate highway I-35 to demonstrate this technology (Patten, 1998, 1999; Kuehn et al., 1999) shown in Figs. 2–3. Figure 4 shows the effectiveness of the SAVA system. This experiment constitutes the first full-scale implementation of structural control in the US.

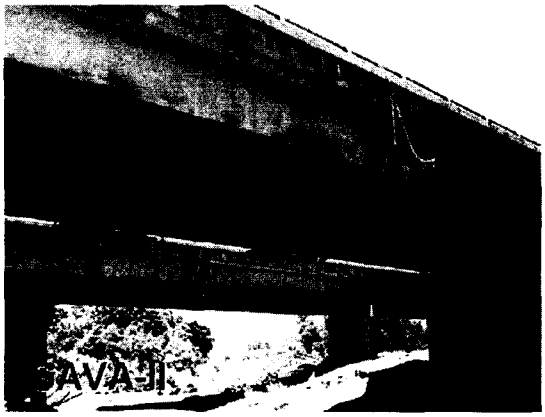

Figure 2. First Full-Scale Implementation of Smart Damping in the US.

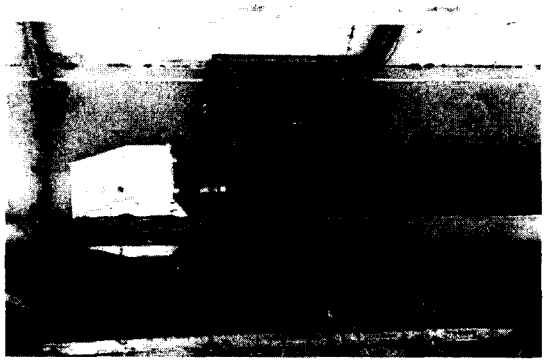

Figure 3. SAVA-II variable-orifice Damper.

Conceived as a variable-stiffness device, Kobori et al. (1993) and Kamagata and Kobori (1994) implemented a full-scale variable-orifice damper in a semiactive variable-stiffness system (SAVS) to investigate semiactive control at the Kajima Technical Research Institute. The overall system is shown in Fig. 5 where SAVS devices were installed on both sides of the structure in the longitudinal direction. The results of these analytical and experimental studies indicate that this device is effective in reducing structural responses.

More recently, a smart damping system was installed in the Kajima Shizuoka Building in Shizuoka, Japan. As seen in Fig. 6, semiactive hydraulic dampers are installed inside the walls on both sides of the building to enable it to be used as a disaster relief base in post-earthquake

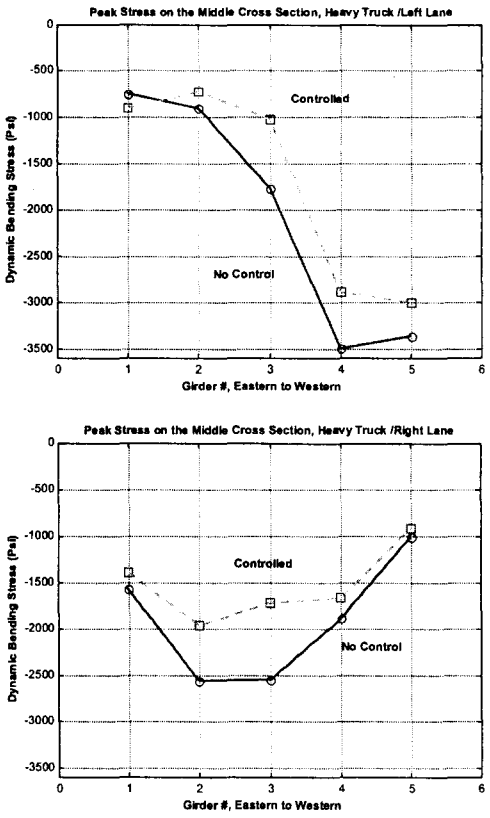

Figure 4. Comparison of Peak Stresses for Heavy Trucks.

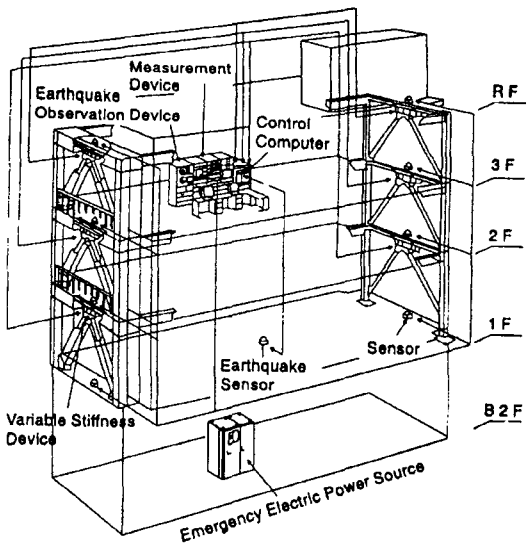

Figure 5. SAVS System Configuration.

situations (Kobori, 1998; Kurata et al., 1999). Each damper contains a flow control valve, a check valve and an accumulator, and can develop a maximum damping force of 1000 kN (see Fig. 7). Figure 8 shows a sample of the response analysis results based on one of the selected control schemes and several earthquake input motions with the scaled maximum velocity of 50 cm/sec, together with a simulated Tokai wave. Both story shear forces and story drifts are seen to be greatly reduced with control activated. In the case of the shear forces, they are confined within their elastic-limit values (indicated by E-limit) while, without control, they would enter the plastic range.

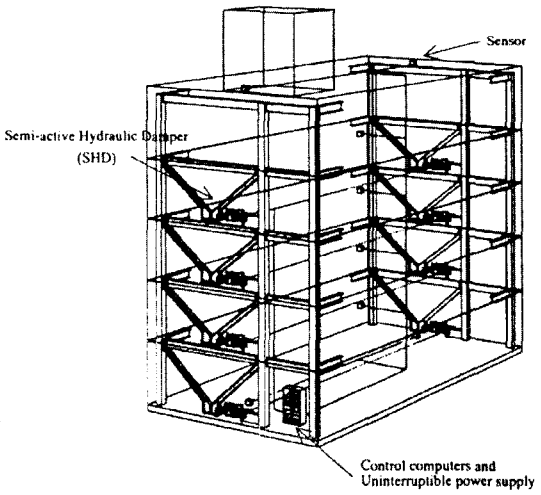

Figure 6. Kajima Shizuoka Building Configured with Semiactive Hydraulic Dampers.

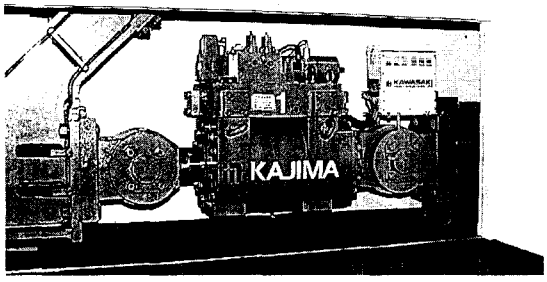

Figure 7. Shizuoka Building variable-orifice Damper.

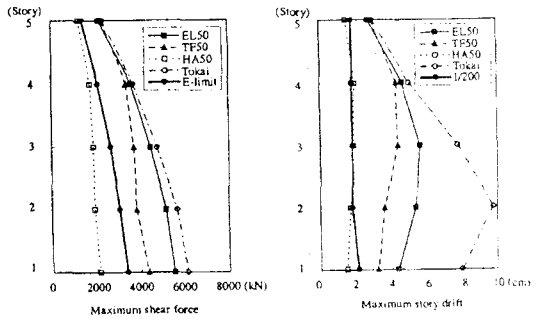

(a) w/ control (b) w/o control

Figure 8. Maximum Responses (El Centro, Taft and Hachinohe Waves with 50 cm/sec. and Assumed Tokai Waves).

The use of the variable-orifice damper has blossomed in Japan. In the Tokyo Siodome area, 4 new buildings are currently under construction (Kobori 2002). One of these structures is the Kajima K-Building, 38-story building with 88 variable-orifice dampers and 2 hybrid mass dampers. In another area of Tokyo, the Kajima R-Building, a 54-story building with 356 variable-orifice dampers and 192 passive dampers distributed throughout, is under construction. When these projects are completed, a total of more than 700 variable-orifice dampers will be installed in building structures in Japan.

2.2 Controllable Fluid Dampers

In comparison with variable-orifice damper systems, another class of relatively new smart damping devices uses controllable fluids, schematically shown in Fig. 9. In comparison with smart damping systems described above, an advantage of controllable fluid devices is that they contain no moving parts other than the piston, which makes them simple and potentially very reliable.

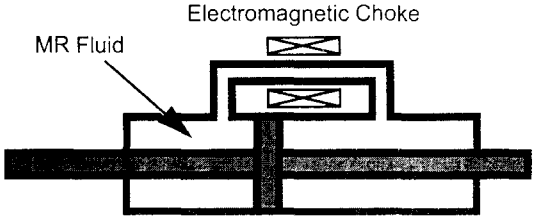

Figure 9. Schematic of MR Damper.

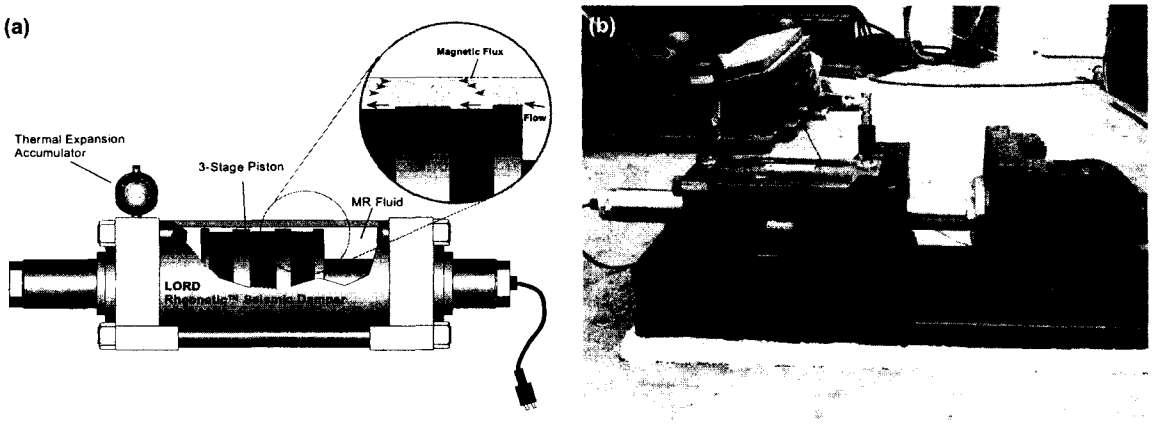

Figure 10. (a) Schematic of 20-ton MR fluid damper; (b) Experimental setup.

The essential characteristics of controllable fluids is their ability to reversibly change from a free-flowing, linear viscous fluid to a semi-solid with a controllable yield strength in milliseconds when exposed to an electric (for electrorheological (ER) fluids) or magnetic (for magnetorheological (MR) fluids) field.

In the case of magnetorheological fluids, they typically consist of micron-sized, magnetically polarizable particles dispersed in a carrier medium such as mineral or silicone oil. When a magnetic field is applied to the fluid, particle chains form, and the fluid becomes a semi-solid and exhibits viscoplastic behavior. Transition to rheological equilibrium can be achieved in a few milliseconds, allowing construction of devices with high bandwidth. Additionally, Carlson and Weiss (1994) indicated that high yield stress of a magnetorheological fluid can be achieved and that magnetorheological fluids can operate at temperatures from –40°C to 150°C with only slight variations in the yield stress. Moreover, magnetorheological fluids are not sensitive to impurities such as are commonly encountered during manufacturing and usage, and little particle/carrier fluid separation takes place in magnetorheological fluids under common flow conditions. Further, a wider choice of additives (surfactants, dispersants, friction modifiers, antiwear agents, etc.) can generally be used with magnetorheological fluids to enhance stability, seal life, bearing life, and so on, since electrochemistry does not affect the magnetopolarization mechanism. The magnetorheological fluid can be readily controlled with a low voltage (e.g., 12-24 V), current-driven power supply outputting only 1-2 amps.

Carlson and Spencer (1996) and Spencer et al. (1997, 1998) and Yang *et al.* (2002) report on the design of a full-scale, 20-ton magnetorheological damper (see Fig. 10–11) showing that this technology is scalable to devices appropriate for civil engineering applications. At design velocities, the dynamic range of forces produced by this device is over 10 (see Fig. 11), and the total power required by the device is only 20-50 W.

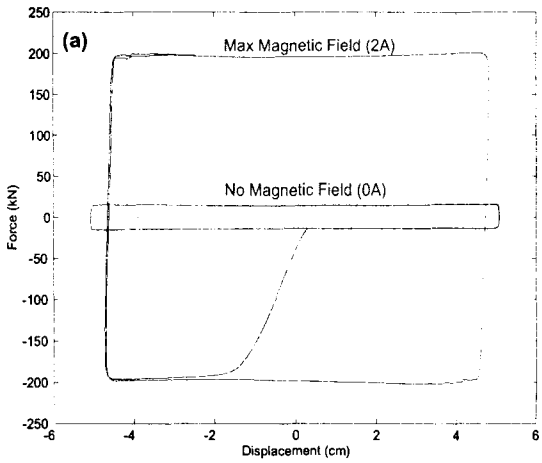

Figure 11. Measured force-displacement loops at 5.4 cm/sec.

Recently, Sunakoda, *et al.* (2001) have also presented encouraging results regarding design, construction, and commercial manufacturing of large scale MR dampers.

In 2001, the first full-scale implementation of MR dampers for civil engineering applications was achieved. The Nihon-Kagaku-Miraikan, the Tokyo National Museum of Emerging Science and Innovation shown in Fig. 12, has two 30-ton, MR Fluid dampers installed between the 3rd and 5th floors. The dampers were built by Sanwa Tekki using the Lord Corporation MR fluid.

Currently being retrofitted with stay-cable dampers, the Dongting Lake Bridge in Hunan, China will constitute the first full-scale implementation of MR dampers for bridge structures. Long steel cables, such as are used in cable-stayed bridges and other structures, are prone to vibration induced by the structure to which they are connected and by weather conditions, particularly wind

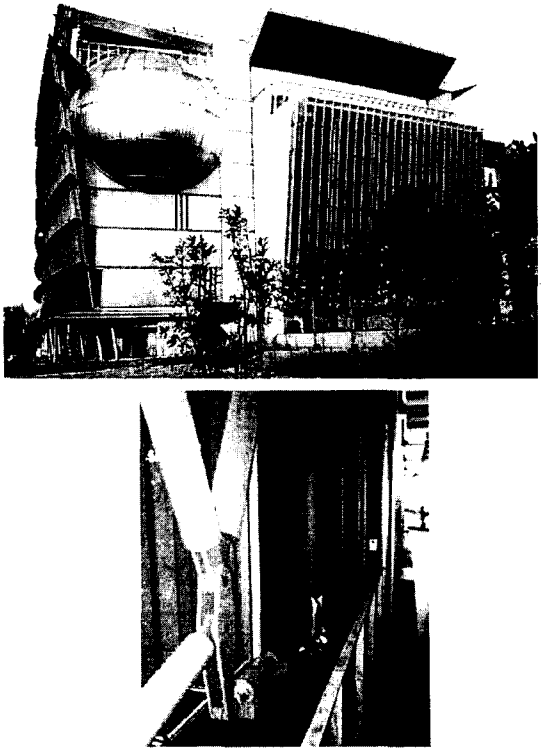

Figure 12. Nihon-Kagaku-Miraikan, Tokyo National Museum of Emerging Science and Innovation.

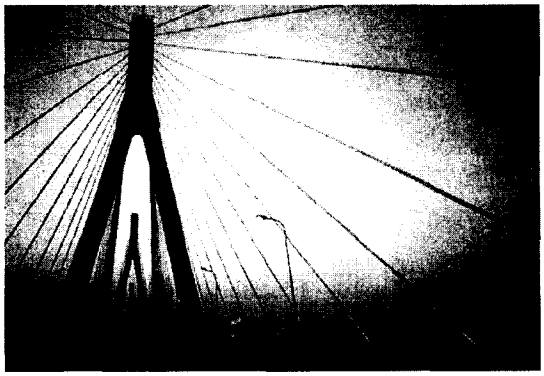

Figure 13. Dongting Lake Bridge, Hunan, China.

combined with rain, that may cause cable galloping. The extremely low damping inherent in such cables, typically on the order of a fraction of a percent, is insufficient to eliminate this vibration, causing reduced cable and connection life due to fatigue and/or breakdown of corrosion protection. Two Lord SD-1005 (www.rheonetic.com) MR dampers are being installed on each cable to mitigate cable vibration.

3.0 CONCLUSIONS

Although in their infancy, control strategies based on smart damping devices appear to combine the best features of both passive and active control systems and to offer a viable means of protecting civil engineering structural systems against earthquake and wind loading. In particular, they provide the reliability and fail-safe character of passive devices, yet possess the adaptability of fully active devices. Because of their mechanical simplicity, low power requirements and high force capacity, magnetorheological (MR) dampers constitute a class of smart damping devices that meshes well with the demands and constraints of civil infrastructure applications and will likely see increased interest from the engineering community.

ACKNOWLEDGMENT

The author gratefully acknowledges the support of this research by the National Science Foundation under grant CMS 99-00234 (Dr. S.C. Liu, Program Director) and the Lord Corporation.

REFERENCES

Carlson, J.D. and Weiss, K.D. "A Growing Attraction to Magnetic Fluids," *Machine Design*, August, pp. 61–64, 1994.

Dyke, S.J., Spencer Jr., B.F. Sain, M.K. and Carlson, J.D. "An Experimental Study of MR Dampers for Seismic Protection," *Smart Materials and Structures*, Vol. 7, pp. 693–703, 1998.

Housner, G.W., Bergman, L.A., Caughey, T.K., Chassiakos, A.G., Claus, R.O., Masri, S.F., Skelton, R.E., Soong, T.T., Spencer, B.F. and Yao, J.T.P. "Structural Control: Past, Present and Future," *Journal of Engineering Mechanics, ASCE,* Vol. 123, No. 9, pp. 897–971, 1997.

Kamagata, S. and Kobori, T. "Autonomous Adaptive Control of Active Variable Stiffness Systems for Seismic Ground Motion", *Proceedings of the 1st World Conference on Structural Control*, pp. TA4:33-42, Pasadena, CA, 1994.

Kobori, T. "Future Direction on Research and Development of Seismic-Response-Controlled Structure," *Proceedings of the 1st World Conference on Structural Control*, Panel:19–31 (1994).

Kobori, T. "Mission and Perspective Towards Future Structural Control Research", *Proceedings of the 2nd World Conference on Structural Control*, 1, pp. 25-34, Kyoto, Japan, 1998.

Kobori, T. "Past, Present and Future in Seismic Response Control in Civil Engineering Structures," *Proceedings of the 3rd World Conference on Structural Control,* 2002.

Kobori, T., Takahashi, M., Nasu, T., Niwa, N. and Ogasawara, K. "Seismic response controlled structure with active variable stiffness system", *Earthquake Engineering and Structural Dynamics*, 22, pp. 925-941, 1993.

Kuehn, J., Song, G. and Sun, J. "Experimental Verification of a NON-Protruding Intelligent Stiffener for Bridges (ISB)", *Proc. Int. Post-SMiRT Conf. Seminar on Seismic Isolation, Passive Energy, Dissipation and Active Control of Vibrations of Structures*, Cheju, Korea, August 23-25, 1999.

Kurata, N., Kobori, T., Takahashi, M., Niwa, N. and Midorikawa, H. "Actual Seismic Response Controlled Building with Semi-active Damper System," *Earthquake Engineering and Structural Dynamics*, Vol. 28, pp1427-1447, 1999.

Patten, W.N. "The I-35 Walnut Creek Bridge: An Intelligent Highway Bridge Via Semi-active Structural Control", *Proceedings of the 2nd World Conference on Structural Control*, Vol. 1, pp. 427-436, Kyoto, Japan, 1998.

Patten, W., Sun, J., Li, G., Kuehn, J. and Song, G. "Field Test of an Intelligent Stiffener for Bridges at the I-35 Walnut Creek Bridge". *Earthquake Engineering and Structural Dynamics*, Vol. 28, No. 2, pp. 109-126, 1999.

Sack, R.L. and Patten, W. "Semiactive Hydraulic Structural Control", *Proceedings of the International Workshop on Structural Control*, USC Publication No. CE-9311, pp. 417-431, Honolulu, Hawaii, 1993.

Sodeyama, H. Sunakoda, K., Suzuki, K., Carlson, J.D. and Spencer Jr., B.F. "Development of Large Capacity Semi-Active Vibration Control Device using Magneto-Rheological Fluid," *PVP-Vol. 428-2, Seismic Engineering–Volume 2*, pp. 109–114, 2001.

Soong, T.T. *Active Structural Control: Theory and Practice*, Longman Scientific and Technical, Essex, England (1990).

Soong, T.T. and Spencer Jr., B.F. "Supplementary Energy Dissipation: State-of-the-Art and State-of-the-Practice," *Engineering Structures*, Vol. 24, pp. 243–259, 2002.

Spencer Jr., B.F., Carlson, J.D., Sain, M.K. and Yang, G. "On the Current Status of Magnetorheological Dampers: Seismic Protection of Full-scale Structures", *Proceedings of the American Control Conference,* pp. 458-462, Albuquerque, NM, 1997.

Spencer Jr., B.F. and Sain, M.K. "Controlling Buildings: A New Frontier in Feedback," *IEEE Control Systems Magazine: Special Issue on Emerging Technologies* (Tariq Samad, Guest Ed.), Vol. 17, No. 6, pp. 19–35, 1997.

Spencer Jr., B.F., Yang, G., Carlson, J.D. and Sain, M.K. "Smart dampers for seismic protection of structures: A full-scale study", *Proceedings of the 2nd World Conference on Structural Control*, 1, pp. 417-426, Kyoto, Japan, 1998.

Spencer Jr., B.F., Johnson, E.A. and Ramallo, J. C. "'Smart' Isolation for Seismic Control," *JSME International Journal: Special Issue on Frontiers of Motion and Vibration Control*, Series C, Vol. 43, No. 3, pp. 704–711, 2000.

Spencer Jr., B.F., Yang, G., Carlson, J.D. and Sain, M.K. "Large-Scale MR Fluid Dampers: Modeling and Dynamic Performance Considerations," *Engineering Structures*, Vol. 24, pp. 309–323, 2002.

Research and Development Programs on Timber Structures in Japan

Hiroshi Isoda[1], Hisashi Okada[2], Naohito Kawai[3] and Nobuyoshi Yamaguchi[1]

ABSTRACT

Recently there have been many projects pertaining to timber structures, mainly dealing with seismic behavior. This paper outlines two main projects that currently are being promoted by several committees within BRI and external to BRI, which report to the BRI project team. They are also being developed collaboratively with public corporations, and international institutes. The Final target of one project is to develop high-performance hybrid timber members and hybrid timber structures, which consist of timber and other materials, to develop the performance evaluation methods for these hybrid timber structures, and to develop the design method for some typical hybrid timber structures. The other target is to develop the seismic rehabilitation system for existing inferior, low-rise wooden buildings. These projects have several goals including developing reliable and economical ways of improving performance of residential wooden houses as well as minimizing the environmental costs in the construction of new homes. The effective utilization of timber is urged from the point of preservation of natural resources and global environment also in Japan.

KEYWORDS: timber structures, advanced hybrid timber members and structures, seismic performance, seismic rehabilitation, fireproof performance

1. INTRODUCTION

Recently Building Research Institute is promoting research and development programs on timber structures as one of important tasks. The research motivation is that timber structures represent one of society's largest investments in the built environment; however, one clear issue is the lack of understanding of the seismic behavior of timber structures. The level of confidence associated with the seismic analysis and design of timber structures is much lower than for reinforced concrete and steel structures. As the result, timber structures are very vulnerable during big earthquakes. In a project, which is called "A Research ad Development Project on Hybrid Timber Building Structures" the main objective to improve the structural performance is summarized in the following three items.

1) Develop high performance hybrid timber members consisting of timber and other materials

[1] Senior Research Engineer, Building Research Institute, Tsukuba-shi, Ibaraki-ken 305-0802

[2] Group Leader, Building Research Institute

[3] Head, National Institute for Land and Infrastructure Management

2) Develop high performance joints to connect timber members ,and between timber and other materials

3) Develop hybrid timber structures incorporating timber with other types of structures such as reinforced concrete or steel frame.

In this paper, the current activities are summarized.

On the other hand, it is very important to improve seismic performance for existing inferior and low-rise wooden buildings in Japan. The project for their seismic rehabilitation has started since 2002. The research review and future plan also describes in this paper.

2. HYBRID TIMBER STRUCTURAL SYSTEM

The effective utilization of timber is urged from the point of preservation of natural resources and global environment also in Japan. And the effective mixture of timber and other materials is expected to extend the possibility of building structures because of the possibility to realize high performance in both structural safety and fire safety. The Building Standard Law of Japan was revised in June 1998 and the potential to accept large-scale and high-rise timber buildings with its provision of performance based code. The objectives of this research and development project are, to develop high-performance hybrid timber members and hybrid timber structural systems, to develop the performance evaluation methods for structural and fire safety of these buildings, and to develop the design methods for typical hybrid timber buildings.

This project started in 1999 as a five-year national project. There are some preceding researches or designs in this area, such as timber beams reinforced by steel or fibers, floor systems with timber and reinforced concrete, structural systems with reinforced concrete or steel core structure surrounded by timber frames, and so on. These preceding researches are, of course, very useful for our starting of the projects. However, one of the most important issues for the structural performance of hybrid timber structure in Japan is the dynamic behavior of the structures against strong grand motions. There are some research needs adding these preceding researches from the point of seismic performance of such kind of buildings.

2.1 Research Plan and Organization

2.1.1 Research Organization

Fig. 1 shows the original organization of research program. The members of the research committee are scholars and persons of experience, structural engineers, and from the Ministry. This committee adjusts and unifies all research items of each sub-committee into themes of the project. The sub-committees carry out concrete research and development on hybrid timber buildings. The working groups were established in order to solve efficiently each item of research and development. Until fiscal year 2000, the research committee, two sub-committees, and six working groups were organized and the sub-committee on fireproof stared from 2001.

2.1.2 Research Plan

Table 1 shows the annual plan in the every fiscal year. In the first fiscal year several investigations have been carried out to confirm the feasibility and social needs of hybrid timber buildings and to clarify the final target of this project. And in fiscal year 2000, concrete research activities have been started.

2.1.3 Final Targets

The final targets in the sub-committee on the member and joint are summarized as:

Development of high-performance and high-reliable hybrid timber members and joints,

Development of general test and evaluation procedures for hybrid timber members and joints,

Development of some design methods for typical hybrid timber members and joints.

The final targets in the sub-committee on the structural systems are summarized as:

Development of the rational and efficient hybrid timber structures,

Development of general performance evaluation method for hybrid timber structural systems,

Development of some structural design methods for typical hybrid timber structural systems.

2.2 Research Themes and Tentative Findings

2.2.1 Investigations

In fiscal year 1999, following investigations were executed to confirm the social needs and the feasibility of hybrid timber buildings.

Investigation of demand for timber-based middle-rise buildings,

Investigation of existing composite timber-based members, joints and structures,

Investigation of patents on composite timber-based members, joints and structures,

Investigation of oversea and international standards and codes,

Review of the background of provisions for timber buildings in Japanese current regulations.

2.2.2 Hybrid Members

In the WG on Members, hybrid timber members, such as glulam reinforced by steel or fiber, are classified and their performance was roughly evaluated reviewing the preceding researches. And the theoretical equations to predict generally the strength and equivalent stiffness were derived. Now a series of static loading tests and creep tests on several types of hybrid beams are prepared to validate the theoretical equations. Table 2 shows the outline of the test plan.

For the evaluation of structural performance and the design methods of these members, probabilistic approach seems essential due to the variability of properties in timber-based materials.

2.2.3 Joints Between Members

Joints between timber and steel, between timber and reinforced concrete and joints between hybrid timbers are treated in the sub-committee. Additionally, timber joints using some new materials, such as carbon fiber, are also investigated. At first, classification of

these joints were made according to the location in buildings, component materials, the stress transferred and so on.

In hybrid timber buildings of dual structure type, joints with glued-in rods seem effective joints to connect timber and other materials. And in hybrid timber buildings such as middle rise office buildings, the stress level may be higher and more effective timber joints will be required. Carbon fiber sheets or other materials can be used for the reinforcement to prevent the rapture perpendicular to grain. Some series of tests on some types of joints to connect timber and reinforced concrete and some joints reinforced by fibers, rods, steel plates or timber-based materials are now prepared for tests.

Although creep behavior of these joints is important problem for the structural performance evaluation and design, there are not so many researches on this matter. Now the prediction method of the creep deformation and the test plans are discussed in the WG on joints between members.

2.2.4 Joints Between Structures

Joint system between structures is essential research theme for the development of dual structure systems. The WG on joint between structures first picked up the problems which occur in the joints between structures, such as deference of creep behavior, deference of shrinkage, deference of structural behavior against lateral load, problems due to condensation on the surface of concrete or steel, and so on. Next the stress types and stress levels were investigated for some particular structural systems, and the effective joint details were discussed.

2.2.5 Floor Systems

The WG on floor systems deals with various kinds of floor systems, which are acceptable for hybrid timber structures, such as timber beams with plywood, timber beams with reinforced concrete slab, timber deck, and timber deck with reinforced concrete slab. In the WG these floor systems were classified and the performance of structure, fireproof, sound insulation, etc. were roughly discussed.

For structural performance of floor systems, not only the strength and stiffness against vertical load, but also the shear strength and stiffness in plane are discussed considering the structural function as diaphragm against wind and earthquake load. This function is important especially, for example, in the structural design with reinforced concrete core systems later mentioned. And the distribution of design earthquake load for these buildings is an important research theme. Some studies using time history analysis considering shear deformation of horizontal frames are executed to obtain proper earthquake design load. There are not so many preceding researches for the shear stiffness and strength in plane of floor systems. Fig. 3 shows the plan of shear loading tests on some floor systems.

2.2.6 Dual Structure Systems

Dual structure systems are considered to be feasible hybrid timber structures. Fig. 4 shows some conceptual models. As a case study, building design is now tried on three types of buildings, which are reinforced concrete core

system, reinforced concrete shear wall and timber frame system, and system of timber frames surrounded by steel frames. This case study is useful to figure out the image of target hybrid timber structures, and to find out the problems for structural performance evaluation and structural design methods.

2.2.7 Timber Based Structure Systems

Timber-based systems includes two types, one is the structure system using hybrid timber members and joints and another is the combined system with different types of timber structures, such as wall system and frame system. In the WG on timber-based systems, these hybrid systems were classified and the problems for structural performance evaluation are drawn out and arranged.

3. SEISMIC REHAVILITATION OF EXISTING WOODEN BUILDINGS

The origin of this project is the collaboration research program with CUREE-Caltech woodframe project, which had been conducted from 1998 to 2001. The objective was to improve the unreliable performance of wooden houses. The following items were examined by integrating current static and dynamic tests, and developing new tests if necessary.

1) Understand the dynamic collapse mechanisms of wooden houses, 1-1) Collect system testing data for analyzing seismic behavior 1-2) Develop three dimensional seismic analysis model (software) for wooden houses

2) Control the catastrophic collapse of wooden houses, 2-1) Develop joint and shear wall systems to avoid a catastrophic collapse 2-2) Evaluate rehabilitation technologies

3) Propose international harmonious testing protocol and evaluation of testing results, 3-1) Testing protocol and evaluation for joints 3-2) Testing protocol and evaluation for shear walls

4) Discuss international harmonious design procedure for wooden house, 4-1) Specification procedure 4-2)Performance-based design procedure

In 2002, the main target was revised in accordance with society problem. The seismic rehabilitation systems are required as soon as possible to ensure life safety. The typical seismic rehabilitation methods and their seismic performance evaluation procedure will be proposed within the fiscal year 2002.

4. CONCLUSIONS

The project on hybrid timber structures started in 1999 as a five-year national project. In fiscal year 1999, some investigations were executed to confirm the demand and feasibility of middle-rise timber-based buildings. In fiscal year 2000, concrete research activities started in six working groups. The main research themes are, general equation for strength and stiffness of hybrid members and joints, prediction of creep behavior of hybrid members and joints, test and evaluation methods for structural performance of members and joints, structural behavior of floor systems against both vertical and lateral load, development of effective hybrid structural systems, and enumeration and solution of some problems in joints

between structures. The final targets of this project are to establish general evaluation methods for structural and fireproof performance of hybrid timber buildings and to make some design methods for typical hybrid timber buildings. It will enable to construct middle-rise and large-scale hybrid timber buildings in general and also to stem global warming by minimizing emission of carbon dioxide. It is also important to improve the seismic performance of existing inferior and row-rise wooden structures. Their rehabilitation scheme began from the fiscal year 2002.

5. Acknowledgements

Authors would like to thank all the members of research committees (Chairperson: Isao Sakamoto of University of Tokyo), sub-committees and working groups under the research and development project on hybrid timber building structures.

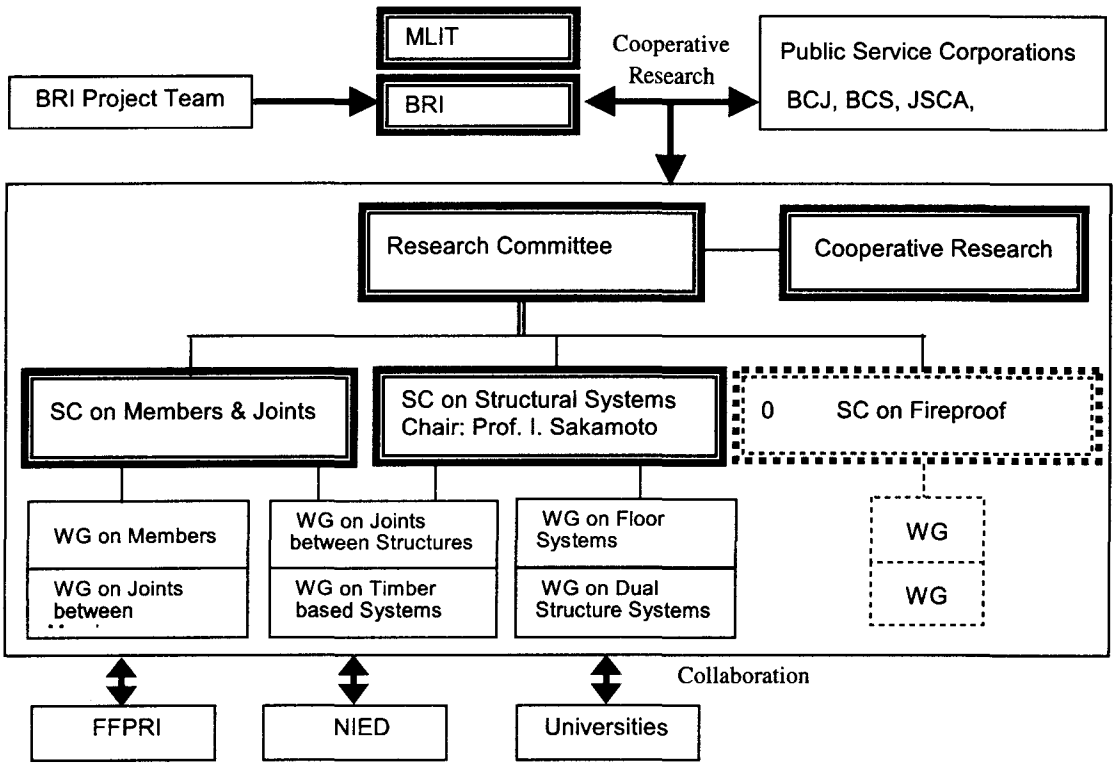

BRI: Building Research Institute, MLIT: Ministry of Land, Infrastructure and Transport, BCJ: The Building Center of Japan, BCS: Building Contractors Society, JSCA: Japan Structural Consultants Association, HOWTEC: The Foundation of Japan Housing and Wood Technology Center, FFPRI: Forestry and Forest Products Research Institute, NIED: National Research Institute for Earth science and Disaster Prevention

Fig. 1Research Organization

Table 1 Research Plan

ITEMS	F.Y. 1999	2000	2001	2002	2003
Development of members & joints					
1) Investigation of current status					
2) Research on mechanical behavior - Creep Tests - Tests on mechanical behavior - Evaluation of mechanical performance					
3) Development and analysis - Proposal of basic concept - Development of members & joints - Tests & analysis					
4) Research on fireproof performance - Clarification of performance requirement - Performance evaluation of members & joints					
5) Design methods & performance evaluation methods - Establishment of basic concept - Proposal					
Development of hybrid timber structural systems					
1) Investigation of current status					
2) Decision of target structural systems - Enumeration of hybrid structural systems - Case study for enumerated systems - Decision of target structural systems					
3) Development and analysis - Basic analysis for proposed systems - Basic tests for proposed systems - Full scale tests for proposed systems					
4) Research on fireproof performance - Clarification of performance requirement - Performance evaluation of proposed systems					
5) Design methods & performance evaluation methods - Establishment of basic concept - Proposal					

Table 2 Test Plan of Hybrid Timber Members

Type of Member		Section of Glulam (mm)	Section of reinforcement (mm)	Connector or Adhesive (mm)	Span of 3-point bending (mm)
Glulam beam reinforced by steel in bith sides		100×200	6×65	2-LS*(d=9, l=75)@70	4,000 and 2,000
				LS (d=9, l=75)@70	4,000
				LS (d=9, l=75)@140	4,000 and 2,000
Glulam beam reinforced by steel in tension sides		100×200	6×65	2-LS (d=9, l=75)@70	4,000
				LS (d=9, l=75)@70	
				LS (d=9, l=75)@140	
Glulam Beam reinforced by carbon fiber sheet in bith sides		100×200	1.4×100	Resorcinol	4,000 and 2,000
			2.8×100		4,000
			4.2×100		4,000 and 2,000
Glulam Beam reinforced by carbon fiber sheet in tension side		100×200	1.4×100	Resorcinol	4,000
			2.8×100		
			4.2×100		

*LS: Lugscrew

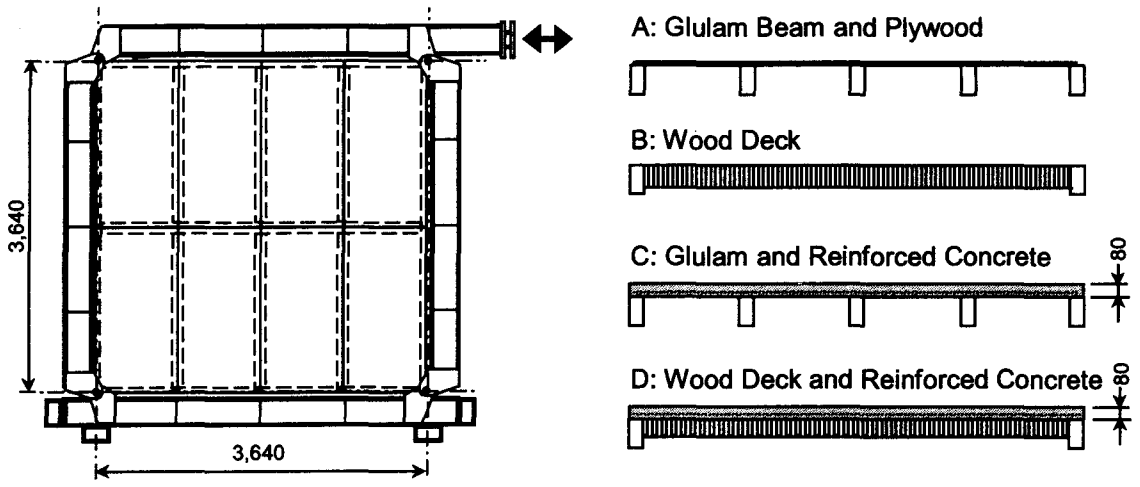

Fig. 3Test plan on floor systems for shear stiffness and strength in plane

a. RC Core & Timber Frame

b. RC Wall & Timber Framec. RC (or Steel) Frame & Timber Frame

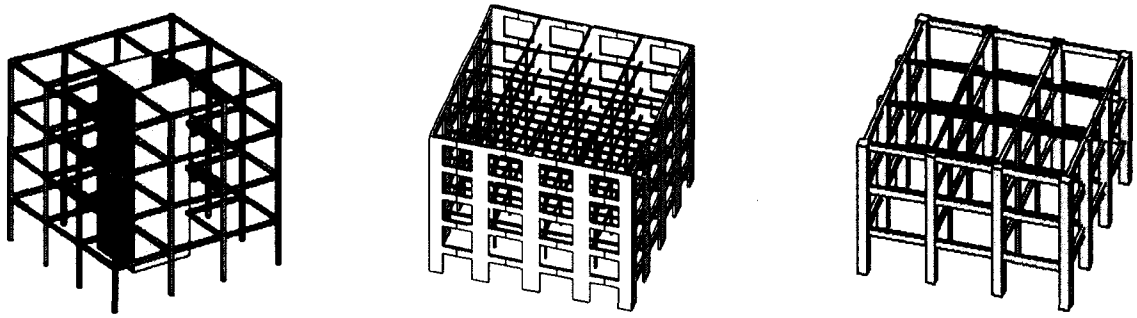

d. RC Wall & Timber Floor and Roof

e. RC Wall & Timber Frame

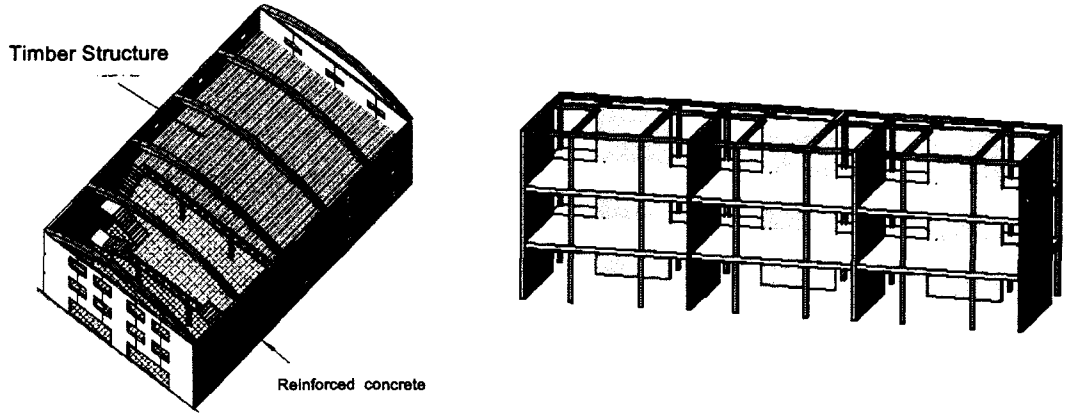

Fig. 4 Conceptual Models of Dual Structural Systems

Modeling Regional Economic Resiliency to Earthquakes: A Computable General Equilibrium Analysis of Lifeline Disruptions

by

Adam Rose and Shu-Yi Liao[1]

ABSTRACT

Business interruption losses from natural hazards and terrorist attacks can be as costly as property damage. They can occur even when no physical damage takes place, as when a business is cut off from one of its utility lifelines. Moreover, such disruptions set off a chain reaction of further production cutbacks among successive rounds of customers and suppliers spreading through the entire regional economy. This paper refines an advanced modeling technique called computable general equilibrium (CGE) analysis to make it suitable for the assessment of the regional economic impacts of lifeline disruptions in the aftermath of a disaster. CGE is the state of the art of regional economic impact analysis but has several weaknesses. We develop a methodology for recalibrating key model parameters in light of empirical data on responses to lifeline disruptions that reflect individual business and regional resiliency. The methodology is applied to analyzing the economic impacts of a disruption to the Portland, Oregon water supply system in the aftermath of an earthquake. Comparison is made between impacts of a business-as-usual scenario and one that reflects the replacement of cast-iron pipe by advanced materials.

KEYWORDS: economic impacts of disasters, business interruption losses, resiliency, computable general equilibrium analysis

1.0 INTRODUCTION

Recent studies indicate that utility lifeline supply disruptions can have significant impacts on regional economic activity in the aftermath of an earthquake, other natural disaster, or terrorist attack (see, e.g., Chang et al., 2000). Even businesses that incur no physical damage are likely to have to curtail their production if they are cut off from their electricity, natural gas, water, or communication links. Moreover, such disruptions will set off a chain reaction of further production cutbacks among successive rounds of customers and suppliers spreading through the entire regional economy. Surveys following the Loma Prieta and Northridge earthquakes, Hurricane Andrew, and the 1993 Midwest floods indicated that business interruption losses stemming directly or indirectly from lifeline failures rivaled property damage in dollar terms (see Webb et al., 2000).

Research on this subject has until now been dominated by the application of input-output (I-O) models, which are linear, rigid and characterized by simplistic responses; and by

[1] The authors are, respectively, Professor and Head, Department of Energy, Environmental, and Mineral Economics, The Pennsylvania State University, University Park, PA 16802; and Economist, Demand Analysis Office, California Energy Commission, Sacramento, CA 95814. The research in this paper was supported by a grant from the National Science Foundation (Grant No. 9802151), and by several grants from the NSF-sponsored Multidisciplinary Center for Earthquake Engineering Research. The authors acknowledge the contribution of Chunsheng Shang, Gauri Guha, Ram Ranjan, and Debo Oladosu for research related to the paper. We are also grateful to Stephanie Chang for providing us with background information on the Portland Bureau of Water Works network and sharing with us results of her analysis study of network vulnerability, direct economic impacts of earthquake disruptions, and maintenance and mitigation costs. Helpful comments on an earlier draft were provided by Ann Fisher. The views expressed in this paper of those of the authors and do not necessarily represent the positions of any sponsoring organization or organizations to which the authors are affiliated. The authors are solely responsible for any errors and omissions.

mathematical programming models, which omit any behavioral responses to prices and markets (see, e.g., Cole, 1995; Rose et al., 1997). Computable general equilibrium (CGE) analysis would appear to be the superior alternative for the next generation of regional economic impact methodologies. It is comprehensive, non-linear, based on individual behavior in response to market prices, and explicitly incorporates a broad range of constraints (see, e.g., Rose, 2002; Rose and Guha, 2002).

One of the few advantages of I-O over CGE modeling is the clear distinction between direct and indirect impacts in the former. Interdependence is even stronger in the CGE framework because of its price-quantity interconnectedness. Thus, CGE results are typically presented in terms of total impacts only and are difficult to decompose. Another shortcoming of CGE models is the lack of data for estimating the many additional key parameters they require, especially elasticities of substitution.

The methodology in this paper provides an alternative to the usual non-survey "adaptation" approach to CGE model parameter estimation. It utilizes primary data on direct economic losses and a sophisticated computational algorithm to recalibrate sectoral production functions in response to a water lifeline service disruption in the aftermath of a major earthquake. It also measures how resiliency improves when mitigation is implemented in the form of replacing old cast-iron pipe with the latest generation of durable materials. Our modeling advances are inspired by the extensive empirical work on business interruption in the aftermath of earthquakes by Tierney (1997), Chang (2001) and others. Our parameter adjustments are linked to specific real world examples of business resiliency (e.g., conservation, use of back-up supplies and equipment, increased substitutability). The approach also enables us to distinguish between direct and indirect losses in a CGE context. This refinement is important because, while each of these adjustments may be capable of reducing the economic shock to the same minimum direct reduction in output, each has different implications for indirect impacts (see, e.g., Rose and Lin, 1995).

2.0 CGE MODEL ADVANTAGES

Computable General Equilibrium (CGE) analysis is the state-of-the-art in regional economic modeling, especially for impact and policy analysis. It is defined as a multi-market simulation model based on the simultaneous optimizing behavior of individual consumers and firms, subject to economic account balances and resource constraints (see, e.g., Shoven and Whalley, 1992). The CGE formulation incorporates many of the best features of other popular model forms, but without many of their limitations (Rose, 1995).

The basic CGE model represents an excellent framework for analyzing natural hazard impacts and policy responses (Boisvert, 1992; Brookshire and McKee, 1992; Rose and Guha, 2002). CGE models can be finely disagggregated to better distinguish the various degrees of vulnerability to hazards across sectors. The production functions are inclusive of all inputs, not just primary factors as in the case of many other economic models, which facilitates identification of materials shortages. At the same time, CGE models allow for the possibility of input substitution, which mimics real world responses beyond the very short run in minimizing hazard impacts. They also allow for the substitution of imported goods for regionally produced goods. CGE models are non-linear in form, thereby more closely reflecting real world conditions, such as economies of scale and non-linear damage functions. CGE models are more capable of analyzing disjoint change than are model forms based on time series data and which therefore simply extrapolate the past. They can also more readily accommodate engineering data or data based on informed judgment.

Another set of CGE model advantages pertains to the important role of prices and markets. Related to this is explicit consideration of behavioral response, and not just simple optimization but also

instances of bounded rationality, applicable to both mitigation and recovery behavior.

Finally, CGE models are superior to some other alternatives in modeling the role of lifelines and infrastructure, which include societal necessities such as electricity, water delivery, transportation, and communication. Many of these services are especially vulnerable because they are provided in linear links so that if one is disrupted, so are all downstream extensions. A CGE model can place a valuation on these services, even for public sector outputs that are typically unpriced. This is more than an academic exercise, because "shadow values" might serve as temporary prices to ration these services through the market rather than by administrative decree (Rose and Benavides, 1999).

3.0 RESPONSES TO HAZARDS IN A CGE CONTEXT

The production side of the CGE model used in this paper is composed of a multi-layered, or multi-tiered, constant elasticity of substitution (CES) production function for each sector. The CES has several advantages over more basic forms such as the Leontief (linear) or Cobb-Douglas (simple multiplicative) functions (see, e.g., Perroni and Rutherford, 1993). It can incorporate a range of input substitution possibilities (not just the zero and unitary values of the aforementioned functions). The multiple tiers allow for the use of different substitution elasticities for different pairs of inputs (the elasticity is constant for a given tier, but elasticities can vary across tiers). The production function is normally applied to aggregate categories of major inputs of capital, labor, energy, and materials, with sub-aggregates possible for each (e.g., the energy aggregate is often decomposed by fuel type—electricity, oil, gas, and coal). Water is usually omitted or incorporated as one of the materials (intermediate goods producing) sectors. We explicitly separate water as a major aggregate in the top tier of the production function so that we can analyze the impacts of a water service disruption. Again, our methodology provides a way of improving the empirical estimates of key elasticities.

3.1 CES Production Function

Our constant elasticity of substitution (CES) production function has the following nested form for five aggregate inputs capital, labor, energy, materials, and water:

$$Y = A_1\left(\alpha_1 A_{1W} W^{-\rho_1} + \beta_1 KLEM^{-\rho_1}\right)^{-\gamma/\rho_1} \quad (1)$$

$$KLEM = A_2\left(\alpha_2 M^{-\rho_2} + \beta_2 KEL^{-\rho_2}\right)^{-\gamma/\rho_2} \quad (2)$$

$$KEL = A_3\left(\alpha_3 L^{-\rho_3} + \beta_3 KE^{-\rho_3}\right)^{-\gamma/\rho_3} \quad (3)$$

$$KE = A_4\left(\alpha_4 K^{-\rho_4} + \beta_4 E^{-\rho_4}\right)^{-\gamma/\rho_4} \quad (4)$$

where:

A_i is the factor-neutral technology parameter, $A_i > 0$

A_W is the water-specific technology parameter

α_i, β_i are the factor shares, $0 \le \alpha_i,\ \beta_i \le 1$

σ_i is constant elasticity of substitution, $\sigma_i = \dfrac{1}{1+\rho_i}$

Y is output

K,L,E,M,W are individual capital, labor, energy, material and water aggregates

$KLEM$ is the capital, labor, energy, and material combination

KEL is the capital, energy and labor combination

KE is the capital and energy combination

The fixed coefficient production function of an I-O model would yield an upper-bound estimate of direct output losses from water input disruption, where the percentage loss of the former would be equal to the percentage loss for the latter. All other types of production functions would yield percentage output losses lower than the percentage decrease in water availability because of substitution possibilities.

We define *individual business resiliency* as the difference between the fixed coefficient (proportional) result and the flexible input (disproportional) result, and which is attributable both to the various response mechanisms related to water services (1st Tier) and inherent in the overall production function with respect to other inputs (Tiers 2-4).

CGE models used for hazard analysis are likely to yield estimates of business disruptions for some if not all sectors of an economy that differ significantly from the direct loss estimates provided by empirical studies. This is because production function parameters are not typically based on solid data, or, even where they are, the data stem from ordinary operating experience rather than from emergency situations. Hence, it is necessary to explicitly incorporate the resiliency responses below into the analysis. This is accomplished here by altering the parameters, and, in one case, the variables in the sectoral production functions of the CGE model.

3.2 Production Responses to Natural Hazards

Below we summarize types of response to natural hazards, linked to the production function tier and parameters to which each relates and to the recovery/reconstruction stage (time period) to which each is applicable (see Rose and Liao, 2002, for the mathematical derivation of the major production function responses). These responses include:

1. Conservation of Water. This response can be implemented immediately and continued through the long-run, i.e., be incorporated into the production process on a permanent basis. One of the silver linings of disasters is that they force businesses to reconsider their use of resources, and often not just at the margin for a single input but also holistically (as noted in item 7 below). The parameter changes for this response in the case of water pertain to the technology trend variable in the first tier of the production function specified above. More generally, in each tier of the production function, the productivity term, A_i, is specified as covering all inputs, i.e., factor neutral. Adjustment of the productivity term for an individual factor, such as the A_{1W} term in equation (1a), biases the productivity improvement in the direction of that factor.

2. Conservation of Other Inputs. This is analogous to water conservation and can be applied to any of the tiers. However, it can often take on more permanence than water conservation, which is a dire necessity in many cases, and it is listed in Table 1 as constant over the applicable period rather than decreasing. Examples would include a reduction in number of trucks or maintenance personnel. One other adjustment option can be thought of as a sub-case—an increase in the use of non-water inventories, though only through the very short run.[2]

3. Increased Substitutability of Other Inputs for Water System Deliveries. This response would be exemplified primarily by purchasing water from other sources (by the bottle or truckload), or by moving to another location where less water is needed.

4. Back-up Supplies. This response is often implemented in the immediate aftermath of an earthquake in the short-run. It includes adjustments that incur costs, such as the digging of wells, and rather costless measures, such as collecting rainfall or using riverine water. The costless alternatives can be modeled in a manner similar to conservation and the cost-incurring ones similar to substitution. The use of water inventories (stored water) is best addressed as discussed above. As with the inventory item discussed above, there is some flexibility in how costs are considered temporally.

5. Water Importance. This response requires more explanation because of the widespread use

[2] Actually, an increase in inventory use may be more like response number 5 below because material is actually used and not saved; however, it is listed here because the purchase has been made in an earlier time period (and will likely be replenished in later one).

of the term "importance" in its broadest sense in the earthquake research literature. Sometimes, it has been used to encompass all of the responses noted in Table 1. In ATC-25 (1991), utility lifeline importance was quantified as the percentage change in a sector's output that would result from a one percent change in input availability. If water were used everywhere in the production process and no resiliency measures were possible, a one percent decrease in water would lead to a one percent decrease in output, or an importance factor of 1.0 (the same as the I-O fixed coefficient production function). The existence of various responses lowers the importance factor, which had a value as low as .30 for the Transportation and Warehouse sector in ATC-25. Here we go to the opposite extreme in the use of the term as the percentage of production activities in a given sector that do not require water to operate. Thus, it refers to the inherent resiliency of a production process in the absence of any explicit adjustment. The presence of this factor is labeled as constant in Table 1; any increase in it over time would mean further technology adjustment and would come under the headings of responses 1 or 7.[3]

6. Time-of-Day Usage. This is a passive response that pertains to hours during which the business is closed, and hence where loss of water has no effect on output (see, e.g., Rose and Lim, 1997, for an example of how this adjustment greatly reduced loss estimates from electricity disruptions in the aftermath of the Northridge Earthquake). It is listed here for the sake of comprehensiveness.[4]

7. Change in Technology. This refers to long run (permanent) changes in the overall process, such as replacing open systems, which do not recycle water, with closed systems. It may require the reformulation of the entire production function.

4.0 PORTLAND ECONOMY AND WATER SYSTEM

4.1. The Portland Water System

The Portland Bureau of Water Works (PBWW) is a rate-financed, City-owned utility that serves 840,000 people in portions of the Portland Metro Area (including businesses responsible for 98% and 72% of sales in Multnomah County and Washington County, respectively). In 1999, PBWW water sales amounted to 39 billion gallons. The largest customers are major manufacturing companies, the Portland City Bureau of Parks and Recreation, and several hospitals.

The PBWW transmission and distribution is comprised of nearly 2000 kilometers of pipelines, 29 pump stations, and 69 major storage tanks. Construction of the PBWW dates back to 1894. About 70% of the system still consists of cast iron pipes, even though the agency began installing ductile iron in the 1960s. Additional information on the PBWW, its maintenance and earthquake mitigation costs, and its earthquake vulnerability can be found in Chang (2001).

4.2 Portland CGE Model

We constructed a CGE model of the portion of Portland Metropolitan Area economy that overlaps with the Portland Bureau of Water Works (PBWW) Service Area. The main data upon which the empirical model is based are the 1998 IMPLAN Social Accounting Matrix (SAM) and Input-Output Table for Multnomah County and Washington County (MIG, 2000). It is divided into several partitions that reveal

[3] Note that ATC-25 assumed that the first 5 percent of lifeline service disruption would not result in any loss of output by customers due to various resiliency measures, such as the others noted in Table 1. Hence, there is some ambiguity about the extent to which the ATC-25 importance factor is intended to be limited just to separable production activities as in the definition in this paper.

[4] In a more extensive model involving dispatch decisions in which water or electricity might be rationed by time of day to shave peak production, this adjustment comes into play for firms that cannot switch production to off-hours.

the structure of the regional economy, including the industry, commodity, factor income, household, government, capital, and trade accounts.

The SAM industry accounts contain 20 sectors, with the Water & Sanitary Services separated from other utility services in order to pinpoint economic impacts of water supply disruptions in the aftermath of an earthquake. The Total Gross Output of the Portland Metro economy in 1998 is $71.2 billion, including $42.1 billion in interindustry transactions and $29.1 billion of total value-added. The total domestic commodity supply and exports of the Portland Metro Area in 1998 are $43.3 billion and $27.9 billion, respectively, implying the region is moderately self-sufficient. This is further evidenced by the trade accounts. The net domestic trading surplus is about $3.4 billion and the net foreign trading deficit is about $5.2 billion. Major features of the Portland CGE model are described in Rose and Liao (2002).

4.3 Model Solution Algorithms

Previous research on the application of CGE models to lifeline disruptions (see, e.g., Rose and Guha, 2001) has made use of the basic nonlinear programming features of the General Algebraic Modeling System (GAMS) software (Brooke et al., 1988). However, GAMS was not able to incorporate the range of substitution elasticity values required. We constructed the Portland CGE model using MPSGE, a subsystem of GAMS that facilitates the formulation and analysis of applied general equilibrium models through complementarity programming (Rutherford, 1995), and which allows for a broader range of parameter values and the inclusion of a broader range of constraints (e.g., sectorally differentiated supply availabilities of lifeline services). Basic elasticity of substitution values in the model were based on a careful synthesis of the literature (see Rose and Guha, 2002). Because we are modeling a very short-run response we further modified all input and trade substitution elasticities (except input elasticities pertaining to water as discussed below) so that they were 10% of their initial values.

The recalibration of the elasticity of substitution (σ_1) between water (W) and the capital, energy, labor, and material aggregate ($KELM$) could only be undertaken with a numerical solution, in this case the numerical bisection method, which is a converging root search routine.[5] Given sectoral water availability and the corresponding output reduction rate, the recalibration involves three iterative steps: First, find a lower bound of σ_1. To obtain an initial unadjusted output reduction rate higher than Chang's estimate for all sectors, 0.05 was used as the lower bound for all sectors. Second, find an upper bound of σ_1. Our initial guess of the upper bound of σ_1 was 0.15, which yielded a corresponding output reduction rate lower than Chang's estimate for all sectors. Third, calculate the arithmetic average of the lower and upper bounds of σ_1 and its corresponding output reduction rate. If the output reduction rate is higher (lower) than the direct output loss estimate, then the arithmetic average can be used as the new lower (upper) bound of σ_1 for the next iteration. The iterative procedure is continued until the deviation between the calculated output reduction rate and the empirical direct loss estimate is less than 0.01%. In our model, the routine converged to the recalibrated σ_1 in less than 10 iterations for each sector.

The computational procedure we have developed to improve model accuracy also generates an additional dividend of enabling us to decompose loss estimates. Our estimation of indirect losses involves the following procedure:

1. Extract the sectoral production functions from the CGE model and adjust parameters and variables in them one at a time to match empirical direct loss estimates.

2. Reinsert the recalibrated sectoral production functions into the CGE model, reduce input

[5] Other parameters, such as A_W, can be solved analytically (see Rose and Liao, 2002).

supply to a level consistent with empirical estimates, and compute total regional losses.

3. Subtract direct losses from total losses to determine indirect losses.

5.0. SIMULATING THE RESPONSE TO NATURAL HAZARDS

5.1 Earthquake Parameters

The Portland Area is characterized by moderate seismic activity stemming from the ocean floor Cascadian Subduction Zone and a series of shallow crustal faults. Two damaging earthquakes have taken place in the past 40 years measuring M5.5 and M5.6. However, large subduction earthquakes as great as M9.0 have taken place as recently as 1700 (see Wong et al., 2000).

Although PBWW service has not been disrupted by earthquakes, a recent study by EQE (1999) found that operators of the system consider it vulnerable. The study also identified mitigation measures that might help meet the System's safety performance standards desired by stakeholders.

Chang (2001) simulated the effects of three alternative mitigation measures (no action, cast-iron pipe replacement, and tank/pump upgrade). The analysis was undertaken in the context of a life-cycle cost model that factored in not only the cost of mitigation over time and its ability to reduce system vulnerability through the year 2050, but also the savings of ordinary maintenance costs. In the analysis below, we will confine our attention to the Year 2000. Also, we will focus on the direct and indirect effects of system disruptions before and after mitigation (through cast-iron pipe replacement by the latest generation of advanced materials) and will leave to another paper our analysis of the regional impacts of implementing the mitigation measures.[6]

[6] Chang (2001) estimates the cost of tank pump upgrades as only $2.1 million, but that of pipe replacement as $380 million.

5.2 Empirical Measurement of Resiliency

Chang (2001) performed simulations for alternative combinations of earthquake types, calendar years, and mitigation options, using several sophisticated geological and engineering models. Each case was subject to 100 Monte Carlo simulations. These simulations were used to estimate direct losses in sectoral output, factoring in resiliency. Based on the work by ATC (1991) and Tierney (1997), resiliency is defined by Chang as "the remaining percentage of output that an industry can still produce in the event of total water outage." Sectoral resiliency measures range from a low of 21 percent for Health Services to a high of 49 percent for Transportation and for Communications and Utilities. Note that the definition of resiliency we provided above is a generalization of Chang's definition to cases where the water outage is not a total one. Note also that the ATC definition assumes a linear relationship, but that non-linear relationships are likely to be more realistic. Our analysis below can be used to estimate non-linear relationships between water service disruptions and output reduction and hence represents a non-linear measure of resiliency.

6.0 WATER DISRUPTION SIMULATION RESULTS

Simulations were conducted of the regional economic impact of an earthquake-induced water supply disruption in the Portland Metro Area. The analysis is based on the simulation of the systems analysis of the Portland water utility system and the direct loss estimation simulations of Chang (2001) described above. Although Chang's engineering vulnerability and direct loss simulations involve many scenarios relating to alternative earthquake magnitudes, outage durations, and resiliency responses, this paper focuses on a subset of scenarios characterized by:

1. One earthquake type (Bolton crustal fault) of magnitude 6.1.
2. Impacts in the Year 2000.
3. Scenarios for Business as Usual (No Mitigation) and Cast-Iron Pipe Replacement.
4. Outages of varying lengths from 3 to 9 weeks.
5. Resiliency responses involving only the substitution of other inputs for water services.

We focused on the first characteristic because it represented the "most likely" case and characteristics 2-4 to keep the number of simulations manageable. We confined ourselves to the characteristic 5 because we have not yet fully developed the methodology to implement changes in other parameters.

Note, one other important dimension of our simulations, which relates to pricing of water delivery. Ordinarily, CGE simulations allow prices to fluctuate freely in response to changing supply and demand conditions. However, two features of this situation warrant simulations with fixed water prices. The first is the fact that businesses often resist raising their prices in the aftermath of a natural disaster for reasons of altruistic community concern and to avoid the image of price gouging. Second, the PBWW is not a typical enterprise with fluctuating prices but rather one in which rates are adjusted only periodically in the context of open public hearings.

6.1. No Pre-Event Mitigation; Post-Event Water Substitution

The results of our simulations for the Business as Usual Scenario (no mitigation) are presented in Table 1. Note that the duration of this outage is projected to be 4 weeks, but the table summarizes the situation for the maximum disruption, which takes place during the first week. Results for the total outage period are summarized more briefly below.

The sector labels on the left-hand side of Table 1 refer to the economic producing units of the Portland CGE model, and direct water disruption for each sector is presented in column 2. In 2000, for example, unmitigated sectoral water disruptions sum to a 50.5 percent. As discussed further below, negative indirect effects on sectors such as Construction are so great as to reduce water demand significantly below the post-earthquake availability levels. Baseline output is presented in Column 3 and reflects the relative prominence of sectors in Portland Metro economy; it also serves as a reference point for our impact simulations. Note that the Water sector (11) gross output represents only 0.44 percent of the regional economy.

Column 4 of Table 1 presents the direct output losses equaling 49.1 percent that are estimated in our model before any resiliency adjustment. Chang's estimates of direct output losses amounting to only 33.7 percent, which incorporate the extent of resiliency, are presented in Column 5.[7] Our direct loss estimates are based on input substitution elasticities of 0.05 presented in the next to the last column in Table 1. Note that our direct loss estimates exceed those of Chang in every sector because ours omit all resiliency options except normal input substitution (and at very low levels). The final column shows the elasticities necessary to incorporate resiliency measures for our model results to be consistent with the Chang estimates (these range from a low increase of 36 percent in Sector 18 to a high increase of 130 percent in Sector 11 itself).

Our estimates of the indirect and total regional economic impacts of the water lifeline disruption are presented in Columns 7 and 8. Overall, they yield a 10.7 percent indirect reduction in regional gross output and a 44.4 percent total reduction in regional gross output

[7] One measure of resiliency would be the extent to which the actual direct output reduction deviated from the likely (fixed-coefficient) maximum, which is equivalent to the percentage water input disruption. The measure would be 33.3 percent in this scenario [(50.5-33.7) ÷ 50.5].

for the week. The former represents $586 million and the latter $2,431 million. Chang (2001) assumes that restoration takes place in a straight-line manner, so the total loss in economic output for the Region is estimated to be $4,862 million. Moreover, for an actual earthquake, damage to other utilities and buildings would likely lead to losses much greater than this, though care needs to be taken to avoid double-counting losses to the same business from several sources (see Chang et al., 1996).

Some interesting aspects of general equilibrium (indirect) losses for the first case are indicated by Table 1. First, they are only about 32 percent the size of direct losses. In the context of an input-output model, this would be a multiplier of only about 1.32. The Portland Metro economy-wide output multiplier is significantly larger than this, but the CGE model incorporates many other factors that mute the uni-directional and linear nature of the pure interdependence effect of the I-O model. For example, it is able to capture price changes for intermediate goods from cost and demand pressures, various substitutions aside from those relating to water, and various income, substitution and spending considerations on the consumer side. The sector suffering the largest indirect decline is Construction (a leading indicator of economic activity); however, if post-earthquake recovery and reconstruction were to be factored in, the Construction decline would be offset significantly. In addition, several sectors are characterized by positive or minimally negative indirect effects, most notably basic necessities, such as Food Processing and Health Services.

6.2 Pre-Event Pipe Replacement and Post-Event Water Substitution

The results of the scenario of an M6.1 crustal fault earthquake but with cast-iron pipe replacement are presented in Table 2. We realize this scenario is somewhat unrealistic because it accelerates the replacement of cast-iron pipes at an unrealistic pace but believe this provides a useful illustration of the potential advantages of mitigation. Note also that the results represent a lower bound of the gains in this type of mitigation in future years, since pipe replacement would be even more valuable as the current system deteriorates, thereby incurring increasingly higher ordinary maintenance cost and likely greater earthquake vulnerability.

In this second Scenario, the direct water outage is reduced from 50.5 percent to 31.0 percent (see column 2 of Table 2). Our initial estimates of direct output losses are 30.7 percent, compared to Chang's empirical estimates of 21.3 percent.[8] The substitution elasticity adjustments needed for the model to replicate the Chang direct loss estimates are presented in the final column of Table 2. They are lower than the corresponding water input changes in each sector because the direct output losses are projected to be lower in each.

Interestingly, our estimate of general equilibrium ("indirect") losses in Scenario 2 is 11.2 percent, which is a 52.6 percent greater than direct losses. Moreover, not only is the percentage increase over direct losses higher in Scenario 2 than in Scenario 1 but the absolute level is as well. The latter is quite surprising at first glance. It would seem to be an impossibility, for example, in the context of an I-O model (where multiplier values are the same at all scales). However, our CGE model is non-linear. Secondly, we should not forget that we have changed parameters (with respect to water substitution), so even in an I-O context multipliers would differ (though only slightly given the small size of our parameter changes, which would correspond to the coefficient

[8] The resiliency index defined in endnote 7 is 31.3 percent in this case. Resiliency would seem to decrease from the 33.3 percent of Scenario 1, but this is likely due to the fact that resiliency opportunities decrease as the size of the disruption decreases (and vice versa, though some threshold may exist for especially large disruptions that overwhelm the resiliency capabilities). Note also that mitigation effectiveness, with respect to the difference in direct water losses between the two scenarios, could be measured by a similar index and would equal 38.6 percent [(50.5-31) ÷ 50.5].

changes that would be utilized in an I-O model). The major explanation of the relatively higher percentage of general equilibrium effects in Scenario 2 is due to the difference in the sectoral mix of direct water disruptions in relation to Scenario 1. This changes relative prices, and the model, despite its relatively low substitution elasticities, is quite responsive. For example, sectors 3, 5, and 7 all incur indirect effects greater than direct ones, and these sectors, as well as 6, 12, 16, and 20, incur greater indirect losses in Scenario 2 than in Scenario 1, despite lower direct losses in the former.

Overall, Scenario 2 is estimated to incur a 32.5 percent loss in gross output in the Portland Metro economy in the Year 2000 during the first week of water service disruption. In dollar terms, this translates into $1,800 million. Chang (2001) estimates the system can be restored to full service within three weeks in this case, so, again assuming a linear restoration path, total output loss is $2,700 million, for an overall reduction from business as usual of 44.5 percent. We now decompose this improvement into its various constituents. The greatest contribution of cast-iron pipe mitigation is the reduction in restoration (-24.4 of the -44.5 percent) time, followed closely by the decrease in direct losses (-21 percent). Indirect losses (0.8 percent) are beyond the control of policymakers, and, although they undercut the effectiveness of this mitigation alternative in this case, their influence is minimal. Moreover, in most cases they are likely to be reinforcing.[9]

7.0. CONCLUSION

This paper has presented major methodological advances in computable general equilibrium modeling for application to estimating the regional economic impacts of earthquakes and other disasters. First, we have provided an operational methodology for recalibrating model parameters in light of empirical estimates of production losses due to a lifeline supply disruption. Second, the methodology enables the analyst to decompose loss estimates into direct and indirect components. Our application to a disruption of water services of the Portland Metro economy showed that indirect economic losses can vary substantially according to the overall level and sectoral mix of water shortages.

Overall, our results appear to be reasonable for the economy as a whole, for individual sectors, and for individual impact stages (direct and indirect). We have, however, modeled only one resiliency measure, albeit one of the most important ones—increased substitutability of other inputs for water utility services. As discussed earlier, different types of resiliency responses would generate different types of indirect impacts. However, only a full simulation will provide a definitive conclusion.

[9] Note that we also simulated cases (not shown) in which water prices were allowed to fluctuate in response to changing conditions of supply and demand. Interestingly, despite a 33 percent increase in water prices in this variant of Scenario 2 the overall results were similar, though indirect effect losses did decrease from 11.2 percent to 10.5 percent, or lower than the 10.7 percent of the Business as Usual Scenario. The reason for this improvement is that resources are allocated more efficiently when prices are not fixed, though the price increase will be especially burdensome to marginal businesses and low income consumers. This points out one of the important equity-efficiency tradeoffs in the mitigation of natural hazards impacts. Mitigation is often just associated with pre-event activities, but it also pertains to post-earthquake responses, such as reducing restoration times or modifying pricing, both of which can have the effect of reducing overall losses or losses to various stakeholders (see also Rose et al., 1997; Shinozuka et al., 1998).

8.0 REFERENCES

Applied Technology Council (ATC). 1991. Seismic Vulnerability and Impact of Disruption of Lifelines in the Conterminous United States, Report ATC-25. Redwood City, CA: ATC.

Boisvert R. 1992. Indirect losses from a catastrophic earthquake and the local, regional, and national interest, in Indirect Economic Consequences of a Catastrophic Earthquake, Washington, DC: FEMA0.

Brooke A., Kendrick D, Meeraus A. 1988. GAMS: A User's Guide. South San Francisco, CA: The Scientific Press.

Brookshire D, McKee M. 1992. Other indirect costs and losses from earthquakes: issues and estimation," in Indirect Economic Consequences of a Catastrophic Earthquake, Washington, DC: FEMA.

Chang S. 2001. Evaluating social benefits of disaster mitigation, Department of Geography, University of Washington, Seattle, WA.

Chang S, Seligson H, Eguchi R. 1996. Estimation of the economic impact of multiple lifeline disruption: Memphis Light, Gas, and Water Case Study, Buffalo, NY: National Center for Earthquake Engineering Research.

Chang S, Rose A, Shinozuka M, Svekla W, Tierney K. 2000. Modeling earthquake impacts on urban lifeline systems: advances in integration, in Research Progress and Accomplishments, 1999-2000, Buffalo, NY: Multidisciplinary Center for Earthquake Engineering Research.

Cochrane H, et al. 1997. Indirect economic losses, in Development of Standardized Earthquake Loss Estimation Methodology Vol. II, Menlo Park, CA: RMS, Inc.

Cole S. 1995. Lifelines and livelihood: a social accounting matrix approach to calamity preparedness, Journal of Contingencies and Crisis Management 3: 1-11.

French S. 1998. Spatial analysis techniques for linking physical damage to economic functions and Shinozuka M, Rose A, Eguchi R (eds.), Engineering and Socioeconomic Impacts of Earthquakes: An Analysis of Electricity Lifeline Disruptions in the New Madrid Area, Buffalo, NY: MCEER.

(MIG) Minnesota IMPLAN Group. 2000. Impact Analysis for Planning System (IMPLAN), Stillwater, MN.

Perroni C, Rutherford T. 1993. Regular flexibility of nested ces functions, European Economic Review 39: 335-43.

Prywes M. 1986. A nested ces approach to capital-energy substitution, Energy Economics 8: 22-28.

Rose A. 1995. Input-output economics and computable general equilibrium models, Structural Change and Economic Dynamics 6: 295-304.

Rose A. 2002. Model validation in estimating higher-order economic losses from natural hazards, in Taylor C, VanMarcke E (eds.) Acceptable Risk to Lifeline Systems from Natural Hazard Threats, New York: American Society of Civil Engineers.

Rose A, Benavides J. 1999. Optimal allocation of electricity after major earthquakes: market mechanisms versus rationing, in Lawrence K (ed.) Advances in Mathematical Programming and Financial Planning, Greenwich, CT: JAI Press.

Rose A, Guha G. 2002. Computable general equilibrium modeling of electric utility lifeline losses from earthquakes, Forthcoming in Chang S, Okuyama Y (eds.), Modeling the Spatial Economic Impacts of Natural Hazards Heidelberg: Springer

Rose A, Liao S. 2002. Modeling regional economic resiliency to earthquakes: a computable general equilibrium analysis of

lifeline disruptions, Department of Energy, Environmental, and Mineral Economics, The Pennsylvania State University, University Park, PA.

Rose A, Lin S. 1995. Regrets or no regrets—that is the question: is conservation a costless CO_2 mitigation strategy? Energy Journal 16: 67-87.

Rose A, Benavides J, Chang S, Szczesniak P, Lim D. 1997. The regional economic impact of an earthquake: direct and indirect effects of electricity lifeline disruptions, Journal of Regional Science 37: 437-58.

Rose A, Liao S, Ranjan R, Guha G. 2001. Estimating economic losses from earthquakes: a computable general equilibrium analysis of the effects of electric utility lifeline losses, Department of Energy, Environmental, and Mineral Economics, The Pennsylvania State University, University Park, PA.

Rutherford T. 1995. Computable general equilibrium modeling with MPSGE as a GAMS subsystem: an overview of the modeling framework and syntax, http://www.gams.com/solbers/mpsge/syntax.htm.

Shinozuka M, Rose A, Eguchi R/ (eds.). 1998. Engineering and Socioeconomic Impacts of Earthquakes, Buffalo, NY: Multidisciplinary Center for Earthquake Engineering Research.

Shoven J, Whalley J. 1992. Applying General Equilibrium, New York: Cambridge University Press.

Tierney K. 1997. Impacts of recent disasters on businesses: the 1993 midwest floods and the 1994 northridge earthquake, in Jones B (ed.), Economic Consequences of Earthquakes: Preparing for the Unexpected, Buffalo, NY: National Center for Earthquake Engineering Research.

Webb G, Tierney K, Dahlhamer J. 2000. Businesses and disasters: empirical patterns and unanswered questions, Natural Hazards Review 1: 83-90.

Wong I, et al. 2000. Earthquake scenarios and probabilistic ground shaking maps for the Portland, Oregon, Metropolitan Area, Interpretative Maps Series IMS-16, State of Oregon, Department of Geology and Mineral Industries, Portland, OR.

TABLE 1. ECONOMIC IMPACTS OF WATER SERVICE DISRUPTIONS IN THE PORTLAND METRO AREA, 2000: NO MITIGATION
(fixed water service price)

Sector	Water Input			Output	Output Change From Water Outage				Elasticity (σ)	
	Baseline (million $)	Direct Disruption	Total Unused	Baseline (million $)	Our Direct w/o Adjust[a]	Chang's Direct	Indirect	Total[b]	Without Adjustment	With Adjustment
1. Agriculture	0.9	-48.0%	-48.4%	297.4	-46.0%	-33.7%	-1.8%	-35.5%	0.050	0.074
2. Mining	0.0	-48.6%	-48.9%	57.7	-46.7%	-26.5%	-11.5%	-38.0%	0.050	0.078
3. Construction	8.4	-51.5%	-60.0%	5160.4	-49.5%	-27.8%	-31.1%	-59.0%	0.050	0.089
4. Food Products	3.1	-49.9%	-50.0%	1862.7	-48.0%	-33.5%	1.8%	-31.7%	0.050	0.077
5. Manufacturing	27.8	-54.5%	-59.1%	16509.7	-52.5%	-36.2%	-21.7%	-57.9%	0.050	0.083
6. Petroleum	0.4	-54.5%	-54.8%	127.7	-52.5%	-36.2%	-16.7%	-52.9%	0.050	0.083
7. Transportation	27.8	-47.8%	-48.0%	3210.3	-45.9%	-24.3%	-20.7%	-45.0%	0.050	0.098
8. Communication	1.2	-48.0%	-48.5%	1453.1	-46.1%	-25.0%	-8.1%	-33.0%	0.050	0.083
9. Electric Utilities	2.4	-48.0%	-48.1%	1992.8	-46.1%	-25.0%	-4.8%	-29.7%	0.050	0.085
10. Gas Distribution	0.1	-48.0%	-48.5%	570.7	-46.1%	-25.0%	-0.5%	-25.5%	0.050	0.078
11. Water & Sanitary Services	4.9	-48.0%	-53.5%	315.4	-46.2%	-25.0%	-13.5%	-38.5%	0.050	0.115
12. Wholesale Trade	12.3	-51.8%	-51.9%	7122.6	-49.8%	-33.1%	-13.3%	-46.4%	0.050	0.083
13. Retail Trade	14.1	-50.9%	-50.9%	4994.2	-48.9%	-36.1%	2.7%	-33.4%	0.050	0.078
14. F.I.R.E.	32.5	-48.9%	-49.0%	10158.0	-46.9%	-36.4%	2.4%	-33.9%	0.050	0.073
15. Personal Services	9.1	-50.9%	-50.9%	1521.1	-48.9%	-35.0%	-0.3%	-35.4%	0.050	0.082
16. Business & Prof. Services	13.7	-51.2%	-50.9%	7971.4	-49.2%	-34.6%	-8.0%	-42.6%	0.050	0.078
17. Entertainment Services	1.5	-50.0%	-50.3%	459.6	-48.0%	-34.6%	-1.1%	-35.7%	0.050	0.077
18. Health Services	7.5	-52.7%	-52.9%	3006.9	-50.7%	-42.5%	12.2%	-30.2%	0.050	0.068
19. Education Services	0.8	-51.9%	-51.9%	587.3	-49.9%	-36.3%	4.0%	-32.3%	0.050	0.075
20. Other Services	9.6	-49.3%	-49.3%	3981.2	-47.4%	-34.0%	-10.3%	-44.3%	0.050	0.077
Total	178.2	-50.5%	-51.0%	71188.9	-49.1%	-33.7%	-10.7%	-44.4%		

[a]From partial equilibrium analysis.
[b]Following CGE simulation.

TABLE 2. ECONOMIC IMPACTS OF WATER SERVICE DISRUPTIONS IN THE PORTLAND METRO AREA, 2000: PIPE REPLACEMENT
(fixed water service price)

Sector	Water Input			Output	Output Change From Water Outage				Elasticity(σ)	
	Baseline (million $)	Direct Disruption	Total Unused	Baseline (million $)	Our Direct w/o Adjust[a]	Chang's Direct	Indirect	Total[b]	Without Adjustment	With Adjustment
1. Agriculture	0.9	-30.9%	-30.8%	297.4	-29.5%	-21.4%	2.2%	-19.1%	0.050	0.064
2. Mining	0.0	-30.2%	-37.1%	57.7	-28.8%	-16.4%	-3.5%	-19.9%	0.050	0.065
3. Construction	8.4	-32.7%	-52.1%	5160.4	-31.2%	-17.8%	-36.9%	-54.6%	0.050	0.071
4. Food Products	3.1	-30.2%	-30.1%	1862.7	-28.8%	-20.5%	8.6%	-11.9%	0.050	0.063
5. Manufacturing	27.8	-35.3%	-52.0%	16509.7	-33.7%	-23.8%	-27.6%	-51.3%	0.050	0.067
6. Petroleum	0.4	-35.3%	-45.2%	127.7	-33.7%	-23.8%	-21.4%	-45.1%	0.050	0.067
7. Transportation	27.8	-24.5%	-32.1%	3210.3	-23.3%	-13.4%	-19.8%	-33.2%	0.050	0.070
8. Communication	1.2	-28.3%	-28.0%	1453.1	-27.0%	-14.8%	-2.8%	-17.6%	0.050	0.066
9. Electric Utilities	2.4	-28.3%	-29.0%	1992.8	-27.0%	-14.8%	2.1%	-12.7%	0.050	0.068
10. Gas Distribution	0.1	-28.3%	-28.3%	570.7	-27.0%	-14.8%	7.1%	-7.7%	0.050	0.064
11. Water & Sanitary Services	4.9	-28.3%	-44.2%	315.4	-27.1%	-14.8%	-5.0%	-19.8%	0.050	0.086
12. Wholesale Trade	12.3	-31.9%	-38.0%	7122.6	-30.4%	-20.7%	-16.4%	-37.1%	0.050	0.066
13. Retail Trade	14.1	-33.5%	-33.9%	4994.2	-32.0%	-23.5%	6.7%	-16.8%	0.050	0.066
14. F.I.R.E.	32.5	-29.8%	-30.0%	10158.0	-28.4%	-22.2%	5.4%	-16.7%	0.050	0.062
15. Personal Services	9.1	-32.4%	-31.9%	1521.1	-31.0%	-22.3%	3.6%	-18.7%	0.050	0.067
16. Business & Prof. Services	13.7	-32.0%	-31.9%	7971.4	-30.5%	-21.8%	-8.2%	-30.0%	0.050	0.064
17. Entertainment Services	1.5	-31.6%	-31.8%	459.6	-30.1%	-21.8%	2.8%	-18.9%	0.050	0.065
18. Health Services	7.5	-34.9%	-34.8%	3006.9	-33.3%	-28.0%	18.9%	-9.2%	0.050	0.060
19. Education Services	0.8	-35.0%	-35.1%	587.3	-33.4%	-24.1%	12.8%	-11.3%	0.050	0.065
20. Other Services	9.6	-30.7%	-33.4%	3981.2	-29.3%	-21.1%	-14.4%	-35.5%	0.050	0.064
Total	178.2	-31.0%	-36.5%	71188.9	-30.7%	-21.3%	-11.2%	-32.5%		

[a]From partial equilibrium analysis.
[b]Following CGE simulation.

SESSION 3

WIND ENGINEERING

Aerodynamic Stability of a Super Long-Span Bridge with Slotted Box Girder

by

Hiroshi Sato[1], Nobuyuki Hirahara[2], Koichiro Fumoto[3], Shigeru Hirano[4] and Shigeki Kusuhara[5]

ABSTRACT

Aerodynamic stability is one of the most important themes in the design of super long-span bridges. In order to improve the aerodynamic stability, various researches were conducted and it was confirmed that slotted box girder with some devices shows the good aerodynamic stability. In this paper, the results of full aeroelastic model test and flutter analysis for a generic super long-span bridge, whose main span is 2.8km, are described. And it was confirmed that slotted box girder was applicable for the super long-span bridge from the reason that it is excellent in economical efficiency and aerodynamic stability.

KEYWORDS: aerodynamic stability; super long-span bridge; flutter analysis; full aeroelastic model; slotted box girder

1. INTRODUCTION

There are several plans or ideas of strait crossing road projects in Japan. In these projects, super long-span bridges longer than the Akashi Kaikyo Bridge may be included. In the design of such super long-span bridges, aerodynamic stability is one of the most important themes. Furthermore, reduction of construction cost is also required. Therefore, Independent Administrative Institution Public Works Research Institute (IAIPWRI) and Honshu-Shikoku Bridge Authority (HSBA) have been conducting cooperative study on super structure of super long-span bridges that have good aerodynamic stability and economical efficiency.

In the previous studies [1][2] by the authors, it was found that a slotted box girder with some devices has good aerodynamic characteristics. Therefore, the slotted box girder was applied to a generic super long-span bridge, and full aeroelastic model test was conducted. And the result was compared with 3-dimensional flutter analysis.

In this paper, main results of the previous study on the slotted box girders are outlined first. Then the results of full aeroelastic model test and flutter analysis for a generic super long-span bridge, whose main span is 2.8km, are described.

2. FLUTTER CHARACTERISTICS OF SLOTTED BOX GIRDERS [1]

The effect of location and size of slot on aerodynamic characteristics was examined through section model wind tunnel tests. Reduced mass μ (=m/(ρ B^2), m: mass per unit

[1]Director, Structures Research Group, Public Works Research Institute, Independent Administrative Institution

[2]Manager, Maintenance Planning Division, Maintenance Department, Honshu-Shikoku Bridge Authority (Formerly, Leader of Bridge Structure Research Team, Structures Research Group, ditto)

[3]Senior Research Engineer, Bridge Structure Research Team, ditto

[4]Director, Tarumi Maintenance Work Office, The 1st Maintenance Bureau, Honshu-Shikoku Bridge Authority (Formerly, Manager, Engineering Management Division, Long-span Bridge Engineering Center, HSBA)

[5]Deputy Manager, Engineering Management Division, ditto

length, ρ : air density, B: girder width), reduced polar moment of inertia ν (=I/(ρ B^4), I: polar

moment of inertia per unit length), and natural frequency ratio ε (=f_θ/fz, f_θ: torsional natural frequency, fz: vertical bending natural frequency) were 16, 2.1, and 2.1, respectively. The cross section of the model is shown in Fig.1. From the test results, it was found that the slot at the center increased the flutter onset wind speed. It was also found that the flutter onset wind speed was increased with the width of slot at the center of the girder (Fig.2).

In order to understand the effect of slot at the center of girder, preliminary analysis was conducted for slotted plate. For the analysis, aerodynamic forces acting on each plate was calculated using the Theodorsen's function. The aerodynamic interference between the 2 boxes was neglected. Using these aerodynamic forces, two degree-of-freedom flutter analysis was conducted by U-g method. The result of the flutter analysis (Fig.2) indicated that the flutter onset wind speed increased with size of slot. The differences between the analysis and the experiment seemed to be caused by aerodynamic interference between the 2 boxes.

Although wide slot at the center of the girder improves flutter characteristics, narrower slot would be preferable from the viewpoint of construction cost of towers and foundations. To improve aerodynamic characteristics, the effect of some devices was studied by section model tests. The tested devices are illustrated in Fig.3. The results showed that the center barrier and guide vanes improved flutter characteristics very well (Fig.4). However, the flutter speed was not so high when angle of attack was -3 deg. It was found that the guard rails at the bottom deck increased the flutter speed considerably at this angle of attack (Fig.5).

3. UNSTEADY AERODYNAMIC FORCES OF SLOTTED BOX GIRDERS [2]

From the above studies, it was found that slotted plates and slotted box girders have better flutter characteristics than single plates and single box girders. It was also found that the devices such as center barrier and guide vanes are effective to improve flutter characteristics of slotted box girders.

In order to understand causes of flutter characteristics of slotted plates and box girders more precisely, unsteady aerodynamic forces were measured for three models: model A (single box girder, b=0 in Fig.1), model B (slotted box girder, b=0.22B in Fig.1) and model C (slotted box girder with devices, Fig.3). The measurement was made by forced oscillation method with angle of attack 0 degree. Coefficients of the unsteady aerodynamic forces were defined as follows:

$$L=\pi\rho\{B^2[L_{ZR}\omega^2 z+L_{ZI}\omega z']+B^3[L_{\theta R}\omega^2\theta+L_{\theta I}\omega\theta']\} \quad (1.1)$$

$$M=\pi\rho\{B^3[M_{ZR}\omega^2 z+M_{ZI}\omega z']+B^4[M_{\theta R}\omega^2\theta+M_{\theta I}\omega\theta']\} \quad (1.2)$$

where, L: lift (upward positive), M: aerodynamic moment (head up positive), z: vertical displacement (upward positive), θ : torsional displacement (head up positive), ω: circular frequency, ( )': d( )/dt, L_{xx} or M_{xx}: coefficients of unsteady aerodynamic forces ($_Z$: caused by vertical vibration, $_\theta$: caused by torsional vibration, $_R$: in phase with displacement, $_I$: in phase with velocity).

In general, it is difficult to predict coupled flutter characteristics directly from these coefficients. For 2-degrees of freedom system, Nakamura [3] showed approximate relationship between unsteady aerodynamic coefficients M_{ZI}, $M_{\theta I}$, $L_{\theta R}$ and $M_{\theta R}$ and some flutter properties as follows:

$$\delta a \fallingdotseq -\pi^2 M_{ZI} X/\nu - \pi^2 M_{\theta I}/\nu \quad (2.1)$$

$$X \equiv z_0/\theta_0/B \fallingdotseq \pi L_{\theta R}/(-1+(f_Z/f_\theta)^2\sigma^2)/\mu \quad (2.2)$$

$$\sigma^2 \equiv (f_\theta/f)^2 \fallingdotseq 1+\pi M_{\theta R}/\nu \quad (2.3)$$

where, δ a: aerodynamic damping in logarithmic decrement.

If onset of flutter is defined as $\delta a \leqq 0$, simpler condition for onset of flutter can be derived from (2.1)-(2.3) as follows:

$$\alpha M_{ZI} L_{\theta R}/M_{\theta I} + \beta M_{\theta R} \geqq 1 \qquad (3.1)$$

$$\alpha \equiv (\varepsilon^2/(\varepsilon^2-1))(\pi/\mu) \qquad (3.2)$$

$$\beta \equiv (1/(\varepsilon^2-1))(\pi/\nu) \qquad (3.3)$$

The left hand side of inequality (3.1) was calculated for the Models A, B and C using measured unsteady aerodynamic forces, as well as for single plate and slotted plate using the Theodorsen's function. ε, μ and ν were assumed as 2.0, 15 and 2.0, respectively. The results are shown in Fig.6. The slotted box girders and slotted plate show higher flutter speed than the single box girder or single plate. Since the first term of the left hand side of inequality (3.1) is much larger than the second term, it can be said that this higher flutter speed was caused mainly by the property of $M_{ZI} L_{\theta R}/M_{\theta I}$.

In Fig.6, reduced flutter speed U/(fB) of slotted box girder with devices is almost identical with that of slotted box girder. In Fig.7, the results are plotted with $f_\theta B/U$. Flutter speed of slotted box girder with devices is higher than that without devices. It means that the effect of devices came from small value of $M_{\theta R}$, which affected apparent frequency in wind as was shown in Equation (2.3).

4. WIND TUNNEL STUDY WITH A FULL AEROELASTIC MODEL

4.1 Full aeroelastic model

A suspension bridge, whose main span length is 2,800m and total length is 5,000m (Fig.8), was assumed as a prototype bridge of this study. The cross section of stiffening girder is shown in Fig.9. This box girder has 4-lanes, whose 2-lanes are on the grating installed on the slot in consideration of economical efficiency.

Wind tunnel test was conducted at the large boundary wind tunnel facility in Tsukuba. It was built in 1991 as one of the cooperative efforts between PWRI and HSBA in order to verify the aerodynamic stability of super long-span bridge such as the Akashi Kaikyo Bridge, and to establish the wind resistant design method for super long-span bridges considering 3-dimentional effects of structure and flow. The test section of this wind tunnel is 41m wide, 4m high and 30m long, and maximum wind speed is 12m/s. It is one of the largest boundary layer wind tunnels in the world.

The scale ratio of a full aeroelastic model of the assumed super long-span bridge was 1/125. Structural dimensions of the bridge and the model are shown in Table 1.

4.2 Wind tunnel test results for the full aeroelastic model

Static deformation by wind load is shown in Fig.10 and Photo 1. Large horizontal deformation (leeward side) and large torsional deformation (head down) were measured at the center of main span.

Logarithmic decrement at each wind speed is shown in Fig.11. It increased gradually with wind speed, and began decreasing at wind speed of about 6m/s. After that, logarithmic decrement decreased, and changed to negative value at 8.8m/s, and flutter started. According to the similarity law of Froude's number, flutter speed for the assumed bridge would be about 100m/s.

5. FLUTTER ANALYSIS FOR THE FULL AEROELASTIC MODEL

3-dimensional flutter analysis for the full aeroelastic model was conducted by using the measured unsteady aerodynamic forces. The analytical method was the same as the one that was used for the Akashi Kaikyo Bridge [4]. The conditions of 3-dimensional flutter analysis are shown in Table 2. In the analysis, static deformation was calculated first, then unsteady aerodynamic forces corresponding to attack angle of the girder were introduced. After that, eigenvalues were calculated using 50 vibrational modes in still air. Modified torsional stiffness was used for the calculation so that torsional natural frequency might become equal to the measured value.

The analytical results of static deformation were

shown in Fig.12. As for horizontal displacement and vertical displacement, the analytical values agreed well with experimental values. However, the analytical value (absolute value) for the torsional deformation was a little smaller than experimental value. Since aerodynamic characteristics are sensitive to attack angles, the flutter analysis was carried out using the measured torsional deformation.

The change of apparent damping of the 1st torsional symmetrical mode (mode 19) is shown in Fig.13 by triangle mark. The flutter speed from the 3-dimensional flutter analysis was 7.9m/s. It agreed fairly well with the experiment.

Since the mass and polar moment of inertia of the model were larger than the values required from the similarity laws, flutter analysis was conducted for the required values of the model. The flutter speed was 7.6m/s. Therefore, flutter speed for the assumed bridge would be estimated about 85m/s, which confirmed its aeroelastic stability

6. CONCLUSIONS

Full aeroelastic model test and 3-dimentional flutter analysis was conducted for a generic super long-span bridge. Results and conclusions obtained are summarized as follows:

1) The slotted box girder was applied to a generic super long-span bridge, whose main span length was assumed to be 2.8km. Wind tunnel study was conducted with a 1/125 full aeroelastic model in smooth flow. It was confirmed that its flutter speed was high enough.

2) Three-dimensional flutter analysis was conducted for the full aeroelastic model. In the analysis, unsteady aerodynamic forces corresponding to attack angles of the girder deformed by steady wind forces were introduced. The calculated flutter speed agreed fairly well with the experiment.

In order to predict the torsional deformation and the flutter speed more accurately, improvement of the analytical model for the bridge is in progress.

REFERENCES:

[1] Sato H. and Ogihara K., Aerodynamic characteristics of slotted box girders, Proceedings of the 28th Joint Meeting of the Panel on Wind and Seismic Effects, UJNR, 1996

[2] Sato H., Ogihara K. and Ogi K., Consideration on flutter characteristics of super long-span bridges, Proceedings of the 30th Joint Meeting of the Panel on Wind and Seismic Effects, UJNR, 1998

[3] Nakamura, Y., An analysis of binary flutter of bridge deck sections, J. of Sound and Vibration, 57(4), 1978

[4] Miyata T., Sato H. et al., Full model wind tunnel study on the Akashi Kaikyo Bridge, Proceedings of the 9th International Conference on Wind Engineering, 1995, pp.793-798

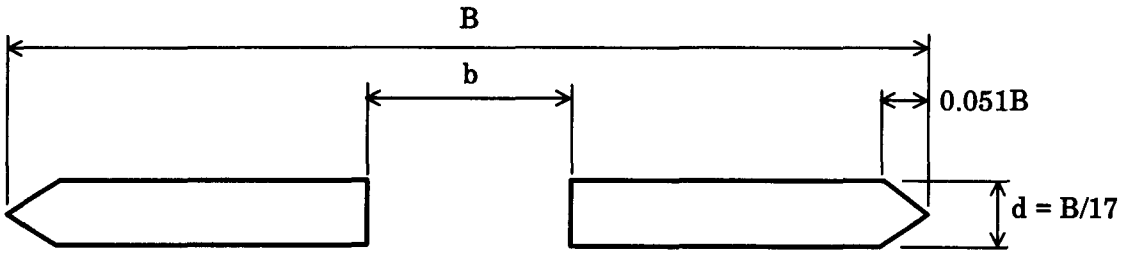

Fig.1 Cross Section of Slotted Girder

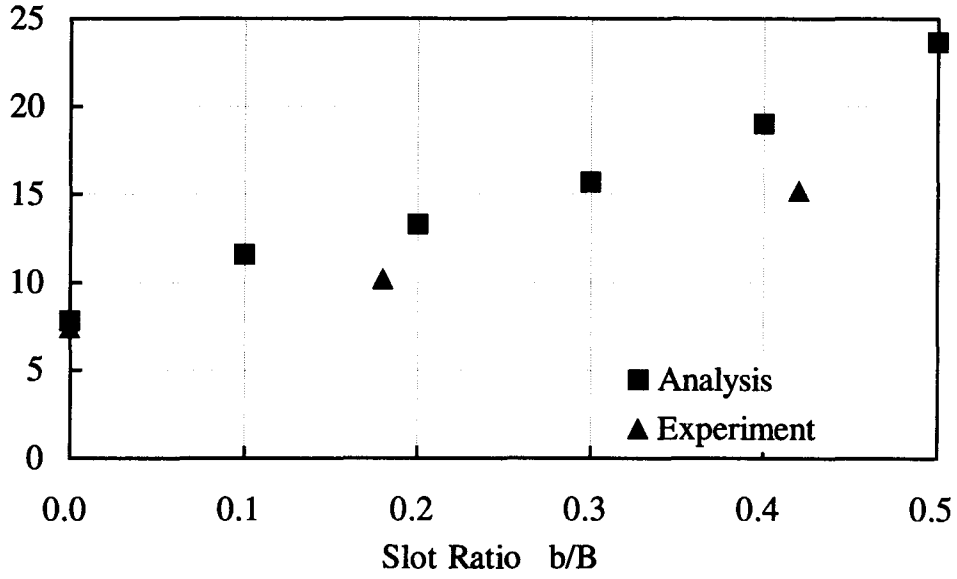

Fig. 2 Flutter Onset Speed and Slot Ratio

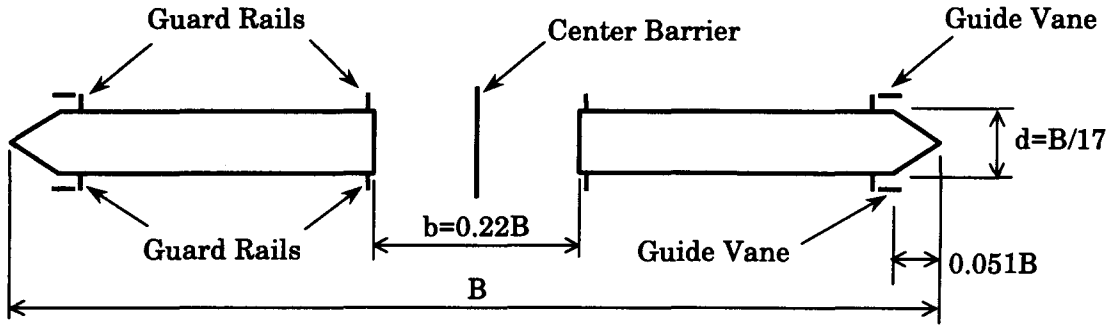

Fig.3 Slotted Box Girder with Devices

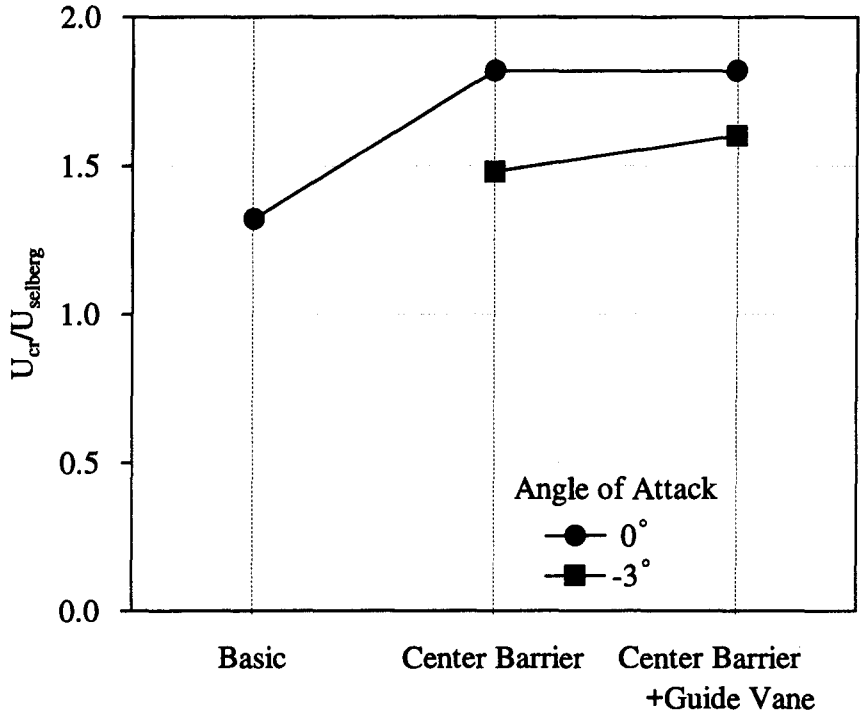

Fig.4 Effect of Tested Devices

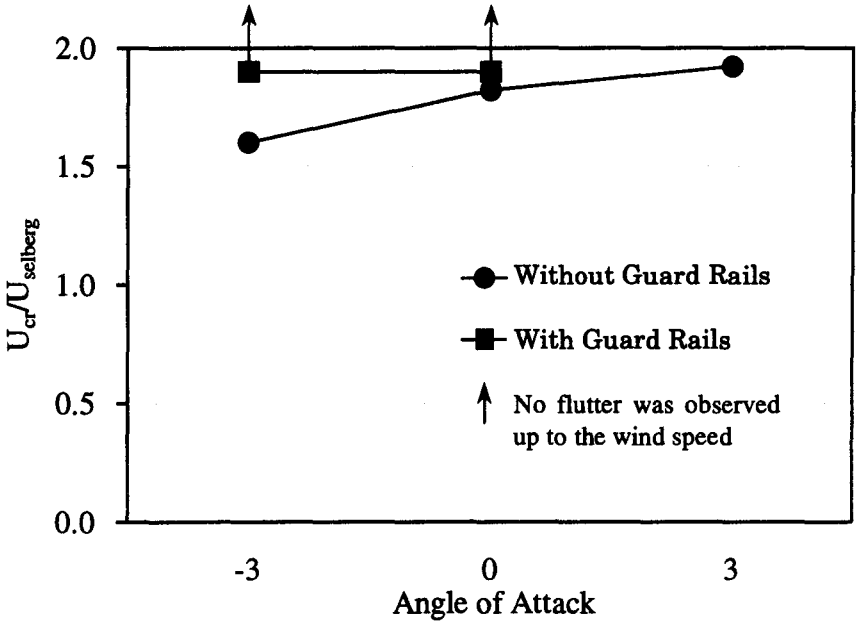

Fig.5 Effect of Guard Rails at Bottom Deck

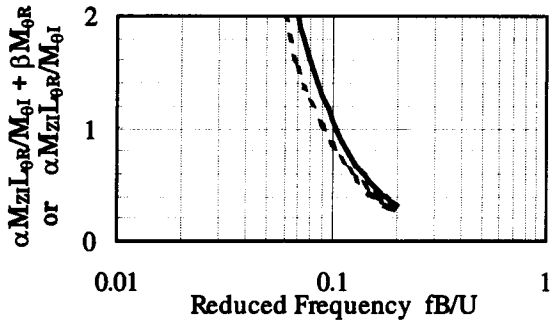

(a) Single Plate

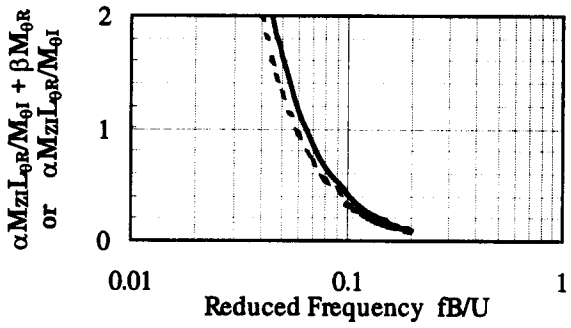

(b) Slotted plate

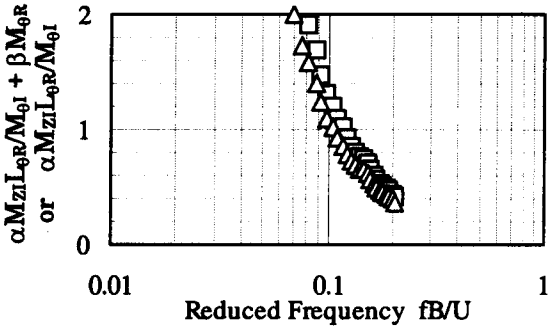

(c) Single Box Girder

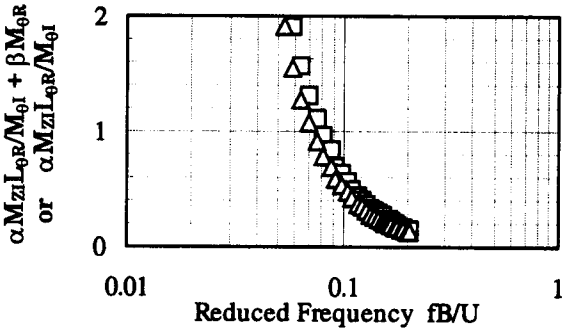

(d) Slotted Box Girder

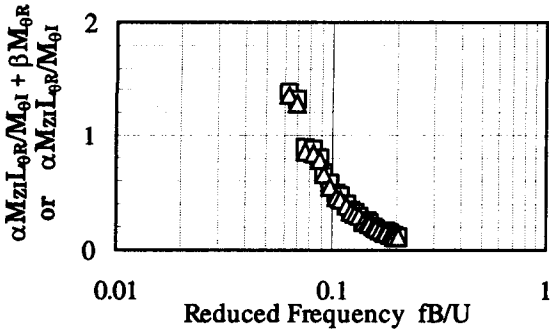

(d) Slotted Box Girder with Devices

Fig.6 Prediction of Flutter Onset (plotted with fB/U)

[Flutter will take place when :$\alpha M_{zI}L_{\theta R}/M_{\theta I} + \beta M_{\theta R} \geqq 1$]

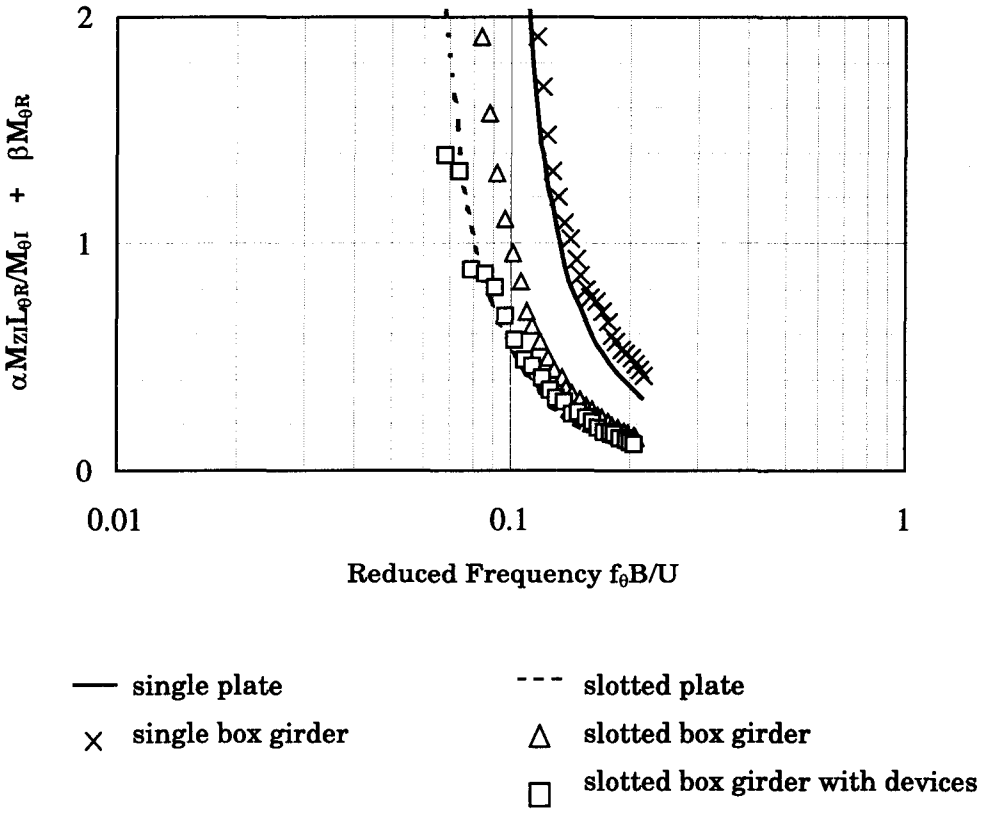

Fig.7 Prediction of Flutter Onset (plotted with $f_\theta B/U$)
[Flutter will take place when : $\alpha M_{ZI}L_{\theta R}/M_{\theta I} + \beta M_{\theta R} \geqq 1$]

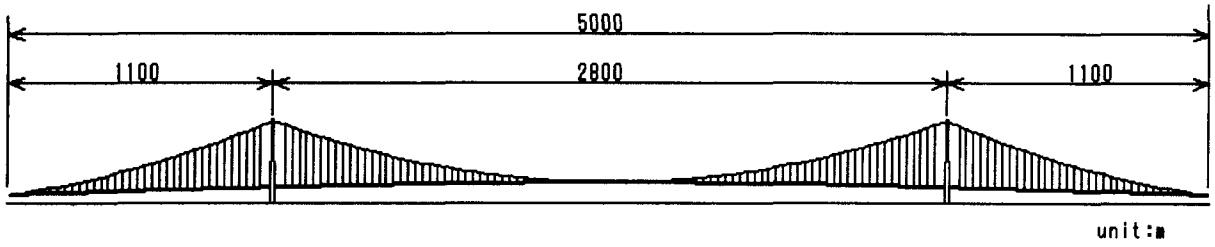

Fig. 8 Assumed super long-span bridge

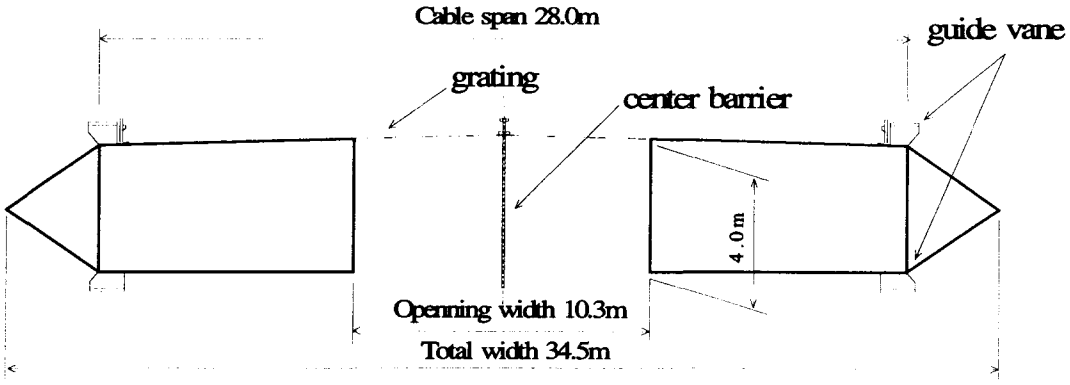

Fig. 9 Cross section of slotted box girder

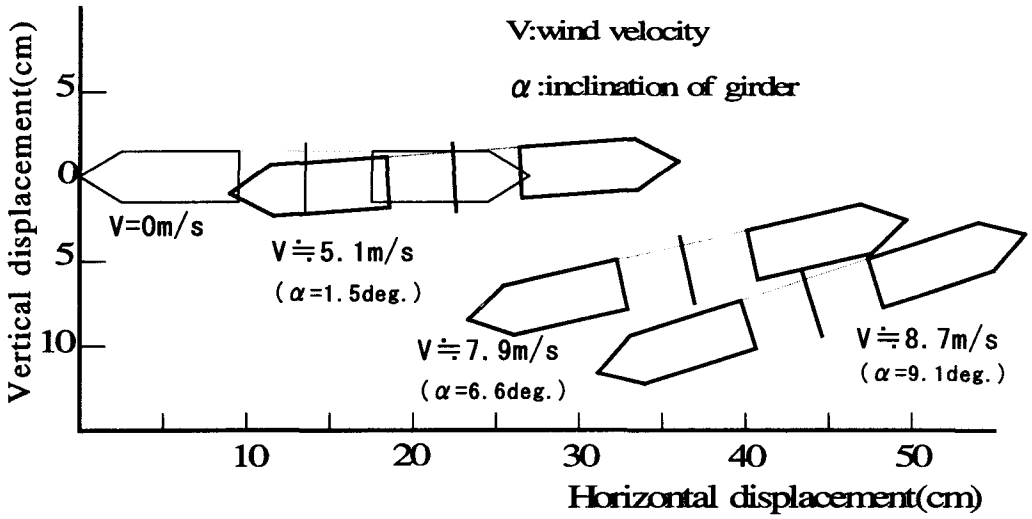

Fig.10 Deformation of girder

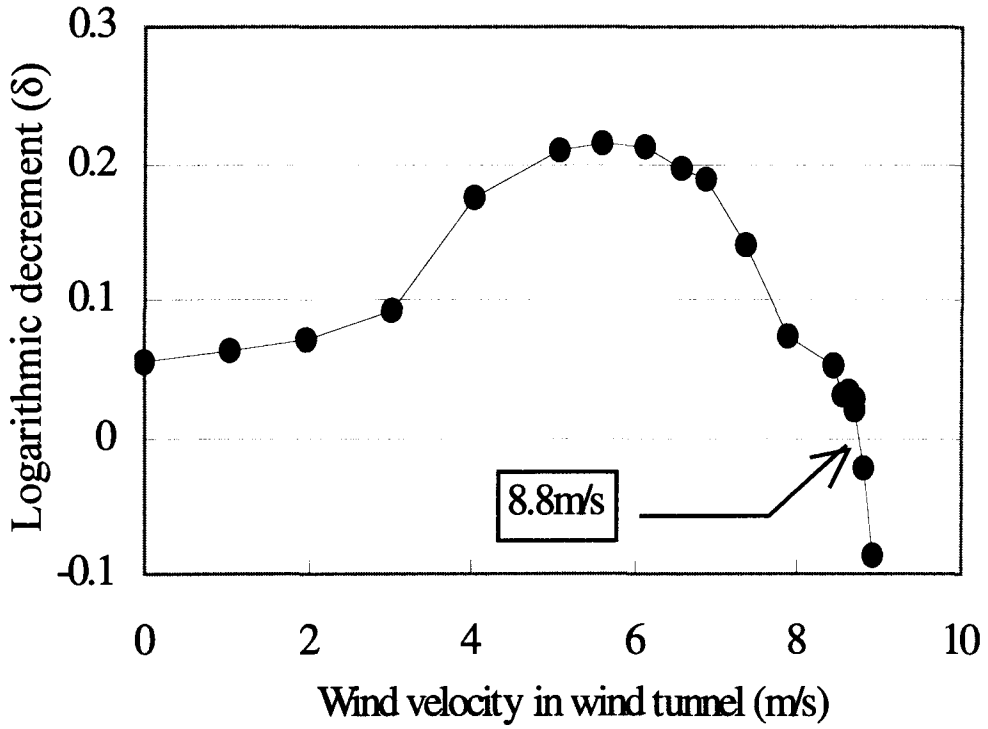

Fig. 11 Apparent damping – wind velocity

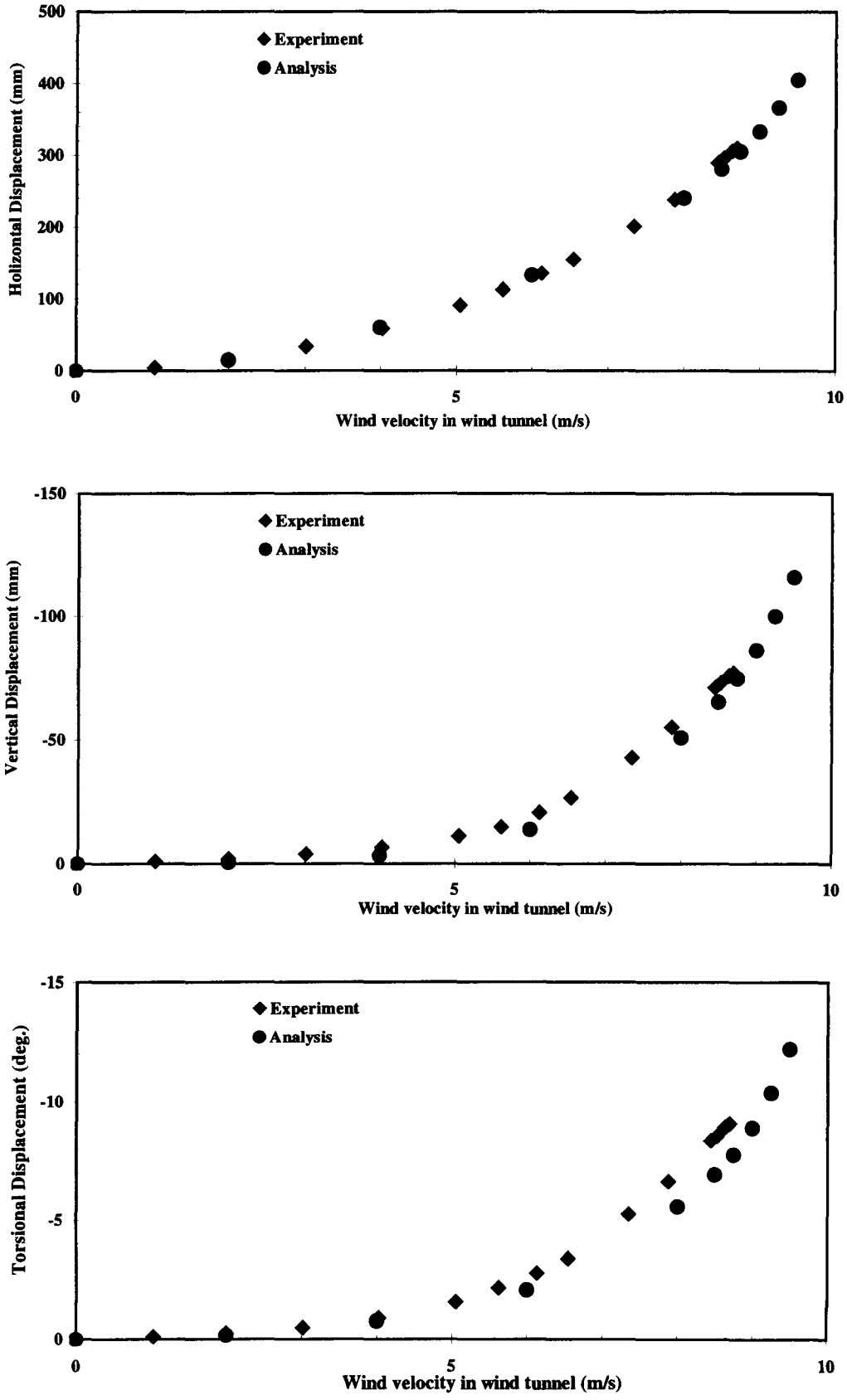

Fig. 12 Results of static deformation

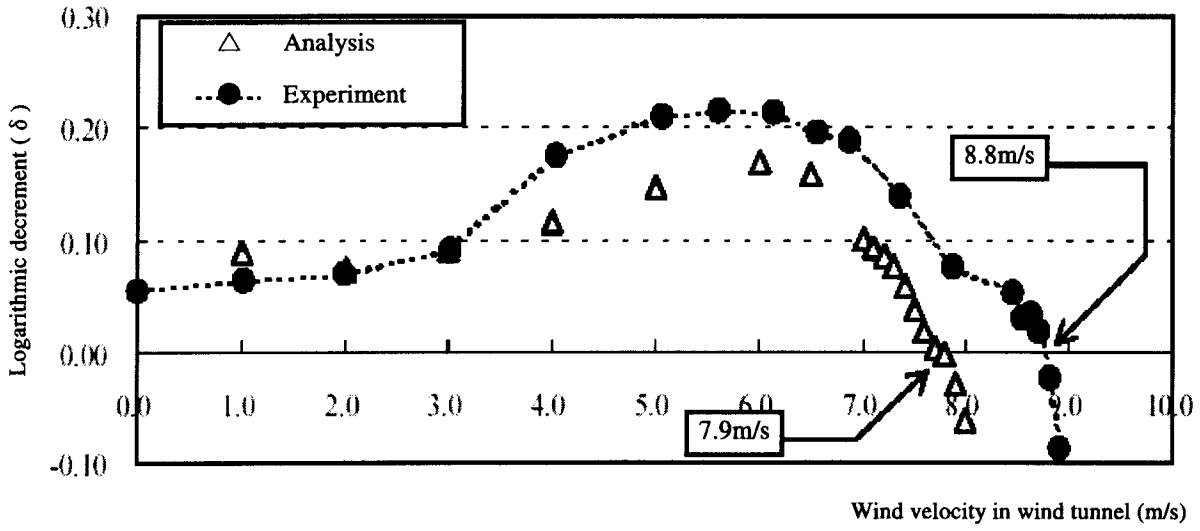

Fig. 13 Apparent damping – wind velocity (1st torsion symmetrical mode)

Photo 1 Static deformation of super long-span bridge (wind speed=8m/s)

Table 1 Structure dimensions of super long-span bridge

			Assumed bridge	Model value		(b)/(a)
				Required (a)	Measured (b)	
Scale			-	1/125	1/125	-
Mass		M	28.41t/m	1.818kg/m	2.100kg/m	1.156
Polar moment of inertia		I_P	388t·m²/m	0.00159kg·m²/m	0.00246kg·m²/m	1.547
Girder size	Width	B	34.5m	0.276m	0.276m	1.000
	Depth	D	4.0m	0.032m	0.032m	1.000
Stiffness	Vertical	EI_V	1.707kNm²/box	9.384Nm²/box	12.277Nm²/box	1.308
	Horizontal	EI_H	3.107kNm²/box	48.828Nm²/box	12.277Nm²/box	0.251
	Torsional	GJ	1.090kNm²/box	6.906Nm²/box	6.853Nm²/box	0.992
Natural frequency	Vertical	1st	0.0621Hz	0.693Hz	0.674Hz	0.973
		2nd	0.0990Hz	1.111Hz	1.106Hz	0.995
		[1st]	0.0610Hz	0.683Hz	0.703Hz	1.029
		[2nd]	0.0831Hz	1.499Hz	1.494Hz	0.997
	Torsional	1st	0.1256Hz	1.369Hz	1.321Hz	0.965
		[1st]	0.1466Hz	1.600Hz	1.597Hz	0.998
	Horizontal	1st	0.0316Hz	0.352Hz	0.352Hz	1.000
		[1st]	0.0550Hz	0.502Hz	0.491Hz	0.978

[ ] means asymmetrical mode

Table 2 The conditions of flutter analysis

Item	Analysis condition
Analytical method	Mode combination method. Using lower 50 modes.
Air density	0.12 kg/m³
Structural damping	All modes δ =0.02
Coefficients of aerodynamic forces	Main girder Force / Vertical / Torsional / Horizontal Lift: ○ / ○ / △ Moment: ○ / ○ / △ Drag: ○ / ○ / △ ○;Unsteady aerodynamic forces △;Quasi-steady aerodynamic forces Cable Quasi-steady drag and lift force (C_D=0.7) Tower Not considered

Wind Effects on Long Span Cable Stayed Bridges: Assessment and Validation

by

Nicholas P. Jones[1] and Ender Ozkan[2]

ABSTRACT

The well-known collapse of Tacoma Narrows Bridge in 1940 clearly identified the importance of aeroelastic effects on long-span bridge performance. Extensive research has been carried out since then to better understand the effects of wind on long-span bridges, producing various analytical response prediction techniques. An example of the application of such techniques will be presented. However, due to challenges related with full-scale measurements, these prediction techniques have commonly been validated using only wind-tunnel experiments. Recent research has revolved around the conduct of long-term full-scale measurements on a cable-stayed bridge to compare actual bridge performance with those of analytical predictions. In order to ensure the reliability of predicted response, the input parameters, such as wind conditions at the site and modal properties of the bridge are also calibrated using corresponding measured quantities. This paper will also summarize some of the preliminary results and outline their implications.

KEYWORDS: bridge engineering, wind engineering, flutter, buffeting, long-span bridges

1.0 INTRODUCTION

The maximum span of long-span bridges has been extended in recent decades to where today, the Akashi-Kaikyo Bridge (central span 1991 m) has been completed, and longer bridges are planned (e.g., Messina Straits (3300 m), Gibraltar Straits (5000m)). These successes are due in particular to progress in wind-resistant design; a primary component in the design of long-span bridges. Recently, multi-mode flutter and buffeting analysis procedures have been developed. These procedures, which were based on frequency-domain methods, take into account the fully coupled aeroelastic and aerodynamic response of long-span bridges to wind excitation.

The current methodology for the estimation of the response of long-span bridges to wind loads incorporates the following components:

- Measurement of a comprehensive set of aerodynamic and aeroelastic parameters for a given cross section using a suitably (i.e., aerodynamically) scaled section model. These parameters include: the static coefficients (lift, moment, and drag at a number of different angles of attack) and the flutter derivatives, generally also at several positive and negative angles of attack. It is emphasized that these quantities are intended to be sectional quantities that will be used in the analytical model. Examples of procedures can be found in Sarkar et al. (1994) and Singh et al (1996).
- A detailed numerical (generally finite element) dynamic model for the bridge under consideration. This model will be expected to provide a set of eigenvalues and eigenvectors for the structure and a corresponding set of generalized inertias. Generally, this will include at least 20 modes, but in some cases more may be required (e.g., up to 50 for very long structures).
- An analytical framework and computational aids for synthesizing the above data. Scanlan and Jones (1990) provide a comprehensive overview of the single-degree of freedom theory, while Jain et al. (1996a, 1996b) and Katsuchi et al. (1998a, 1998b,1999) outline the extension of this theory to consider the interaction of multiple modes.

In addition to the above components, knowledge

[1] Professor and Chair, Dept. of Civil Engineering, Johns Hopkins University, Baltimore, MD 21218, USA
[2] Graduate student, Dept. of Civil Engineering, Johns Hopkins University, Baltimore, MD 21218, USA

or assumptions about modal damping values and the wind environment are also required.

One of the most commonly used prediction techniques is the frequency-domain analysis described by Scanlan and Jones (1990), Jain et al. (1996a) and Katsuchi et al. (1999), and is based on modal analysis in the frequency domain. A suite of computer programs has been created to enable fast and efficient implementation of multi-mode frequency-domain prediction methods. For brevity, details are not included here; interested readers are referred to the above-referenced publications for this material.

2.0 EXAMPLE APPLICATION

This section summarizes the results of the flutter and buffeting analysis carried out for a cable-stayed bridge: a 1169 ft. main span structure and shows the capabilities of frequency-domain-based analysis tools. The input parameters in Table 1 were used in the analysis to model the structural and climatological properties of the bridge. Table 2 lists this first ten modal frequencies of the bridge, and their associated descriptions. The A_2^* flutter derivative for different wind directions and angles of attack are shown in Figure 1. The potential flutter susceptibility is indicated by the crossing of the A_2^* from negative to positive at a reduced velocity (U/nB) of about 4.

2.1 Flutter analysis

For some long-span bridges, the lowest torsional mode may couple with the first vertical mode of the bridge to cause flutter at a lower wind velocity than predicted from the single-mode analysis alone. To evaluate the possible coupling of modes, a two-mode flutter analysis was carried out for the bridge using Modes 2 and 7 (first vertical and first torsional). The two-mode flutter analysis was repeated using all of the flutter derivative sets; results are summarized in Table 3.

According to these results, the most critical condition corresponds to a south with an angle of attack of -3 degrees. Coupling was observed to be minimal in this case: this is primarily a single-mode flutter, as would generally be expected for a structure of this size.

2.2 Buffeting Analysis

Buffeting analysis of the structure was carried out using two sets of flutter derivative data, one with force coefficients corresponding to a north wind at zero degrees) and one with force coefficients corresponding to a south wind at zero degrees. In the results reported herein, the mean wind speed U is taken as 33 m/s (109 ft/s).

Table 3 summarizes the results of this investigation, and Figures 2 and 3 show the RMS vertical and torsional displacement estimated as a function of span location for varying number of modes included in the analysis. Note that the responses converge rapidly after the significant modes that contribute are included in the analysis. Figures 4 and 5 show spectra of response at midspan and quarter-span points, and demonstrate the different modal contributions expected at these locations. Again, analysis confirmed that the modal coupling in this structure is insignificant, and analysis using a mode-by-mode approach is generally adequate.

3.0 FULL-SCALE MEASUREMENTS

As noted above, few opportunities have existed to quantitatively verify the above results at full scale. A long-term measurement program is currently underway at the Fred Hartman Bridge in Texas to continuously monitor its response to ambient loading conditions. The Fred Hartman Bridge (Fig. 6) is a twin-deck cable-stayed bridge with a main span of 380 m. and two side spans of 147 m. The decks are carried by a total of 192 cables, arranged in four inclined planes and connected to the deck at 15 m intervals.

Measurements are carried out using a PC-based self-triggering system that collects data on the basis of exceedance of threshold motion and wind levels. This system has been in use for over 4 years, collecting in excess of 20000 trigger files. Each file contains 5-minute trigger runs collected at 40 Hz, which are stored on high-capacity disks. The recorded files are later processed to extract deck and

cable accelerations, cable displacements and loads, wind speeds and other relevant meteorological factors, all of which are summarized in a comprehensive database for subsequent analysis. Further details of data collection and processing can be found in Ozkan et al. (2001a).

As noted earlier, there are three main components used in a bridge wind analysis: knowledge of the meteorological conditions at the bridge site, information on the modal properties of the structure and the experimentally determined flutter derivatives and associated aerodynamic parameters associated with the cross section. The first component, through the wind spectra, can be evaluated directly using measured wind speeds and compared to theoretical meteorological models. Preliminary comparison of wind spectra show reasonable agreement (see Figure 7); detailed results will not be reported herein.

The modal properties predicted for the bridge can also be evaluated directly from the measured deck frequencies through comparison to the results obtained from a 3-D finite element model of the bridge; good agreement has generally been obtained. It should be noted here that due to the inherent flexibility of long-span bridges, self-excited forces play a role in the overall stiffness and damping of the structure, making them wind-speed dependent. This characteristic is modeled through the flutter derivatives, the effects of which can be seen in histograms of modal frequencies, which show a range of values for each mode. Studies are also being performed to better evaluate the wind-speed dependence of frequency and damping of the structure and relate them to the flutter derivatives.

Comparison of overall bridge response is made using root-mean-square (RMS) acceleration and displacement response of the bridge. Since multiple modes contribute to the response, RMS displacement is estimated for each mode individually. This is done for each record, and the results consequently compared to analytical predictions obtained from the programs mentioned above. However, the nature of the structure and the measurement program gives rise to observations that should be considered carefully to ensure the reliability of results. An example of these is the localized effect of cable vibrations. These are instances of large-amplitude cable vibrations that are recorded by deck transducers (Ozkan et al. 2001a). Measurements taken after the installation of dampers on the cables show a much-reduced level of such vibrations and more evident global vibrations of the deck. Another interesting observation is the instances of cable-deck interaction, initiated by moderate vibrations of the deck that induces oscillation of cables (Ozkan et al. 2001b).

3.1 Deck Vibration Measurements and Data Analysis

A significant challenge related with long-term monitoring projects is the process of analyzing large quantities of data without loss of interesting information that might not have been expected. More than 20000 trigger files have been recorded during the three years of the test program and more are continuously being collected. Analyzing such a large number of data files demands extensive use of automated procedures. However, the use of such procedures must be carefully controlled to ensure that flawed or questionable data are not included in the study. The data analysis techniques used in this project have been automated to the greatest extent considered prudent, with careful consideration to maintaining the integrity and accuracy of the data and not missing important features of individual records.

The recorded files are initially processed to determine the general features of the raw data. These features include the mean, standard deviation and other higher moments of the data as well as one-minute average wind speeds and directions, accelerations and displacements, all of which are automatically added to a database. The database provides for easy analysis and correlation of these statistical quantities. It is also possible to readily interrogate the data using queries created and stored in the database.

Modal frequencies and mode shapes have been found and these values have been compared with values obtained from finite element (FE) analysis. Preliminary results of this comparison have been

presented previously (Ozkan et al. 2001a). Table 5 shows the comparison of measured modal frequencies with those obtained from a FE analysis for the first 20 modes. In general, good agreement between the two data sets is observed. Similarly, the mode shapes have been found for the first 20 modes, showing reasonable agreement with those calculated from the FE analysis (Ozkan et al. 2001a).

To investigate the wind-vibration characteristics of the bridge deck, plots of root mean square (RMS) displacement of the deck versus wind speed have been made (Figure 8). A general trend of increasing RMS acceleration with wind speed can be observed from this figure. Comparison with predicted responses using the procedure outlined above and parameters suitable for the recording environment show reasonable agreement in large measure; "outliers" are currently being studied in more detail.

3.2 Deck-Stay Interaction

An example of an interesting record is given in Fig. 9. This record forms the initial five-minutes of a series of triggers during the passage of a meteorological event. For this specific record, Fig. 9(a) and (b) show the time-histories and power spectral densities (PSD's) of vertical deck acceleration at midspan and of the adjacent stay cable AS24 (length 198 m; natural frequency approximately 0.59Hz), respectively. Fig. 9(c) shows the wind speed at deck level. These figures, and others similar that have been made for different deck instruments, show a dominant frequency of vibration at approximately 0.58 Hz. It is important to note that this frequency corresponds to the third symmetric vertical mode of the deck (given as approximately 0.56 Hz in Table-1), and is also close to the first mode of the stay cable AS24. This is an interesting and important observation since the first-mode vibrations of a cable at this level of acceleration are generally associated with large displacements. In fact, by integrating the acceleration time-history, a displacement amplitude of approximately one meter (peak to peak) was estimated.

Furthermore, by observing the time-histories it can be seen that the significant vibrations are initially observed at the deck instead of the cable. This observation, as well as the similarity of modal frequencies suggests that the deck is driving the cable to vibrate with large amplitude in its fundamental mode. Vortex-induced vibration of the deck is thought to be the driving mechanism for this motion. Further studies are continuing to better understand the underlying mechanisms involved in this behavior and its consequences, and will be reported in future publications.

4.0 CONCLUDING REMARKS

The preceding paper presents an overview of long-term efforts to monitor a cable-stayed bridge for a variety of purposes, including understanding the modal characteristics and wind-induced responses under ambient wind conditions. Using data files collected during various meteorological conditions, natural frequencies and mode shapes of the deck were found using an automated data analysis procedure. The measured modal frequencies, mode shapes, and RMS responses are observed to agree with the predicted values found from a finite element and aerodynamic analysis.

The analysis and comparison described above demonstrates acceptable performance of the analytical model in its ability to predict the response of long-span bridges to wind loading. The analytical model (with suitable choice of parameters) may therefore be considered suitable for the prediction of the prototype response. Overall, the methodology employed in the present paper represents the general versatility of the analytical and experimental techniques for the aeroelastic design of long-span bridges.

It is noted that while automated data analysis procedures are clearly necessary for such large volumes of data, care must be taken not to miss or obscure important phenomena or characteristics through this approach. The interaction observed between the deck and a stay is a good example of a situation where careful interpretation of the data is required to fully understand the relevant underlying mechanics.

5.0 ACKNOWLEDGEMENTS

The authors would like to thank Dr. Jon Raggett of West Wind Lab, Carmel, CA for performing the aerodynamic and aeroelastic section model tests reported in this paper. URS Corporation was responsible for the finite element analysis of the first structure analyzed herein that provided the structural dynamic data.

The support of both authors by the National Science Foundation is also gratefully acknowledged. The authors would also like to acknowledge the Texas Department of Transportation, the US Federal Highway Administration, the US Department of Defense (NDSEG Fellowship) and the Department of Civil Engineering at Johns Hopkins University for the support of various components of this work.

6.0 REFERENCES

Jain, A., Jones, N.P. and Scanlan, R.H. (1996a). "Coupled Flutter and Buffeting Analysis of Long-Span Bridges." J. Str. Engrg., ASCE. 122(7), 716-725.

Jain, A., Jones, N.P., and Scanlan, R.H. "Coupled Aeroelastic and Aerodynamic Analysis of Long-Span Bridges." J. Wind Eng. and Indust. Aero, 60 (1996b), 69-80.

Jain, A., Jones, N.P., and Scanlan, R.H. "Effect of Modal Damping on Bridge Aeroelasticity." J. Wind Eng. and Indust. Aero, 77&78, 421-430, (1998).

Katsuchi, H., Jones, N. P., Scanlan, R. H. and Akiyama, H. (1998a). "A Study of Mode Coupling in Flutter and Buffeting of the Akashi-Kaikyo Bridge." J. Struct. *Mech. and Earthquake Engrg.*, JSCE, No 598 / I-44.

Katsuchi, H., Jones, N. P., Scanlan, R. H. and Akiyama, H. "Multi-Mode Flutter and Buffeting Analysis of the Akashi-Kaikyo Bridge." J. Wind Eng. and Indust. Aero, 77&78, 431-441, (1998b).

Katsuchi, H., Jones, N.P., Scanlan, R.H., and Akiyama, H. "Multimode Coupled Buffeting and Flutter Analysis of the Akashi-Kaikyo Bridge". J. Struct. Eng. ASCE, 125(1), 60-70, January, 1999.

Ozkan, E., Main, J. and Jones, N. P. (2001a). "Long-Term Measurements on a Cable Stayed Bridge", *Proc. 19th Inter. Modal Analysis Conf.*, Kissimmee, Florida, p. 48-50.

Ozkan, E., Main, J. and Jones, N. P. (2001b). "Full-Scale Measurements on the Fred Hartman Bridge", *Proc. 5th Asia-Pacific Conf. on Wind Engrg.*, Kyoto, Japan.

Sarkar, P.P., Jones, N.P. and Scanlan R.H. "A Recursive Time-Domain System-Identification Procedure for Extraction of Aeroelastic Parameters." Journal of Engineering Mechanics, 120(8), ASCE, August, 1994, 1718-1742.

Scanlan R.H. and Jones N.P. "On Aerodynamic Admittance in Bridge Aeroelastic Analysis." J. Fluids and Structures, 13, 1017-1027 (1999)

Scanlan, R.H. and Jones, N.P. (1990). "Aeroelastic Analysis of Cable-Stayed Bridges." J. Struct. Engrg., ASCE, 116(2), 279-297.

Scanlan, R.H.. "State-of-the-Art Methods for Calculating Flutter, Vortex-Induced, and Buffeting Response of Bridge Structures." Federal Highway Administration Report No. FHWA/RD-80/50 (1981).

Simiu, E. and Scanlan, R.H., Wind Effects on Structures, Third Edition, John Wiley and Sons, New York, N.Y., 1996

Singh, L., Jones, N.P., Scanlan, R.H. and Lorendeaux, O. "Identification of Lateral Flutter Derivatives of Long-Span Bridges." J. Wind Eng. and Indust. Aero, 60 (1996), 81-89.

Table 1: Parameters for Example Structure

ζ (structural damping)	0.003
B (width) – ft	76.75
L (total length) – ft	1169.0
Air Density, ρ, – lbs^2/ft^4	0.002378
Lift coeffcient C_L	-0.0344
Drag coeffcient C_D	0.134
Moment coeffcient C_M	-0.0293
Derivative of lift coefficient C_L'	5.107
Derivative of moment coefficient C_M'	0.332
Z (deck height) - ft	78
Z_0 (roughness length) - ft	0.25
Correlation Constant	5

Table 2: Modal frequencies

Mode No.	Frequency (Hz.)	Period (Second)	Description
1	0.172	5.825	1st Longitudinal Deck Mode
2	0.294	3.398	1st Vertical Deck Mode
3	0.446	2.241	1st Lateral Deck Mode
4	0.473	2.113	
5	0.718	1.392	
6	0.723	1.383	1st Torsional Deck Mode
7	0.784	1.276	
8	0.867	1.153	
9	0.919	1.088	
10	0.933	1.072	

Table 3: Critical flutter velocities

Angle of Attack	Critical Flutter Velocity
North 0 deg	163 mph
North +3 deg	>191 mph
North -3 deg	158 mph
South -3 deg	145 mph
South 0 deg	161 mph
South +3 deg	>178 mph

Table 4: Buffeting analysis results (0.5% damping)

Configuration	Modes Analyzed	Vertical RMS Disp. at Midspan (inch (cm))
North Wind	1&2	4.44 (11.3)
	1, 2 & 3	4.45 (11.3)
	10 Modes	4.48 (11.4)
	18 Modes	4.49 (11.4)
South Wind	1 & 2	4.52 (11.5)
	1, 2 & 3	4.53 (11.5)

Table 5: Comparison of measured deck modes with FE analysis

Mode	Long-Term Measured Frequency (Hz)	FEM Frequency (Hz)	Percentage Difference	Phasing (I :in-phase O: Out-of-phase)	Description of the Mode (FE)
1	0.290	0.286	1.4	I	Vertical
2	0.299	0.291	2.8	O	Vertical
3	0.375	0.366	2.5	I	Vertical
4	-	0.377	-	O	Vertical
5	0.432	0.410	5.4	O	Lateral
6	-	0.426	-	I	Lateral
7	0.564	0.556	1.4	I	Vertical
8	-	0.562	-	O	Vertical
9	-	0.612	-	O	Torsional
10	0.586	0.625	6.2	I	Vertical
11	-	0.634	-	O	Vertical
12	0.665	0.658	1.1	I	Vertical
13	-	0.659	-	-	Torsional-Lateral
14	0.683	0.662	3.2	-	Torsional-Bending
15	0.714	0.735	2.9	I	Vertical
16	-	0.736	-	O	Vertical
17	-	0.756	-	I	Torsional
18	0.784	0.757	3.6	O	Vertical
19	-	0.817	-	I	Torsional
20	0.924	0.856	7.9	I	Vertical

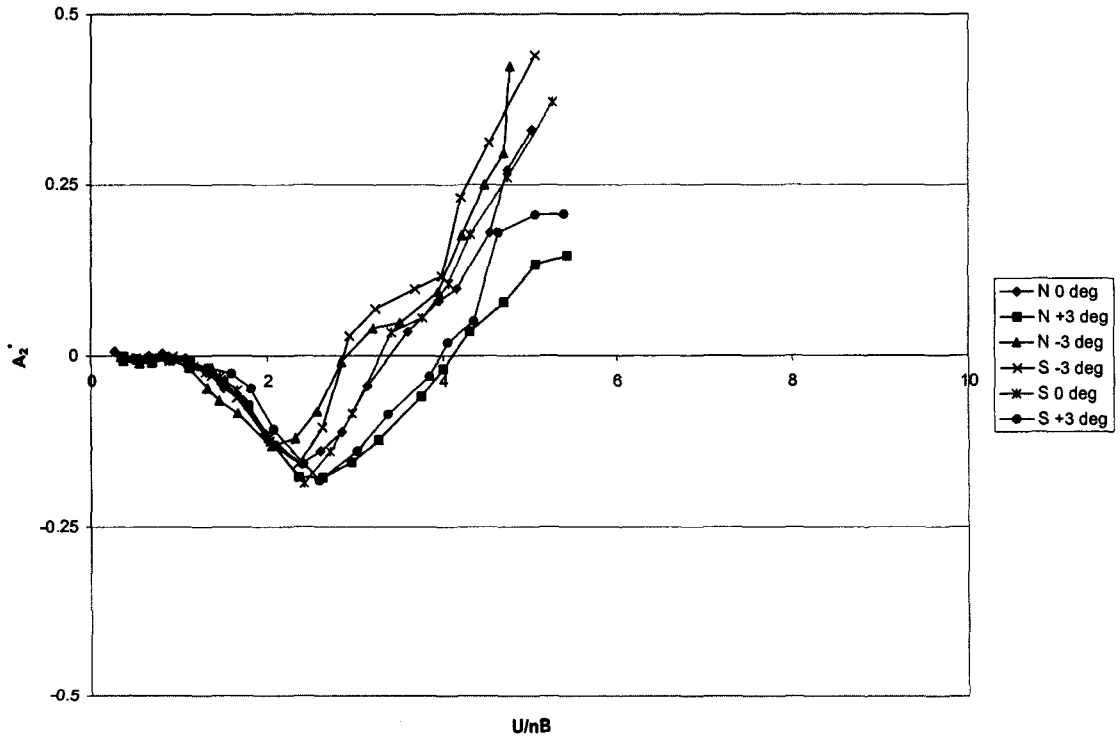

Figure 1: Flutter derivative A_2^* for various wind directions and angles of attack.

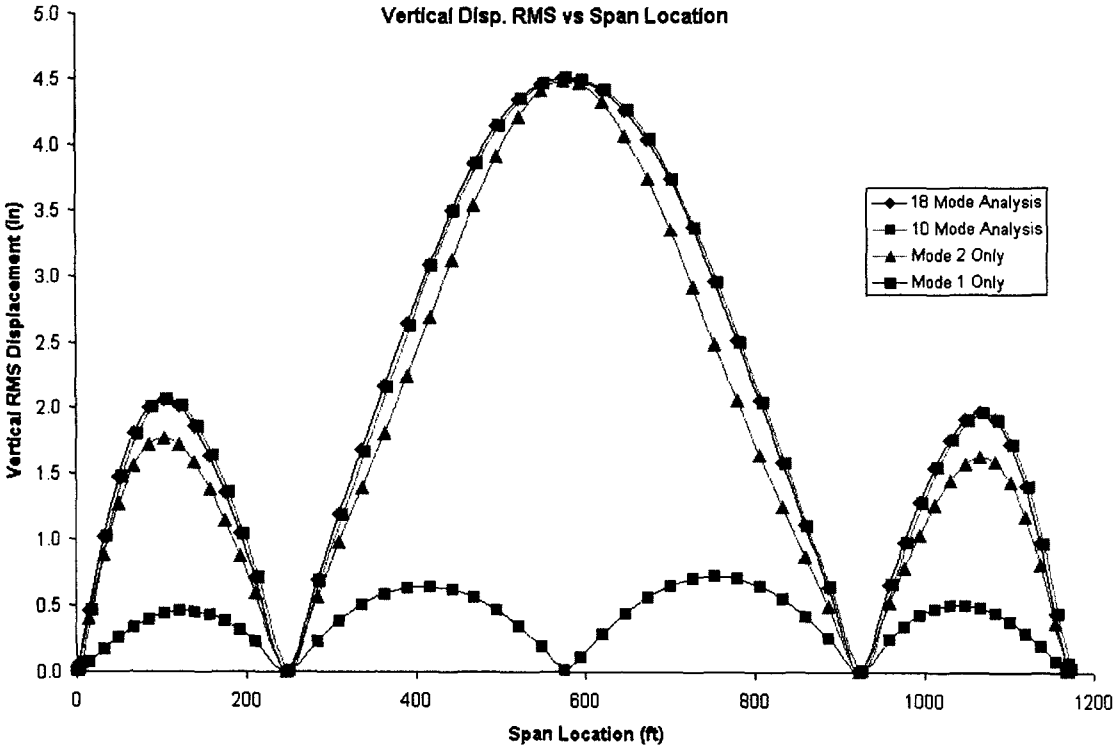

Figure 2: RMS Vertical displacement vs span location: North wind; 0.5% damping

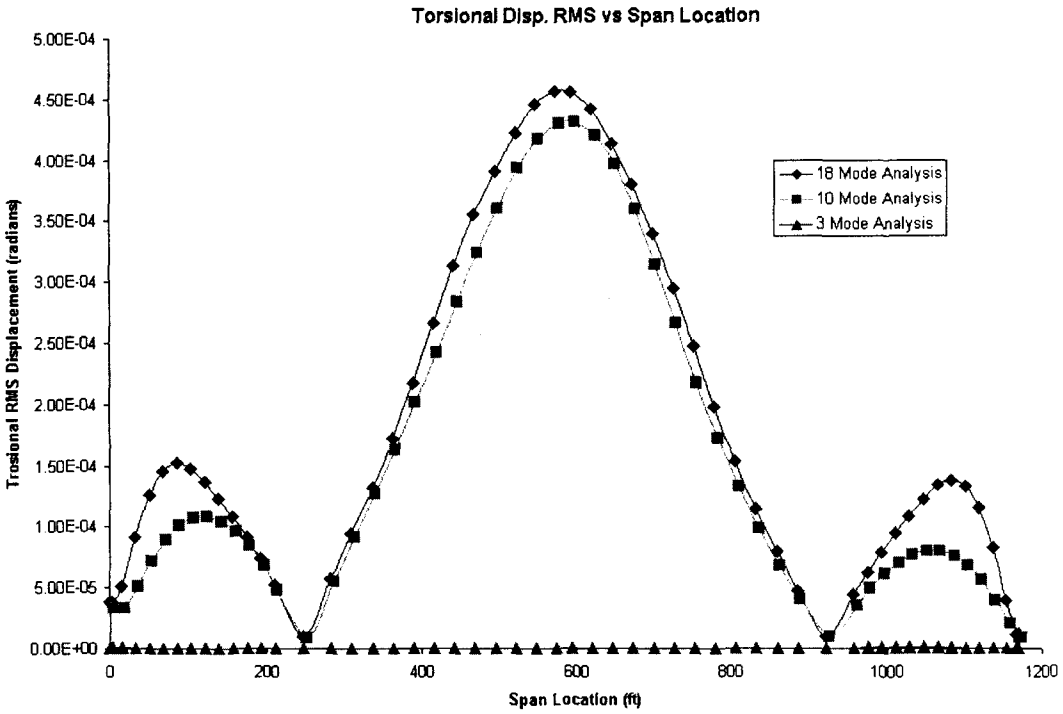

Figure 3: RMS Torsional displacement vs span location: North wind; 0.5% damping

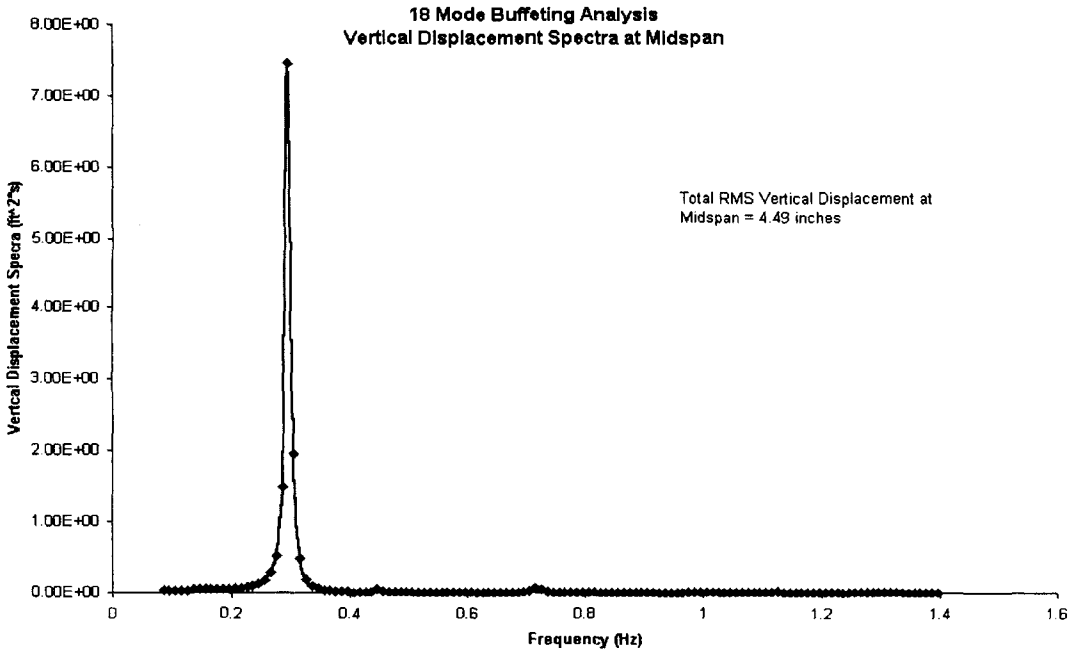

Figure 4: Vertical displacement spectrum at midpsan: 18 mode analysis; North wind; 0.5% damping

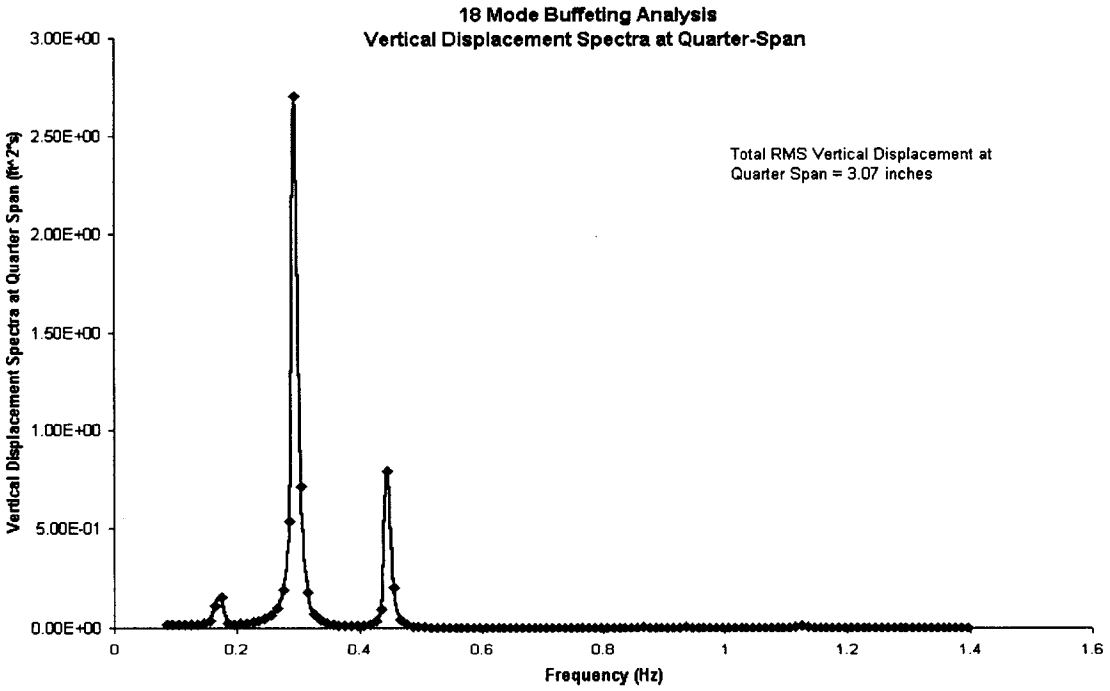

Figure 5: Vertical displacement spectrum at quarter-span: 18 mode analysis; North wind; 0.5% damping

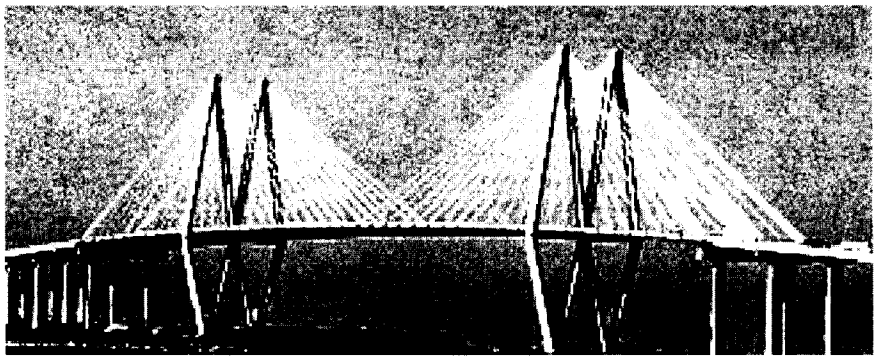

Figure 6. The Fred Hartman Bridge

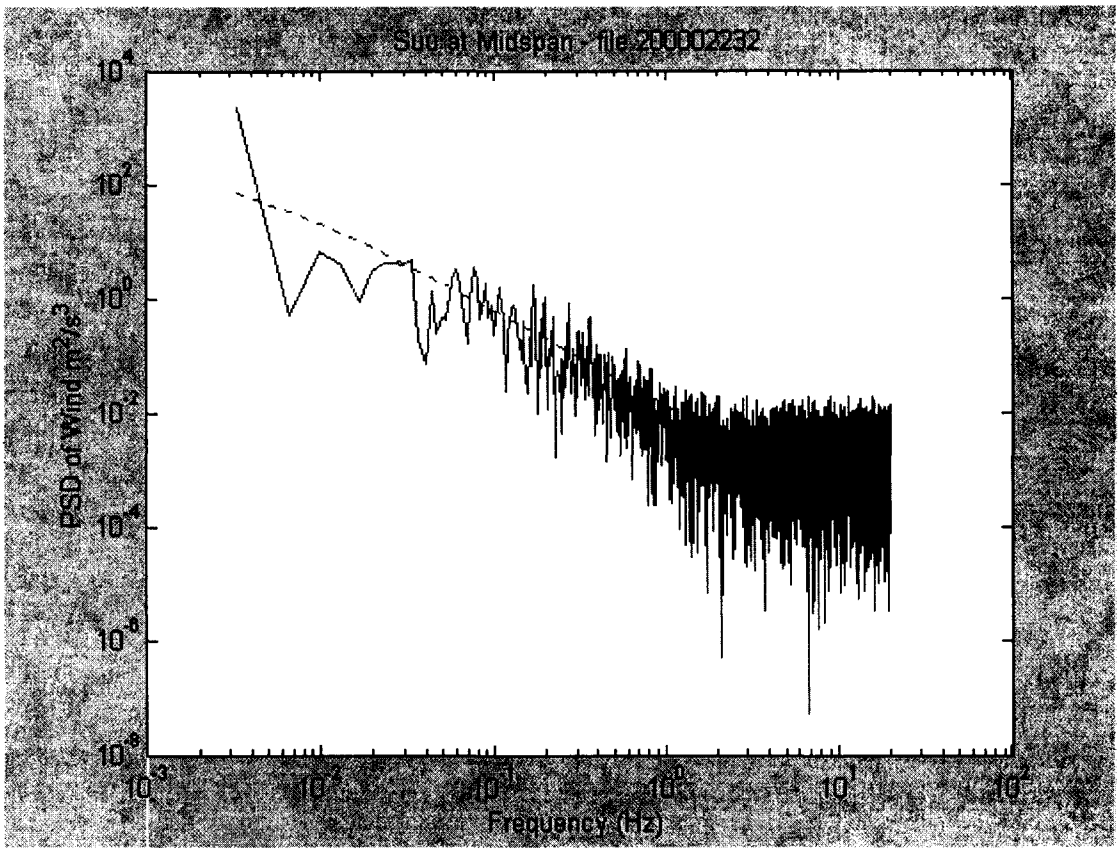

Figure 7. Example wind speed spectrum: Measured and predicted.

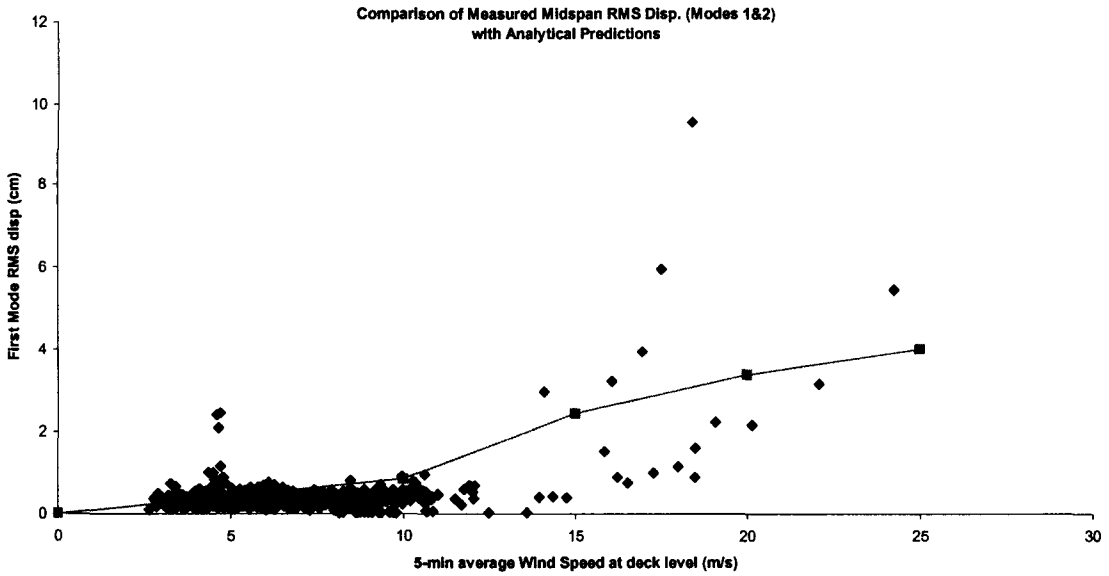

Figure 8. RMS Midspan Displacement in first two modes: Measured and predicted

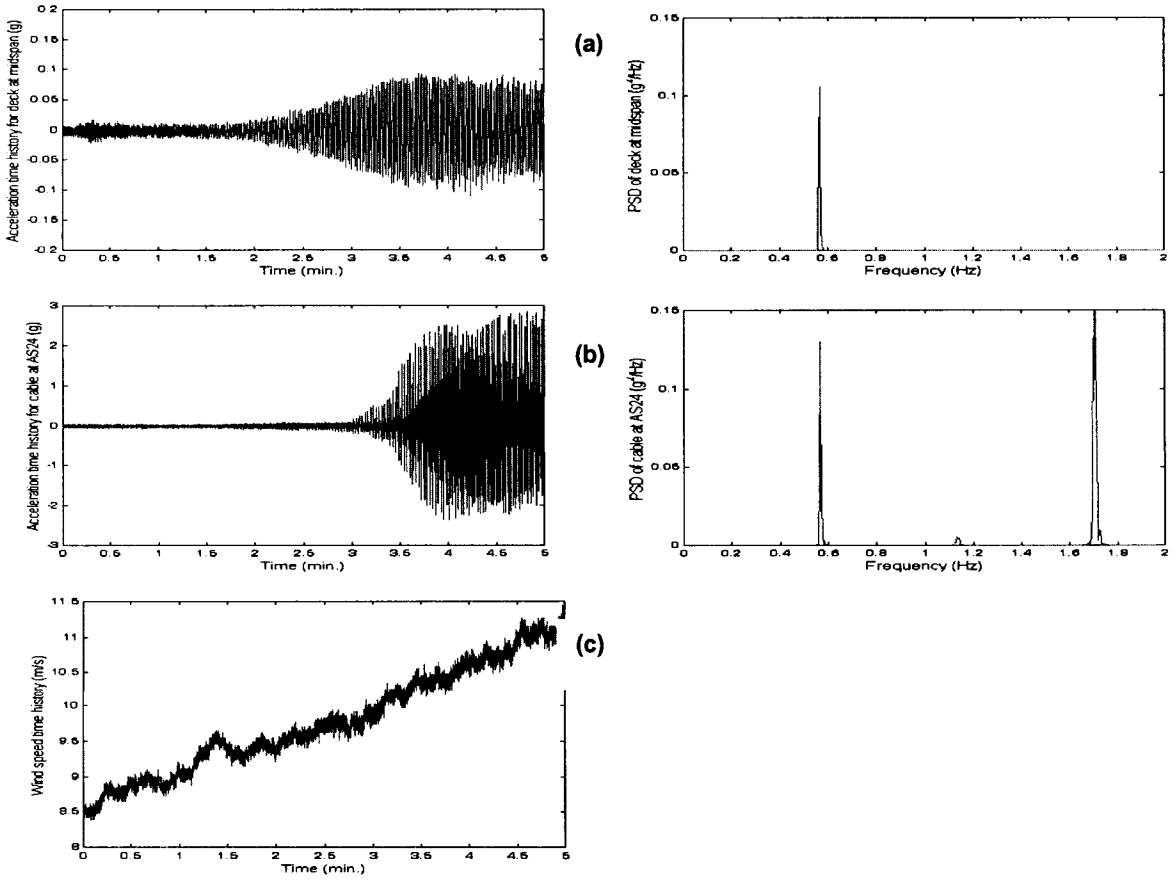

Figure 9. Time history and power spectral density (PSD) of acceleration for a) deck at midspan (vertical dir.), b) cable at AS24 (in-plane dir.) and c) deck level wind speed.

Strategy on Wind Engineering Research in BRI and NILM

by

Hisashi Okada[1], Yasuo Okuda[2], Hitomitsu Kikitsu[3] and Masamiki Ohashi[4]

ABSTRACT

This paper describes current strategy on wind engineering researches in the Building Research Institute (BRI) and the National Institute for Land and Infrastructure Management (NILIM). As for the strategy on wind engineering researches, based on performance-based structural design of buildings, it is significant to evaluate more reasonable wind loads on buildings by means of numerical simulations, wind tunnel experiments and field measurements. The outputs of such evaluations may be complementary to the new wind load provision[1] revised in 2000. The strategy presented here includes various themes of wind engineering about not only a building structural aspect but also meteorological or social/economical aspects.

KEYWORDS: Performance-Based Design
Index of Roughness Terrain
Numerical Simulation
Wind Tunnel Experiment
Strong Wind Damage
High-Rise Building

1. INTRODUCTION

Every year relatively strong and large-scale typhoon hit Japan, so it is indispensable to design buildings considering serviceability and safety limit criteria based on wind engineering. In Japan, structural designers usually refer several design regulations and standards on wind engineering, which are the Building Standard Law of Japan, Recommendations for Loads on Buildings of Architecture Institute of Japan (AIJ)[2] and so on. BRI and NILIM have already had important roles in making out drafts of them. As for the Building Standard Law of Japan, it was revised in 1998 and it is a so-called performance-based regulation. The new wind load provision entrusted by the Building Standard Law of Japan consists of several new design concepts based on Recommendations for Loads on Buildings of AIJ and other national or international standards such as ISO4354, and the main concepts[1] are as follows:

- Setting return period of design wind speed
- Introduction of exposure factor and gust effect factor
- Definite separation of loads for design of structural frames and design of claddings

However, there is still further discussion for reasonable improvement in the new wind load provisions.

Under the present circumstances as mentioned

[1] Group Leader, Department of Structural Engineering, Building Research Institute, 1 Tachihara, Tsukuba, Ibaraki, 305-0802, JAPAN

[2] Chief Research Engineer, ditto

[3] Research Engineer, ditto

[4] Researcher, Urban Planning Department, National Institute for Land and Infrastructure Management, 1 Tachihara, Tsukuba, Ibaraki, 305-0802, JAPAN

above, it is more important to design buildings based on performance-based design of wind loads. BRI and NILIM have set up the strategy on wind engineering researches for more rational wind load provisions and some themes of the strategy have been already started. The outlines of them are introduced in this paper. We consider that the following themes will get satisfactory results under international collaboration with US and Japan.

2. STRATEGY ON WIND ENGINEERING RESEARCHES

2.1 Establishment of Design Wind Load Based on Numerical Index of Roughness Terrain

New wind load provision in the Building Standard Law of Japan regulates four roughness terrain categories in Table 1 for the exposure factor as pointed out in the Introduction. Fig.1 shows Er for each roughness terrain category. For example, it defines very flat area as Category I and high density metropolitan area as Category IV , respectively. Originally, Recommendations for Loads on Building of AIJ as well as other national or international standards define roughness terrain categories by descriptive expressions and/or photographs of typical examples. But the way to define them was considered to have a possibility of misunderstanding.

Therefore, in the new wind load provision, a clear definition was required from the viewpoint of administrative control of building construction and it has been developed as follows. The roughness terrain categories are regulated with considerations whether the construction site is inside the city planning area or not and how is the building height and the distance from seafront or lakefront in Fig.2. The area of Category I is designated in the area of Category II , and the area of Category IV is designated in the area of Category III, respectively.

It is true that the way to define roughness terrain categories is distinct administratively, but it is not always reasonable evaluation from the viewpoint of wind engineering since the effects of configuration parameters such as element density[3] are not evaluated numerically in the provision. Therefore, we are now planning new research theme concerning the above problem. Recently the local height of each building in the roughness terrain has been able to be measured numerically by means of remote sensing laser devices on the airplane which can precisely measure the distances from the airplane to objects on the ground. Such measured digital data become available in major cities, the populations of which are more than 150 thousands in Japan. They can be classified into two models which are called Digital Surface Model (DSM) and Digital Elevation Model (DEM). DSM contains digital information of absolute heights above sea level of surface objects such as buildings or trees as shown in Fig.3, while DEM contains digital information of absolute height above sea level of the ground level enveloped from DSM. The main purpose of the theme is proposition of new numerical index of roughness terrain category which reflects uneven of the surface of the ground by means of DSM and DEM.

We have already engaged in measuring wind speed at some field points. One of them is located at the rural area in Tsukuba as shown in Fig.4[4]. The others are located just near the coast of the Pacific Ocean in Wakayama and the coast of Tokyo Bay in Chiba. The roughness terrain category of them may be different by the possible index, though the roughness terrain categories of them are the same in the new wind load provision. Fig.5 shows the power law index α of the wind profile near the ground observed at Tsukuba. The roughness terrain category around Tsukuba also should be III in the

new wind load provision, but the results in Fig.5 shows between category II and III. And the Boundary Layer Wind Tunnel in BRI will introduce automatic roughness element system in this year. So we can evaluate validity of the possible index by both of field data and experimental data. We consider that the index will be more useful for the reasonable design wind load.

2.2 Estimation of Urban Disaster by the Strongest Typhoon

Lots of strong typhoons have hit Japan almost every year, while the maximum instantaneous wind speed in history is 105m/s at Guam in 1997 by Typhoon Paka. From now on we cannot deny the possibility that such a strong typhoon will hit Japan owing to the greenhouse effect of the earth. Therefore, it is important to evaluate the possibility of attack of such typhoons by means of probabilistic and numerical simulation. BRI and NILIM have already started the research in collaboration with Tokyo Institute of Technology, Kyoto University, Meteorological Research Institute and Property and Casualty Insurance Rating Organization of Japan. The outline of the research is as follows.

2.2.1 Estimation of Possibility about Hitting of the Strongest Typhoon

In the probabilistic viewpoint, probabilistic data about the generating area and magnitude of the typhoon are necessary to collect and then the probabilistic estimation will be carried out considering unusual meteorology, the greenhouse effect and so on. In the numerical viewpoint, on the other hand, the estimation model of generation of the strongest typhoon will be developed and numerical simulation will be carried out. From these results, it will be possible to discuss how often and where the strongest typhoon hits, how the structure of the strongest typhoon is and what meteorological phenomena including meso-scale cyclone are generated following it.

2.2.2 Estimation of the Generation of Strong Wind in Urban Area

Recently local digital data of roughness terrain over Japan are going to be available as explained in section 2.1 and Fig.2. Doppler radar is useful for measuring wind speed in the sky of urban area[5]. Moreover, as for the meteorological measuring network, Atmospheric Environmental Regional Observation System (AEROS)[6] by Ministry of the Environment and measuring network by Fire and Disaster Management Agency as well as the Automated Meteorological Data Acquisition System (AMeDAS)[7] are now provided. We gathered the surface meteorological data of Typhoon Vicki in Kansai distinct in 1998 and showed the distributions of the meteorological elements on the ground[8]. In this study, we will evaluate how the strong wind generates in urban area by the numerical simulation such as Large Eddy Simulation (LES) in Fig.6. These digital data of roughness terrain and measured meteorological data are useful as the boundary condition of this simulation. And then in order to estimate wind loads on buildings on the ground, it is important to understand the correlation of the wind speed above the buildings and the wind speed around the buildings on the ground. By the numerical simulation which takes into account such boundary conditions and the correlation of the wind speeds in different heights, it is possible to evaluate tendency of strong wind around buildings and estimate the degree of the structural damage of buildings.

2.2.3 Estimation of the Disaster Caused by the Strongest Typhoon in Urban Area

Based on the results of numerical simulation, it is necessary to estimate not only structural damage of

buildings but also social or economical damages in order to understand the whole damage induced by the strongest typhoon. Therefore, the main outcome in this theme is presenting risk management system against the strongest typhoon in urban area.

2.3 Making out of Database on Buildings Damaged by Strong Wind

In this study, the main purpose is making out database of damaged low rise buildings based on technical reports[9] on past disaster by strong wind classifying damaged buildings into several patterns such as structure, height, shape of roof, roughness terrain and so on. Since above all low- rise wooden or lightweight buildings are relatively subject to attack of the strong typhoon and may end in collapse as shown in Fig.7, the damages of them must be discussed at the safety viewpoint as well as serviceability viewpoint. We consider this study will be useful for developing precise fragility curve of risk evaluation system against strong wind and for limit state design of low-rise wooden or lightweight buildings.

2.4 Evaluation of Characteristics of Across-Wind Response of High-Rise Buildings

In order to design structures of high-rise buildings, wind load is supposed to be more considered rather than seismic load since across-wind response is significant under strong wind. In BRI, several wind tunnel experiments about across-wind response using tall building dynamic models have been already carried out and the tendency of the configuration of building section to influence across-wind response and aerodynamic damping effect has been evaluated[10].

As next study, it is important to understand how strong wind velocity surrounding the building model has an influence on across-wind aerodynamic responses. In order to understand it, we will introduce PIV (Particle Image Velocimetry) system and measure the wind velocities around the building model by the synchronous measurements of wind pressures or across-wind deflections. This concept of a new wind tunnel experiment can be useful for evaluation of aerodynamic interaction.
Fig.8 shows an example of a synchronous measurement of wind velocities around a cubic model and wind pressures in a wind tunnel experiment. This measuring system can clarify the instantaneous complex wind flows around a body and wind pressure distributions on it, which have been evaluated only by numerical methods.

2.5 Harmonization of Wind Pressure Coefficient among Several Codes or Standards

BRI has already held some international workshops on performance-based design as follows:

- International Workshop on Harmonization of Performance-based Buildings Structural Design in Countries surrounding the Pacific Ocean (Dec. 1997) [12]
- International Workshop on Performance Based Building Structural Design(Nov. 2000) [13].

In these workshops, importance of the harmonization of design load among countries was stressed. However, as for wind pressure coefficient of several codes or standards, there are differences among them since there are differences in averaging time of basic wind speeds and the reference heights of the velocity pressure, though the basic concepts of them are similar[14]. Therefore, from now on we will propose how to harmonize wind load among codes and standards in the international meeting like the above workshops.

3.CONCLUSIONS

In this paper outlines of the strategy of wind engineering researches have been introduced. We consider that the output of these researches will contribute to estimating reasonable wind load affecting low-rise and high-rise buildings on the basis of performance-based structural design and also stress that wind engineering area on wind load which has ever focused on almost only building structures has necessity to take account of meteorological or social/economic aspects as well.

REFERENCES:

[1] H.Okada et al., Wind Load Provisions of the Revised Building Code in Japan, Preprint of the 33rd UJNR Joint Meeting, 2001

[2] Architectural Institute of Japan, Recommendations for Loads on Buildings, 1996.

[3] T. Maruyama, On the configuration of roughness elements in the urban area, J. of Wind Engineering, No.57, 1993 (in Japanese).

[4] Y.Sasaki et al., Full-scale Measurements on a Tower-like Structure, Summaries of Technical Papers of Annual Meeting Architectural Institute of Japan, 2002 (in Japanese).

[5] http://www.mri-jma.go.jp/Dep/sa/MRI-MSOSRD.html

[6] http://w-soramame.nies.go.jp/

[7] http://tenki.jp/amedas.html

[8] Y.Okuda et al., Weather Situation on Ground Observed at Fire Stations -Case of Typhoon Vicki, Proc. of the 32nd UJNR Joint Meeting, 2000

[9] For example, T. Murota et al., Report on Damage to Buildings Due to Bobara Tornado on December 11, 1990, Kenchiku Kenkyu Shiryo, No.78, 1992

[10]H. Kikitsu et al., Characteristics of Across- Wind Response of Tall Building with Open Passage, Proc. of 16th National Symposium on Wind Engineering, 2000 (in Japanese).

[11]H. Kikitsu et al., Synchronous Measurements of Wind Flows around a Building and Wind Pressures on a Building, Summaries of Technical Papers of Annual Meeting Architectural Institute of Japan, 2002 (in Japanese).

[12]Proc. of International Workshop on Harmonization of Performance-based Buildings Structural Design in Countries surrounding the Pacific Ocean, BRI, Dec. 1997.

[13]Proc. of International Workshop on Performance-Based Building Structural Design, BRI, Nov. 2000(CD-ROM).

[14]R.Yoshie et al., Comparison of peak pressure coefficients for wind load on cladding in national and international standards, J. of Wind Engineering, No.89, 2001.

Table1 Parameters of E_r

Terrain Category	Z_b (m)	Z_G(m)	α
I	5	250	0.10
II	5	350	0.15
III	5	450	0.20
IV	10	550	0.27

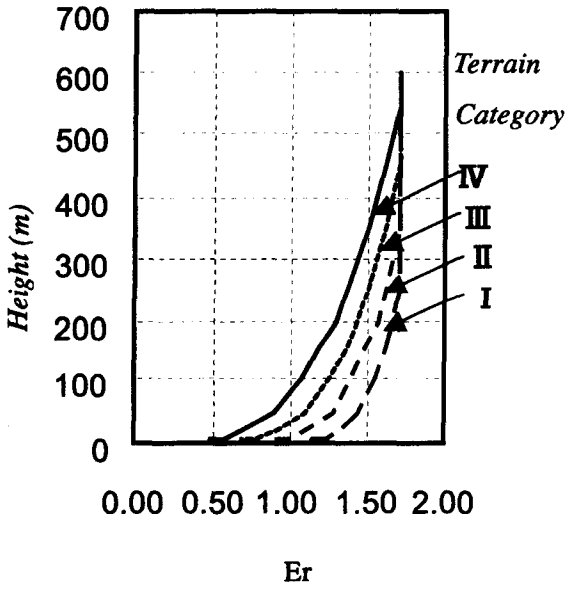

Fig.1 E_r (=Vertical Distribution Coefficient for Mean Wind Speed)

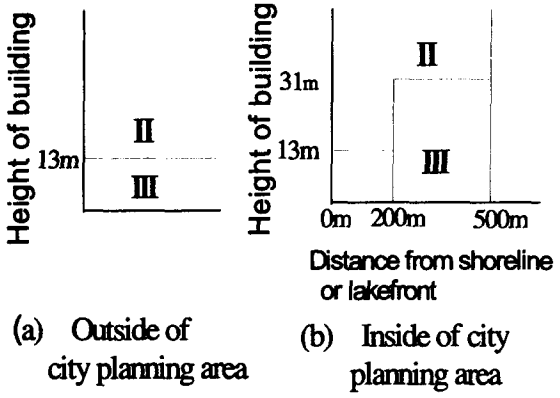

Fig. 2 Categories of Exposure Factor

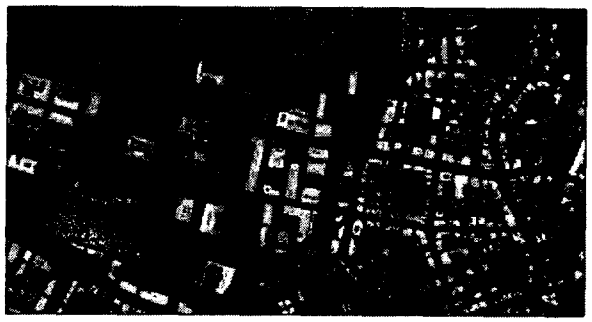

Fig.3 Example of Digital Surface Model at Maruno-uchi, Tokyo

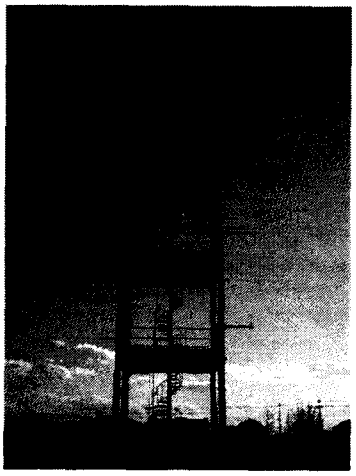

Fig.4 Overview of Tower-Like Structure in Tsukuba

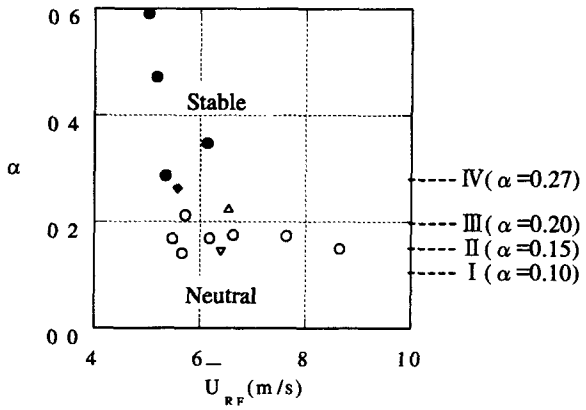

Fig.5 Power Law Index of Wind Profile near the Ground[4]

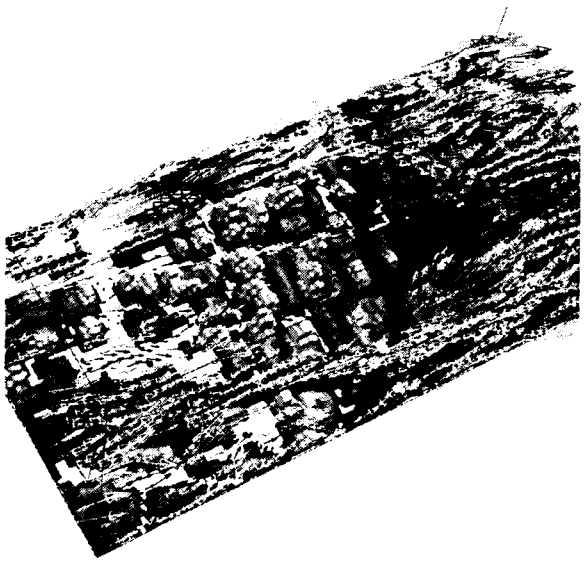

Fig.6 Example of Urban Area Simulated by LES with Local Digital Data of Roughness Terrain, Maruno-uchi, Tokyo

Fig.7 Example of Building Damaged by Typhoon Bart (Sep. 1999) The maximum instantaneous wind speed in Japan was recorded 83.9m/s.

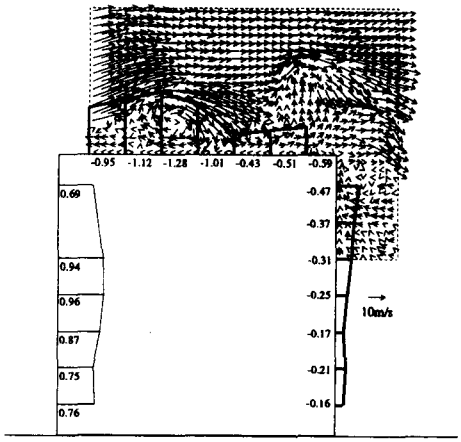

Fig.8 Synchronous Measurement of Wind Velocity around a Cubic Model and Wind Pressure[11]

Next Generation Wind Tunnels for Simulation of Straight-Line, Thunderstorm- and Tornado-Like Winds

by

Partha P. Sarkar[1] & Fred L. Haan, Jr.[1]

ABSTRACT

Researchers at Iowa State University (ISU) are developing next generation wind tunnels for studying primarily wind effects on structures. The Wind Simulation and Testing Laboratory in the Department of Aerospace Engineering and Engineering Mechanics will house facilities that simulate straight-line, thunderstorm- and tornado-like winds. This paper describes the motivation for advancing the state of the art of wind-structure interaction problems and the work currently underway at ISU.

A closed-circuit wind tunnel at ISU is currently being designed to accommodate two test sections (2.44 m x 1.83 m and 2.44 m x 2.29 m) with maximum wind speed capabilities of 50 m/s for aerodynamic testing and 40 m/s for testing in boundary-layer wind. It will have a gust generator that is capable of producing gusts up to 125% of the mean speed and an active lateral-turbulence generator that is capable of replicating the turbulence in hurricane winds. In addition, a microburst simulator and a tornado simulator are being designed. While the microburst simulator can produce a stationary/translating downdraft of 1.60 m in diameter and 25 m/s wind speed, the tornado simulator will produce a stationary or translating tornado-like vortex of up to 1.22 m in diameter with a swirl ratio of up to 2.0.

KEYWORDS: atmospheric boundary layer; next generation wind tunnel; thunderstorm simulation; tornado simulation; wind loads.

1.0 INTRODUCTION

Building wind tunnels with advanced capabilities will aid research efforts to understand the complex fluid structure interaction problems encountered in wind engineering design. Computer simulations currently are inadequate for design calculations because of the complexity of the fluid dynamics problems involved. Wind tunnels remain an integral component of the design process for wind sensitive structures.

Whether dealing with the aerodynamics of buildings, bridges or towers many issues remain to be fully resolved—including the role of non-stationary gust interactions, Reynolds number effects, and the significance of small-scale turbulence. Research into these issues is currently limited by the capabilities of existing wind tunnels. Building the next generation of such wind tunnels will contribute to the research infrastructure necessary to meet the challenges of wind hazards in this country. Better simulations of atmospheric flows will enhance our understanding of the various fluid structure interaction phenomena involved and greatly enhance our ability to develop mitigation measures.

[1] Wind Simulation and Testing Laboratory, Department of Aerospace Engineering and Engineering Mechanics, Iowa State University, 2271 Howe Hall, Room 1200, Ames, IA 50011-2271 USA

Understanding how the construction of wind tunnels with advanced capabilities constitutes a worthy endeavor requires some background into the use of wind tunnels in wind engineering and into the technical problems faced by wind engineers. This section provides such background by providing a general introduction to atmospheric boundary layer (ABL) wind tunnels—the wind engineer's tool of choice for the past several decades. Following this introduction, three distinct types of wind tunnels—for straight-line, thunderstorm-like and tornado-like winds—will be described.

2.0 BACKGROUND

2.1 Boundary-Layer Wind Tunnel

Wind tunnel simulation of the earth's atmospheric boundary layer is a well-established practice. Numerous researchers have contributed to the set of tools now in use for generating wind tunnel boundary layers that are several feet deep (for example, Cermak, 1971; Davenport, 1966; Cook, 1973; Farell and Iyengar, 1999). Conventional approaches employ a combination of passive devices such as spires, barrier walls, and floor roughness to generate boundary layers of the same scale as the geometric scaling of structural models placed in them.

It is assumed that atmospheric velocity variations can be adequately modeled by stationary mean and turbulent flow properties. This assumption means that despite the fact that hurricanes and gust fronts can have non-stationary characteristics, wind sensitive structures are tested in stationary flow environments. Wind tunnel turbulence intensities are matched to site values, and wind tunnel integral scales are scaled with the geometric scale of the structural models. While this conventional approach has served (and still serves) research and industrial needs for some time, the following two sections summarize how new tunnel capabilities can answer questions that cannot be addressed with the current generation of wind tunnels.

2.1.1 Turbulence Effects

The role of turbulence in the relevant fluid-structure interaction problems will influence the wind tunnel design. While some of the characteristics of atmospheric turbulence have been simulated sufficiently well for some time (for example, boundary layer velocity profiles, scaling of turbulence integral scales with model dimensions, etc.) other turbulence characteristics cannot be simulated precisely at all or cannot be simulated without considerable effort. This section briefly describes the role that turbulence plays in wind engineering and how new capabilities in wind tunnels can improve our understanding of these complex fluid-structure interaction problems.

Civil engineering structures do not, in general, have aerodynamic performance as their primary design goal. As a result, most civil engineering structures can be classified as bluff rather than streamlined bodies. Bluff bodies experience flow separation over significant portions of their surface. Bluff body aerodynamics differs from aerodynamics of streamlined bodies in that flow separation and reattachment play primary roles in pressure distributions about bodies of interest.

Free stream turbulence can modify the behavior of shear layers separating from bluff bodies. These modifications lead to flow structure changes and pressure distribution changes.

The role of turbulence in the aerodynamics of bluff bodies has been extensively documented in the literature (e.g., Gartshore, 1973; Kareem & Cermak, 1979; Hillier & Cherry, 1981; Bearman & Morel, 1983; Nakamura & Ohya, 1984; Kiya & Sasaki, 1985; Saathoff & Melbourne, 1997; and others). What is clear is that turbulence scales influence aerodynamic properties (such as rms and peak pressure coefficients). What is not clear is the extent of these influences or the precise mechanism of these influences.

When considering the smallest scales of turbulent velocity fluctuations, the inertial subrange is a relevant concept. The "inertial subrange" of a turbulent flow refers to that range of turbulent eddy scales between the large inviscid energy-containing scales and the small viscous diffusion scales. The size of the small, energy dissipating scales decreases

with increasing Reynolds number—which accompanies an increase in the size of the inertial subrange. The size of the inertial subrange is relevant to bluff body aerodynamics because the size of the subrange impacts the amount of turbulent energy residing at small scales. Small scale content—particularly scales on the order of the thickness of the separated shear layer—has been shown by a number of researchers to have a significant effect on separated shear layer flow structure (Gartshore, 1973; Tieleman & Akins, 1990).

A significant difference in small-scale turbulence content can exist between wind tunnel and full-scale flows because wind tunnel Reynolds numbers can be as much as three orders of magnitude lower than those of atmospheric flows. To quantify small-scale content, a "small-scale spectral density parameter" was originally suggested by Melbourne (1979) and subsequently used by Tieleman and Akins (1990). This parameter is essentially a *scale-specific* turbulence intensity. Tieleman and Akins reported that wind tunnel simulations with insufficient small scale content resulted in poorer comparisons of pressure coefficients between model and full-scale results.

The above may not fully address all issues relating to Reynolds number mismatches. Rather, it illustrates one of the ramifications of failing to match Reynolds numbers in wind tunnel simulations. Decreasing Reynolds number disparities between model and prototype flows will increase our confidence in test results. Understanding the physics of *how* flows depend on Reynolds number will decrease the uncertainty associated with imperfect turbulence simulation. Wind tunnels capable of higher Reynolds numbers would enable study of such questions.

2.1.2 Non-Stationary Flow Simulation

In addition to Reynolds number and small-scale turbulence issues, large-scale turbulent gusts also constitute an important aspect of wind tunnel simulation. Passive turbulence generation techniques (such as the obstacles described previously) have been shown to produce only a limited range of possible integral scales (Bienkiewicz et al., 1983). These scales are often not large enough to match prototype scales. As a result, active turbulence generation schemes have been developed to produce integral scales up to an order of magnitude larger than those of passive techniques. These techniques generally involve grids, flaps, airfoils (and combinations of them) that are forced to oscillate (Bienkiewicz et al., 1983; Kobayashi et al., 1994; Cermak et al., 1995).

While such devices are useful for generating stationary velocity fluctuations, they have not generally been used to simulate the non-stationary gusts that can occur in hurricanes. Anemometry data from hurricanes has shown that velocity records are non-stationary at times (Schroeder & Smith, 1999). Thus far, however, no wind tunnel studies have investigated the impact of such non-stationarity on aerodynamic pressures on structures. The next generation of ABL wind tunnel should have the capability to conduct such tests.

In addition to simulating large-scale gusts, wind direction changes can be simulated with active turbulence generation equipment. Wind direction changes have been observed to significantly affect pressure distributions on building models in wind tunnels (Wu et al., 2001a; Wu et al., 2001b). Next generation ABL wind tunnels will also be used for furthering research of this type.

2.2 Thunderstorm Winds

Microbursts occur in thunderstorms where the weight of the precipitation and the cooling due to microphysical processes acts to accelerate the air downwards. They are characterized by a strong localized down-flow and an outburst of strong winds near the surface. Strong outflow winds develop as the downdraft air is forced to spread horizontally near the ground level.

Fujita (1985) termed microburst as a small downdraft having an outburst of damaging winds with the horizontal extent of the damaging winds being less than 4 km. This definition has been modified by radar meteorologists: they require the peak-to-peak differential Doppler Velocity across

the divergent center to be greater than 10 m/s and the distance between these peaks be less than 4 km.

Thunderstorm winds have significant vertical velocity components and mean horizontal velocity distributions different from usual boundary-layer winds. It is also believed that the gust structure in a downdraft is much better correlated over its width than in more traditional boundary-layer flow, and hence will lead to larger overall loading of long structures. Thunderstorms are responsible for about 1/3 of the extreme gust speeds in the United States (Thom, 1969). In recent studies of extreme wind speeds in the United States, Vickery and Twisdale (1995) found that, outside of hurricane regions, up to 75% of the peak gust wind speeds occurred during thunderstorms. Selvam and Holmes (1992) undertook numerical modeling of the thunderstorm downdraft phenomenon, and were able to demonstrate reasonable agreement between a numerical model and limited full-scale data. Later, Holmes (1999) and Letchford and Illidge (1999) undertook physical model studies of a jet impinging on a wall and again found reasonable agreement between the numerical model, physical model and full-scale observations of a jet outflow velocity profile.

2.3 Tornado Winds

Tornadoes are vortices with significant tangential and vertical velocity components. Therefore, the flow field in a tornado is much different from the straight-line boundary-layer wind. Each year people die and civil infrastructure sustains damage due to tornados. According to Wind Hazard Reduction Coalition statistics (for more information, see www.windhazards.org), each year an average of 800-1000 tornados occur in the U.S. and cause 80 deaths (on average), 1500 injuries, and $850 million worth of damage. Although mostly associated with the region in the central states often referred to as "tornado alley," tornados have occurred in all fifty states and also occur in coastal regions as hurricanes make landfall.
In spite of causing significant losses, tornados have received little attention from wind engineers. Statistics show that 90% of all recorded tornados are rated F2 or less (Bluestein, 1993) on the Fujita Scale—that is, they involve wind speeds less than 157 mph. It may be economically feasible to design structures to resist F2 tornados. For cases where structures cannot be designed to survive, shelters below or above ground can be designed to protect people from tornados. It can be argued that certain essential facilities such as power plants, hospitals, and airports should be designed for tornados of F3 intensity or higher. Any such design work, however, requires accurate information about the nature of the wind loads on structures due to tornados.

Determining tornado-induced wind loads is difficult for two reasons—because quantifying wind velocity magnitudes in tornados is difficult and because simulating tornados in a laboratory while measuring wind pressures on structures is non-trivial and has not been attempted systematically. Laboratory simulation of tornados to obtain wind loads on structures is considered later. With the latest instruments, equipment, and computing facilities, it is now possible to pursue these goals through fieldwork and through numerical and laboratory simulation.

2.3.1 Field Measurements

Beyond the use of storm damage, recent advances in field measurements have greatly enhanced current knowledge of tornados and the supercells that spawn them. For example, the VORTEX project (which stands for "Verification of the Origins of Rotation in Tornadoes Experiment") (Rasmussen et al., 1994) was an effort to use advanced remote sensing equipment to conduct field measurements of tornados and tornadic storms.

One particular piece of field equipment that has proved to be useful is the "Doppler on Wheels" system (DOW). DOW systems measure wind velocities directly during a storm from single or multiple truck-based radars (e.g., Wurman, 1998, Wurman & Gill, 2000). In more recent years two DOW radars have been deployed in a pattern to allow dual-Doppler analysis. Whereas a single radar can measure the component of the wind along the line of site of the radar, a dual-Doppler analysis can determine the 3D characteristics of the flow field.

The DOW radars have been upgraded to include a 2.33 m dish, with a 0.9 degree beam width. In a violent tornado in South Dakota, one of the radars was deployed within 1.7 km of the tornado, so that wind data were collected with resolution of 30 m x 30 m x 38 m (Wurman 1998). These wind observations from radar are both supporting existing theories, and in some cases, raising questions about the previous views of tornado behavior. For example, Doppler measurements are finding that the decay rate of the wind does not follow a Rankine curve, as is often assumed (Wurman & Gill 2000).

2.3.2 Numerical Simulation

Because of prior difficulties in collecting small-scale observations within and near a tornado, numerical simulations of tornadic flow have been performed as a tool to improve understanding of tornado dynamics, small-scale flow characteristics, and possible genesis mechanisms (e.g., Lewellen et al., 1997; Lewellen et al. 2000a). Many of the numerical models developed were patterned after existing laboratory simulators, and were based upon simplified forms of the governing equations.

In most of the prior studies conducting numerical simulation of tornados, the emphasis has been on processes influencing the general tornadic wind flow or on potential mechanisms for tornadogenesis or tornado dissipation. Such issues can be explored with grid spacings larger (roughly 50-100 m) than what is required to examine the fine-scale details of tornado wind structure near the ground. Because of the different focus of these earlier works, little information has been provided about wind variations near enough to the ground to impact most built structures. For instance, Lewellen (1993) states that the *maximum velocities will occur below the top of the ground boundary layer (roughly 100 m above surface)*—a result that has great significance for determining tornado-induced wind loads. Therefore, much more detail about the near-ground winds is needed.

2.3.3 Laboratory Simulation

Simulating tornados in laboratory environments is not a new concept. Many laboratory simulator designs have been based on the pioneering work of Ward (1972). The Ward simulator essentially consisted of a fan providing updraft at the top of a cylinder above a test area and guide vanes and rotating screens around the test area to provide angular momentum to converging flow. Subsequent efforts—based on the Ward model—at Purdue University (Church et al., 1979), the University of Oklahoma (Jischke & Light, 1983) and that of Davies-Jones (1976) employed various means to improve the similarity between laboratory simulations and full-scale tornado events.

These laboratory simulations were aimed at greater understanding of the tornado vortex itself. However, numerical simulation has overtaken physical simulation as the tool of choice for tornado studies—both because of cost and because of versatility. While both laboratory and numerical simulation efforts have revealed a great deal about tornado structure (Lewellen, 1993), physical simulation of tornados *for the purpose of studying the tornado* may no longer be useful. For the purpose of quantifying tornadic wind loads on structures, however, physical simulation is a necessity.

The fluid mechanical complexity of flow-structure interaction problems relevant to buildings and engineered structures require that physical modeling (usually wind tunnels) be a fundamental design tool. Computers, in most cases, do not have the capacity for the Reynolds numbers and geometric complexity involved. This is also true of flow-structure interactions problems involving tornados.

Chang (1971) and Jischke & Light (1983) both modified the basic Ward design and added a small building model with pressure taps. These efforts found mean surface pressures to be significantly higher (3-5 times) in swirling, tornado-like vortices than in straight-line boundary layer flows. This suggests that when estimating tornado-induced wind loads on structures, it is not sufficient to use a conventional wind tunnel running with tornado wind velocities.

3. CURRENT WORK

3.1 Boundary-Layer Wind Tunnel Facility

At this point, much of the rough design of the wind tunnel has been completed. Rough sizing and layout of various components including the test sections, turning sections, and fan has been completed (Figure 1). This design incorporates non-stationary flow capabilities and a high velocity capacity of 50 m/s (112 mph) along with a large cross section to accommodate realistic models. The wind tunnel will be of closed-circuit type with the option of running in an open-circuit mode. It will have two test sections, one for aerodynamic testing that is 2.44 m (8 ft) wide by 1.83 m (6 ft) high followed by a test section to simulate atmospheric boundary layer wind that is 2.44 m (8 ft) wide by 2.29 m (7.5 ft) high. The maximum speed in the ABL test section will be 40 m/s (89 mph). Increased velocity capability will allow larger Reynolds numbers—with the accompanying increase in small-scale turbulent spectral content. A large working cross section will accommodate both large-scale models and large-scale velocity structures.

The major component remaining to be designed is the gust front generator that will involve bypass venting for the wind tunnel. This bypass vent will connect a portion of the tunnel upstream of the test section with a portion downstream. Computer-controlled valves will be used to control how much air is vented through the test section thus modifying the velocity in the test section. Preliminary calculations show that variations in flow velocity of up to 25% of the mean wind speed can be obtained.

Other design details include final specifications for all parts including the fan, the motor, turning vanes, turbulence screens, honeycomb sections, etc. The selected fan is of 2.74 m (9ft) diameter with capability of 220 m^3/s (465,000 cfm) flow rate driven by a 260 kW (350 hp) AC motor. The open circuit mode will be achieved by removing the set of turning vanes at the two successive corners that follow the test sections. The turning vanes will be moved on rails to the duct that connects these corners and this duct will be isolated from rest of the wind tunnel to make the flow circuit U-shaped. It is also planned to use one set of turning vanes as a heat exchanger to minimize the pressure losses in the tunnel.

3.2 Microburst Simulation

The schematic diagram for a downdraft flow is shown in Figure 2, and the experimental setup for the microburst simulator is shown in Figure 3. A honeycomb and two screens were used to reduce the turbulence of the issuing jet. A 3:1 area contraction was used at the nozzle end to make the velocity of the issuing jet uniform. The diameter (D) of the jet nozzle was 203 mm (8"). The distance (H) of the ground plane or impinging platform from the jet nozzle could be varied from a minimum of 203 mm (8") to a maximum of 826 mm (32.5"). For the current work, H/D = 2.89 and H/D = 4.06 were used. Henceforth, these two heights are termed as H23 and H32, respectively. The H/D ratio for this study was chosen to be around the median H/D value of a microburst that varies in between 0.75 to 7.5. Two jet velocities were used, V_0 = 9.57 m/s (31.4 ft/s) and V_0 = 16.17 m/s (52.0 ft/s). Henceforth, these two velocities are termed as V31 and V52, respectively. The velocity profiles were measured at distances of 2D and 3D from the center of the jet and the pressures on the buildings were also measured at those two locations as well as directly under the jet (i.e., at 0D). The building model used was a 25.4 mm (1") cube with 21 pressure taps uniformly spaced along its centerline; 7 taps on each of the front, roof and rear of the building. Pressures on the ground plane along the centerline of the jet were measured using 22 taps.

Velocity measurements were done using a DANTEC MiniCTA with a single hot wire. Flow visualization was achieved using a smoke generator, and pressure measurements were conducted using seven Validyne DP-45 transducers with each having a maximum capacity of ±0.89 inH_2O.

Smoke flow visualization is shown in Figure 4 for a stationary jet. The horizontal velocity profiles at 2D (distance from the center of the jet) are plotted for two different heights of the jet as shown Figure 6.

The profiles are compared with the empirical profile of Rajaratnam (1976), (Blevins, 1984), given by

$$\frac{U}{U_m} = e^{-0.693[(z-\delta)/b]^2}, \quad z \geq \delta, \qquad \text{Eqn. 1}$$

where δ is the height z from the ground plane at which the horizontal velocity U is maximum (U_m), and b is the height z where velocity is $U_m/2$ (Figure 5). Also plotted is Wood's (1999) empirical profile given by

$$\frac{U}{U_m} = 1.55\left(\frac{z}{b}\right)^{1/6}\left[1 - \text{erf}\left(0.7\frac{z}{b}\right)\right], \qquad \text{Eqn. 2}$$

where the variables U, U_m, z and b have been defined earlier and erf( ) is the error function. There is close agreement between the experimental and the empirical profiles. They are also compared with the experimental profile of Letchford & Illidge (1999).

3.3 Tornado Simulation

Small-scale models of the tornado simulator were built as design tools for the prototype. These were built to test concepts that advance the state of the art of laboratory tornado simulators beyond that based on the Ward simulator (Ward, 1972).

The first of the two simulators consists of a circular duct (diameter of 356 mm, 14 in.) that is vertically fixed to a trolley (Figure 7). It is covered at the top. A motor (0.75 kW or 1 hp, maximum 1750 rpm) drives a 5-blade vane located inside the duct through a pulley and shaft arrangement. The duct has a clearance of 127 mm (5 in.) from the top followed by a 102 mm (4 in.)–thick honeycomb plus screens. The 5-blade vane is 152 mm (6 in.) in length and is located below the honeycomb. There is a 356 mm (14 in.) gap between the vane and the exit of the duct. There is a deflector mounted at the duct exit to separate the updraft from the downdraft that occurs near the periphery of the duct. A variable speed motor drives the trolley so that the effect of translation speed on the tornado-like vortex can be studied. The distance between the ground plane and the bottom of the duct can be varied up to 584 mm (23 in.). There are two ground planes that can be separately used in this experimental setup. The first one has a circular opening covered by a slotted plate for injecting smoke or mist from underneath the ground plane to help visualize the flow. Two mist generators were used to produce mist for visualizing the vortex (Figure 8). The second ground plane has several pressure ports connected to a dedicated set of Validyne transducers to measure pressures on the ground surface underneath the vortex. The surface ground pressures were measured underneath the vortex (Figure 9) and compared with those obtained using Rankine vortex theory. They are comparable, but some differences exist. This is expected because the tornado vortex is somewhat different from a Rankine vortex in the free vortex region near the ground plane.

For the purpose of exploring different design configurations of the tornado simulator, a water-based simulator was also constructed (Figure 10). Water is often a better visualization medium than air. The water tank used here is a hexagonal glass tank. The height of the tank is 0.76 m (30 in.). The across panel dimension is 0.56 m (22 in.). The basic design of this simulator is the same as the tornado simulator mentioned earlier with minor differences. Due to the small size of this simulator, creating additional components are relatively inexpensive compared to the air-based tornado simulator. New blade assemblies and ducts can be interchanged with ease. This will aid the design process in terms of determining the best blade and duct assembly configuration for producing accurate representations of tornado vortices.

Visualization is accomplished by introducing glitter into the water and by using Particle Image Velocimetry (PIV) whose setup is shown in Figure 10. The velocity vectors were obtained on horizontal and vertical planes. The tangential velocity vectors at Z = 25 mm from the ground plane for the case where a screen (102 mm in diameter and 102 mm in height) was used without any surrounding duct at a height of 204 mm from the ground plane are shown in Figure 11.

Table 1 shows several parameters by which similarity between atmospheric and laboratory tornado vortices can be quantified. Aspect ratio is defined as the height of the vortex divided by the radius of the vortex core. Swirl ratio is the ratio of the vortex circulation compared to the accompanying flow rate into it. Radial Reynolds number is calculated using the radial velocity component of the tornado vortex flow. The parameters in this table for the ISU prototype simulator have been estimated based on the design and should be considered target parameters. The diameter of the simulated vortex near the ground for the prototype simulator is expected to be about 1.22 m (4 ft.) for a swirl ratio of 1.0 when the ground plane is 1.83 m (6 ft) from the ground. The diameter of the vortex will increase with reduced distance of the ground plane from the bottom of the rotating mechanism. This will allow structural model scales from 1:100, required for low-rise buildings, to 1:500, required for high-rise buildings and large structures. The surface friction on the ground plane will be scaled as per the geometric scale used for each model. The prototype simulator can translate for a distance of 3.05 m (10 ft) at a constant speed of 4.5 m/s (10 mph). The test section will be 6.1 m (20 ft) wide by 1.83 m (6 ft) high and 9.1 m (30 ft) length.

4.0 SUMMARY

This paper presents the need for the next generation wind tunnels for simulation of straight-line, thunderstorm and tornado-like winds and describes the current effort that is underway at Iowa State University.

5.0 REFERENCES

Bearman, P.W., Morel, T., "Effect of Free Stream Turbulence on the Flow Around Bluff Bodies," *Prog. Aerospace Sci.*, v. 20 (1983) 97-123.

Bienkiewicz, B., Cermak, J.E., Peterka, J.A., Scanlan, R.H., "Active Modeling of Large-Scale Turbulence." *Journal of Wind Engineering and Industrial Aerodynamics*, v. 13 (1983) 465-475.

Blevins, R. D, *Applied Fluid Dynamics Handbook*, Van Nostrand Reinhold Co, New York (1984).

Bluestein, H. B., "A Review of Tornado Observations," *The Tornado: Its Structure, Dynamics, Prediction, and Hazards*, ed. Church, Burgess, Doswell, Davies-Jones, American Geo. Mon. 79 (1993).

Cermak, J.E., "Laboratory simulation of the atmospheric boundary layer," *AIAA Journal*, 9, 9, (1971).

Cermak, J.E., Leighton, S.C., Leffler, R.D., "Wind-tunnel modeling of the atmospheric surface layer." *Journal of Wind Engineering and Industrial Aerodynamics*, v. 54/55 (1995) 505-513.

Church, C.R., J.T. Snow, G.L. Baker, E.M. Agee, "Characteristics of tornado-like vortices as a function of swirl ratio: A laboratory investigation," *Journal of the Atmospheric Sciences*, v. 36, (1979) 1755-1776.

Chang, C.C., "Tornado Effects on Buildings and Structures with Laboratory Simulation," *Proc. Third International Conference on Wind Effects on Buildings and Structures*, Tokyo, Japan, (1971) 231-240.

Cook, N.J., "On Simulating the Lower Third of the Urban Adiabatic Boundary Layer in a Wind Tunnel." *Atmospheric Environment*, v. 7 (1973) 691-705.

Davenport, A.G., "The treatment of wind loading on tall buildings," Proc. Symp. On Tall Buildings, (1966).

Davies-Jones, R.P., "Laboratory Simulation of Tornadoes," *Proceedings of the Symposium on Tornadoes, Assessment of Knowledge and Implications for Man*, ed. R.E. Peterson, Texas Tech University, (1976) 151-174.

Farell, C., Iyengar, A.K.S., "Experiments on the wind tunnel simulation of atmospheric boundary layers," *Journal of Wind Engineering and Industrial Aerodynamics*, v. 79 (1999) 11-35.

Fujita, T. T. *The Downburst: Microburst and Macroburst*, The University of Chicago Press, (1985).

Gartshore, I.S. *The effects of free stream turbulence on the drag of rectangular two-dimensional prisms*. Boundary Layer Wind Tunnel Laboratory 4-73, University of Western Ontario, (1973).

Hillier, R., Cherry, R.J., "The effect of stream turbulence on separation bubbles." *Journal of Wind Engineering and Industrial Aerodynamics*, v. 8 (1981) 49-58.

Holmes, J.D., "Modelling of extreme thunderstorm winds for wind loading of structures and risk assessment," 10th Int. Conf. on Wing Engineering, Copenhagen, 21-24 June, (1999).

Jischke, M. C., Light, B. D., "Laboratory Simulation of Tornadic Wind Loads on a Rectangular Model Structure," Proc. Sixth International Conference on Wind Engineering, v. 1, Australia & New Zealand (1983).

Kiya, M., Sasaki, K., "Structure of large-scale vortices and unsteady reverse flow in the reattaching zone of turbulent separation bubble." *Journal of Fluid Mechanics*, v. 154 (1985) 463-491.

Kareem, A., Cermak, J.E., "Wind-tunnel simulation of wind structure interactions." *ISA Transactions*, v. 18, n. 4 (1979) 23-41.

Kobayashi, H., Hatanaka, A., Ueda, T., "Active simulation of time histories of strong wind gust in a wind tunnel." *Journal of Wind Engineering and Industrial Aerodynamics* v. 53 (1994) 315-330.

Letchford, C.W. and Illidge, G. "Turbulence and topographic effects in simulated thunderstorm downdrafts by wind tunnel jet", 10th Int. Conf. on Wing Engineering, Copenhagen, 21-24 June, (1999).

Lewellen, W. S., "Tornado Vortex Theory," in Church et al., eds., *The Tornado: Its Structure, Dynamics, Prediction, and Hazards*, Geophysical Monograph 79, American Geophysical Union, (1993) 19-39.

Lewellen, W. S., D. C. Lewellen, R. I. Sykes, "Large-eddy simulation of a tornado's interaction with the surface," *J. Atmos. Sci.*, v. 54, (1997) 581-605.

Lewellen, D. C., W. S. Lewellen, J. Xia, "The influence of a local swirl ratio on tornado intensification near the surface," *J. Atmos. Sci.*, v. 57, (2000a) 527-544.

Melbourne, W.H., "Turbulence Effects on Maximum Surface Pressure – A Mechanism and Possibility of Reduction." *Wind Engineering, Proc. of Fifth International Conference.* Pergamon Press, (1979).

Nakamura, Y., Ohya, Y., "The effects of turbulence on the mean flow past two-dimensional rectangular cylinders." *Journal of Fluid Mechanics*, v. 149 (1984) 255-273.

Rajaratnam, N., *Turbulent Jets*, Developments in Water Science, 5, Elsevier Scientific Publishing Company, Amsterdam (1976).

Rasmussen, E.N., Straka, J.M., Davies-Jones, R., Dowell III, C.A., Carr, F.H. Milts, M.D., MacGorman, D.R. "Verification of the origins of rotation in tornadoes experiment: VORTEX," *Bulletin of the American Meteorological Society*, v. 75, (1994) 995-1006.

Saathoff, P.J., Melbourne, W.H., "Effects of free-stream turbulence on surface pressure fluctuations in a separation bubble." *Journal of Fluid Mechanics*, v. 337 (1997) 1-24.

Selvam, R.P. and Holmes, J.D. Numerical simulation of thunderstorm downdrafts", JWEIA, 41-44, pp. 2817-2825, (1992).

Schroeder, J.L., Smith, D.A., "Hurricane Bonnie wind flow characteristics as determined from WEMITE." *Wind Engineering into the 21st Century, Proc. of Tenth International Conference on Wind*

Engineering, (1999) 329-335.

Thom, H.C.S. New distributions of extreme wind speeds in the United States, J. Structures Div., ASCE, 94, 1787-1801, (1969)

Tieleman, H.W., Akins, R.E., "Effects of Incident Turbulence on Pressure Distributions on Rectangular Prisms." *Journal of Wind Engineering and Industrial Aerodynamics,* v. 36, (1990) 579-588.

Vickery, P. J. and Twisdale, L.A. Analysis of thunderstorm occurrences and wind speed statistics, JWEIA, 55, 813-821, (1995).

Ward, N.B. (1972) The Exploration of Certain Features of Tornado Dynamics using a Laboratory Model. *J. of the Atmospheric Science*s, 29, 1194-1204.

Wood, G. S and Kwok, K. C. S. "Physical and Numerical Modeling of Thunderstorm Downbursts", Wind Engineering into the 21st Century, Proc. of the 10th Intl. Conf. on Wind Eng., eds. A. Larsen et al., Denmark, June (1999), pp. 1919–1924.

Wu, F., Sarkar, P.P., Mehta, K.C., "Full-scale study of conical vortices and roof corner pressures." *Wind & Structures*, v. 4, n. 2 (2001) 131-146.

Wu, F., Sarkar, P.P., Mehta, K.C., Zhao, Z. "Influence of incident wind turbulence on pressure fluctuations near flat-roof corners." *Journal of Wind Engineering and Industrial Aerodynamics,* v. 89, (2001) 403-420.

Wurman, J. "Preliminary results from the ROTATE-98 tornado study," *Preprints, 19th Conf. on Severe Local Storms*, Minneapolis, MN, 14-18 September, (1998) 120-123.

Wurman, J., Gill, S. "Finescale radar observations of the Dimmitt, Texas (2 June 1995), tornado," *Mon. Wea. Rev.*, v. 128, (2000) 2135-2164.

TABLE 1. LABORATORY TORNADO SIMULATOR PARAMETERS

	Swirl Ratio	Aspect Ratio	Radial Reynolds No.
Atmospheric Range	0.050-2.0	0.2-3.0	1e9-1e11
Dallas Tornado	0.8	3.0	2e9
Purdue Simulator	0.1-1.0	0.3-3.0	4.1e3-1.2e5
Oklahoma Simulator	0.0-0.8	1.2	-
ISU Simulator	0.1-2.0	0.5-3.0	up to 1e6

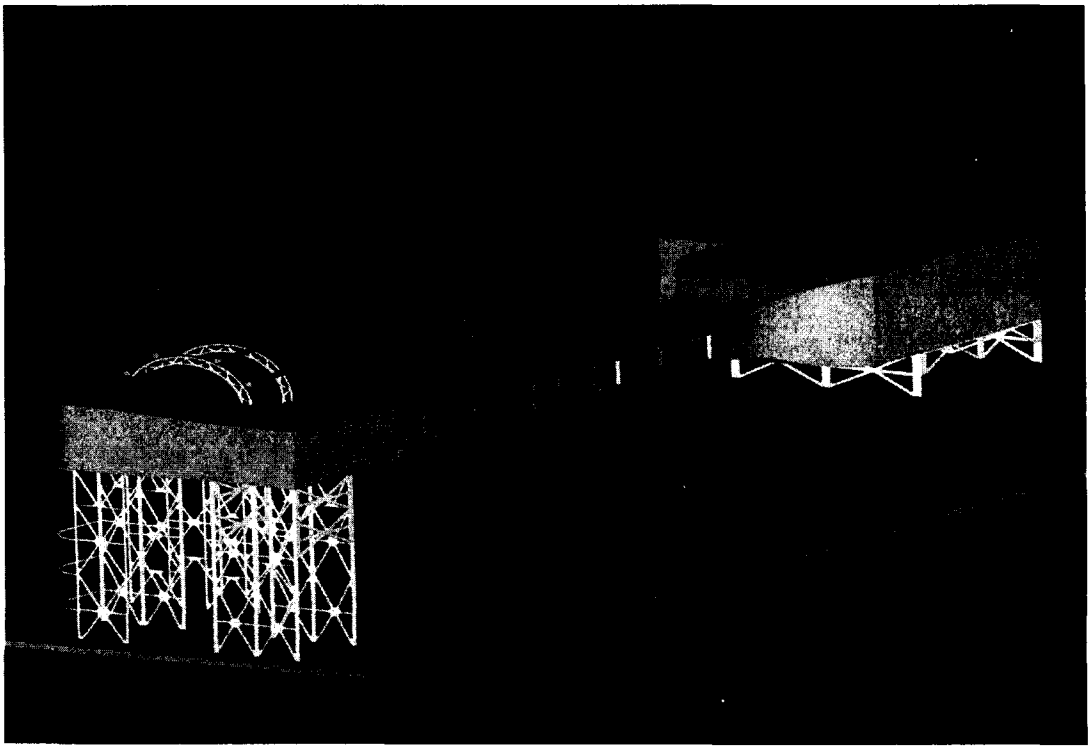

Figure 1 Three-dimensional rendering of the design for the atmospheric boundary layer wind tunnel.

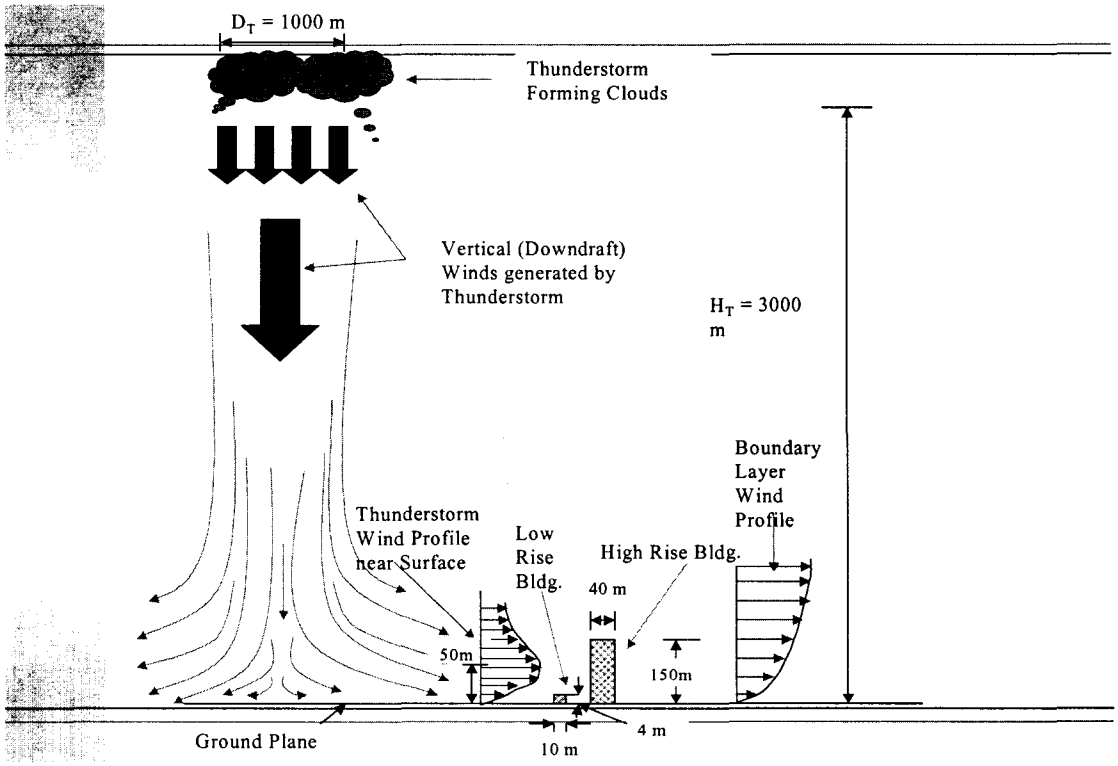

Figure 2. Schematic view of a typical downdraft flow showing the developed boundary-layer profile of horizontal flow field as compared to a straight-line boundary-layer wind profile

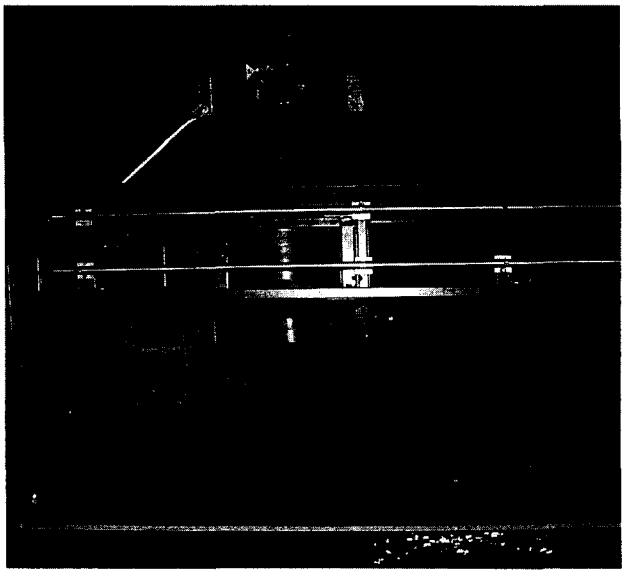

Figure 3. Experimental setup for the model microburst simulator

Figure 4. Microburst flow visualization with smoke

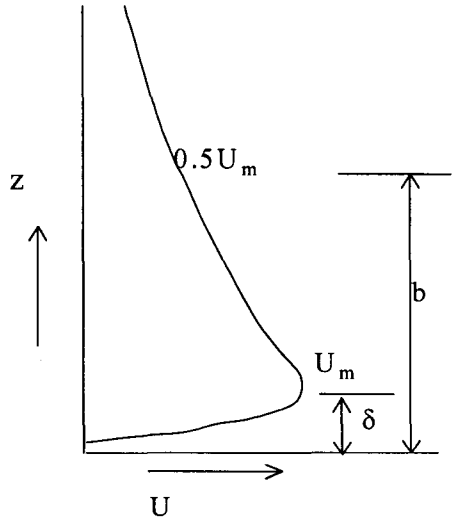

Figure 5. Boundary-layer horizontal velocity profile in an impinging jet

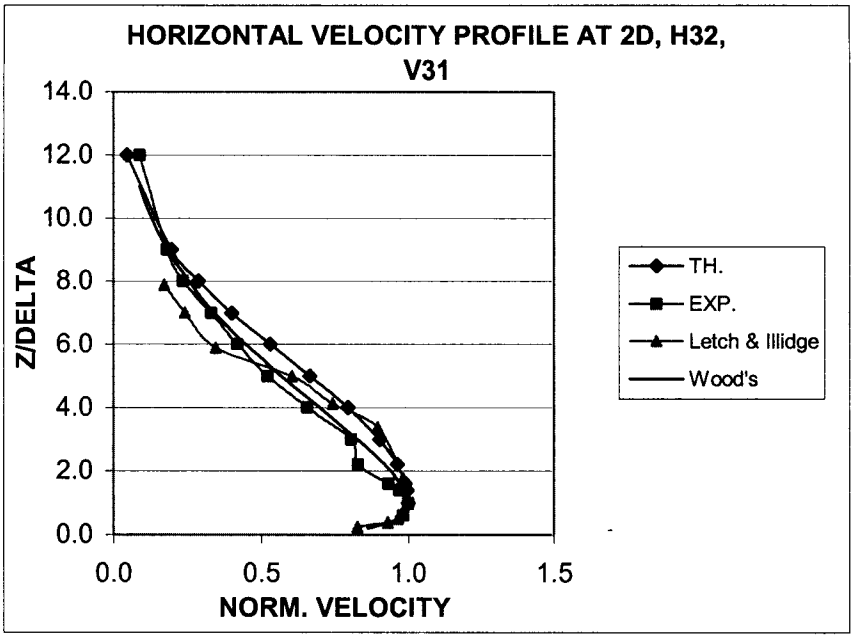

Figure 6. Comparison of normalized velocity profiles at 2D distance from the center of the microburst (D diameter). EXP. ISU experiment, TH. Blevin's (1984) Profile

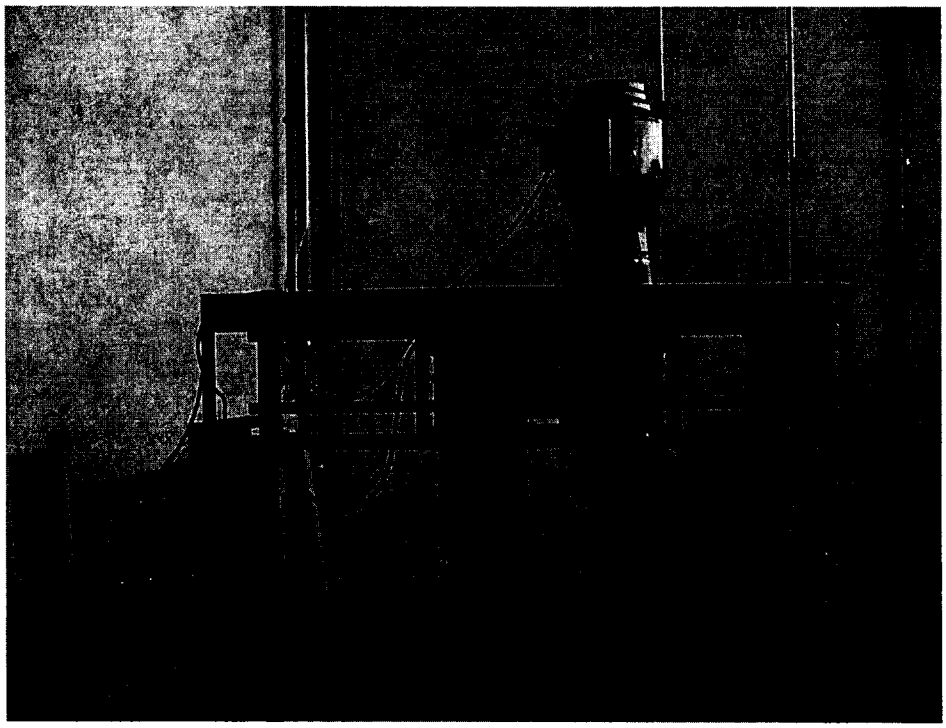

Figure 7. View of the model microburst/tornado simulator (1:5 scale) at ISU

Figure 8. Tornado flow visualization with mist (fine water particles in air)

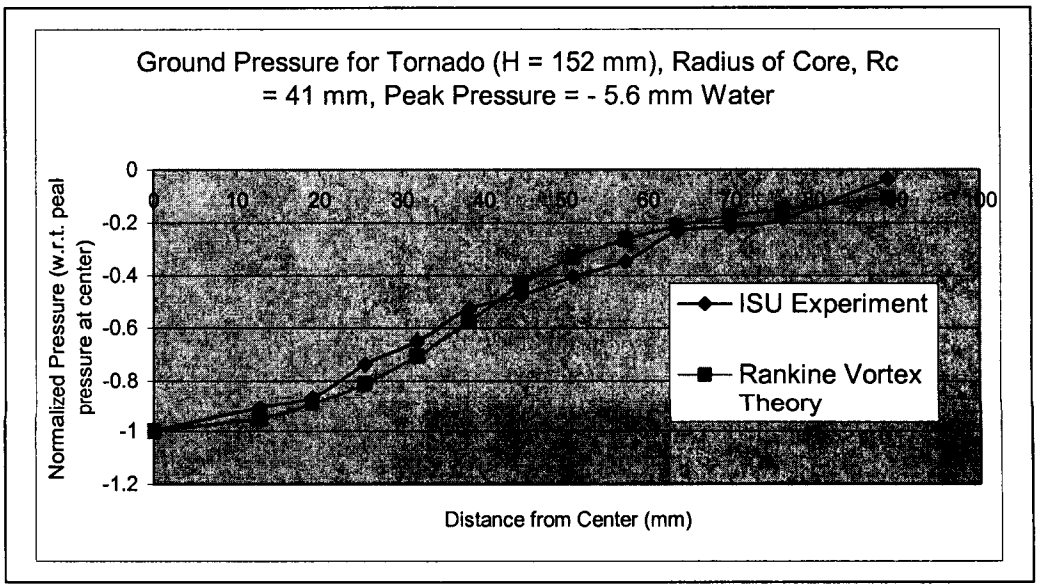

Figure 9. Normalized pressure distribution as measured underneath the tornado-like vortex on the ground plane compared with Rankine vortex

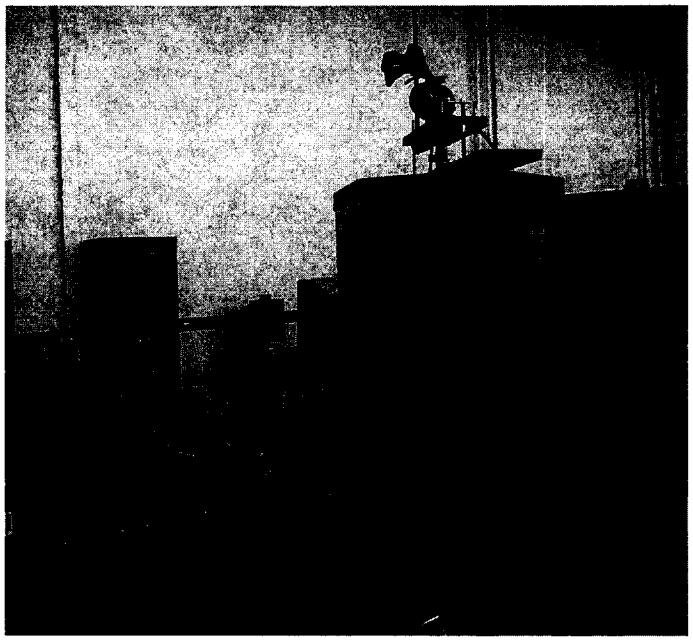

Figure 10. Experimetal setup for PIV measurement for flow visualization and measurement in water simulator

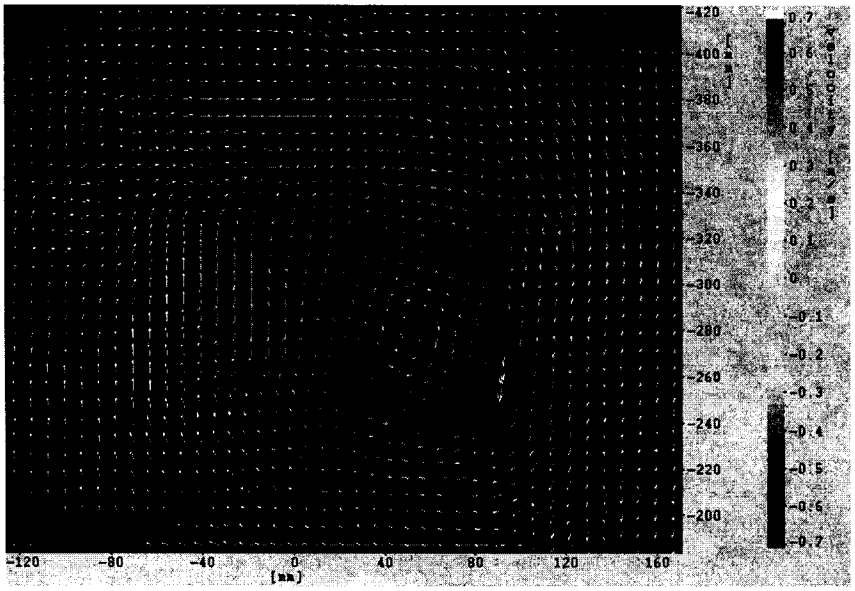

Figure 11. Tangential velocity vectors in the water simulator at z = 25 mm from ground plane. A screen (102 mm D and 102 mm H) without duct at 203 mm from ground plane was used to generate the vortex.

SESSION 4

DAMS

Seismic Performance Evaluation of Intake Towers

by

Richard C. Dove[1] and Enrique E. Matheu[2]

ABSTRACT

In the event of an earthquake, it is vitally important that the catastrophic failure of a dam and subsequent sudden release of the reservoir be prevented. An important part of the prevention of such a failure is maintaining the ability to control the release of water after the earthquake. For most earthen dams, and some concrete dams, the release of water is controlled through a reinforced concrete intake tower. The functional survival of such towers has been the main concern of a multi-year research effort sponsored by the U.S. Army Corps of Engineers (USACE). Most intake towers in the current USACE inventory are lightly reinforced. The functional survival of such lightly reinforced structures is thus the main concern of this research effort. The ultimate objective of this research work is the development of analysis procedures for seismic evaluation of these structures. This paper presents some of the results of this effort.

KEYWORDS: Reinforced concrete, ductility, intake towers, seismic evaluation, displacement-based approach, shaking table tests.

1.0 INTRODUCTION

Earthquake engineering research efforts in the area of reinforced concrete intake towers are currently focused on understanding the nonlinear response of lightly reinforced intake towers. The ultimate objective is the evaluation and/or development of simplified analysis procedures for the seismic evaluation of these structures. The work presented in this paper is part of a larger research effort that began with a statistical analysis of the USACE inventory of existing intake towers. This tower inventory analysis quantified the distribution and variation of the structural characteristics of the towers as relating to their earthquake location hazard (Dove, 1996). The information collected was used in planning the second phase of this research program, referred to as the Intake Tower Substructure (ITS) experimentation series (Figure 1), which was conducted during 1996 and 1997 (Dove, 1998) at the Geotechnical and Structures Laboratory (Vicksburg, Mississippi).

Figure 1. Typical 1/8-scale static experiment.

The results from this experimental effort, which included monotonic and cyclic loading tests of 1/8-scale models, showed that substantial ductility is available (Figure 2). The objectives of these experiments were not only to observe the response of reduced scale models of typical intake towers and quantify the ductility available, but also to use the information generated for the development of approximate and/or simplified evaluation procedures for existing intake towers.

[1] Geotechnical and Structures Laboratory, U.S. Army Engineer Research and Development Center, Vicksburg, MS 39180 (USA).

[2] Department of Civil and Environmental Engineering, Louisiana State University, Baton Rouge, LA 70803 (USA).

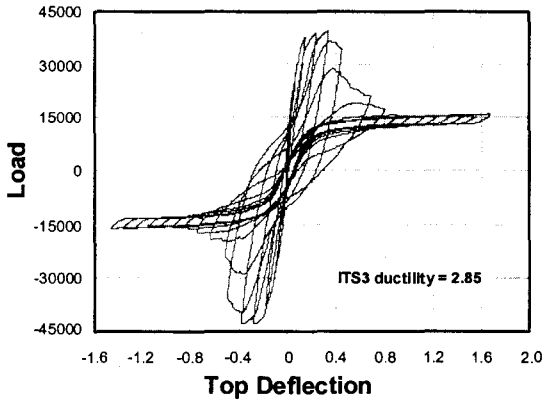

Figure 2. Typical load-deflection curve exhibiting substantial ductility.

Based on the results of the ITS experiments, it was concluded that additional information was required for the application of the simplified analysis procedures under development. Specifically, a method was needed to properly estimate the ultimate deflection capacity of existing intake towers. During 1999 and 2000, fourteen 1/2-scale experiments were conducted to provide a statistically significant basis for the development of an empirical estimation of the parameters needed (Dove, 2000). As a result of these tests, a modified displacement-based analysis procedure was generated incorporating the available experimental information. This analysis procedure is discussed in the next section. More recent research efforts have mainly focused on the validation and calibration of the proposed analysis procedure and its underlying assumptions by means of an extensive series of shaking table tests. The first series of tests were recently performed at the facilities of the Construction Engineering Research Laboratory (Urbana, Illinois). The corresponding results and preliminary conclusions are discussed in following sections.

2.0 DISPLACEMENT-BASED ANALYSIS

The nonlinear response and ductility of lightly reinforced intake towers has been the focus of recent analytical and experimental efforts. It has been shown that lightly reinforced intake towers can exhibit ductility but with a very localized failure. When a lightly reinforced intake tower is excited by a seismic event, a single crack forms at the base of the tower or at the location of a major stiffness change. Experimentation has shown that ultimate failure is dependent on the response of the rebar within the crack (Dove, 2000). An analysis technique has been developed that reflects this localized failure mode and includes explicit consideration of the earthquake-induced displacements of a structure. It also attempts to account for the shift of the fundamental frequencies with formation of plastic regions in the structure. The proposed analysis procedure will be presented by applying it to a representative rectangular intake tower.

The structure analyzed has been used as an example problem in past and current USACE guidance documents (U.S. Army Corps of Engineers, 2002). The analysis presented here is essentially a modification of the prior analysis presented in this reference. The structure is a generic tapering rectangular tower about 61 m tall, 14.6 m by 11.6 m wide with a wall thickness 1.83 m at the base, as shown in Figure 3. Primary reinforcement consisted of #11 bars at 30.48 cm on center.

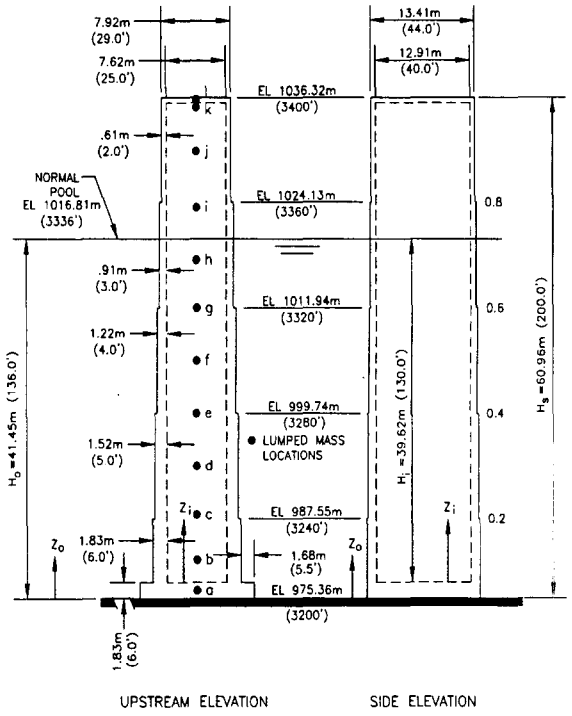

Figure 3. Layout of example intake tower.

The assumed analytical model consists of a simple cantilever beam attached to a rotational spring. The spring approximates the response of the cracked region. The beam models the response of the uncracked tower above the base. The definition of the rotational spring stiffness requires the calculation of the moment-curvature (M-ϕ) relationship. Based on this relationship, it is then possible to calculate the corresponding moment-rotation relationship (M-θ), which is obtained by multiplying the curvature by an assumed plastic hinge length. The M-θ relationship represents the stiffness of the rotational spring.

The M-θ relationship is often strongly bilinear, and therefore a simplification is required in order to conduct a response spectrum analysis. The M-θ relationship is linearized such that it encloses the same area for the same maximum rotation. This approximation allows the calculation of the expected deflection under the given earthquake loads. Given the linear spring stiffness, the element properties, and any added mass due to water, a response spectrum analysis can be readily conducted. The maximum deflection calculated represents the deflection demand of the tower under the input earthquake.

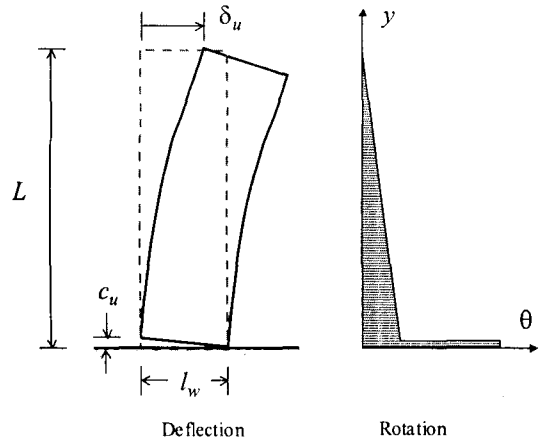

Figure 4. Deflection capacity.

In order to complete the analysis, it is necessary to determine the ultimate deflection capacity δ_u (Figure 4), which is calculated as follows:

$$\delta_u = \frac{\phi_E L^2}{3} + \delta_{cu} \quad (1)$$

where ϕ_E is the ultimate elastic curvature at the base of the tower, also known as the cracking curvature; θ_P represents the plastic rotation at failure; l_w denotes the depth of the section, L is the height of the intake tower; and δ_{cu} represents the deflection contribution caused by the base crack.

This model assumes that the ultimate lateral deflection consists of the sum of two parts. The first part is the elastic response of the body of the intake tower above the cracked section. The elastic curvature ϕ_E can be computed as

$$\phi_E = \frac{M}{EI_g} \quad (2)$$

where M denotes the yielding moment, E the elastic modulus, and I_g the uncracked moment of inertia. The second part is a rigid body rotation of the tower as the crack opens at the base of the elastic section, and the tower rotates about the neutral axis of the cracked section. It is conservative to assume that the neutral axis is coincident with the edge of the tower. Hence, the lateral rigid-body deflection at the top of the tower varies directly with the crack width, and its maximum value is as a ratio of the tower height and the tower width, times the ultimate crack width. Therefore,

$$\delta_{cu} = \theta_P L = \frac{c_u}{l_w} L \quad (3)$$

The principal unknown in the above equation is c_u, i. e., the ultimate crack width at failure, which is a function of the ultimate strain of the rebar and the strain penetration. Experiments have indicated that for a single crack response, the crack widths are largely predicted by the ultimate strain capacity of the rebar and rebar diameter. An empirical equation for c_u was generated as follows:

$$c_u = 0.12 + 2.47\varepsilon_u + 0.79 d_b \quad (4)$$

where ε_u is the ultimate strain at failure of the rebar as measured over the standard gage length (20.3 cm or 8 inch) and d_b is the diameter of the reinforcing bar in cm.

Application of the proposed displacement-based procedure to the design example begins with the calculation of the M-ϕ relationship for the bottom section of the tower in two directions (weak and strong axis). This follows the assumption that the failure mechanism of the tower will be the formation of a single crack at the base of the bottom section. The vertical dead load of the tower self weight was included. Assuming an 18 percent ultimate strain, the ultimate crack width calculated from the above empirical equation to be 1.40 cm. The strain penetration length (L_s) can be calculated from the following equation:

$$L_s = \frac{c_u}{\varepsilon_u} \qquad (5)$$

This gives a strain penetration length of 7.52 cm. Multiplying the M-ϕ diagram by this strain penetration length gives the corresponding M-θ relationship. Proceeding as described above, the equivalent rotational spring stiffness is calculated such that the total area under the equivalent rotational spring is the same as that for the corresponding weak and strong axis M-θ relationships. The resulting equivalent spring constants are given by 2.107E+12 N-m/rad and 3.561E+12 N-m/rad for the weak and strong axes, respectively. Based on these properties, and assuming a finite-element discretization of the structure using standard beam elements, a response spectrum analysis was conducted using the MDE response spectrum for 5% damping indicated in Figure 5. The results of this analysis indicate a top deflection of 9.6 cm for rotation about the strong axis and 10.1 cm for rotation about the weak axis.

Finally, it is necessary to calculate the ultimate deflection capacity δ_u. Given the ultimate crack width and section width at the base of the model, the ultimate base rotation θ_P can be calculated. The elastic curvature ϕ_E at the base of the intake tower (also known as the cracking curvature) is determined from the M-ϕ relationship for the section. Based on these parameters, the deflection capacity of the tower is calculated as 9.6 cm for rotation about the strong axis and 12.6 cm about the weak axis. Therefore, the tower passes the analysis.

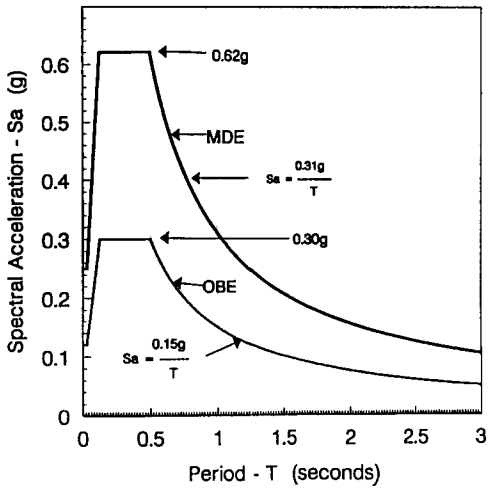

Figure 5. Standard spectra used in analysis.

3.0 SHAKING TABLE EXPERIMENTS

As part of a continuing effort to validate the displacement-based analytical procedure, a series of shaking table experiments was performed. The experiments were conducted on a 1/8-scale model of a typical intake tower, of the same design as used for the ITS3 cyclic loading tests. The objective of these tests was to compare the failure mode under dynamic conditions with the failure mechanism previously observed under monotonic and cyclic loading. These tests also served the purpose of providing additional data for the evaluation and validation of current analytical models.

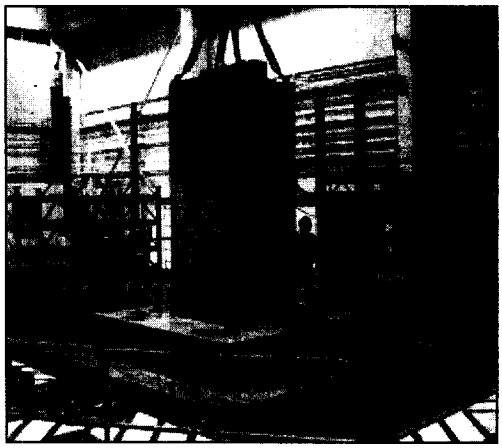

Figure 6. Intake tower model on top of shaking table at the Construction Engineering Research Laboratory (Urbana, Illinois).

The tests were completed by early July 2001. The intake tower model (Figure 6) was tested laterally with uniaxial sinusoidal support motions, near the tower's natural frequency in the short direction of the tower. Test levels were increased until failure occurred. Pre- and post-failure responses of the model as well as the corresponding failure mechanism were systematically documented. The extensive results collected from this testing program will facilitate a direct comparison between the measured responses and the behavior predicted by numerical models and previous static cyclic tests.

The intake tower model was 3.05 m tall with a hollow rectangular cross-section that was 1.32 m wide in the east-west direction and 1.02 m wide in the north-south direction. The walls were 0.14 m thick, constructed of normal strength concrete with scaled aggregate and reinforcing steel. The weight of the tower was calculated as 4.29 metric tons. Figure 7 shows a schematic drawing of the intake tower model, which was placed on top of a heavily reinforced base beam. The base beam was square, with a width of 2.74 m and a thickness of 0.46 m.

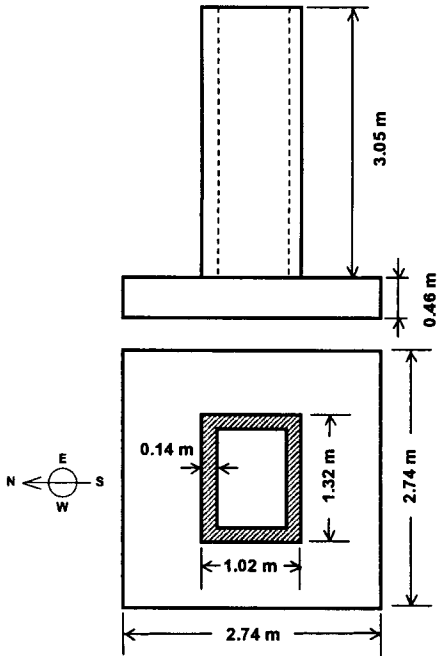

Figure 7. Schematic view indicating intake tower model dimensions.

The model was extensively instrumented with accelerometers attached to the base beam and the external faces, linear variable differential transducers (LVDT) installed between the base beam and tower, and several deflection gages. In addition, the vertical reinforcing steel was instrumented with strain gages. Progression of damage was extensively documented with digital photographs and video. Two digital camcorders were used: one recorded the overall model response from the east-north-east side, whereas the other camcorder zoomed in on the cold joint at the bottom of the model on the west face of the model (Figure 7).

Table 1. Scaling relationships

Variable	Scaling factors	
	$\lambda_L, \lambda_E, \lambda_\rho$	$\lambda_L, \lambda_E = \lambda_\rho = 1$
Time	$\lambda_t = \lambda_L \sqrt{\frac{\lambda_\rho}{\lambda_E}}$	$\lambda_t = \lambda_L$
Frequency	$\lambda_f = \frac{1}{\lambda_L}\sqrt{\frac{\lambda_E}{\lambda_\rho}}$	$\lambda_f = \frac{1}{\lambda_L}$
Force	$\lambda_F = \lambda_E \lambda_L^2$	$\lambda_F = \lambda_L^2$
Stress	$\lambda_\sigma = \lambda_E$	$\lambda_\sigma = 1$
Strain	$\lambda_\varepsilon = 1$	$\lambda_\varepsilon = 1$
Displacement	$\lambda_u = \lambda_L$	$\lambda_u = \lambda_L$
Velocity	$\lambda_{\dot{u}} = \sqrt{\frac{\lambda_E}{\lambda_\rho}}$	$\lambda_{\dot{u}} = 1$
Acceleration	$\lambda_{\ddot{u}} = \frac{\lambda_E}{\lambda_L \lambda_\rho}$	$\lambda_{\ddot{u}} = \frac{1}{\lambda_L}$

Table 1 displays the scaling relationships that govern this type of problem, in terms of 3 main scaling factors: λ_L (geometry), λ_E (modulus of elasticity), and λ_ρ (density). The model geometry was 1/8 of the prototype, that is, $\lambda_L = 8$. Standard strength concrete was used for the model, and therefore $\lambda_E = \lambda_\rho = 1$. The third column of the table contains the resulting scaling relationships for this case, which is characterized by an acceleration scaling factor that is the reciprocal of the geometric scaling factor. Therefore, inertial and gravity effects for the

model should be increased $\lambda_L = 8$ times with respect to prototype conditions. The scaling of inertial effects was achieved by increasing the magnitude of the imposed base accelerations by a factor of 8.

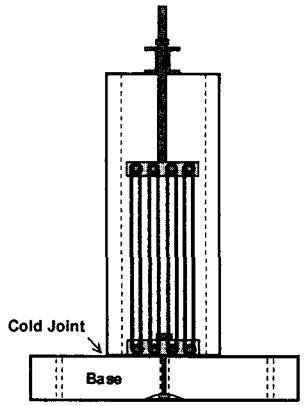

Figure 8. Schematic view depicting modeling of gravity load effects.

The scaling of gravity effects was achieved by means of 80 loops of 2.54cm diameter elastic cord connected between the top and the base of the tower model (Figure 8). The extremely flat load-deflection characteristics of these elastic cords allowed them to be used in such a way that the corresponding vertical loads did not vary significantly with the rocking response of the tower with respect to the base. The cords were designed to provide an additional vertical load equal to 30 metric tons. Including this load, the resulting vertical compressive stresses at the base of the model due to gravity effects were 575 kPa.

The model was initially tested with low-level random motions to measure natural frequencies, mode shapes and damping. These tests were conducted in the X (north-south) and Y (east-west) directions. The amplitude of the input motions were initially very low (0.02 g). The random motion tests were then repeated at increasing amplitudes until clear modal information was acquired in both horizontal directions.

The model was initially excited using sinusoidal base motions in the X direction at a frequency of 28 Hz (3.5 Hz, prototype scale). The imposed base motions ramped up to full amplitude in 0.5 seconds; held a constant amplitude for 2.0 seconds; and ramped down in 0.5 seconds, for a total test duration of 3.0 seconds. For each test run, the amplitude of the sinusoidal support motion was gradually increased with respect to the previous one while keeping the excitation frequency constant. Previous static tests performed on similar 1/8-scale models indicated that the base of the model cracked at a value of top lateral deflection between 1.3 and 1.8 mm, with applied lateral loads between 130 and 170 kN.

The model failed by cracking at the cold joint at the base. Once it cracked across the entire cold joint surface, the model softened significantly. The change in the fundamental frequency was a very effective damage indicator. Damage evolution was carefully monitored by the LVDT measurements along the base of the model.

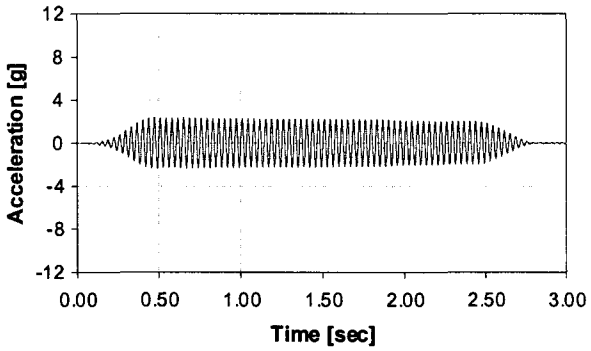

Figure 9. Base acceleration, A6x (run 18).

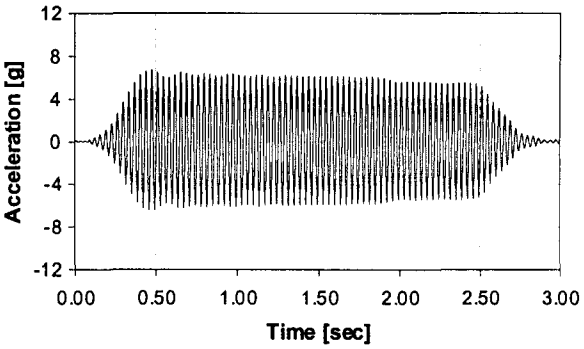

Figure 10. Top acceleration, A14x (run 18).

Figures 9 and 10 show acceleration responses measured during test run 18, corresponding to an excitation level of 2.04 g (0.255 g, prototype

scale). These responses correspond to sensors A6x and A14x, located at the bottom and top of the north face of the model, respectively. Figure 11 shows the time history measured by one of the deflection gages installed at the top of the model (D5x). The amplitude of oscillation is about 2 mm.

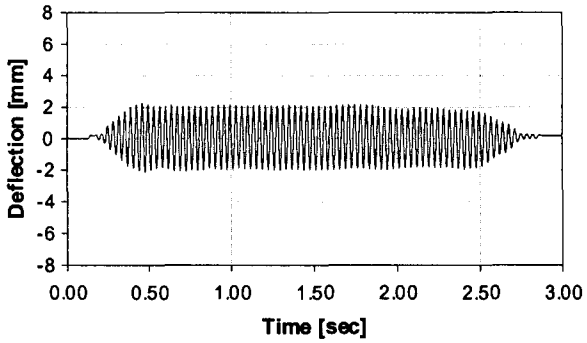

Figure 11. Top deflection, D5x (run 18).

After significant damage was identified, the model was again tested with random motions to determine updated modal properties associated with the damaged condition. Cracking of the model across the entire cold joint surface softened the structure, as evidenced by the shift in the fundamental vibration frequency. Figure 12 shows the transfer functions between the top model acceleration (A14x) and the base beam acceleration (A1x) corresponding to two different series of random motion tests. As shown in the figure, the fundamental frequency decreases from 29 Hz to 24 Hz.

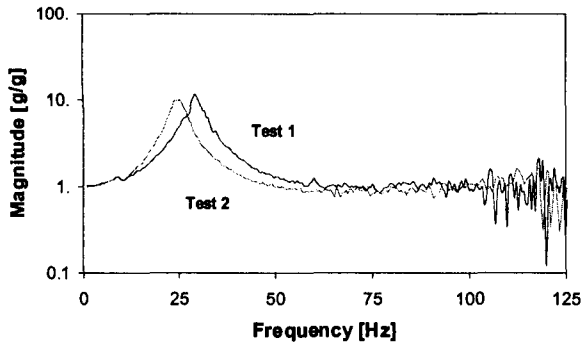

Figure 12. Transfer functions A14x/A1x for different series of random excitation tests.

Additional sinusoidal tests were conducted with an excitation frequency of 22 Hz (2.75 Hz, prototype scale), gradually increasing the amplitude of the motions as in the previous case. Figures 13 and 14 show acceleration responses measured at the top and bottom of the model during test run 37, corresponding to an excitation level of 6.00 g (0.75 g, prototype scale).

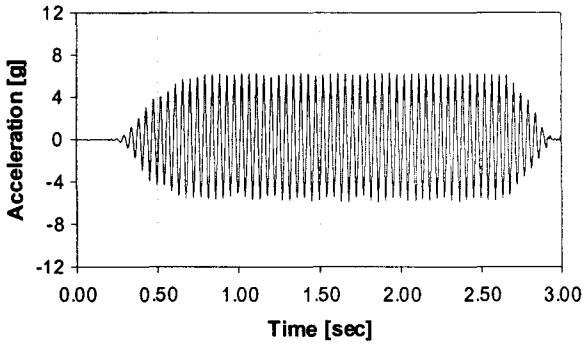

Figure 13. Base acceleration, A6x (run 37).

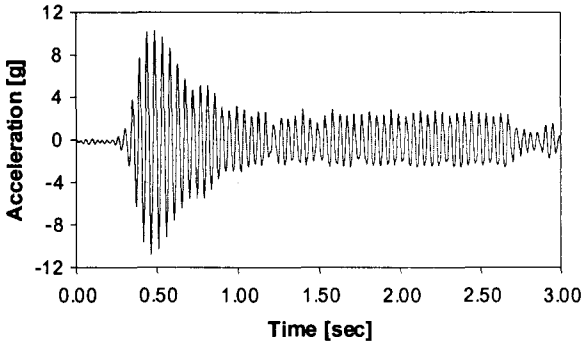

Figure 14. Top acceleration, A14x (run 37).

As seen in these figures, the behavior of the model at this stage exhibits different response characteristics that are induced by the significant damage and rotation at the base. Similar conclusions can be drawn by considering the top deflection of the model, shown in Figure 15.

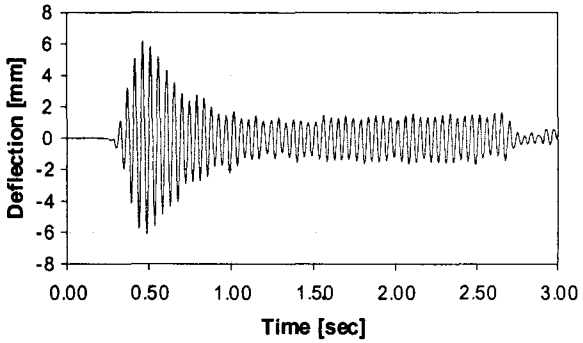

Figure 15. Top deflection, D5x (run 37).

Extensive quantitative information regarding the behavior of the failure surface (cold joint at the base of the model) was gathered by the vertical LVDT gages at that location. Figure 16 shows the time history for the sensor L2Z, illustrating the opening and closing of the single base crack.

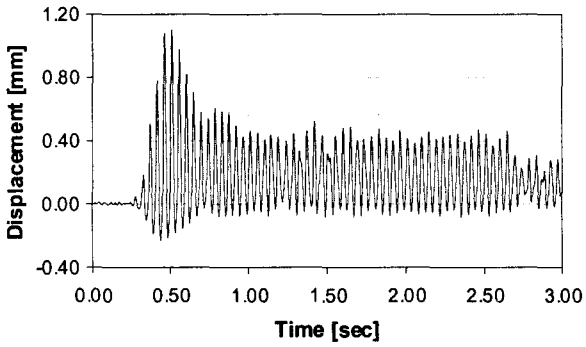

Figure 16. Base LVDT, L2z (run 37).

4.0 CONCLUSIONS

These experiments demonstrated that the failure mode under dynamic conditions was very similar to the failure mechanism previously observed under monotonic and cyclic loading. The same single crack response with significant ductility was witnessed in both the static and dynamic experiments. As expected, the natural frequency of the model decreased substantially after cracking. The experiment validates the calculation of the deflection capacity based on the results of static experimentation. Future dynamic experiments will model the response of a tower to an individual earthquake. This will further validate the complete displacement-based analysis process.

5.0 ACKNOWLEDGEMENTS

This work was sponsored by the Direct–Allotted Civil Works Earthquake Engineering Research Program of the U.S. Army Engineer Research and Development Center (ERDC) in Vicksburg, Mississippi. The authors appreciate the cooperation of the authorities at the ERDC, which permitted the presentation and publication of this study. Permission to publish this paper was granted by the Chief of Engineers, U.S. Army Corps of Engineers.

6.0 REFERENCES

Dove, Richard C. (1996). "Structural Parameter Analysis of U.S. Army Corps of Engineers Existing Intake Tower Inventory," Technical Report SL-96-1, U.S. Army Engineer Waterways Experiment Station, Vicksburg, MS.

Dove, Richard C. (1998). "Performance of Lightly Reinforced Concrete Intake Towers under Selected Loadings," Technical Report SL-98-1, U.S. Army Engineer Waterways Experiment Station, Vicksburg, MS.

Dove, Richard C. (2000). "Performance of Lightly Reinforced Concrete Intake Towers under Selected Loadings," Technical Report ERDC/SL TR-00-6, U.S. Army Engineer Research and Development Center, Vicksburg, MS.

Headquarters, U.S. Army Corps of Engineers (2002). "Structural Design of Spillways and Outlet Works," Engineer Manual EM 1110-2-2400, Washington, DC (in publication).

Present State of Measurement of Earthquake Motion and Nation-wide Networking of Seismographs at Dam Sites in Japan

by

Tadahiko Sakakomo[1], Syuji Takasu[2], Hitoshi Yoshida[3],
Yoshikazu Yamaguchi[4], Takashi Sasaki[5] and Kenji Inagaki[6]

ABSTRACT

The SMAC-type strong motion recorder was installed in the Sarutani Dam in the Kinki Region, Japan in 1957, and strong motion observation on dam structures under the jurisdiction of the MLIT, the Ministry of Land, Infrastructure, and Transport (formally the Ministry of Construction) had been started. Since the Niigata Earthquake in 1964, the necessity of strong motion observation has been widely recognized and the Ministry has been positively promoted the installation of seismometers in dams.

Nowadays, the 413 dams under the jurisdiction of the Ministry have seismometers and the high-density observation of earthquake records can be conducted. Furthermore, the network of observation of earthquake records at dam sites has been speeded, the 236 seismometers at 50 dam sites have been connected to the Public Works Research Institute (PWRI), presently the National Institute for Land and Infrastructure Management (NILIM).

This report describes the present state of earthquake data measurement at dams under jurisdiction of MLIT, the characteristics of collected data, and the outline of the dam-site seismograph network that is now being constructed.

KEYWORDS: Strong motion records, Dam, Seismometer, Network of observation of earthquake record

1. INTRODUCTION

Many large earthquakes struck Japan and caused severe damage on important infrastructures and private properties. Fortunately, no dams in Japan has suffered damage that threatened its safety, but clarifying and securing the earthquake safety of dams is one of the most important missions that must be faced in densely populated Japan. To respond to a strong demand for the advancement of evaluating methods of the earthquake safety of new and existing dams, it is important to study the characteristics of seismic motion at rock foundation and the dynamic behavior of actual dams based on observed records measured at various dam sites. Installing seismographs at dams have been speeded since the 1995 Hyogo-ken Nanbu Earthquake (the Kobe Earthquake) and all dams have seismographs under jurisdiction of the MLIT now.

[1] Chief Executive, Public Works Research Institute (PWRI), 1-6 Minami-hara, Tsukuba-shi, 305-8516, JAPAN
[2] Group Leader, Hydraulic Research Group (HRG), PWRI
[3] Research Coordinator for Watershed Management, River Department, National Institute for Land and Infrastructure Management (NILIM), Ministry of Land, Infrastructure, and Transport (MLIT), 1 Asahi, Tsukuba-shi, 305-0804, JAPAN
[4] Head, Dam Structures Research Team, HRG, PWRI
[5] Senior Researcher, Dam Structures Research Team, HRG, PWRI
[6] Researcher, Water Management and Dam Division, River Department, NILIM, MLIT

2. PRESENT STATE OF MEASUREMENT OF EARTHQUAKE MOTION AT DAMS IN JAPAN

2.1 Background

The measurement of earthquake motion at dams began in 1957 when the Ministry of Construction (presently the MLIT) installed a SMAC-type strong motion seismograph at the Sarutani Dam to obtain data vital for dam safety management and to advance seismic resistant design. The installation of strong motion seismographs was promoted in response to a growing awareness of the need for strong motion observations following the Niigata Earthquake in 1964.

At the Kobe Earthquake in 1995, a lot of several strong motion records at dam sites were observed, but some dams near the earthquake faults didn't have seismometers, so the strong motion records at dam sites near the earthquake faults were not got unfortunately. The Ministry, therefore, decided to place the seismometers in all dam sites under its jurisdiction, and to replace the old-fashioned analog seismometers to the new digital seismometers. By the end of 2000, all dam got the seismometers.

2.2 State of installation of strong motion seismographs

By the time of the Hyogo-ken Nanbu Earthquake, 443 strong motion seismographs were installed at 140 dams (MLIT's dams: 48, Water Resources Development Public Corporation's dams: 10, Subsidized prefectural dams: 82) , but 1,152 have now been installed at 413 dams (MLIT's dams: 78, Water Resources Development Public Corporation's dams: 20, Subsidized prefectural dams: 315) . Figure 1 shows the locations of the dams where the installation of strong motion seismographs has been completed, and Figure 2 shows changes in the number of strong motion seismographs in operation.

2.3 Standard installation method of seismographs at dams

Strong earthquake motion observations at dams play an important role in dam safety management and studies of the response of the dam to strong motion in bedrock. Therefore, in principle, installation of seismographs is done at the base and at the crest of each dam in the maximum cross section. But because differing responses appear at bridges and pier structures on dam crest, installing seismographs at these locations is avoided generally. Table 1 shows a breakdown of strong motion seismograph installation locations. Dam base mainly means the gallery near the base of concrete dams or the gallery beneath the impervious zone of rockfill dams. Other locations include rim grouting tunnels, water intake systems, and management offices. Data observed at foundations under the dam include reflected waves from on the dam body. Therefore, installation of seismographs on the downstream free field is recommended [1].

The components measured by a seismograph are set of course as 2 horizontal components and 1 vertical component. Vibration of dam body occurs most easily at right angles to the dam axis because of the vibration characteristics of dams. Therefore, the directions of the horizontal components are, in principle, right angles to the dam axis and the dam axis direction.

Earthquake observations are normally performed in trigger mode; the seismographs are all linked and begin recording simultaneously when a certain standard value is exceeded. In general, trigger seismograph is located at dam base.

Strong motion seismographs that are now installed at dam sites include analog type seismograph and digital type seismographs. Figure 3 shows the state of installation of analog type and digital type seismographs. Initially, most were analog type equipped with a moving pendulum to record earthquake motion on paper, but most of those now in use are digital type that converts earthquake motion to electrical output that is then digitized by an AD converter and recorded on an IC card etc. In the

case of new installation, only digital type seismographs are now selected.

3. CHARACTERISTICS OF ACCELERATION AT ROCK FOUNDATION OF DAM SITE

Two reports about the collection of observed acceleration data at dam sites by the PWRI were published in January, 2001. The first report[2] is about the information of the locations and the specifications of seismographs in each dam at the time of 2000. The second report[3] summarizes the acceleration data and spectrum, and information of earthquakes. The number of records dealt with in this report is 2,960 collected in from 1966 to 2000.

In this paper, the characteristics of horizontal acceleration records in dam foundations have been examined based on records of observed earthquake data. Dams under the jurisdiction of the MLIT were all constructed on rock foundations. The S-wave velocities of dam foundations are therefore, expected to be at least 1,000 m /sec.

The 143 sets of, 286 in total of horizontal acceleration records were used in this study. These data were collected during earthquakes with a magnitude of 5 or more and observed at an epicentral distance of 200 km or less. Figure 4 shows the distribution of the earthquake epicenters and Figure 5 shows the relationships of the magnitude, hypocenter depth, and peak acceleration with the epicentral distance. The distribution of observed results is relatively dispersive.

Figure 6 shows the relationship of the epicentral distance with the peak acceleration. The data are shown with the presumption values by the attenuation relationship equations by Fukushima et al.[5] and An-naka et al.[6] These two attenuation relationship equations are based on the data mainly collected on hard soil foundation. The data of dam sites seem to be small as compared with the presumption values.

Figure 7 shows acceleration response spectra. And, Figure 8 shows acceleration response magnification spectra.

Figure 9 shows acceleration response spectra for different epicentral distances. Figure 10 shows acceleration response magnification spectra obtained by dividing acceleration response spectra by the peak acceleration values. In order to investigate the characteristics of the relatively strong motions, the data shown in these figures are reduced data observed earthquakes of a magnitude 6 or more and within 100 km of the epicentral distance. The number of extracted data is 122. The peak value of response magnification spectrum is about 2 for all earthquake magnitude and epicentral distance, and the peak values mostly appear within the periods of 0.1-0.2s. The response magnification spectrum decreases rapidly for the period over 1 sec, and the larger earthquake magnitude is, the smaller the decreasing rate of the response magnification spectrum according to the period is.

4. DAM SEISMOGRAPH NETWORK

Because the observed data are very valuable and indispensable for the investigation of seismic resistance of dams, the MLIT have been made a periodical collection of the data observed at dams under its jurisdiction. Now, the dam offices should report the earthquake records to once a year and the information of observation system in the event of new installation or updating of seismographs to the NILIM, the MLIT. The detailed format is fixed for the report and the data in fixed format is sent to the NILIM by floppy disks.

The MLIT is connecting seismographs installed at dams in a network to construct a system that can monitor earthquakes in real time for responding to demand of earthquake disaster management. The dam seismograph network is connected by the direct microwave circuit, and enables quick collection of not only the maximum acceleration values but also time-history acceleration data. This network system is now monitoring 50 dams of the MLIT.

This system consists of earthquake information monitoring parts and a data base system. Figure 11 shows the outline of the network system, and Figure

12 shows a sample screen on a display terminal.

4.1 Monitoring

The seismograph network monitors earthquakes by connecting a server at the NILIM with relay devices installed at each dam using microwave circuits which is dedicated to the MLIT.

4.2 Data base

The database consists of basic information of dam, information of seismograph, earthquake information and measure data. The following is the actual examples of the items in database.

a) Basic information of dam

Dam height, dam length, latitude, longitude, epicentral distance, dam type, slope gradient , etc.

b) Seismograph information

Seismograph model number, specification of seismograph, installation position, installation elevation, etc.

c) Earthquake information

Occurrence time, epicenter location, depth, magnitude, etc.

d) Measure data

Components, peak acceleration, number of samples, number of data, etc.

4.3 Function and operation

At the instant that a seismograph at a dam detects an earthquake, the peak acceleration and the measured seismic intensity of the earthquake are transmitted through relay devices to the NILIM database. When the earthquake information arrives at the NILIM from a dam relay device, a message that an earthquake has occurred is displayed on a terminal screen at the same time as an alarm is sounded. And this system automatically starts the collecting of earthquake records from dams nearby the dam that firstly send a data. The dam seismograph network is connected to other seismograph networks[6] for national facilities related rivers and roads, and is sharing data such as the peak acceleration and measured SI value etc.

The shared information is utilized for immediate expectation of disaster occurrences such as the ground liquefaction the damage of bridge etc. Some kind of digital data such as the peak accelerations opens public through the Internet.

For maintaining of system functions, the state of the system is constantly monitored once a day by confirmations of the soundness of each relay device, and by checking of the existence of untransmitted earthquake data.

5. FUTURE PLANS

The researches on evaluation methods of seismic safety of dams have been conducted using data are accumulated in the PWRI and the NILIM.

According as the system to collect the observed earthquake data from jurisdictional dams has been completed and networking of seismographs has been progressing, the related researches are expected to be advanced. Future plans for the seismograph network include cooperating with prefectural governments to link the network to seismographs at all prefectural dams in order to create a more precise, more highly concentrated earthquake motion monitoring environment.

The networking of seismographs enables quick collection of the earthquake information. The network is, therefore, counted on to make a big contribution to supporting an efficient and appropriate initial emergency action: evaluating the need for inspections of managed facilities, predicting the state of damage etc. immediately after the earthquake when little information is available.

It is, moreover, very important to share earthquake information each other in organizations responsible to the disaster prevention.

And the collection and accumulation of recordings of actual seismic data are essential to researches on the dynamic analysis methods of dams. Therefore, one of important subjects of the network is linkage to the

database of detailed data of foundation and dam material for the precise estimation of earthquake motion distribution and dam behavior.

When the networking of seismographs of all dams under jurisdiction of the MLIT, the collection data by the NILIM through the network will be take the place of the report of earthquake data form dam offices to the NILIM. For improvement of the reliance of the network system, the supervising function of system should be strengthened to be preventing the functional trouble and deterioration.

REFERENCES:

1) Y. Yamaguchi, T. Iwashita: Earthquake Motions at an Embankment Dam Site and an Estimation Method of Incident Seismic Waves Using the Observations, Proceeding of the 32nd Joint Meeting of UJNR Panel on Wind and Seismic Effects, pp. 253-262, 2001

2) Y. Yamaguchi, T. Iwashita, J. Matsuura: Seismometers Installed in the Dams Under the Jurisdiction of the Ministry of Land, Infrastructure and Transport, Technical Memorandum of PWRI, No.3768, 2001.

3) Y. Yamaguchi, T. Iwashita: Earthquake Motion at Rock Foundation and Response of Embankment Dams by Acceleration Records at Dams in Japan, Technical Memorandum of PWRI, No.3780, 2001.

4) Fukushima et al.: Shimizu Tech. Res. Bull., Vol.10, 1-11, 1991 (in Japanese)

5) An-naka et al.: 19th JSCE Earthquake Engineering Symposium, 129-132, 1987 (in Japanese)

6) H. Sugita, T. Hamada: Development of Real-time Earthquake Damage Estimation System for Road Facilities, 7th U.S-Japan Workshop on Earthquake Disaster Prevention for Lifeline Systems, 1997

Table 1 Seismograph installation locations

Location	Number of Seismographs	Ratio (%)
Dam base	400	34.7%
Dam crest	426	37.0%
Free field	290	25.2%
Other	36	3.1%
Total	1152	100.0%

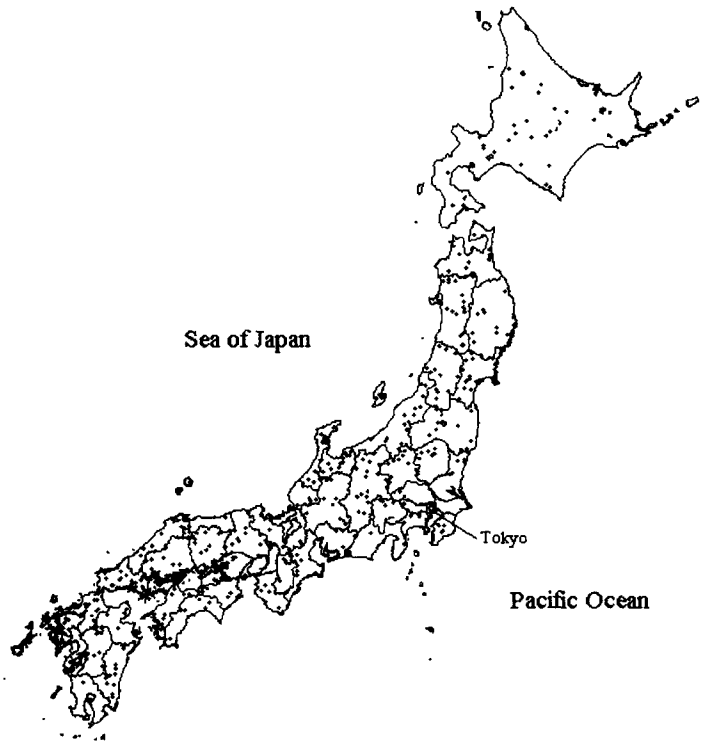

Figure 1 Distribution of dams where seismograph installation is completed

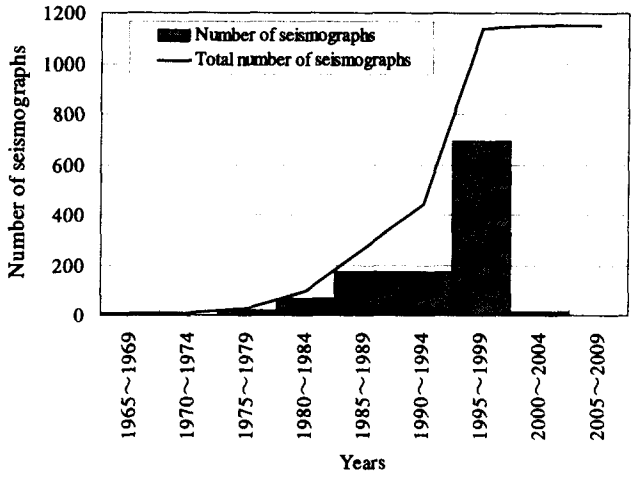

Figure 2 Changing number of seismographs

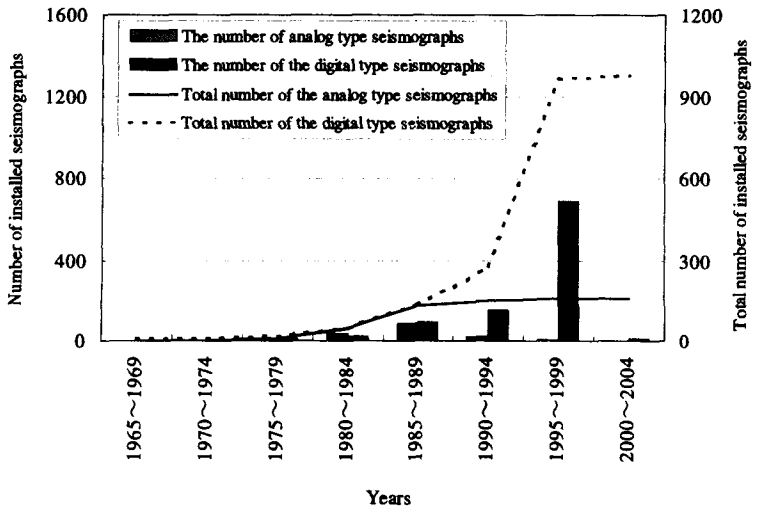

Figure 3 Transition of number of analog type and digital type seismographs

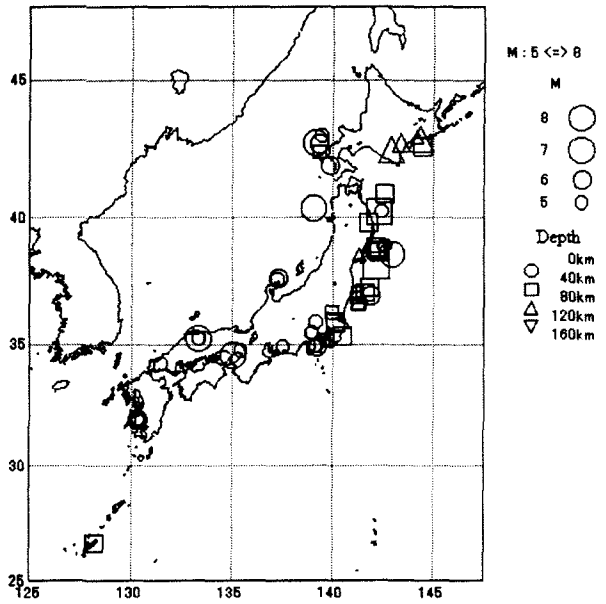

Figure 4 Distribution of earthquake epicenters

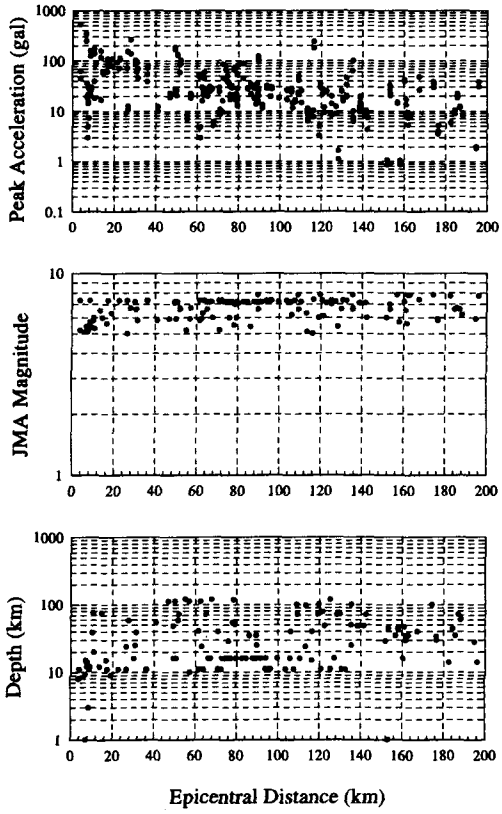

Figure 5 Relationship of magnitude, hypocenter depth, and peak acceleration with epicentral distance

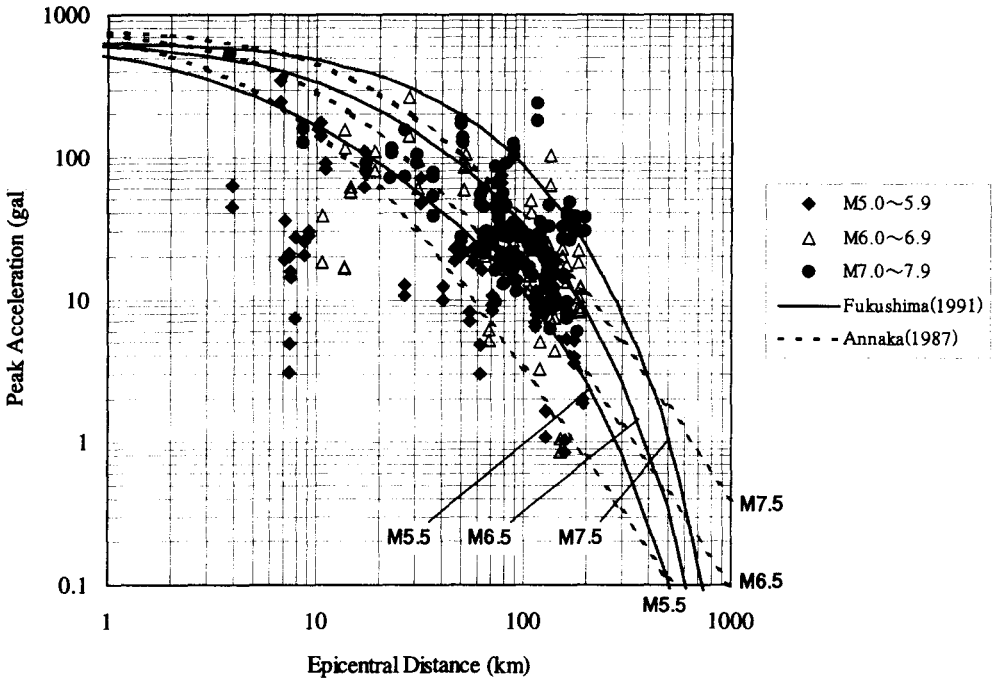

Figure 6 Relationship of epicentral distance and peak acceleration

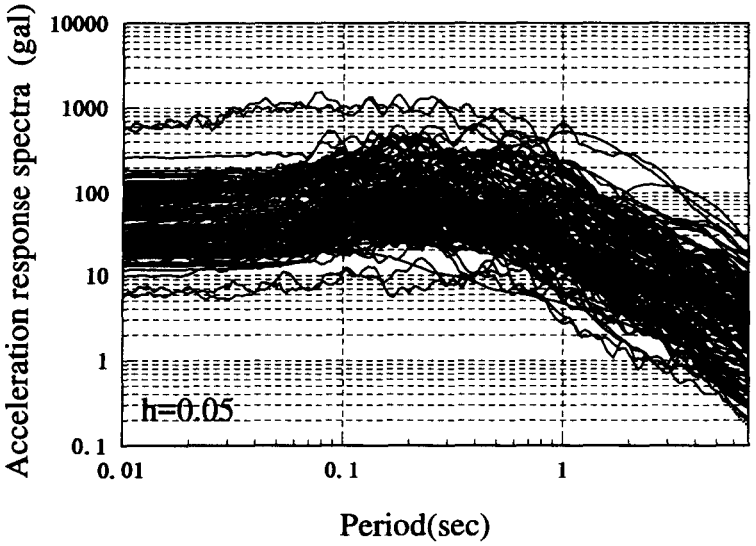

Figure 7 Acceleration response spectra (dam base, horizontal)

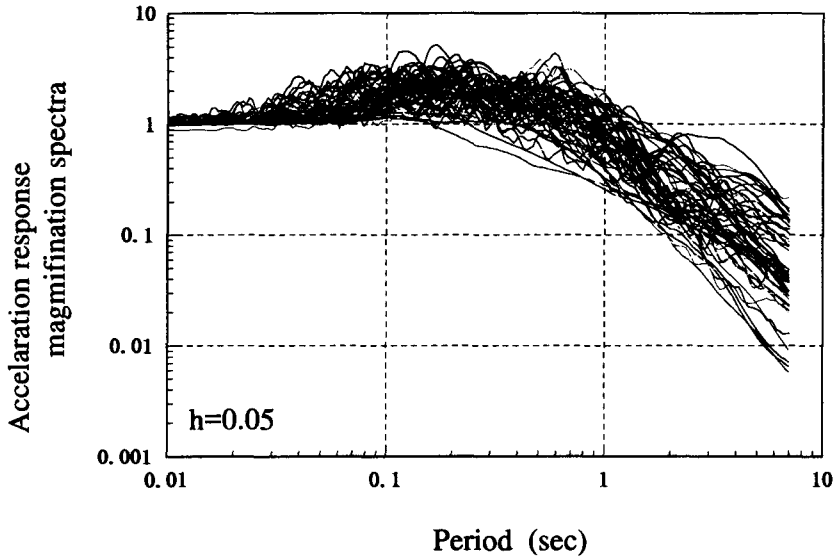

Figure 8 Acceleration response magnification spectra (dam base, horizontal)

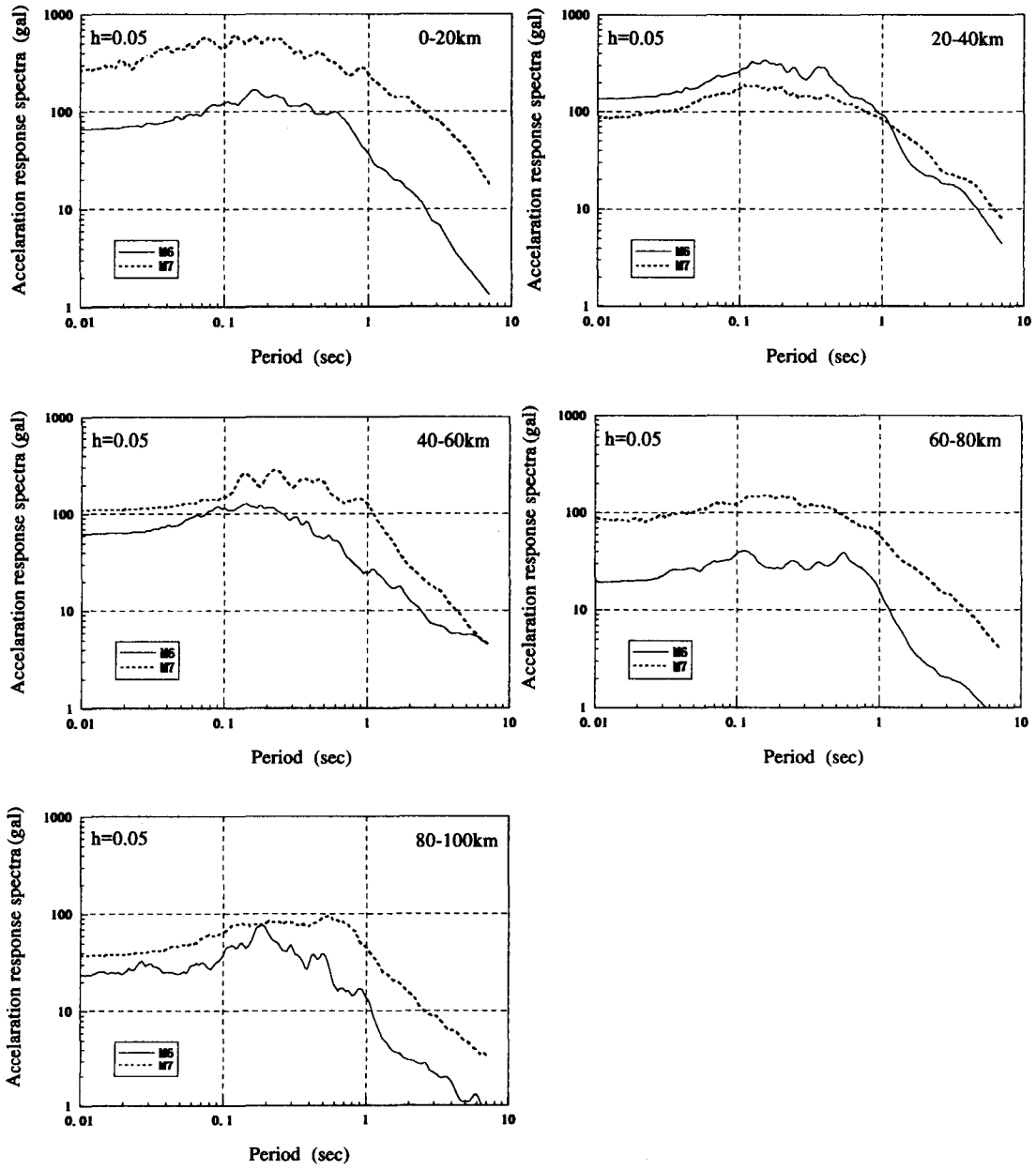

Figure 9 Acceleration response spectra by epicentral distance interval of 20km
(average, dam base, horizontal)

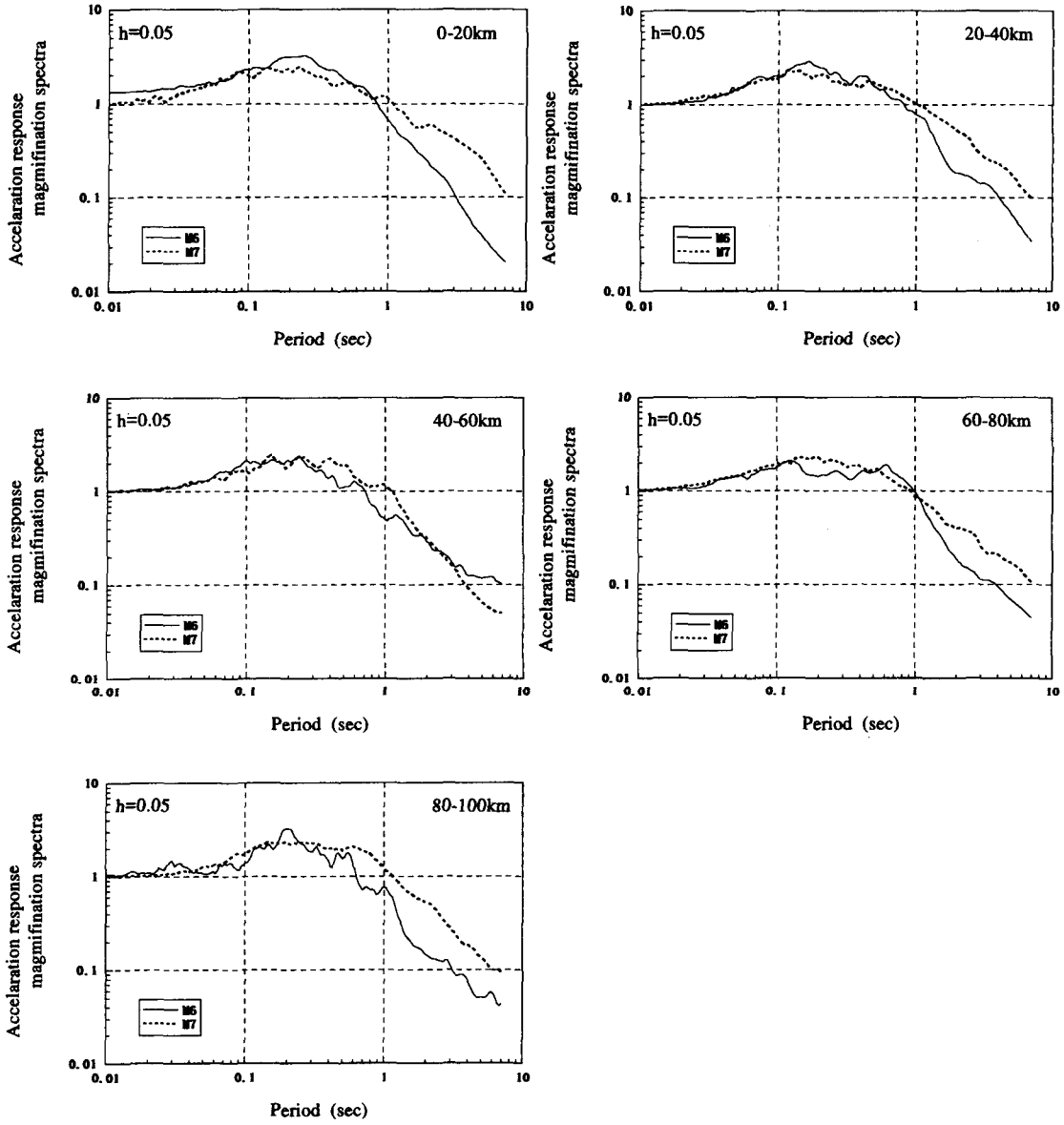

Figure 10 Acceleration response magnification spectra by epicentral distance interval of 20km (average, dam base, horizontal)

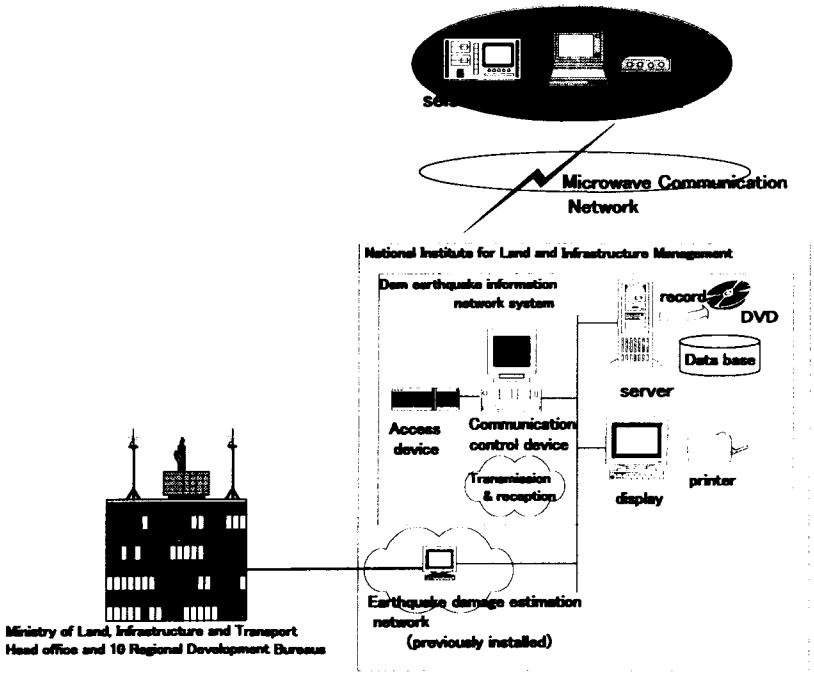

Figure 11 System configuration of the real-time dam seismograph network system

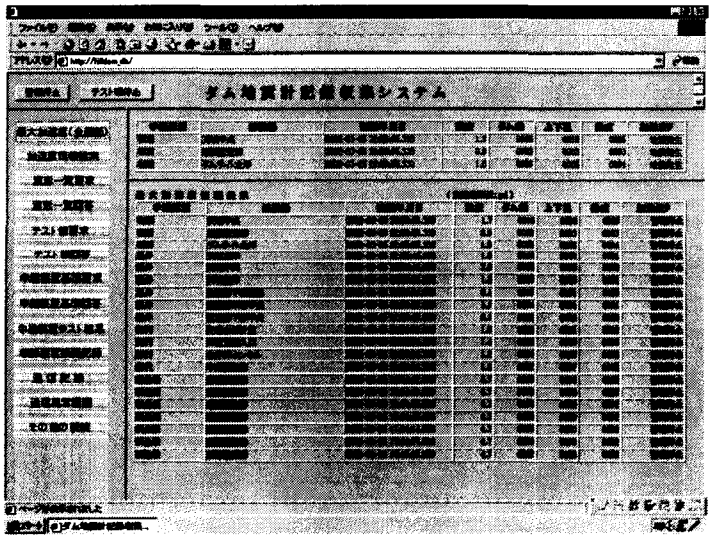

Figure 12 Example of screen shot of a seismograph network information terminal

Cyclically-Induced Pore Pressure at High Confining Stress

by

Michael K. Sharp[1] and R. Scott Steedman[2]

ABSTRACT

Experiments were conducted by the ERDC Centrifuge Research Team to investigate effective confining stress effects on liquefaction potential of fine, clean, Nevada sand, under the boundary and loading conditions of a centrifuge model. For this test series, twenty-six level ground models with either a dense layer over a loose layer or homogeneous profile were tested in an equivalent-shear-beam box. Some models were subjected to sequential earthquakes, and some models were overconsolidated, to observe stress-history effects on pore pressure development. The purpose of this paper is to make the initial liquefaction and confining stress studies, centrifuge test procedures, results, and validation efforts conducted to date known to the professional community.

KEYWORDS: Centrifuge; confining stress; dams; earthquakes; liquefaction; pore-pressure

1.0 INTRODUCTION

The concern over earthquake resistance of older embankment dams drives the need for remedial construction costing hundreds of millions of dollars of public funds annually. This concern is not generated by actual experience from failures of well-designed dams but from predictions based on scientifically sound principles of soil mechanics. Yet the mechanical response of an embankment dam depends on so many factors that interact non-linearly that implementation of these principles in a predictive tool is still as much an art as it is a science. Thus the decision-maker is faced with the dilemma of making large investments in the absence of experience versus protecting the public from the catastrophic consequences that loss of a major dam would entail.

Liquefaction is the most critical factor to the earthquake resistance of embankment dams. Foundation materials that are structurally ideal under static loading can be severely weakened by pore pressures induced from earthquake motions. Many dams built before awareness of liquefaction must now be reexamined in light of potential damage from this threat. An open question in these reexaminations is the effect of depth on liquefaction potential. Historically, there have been no observations of liquefaction at depths greater than about 30 m or 100 ft (as summarized in Youd and Idriss, 1997), suggesting that the high confining stress beneath most embankment dams wound not be conducive to significant pore pressure response. If so, remedial construction could be avoided or simplified in many dams now under investigation. Studies to investigate these and other liquefaction questions relevant to earth dams are in progress at the U.S. Army Corps of Engineers, Engineering Research and Development Center (ERDC), Vicksburg, MS. Recent findings, focused on level ground stress conditions, are reported in this paper.

2.0 ERDC CENTRIFUGE TESTS

This section describes the test plan, description of the soils tests, equipment used to conduct the tests, as well as model construction, quality control and instrumentation. The results and an interpretation of results conclude the section.

[1] Centrifuge Research Center, Engineer Research and Development Center, Vicksburg MS (USA)
[2] Whitby Byrd and Associates, London England (UK)

2.1 Test Plan

The centrifuge experiments, summarized in Table 1, were designed to investigate liquefaction potential of a loose, saturated sand layer with initial vertical effective confining stresses ranging from 1 to 10 atm. Level ground stress conditions were used in all tests. As shown in Table 1, the models are grouped in series that correspond to different target ranges of vertical effective overburden stress near the bottom of the deposit. All models were shaken initially at a 50g spin rate with subsequent shakings at either 50g, 80g, 100g, or 125g. The results reported in this paper concentrate on the first shakings at 50g, unless specifically stated otherwise. Some models were overconsolidated by a factor of 2.5 prior to shaking (achieved by running the centrifuge up to 125g, then back down to 50g for the shaking event).

Table 2 provides further details on each experiment, including the densities achieved in the specimen, the number of earthquake events and the initial vertical effective stress near the bottom of the deposit. For the two-layer models, the target relative density for the upper medium dense layer was 75 percent while the target relative density for the lower layer was 50 percent. For the uniform deposits, the target relative density was 50 percent.

The cross-sections for the different series of experiment are shown in Figure 1. A variety of techniques were used to achieve higher confining stresses while maintaining the same g level. In some specimens, the water table or phreatic surface was lowered; in others a surcharge (lead weights) was added on the surface.

The thickness of the loose sand layer, for the two-layer case, was constant in all the experiments (160mm or 8m equivalent field thickness when tested at 50g). The thickness of the overlying deposits, and selection of water table or surcharge were adjusted to achieve the target effective vertical stress at its mid-depth. The overall depth of sand within each specimen was either 300mm or 525mm (15m or 26.25m respectively, when tested at 50g).

2.2 Soils Used in Centrifuge Models

The Nevada sand used in the models was characterized by standard laboratory tests to determine parameters such as dry density and gradation. The constitutive behavior for Nevada sand based on laboratory triaxial and simple tests is given by (Arulmoli et al., 1992). These tests show the typical reduction with K_σ at elevated confining pressure. As a reference, the K_σ relationship for this sand is shown in Figure 2, which clearly displays the effect of confining pressure. A linear extrapolation of cyclic strength from low confining pressures would result in over estimates of the available strength at high confining stresses.

2.3 Pore Fluid

All models were saturated with a glycerin-water solution which comprised an 80 percent by weight mixture of glycerin and water, determined after study of the sensitivity of the viscosity to changes in temperature and the mix proportions, Steedman (1999). The viscosity of the fluid at 1g was selected to maintain proper scaling of the permeability at 50g. Tables 3 and 4 present key material parameters for Nevada sand, and the glycerin-water solution respectively.

The density of the glycerine-water mix was calculated from as follows.

$$\rho_m = \rho_g(m_g + m_w)/(m_g + \rho_g m_w)$$

In this equation ρ_m is the density of the mix, ρ_g is the density of glycerine, m_g is the mass of glycerine, and m_w is the mass of water.

2.4 Earthquake Simulation

The earthquake actuator used in the ERDC experiments is a mechanical shaker designed to provide a single frequency input motion of variable duration to the base of the specimen container. The displacement of the platform is

constant at +/- 1mm; the frequency and hence amplitude is readily changed by varying the speed of the shaft. The use of a single frequency of input motion facilitates comparisons with laboratory tests and practical liquefaction analysis procedures based on equivalent, uniform cycles. Table 5 gives the pertinent characteristics of the input motion for each model reported in this paper.

2.5 Equivalent Shear Beam Model Container (ESB)

The soil specimen is built within a hollow rectangular model container (termed an equivalent shear beam, or ESB container) comprised of a series of aluminum alloy rings stacked one above the other, and separated by an elastic medium. Several of these chambers have been constructed, and extensive dynamic analysis and testing have been carried out to determine their dynamic response characteristics (Butler 1999).

The ESB concept is to create an equivalent shear beam with an average stiffness comparable to the stiffness of the soil specimen during the initial stages of the shaking, so that the dynamic response of the box does not significantly influence the behavior of the soil specimen inside. A chamber with no stiffness simply adds mass to the soil specimen, again changing its dynamic response. In experiments involving liquefaction of large volumes of soil inside the container, the stiffness (and hence dynamic response) of the soil changes throughout the base shaking.

The ERDC ESB model container has internal dimensions of 627mm deep by 315mm wide by 796mm long. Each of the 11 aluminum alloy rings was 50 mm high and had a plan area of 0.0675 m^2. The rings are not stiff enough along their long dimension to support the outward pressure from the soil inside under high g, therefore the container relies on vertical reaction walls, independent of the shaker unit itself, for lateral support. A rubber sheet separates the rings from the steel walls on either side, and is designed to be incompressible but very flexible in shear. This system has undergone extensive study to verify that the ESB box is not being impeded from moving with the shaker platform even though the container expands during spin up to 50 g and sits snugly against the reaction walls.

The end walls of the ESB have thin metal sheets, termed shear sheets, fixed securely to the base of the chamber, Steedman et al. (2000). The shear sheets transmit the complementary shear force generated by the horizontal shaking on vertical planes within the specimen to the base of the container. This improves the uniformity of the stress field at each elevation along the model, reducing the tendency for the chamber to rock thus better representing the stress state boundary condition that exists in the field.

Butler (1999) conducted a thorough theoretical and experimental analysis of the dynamic response of the coupled soil-container system. At high g the soil and container act as a coupled system, where the lower stiffness of the container reduces the natural frequency (slightly) of the combined system compared to the soil column alone. However, provided the driving frequency is low relative to the natural frequency of the coupled system, Butler (1999) demonstrated that the displacement response of the system is unaffected compared to the soil acting independently.

2.6 Model Construction

The specimens were all 300mm wide and 781mm long, between the vertical sidewalls of the ESB. The specimen was constructed within the ESB container by pluviating dry Nevada sand, forming a level sand bed. Instruments were placed at different depths, during the pluviation process, to measure pore pressures and accelerations. The volume and density of sand poured for each layer was checked to verify the target relative density. Once complete, the specimen was fully submerged by introducing the viscous fluid into the model from the bottom by gravity over a period of several days.

As the equivalent field depth was increased in successive experiments, the options were to shake the models at a higher g level (spin rate),

to depress the water table or phreatic surface, or to use surcharging to achieve the target overburden. It was determined that the models should all be shaken at 50g, and that surcharging would be adopted to reach the required stress levels. In the Model 4 series, two models used a depressed phreatic surface and two used surcharging. In the Model 5 series, the equivalent field depth was too great to be achieved without surcharging. The surcharge comprised lead strips laid lengthwise along the surface of the specimen, with additional lead plate on top where necessary. The phreatic surface was then maintained at the surface of the sand bed.

The centrifuge was operated at 50g (for the majority of tests reported in this paper unless otherwise specified), creating a field-equivalent of a site approximately 40 m long by 15 m wide by over 26 m deep (for the deepest specimens). Surcharges, variations in the depth of the phreatic surface, and increased g level were used to achieve higher effective overburden stresses, up to 10 atm, as described earlier.

3.0 EXPERIMENTAL RESULTS

In the initial experiment series, Table 2 (model code 2a – 2f), the behavior of a soil column 15m deep, with about 1 atm vertical effective stress in the lower layer was studied. The soil deposit had a 7m thick upper layer of denser Nevada sand (relative density of 73 to 83 percent), and a lower layer of looser sand (relative density of 43 to50 percent). The entire model was fully submerged. Example results for this model series are shown in Figure 3, for model 2f. This model has an overconsolidation ratio of 2.5. The effect of overconsolidation for this series was to slow the rate of pore pressure increase throughout the column. Accelerometer records are shown for depths of 1.5, 3.8, 6.5, 11.3, 14.5, and 15m. Pore pressure transducer records are shown for depths of 3.5, 6.9, 11, and 14.8m. The input motions are applied at 0.54 Hz, and the fundamental period of the soil column is estimated to be 4x15m/300mps = 0.2 seconds.

Pore pressures begin to rise simultaneously at all 4 transducer depths at 1.5 cycles or 3 seconds of shaking. During this time, the accelerations are ramping up to 0.10g uniformly in the 4 upper accelerometers, and to 0.12g in the input motion at 15m and the deepest accelerometer at 14.5m. At 7.8 seconds, acceleration peaks at 0.18g for 1.5m, and at 0.15g for 3.8 and 6.5m. From 7-10 seconds, amplitudes decrease slightly to about 0.10g in the lower 2 accelerometers and input motion. At 7 seconds, the rate of pore pressure buildup increases in the 14.8m transducer, slows in the 11m transducer, and remains steady in the 6.9m transducer. At 10 seconds, strong shaking stops in the 1.5m accelerometer, and remains steady at all other depths. Pore pressures are 100 percent at 1.5m, 35 at 6.9m, 40 at 11m, and 70 percent at 14.8m.

At 26 seconds, pore pressures reach their maximum values of 100 percent for 6.9m and 95 percent for 11m. Input motions increase from 0.10g to 0.25g, and remain constant at 0.10g at 14.5m. Accelerations decrease to about 0.05g at 3.8, 6.5, and 11.3m. Accelerations reduce to near zero at 1.5m. Accelerations and pore pressures remain relatively constant at all depths through the end of shaking at 65 seconds. Little or no pore pressure dissipation is observed during the 21 seconds since shaking stopped.

More generally, in the model code 2 series, excess pore pressures rose fairly rapidly to 100 percent or near 100 percent of the initial vertical effective stress (R_u = 1) throughout the column within a few cycles. The acceleration time histories decrease in amplitude as the R_u approaches 1. Despite the higher density of the upper layer, excess pore pressures within it reach high levels.

As the effective vertical confining stress is increased, the pattern of behavior is initially repeated. Models 3a-3d in Table 2 were designed to have an initial vertical effective stress of 2 atm in the lower, looser layer. All series 3 models had 18.25m of dense sand, relative densities of 73-80 percent, on top of 8m of loose sand, relative densities of 34-54 percent. All series 3 models were fully submerged. Example results for this model series are shown in Figure 4, for model 3c. This model was normally consolidated. Accelerometer records

are shown for depths of 1, 5.5, 14.5, 18.3, 22.3, 25.8m, and the input motion depth of 27m. Pore pressure transducer records are shown for depths of 0.75, 5.3, 10.8, 14.4, 18, 22, and 25m. The input motions are applied at 0.54 Hz, and the fundamental period of the soil column is estimated to be 4x26.25m/300mps = 0.35 seconds.

The input motions ramped up to a maximum of 0.09g at 3 seconds and dropped down to a steady 0.06g for the rest of cycling. At 25.8m, accelerations peaked in the 2nd cycle at 0.14g, and remained constant at 0.12g for the remainder of cycling. At 22.3m, accelerations ramped up to 0.09g. Accelerations peaked at 0.035g in 4 seconds at 18.3m. At 5 seconds, accelerations peaked at 0.035g for 14.5m, 0.022g for 5.5m, and 0.036g for 1m. Pore pressures begin to rise at all depths as soon as shaking starts. There is no lag as observed at 1 atm. At 5 seconds, pore pressures are 100 percent at 0.75m, 80 percent at 5.3m, 70 percent at 10.8m, 55 percent at 14.4m, and 87 percent at 18, 22, and 25m. Pore pressures reached maxima of 100 percent in 5 seconds at 0.75m, 16 seconds at 5.3m, 22 seconds at 10.8m, 51 seconds at 14.4m, 7 seconds at 18 and 22m, and 30 seconds at 25m. After shaking stopped, excess pore pressures remained constant at 100 percent.

Above an initial vertical effective stress of around 250 –300 KPa (3 atm), however, a different behavior was observed. Under high effective confining stresses, it was noted that in many cases, excess pore pressures did not reach the initial vertical effective stress. Figure 5 shows the results from Model 4d, a deep soil column with a target vertical effective stress of 500 KPa (5 atm) near the bottom of the model. Model 4d was subjected to a relatively low level of shaking amplitude. Nevertheless, in the initial stages of shaking, the excess pore pressure development within the loose layer is positive. Within around 20 cycles, the excess pore pressure reached 45 percent of the effective overburden stress. Shortly after this, the rate of generation of pore pressures all but ceases. There is a slight reduction in the amplitude of the acceleration, reflecting the increase in excess pore pressure but the displacement (strain) cycles continue for a considerable period without further increase in excess pore pressure. One concern was that the low amplitude of shaking might be the reason for this plateau in pore pressure at only 45 percent of the initial vertical effective stress. Subsequent models similar to model 4d were tested with higher levels of input shaking, revealing the same pattern as shown in Figure 5.

Figure 6 shows the results of a model very similar to model 4d, shown in Figure 5, but now the model is homogeneous rather than a two layer case. Model 4j had slightly less weights used for surcharging resulting in an initial vertical effective stress near the bottom of the model of around 400 KPa (4 atm). Notice that the level of input shaking is more than double that of model 4d, from 0.11 g to 0.25 g. Pore pressure transducers located in the deep loose layer (33 m and 36 m depths) reach a limit of 78 percent for this case. The largest excess pore pressure (90 percent) occurs at a depth of 28.5 m.

A second homogeneous model was tested, without the use of weights for surcharging as was used in model 4j. The results of this test, model 4k, are shown in Figure 7. Model 4k depicts a 26 m deep homogeneous deposit of D_r = 49 percent clean sand. The input peak horizontal acceleration in the model was 0.31g. The model did not contain any lead weight surcharging; the increase in confining stress was accomplished by testing the model at increasing g levels. The results shown in Figure 7 are those from a 50g test, which produces an initial effective confining stress near the bottom of the model of 230 KPa (2.3 atm). As expected, with a confining stress of only 2.3 atm, the entire model liquefied. This model was also tested at higher g levels of 80g, 100g, and 125g, the results of the testing at 100g are discussed next.

Figure 8 shows the results of model 4k tested at a centrifugal acceleration of 100g, which produces an initial effective confining stress near the bottom of the model of 400 KPa (4 tsf). The results shown are after the model was initially tested (input shaking applied) at 50g,

held at 50g for several minutes to allow the pore pressures to dissipate, spun up to 80g and tested, held at 80g for several minutes to allow pore pressure dissipation, and then spun up to 100 g and tested. Pore pressures initially increase rapidly, and then more slowly, and reach 100 percent or near 100 percent of the vertical effective stress. At depths of 44.5 and 52 m, the pore pressures plateau at approximately 82 percent.

The last sets of data are presented in Figures 9 and 10, representing models 5a and 5d respectively. These results represent two-layer models surcharged with a large amount of lead weights and tested at 50g. For model 5a shown in Figure 9, the confining stress near the bottom of the deposit is 740 KPa (7.4 tsf). Peak input acceleration at the base is about 0.1g. In this test, the pore pressure transducers at depths of 50 and 53 m, corresponding to the relatively loose soil (relative density about 51 percent), reach a peak value of only about 50 percent, even with numerous additional cycles of loading. Very little to no excess pore pressure was recorded in the soil column above 50 m.

Nearly identical results are seen in Figure 10, model 5d. This model had slightly larger lead weights resulting in a confining stress near the bottom of the deposit of 920 KPa (9.2 tsf). The level of shaking was also increased from that applied in model 5a from 0.1 g to 0.3 g. At a depth of 63 m, the pore pressure peaked at a value of 55 percent, and at a depth of 59 m the pore pressure peaked at a value of 40 percent. Very little to no excess pore pressure was recorded in the soil column above 59 m.

4.0 DISCUSSION OF RESULTS

In the homogeneous models, excess pore pressures rise more quickly and to higher levels throughout the column than in the two-layer models. Post-shaking pore pressure redistribution is difficult to see because the whole column liquefied, so the gradients are smaller. These observations suggest that pore pressures are being generated cyclically within each layer (local generation) in addition to redistribution effects. The pore pressures do not reduce within 20 sec after shaking stops, so, dissipation is not observed. Also notice the sharp correspondence between accelerations and pore pressure responses. The sharp pore pressure peaks and liquefaction observations indicate that sufficient saturation was achieved with the employed model saturation and consolidation procedures.

The rate at which PWP is increasing in the shorter columns appears to be too fast to be explained by pore pressure redistribution (flow) alone. Rather, a pressure wave effect may be occurring in the column. Communication of a high increment of pore pressure originating in a lower layer may be nearly instantaneous throughout the soil column. Whereas consolidation requires drainage to take place, the initial response is essentially undrained, and the speed of propagation of a compressive wave in the pore fluid will be many times the velocity of the shear wave through the soil skeleton. Thus it is feasible for a pore pressure increment, which arises during part of a cycle of loading to be communicated upwards through the soil column in advance of the shear wave that created it. As the increments of excess pore pressure tend to be large at depth, then the potential impact on the response of the upper layer is increased.

The surcharge has a distinct effect on the behavior of the soil column. The effect appears to be even more pronounced in the two layer models. For the deep two-layer models, excess pore pressures are generated only in the deeper layers. Dissipation or redistribution effects can be seen in the pore pressure response during and after shaking stops.

5.0 SUMMARY AND CONCLUSIONS

The relationship between effective confining stress and liquefaction potential, in terms of cyclically induced excess pore water pressure, has been extensively studied in the laboratory using traditional triaxial, torsional and simple shear devices. The laboratory studies show that there is a less-than-linear increase in cyclic shear strength with increasing effective confining stress. Laboratory tests indicate that 100 percent pore pressure response (liquefaction) can occur

at high confining stresses in the range 3 to 12 atm. At lower confining stresses, less than 3 atm, stress history strongly influences liquefaction resistance, K_σ relationships, and threshold cyclic shear strain required to develop high pore pressures.

Experiments were conducted by the ERDC Centrifuge Research Team to investigate effective confining stress effects on liquefaction potential of fine, clean, Nevada sand, under the boundary and loading conditions of a centrifuge model. For this test series, twenty-six level ground models with either a dense layer over a loose layer or homogeneous profile were tested in an equivalent-shear-beam box. Some models were subjected to sequential earthquakes, and some models were overconsolidated, to observe stress-history effects on pore pressure development. A representative number of the models tested have been reported in this paper.

6.0 REFERENCES

Arulmoli, K., Muraleetharan, K.K., Hossain, M.M., and Fruth, L.S., (1992). "VELACS Verification of Liquefaction Analyses by Centrifuge Studies Laboratory Testing Program Soil Data Report." National Science Foundation Report.

Butler, G.D., (1999). A dynamic analysis of the stored energy angular momentum actuator used with the equivalent shear beam container, PhD thesis, Cambridge University.

Steedman, R.S., (1999). Earthquake engineering support, Phase 3, Final Technical Report, N68171-99-C-9021, European Office of the U.S. Army, London, November.

Steedman, R.S., Ledbetter, R.H., and Hynes, M.E., (2000). "Liquefaction of sands under high initial effective confining stresses." Proc. GeoDenver 2000, ASCE Geotech. Spec. Pub., August.

Youd, L. and Idriss, I. M., Editors (1997). "Workshop on Evaluation of Liquefaction Resistance of Soils." Proceedings, Salt Lake City, Technical Report NCEER-97-0022, sponsored by FHWA, NSF and WES, published by NCEER

TABLE 1. Outline summary of centrifuge model test program

Model series	Models in series	Effective overburden stress near bottom	Equivalent field depth (approx)	Depth of specimen	Notes (all specimens constructed from Nevada Sand, tested at 50g unless indicated)
2	a, b, c, d, e, f	1 tsf	15 m	300 mm	Fully submerged
3	a, b, c, d, e	2 tsf	26 m	525 mm	Fully submerged
4	a, b, c, d	3 – 5 tsf	26 – 40 m	525 mm	Lowered water table or surcharge (weights)
	e, f, g, h, i, j	3.9 – 9.7 tsf	30 – 60 m	525 mm	Surcharge (weights) and change in g level, fully submerged
	k	1.9 – 4.8 tsf	25 – 39 m	525 mm	Change in g level, no surcharge, fully submerged
5	a, b, c, d, e	7 – 10 tsf	54 – 63 m	525 mm	Surcharge (weights), fully submerged

TABLE 2. Summary description of centrifuge model test program						
Model Code	**Dpth. (mm)**	**Relative Density (D_r)***	**σ_v' near bottom of deposit (tsf)**	**OCR**	**Number of Eqks.**	**Comments: All models constructed from Nevada Sand and tested at 50g unless specified****
2a	300	44% loose, 83% dense	1	1	3	Fully submerged
2b	300	50% loose, 75% dense	1	1	2	Fully submerged
2c	300	49% loose, 74% dense	1	1	5	Fully submerged
2d	300	50% loose, 75% dense	1	1	4	Fully submerged
2e	300	49% loose, 73% dense	1	2.5	4	Fully submerged
2f	300	50% loose, 75% dense	1	2.5	4	Fully submerged
3a	525	34% loose, 73% dense	2	1	2	Fully submerged
3b	525	49% loose, 77% dense	2	1	3	Fully submerged
3c	525	49% loose, 79% dense	2	1	3	Fully submerged
3d	525	54% loose, 80% dense	2	2.5	4	Fully submerged
4a	525	49% loose, 80% dense	3	1	4	Saturated to top of loose layer only.
4b	525	56% loose, 74% dense	3	2.5	4	Saturated to top of loose layer only.
4c	525	50% loose, 75% dense	4.7	1	4	Fully submerged, surcharge (weights)
4d	525	50% loose, 68% dense	4.7	2.5	4	Fully submerged, surcharge (weights)
4e	525	47% uniform	3.9 – 7.8	1	2,1,1**	Fully submerged, surcharge (weights), **Shaking at 50, 80, 100g
4f	525	55% uniform	3.9 – 9.7	1	1,1, 2,1**	Fully submerged, surcharge (weights), **Shaking at 50, 80, 100, 125g
4g	525	50% uniform	3.9 – 9.7	1	1,1, 1,2**	Fully submerged, surcharge (weights), **Shaking at 50, 80, 100, 125g
4h	525	50% uniform	3.9 – 9.7	1	1,1, 1,1**	Fully submerged, surcharge (weights), **Shaking at 50, 80, 100, 125g
4i	525	50% uniform	3.9 – 9.7	1	1,1, 1,1**	Fully submerged, surcharge (weights), **Shaking at 50, 80, 100, 125g
4j	525	50% uniform	3.9 – 9.7	1	1,1, 1,2**	Fully submerged, surcharge (weights), **Shaking at 50, 80, 100, 125g.
4k	525	50% uniform	1.9 – 4.8	1	1,1, 1,2**	Fully submerged, no surcharge, **Shaking at 50, 80, 100, 125g.
5a	525	51% loose, 72% dense	7.4	1	4	Fully submerged, surcharge (weights)
5b	525	49% loose, 76% dense	7.4	2.5	4	Fully submerged, surcharge (weights)
5c	525	52% loose, 75% dense	9.2	1	3	Fully submerged, surcharge (weights)
5d	525	57% loose, 80% dense	9.2	1	1	Fully submerged, surcharge (weights)
5e	525	50% uniform	8.4	1	7	Fully submerged, surcharge (weights)

*Relative density of the portion of the model termed 'loose', always refers to a 160 mm thick layer at the bottom of the model. Relative density of the portion of the model termed 'dense', refers to that portion of the model above the 'loose' layer (ranges in thickness from 140 to 365 mm)

Table 3. Nevada Sand Properties (as measured)	
Specific Gravity	2.64
Maximum void ratio	0.757 (density 1502.53 kg/m^3)
Minimum void ratio	0.516 (density 1741.21 kg/m^3)
D_{50}	0.18 mm
D_{10}	0.11 mm

Table 4. Pore Fluid Properties (as measured)	
Density	1200 kg/cm^3
Viscosity	50 cs
Specific Gravity	1.26
Composition	85% glycerine, 15% water (by weight)

Table 5. Characteristics of Input Motion			
Model	**Freq., Hz**	**A_{max}, g**	**Number of cycles**
2f (Figure 3)	0.54	0.25	34
3c (Figure 4)	0.54	0.09	35
4d (Figure 5)	0.54	0.11	50
4j (Figure 6)	1.18	0.25	57
4k (50g), (Figure 7)	1.17	0.32	57
4k (100g), (Figure 8)	0.88	0.42	85
5a (Figure 9)	0.54	0.10	35
5d (Figure 10)	0.86	0.32	51

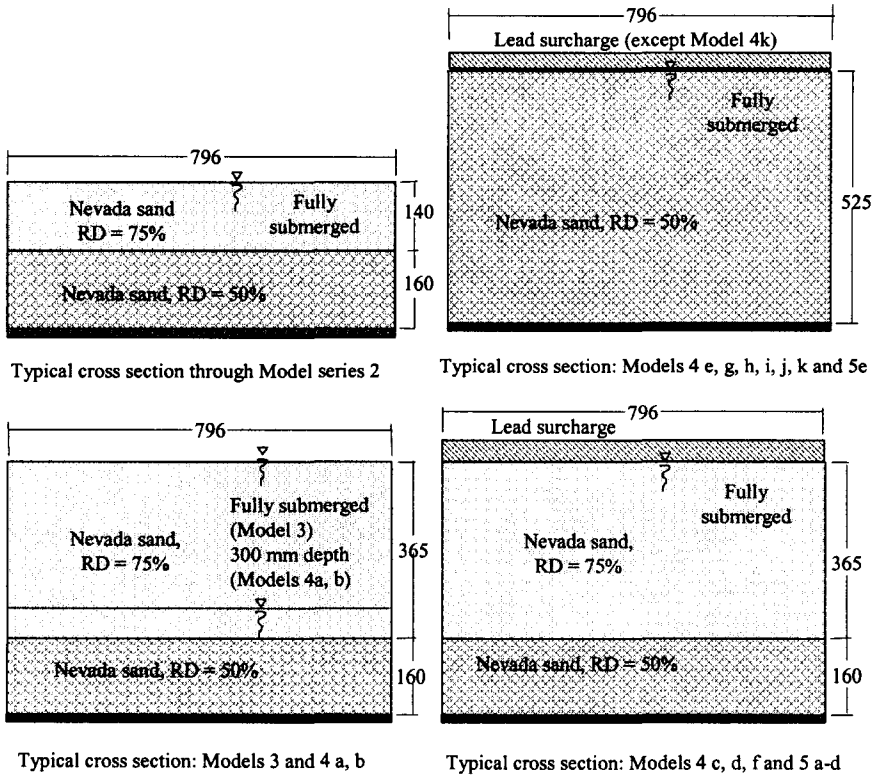

Figure 1. Cross sections through different centrifuge models (all dimensions in mm)

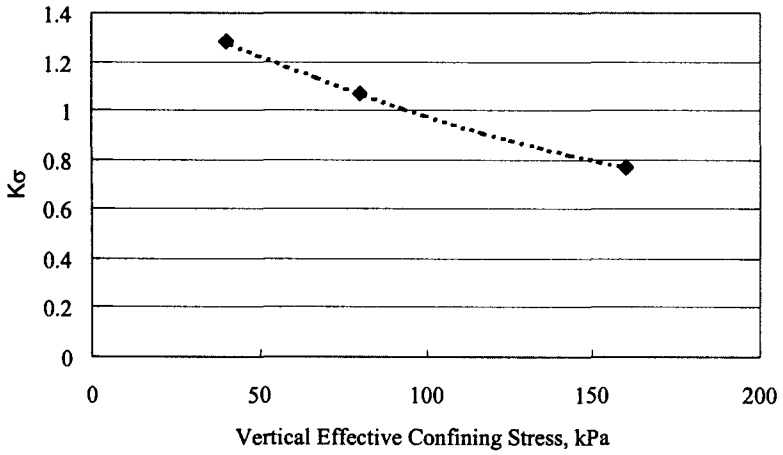

Figure 2. K_σ relationship for Nevada sand based on cyclic triaxial test data as reported by Arulmoli et al., 1992.

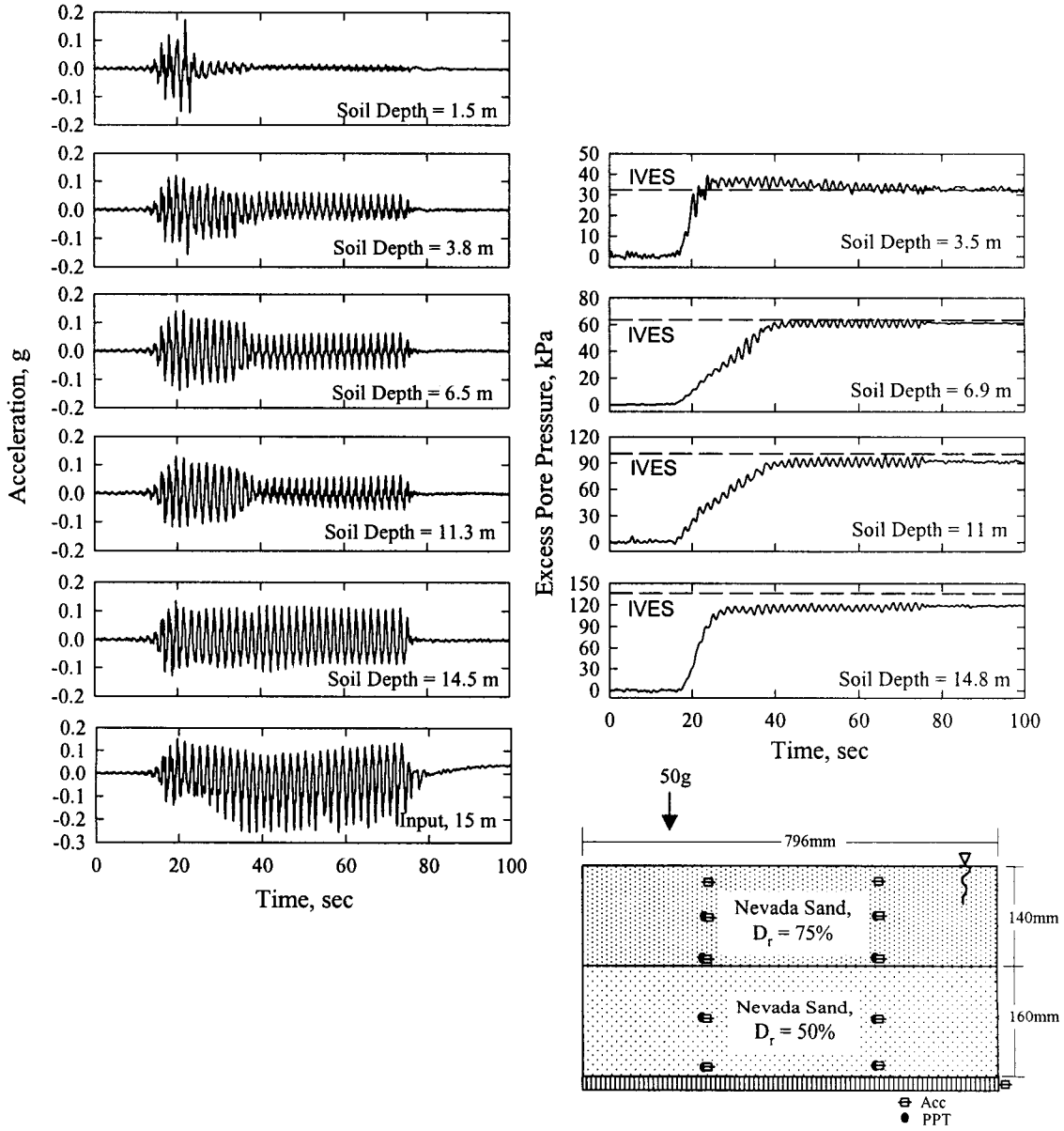

Figure 3. Results from model 2f showing recorded accelerations and excess pore pressure

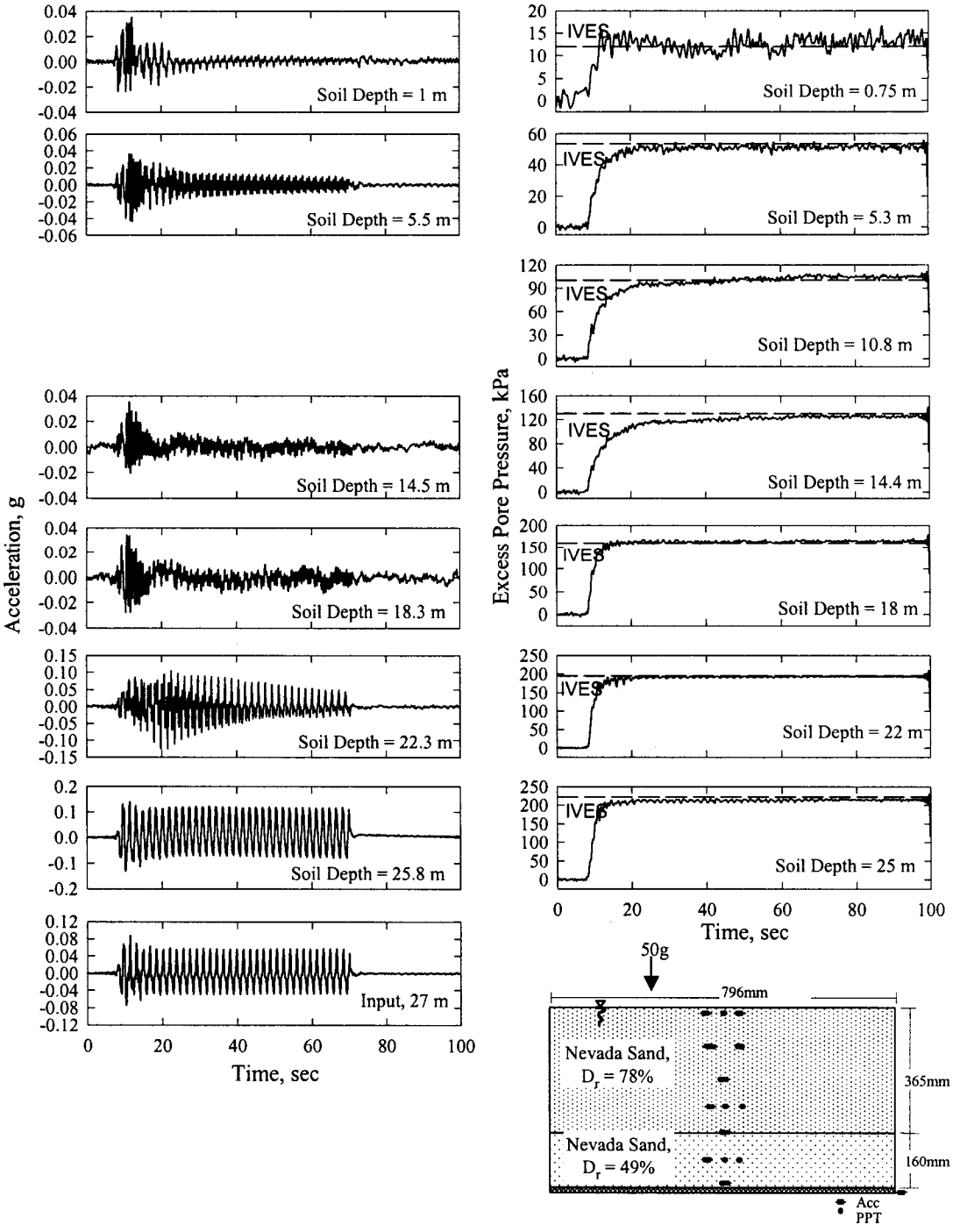

Figure 4. Results from model 3c showing recorded accelerations and excess pore pressure

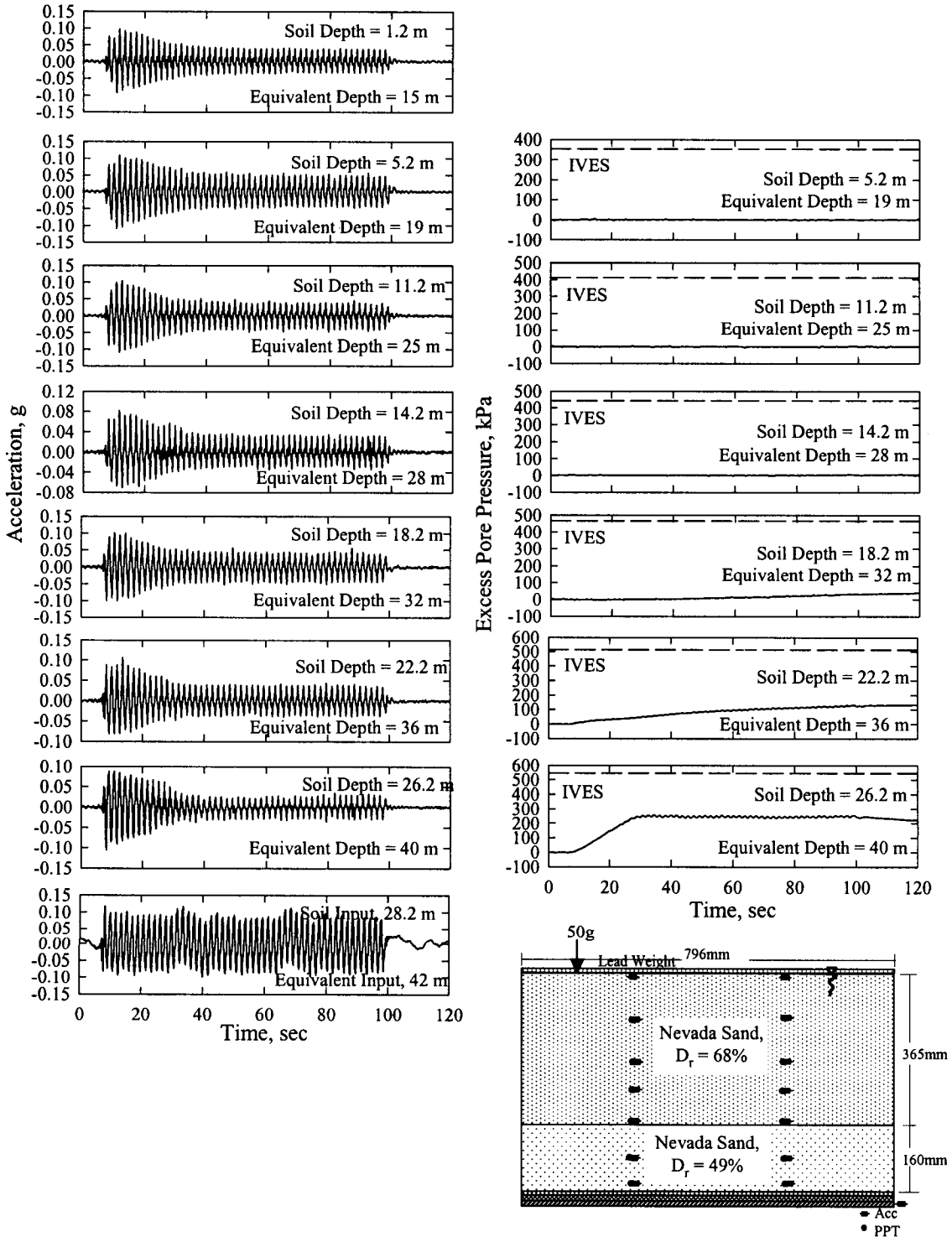

Figure 5. Results from model 4d showing recorded accelerations and excess pore pressure

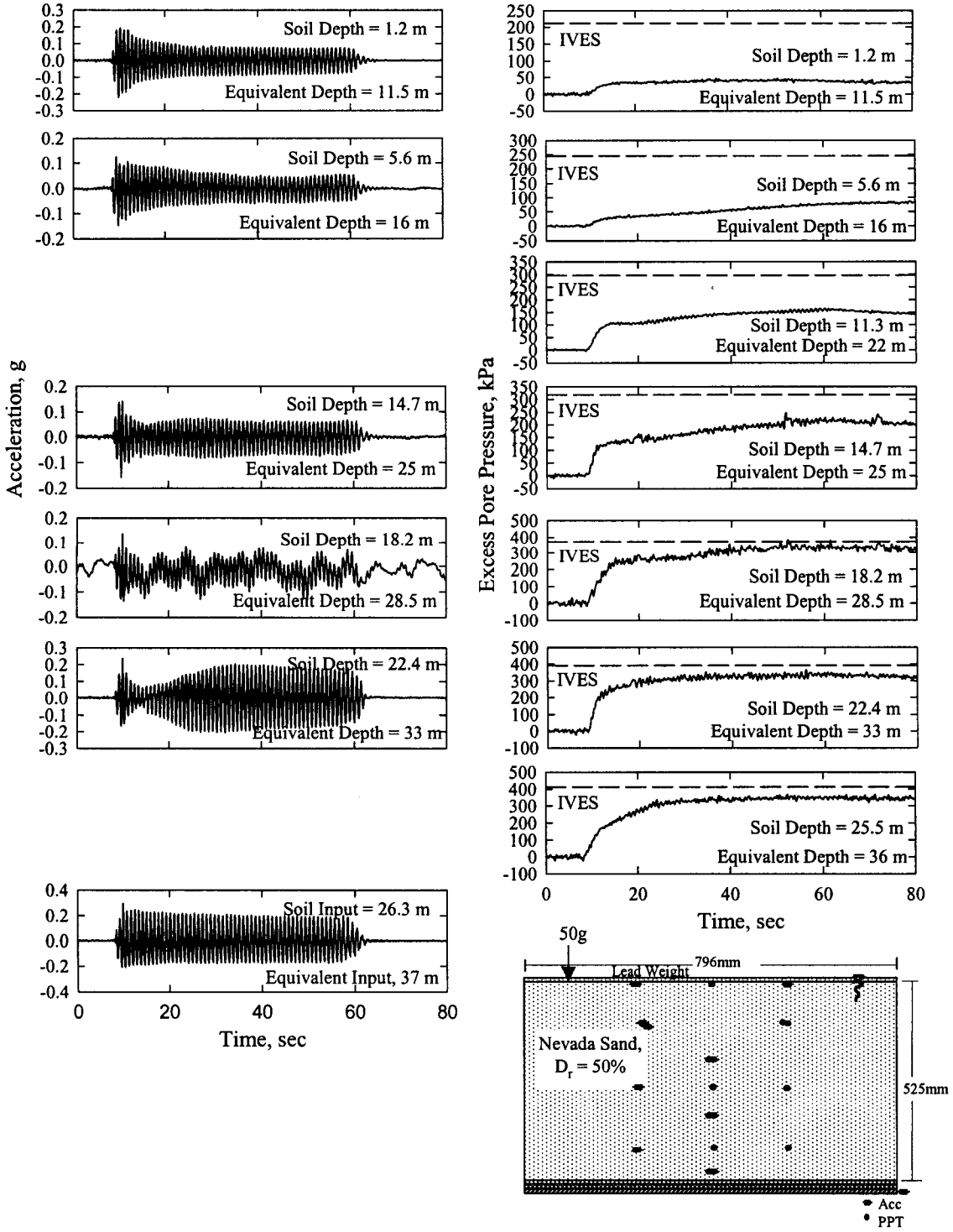

Figure 6. Results from model 4j showing accelerations and excess pore pressures.

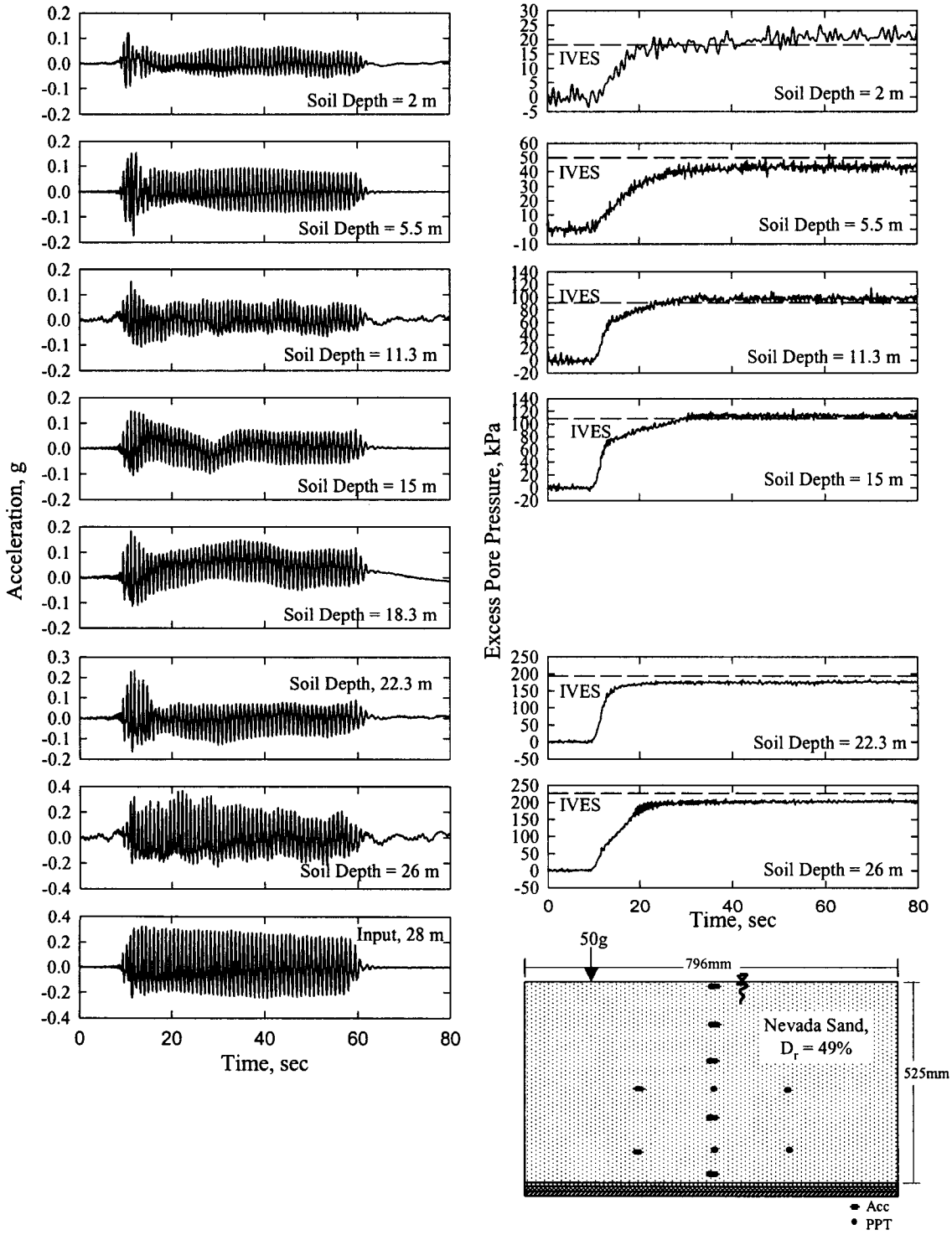

Figure 7. Results from model 4k, 50 g showing accelerations and excess pore pressure.

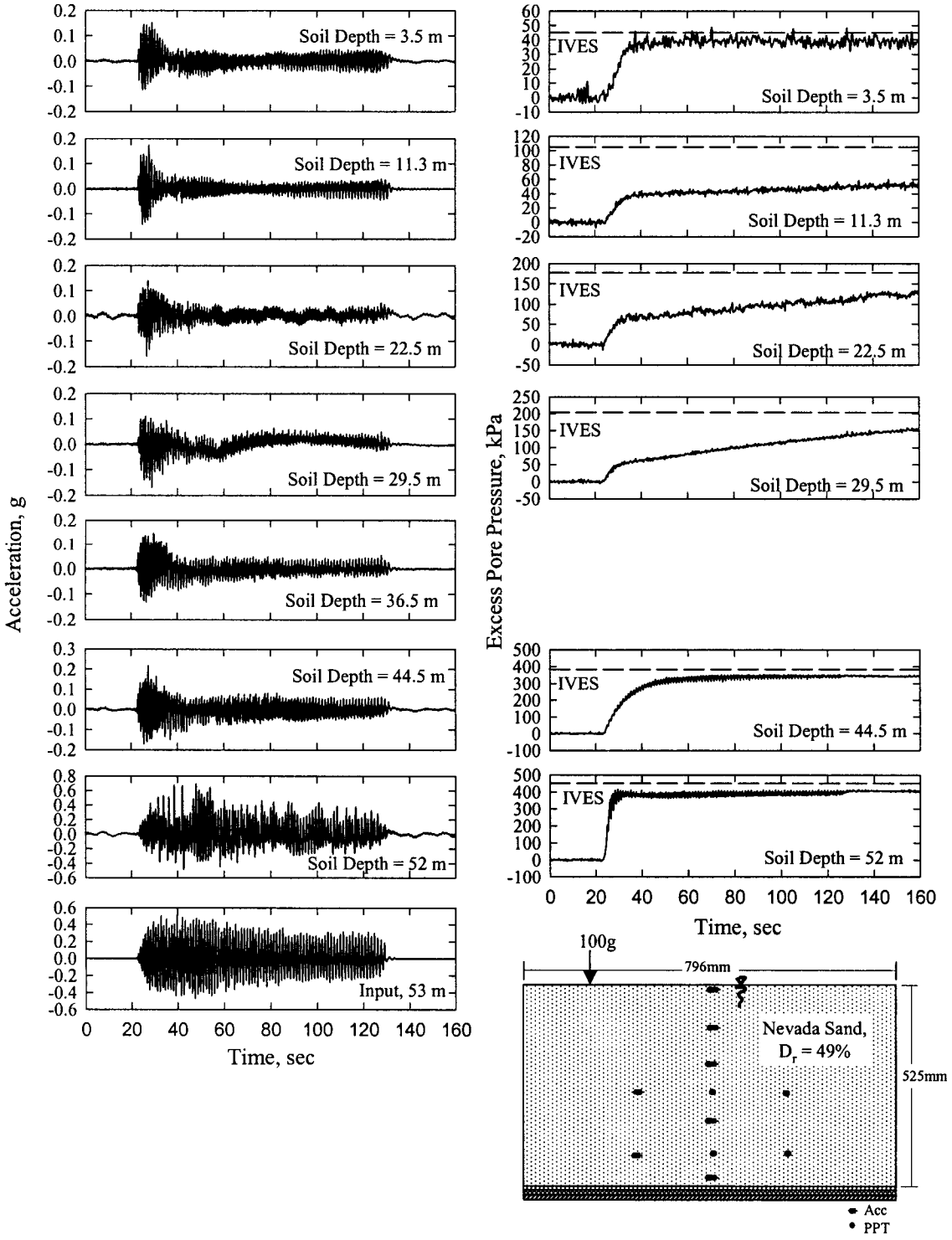

Figure 8. Results from model 4k, 100g showing accelerations and excess pore pressures.

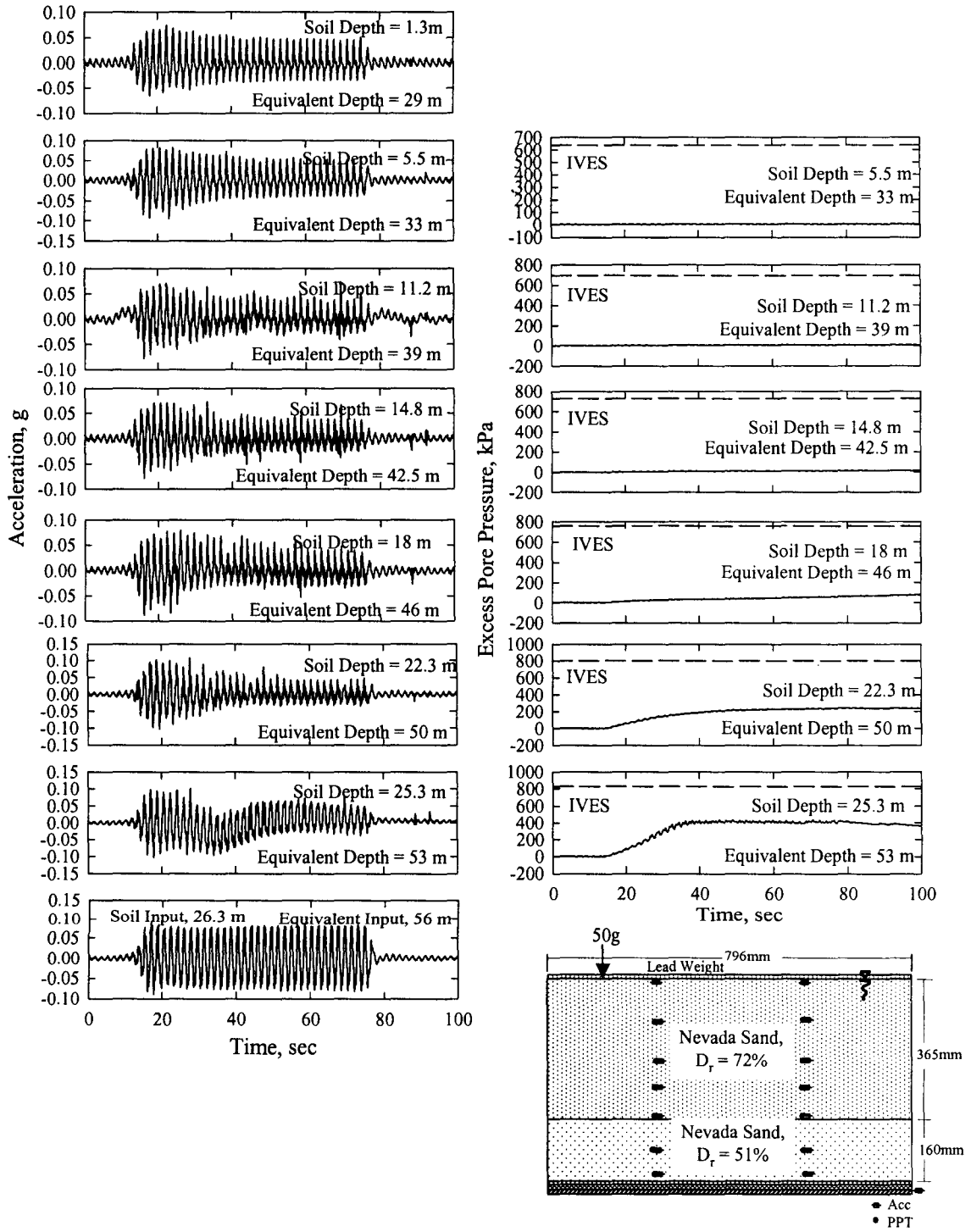

Figure 9. Results from model 5a showing accelerations and excess pore pressure.

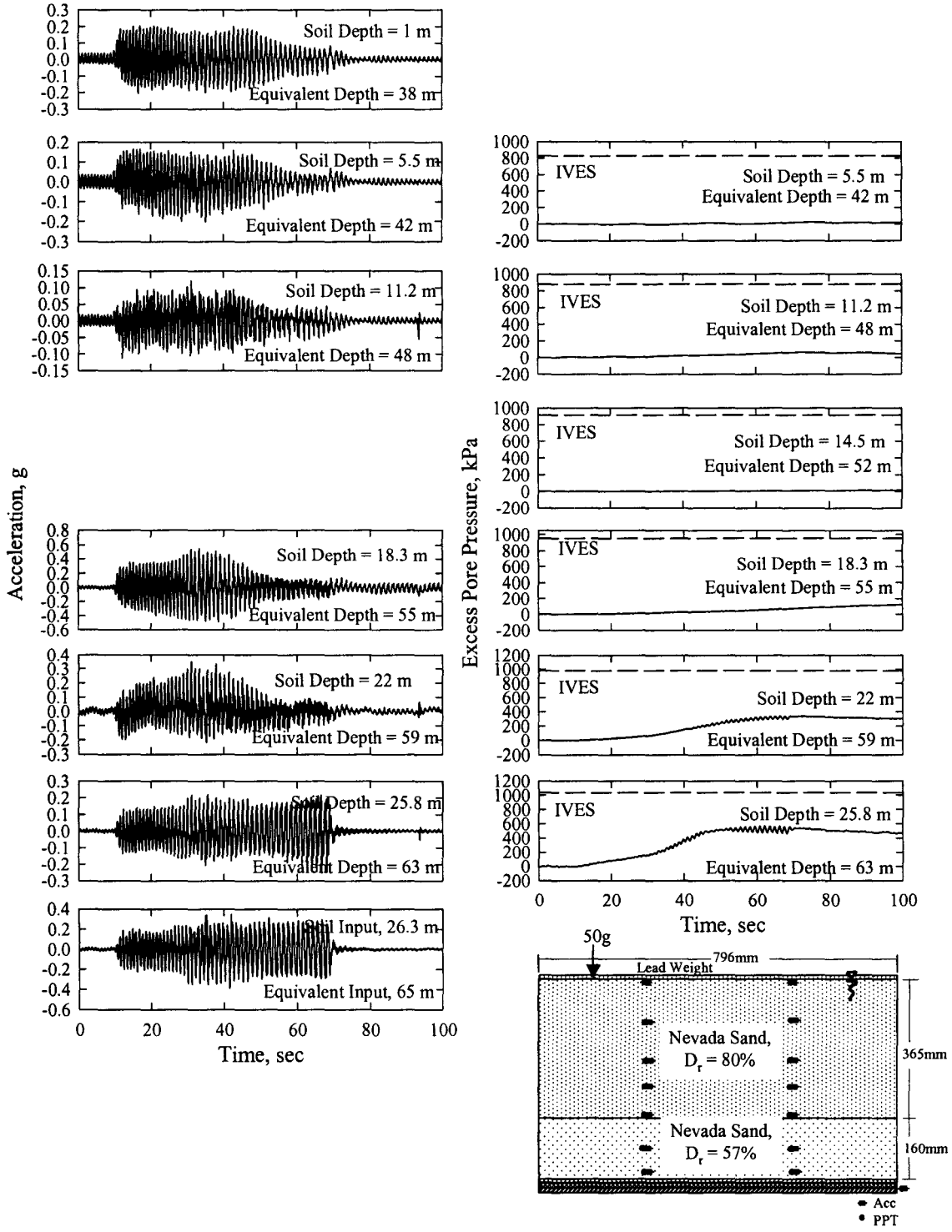

Figure 10. Results from model 5d showing accelerations and excess pore pressures.

SESSION 5

TRANSPORTATION SYSTEMS

An Evaluation of the Force Reduction Factor in the Force-Based Seismic Design

by

Gakuho Watanabe[1] and Kazuhiko Kawashima[1]

ABSTRACT

This paper presents an analysis of the force reduction factors used in the force-based seismic design of structures. The force reduction factors are evaluated based on 70 free-field ground motions. Scattering of the force reduction factors depending on ground motions and the effect of damping rations assumed in linear and nonlinear responses are clarified. A new formulation of the force reduction factors is presented.

KEY WORDS:
Seismic design, Forced-based design, Response modification factor, Force modification factor, Seismic response

1. INTRODUCTION

In the force based seismic design, it is usual to estimate the demand from a linear response of a structure by dividing it by the force reduction factor. The force reduction factor or response modification factor, which is often called q-factor or R-factor, has an important role in the estimation of design force of a structure. An early study by Newmark and Hall (1973) revealed the fact that the equal displacement assumption and the equal energy assumption provide a good estimation of the force reduction factors at long and short periods, respectively. This affected an important effect to seismic design criteria worldwide. Various researches such as Nassar and Krawinkler (1991) and Miranda and Bertero (1994) have been conducted on the force reduction factors. In particular, Miranda and Bertero provided a detailed review on the force reduction factors.

However, in spite of the importance in seismic design, less attention has been paid to large scattering of the force reduction factors depending on ground motions. Since the scattering is so large, only the mean values of the force reduction factor is not sufficient to evaluate a force reduction factor for design. Assumption of damping ratio for evaluating the linear and nonlinear responses is another important point. Although it has been general to assume the same damping ratio for the linear and nonlinear responses, it depends on how the force reduction factors are used.

This paper present an analysis on the force reduction factors based on 70 free-field ground motions. The scattering of the force reduction factors depending on ground motions and the effect of assumption of damping ratios in linear and nonlinear responses are clarified.

2. DEFINITION OF FORCE REDUCTION FACTOR

If one idealizes a structure in terms of a single-degree-of-freedom (SDOF) oscillator with an elastic perfect plastic bilinear hysteretic behavior as shown in Fig. 1, the force reduction factor R_μ may be defined as

[1]Tokyo Institute of Technology, O-Okayama, Meguro, Tokyo, Japan, 152-8552

$$R_\mu(T,\mu_T,\xi_{EL},\xi_{NL})=\frac{F_R^{EL}(T,\xi_{EL})}{F_Y^{NL}(T,\mu_T,\xi_{NL})} \quad (1)$$

in which T : natural period, F_R^{EL} and F_Y^{NL} : maximum restoring force in an oscillator with a linear and a bilinear hysteresis, respectively, μ_T : target ductility factor, and ξ_{EL} and ξ_{NL} : damping ratio assumed in the evaluation of linear and bilinear responses, respectively. The natural period T may be evaluated based on the cracked stiffness of columns. Representing u_y the yield displacement where the stiffness changes from the cracked stiffness to the post-yield stiffness, a target ductility factor μ_T may be defined based on the yielding displacement u_y as

$$\mu_T=\frac{u_{\max T}}{u_y} \quad (2)$$

in which $u_{\max T}$ is a target maximum displacement of an oscillator. The post-yield stiffness is assumed to be 0 in the present study.

Since the damping controls structural response, it has to be clarified carefully. A structure under a strong excitation generally exhibits strong hysteretic behavior, and this results in an energy dissipation in a structure. For example, the flexural inelastic deformation of columns contributes to energy dissipation in a bridge. Hence, the evaluation of damping ratio depends on the idealization of such an energy dissipation. If one idealizes the energy dissipation in nonlinear structural components by incorporating nonlinear elements that represent the hysteretic behavior, the energy dissipation in the nonlinear structural components is automatically included in the analysis. On the other hand, if one idealizes the nonlinear structural components by elastic linear elements, the energy dissipation in the nonlinear structural components has to be included in the analysis by other means. The equivalent viscous damping ratio ξ_h is generally used for such a purpose as

$$\xi_h=\frac{1}{4\pi}\cdot\frac{\Delta W}{W} \quad (3)$$

in which ΔW and W represent an energy dissipation in a hysteretic excursion and the elastic energy, respectively. For example, in an oscillator with an elastic perfect-plastic bilinear hysteresis, the equivalent damping ratio ξ_h is

$$\xi_h=\frac{2}{\pi}\frac{\mu-1}{\mu} \quad (4)$$

Fig. 2 shows the equivalent damping ratio by Eq. (4). It is generally very large such as 0.4 at the target ductility factor of 3-5.

In addition to such hysteretic energy dissipation, there must be some other sources of energy dissipation (for example, Kawashima, Unjoh, Tsunomoto 1993). The radiation of energy from a foundation to surround ground contributes to energy dissipation. Structural damping such as friction at connections may be important in many structures (for example, Kawashima and Unjoh 1989). Viscous damping due to friction with air is generally predominant in a structure with a long natural period. It is general to idealize those sources of energy dissipation in terms of the equivalent viscous damping.

If one considers a structure in which the flexural hysteretic energy dissipation is predominant with other sources of energy dissipation being a secondary importance, the total damping ratio ξ_{eq} of a SDOF oscillator may be provided as

$$\xi_{eq}=\xi_h+\xi_{oth} \quad (5)$$

in which ξ_h is the damping ratio that accounts the hysteretic energy dissipation by Eq. (3), and ξ_{oth} is the damping ratio that accounts the energy dissipation other than the hysteretic energy dissipation.

In the evaluation of the force reduction factor R_μ based on Eq. (1), how damping ratios are assumed in the evaluation of the linear and the nonlinear responses is important. If one assumes the damping ratios as

$$\xi_{EL} = \xi_{eq} \text{ and } \xi_{NL} = \xi_{oth} \quad (6)$$

the energy dissipation is essentially the same between the linear and the nonlinear responses. Hence, the force reduction factor by Eq. (1) represents the difference of restoring force between the linear and nonlinear responses. Thus, Eq. (1) reflects the effect of nonlinear response of an oscillator.

On the other hand, if one assumes the damping ratios as

$$\xi_{EL} = \xi_{NL} = \xi_{eq} \quad (7)$$

or,

$$\xi_{EL} = \xi_{NL} = \xi_{oth} \quad (8)$$

the force reduction factor by Eq. (1) includes the effect of different energy dissipation between the linear and nonlinear responses, in addition to the effect of nonlinear response. By assuming Eq. (7) in the evaluation of nonlinear response, the hysteretic energy dissipation in the nonlinear structural components is counted by the equivalent viscous damping in addition to the inelastic excursion in the nonlinear elements. As a consequence, the hysteretic energy dissipation in the nonlinear structural components is counted twice in the evaluation of nonlinear response. On the other hand, if one assumes Eq. (8), the hysteretic energy dissipation is not taken into account in the evaluation of linear response.

It should be noted here that which is appropriate among Eqs. (6), (7) and (8) depends on how the force reduction factor is used. Based on the original definition inherent to the force reduction factor, it seems that Eq. (6) is the most appropriate. Eq. (8) generally provides conservative estimation for the force reduction factors. If $\xi_{oth} \approx 0$, the difference of the force reduction factors among Eqs. (6), (7) and (8) is limited. It should be noted that ξ_h, ξ_{oth} and ξ_{eq} depend on the type of a structure, mode shape, hysteresis and the target ductility factor.

Although the equivalent damping ratio ξ_h is very high as shown in Fig. 2, it is not general to assume such a high damping ratio in seismic design of a bridge structure. It is because a bridge structure is generally more complex than a SDOF oscillator, and this makes the relative contribution of the hysteretic energy dissipation of columns less significant. Since it is general practice in a standard bridge structure to assume about 0.05 for the damping ratio including hysteretic energy dissipation of columns, ξ_{eq} is assumed to be 0.05 in the present study based on Eq. (6). Hence, it is assumed here that ξ_h and ξ_{oth} is 0.03 and 0.02, respectively.

Using those damping ratios, the force reduction factors are evaluated in this study based on Eq. (6). However, an analysis assuming Eqs. (7) and (8) is also conducted for comparison with the previous studies.

3. REVIEW OF THE PAST INVESTIGATIONS

An early study for the force reduction factor was conducted by Newmark and Hall (Newmark and Hall 1973). They used 10 ground motions recorded in the 1940 Imperial Valley Earthquake. They assumed $\xi_{EL} = \xi_{NL} = 0.05$, and proposed a force reduction factor as

$$R_\mu = \begin{cases} 1 \cdots\cdots\cdots (0 \le T \le T_1/10) \\ \sqrt{2\mu-1}\left(\dfrac{T}{4T_1}\right)^{2.513\log\left(1/\sqrt{2\mu-1}\right)} \\ \qquad \cdots\cdots\cdots (T_1/10 \le T \le T_1/4) \\ \sqrt{2\mu-1} \cdots\cdots\cdots (T_1/4 \le T \le T_1') \\ T\mu/T_1 \cdots\cdots\cdots\cdots\cdots (T_1' \le T \le T_1) \\ \mu \cdots\cdots\cdots\cdots\cdots (T_1 \le T \le T_2) \end{cases} \quad (9)$$

where,

$$T_1 = 2\pi \frac{\phi_{ev} V}{\phi_{ea} A}$$

$$T_1' = T_1 \frac{\mu}{\sqrt{2\mu - 1}} \tag{10}$$

$$T_1 = 2\pi \frac{\phi_{ed} D}{\phi_{ev} V}$$

in which, A, V and D represent peak ground acceleration, velocity and displacement, respectively, and ϕ_{ea}, ϕ_{ev} and ϕ_{ed} represent the amplification for acceleration, velocity and displacement, respectively.

Nassar and Krawinkler proposed a force reduction factor, assuming $\xi_{EL} = \xi_{NL} = 0.05$, based on an analysis for 15 ground motions as (Nassar and Krawinkler 1991)

$$R_\mu = \{c(\mu - 1) + 1\}^{1/c} \tag{11}$$

where

$$c(T, \alpha) = \frac{T^\alpha}{1 + T^\alpha} + \frac{b}{T} \tag{12}$$

in which α represents a ratio of the post-yield stiffness to the initial elastic stiffness, and a and b are coefficients depending on α. Nassar and Krawinkler precisely analyzed the effect of stiffness deterioration, and provided the coefficients a and b depending on α.

Miranda and Bertero proposed a force reduction factor, assuming $\xi_{EL} = \xi_{NL} = 0.05$, based on an analysis for 124 ground motions as (Miranda and Bertero 1994)

$$R_\mu = \frac{\mu - 1}{\Phi(T, T_g)} + 1 > 1 \tag{13}$$

where,

$$\Phi = \begin{cases} 1 + \dfrac{1}{10T - \mu T} - \dfrac{1}{2T} \exp\left\{ -\dfrac{3}{2}\left(\ln T - \dfrac{3}{5} \right)^2 \right\} \\ \qquad \cdots\cdots\cdots\cdots\cdots\cdots \text{(rock)} \\ 1 + \dfrac{1}{12T - \mu T} - \dfrac{2}{5T} \exp\left\{ -2\left(\ln T - \dfrac{1}{5} \right)^2 \right\} \\ \qquad \cdots\cdots\cdots\cdots\cdots\cdots \text{(alluvium)} \\ 1 + \dfrac{T_g}{3T} - \dfrac{3T_g}{4T} \exp\left\{ -3\left(\ln \dfrac{T}{T_g} - \dfrac{1}{4} \right)^2 \right\} \\ \qquad \cdots\cdots\cdots\cdots\cdots\cdots \text{(soft)} \end{cases} \tag{14}$$

in which T_g represents a most predominant period.

It has been known that the equal energy assumption provides a good estimation for the force reduction factor at short periods while the equal displacement assumption at long periods. The force reduction factor provided by the equal energy and the equal displacement assumptions are given as

$$R_\mu = \sqrt{2\mu - 1} \quad \text{(equal energy)} \tag{15}$$

$$R_\mu = \mu \quad \text{(equal displacement)} \tag{16}$$

Application of Eqs. (15) and (16) and a comparison of the present study to the previous models will be described later.

4. FORCE REDUCTION FACTOR FOR BILINEAR OSCILLATORS

Force reduction factors were evaluated for target ductility factor μ_T of 2, 4, 6 and 8 assuming an elastic perfect-plastic bilinear hysteresis. Damping ratio in the linear and nonlinear analyses is assumed as $\xi_{EL} = 0.05$ and $\xi_{NL} = 0.02$ based on Eq. (6). Seventy free field ground accelerations by 64 shallow earthquakes with depth less that 60 km were used for analysis. They are classified into three soil conditions depending on the fundamental natural period of subsurface ground

T_g; stiff ($T_g < 0.2$ s), moderate ($0.2 \le T_g < 0.6$ s) and soft ($T_g \ge 0.6$ s) (Japan Road Association 2002). Number of records in the stiff, moderate and soft categories is 16, 39 and 15, respectively. Distribution of peak ground accelerations on the earthquake magnitudes and epicentral distances is shown in Fig. 3. The peak accelerations are in the range of 0.1-8m/s^2, and the epicentral distances are in the range of 10-500 km.

Fig. 4 shows the force reduction factors for the 70 ground motions. Only the results for μ_T=4 and 6 are presented here since the results for other target ductility factors show the similar characteristics. It is seen in Fig. 4 that scattering of the force reduction factors depending on ground motions is significant. For example at natural period of 1 second, the force reduction factors varies from 1.9 to 10.3 depending on ground motions for μ_T=4 at the moderate soil sites. It is apparent that such a large scattering of the force reduction factors result in a large change of sizing of a structure in seismic design. Obviously smaller force reduction factors should be assumed in design to provide conservative design. It is observed in Fig. 4 that the dependence of force reduction factors on the soil condition is less significant. This will be discussed later.

Since the scattering of the force reduction factors depending on ground motions is so large that the means +/- one standard deviations of the force reduction factors were obtained for each target ductility factor, natural period and soil condition. Fig. 5 shows the mean values and the mean values +/- one standard deviations of the force reduction factors presented in Fig. 4. The force reduction factors predicted by Eqs. (15) and (16) based on the equal displacement and the equal energy assumptions are also presented here for comparison. The mean values of force reduction factors increase as the natural periods increase, and then they approach to μ_T at long period. It has been pointed out in the previous researches that the Eq. (15) provides a good estimation to the force reduction factor. However, it is noted that Eq. (15) provides a good estimation to the mean values, but it considerably underestimates the force reduction factors corresponding to the mean values minus one standard deviations. On the other hand, Eq. (16) provides better estimation to the mean values minus one standard deviations. Taking account of the force reduction factors having considerable scattering depending on ground motions, it seems reasonable to consider a certain redundancy in the estimation of the force reduction factor in design. Based on such a consideration, it is more conservative to assume Eq. (16) instead of Eq. (15) for a design purpose.

Fig. 6 shows the dependence of the standard deviations of force reduction factors $\sigma(R_\mu)$ on the natural periods T and the soil condition. Similar to the mean values, the standard deviations $\sigma(R_\mu)$ increase as the natural periods increase, and decrease after taking peak values at natural period of 1-2 second. Fig. 7 shows the dependence of the standard deviations $\sigma(R_\mu)$ on the target ductility factors μ_T. The standard deviations $\sigma(R_\mu)$ increase as the target ductility factors increase. The relation may be approximated by a least square fit as

$$\sigma(R_\mu) = \begin{cases} -0.328 + 0.379 \cdot \mu_T & \text{(stiff)} \\ -0.292 + 0.378 \cdot \mu_T & \text{(moderate)} \\ -0.354 + 0.409 \cdot \mu_T & \text{(soft)} \end{cases} \quad (17)$$

As the soil condition dependence of $\sigma(R_\mu)$ is less significant as shown in Fig. 7, Eq. (17) may be approximated as

$$\sigma(R_\mu) \approx -0.3 + 0.4 \cdot \mu_T \quad (18)$$

5. FORMULATION OF FORCE REDUCTION FACTORS

To idealize the mean values of the force reduction

factors in Fig. 5, they are represented as

$$R_\mu = (\mu - 1) \cdot \Psi(T) + 1 \tag{19}$$

where,

$$\Psi(T) = c \cdot \frac{T - a}{e^{b \cdot (T-a)}} + 1 \tag{20}$$

in which a, b and c are parameters to be determined.

Since $R_\mu = \mu$ at $T = a$ in Eq. (20), the parameter a represents the period where R_μ is equal to μ (Point P) as shown in Fig. 8. Because the gradient of R_μ is

$$\frac{dR_\mu}{dT} = c(\mu - 1) \cdot \frac{1 - b(T - a)}{e^{b(T-a)}} \tag{21}$$

it is $c \cdot (\mu - 1)$ at Point P. Consequently, the parameter c represents the gradient at Point c divided by $\mu - 1$. Representing Q as the point where R_μ takes the peak value, $1/b$ represents the period between Points P and Q.

Based on the definition, the following condition has to be satisfied in R_μ

$$\lim_{T \to 0} R_\mu = 0 \tag{22}$$

Hence, the coefficient c can be eliminated as

$$c = 1 / ae^{ab} \tag{23}$$

Substitution of Eq. (23) makes Eq. (20) as

$$\Psi(T) = \frac{T - a}{ae^{bT}} + 1 \tag{24}$$

It is noted that Eq. (19) automatically satisfies the following condition

$$\lim_{T \to \infty} R_\mu = \mu \tag{25}$$

It is a feature of the above formulation that the equation is simpler and the physical meaning of the parameters a and b is clearer than the previous studies.

The mean values of force reduction factors in Fig. 5 were fitted by Eq. (19) using a nonlinear least square method (Press et al 1996). Table 1 represents the a and b as well as the regression coefficients. Although the regression coefficient is not high enough for some combinations such as μ_T=2 and stiff sites, it may be accepted in other conditions. As shown later, the fitting is not necessarily poor for a combination of μ_T=2 and stiff sites.

Fig. 9 shows parameters a, $1/b$ and $a + 1/b$. Parameter a is in the range of 1.0-1.4 second at stiff and moderate sites, and 1.5-2.4 second at soft sites. They are less sensitive to the target ductility factor μ_T between 2 and 8. As described before, a represents the period where $R_\mu = \mu$, which implies that the equal displacement assumption by Eq. (16) provides the best estimation at period a. Consequently, the accuracy of equal displacement assumption is high at 1.0-1.4 second at stiff and moderate sites, and 1.5-2.4 second at soft site.

As shown in Fig. 8, $a + 1/b$ represents the natural period where R_μ takes the peak value. It is 1.5-2 second at stiff and moderate sites, and 2.5-3.5 second at soft site. It slightly increases as target ductility μ_T increases.

The natural periods where R_μ take the values predicted by Eq. (15) based on the equal energy assumption are obtained as shown in Fig. 10. They are in the range of 0.2-0.36 second, 0.26-0.4 second and 0.4-0.6 second at stiff, moderate and soft sites, respectively. They are much shorter than the natural periods where the equal displacement assumption provides the best approximation.

Fig. 11 compares the mean force reduction factors presented in Fig. 5 to the values predicted by Eq. (19). Although some discrepancies are observed at larger target ductility factors, Eq. (19) provides a good estimation for the mean force reduction factors.

Fig. 12 shows the effect of soil condition on the mean force reduction factors estimated by Eq. (19). The effect of soil condition is less significant on the force reduction factors, in particular at small target ductility factors.

As shown in Fig. 4, scattering of the force

reduction factors around the mean values is extensive. Hence, the force reduction factors corresponding to the mean values m substituted by a standard deviation $\sigma(R_\mu)$ are evaluated as shown in Fig. 13. The mean and the standard deviation of force reduction factors were evaluated by by Eq. (19) and Eq. (18), respectively, in this estimation. They are of course close to the force reduction factors of the mean minus one standard deviation directly computed from the 70 ground motions (refer to Fig. 5). The force reduction factors predicted by Eq. (15) based on the equal energy assumption are presented here for comparison. From Fig. 13, it is seen that at μ_T=4, the equal energy assumption provides a good estimation at natural periods longer than 0.5 second at stiff and moderate sites and 1.2 second at soft sites, while it provides underestimation at natural periods shorter than those values. On the other hand, at μ_T=8, the equal energy assumption provides a good estimation at 0.6 second at stiff and moderate sites and 1 second at soft sites. It underestimates and overestimates the force reduction factors corresponding to the mean minus one standard deviation at natural periods shorter and longer, respectively, than the above natural periods.

6. EFFECT OF DAMPING RATIOS

In the preceding analysis, the force reduction factors were evaluated based on Eq. (1) assuming ξ_{EL}=0.05 and ξ_{NL}=0.02. However in the past researches, damping ratios were usually assumed as $\xi_{EL} = \xi_{NL}$ =0.05. Consequently, the same analysis presented in the preceding chapters was conducted by assuming $\xi_{EL} = \xi_{NL}$=0.05 based on Eq. (7) using the same ground motion data set. For comparison, an analysis was also conducted assuming $\xi_{EL} = \xi_{NL}$=0.02 based on Eq. (8).

Tables 2 and 3 show the parameters a and b determined for a combination of $\xi_{EL} = \xi_{NL}$=0.02 and $\xi_{EL} = \xi_{NL}$ =0.05, respectively. Fig. 14 compares a and $a+1/b$ thus determined. Also presented in Fig. 14 are a and $a+1/b$ used in the preceding chapter (ξ_{EL}=0.05 and ξ_{NL}=0.02, refer to Fig. 9). It is seen in Fig. 14 that both a and $a+1/b$ at the same target ductility factors are the shortest for a combination of $\xi_{EL} = \xi_{NL}$ =0.02 and the longest for a combination of ξ_{EL} =0.05 and ξ_{NL} =0.02. Parameters a and $a+1/b$ for a combination of $\xi_{EL} = \xi_{NL}$=0.05 are between the two cases.

Fig. 15 compares the mean values of the force reduction factors based on the three assumptions of damping ratios. Original force reduction factors computed from the 70 ground motions are also presented here for comparison. A systematic difference of the force reduction factors is observed reflecting the dependence of a and $a+1/b$ on the damping rations. The combination of $\xi_{EL} = \xi_{NL}$ =0.02 provides the largest estimation for the force reduction factors, while the combination of ξ_{EL} =0.05 and ξ_{NL} =0.02 provides the smallest estimation. The combination of $\xi_{EL} = \xi_{NL}$ =0.05 provides the estimation between the two cases.

7. COMPARISON WITH THE PREVIOUS STUDIES

Fig. 16 shows a comparison of the force reduction factor in the present study by Eq. (19) to Nassar and Krawinkler by Eq. (11) and Miranda and Bertero by Eq. (13). Since it is assumed in Eqs. (11) and (13) that $\xi_{EL} = \xi_{NL}$=0.05, the same damping ratios are assumed in the present study for comparison. The original mean values of the force reduction factors computed from the 70 ground motions are also presented here for comparison. It is noted that definition of soil conditions is not the same among three researches. Hence they are classified into stiff, moderate and

soft. In the Miranda and Bertero formulation, T_g was assumed 1.5 second at soft (alluvial) site in Eq. (14).

From Fig. 16, it is seen that the present study provides a quite similar result to the formulations by Miranda & Mertero and Nassar & Krawinkler if the same damping ratios are assumed in the evaluation of linear and nonlinear responses.

8. CONCLUSIONS

An analysis was conducted for the force reduction factor based on response of SDOF oscillator using 70 free-field ground motions. Based on the analysis presented herein, the following conclusions may be deduced:

1) A new formulation as shown in Eqs. (19) and (24) was developed. The formulation is simpler than the past formulations. Parameters a and $a+1/b$ express the natural period where R_μ is equal to μ and R_μ takes a peak value, respectively.

2) Difference of the damping ratios assumed in the evaluation of linear and nonlinear responses (ξ_{EL} and ξ_{NL}) provides a systematic difference in the force reduction factors. The combination of $\xi_{EL}=\xi_{NL}=0.02$ provides the largest estimation for the force reduction factors, while the combination of $\xi_{EL}=0.05$ and $\xi_{NL}=0.02$ provides the smallest estimation. The combination of $\xi_{EL}=\xi_{NL}=0.05$ provides the estimation between the two cases. Hence, the damping ratios have to be carefully assumed keeping how the force reduction factors are used in mind.

3) Scattering of the force reduction factors depending on ground motions is significant. Although it has been pointed out that the equal displacement assumption by Eq. (15) provides a good estimation to the force reduction factors, it provides a good estimation only to the mean values; however, it considerably underestimates the mean minus one standard deviation. On the other hand, the equal energy assumption by Eq. (16) provides a better estimation to the force reduction factors corresponding to the mean minus one standard deviation, although it provides too conservative estimation to the mean values. Taking account of the considerable scattering of the force reduction factors depending on ground motions, it is conservative to assume the equal energy assumption instead of the equal displacement assumption.

4) The response modification factors in the present study by Eqs. (19) and (24) provides quite close force reduction factors proposed by Nassar and Krawinkler, and Miranda and Betero, if the damping ratios are assumed as $\xi_{EL}=\xi_{NL}=0.05$.

REFERENCES:

Japan Road association (2002), Part V Seismic design, Design specifications of highway bridges," Maruzen, Tokyo, Japan.

Kawashima, K, MacRae, G. A., Hoshikuma, J. and Nagaya, K. (1998). "Residual displacement response spectra," Journal of Structural Engineering, 124(5), 513-530, ASCE

Kawashima, K. and Unjoh, S. (1989). "Damping characteristics of cable-stayed bridges associated with energy dissipation at movable support," Structural Engineering and Earthquake Engineering, Proc. Japan Society of Civil Engineers, 404/I-11, 123-130.

Kawashima, K., Unjoh, S. and Tsunomoto, M. (1993). "Estimation of damping ratio of cable-stayed bridges for seismic design," Journal of Structural Engineering, 119(4), 1015-1031, ASCE.

Miranda, E. and Bertero, V. (1994). "Evaluation of strength reduction factors for earthquake resistant design," Earthquake Spectra, 10(2), 357-379.

Nassar, A. A. and Krawinkler, H. (1991). "Seismic demands for SDOF and MDOF systems," Report No. 95, The John A. Blume Earthquake Engineering Center, Stanford University, California, USA.

Newmark, N. M. and Hall, W. J. (1973). "Seismic design criteria for nuclear reactor facilities," Report No. 46, Building Practices for Disaster Mitigation, National Bureau of Standards, U.S. Department of Commerce, 209-236.

Press, W.H., Teukolsky, S.A., Vetterling, W.T. and Flannery, B.P. (1996). "Numerical recipes in Fortran 77," Second Edition, The Art of Scientific Computing, Cambridge University Press, 678-683.

Priestley, M. J. N., Seible, F. and Calvi, G. M. (1996). "Seismic design and retrofit of bridges," John Wiley & Sons, New York, USA.

Takeda, T., Sozen, M. A. and Nielsen, N. N. (1970). "Reinforced concrete response to simulated earthquake," Journal of Structural Engineering, 96(12), 2557-2573, ASCE

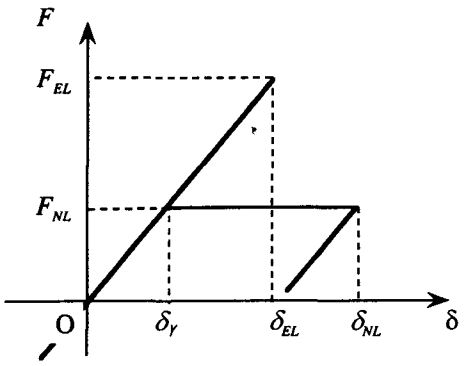

Fig. 1 Definition of Force reduction Factor

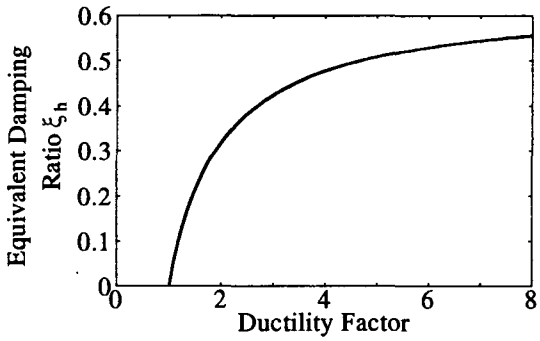

Fig.2 Equivalent Damping Ratio ξ_h by Eq. (4)

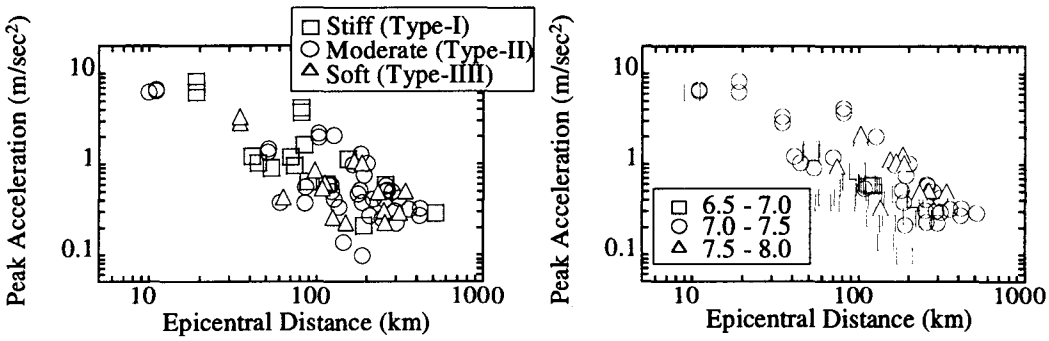

(a) Soil Condition

(b) Earthquake Magnitude

Fig. 3 Classification of Ground Accelerations in Terms of Soil Conditions and Earthquake Magnitudes

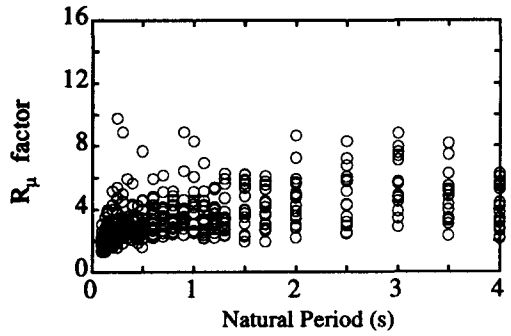

(a) Stiff (Type-I)

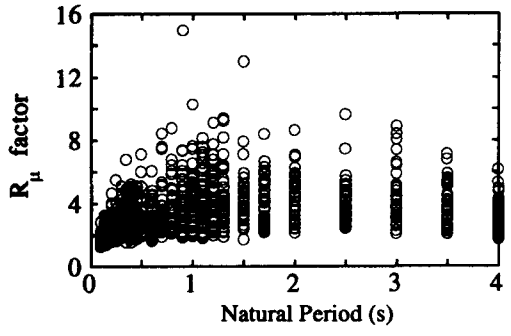

(b) Moderate (Type-II)

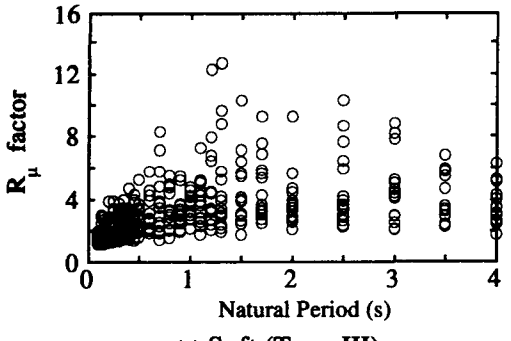

(c) Soft (Type-III)

(1) μ_T =4

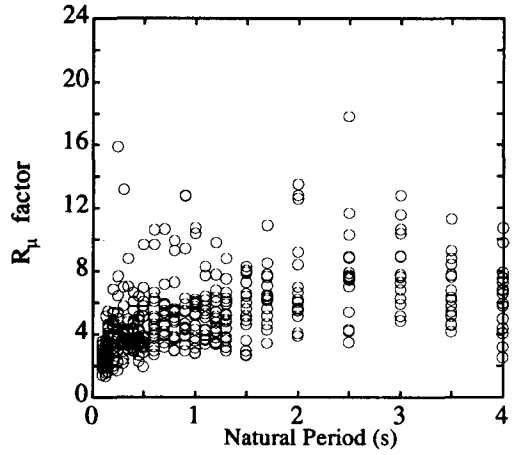

(a) Stiff (Type-I)

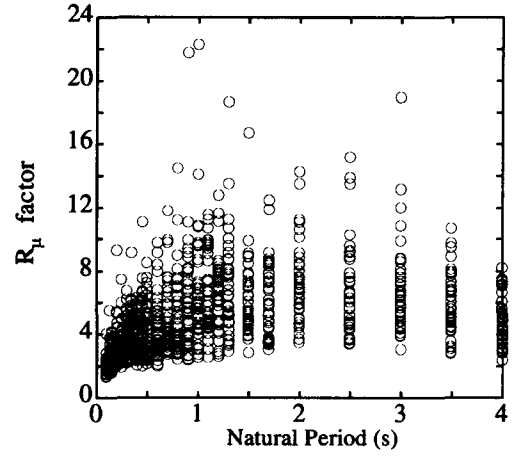

(b) Moderate (Type-II)

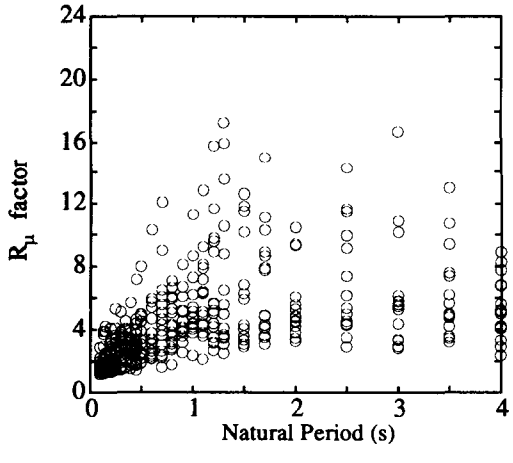

(c) Soft (Type-III)

(2) μ_T =6

Fig. 4 Force Reduction Factors

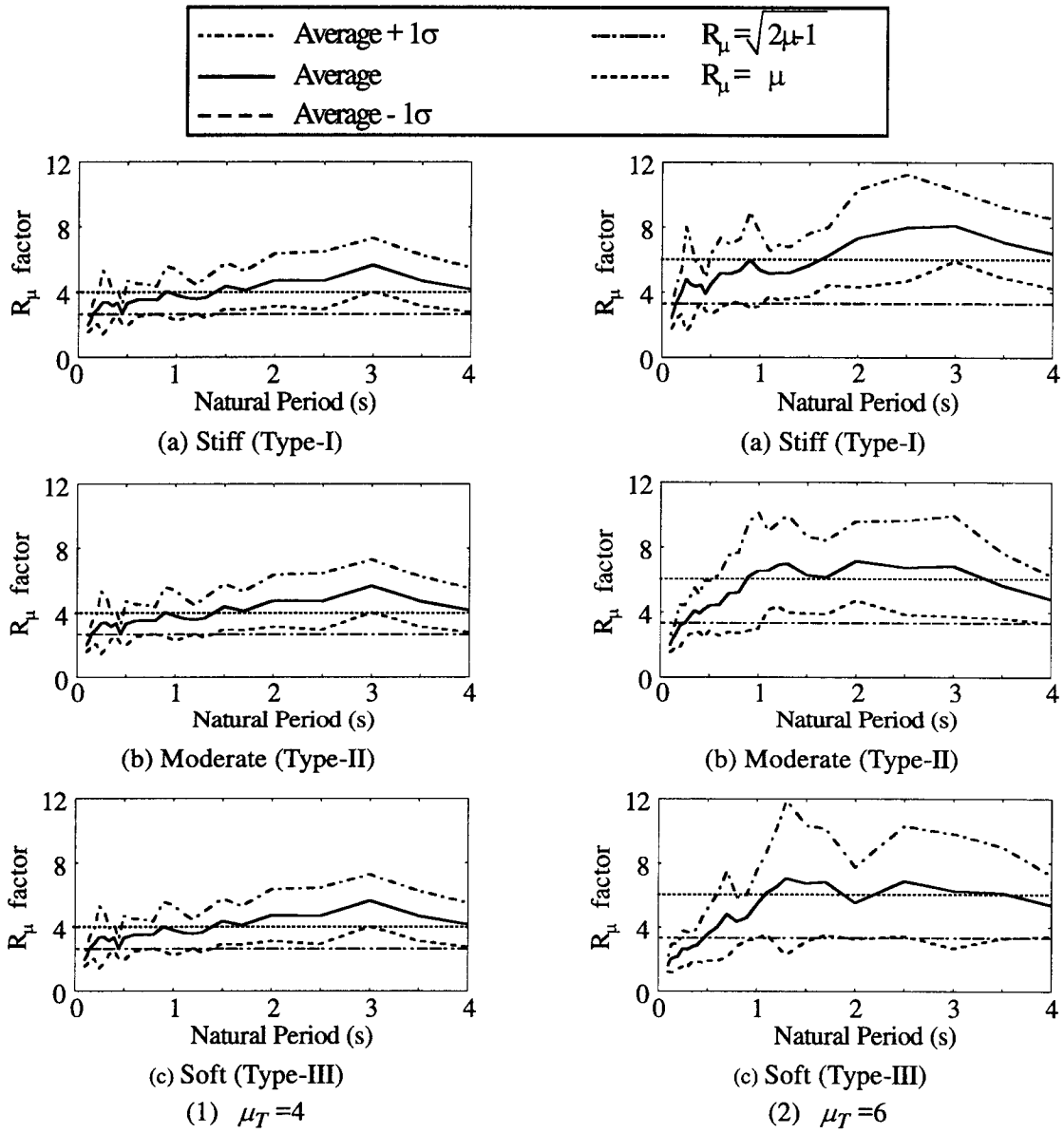

Fig. 5 Mean and Mean +/- One Standard Deviation of the Force Reduction Factors for 70 Ground Motions

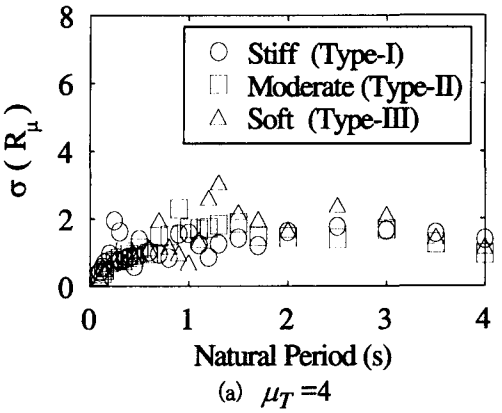

(a) μ_T =4

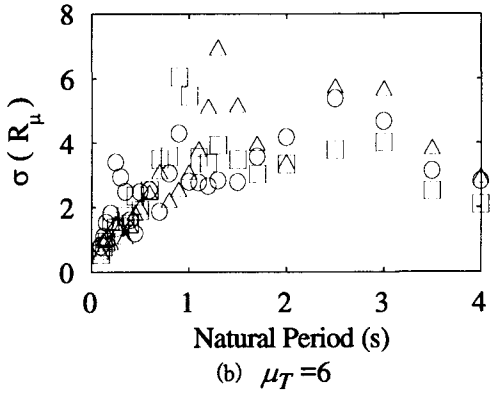

(b) μ_T =6

Fig. 6 Natural Period Dependence of Standard Deviations of the Force Reduction Factors

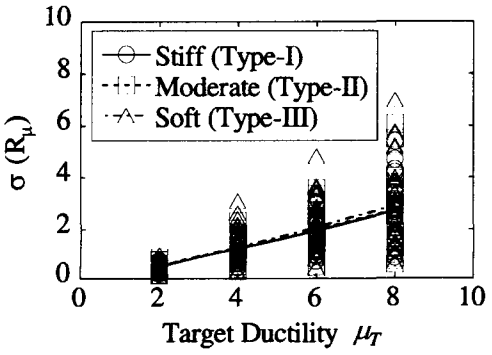

Fig. 7 Target Ductility Factor Dependence of the Standard Deviations of Force reduction Factors

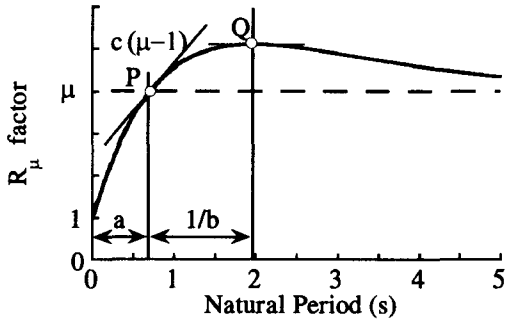

Fig. 8 Idealization of Force Reduction Factors

Table 1 Parameters a and b and Regression Coefficients R (ξ_{NL}=0.02 and ξ_{EL} = 0.05)

η_T	a, b and R	Soil Conditions		
		Type-I	Type-II	Type-III
2	a	1.29	1.12	2.35
	b	2.77	2.18	1.69
	R	0.379	0.701	0.851
4	a	1.24	0.989	1.52
	b	2.39	1.62	1.05
	R	0.673	0.842	0.886
6	a	1.34	1.03	1.85
	b	2.15	1.24	0.821
	R	0.717	0.869	0.878
8	a	1.36	1.20	1.74
	b	1.67	1.11	0.611
	R	0.776	0.899	0.895

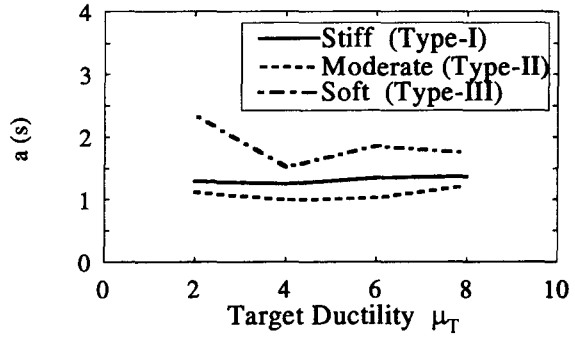

(a) Parameter a

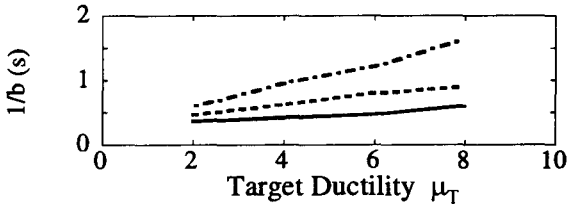

(b) Parameter $1/b$

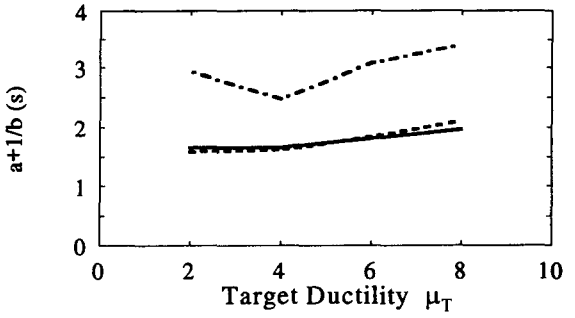

(c) Parameter $a+1/b$

Fig. 9 Parameters a and $a+1/b$ in Eqs. (20)

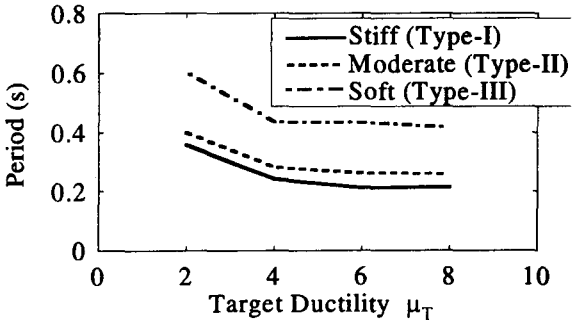

Fig. 10 Natural Periods where Force Reduction Factors Take Values Predicted by the Equal Energy Assumption (Eq. (15))

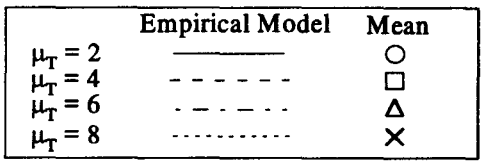

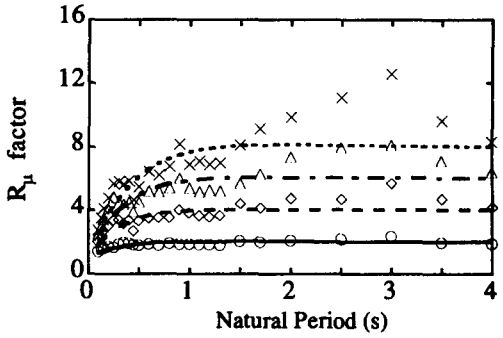

(a) Stiff (Type-I)

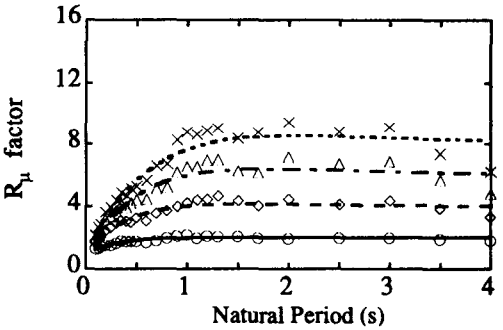

(b) Moderate (Type-II)

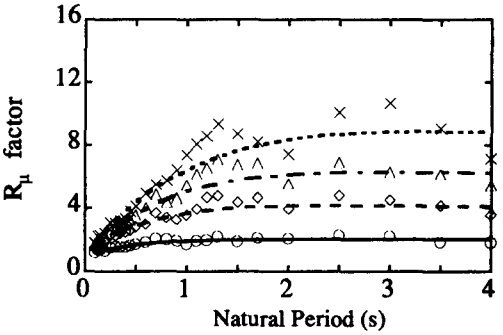

(c) Soft (Type-III)

Fig. 11 Application of Eq. (19) to the Mean Force Reduction Factors Presented in Fig. 5

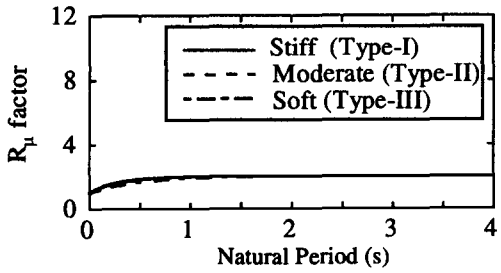

(a) μ_T =2

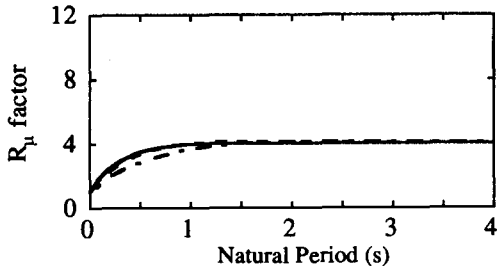

(b) μ_T =4

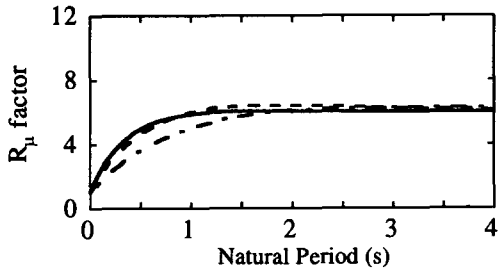

(c) μ_T =6

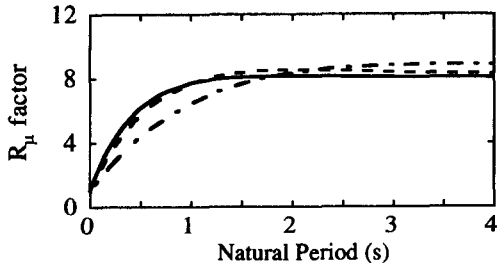

(d) μ_T =8

Fig. 12 Effect of Soil Condition on the Force Reduction Factors Predicted by Eq. (19)

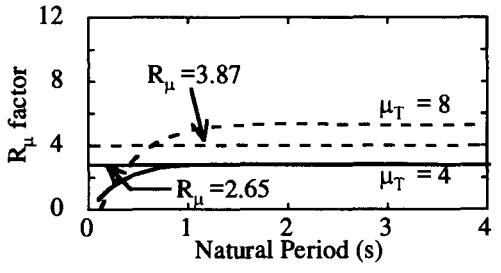

(a) Stiff (Type-I)

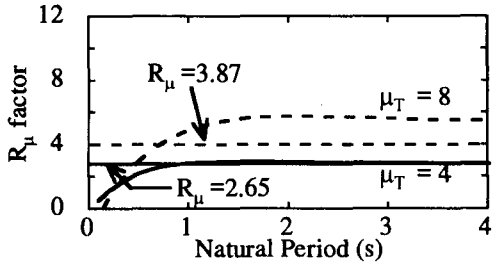

(b) Moderate (Type-II)

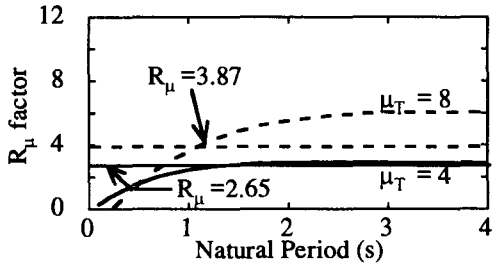

(c) Soft (Type-III)

Fig.13 Force Reduction Factors Corresponding to Means minus One Standard Deviations

Table 2 Parameters a and b ($\xi_{NL}=\xi_{EL}=0.02$)

μ_T	a and b	Soil Conditions		
		Type-I	Type-II	Type-III
2	a	0.152	0.225	0.361
	b	0.289	1.60	1.12
4	a	0.289	0.348	0.600
	b	2.46	1.28	0.902
6	a	0.397	0.432	0.800
	b	1.81	1.14	0.768
8	a	0.507	0.513	0.916
	b	1.14	1.04	0.632

Table 3 Parameters a and b ($\xi_{NL}=\xi_{EL}=0.05$)

μ_T	a and b	Soil Conditions		
		Type-I	Type-II	Type-III
2	a	0.226	0.344	0.521
	b	4.14	1.94	1.34
4	a	0.778	0.572	0.976
	b	3.50	1.35	0.994
6	a	0.981	0.725	1.23
	b	2.93	1.15	0.757
8	a	1.23	0.807	1.28
	b	2.57	0.983	0.569

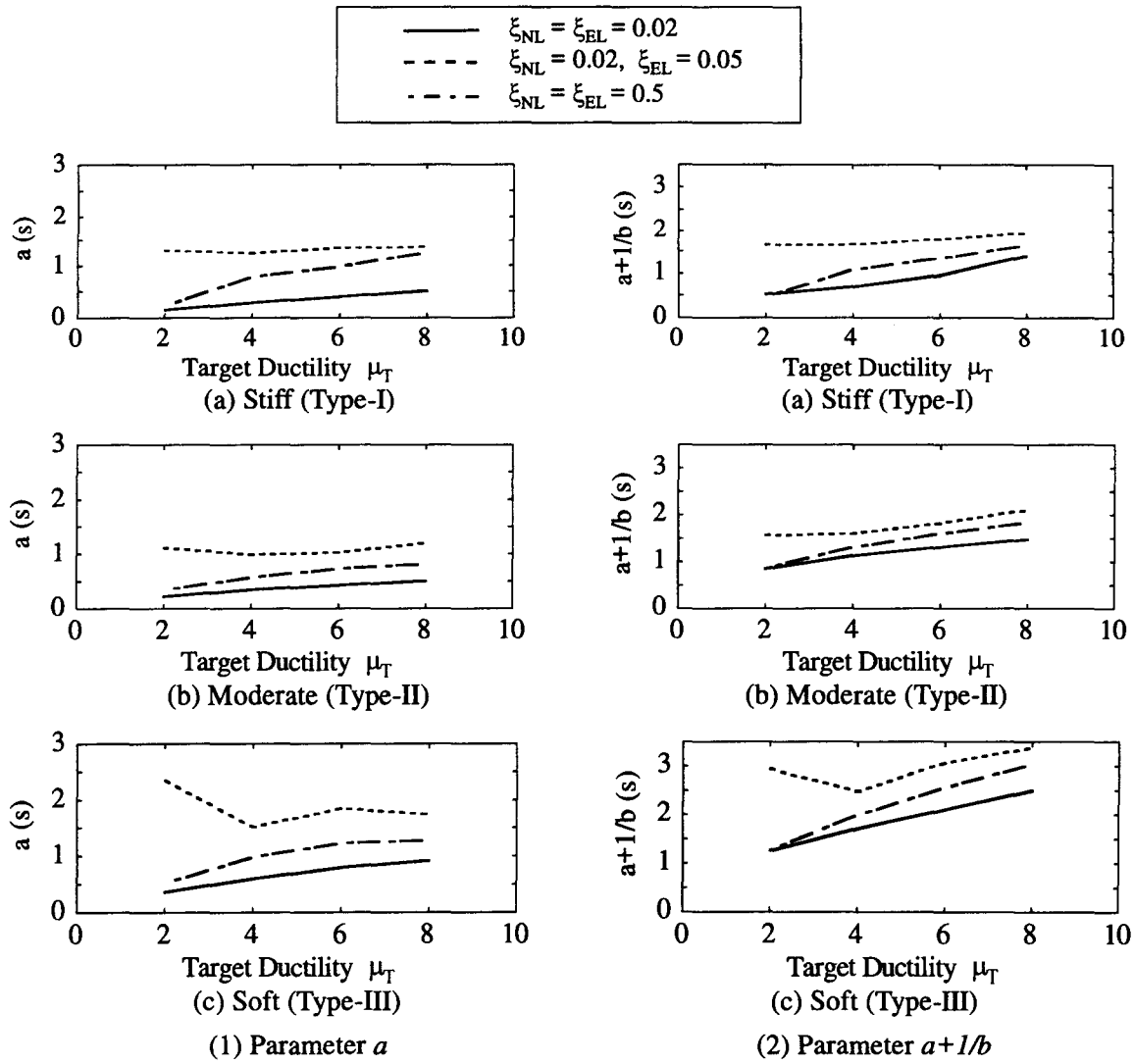

Fig. 14 Dependence of Parameters a and $a+1/b$ on the Assumption of Damping Ratios

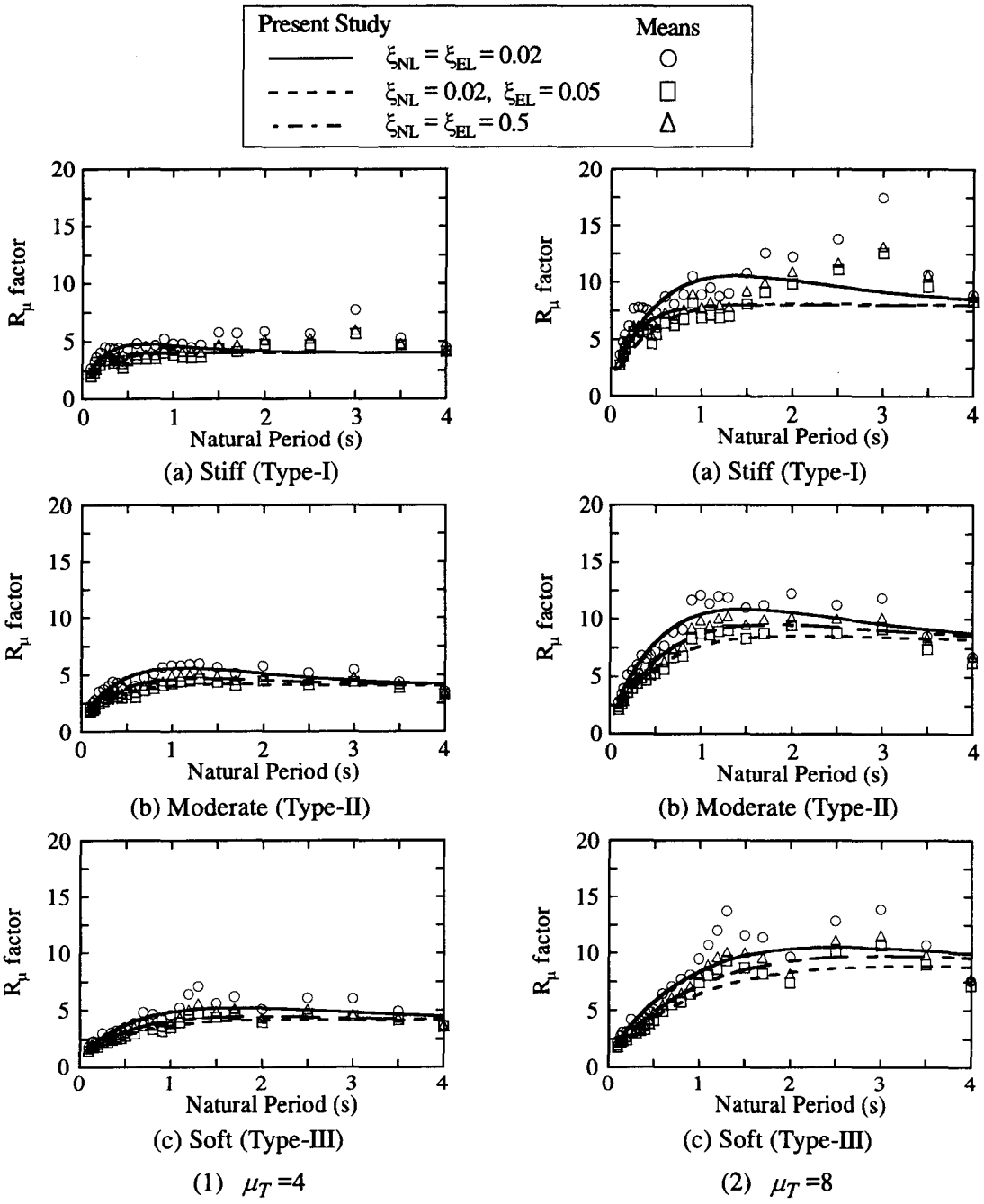

Fig. 15 Dependence of Force Reduction Factors on the Assumption of Damping Ratios

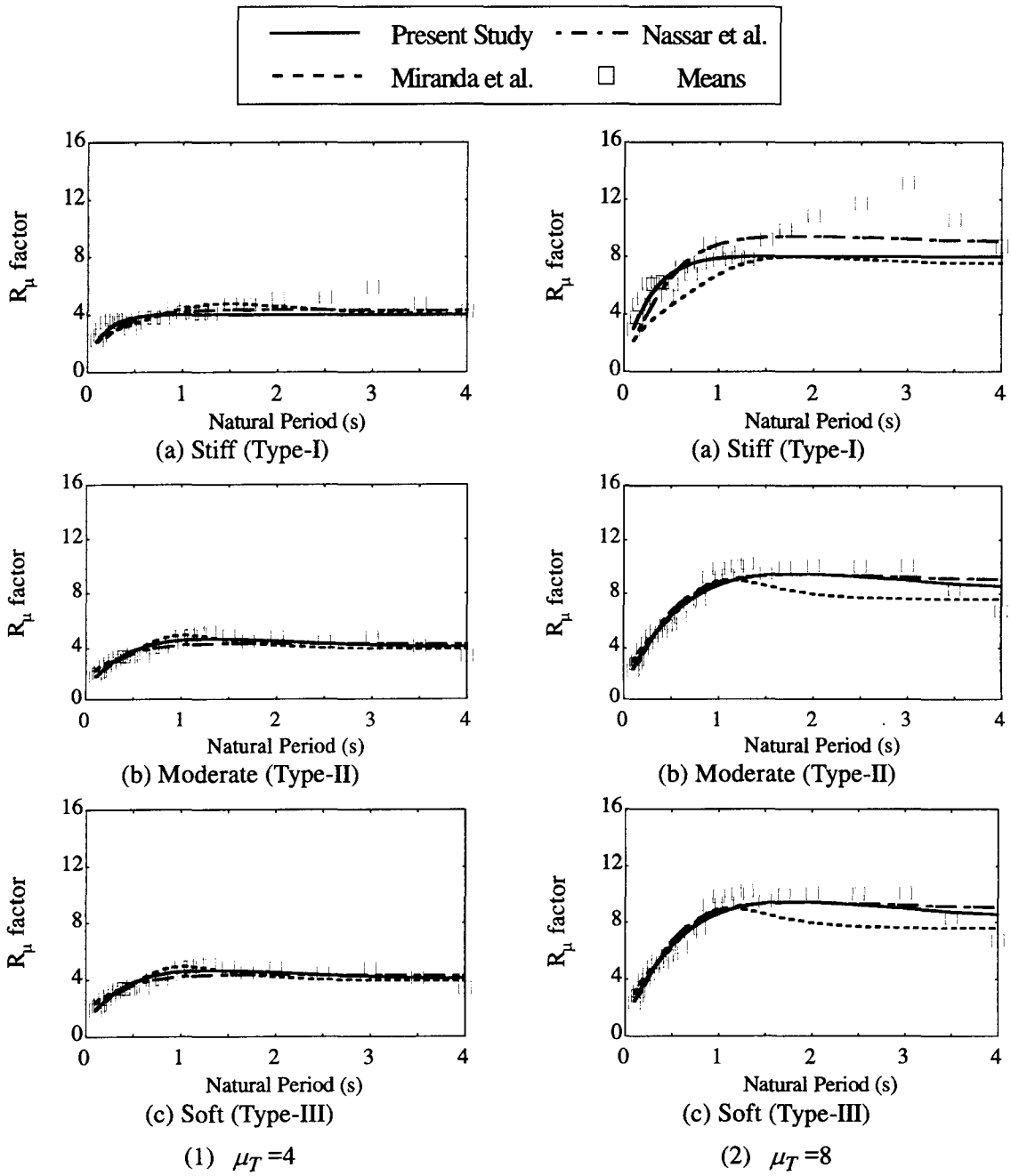

Fig. 16 Comparison with Previous Studies

Bolu Viaduct-1 Subjected to Near-Fault Ground Motion

by

Sunwoo Park[1], Hamid Ghasemi[2], Jerry Shen[1], and Phillip Yen[2]

ABSTRACT

The performance of seismically-isolated Bolu Viaduct-1 in Turkey subjected to a simulated near-fault ground motion during the 1999 Duzce Earthquake was evaluated through nonlinear finite element analysis. The ground motion is characterized by a large residual movement of the ground across the fault rupture that crosses the viaduct. Analysis indicates that the ground motion induces response that exceeds the design capacities of the seismic isolation systems thus resulting in substantial damage to the bearings and energy dissipation units, which is consistent with post-earthquake field observation. The analysis also indicates that shear keys, both longitudinal and transverse, play a critical role in preventing the superstructure collapse.

KEY WORDS: seismic isolation, damping, Viaduct 1, Duzce earthquake, near-fault

1.0 INTRODUCTION

Developments in seismic isolation and energy dissipation devices have permitted considerable advances in seismic protection of highway bridges. However, existing seismic protection strategies are largely based on design ground motions that do not contain near-fault features. Experience with a number of recent earthquakes has pointed to the need for accounting for the effects of near-fault ground motions in the seismic design of highway bridges. In this paper, the effects of a near-fault earthquake ground motion on the performance of a seismically isolated bridge are studied through numerical analysis of Bolu Viaduct 1 subjected to the 1999 Duzce Earthquake.

Bolu Viaduct 1 is located in north central Turkey and is part of the Trans-European Motorway (TEM) running from Ankara to Europe, see Figs 1 and 2. The 2.3-km viaduct, with its 59 dual spans, was approximately 95% complete at the time of the earthquake. The superstructure consists of seven lines of simply-supported, prestressed-concrete box girders seated on sliding bearings with stainless steel/PTFE slider interfaces. The deck slab is monolithic over 10-span segments and each segment is 392 m long and supported by 11 piers. An energy dissipation system of yielding-steel type is also installed on each pier cap to form, together with the sliding bearings, a seismic isolation system for the viaduct.

2.0 NUMERICAL ANALYSIS

Numerical simulation of the response of a typical ten-span segment of the viaduct subjected to a recorded and a simulated earthquake ground motion is conducted via nonlinear time-history analysis. The viaduct's superstructure and piers are modeled using 3-D beam elements, and the foundation conditions at each pier base are modeled by elastic translational and rotational springs. Special nonlinear link elements are used to model energy dissipation units (EDUs), sliding (or friction pot) bearings, and shear keys, see Fig. 3. The schematic illustration of the constitutive behavior of the nonlinear link elements used in the analysis are presented in Fig. 4. The force-displacement hysteretic behavior of the EDU resembles that of a lead-rubber bearing or friction pendulum system, and behavior of the sliding bearing is dictated by the coefficient of

[1] LENDIS Corporation @ Federal Highway Administration, Office of Infrastructure R&D, 6300 Georgetown Pike, McLean, VA 22101, USA
[2] Federal Highway Administration, Office of Infrastructure R&D, 6300 Georgetown Pike, McLean, VA 22101, USA

friction of the sliding surfaces. Seven bearings, each between a girder and pier cap, are modeled by a single bearing element, and multiple transverse shear keys are also modeled by a single gap/hook element, situated between the superstructure and pier. A pedestal for an EDU plays the role of a longitudinal shear key. The displacement capacity of the sliding bearings is 210 mm and the displacement capacities of the EDUs, longitudinal and transverse shear keys are all 480 mm, which presents apparent inconsistency.

A ground motion recorded at the Bolu station in the 1999 Duzce earthquake and a simulated near-fault ground motion are used as the input in the analysis. Figure 5 shows the acceleration histories and spectra of the two horizontal components of the Bolu ground motion. The design spectra shown is based on the 1999 AASHTO Guide Specifications for Seismic Isolation Design (AASHTO, 1999). An acceleration coefficient, A=0.4, and Soil Type II are assumed. The acceleration histories and spectra of the fault-normal and fault-parallel components of the simulated near-fault ground motion at the site of Viaduct 1 are shown in Fig. 6, and the corresponding ground displacement histories are presented in Fig. 7. It is to be noted that the effect of surface fault rupture that crosses the 10-span segment is modeled by specifying a different ground motion to each side of the segment divided by the rupture crossing as indicated in Fig. 8. The surface rupture is oriented at an approximate angle of 25° relative to the axis of the viaduct segment analyzed. The left-hand side of the segment in Fig. 8 is subjected to a motion defined by fault-normal and fault-parallel 1 components shown in Fig. 6, and the right-hand side is subjected to a motion defined by fault-normal and fault-parallel 2 components.

The two fault-parallel components are created by superimposing a pulse motion ("Type-A" by Makris and Chang, 2000) on the E-W component of the Bolu record, and the fault-normal component by superimposing a pulse motion ("Type-B" by Makris and Chang, 2000) on the N-S component of the Bolu record. The two fault-parallel components contain a pulse motion that induces a residual displacement of 0.75 m in opposite directions (representing "fling" effect), thus resulting in a relative displacement of 1.5 m across the surface rupture, see Fig. 7. The ground motions applied to either side of the segment have the same fault-normal component due to kinematic continuity across the fault rupture, and the magnitude of the fault-normal component is estimated from its conjugate relationship to the fault-parallel component in a related problem (Anderson and Luco, 1983). The simulated near-fault ground motion uses the Bolu record as the background far-field motion and is consistent with the field observation of an approximate relative ground movement of 1.5 m across the surface rupture.

3.0 RESULTS OF ANALYSIS

Analysis has focused on the displacement of isolation/damping elements. The bearing displacement at the center pier of the 10-span segment subjected to the Bolu ground motion is shown in Fig. 9. It is to be noted that the displacement of bearing (or EDU) represents the relative displacement between the superstructure and pier. The time histories of the longitudinal and transverse components are shown in Figs. 9(a) and (b), respectively, and the displacement path on the bearing surface in Fig. 9(c). The displacement capacities of sliding bearings and shear keys are indicated in broken lines in Fig. 9(c). It can be seen that the bearing's displacement capacity is exceeded at an early stage of the movement. It is believed that, due to this exceedance, EDUs are distorted and failed before they can be functioned as designed. Post-earthquake field investigations have revealed that the majority of the EDUs were broken for the 10-span segment which was crossed by the fault rupture. In our analysis, different levels of EDU survival were considered, and the results shown in Figs. 9 to 11 are all based on the assumption that the entire EDUs are failed at the beginning. Figure 9 indicates that, while the longitudinal shear key was briefly engaged, the transverse shear key has never been engaged under the Bolu ground motion. Field inspections revealed that transverse as well as longitudinal shear keys of Viaduct 1 were repeatedly engaged during the earthquake. It is believed that the

Bolu ground motion does not induce the observed damage to the viaduct, suggesting that a much stronger near-fault ground motion must have hit the Viaduct 1 site in the 1999 Duzce earthquake.

Figures 10 and 11 respectively show the bearing displacements at the pier immediately left (P1 in Fig. 8) and immediately right (P2 in Fig. 8) of the fault rupture under the simulated near-fault ground motion. The displacement capacity of the sliding bearings is exceeded during the first major cycle of movement, and then both longitudinal and transverse shear keys are engaged. Analysis indicates that the longitudinal shear keys at both piers remain engaged after the event due to the large relative ground movement across the fault rupture, and that the transverse shear key at P1 remain engaged following several interactions between the girder and shear key. The displacement demand due to the static ground movement (1.5 m) is accommodated partly by bearings (until the longitudinal shear key is engaged) and partly by the pier. It is interesting to note that the shear keys, both longitudinal and transverse, are engaged only on one side throughout the motion, which is consistent with findings from field inspection of the shear keys.

Finally, post-earthquake field reconnaissance survey has revealed that the majority of the stainless steel interface plates had distinct scoring that resembled the number "9" as shown in Fig. 12(a) (Ghasemi et al., 2000). The calculated displacement path as shown in Fig. 12(b) is fairly consistent with the field observation. The initial movement consists of a half cycle of displacement with an amplitude of approximately 130 mm followed by movement in the opposite direction that exceeds the bearing's displacement capacity. Due to this exceedance at an early stage of the ground motion, subsequent large movement of the girders (which are already dropped off the bearing plates) on pier-cap table is believed to have caused damage to sliding bearings (including ejection of bearing plates) and EDUs and, as a consequence, the entire seismic isolation/damping systems did not function as designed. However, from a technical point of view, the viaduct performed satisfactorily largely due to shear keys (longitudinal and transverse) that prevented collapse of the superstructure segments.

4.0 CONCLUSIONS

Analysis of the seismically-isolated Viaduct 1 subjected to the ground motion recorded at the Bolu station resulted in displacements exceeding the capacity of the isolation bearings but not large enough to engage shear keys and to cause significant damage to the viaduct as was observed in the post-earthquake investigation. However, analysis with a simulated near-fault ground motion that accounts for relative static ground movement across the surface rupture resulted in displacements far exceeding the capacities of the isolation bearings and EDUs and resulted in engagement of the shear keys, both longitudinal and transverse. The calculated bearing displacement paths are consistent with the "9"-shaped scoring trace observed on the surface of the bearing plates at the site. The close proximity of the fault rupture to the viaduct caused significant superstructure movement relative to the piers resulting in severe damage to bearings, EDUs, and shear keys. The simulation, however, indicates that the shear keys played a critical role in preventing superstructure segments from dropping off the pier caps thus preventing a collapse of the viaduct during the earthquake.

5.0 REFERENCES

AASHTO (1999). *Guide Specifications for Seismic Isolation Design*. American Association of State Highway and Transportation Officials, Washington, DC.

Anderson, J. G. and Luco, J. E. (1983). Parametric study of near-field ground motion for a strike-slip dislocation model. *Bulletin of the Seismological Society of America*, **73**(1), 23-43.

Makris, N. and Chang, S.-P. (2000). Effect of viscous, viscoplastic, and friction damping on the response of seismic isolated structures. *Earthquake Engineering and Structural Dynamics*, **29**, 85-107.

Ghasemi, H., Cooper, J. D., Imbsen, R., Piskin, H., Inal, F., and Tiras, A. (2000). *The November 1999 Duzce Earthquake: Post-Earthquake Investigation of the Structures on the TEM.* Publication No. FHWA-RD-00-146, Federal Highway Administration, U. S. Department of Transportation, Washington, D.C.

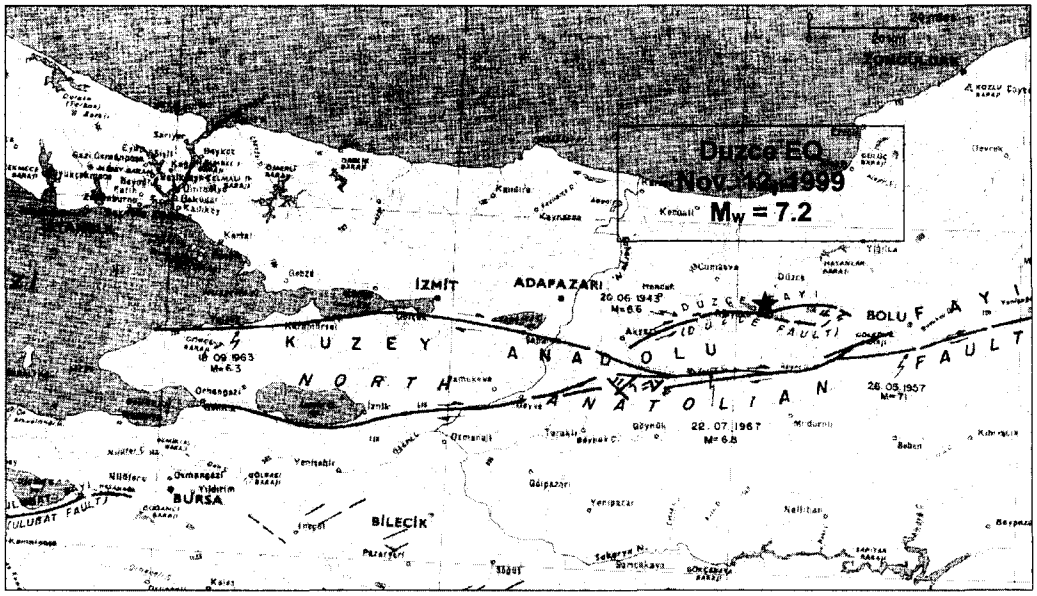

Fig.1. General area map.

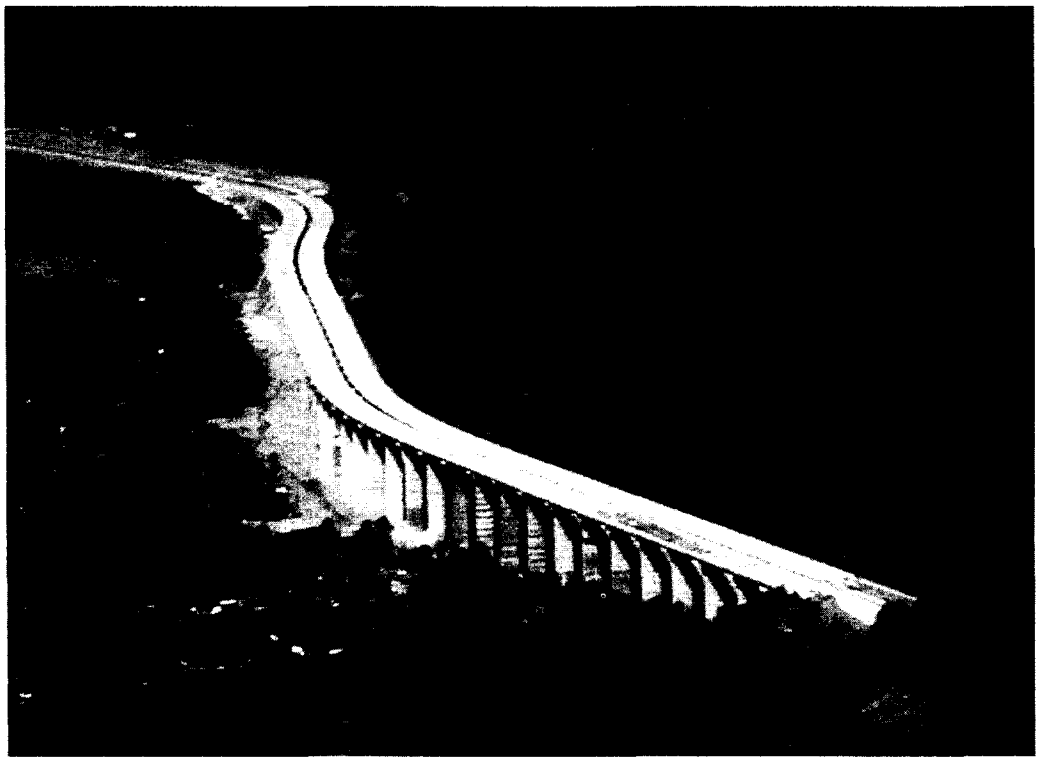

Fig.2. General view of Bolu Viaduct 1

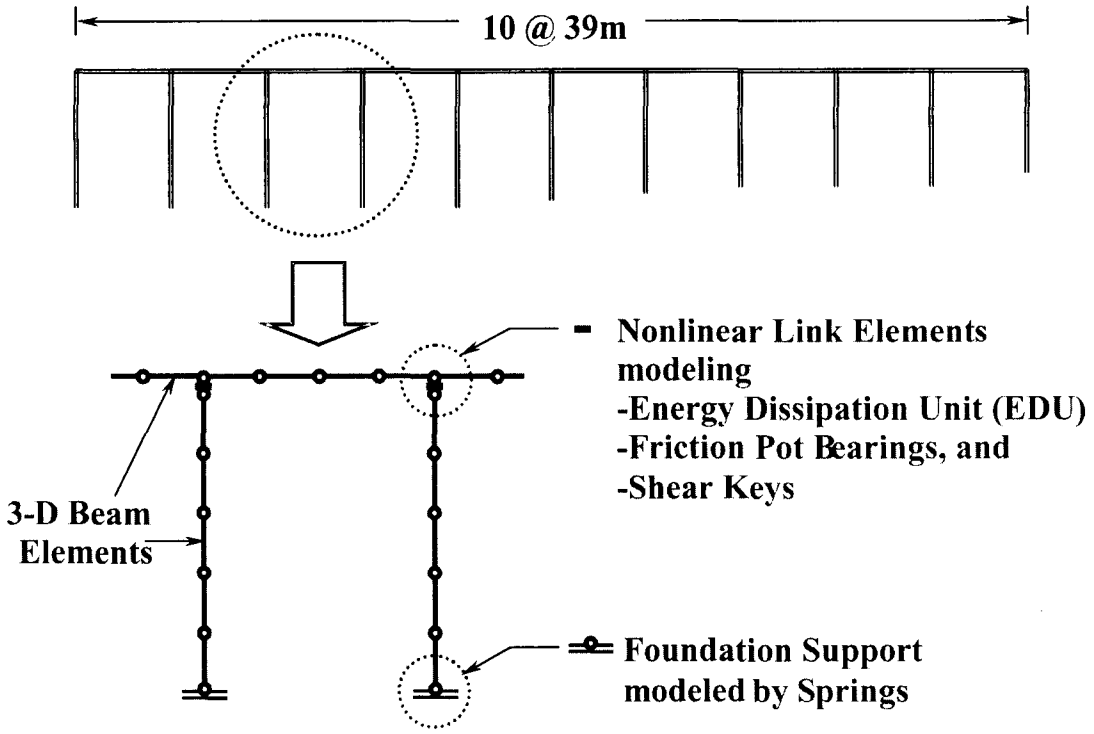

Fig. 3. Finite element discretization of a 10-span segment of Viaduct 1

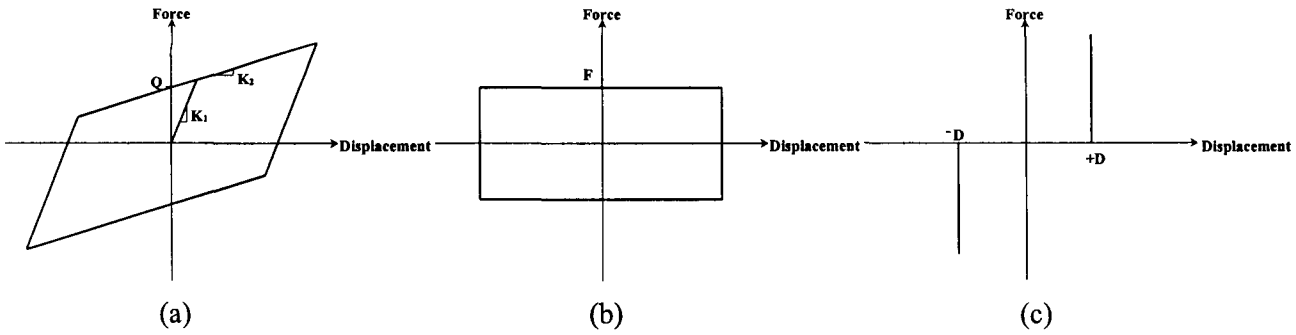

Fig. 4. Schematic illustration of constitutive models for (a) EDUs, (b) friction bearings, and (c) shear keys.

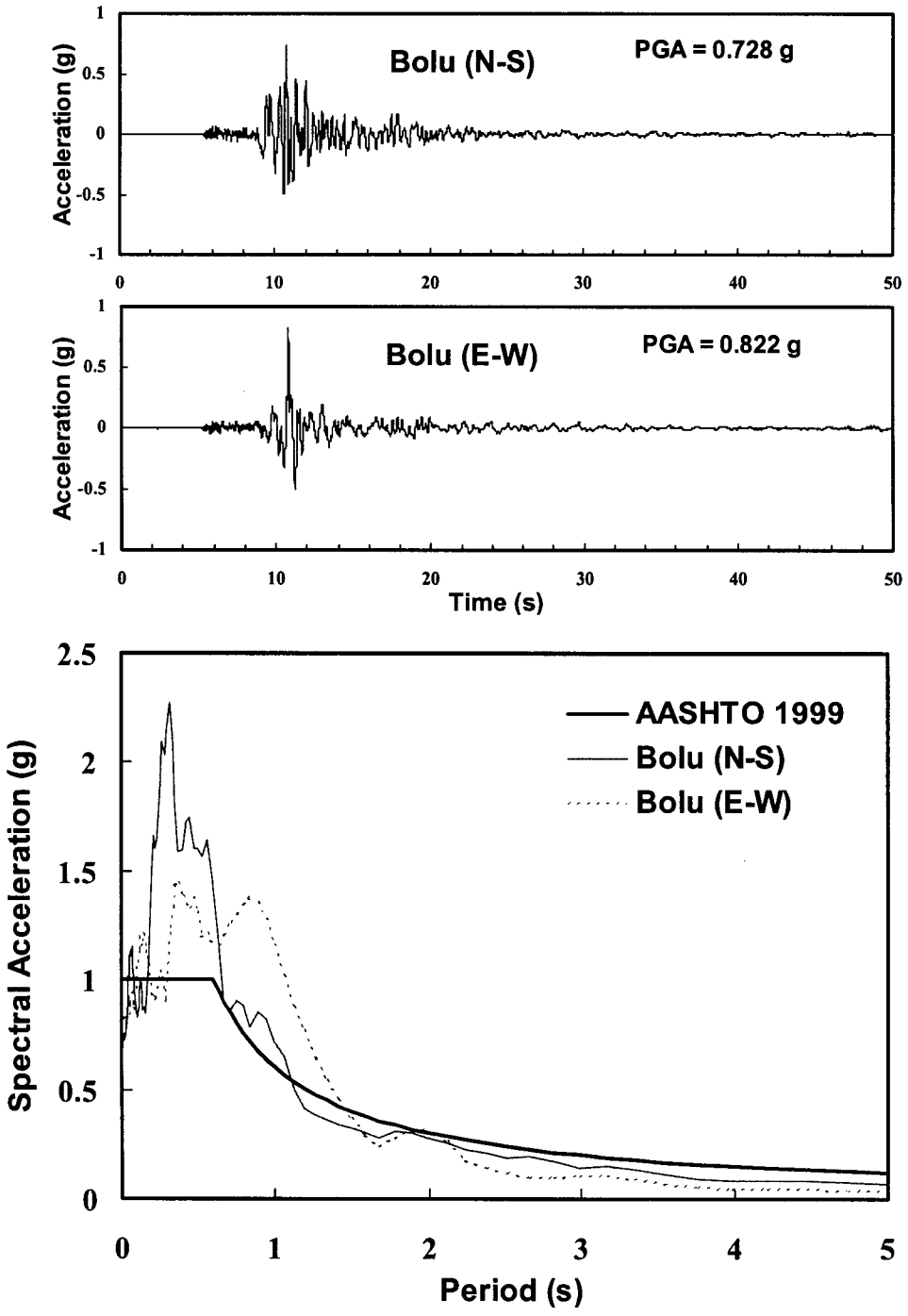

Fig. 5. Acceleration histories and spectra of the ground motion recorded at the Bolu station.

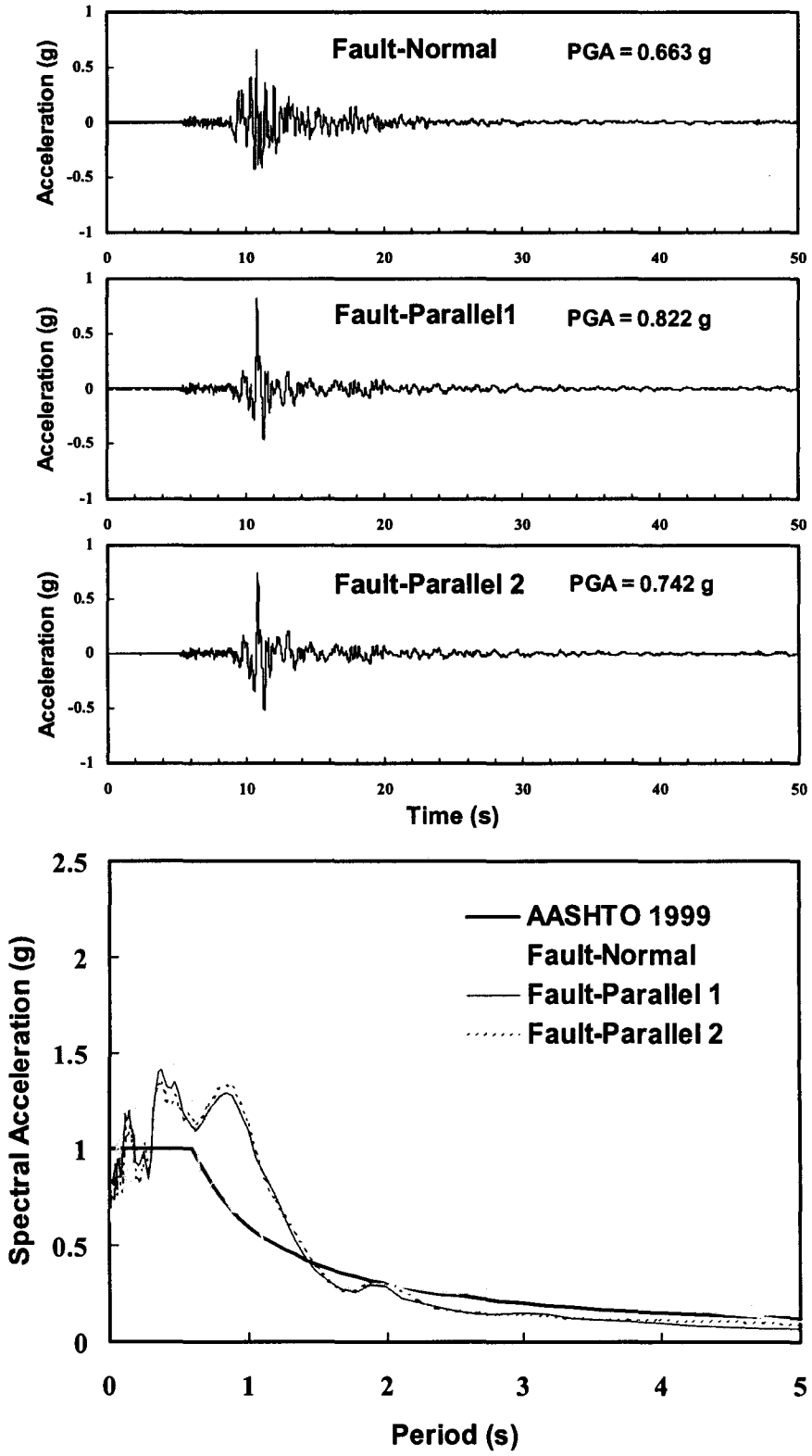

Fig. 6. Acceleration histories and spectra of the simulated near-fault ground motion.

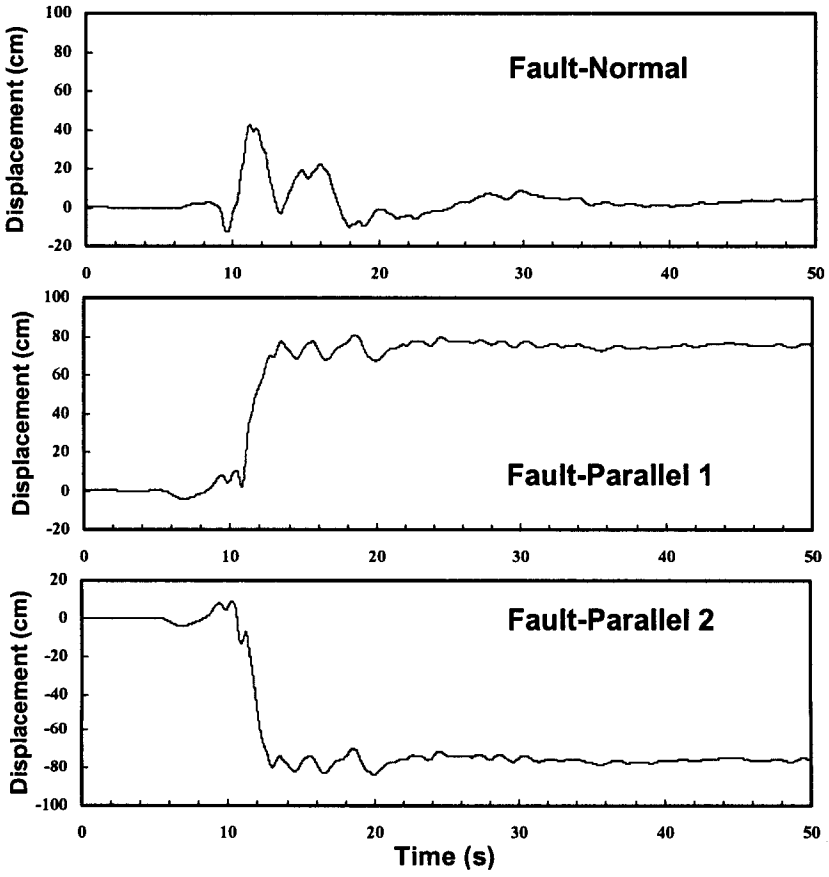

Fig. 7. Displacement histories of the simulated near-fault ground motion.

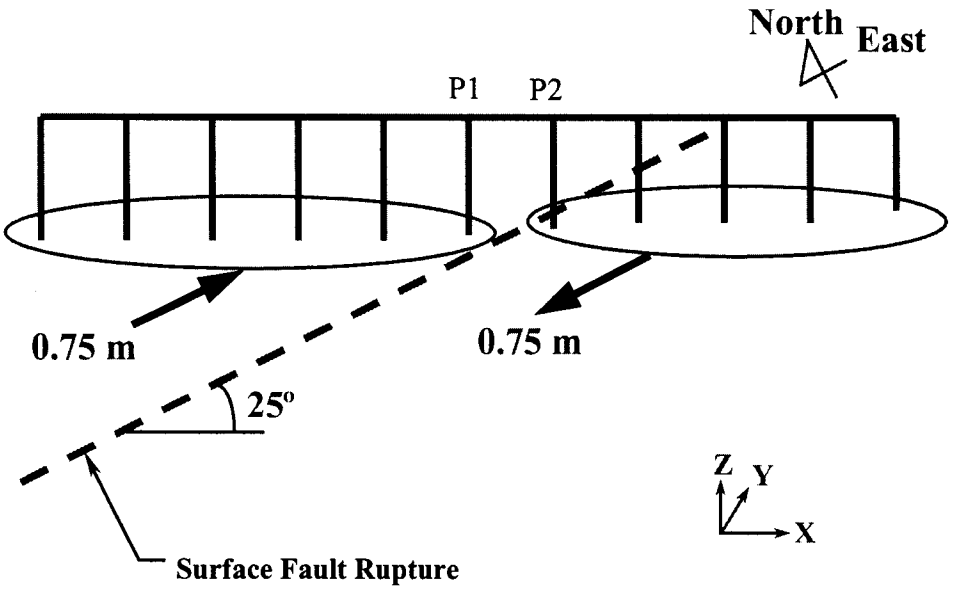

Fig. 8. Orientation of the surface fault rupture and direction of the residual ground movement.

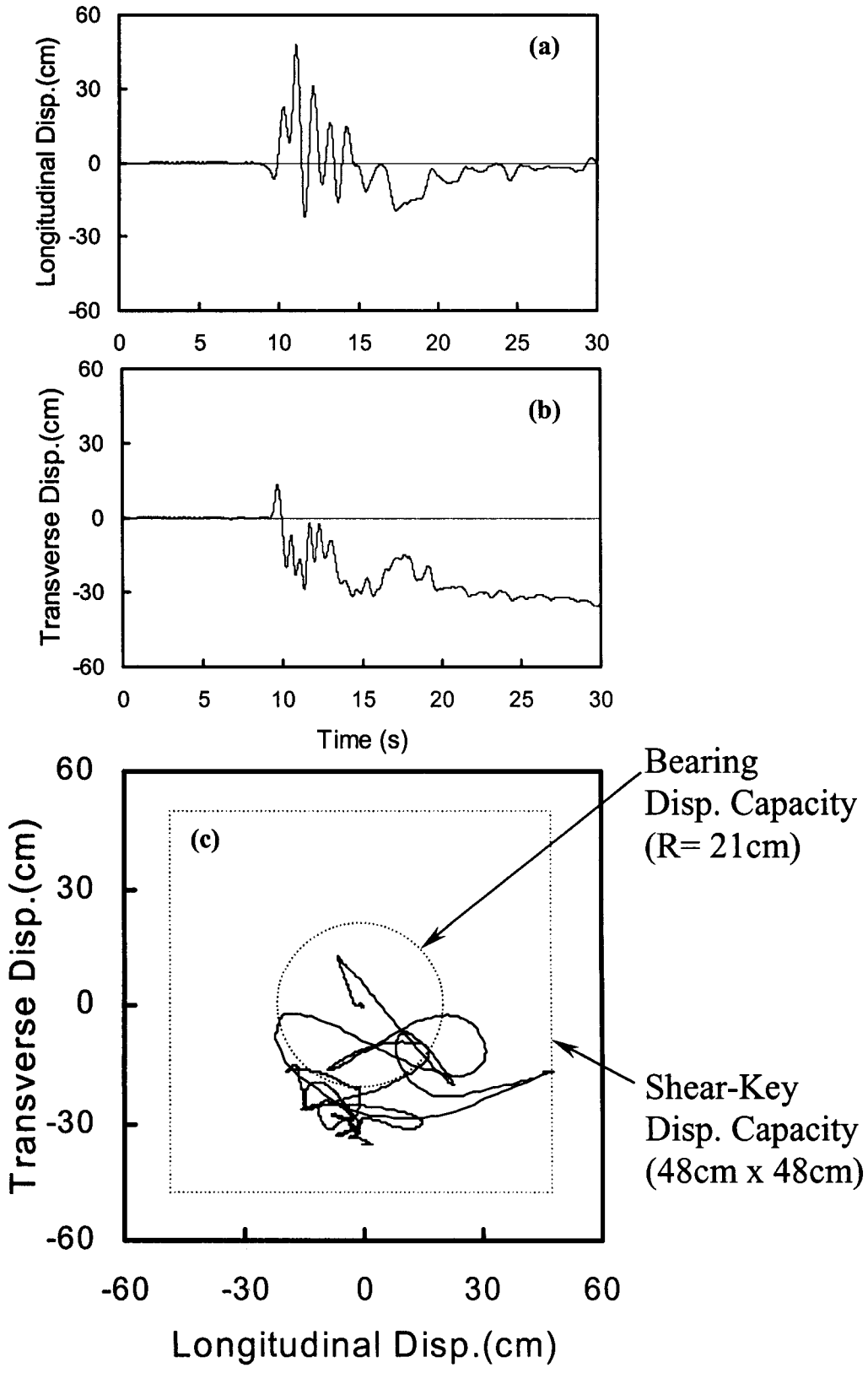

Fig. 9. Bearing displacement at the center pier under the Bolu ground motion: (a) longitudinal displacement history, (b) transverse displacement history, and (c) displacement path on the bearing surface.

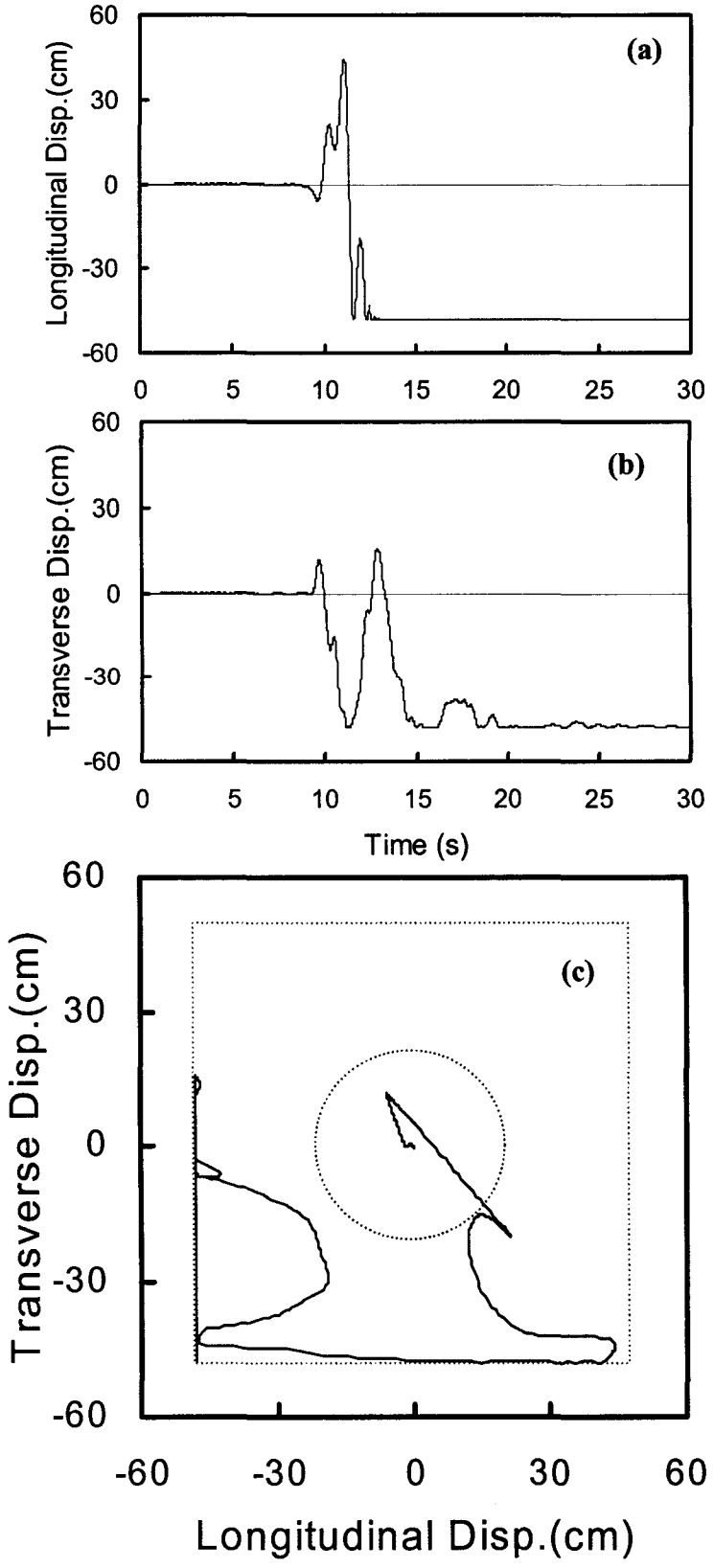

Fig. 10. Bearing displacement at Pier P1 (see Fig. 8) under the simulated near-fault ground motion: (a) longitudinal displacement history, (b) transverse displacement history, and (c) displacement path.

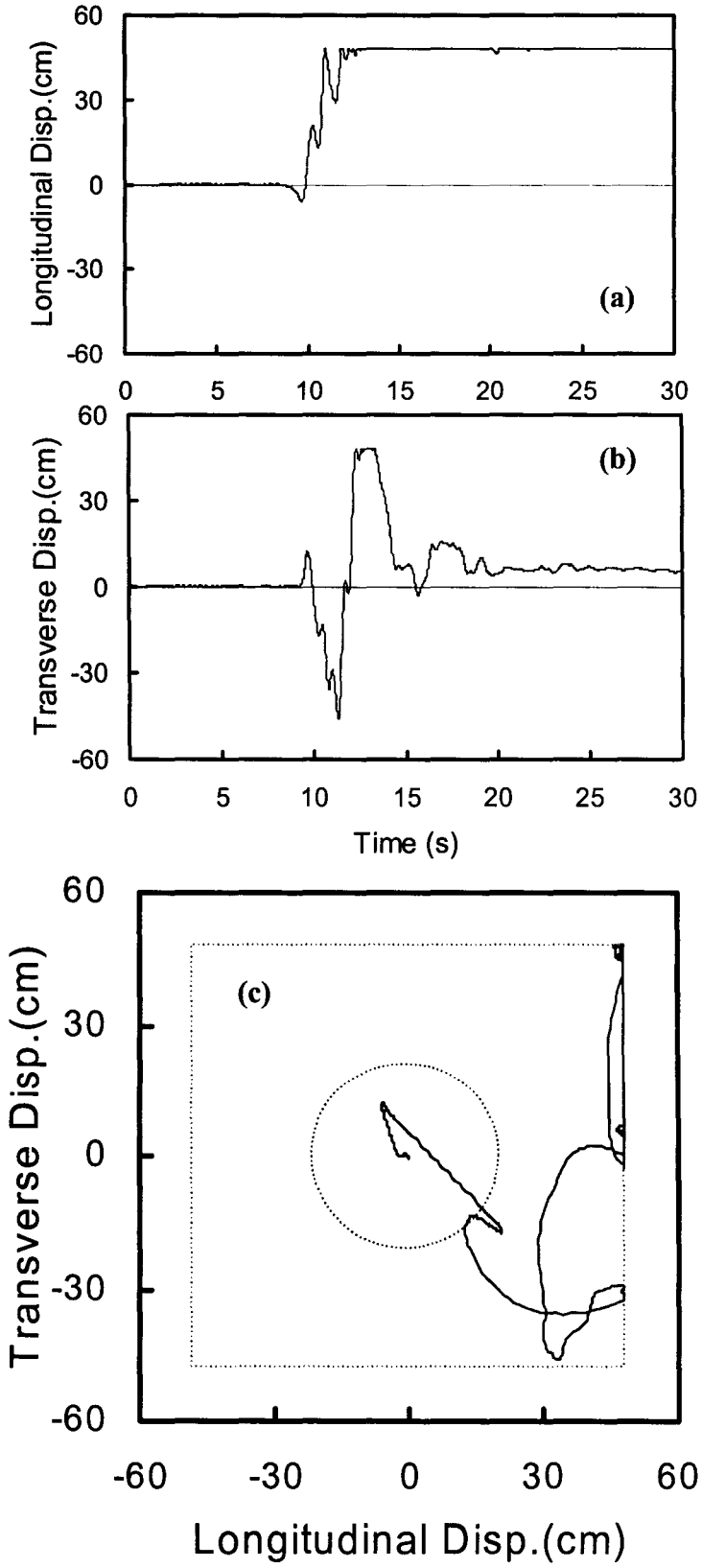

Fig. 11. Bearing displacement at Pier P2 (see Fig. 8) under the simulated near-fault ground motion: (a) longitudinal displacement history, (b) transverse displacement history, and (c) displacement path.

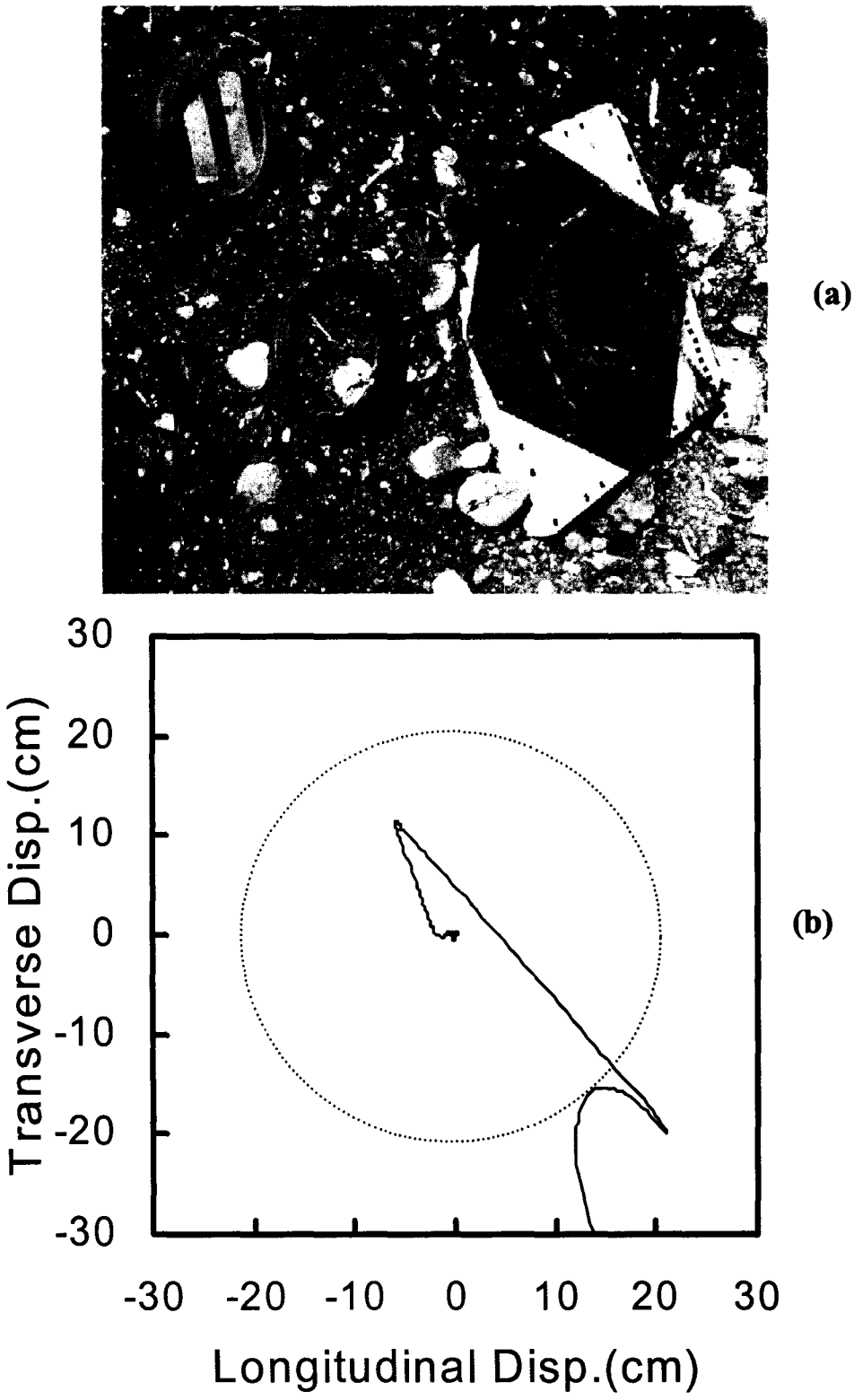

Fig. 12. Displacement path on the bearing surface during the initial stage of movement: (a) observed scoring trace on the bearing plate and (b) calculated displacement path from finite element analysis.

2002 Seismic Design Specifications for Highway Bridges

by

Shigeki Unjoh[1], Sho-ichi Nakatani[2], Kei-ichi Tamura[3]
Jiro Fukui[4] and Jun-ichi Hoshikuma[5]

ABSTRACT

This paper presents the revised Seismic Design Specifications of Highway Bridges, Japan Road Association (JRA), in 2002 [1]. The revised specifications are based on the Performance-based Design Code Concept and the improved knowledges on the seismic design methods for highway bridges are also included. According to the Performance-based Design Code Concept, the design requirements are clearly specified and the existing detailed design methods including the analytical methods and the allowable limits are specified as verification methods and/or the examples of acceptable solutions. The designers can modify or select other verification methods and/or acceptable solutions with appropriate verifications. It is expected that new ideas on the materials and structures will be employed much easier than before. In this paper, the revised major points in the 2002 JRA Seismic Design Specifications are briefly described including the performance-based design code concept, seismic performance levels, the seismic design force, and the ductility evaluation methods for foundations and superstructures.

KEYWORDS: Seismic Design
JRA Design Specifications
Highway Bridges
Performence-based Design Code

1. INTRODUCTION

Seismic design methods for highway bridges in Japan has been developed and improved based on the lessons learned from the various past bitter experiences after the Great Kanto Earthquake (M7.9) in 1923. By introducing the various provisions for preventing serious damage such as the design method against soil liquefaction, design detailing including the unseating prevention devices, a number of highway bridges which suffered complete collapse of superstructures was only a few in the recent past earthquakes. However, the Hyogo-ken-Nanbu Earthquake of January 17, 1995, caused destructive damage to highway bridges. Collapse and nearly collapse of superstructures occurred at 9 sites, and other destructive damage occurred at 16 sites [2, 3]. The earthquake revealed that there are a number of critical issues to be revised in the seismic design and seismic strengthening of bridges. Based on the lessons learned from the Hyogo-ken-Nanbu

[1] Leader, Earthquake Engineering Team, Earthquake Disaster Prevention Research Group, Public Works Research Institute (PWRI), Tsukuba-shi, Ibaraki-ken, 305-8516 Japan
[2] Head, Bridge Division, Road Department, National Institute for Land and Infrastructure Management (NILIM), Ministry of Land, Infrastructure and Transport, Tsukuba-shi, Ibaraki-ken, 305-0804 Japan
[3] Leader, Ground Vibration Team, Earthquake Disaster Prevention Research Group, PWRI
[4] Leader, Foundation Engineering Team, Structures Research Group, PWRI
[5] Senior Research Engineer, Earthquake Engineering Team, Earthquake Disaster Prevention Research Group, PWRI

Earthquake, the design specifications for highway bridges were significantly revised in 1996 [3, 4, 5]. The intensive earthquake motion with a short distance from the inland earthquakes with Magnitude 7 class as the Hyogo-ken-Nanbu Earthquake has been considered in the design.

In the Japan Road Association (JRA), the "Bridge Committee" (Chairman: Dr. Syo-ichi SAEKI, Director of Public Works Research Center) has worked on the revision of the design specifications of highway bridges. The target point of the revision was to be based on the performance-based design code concept and to enhance the durability of bridge structures for a long-term use, as well as the inclusion of the improved knowledges on the bridge design and construction methods. The new Design Specifications of Highway Bridges was issued by the Ministry of Land, Infrastructure and Transport on December 27, 2001. The JRA has released it with the commentary in March 2002. This paper summarizes the new JRA Design Specifications of Highway Bridges, Part V: Seismic Design, issued in March 2002.

2. MAJOR REVISION OF JRA SEISMIC DESIGN SPECIFICATIONS

The major revision point is to be based on the performance-based design code concept. According to the performance-based design code concept, the code structure, in which both the design requirements and the existing detailed design methods are clearly separated and specified, is employed. And the improved knowledges on the seismic design methods are also included.

The major revisions of the Part V: Seismic Design are as follows:

(1) Based on the performance-based design code concept, principle requirements on the seismic performance of highway bridges, determination concept of design earthquake ground motion and principle to verify the seismic performance are clearly specified.

(2) Two earthquake level design concept is used and the design earthquake ground motion with high probability to occur and the design earthquake ground motion with high intensity and low probability to occur is employed as the same as 1996 JRA Specifications. The ground motions are named as Level 1 Earthquake and Level 2 Earthquake, respectively.

(3) Verification methods of seismic performance are rearranged as "Static Analysis" and "Dynamic Analysis." The selection of two design methods is clearly shown. The applicability of the dynamic analysis is much widened and the detailed verification method for the dynamic analysis is specified.

(4) The evaluation method of dynamic earth pressure for the Level 2 Earthquake design is introduced. This is the based on the modified Mononobe-Okabe earth pressure theory. The evaluation method of the dynamic water pressure for the Level 2 Earthquake design is also introduced.

(5) The verification method of the seismic performance of abutment foundations on the liquefiable ground is newly introduced.

(6) The evaluation method of the force-displacement relation models for steel columns with/without infilled concrete is improved.

(7) The verification method of the seismic performance for steel and concrete superstructures are newly introduced.

(8) The evaluation methods of the strength for bearing supports are improved.

(9) References on the back data of the design methods and related information are added at the end of the specifications.

3. PERFORMANCE-BASED DESIGN SPECIFICATIONS

The JRA Design Specifications has been revised

based on the Performance-based design code concept for the purpose to respond the international harmonization of design codes and the flexible employment of new structures and new construction methods. The performance-based design code concept is that the necessary performance requirements and the verification policies are clearly specified. The JRA specifications are employed the style to specify both the requirements and the acceptable solutions including the detailed performance verification methods which are based on the existing design specifications including the design methods and the design details. For example, the analysis method to evaluate the response against the loads is placed as one of the verification methods or acceptable solutions. Therefore, designer can propose the new ideas or select other design methods with the necessary verification.

The most important issue of the performance-based design code concept is the clear specifications of the requirements, which the designers are not allowed to select other methods, and the acceptable solutions, which the designers can select other methods with the necessary verification. In the JRA Specifications, they are clearly specified including the detailed expressions. In future, the acceptable solutions will be increased and widened with the increase of the verification of new ideas on the materials, structures and constructions methods.

The code structure of the Part V: Seismic Deign is as shown in Fig. 1. The static and dynamic verification methods of the seismic performance as well as the evaluation methods of the strength and ductility capacity of the bridge members are placed as the verification methods and the acceptable solutions, which can be modified by the designers with the necessary verifications.

4. BASIC PRINCIPLES OF SEISMIC DESIGN

Table 1 shows the performance matrix including the design earthquake ground motion and the Seismic Performance Level (SPL) provided in the revised JRA Seismic Design Specifications in 2002. There is no revision on this basic principle from the 1996 Version.

The two level ground motion as the moderate ground motions induced in the earthquakes with high probability to occur (Level 1 Earthquake) and the intensive ground motions induced in the earthquakes with low probability to occur (Level 2 Earthquake).

The Level 1 Earthquake provides the ground motions induced by the moderate earthquakes and the ground motion considered in the elastic design method in the past for a long time is employed. For the Level 2 Earthquake, two types of ground motions are considered. The first is the ground motions which is induced in the interplate-typeearthquakes with the magnitude of around 8. The ground motion at Tokyo in the 1923 Kanto Earthquake is a typical target of this type of ground motion. The second is the ground motion developed in earthquakes with magnitude of around 7 at very short distance. The ground motion at Kobe during the Hyogo-ken-Nanbu Earthquake is a typical target of this type of ground motion. The first and the second ground motions are named as Type-I and Type-II ground motions, respectively. The recurrence period of the Type-II ground motion may be longer than that of the Type-I ground motion, although the estimation is very difficult.

In the 2002 revision, the design ground motions are named as Level 1 Earthquake and Level 2 Earthquake. One more important revision on the design earthquake ground motion is that the site-specific design ground motions shall be considered if the ground motion can be appropriately estimated based on the information on the earthquake including past history and the

location and detailed condition of the active faults, ground conditions including the condition from the faults to the construction sites. To determine the site-specific design ground motion, it is required to have the necessary and accurate informations on the earthquake ground motions and ground conditions as well as the verified evaluation methodology of the fault-induced ground motions. However, the area to get such detailed informations in Japan is very limited so far. Therefore, the continuous investigation and research on this issue as well as the reflection on the practical design of highway bridges is expected.

5. GROUND MOTION AND SESIMIC PERFORMANCE LEVEL

The seismic design of bridges is according to the performance matrix as shown in Table 1. The bridges are categorized into two groups depending on their importances; standard bridges (Type-A bridges) and important bridges (Type-B bridges). Seismic Performance Level (SPL) depends on the importance of bridges. For the moderate ground motions induced in the earthquakes with high probability to occur, both A and B bridges shall behave in an elastic manner without essential structural damage (Seismic Performance Level (SPL): 1). For the extreme ground motions induced in the earthquakes with low probability to occur, the Type-A bridges shall prevent critical failure (SPL: 3), while the Type-B bridges shall perform with limited damage (SPL: 2) .

The SPLs 1 to 3 are based on the viewpoints of "Safety," "Functionability," "Repairability" during and after the earthquakes. Table 2 shows the basic concept of these three viewpoints of the SPL.

6. VERIFICATION METHODS OF SEISMIC PERFORMANCE

6.1 Seismic Performance Level and Limit States

As mentioned in the above, the seismic performance is specified clearly. It is necessary to determine and select the limit states of highway bridges corresponding to these seismic performance levels to attain the necessary performance in the design procedure of highway bridges.

In the 2002 revision, the determination principles of the limit state to attain the necessary seismic performance are clearly specified. For example, the basic principles to determine the limit state for SPL 2 is: 1) the plastic hinges shall be developed at the expected portions and the capacity of plastic hinges shall be determined so that the damaged members can be repaired relatively easily and quickly without replacement of main members, 2) the plastic hinges shall be developed at the portions with appropriate energy absorption and with high repairability, 3) considering the structural conditions, the members with plastic hinges shall be combined appropriately and the limit states of members with plastic hinges shall be determined appropriately. Based on the basic concept, the combinations of members with plastic hinges and the limit states of members for ordinary bridge structures are shown in the commentary.

6.2 Verification Methods of Seismic Performance

It is the fundamental policy of the verification of seismic performance that the response of the bridge structures against design earthquake ground motions does not exceed the determined limit states.

Table 3 shows the applicable verification methods of seismic performance used. In the seismic design of highway bridges, it is important to increase the strength and the ductility capacity to appropriately resist the intensive earthquakes. The verification methods are based on the static

analysis and dynamic analysis. In the 1996 design specifications, the lateral force coefficient methods with elastic design, ductility design methods and dynamic analysis were specified and these design methods had to be selected based on the structural conditions of bridges. The basic concept is the same as 1996 one but the verification methods are rearranged to the verification methods based on static and dynamic analyses.

The static verification methods including the lateral force design method and the ductility design method are applied for the bridges with simple behavior with predominant single mode during the earthquakes. The dynamic verification method is applied for the bridges with complicated behavior, in such case the applicability of the static verification methods is restricted. In the 1996 design specifications, for the bridges with complicated behavior both the static and dynamic analyses had to be applied and satisfied. In the 2002 one, the applicability of the dynamic analysis is widened and the dynamic verification method is expected to be used mainly with appropriate design consideration.

6.3 Major Revision Points of the Verification Methods of Seismic Performance

6.3.1 Verification Methods of Abutment-Foundation on Liquefiable Ground against Level 2 Earthquake

In the 1996 design specifications, the performance of the abutment-foundations was not verified in detail. This is because 1) the serious damages to abutment-foundations were not found in the past earthquakes when the soil liquefaction was not developed, 2) abutment-foundation is affected by the backfill soils during earthquakes and the effect of the inertia force of abutment itself is relatively small comparing with the pier-foundations, 3) since abutments generally resist against back-fill earth pressure, the abutment-foundations tend to develop displacement to the direction of the earth pressure that is to the center of bridges, then it is generally low probability to have the unseating of superstructures.

On the other hand, recently, the dynamic earth pressure against Level 2 Earthquake based on the modified Mononobe-Okabe theory has been proposed and the behavior of the abutment-foundations can be evaluated during the Level 2 earthquakes. Based on investigations using the modified Mononobe-Okabe theory, it is shown that the abutment-foundations designed according to the Level 1 Earthquake generally satisfy the performance requirement during the Level 2 Earthquake. Therefore, based on these results, the performance of the abutment-foundations only on the liquefiable ground shall be verified in order to give the necessary strength to the foundations and to limit the excessive displacement even if the nonlinear behavior is expected in the abutment-foundations.

6.3.2 Verification Methods of Strength and Ductility of Steel Column

In the 1996 design specifications, the concrete infilled steel columns was designed according to the static ductility design methods using the response evaluation based on the energy equal theory. The force-displacement relation was based on the experimental data of steel columns. On the other hand, steel columns without infilled concrete was designed based on the dynamic analysis because the applicability of the static response evaluation was not verified.

In the 2002 design specifications, new and more appropriate force-displacement relation models for steel columns with and without infilled concrete are proposed based on the experimental data of steel columns which has been made before and after the last 1996 revision. Using these new

models, the seismic performance is verified based on the dynamic analysis.

6.3.3 Verification Methods of Strength and Ductility of Superstructure

Generally, the seismic design of superstructures is not critical except the portion around the bearing supports which are the connection between superstructure and substructures. However, the seismic design sometimes becomes critical in the design of rigid frame bridges and arch bridges in the longitudinal direction, and in the design of bridges with relatively long spans to the bridge width in the transverse direction.

The nonlinear behavior of superstructures against cyclic loading is investigated in the recent research. Therefore, the verification method of the limited nonlinear performance for the superstructures is newly specified with the assumption of energy absorption at the plastic hinges in the columns.

7. CONCLUDING REMARKS

This paper presented an outline of the revised JRA Seismic Design Specifications of Highway Bridges issued in 2002. Based on the lessons learned from the Hyogo-ken-Nanbu Earthquake in 1995, the "Part V: Seismic Design" of the "JRA Design Specifications of Highway Bridges" was totally revised in 1996, and the design procedure moved from the traditional Seismic Coefficient Method to the Ductility Design Method. Major point of the revision was the introduction of explicit two-level seismic design methods. In the 2002 revision, the target point of the revision is to be based on the performance-based design code concept and to enhance the durability of bridge structures for a long-term use, as well as the inclusion of the improved knowledgs on the bridge design and construction methods. It is expected to have the circumstances to employ the new ideas on the materials, structures and constructions methods to construct safer, more durable and more cost-effective bridges in the future.

Acknowledgments

Drafting of the revised version of the "Part V Seismic Design" of the "2002 JRA Design Specifications of Highway Bridges" was conducted at the "Sub-committee for Seismic Design of Highway Bridges" and was approved by the Bridge Committee, Japan Road Association. The authors served as members of bridge committee and executive member of the sub-committees, respectively. The authors thank all members of the Bridge Committee and the Sub-Committees.

REFERENCES:

1) Japan Road Association: Design Specifications of Highway Bridges, Part I Common Part, Part II Steel Bridges, Part III Concrete Bridges, Part IV Foundations, and Part V Seismic Design, 2002

2) Ministry of Construction: Report on the Damage of Highway Bridges by the Hyogo-ken Nanbu Earthquake, Committee for Investigation on the Damage of Highway Bridges Caused by the Hyogo-ken Nanbu Earthquake, 1995

3) Japan Road Association: Design Specifications of Highway Bridges, Part I Common Part, Part II Steel Bridges, Part III Concrete Bridges, Part IV Foundations, and Part V Seismic Design, 1996

4) Kawashima, K.: Impact of Hanshin/Awaji Earthquake on Seismic Design and Seismic Strengthening of Highway Bridges, Report No. TIT/EERG 95-2, Tokyo Institute of Technology, 1995

5) Kazuhiko Kawashima, et. al.: 1996 Design Specifications for Highway Bridges, 29th UJNR Joint Panel Meeting, May 1996

APPENDIX

2002 JRA Design Specifications for HighwayBridges, Part V: Seismic Design

Table of Contents

Table 1 Seismic Peformance Matrix

Type of Design Ground Motions		Standard Bridges (Type-A)	Important Bridges (Type-B)
Level 1 Earthquake: Ground Motions with High Probability to Occur		SPL 1: Prevent Damage	
Level 2 Earthquake: Ground Motions with Low Probability to Occur	Interplate Earthquakes (Type-I)	SPL 3: Prevent Critical Damage	SPL 2 : Limited Damage for Function Recovery
	Inland Earthquakes (Type-II)		

Note) SPL: Seismic Performance Level

Table 2 Key Issues of Seismic Performance

SPL	Safety	Functionability	Repairabilty	
			Short Term	Long Term
SPL 1 Prevent Damage	Safty against Unseating of Superstructure	Same Function as before Earthquake	No Need of Repair for Function Recovery	Simple Repair
SPL 2 Limited Damage for Function Recovery	Safety against Unseating of Superstrucure	Early Function ercovery can be made	Function Recovery can be made by Temporary Repair	Relatively Easy Permanent Repair work can be made
SPL 3 Prevent Critical Damage	Safety against Unseating of Superstructure	—	—	—

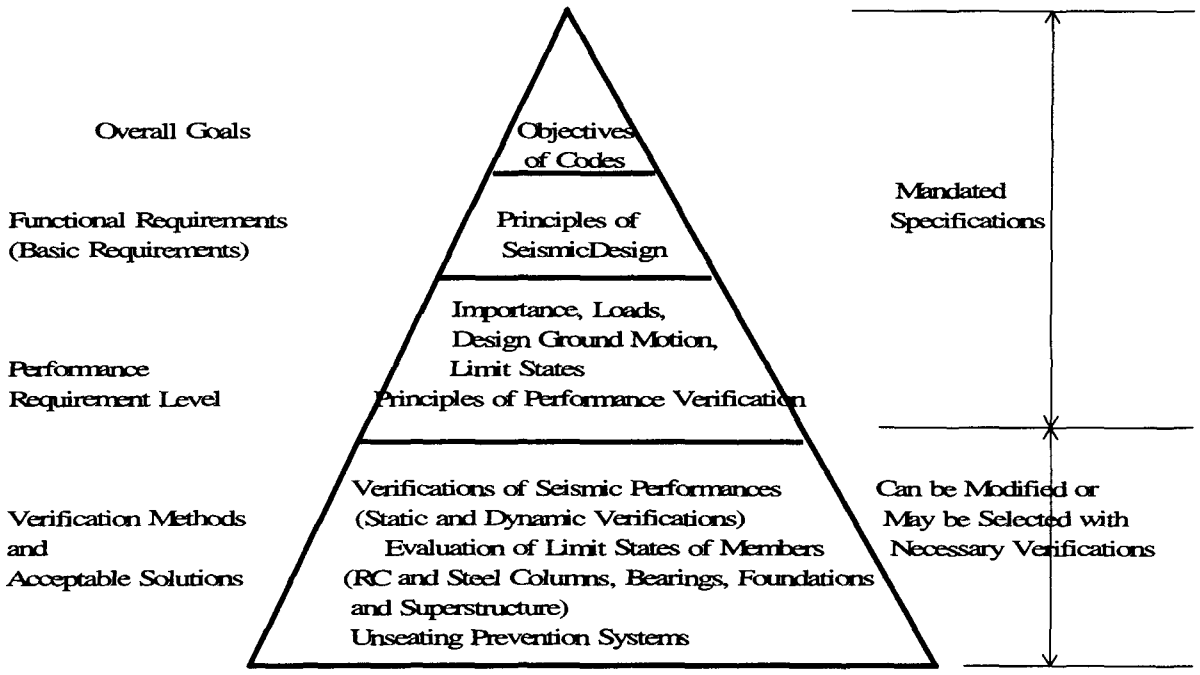

Fig. 1 Code Structure of JRA Design Specifications, Part V: Seismic Design

Table 3 Applicable Verification Methods of Seismic Performance Depending on Earthquake Response Characteristics of Bridge Structures

Dynamic Characteristics / SPL to be verified	Bridges with Simple Behavior	Bridges with Multi Plastic Hinges and withuot Verification of Applicability of Energy Constant Rule	Bridges with Limited Application of Static Analysis	
			With Multi Mode Response	Bridges with Complicated Behavior
SPL 1	Static Verification	Static Verification	Dynamic Verification	Dynamic Verifiatin
SPL 2/SPL 3		Dynamic Verification		
Example of Bridges	Other Bridges	1)Bridges with Rubber Bearings to distribute Inertia Force of Superstructures 2) Seismically Isolated Bridges 3) Rigid Frame Bridges 4) Bridges with Steel Columns	1) Bridges with Long Natural Period 2) Bridge with High Piers	1) Cable-stayed Bridges, Suspension Bridges 2) Arch Bridges 3) Curved Bridges

Development of National Guidelines for Seismic Performance Testing

by

W. Phillip Yen[1], Jerry J. Shen[2], and John O'Fallon[3]

ABSTRACT

In order to make the bridge experiments more efficient in terms of providing reliable and comparable information, Federal Highway Administration has conducted a systematic study on bridge testing methods. The most common procedures and issues are identified. Proper methods on specimen construction, loading procedure, as well as measurements and data format will be established to provide experimental researchers an easy reference that makes test results comparable to results from other tests.

KEYWORDS: Bridge performance testing; earthquakes; guidelines; performance-based approach; performance testing; Seismic testing

1.0 INTRODUCTION

Experimental studying on bridges and components of bridges is an essential need for the improvements on design and construction techniques. As the seismic design concept for bridges gradually turns to performance-based approach, the need for a large amount of comparable tests results increases. In order to make the bridge experiments more efficient in terms of providing reliable and comparable information, the Federal Highway Administration (FHWA) has launched a systematic study on the techniques and procedures of conducting experimental bridge ests. The objective of the study is to develop the National Guidelines for Experimental Tests on Highway Structures.

A literature review covering a wide range of bridge tests were performed. Information of the major experimental research institutes was collected. Some laboratory administrative personnel were or will be interviewed to include their practical experiences. These materials will be summarized and a proposed experimental guidelines will be produced. These results will be made available for experts to review and comment.

2.0 BENEFITS FROM THE GUIDELINES

Each experimental study has its own purpose and unique setup to serve this purpose. The results from experiments always contain more information than they were designed to provide. A large part of the information is often either ignored or not comparable with other tests due to incompatible format and testing conditions. If widely adopted experiment guidelines exist, the part of an experiment that is not essential to its purpose can be conducted in the standard manner. Commonly demanded information will not be ignored. The result can be used for theoretical derivation or empirical model calibration with a solid confidence that the data were obtained from an experiment compliant to a reliable procedure. In the mean time, the tester receives additional credits and publicities because the experimental results appear in more consequent studies.

This guidelines is not similar to some of the

1 Office of Infrastructure, R&D Federal Highway Administration, , 6300 Georgetown Pike, McLean, VA 22101
2 Lendis/FHWA, 6300 Georgetown Pike, McLean, VA 22101
3 Office of Infrastructure, R&D Federal Highway Administration, , 6300 Georgetown Pike, McLean, VA 22101

existing testing standard such as those in ASTM testing manual. Due to the explorative origin of the tests regulated by this guidelines, making changes to the procedure in accordance to the need of the specific test does not immediately disqualify the results. The intention is to provide assistance rather than restriction to the experimental community.

3.0 COMMON METHODS AND PURPOSES FOR BRIDGE COLUMN TESTS

Dynamic structural tests are commonly divided into 3 categories. They are quasi-static tests, pseudodynamic tests, and shake table tests (Kausel, 1998; Dimig et al, 1999). Dynamic tests on bridges are carried out for either discovering element properties that were not clear to engineers or verifying the theoretical predictions. The most common goals for dynamic bridge tests are:

(1) To determine strength and ductility under strong earthquake (capacity)
(2) To determine displacement and force demand
(3) To determine effectiveness of retrofit
(4) To observe failure patterns such as cracking, buckling, etc.
(5) To observe the performance of new design or retrofit methodologies
(6) To develop and verify analytical or empirical models
(7) To inspect existing bridges

Different goal results in different test requirements and test methods. The issues being addressed in this guidelines are those shared by a number of different tests.

4.0 GUIDELINES

There are three major issues in a bridge test: specimen, loading, and data handling. The specimen is a full or reduced replica of the interested part of a real or imaginary bridge. It needs to be designed to best reflect the bridge characteristics. The loading procedure is usually a simulation of load history occurs in a real event. For random-type input such as earthquake and wind, some load histories that are different from the real load but possess certain realistic characteristics are used (e.g. cyclic load). The results of the tests need to be recorded and stored with adequate conditioning and format.

4.1 Model construction

4.1.1 Prototype

For general bridge studies, which may target a group of bridges, the bridge parameters, such as size, shape, designed loads, and detailing, may not be available from the original design agencies. One approach is to conduct a statistical investigation (Lowes and Moehle, 1995, Abo-Shadi et al, 2000) to determine the most representative parameters for the group of bridges. The other approach is to simply use a most common value regardless what group of bridges the test is designed for. The proper guideline provisions to these two scenarios are described below:

(1) The National Bridge Inventory (NBI) Database is a complete collection of bridge external dimensions, functions, locations, ages, etc. This information can be converted to that required by the testers (Lampe and Azizinamini, 2000). This can largely reduce the time spent on preliminary investigation and increase the representativeness of the selected parameters.
(2) When the tester only needs a general bridge model, a set of most common parameters can be provided. For example, a height of 20 ft (6 m), span of 65 ft (20 m), and width of 40 ft (12 m) can be provided. The dead load and live load can be derived from the dimensions given above. For more convenience when only one bent is involved, a dead load of 800 kip (360 ton) and a live load of 200 kip (90 ton) can be provided. The sum of dead load and live load determines the axial load of the column and the dead load alone determines the lateral loads.

4.1.2 Scale

A dimensionless analysis is used to find the proper scaling of each parameter (Moncarz, 1981; Bertero, 1984). In the quasi-static bridge column tests, all time-dependent parameters that relate to velocity and acceleration are ignored. The axial load and lateral load from the superstructure are reduced to an external force applied vertically and horizontally to the top of the column. The material properties, such as elastic modulus, yielding stress, and specific weight, are kept to the same as the prototype (scale factor=1). The parameter that needs to be changed as will is the geometrical dimensions. The resultant scaling factors for quasi-static tests are listed in the 1st column of Table I.

Time and time-dependent variables need to be considered in the scaling for fast tests such as shake table tests. Because of the involvement of the gravitational acceleration (cannot be changed in large structural tests), the scaling is diverted into two courses:

(1) Gravity is insignificant:
The vertical load is either unimportant to the test or is applied externally. The self weight of the entire specimen is negligible to the purpose of the test. Supplementary vertical load (if necessary) is applied through force actuators. The input and response acceleration is allowed to be scaled without changing specific weight. The proper scaling is shown in the 2nd column of Table I.

(2) Gravity is essential:
If the gravity force from the self weight is one of the important factor in the test, the horizontal acceleration needs to be kept the same scale as the gravitational acceleration (unity) because the vertical (gravity) force and horizontal (inertia) force come from the same mass. Due to the difficulty of changing specific weight in specified proportion, the scaling of specific weight is substitute by auxiliary masses. The auxiliary mass needs to be attached to the heaviest places, which is usually the superstructures, without introducing additional stiffness. The proper scaling and auxiliary mass are listed in the 3rd column of Table I.

It has been noticed that the construction materials have different mechanical properties at different size. The mechanical properties such as elastic modulus and yielding or ultimate stress are not only difficult to change by any specific scale but also difficult to maintain constant when size is changed. There are multiple reasons that make the mechanical properties size-dependent, such as different manufacturing process and failure mechanism. Special care should be taken to ensure this does not alter the test result unexpectedly.

4.2 Load histories

The cyclic loading procedure is usually considered to be a good simulation tool for earthquakes when more realistic options, i.e. true dynamic tests, are not feasible. Since it is an approximation of earthquake load, there can be numerous approaches. Most tests done to bridge columns have adopted a progressive pattern cyclic loading procedure (Figure 1). This procedure involves some pilot cycles in the elastic range that provides more accurate estimation for yielding displacement, followed by plastic cycles that contain 2-3 cycles at each deformation level and increase in multiples of yielding displacement. It is believed that two or three cycles for each displacement level is a balance between demonstration of strength degradation and avoidance of undesired early fatigue fracture (Lowes and Moehle, 1995). This procedure was evolved from the standard steel element cyclic procedures (ECCS, 1986; Stone and Cheok, 1989; ATC-24, 1992). This procedure provides a general test condition for earthquake loads.

When specific earthquake record is to be tested on the specimen, a preliminary analysis is required to estimate structural response, and consequently the displacement history of the specimen (El-Bahy et al, 1999).

The shake table test is a real dynamic test. As being more realistic, it is important to be careful controlling the test environment. The loading records need to be properly filtered and scaled.

Elastic tests should be conducted prior to full-scale nonlinear tests. Modal parameters are retrieved in the elastic tests in order to well categorize the model. One or more of the hammer test, harmonic input test, and random vibration test can be used for this purpose.

Pseudodynamic tests represent the balance of actuality and test facility limit. In the slow pseudodynamic tests, the inertia force and viscous damping force are calculated in a computer that controls the loading procedure. The design of the real part and imaginary part as well as the scaling follows the specimen construction part of this guidelines.

4.3 Measurements and data acquisition

The technologies used in measurement systems evolve quickly. New issues emerge while old issues are resolved. It is not easy to setup general guidelines for all tests. However, well-configured measurement and acquisition systems share some similar principles. It is important to layout the principles to be followed.

A few fundamental values, such as lateral load, lateral displacement, and curvature, should be required by the guidelines. Some physical detail that may affect the resultant accuracy should be specified. For example, the range of the curvature measurement (with respect to section size) needs to be sufficient to cover the plastic hinge zone and part of the elastic zone. Any potential slippage surface needs to be monitored on both sides.

The data acquisition systems have all become digital nowadays. Analog filtering is crucial for such systems. For slow static tests, the system can stop at each designated load step and allow the measurements recorded. Analog filters can be conditionally absent if several readings are made and averaged to eliminate the fluctuation from high-pitch electronic or physical noise. For high-speed tests, the analog low-pass filtering range needs to cover the highest frequency of the interested vibration component. The sampling rate should be higher than twice of the filter cut-off frequency.

The study on data format, storage, and transmission is currently one of the major efforts from many experimental institutes lead by the National Science Foundation (NSF). The progress will be closely observed and integrated with this guidelines.

5.0 SUMMARY

Most bridge column tests are either for research purpose or for specific construction or retrofit project. The uniqueness of these tests makes it difficult to set up general guidelines for all. However, as a leading agency in the highway industry, the FHWA will persevere in the effort of laying out the national testing guidelines for bridges due to the anticipated tremendous benefits to the researchers and designers in this country. The first appearance of the product is expected to take place in a short time. This project will not be able to provide premium result without the contributions from bridge testing experts. All suggestions and discussions are highly appreciated.

6.0 REFERENCES

[1] Abo-Shadi, N.; Saiidi, M.; Sanders, D. July 2000. "Seismic Response of Reinforced Concrete Bridge Pier Walls in the Weak Direction," Technical Report MCEER-00-0006.

[2] Applied Technology Council. 1992. "Guidelines for Cyclic Seismic Testing of Components of Steel Structures," ATC-24, Applied Technology Council, Redwood City, CA.

[3] Bertero, V. V.; Aktan, A. E.; Charney, F. A.; Sause, R. 1984. "Earthquake Simulation Tests and Associated Studies of a 1/5th-scale Model of a 7-story R/C Frame-wall Test Structures," Report No. UCB/EERC-84/05, University of California, Berkeley.

[4] Dimig, J.; Shield, C., French, C.; Bailey, F.; Clark, A. Sept. 1999. "Effective Force Testing: A Method of Seismic Simulation for Structural Testing," *Journal of Structural Engineering*. ASCE, 125(9), pp 1028-1037.

[5] El-Bahy, A.; Kunnath, S.; Stone, W.; Taylor, A. September 1999. "Cumulative Seismic Damage of Circular Bridge Columns: Variable Amplitude Tests," *ACI Structural Journal*, 96(5), pp 711-719.
[6] European Convention for Constructional Steelwork, Technical Committee 1, Structural Safety and Loadings; Working Group 1.3, Seismic Design. 1986. "Recommended Testing Procedure for Assessing the Behavior of Structural Steel Elements under Cyclic Loads," First Edition.
[7] Kausel, E. May 1998. "New Seismic Testing Method. I: Fundamental Concepts," *Journal of Engineering Mechanics*, ASCE, 124(5), pp 565-570.
[8] Lampe, N.; Azizinamini, A. Nov. 2000. "Steel Bridge System, Simple for Dead Load and Continuous for Live Load," Proc. Conference of High Performance Steel Bridge, Nov. 30~Dec. 1 2000, Baltimore, Maryland.
[9] Lowes, L., N.; Moehle, J., P. Sept. 1995. "Seismic Behavior and Retrofit of Older Reinforced Concrete Bridge T-Joints," Report No. UCB/EERC-95/09, Earthquake Engineering Research Center.
[10] Moncarz, P. D. 1981. "Theory and Application of Experimental Model Analysis in Earthquake Engineering," Dissertation, Stanford University.
[11] Stone, W.; Cheok, G. Jan. 1989. "Inelastic Behavior of Full-Scale Bridge Columns Subjected to Cyclic Loading," NIST Building Science Series 166.

TABLE I SCALING FACTORS FOR DIFFERENT TESTS

Variable	Slow test	Dynamic test	
		Gravity insignificant	Gravity essential
Geometric size *l*	S_L	S_L	S_L
Time *t*	N/A	S_L	$S_L^{0.5}$
Stress σ	1	1	1
Strain ε	1	1	1
Elastic modulus E	1	1	1
Yielding stress σ_y	1	1	1
Density ρ	N/A	1	1
Force P	S_L^2	S_L^2	S_L^2
Bending moment M	S_L^3	S_L^3	S_L^3
Rotation angle (Δ/L) θ	1	1	1
Curvature ϕ	S_L^{-1}	S_L^{-1}	S_L^{-1}
Displacement U	S_L	S_L	S_L
Acceleration	N/A	S_L^{-1}	1
Auxiliary mass	N/A	0	S_L^2-S_L^3
External damping	N/A	S_L^2	$S_L^{1.5}$
External stiffness	S_L	S_L	S_L

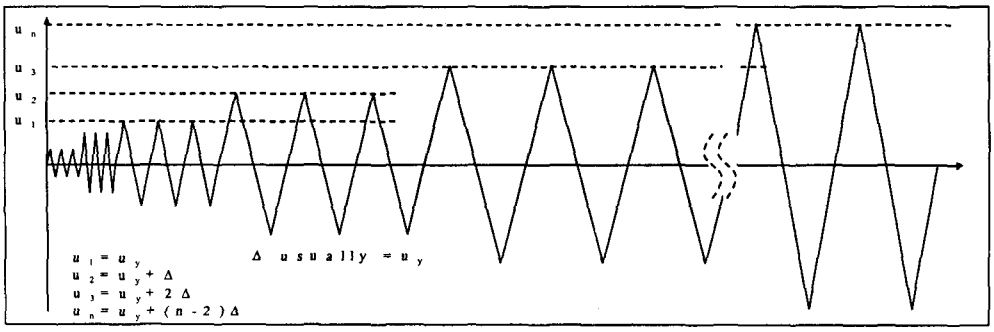

Figure 1 The progressive cyclic load history

SPECIAL THEME 1

TERRORISM: COLLAPSE of the WTC and PENTAGON WEDGE A

Terrorist Threats Against the Pentagon

by

Robert L. Hall[1], James T. Baylot[1], Robert J. Dinan[1], Richard Dove[1], John Hayes[2], W. Matthew Hossley[1], James L. O'Daniel[1], Thomas R. Slawson[1], Stanley C. Woodson[1]

ABSTRACT

The terrorist attack of 11 September 2001 against the Pentagon prompted USACE to perform a 30-day study to assist in the development of anti-terrorist methods for the Pentagon structure. Drawing on years of experience and model development, USACE provided and analyzed structural concepts for the rebuild and renovation of the Pentagon. USACE personnel assisted in the damage assessment immediately following the terrorist event, analyzed the current configuration and design concepts of the Pentagon wall system using simplified engineering-level and high performance computational models, and developed strength measures that were inserted into a PC-based vulnerability assessment code. Recommendations were provided to the Pentagon Renovation Program.

KEYWORDS: blast effects; Pentagon renovation; retrofit; structural assessment; terrorist attack; vulnerability

1.0 INTRODUCTION

Following the 11 September 2001 terrorist attack on the Pentagon, USACE entered into a 30-day study agreement with the Pentagon Renovation Program managers to assist in the evaluation and development of physical anti-terrorist measures for the Pentagon. USACE is uniquely qualified to blend state-of-the-art research, simple and sophisticated analytical techniques, and practical engineering into a focused study to provide concepts for anti-terrorist measures. The bombing of the Marine Corps barracks in Lebanon in 1984 was the motivation for the U.S. Army to establish one of the first research programs to address the effects of terrorist weapons on conventional buildings and develop improved design and retrofit methods for these facilities. During the past 15 years, experimental and analytical studies have resulted in significant improvements in the understanding of the response of conventional aboveground structures to blast effects. The studies have led to the development of guidelines and computer software for assisting engineers in evaluating and designing protective measures.

At the time of the 11 September attack, the Pentagon was undergoing a renovation that included retrofit measures to increase the resistance of the structural envelope to terrorist attack, particularly for blast effects. Although the Pentagon Renovation Project took great advantage of state-of-the-art technology available at the time, this technology is steadily advancing. The opportunity now exists to incorporate recent advances into the areas to be reconstructed, as well as areas not yet renovated.

2.0 PURPOSE

The purpose of the 30-day study was to examine protective measures for the Pentagon for a range of potential types of threats and threat levels that include airblast from explosive detonations, fire hazards, and chemical/biological/radiological weapons. The focus was general protection for all building occupants, rather than localized protection for specific critical assets. The 30-day study was not an effort to design for specific performance in response to a specific defined threat. This paper will summarize the blast response of the unretrofited Pentagon and the added protect provided by the existing retrofit used in wedge 1.

3.0 11 SEPTEMBER 2001 EVENT

U.S. Army Corps of Engineers personnel conducted a Pentagon damage assessment from 14-17 September 2001. The overall purpose of this initial forensic study was to investigate the

extent of the damage caused by the plane that crashed into the Pentagon on 11 September. An important part of this effort was gathering information on the performance of the retrofitted components of the Pentagon. While, the recent retrofit upgrade techniques employed in the building's renovated sections were intended to increase protection against vehicle bombs, the response of the retrofit components under the 11 September loads provides insight into the overall effectiveness of the upgrades. The structure experienced the extraordinarily energetic localized impact of the plane itself, secondary impacts, and the complex external/internal blast and fire loads from the fuel carried within the plane. While the complexity of the loading complicates a quantitative determination of the exact load/response relationship, a qualitative assessment of the relative response of the retrofit components as compared to the non-retrofit components is feasible. This is possible because the plane struck close to the interface between the retrofit and the non-retrofit building sections.

Figure 1 is a schematic of the layout of the Pentagon. Wedge 1 consists of sections 3 and 4 as shown in this figure. The impact location and orientation are also indicated on the figure. The exterior wall near the impact location is shown as Figure 2. The boundary of Wedge 1 (retrofitted) with Wedge 2 (non-retrofitted) is shown near the left side of the figure. The impact occurred near column line 14 of Wedge 1. The collapsed region (Figure 3) extended from the expansion joint near column line 11 to column line 18. Windows near the Wedge 1 - Wedge 2 boundary are shown in Figure 4. Damage to the non-retrofitted windows is higher than damage to the retrofitted windows, although the retrofitted windows are closer to the impact area and subsequent fuel fire/blast.

The retrofit of Wedge 1 was effective in saving lives during the events of 11 September 2001. While, the retrofit upgrades were intended to increase protection against vehicle bombs, they appeared to have been effective in mitigating some of the secondary effects of the plane impact. The retrofit windows responded in a ductile and tough manner to the blast loads and were also able to resist substantial fragment impacts. The windows also remained intact even when apparently engulfed in the fireball of burning fuel, preventing entry of the fire into the upper floors. The tube steel members worked as intended and may also have played a part in the resilience of the building, a possibility that was not evaluated in this study. The annotated photographic documentation of the response of both the non-retrofit and retrofit windows may prove useful in future analytical and experimental efforts to improve protection against terrorist attack.

4.0 UN-RETROFITTED PENTAGON CONFIGURATION

The unretrofitted wall analyzed consists of 5-1/2 inches of limestone facade with an 8-in., two wythe, unreinforced brick infill wall. The floor height varies but is taken as a nominal 10 ft for this analysis. The horizontal span between columns is 10 ft on-center. The construction quality of the edge support conditions of the masonry wall (gap between wall and columns or grout fill) is uncertain, but it is assumed that the wall is supported on all 4 sides (two-way action) without the support rigidity that could induce arching (compressive membrane action). The limestone façade was assumed to respond in one-way action between column lines. In addition, nearly every bay except those on the fifth floor has a window. The window analyzed is 7-feet high by 5-feet wide (outside dimensions), with ¼-inch thick annealed glass.

5.0 EXISTING (WEDGE 1) RETROFIT

The retrofits currently used in the Pentagon renovation (Figure 5) include blast hardened windows, supported by horizontal tubes that frame into vertical tubes that run from floor slab to floor slab. The 6"x6" or 8"x8" tubes transfer the dynamic reactions from the windows and the exterior masonry walls to the floor slabs. The E-Ring retrofit window for the W1 type consists of an insulated, or double pane glazing. The outer pane is ¼ in. thick thermally tempered glass, with a ½ in. air gap. The inner pane is a laminate consisting of 3/8 in. thermally tempered glass, .090 in. PVB inner layer, and 3/8 in. thermally tempered glass. In addition, a

geotextile membrane is used over the interior surface of the masonry wall to prevent the masonry from becoming a debris hazard during a blast event.

6.0 ANALYSIS

The analyses assume that the Pentagon frame is sufficient to resist the loads transferred to it from the exterior walls. Evaluations of the original and retrofitted Pentagon structures were performed using the Antiterrorist (AT) Planner software [1]. AT Planner is a PC-based computer code that assists installation-level personnel in analyzing the vulnerability of buildings and their occupants to the effects of terrorist vehicle bombs. The program also contains information to aid in developing protective measures.

AT Planner is being developed to present concepts and procedures for protecting deploying forces from terrorist/saboteur attack using expedient methods that require a minimum of engineer resources. Recent experience has shown that the demand for military engineering in support of antiterrorism has risen dramatically as the Army is drawn into a succession of operations other than war. In these situations, U.S. troops may be subject to attack by unfriendly civilian or paramilitary groups. AT Planner is a Windows 95-based application suitable for operation on a notebook computer by combat engineer officers, and draws on completed and ongoing research related to the protection of fixed facilities from terrorist attack as well as work on field fortifications. AT Planner is based on references 2-7. AT Planner provides standoff distance evaluations, structural damage and window hazard calculations, protective measures checklist for terrorist threats, and vehicle velocity calculations and barrier recommendations. When a vulnerability analysis from a terrorist bomb is calculated in AT Planner, blast pressure is calculated at the center of each structural bay on a structure. Angle of incidence is considered in calculating airblast levels on structures, but clearing effects and shielding effects are not. AT Planner uses PI (Pressure Impulse) diagrams to allow a user to quickly estimate building damage from a vehicle bomb attack. A description of a PI curve is shown in Figure 6. The hazard/protective levels used by AT Planner in this study are shown in Figure 7. AT Planner has a set of default damage diagrams and the capability to read in user specified diagrams. The AT Planner default building components (excluding windows and non-reinforced masonry walls) are normalized so that the user can modify the span and thickness of the component. The user specified diagram is not normalized; therefore a different diagram must be developed for each different building layout. For this reason, a significant amount of time was spent studying construction diagrams in order to determine nominal specifications before the damage diagrams were developed.

Wall response calculations were performed using the Wall Analysis Code [8] (WAC). WAC is a single-degree-of-freedom (SDOF) model designed specifically to calculate the response of reinforced and unreinforced concrete and masonry walls to airblast loads. Window response/hazard predictions were made with HAZL [9]. These response predictions were used to develop the PI diagrams that were input into AT Planner to perform the blast evaluations. The PI diagrams for the walls were validated by performing analyses using higher-fidelity, finite element (FE) structural response models described in Appendix 3.D.

Range-to-effect (RTE) and PI curves for the Ring E walls and windows were developed and entered into AT-Planner. In addition, PI curves for the reinforced concrete roof panels required to perform AT Planner assessments. Roof panel retrofits were not required for blast protection in subsequent scenarios – the curves used for the roof panels are constant throughout this report. RTE curves for this report are shown for components exposed to normally reflected loads. They are not shown for roof panels since realistic roof loads are closer to incident pressures rather than normally reflected pressures. The damage levels obtained from the supporting FE models match well with the PI diagrams developed using WAC, thus validating the PI diagrams. The PI curves presented above are used in AT Planner to define safe stand-offs

around the Pentagon for the large and small truck bomb threats as shown in Figure 8 (the windows control these stand-offs).

To analyze the existing retrofits response to blast load, SDOF models of the wall and window systems were developed. The wall model did not consider the effects of window failure. The resistance of the wall included the strength of the façade, the masonry wall, and the tubular framing system (dominant contribution). The wall system model was used in WAC to generate RTE and PI curves and these curves were validated with FE analyses. The high level PI curves were used in AT Planner to define safe stand-offs around the Pentagon for the large and the small truck bomb threats. The custom PI diagrams for the window and wall retrofits of the exterior wall of the E-Ring were used for all walls. Damage plot in figure 9 are intended to illustrate damage to the outside of the E-Ring only.

7.0 RECOMMENDED RESEARCH/ EVALUATION

Doors in the exterior wall of the E-Ring need to be designed to resist the same bomb size - standoff combination that the E-Ring exterior walls and windows are designed to. Other components of the exterior shell of the Pentagon need to be evaluated for the same conditions used to design the E-Ring exterior. Components that need to be evaluated include the walls windows and doors on the back of the E-Ring and on the backs and fronts of the A-, B-, C-, and D-Rings. The roofs of the two-story portions of the buildings located between the D- and E-Rings and between the C- and D-Rings also need to be evaluated.

Further blast hardening should be considered in conjunction with proposed plans to relocate public roads and/or further control access to the Pentagon roads and parking areas. The Pentagon should be evaluated against other reasonable threats. The wall/window retrofit or rebuild selected for use in the Pentagon rebuild/restoration should be tested to verify the level of protection provided.

8.0 REFERENCES

1] AT Planner, U.S. Army ERDC, Vicksburg, MS, October 2001.

2] FM 5-114, Engineer Operations Short of War, Headquarters, Department of the Army, 13 July 1992.

3] TM5-853-2/AFMAN 32-1071, Security Engineering Manual, Vols. 1-4, Departments of the Army, and the Air Force, May 1994.

4] "Structures to Resist the Effects of Accidental Explosions," ADA 243 272/TM 5-1300/NAVFAC P-397/AFR 88-22, Departments of the Army, the Navy, and the Air Force, November 1990.

5] Drake, J.L., et. al., "Protective Construction Design Manual," prepared for Air Force Engineering & Services Laboratory, Tyndall Air Force Base, Florida, November, 1989, ESL-TR-87-57.

6] Ferritto, J., Tancreto, J., "User's Guide for Navy Air Attack Simulation Program (NAASP)," Naval Facilities Engineering Command, Alexandria, VA, Program No. Y0995-001-06-010, May 1987.

7] Oswald, C.J., and Skerhut, D., "FACEDAP Theory Manual," Contract No. DACA45-91-D-0019, U.S. Army Corps of Engineers, Omaha District, April 1993.

8] Slawson, T.R., "Wall Response to Airblast Loads: The Wall Analysis Code (WAC)," prepared for the U.S. Army ERDC, Vicksburg, MS, Contract DACA39-95-C-0009, ARA-TR-95-5208, November 1995.

9] "Window Fragment Hazard Level Analysis, the HAZL Model," U.S. Army ERDC, Vicksburg, MS, October 2001.

9.0 ACKNOWLEDGMENT

The authors greatly appreciate the efforts of all members of the study team and the permission to publish granted by the Director, Geotechnical and Structures Laboratory.

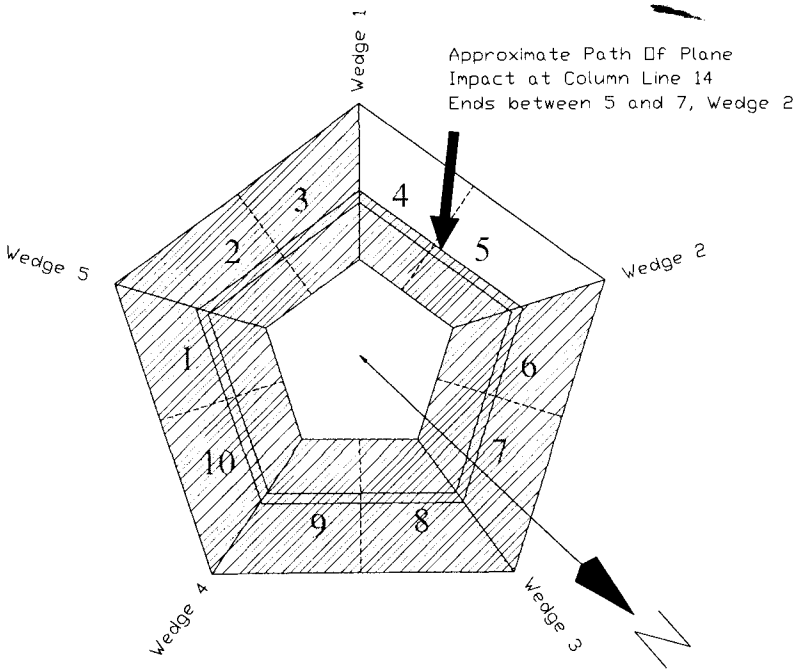

Figure 1. Layout of Pentagon showing impact location.

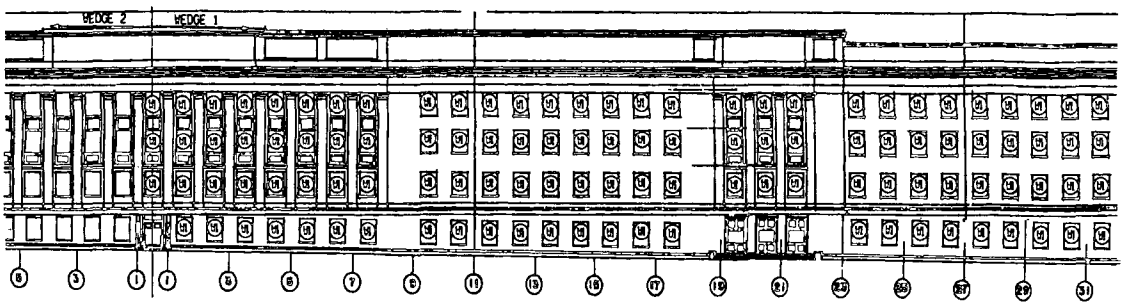

Figure 2. Exterior of E-Ring of Pentagon Wedge 1 and 2 with column line designations. W1 designation on windows denotes non-operable (fixed) retrofit window. Impact occurred near Column Line 14, collapsed region extended from construction joint at Column Line 11 to Column Line 18.

[1] Geotechnical and Structures Laboratory, Engineer Research and Development Center, U.S. Army Corps of Engineers, Vicksburg, MS 39180

[2] Construction and Engineering Research Laboratory, Engineer Research and Development Center, U.S. Army Corps of Engineers, Champaign, IL 61826

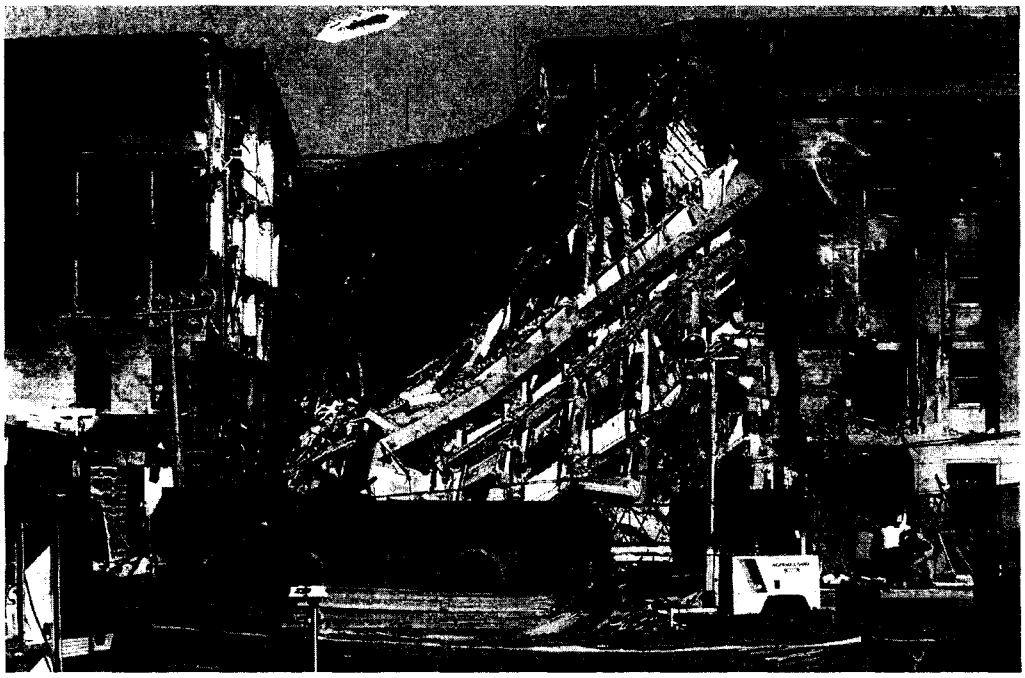

Figure 3. Collapsed section/plane impact area in Wedge 1. Plane entered the 1st floor at an angle of approximately 40 degrees from perpendicular moving toward the left into Wedge 2.

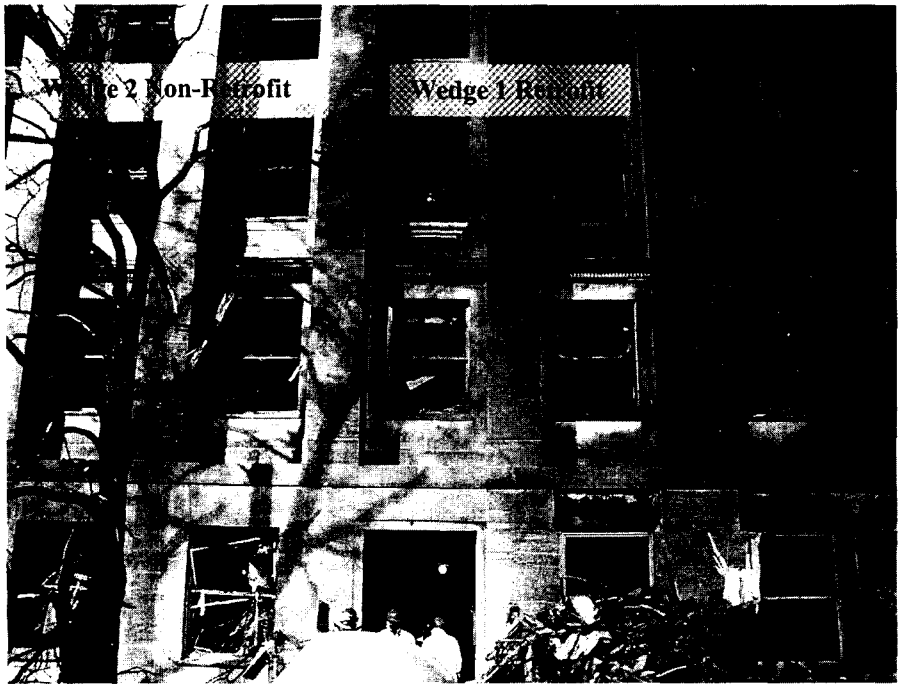

Figure 4. Exterior view of transition between Wedge 1 (on right, retrofit) and Wedge 2 (on left, non-retrofit). First floor non-retrofit window adjacent to transtion may be High Hazard blast response. Second and 3rd floor fire damage. Approximately 135 ft (44.2 m) North of plane impact point.

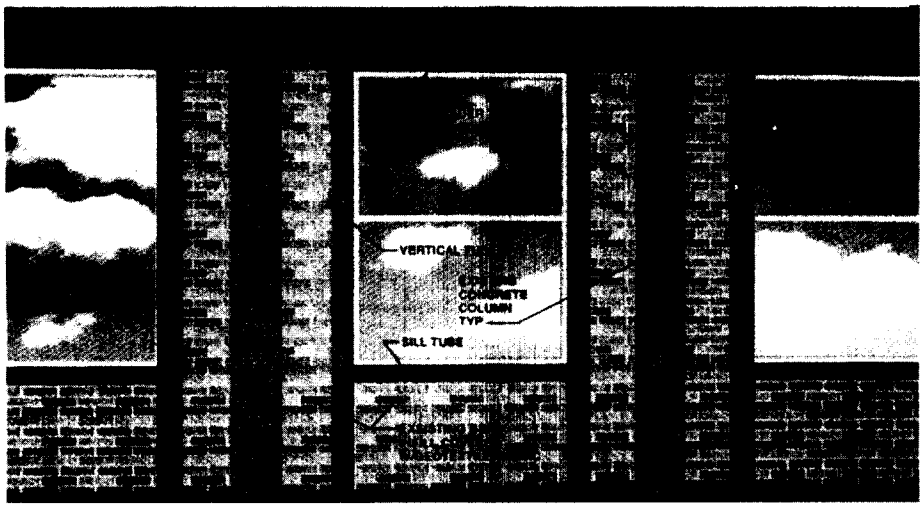

Figure 5. Current retrofits.

Pressure Impulse Curve

A pressure-impulse (PI) diagram is an iso-response curve for a particular structure loaded with a particular load history type.

The PI curve divides the plot into two regions: (1) the area above and to the right where the response level of the PI curve is exceeded and (2) the area below and to the left.

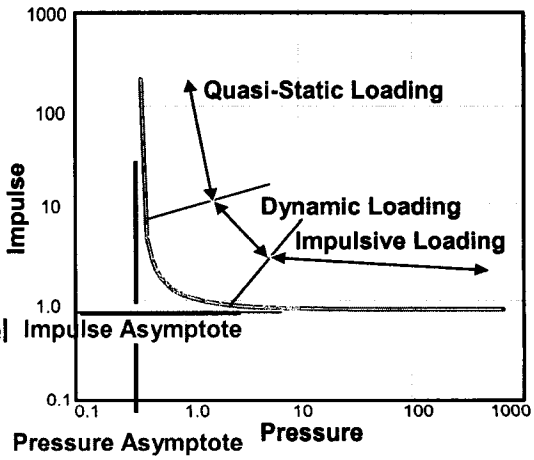

At low impulse (short duration loads), the response is essentially independent of peak pressure and depends only on the impulse.

At low pressures (long duration loads), the response is independent of impulse and depends only on the peak quasi-static load.

Figure 6. PI curve description.

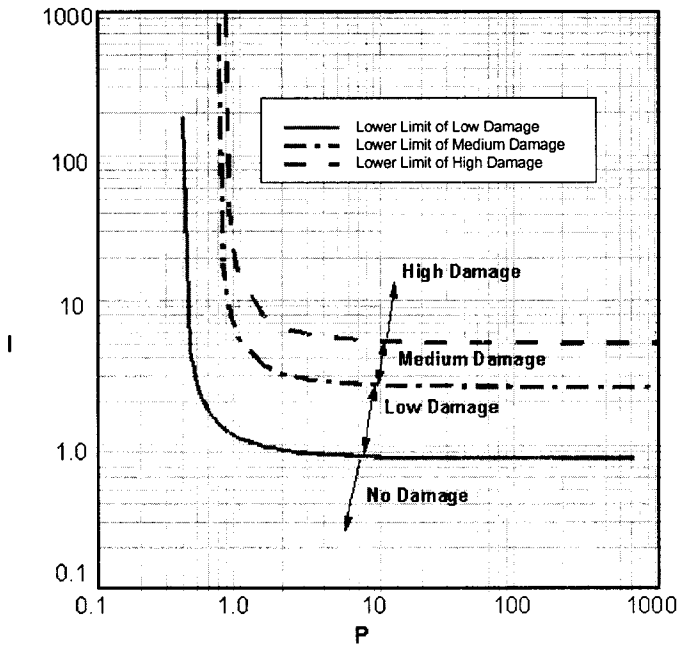

No damage: No appreciable damage; the component is reusable without repair. This damage level can be equated with a **High Level of Protection**.

Low damage: The component is probably repairable and it has provided a generally adequate level of protection to personnel and equipment from the effects of the explosion. This damage level can be equated with **a Medium Level of Protection**.

Medium/Moderate Damage: Repair of the component is not feasible, but it has not collapsed, and it has provided substantial protection to personnel and equipment from the effects of the explosion. This damage level corresponds to the greatest degree of damage that might be accepted, thus it can be equated with a **Low Level of Protection**.

High Damage: The component is definitely beyond repair but it has not necessarily completely collapsed. It has undergone a deformation such that it cannot be counted on with high certainty to protect personnel and equipment from the effects of the explosion. This damage level is equated with "**Collapse**" as it is used in terms of a **Level of Protection**. However, components with 100% damage will most probably not be collapsed in the general usage of this word.

Figure 7. Hazard/Protection Levels.

Figure 8. Stand-offs to prevent high hazard for the large and small truck bombs for the unretrofitted Pentagon.

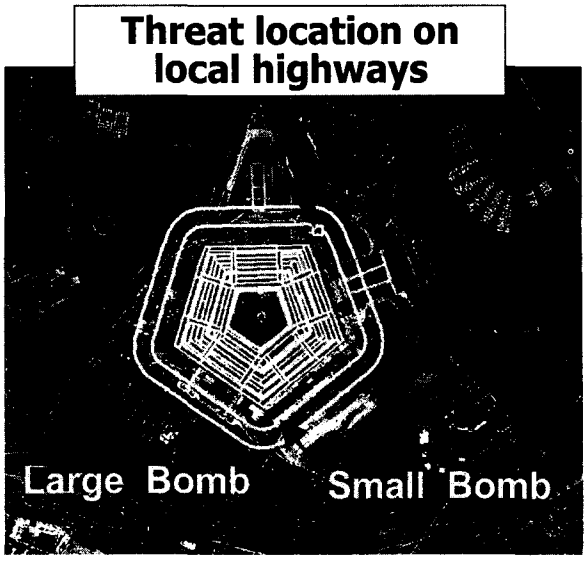

Figure 9. Stand-offs to prevent high hazard for the large and small truck bombs for the current Pentagon retrofits.

SPECIAL THEME 2

DISASTER INFORMATION

Natural-Technologic Events: The Frequency and Severity of Toxic Releases During and After Natural Disasters with Emphasis on Wind and Seismic Events

by

Stacy Young[1]

ABSTRACT

Toxic substances released from storage facilities, industrial plants, or transportation vehicles as the result of technologic emergencies (e.g., equipment failures, severed pipelines) precipitated by natural disasters are known as natural-technologic or *na-tech* events. The risks associated with na-tech discharges are of importance given accelerated technologic and industrial expansion, increasing population density in disaster-prone areas and trends in the more frequent occurrence of natural disasters. These trends increase the probability of catastrophic future disasters and the potential for mass human exposure to toxic agents released during disasters. Half of the natural disasters that occurred in the United States and its territories during the 1990s resulted in at least one na-tech event. We identified and characterized 1,152 na-tech events that occurred during the 1990s. Of these, 580 were related to wind or seismic effects. Greater knowledge of the factors that resolve the occurrence and severity of na-tech events can be used to increase disaster preparedness levels and damage adsorption capacities.

KEYWORDS: Chemicals; Exposure; Health Effects; Na-tech; Natural Disasters; Toxic

1.0 INTRODUCTION

Subterranean stress, surface instability, high winds, and abnormal precipitation or temperature are natural circumstances that threaten human health (*1*). Rapidly moving or rising floodwaters, damaged roadways, and collapsing buildings are hazards commonly associated with extreme natural events. Oil releases, agrochemical pollution, asbestos dust and other toxic materials released during extreme natural events can also endanger human health. Toxic releases that result from technologic emergencies created by natural disasters have been referred to as natural-technologic or *na-tech* events (*10*).

Na-tech releases pose potential threats to human health through both acute and chronic exposures that may occur when environmental integrity is compromised. Oil, chemical, radiological, or biological agent releases may pose extreme fire and explosive hazards, result in the formation of toxic vapors, or lead to contamination of waterways and groundwater sources (*8, 11, 12*). After a 1995 quake in Kobe City, Japan, dust and irritants raised during demolition work were considered a factor in the deteriorating condition of asthma patients (*7*). In the 1989 Loma Prieta earthquake near Santa Cruz, California, hazardous materials exposures accounted for 20% of after-earthquake work-related injuries (*3*), and numerous human exposures to toxic materials (e.g., asbestos and fiberglass insulation, mercury, leaking transformers, broken chemical containers) (*6*).

A lack of standardized record keeping, however, has hampered efforts to assess the frequency and severity of these occurrences (*10*). As a result, the significance of hazardous material releases in the broad scope of disaster-associated risks has yet to be determined. Na-tech events are a preventable consequence of natural disasters. Na-tech occurrence is the result of technologic circumstances in combination with a natural disaster. Though little can be done to modify the nature of a disaster, the technologic component offers a point of intervention that can be used to diminish or eliminate toxic releases resulting from na-tech causes in disaster situations. In this study, we present estimates of the frequency and character of na-tech incidents

[1] National Center for Environmental Health, Centers for Disease Control and Prevention, 1600 Clifton Road, NE (Mailstop E-23), Atlanta, GA 30333 USA

that occurred in the United States and its territories during the 1990s—with emphasis on wind- and seismic-related na-tech events. Characterization of these events will aid disaster preparedness and mitigation.

2.0 METHODS

We used National Response Center (NRC) records to assess oil, chemical, radiological, and biological discharges occurring in the United States and its territories from January 1, 1990, through December 31, 1999. We used Federal Emergency Management Agency (FEMA) records to identify climatological and geophysical events that occurred in the United States during the same period and resulted in Emergency Declarations or Major Disaster Declarations[2]. A toxic release was identified as a na-tech release if all of the following criteria were met: (1) cause of the release was a "Natural Phenomenon," (2) release day fell within a *disaster period*, (3) state of release and state of FEMA declaration matched, and (4) county of release and county of FEMA declaration matched. Toxic releases attributed to non-natural disasters (e.g., the Oklahoma City bombing) and fire events were removed from analysis.

We characterized na-tech events with respect to: type of natural incident, type of declaration, year of occurrence, type of facility/mode of transportation, location of release (e.g., EPA region), total amount of discharge, and chemical class.

3.0 RESULTS

The NRC recorded 275,032 toxic incidents during the 10-year study period. Of these, 177,464 had sufficient information on the cause, date, and location of the toxic release to facilitate identification of na-tech events. FEMA records indicated that 480 natural, non-fire disasters occurred in the United States and its territories during the same period. Over half of the natural events (52.0%) were associated with at least one na-tech release. The remaining events (47.3%) resulted in no na-tech releases. The number of na-tech releases per event ranged from 0 to 42 with an average of 2.4 na-tech releases per natural event. A total of 1,152 na-tech events were identified.

3.1 General Na-tech Characterization

Nearly half (48.2%) of all na-tech events were generated by wind-related storms, with flood-related storms (30.5%), severe winter storms (19.2%) and earthquakes and aftershocks (2.2%) accounting for the remainder (Figure 1). Further analysis presented in this report focus solely on the 580 na-tech events attributed to wind and seismic events during the 10-year period, unless otherwise noted.

The majority of wind- and seismic-related na-tech events were associated with a major disaster declaration (98.5%). Na-tech events were reported more frequently during the latter half of the decade (61.2%) than during the first half (38.8%). Nearly 73% of all discharges were from fixed facilities (e.g., factories, laboratories) with marine-related and pipeline-associated discharges accounting for 14.5% and 8.8% of releases, respectively. EPA Regions IV and VI experienced the greatest number of na-tech releases—190 and 175, respectively (Figure 2).

3.2 Annual and Geographic Na-tech Fractions and Ratios

The crude na-tech fraction for the period from 1990 through 1999 was 2.1 per 1,000 releases (95% confidence interval [CI]: 2.0-2.2 per 1,000 releases). Analysis of na-tech fractions in 2-year intervals suggested that na-tech occurrence increased during the last two years of the decade (Figure 3). Geographically, the highest na-tech fractions of release occurred in EPA regions IV (4.60 [95% CI: 4.57-4.63]), I (2.37 [95% CI:

[2] An Emergency Declaration can be declared when the President determines Federal assistance is needed to supplement State and local efforts in providing emergency services. A Major Disaster Declaration may be presidentially determined for any natural catastrophe resulting in severe damage exceeding the combined capabilities of State and local governments to respond.

2.36-2.38]), IX (1.97 [95% CI: 1.97-1.98]), and VI (1.87 [95% CI: 1.87-1.88]).

Regions VI (7.3 [95% CI: 5.4-9.9]) and IX (2.9 [95% CI: 2.5-3.5]) exhibited the greatest number of na-tech events per natural event. Earthquakes were associated with 5.00 [95% CI: 4.0-6.3] na-tech events per natural events and wind-related storms were associated with 2.7 [95% CI: 2.4-3.1] na-tech events per natural event.

3.3 Amounts of Toxics Released

In 580 na-tech events, 651 toxic materials were released. Measures of the total volume released were available for a limited number of the 580 na-tech events. Earthquakes and aftershocks (n=10) produced a greater median release volume (3880.0 L) than wind-related storms (n=288; 113.6 L). Release volumes and masses during the period from 1990 through 1994 (median=310.4 L; 453.6 kg) were greater than those between 1995 and 1999 (median=111.7 L; 102.1 kg).

3.4 Types of Toxics Released

Of the 651 hazardous materials released during wind- or seismic-related na-tech events, 465 could be characterized on chemical class. The majority of discharged chemicals (324 [69.7%]), were flammable liquids.

4.0 DISCUSSION

Previously, anecdotal accounts and regional surveys lent evidence to the existence of na-tech events during and after natural disasters (*2, 9, 13, 14*). Our identification of 580 wind- and seismic-related na-tech events during the 1990s reinforces anecdotal descriptions and regionally conducted surveys in demonstrating the existence of na-tech threats.

A 1994 survey of hazards mitigation organizations in 20 states showed an increase in the number of na-tech events during the 1980s (*10*). Our data suggest that wind and seismic na-tech occurrence increased during the 1990s. However, our ability to definitively note trends and make comparisons between groups is limited by the quality of the data.

The NRC data are based on initial release accounts made during or immediately after an incident when exact details may be unknown. As a result, only information that is available early on in the incident is available. Rarely do these early reports indicate the exact amounts released or whether injuries or deaths resulted from a release. Inaccurate, insufficient, or missing NRC data limited the quality of some data and continued to be a problem during our na-tech identification process. One-third of all discharges reported to the NRC did not have sufficient information to allow for determining whether they were na-tech discharges. Voids in the data limit our ability to identify trends and make comparisons, but may also increase the likelihood that the approximations of na-tech occurrence presented here are underestimates of the true occurrence.

Despite the limitations of our study, we identified 580 wind and seismic na-tech events that occurred during the 1990s. In our data, natural events of all types had the potential to result in a na-tech disaster. Windstorms produced the greatest number of na-tech events and earthquakes resulted in the greatest quantities of release. Wind-related storms and earthquakes also had the largest ratios of na-tech events per natural event—indicating that how often some types of natural events occur is not the sole factor determining their relevance with respect to na-tech events. Earthquakes have previously been found to pose the greatest na-tech threat (*10*).

While the frequency of na-tech occurrence appeared to increase during the 10-year period, the median volume and mass of releases decreased. One possible explanation for this paradoxical finding may be that safety measures put in place during the 1990s successfully limited large releases and heightened awareness of na-tech threats, thus increasing the reporting of smaller releases.

5.0 CONCLUSION

Our study reported the occurrence of wind- and seismic-related na-tech events during the 1990s, but was unable to identify significant trends in occurrence. The frequency of na-tech events during the study period suggests that na-tech events may be more pervasive than commonly thought and could be occurring with increasing frequency (*4, 10*).

Prevention of future na-tech events is the ultimate goal. Some preventative actions that can be taken are identifying and addressing known hazards, providing adequate information and skills to individuals most likely to be exposed or in-contact with toxic agents during or after natural disasters, and increasing municipal and private awareness of the environmental hazards associated with natural disasters. Our study aids such prevention efforts through characterizing the circumstances by which historical na-tech events have occurred in an effort to identify future hazards. The study is also an effective tool for establishing that toxic exposures are occurring in the wake of natural disasters—potentially increasing awareness of disaster-associated environmental hazards and spurring the development of appropriate mitigation and preparedness plans in disaster-prone states and countries that might otherwise have difficulty generating interest in such activities.

Modifying the NRC database or developing a new surveillance tool would yield more useful information on na-tech frequency and more detailed accounts of incidents. Thoroughly characterizing na-tech events will aid in providing communities with accurate and appropriate information so that preparedness levels and damage adsorption capacities can be raised in an effort to thwart future impacts (*5*).

5.0 REFERENCES

1. S. Binder, L. M. Sanderson, *Annals of Emergency Medicine* **16**, 1081 (1987).
2. K. Breslin, *Environmental Health Perspectives* **101**, 590 (1993).
3. M. E. Durkin , C. C. Thiel , J. E. Schneider, T. DeVriend, *Bulletin of the Seismological Society of America* **81**, 2143 (1991).
4. T. Fields, *Natural Hazards Observer* **24**, 1 (2000).
5. Guha-Sapir, M. F. Lechat, *Disasters* **10**, 232 (1986).
6. R. Nathan, K. R. Olson, G. W. Everson, T. E. Kearney, P. D. Blanc, *Western Journal of Medicine* **156**, 278 (1992).
7. J. Nukushina, *Epidemiologia e Prevenzione* **19**, 226 (1995).
8. Proceeding of the Hazmacon Conference, Santa Clara, CA, April 18-20, (Dames & Moore, Los Angeles, CA, 1989).
9. L. M. Sanderson, in *Hazardous Materials Toxicology: Clinical Principles of Environmental Health*, J. B. Sullivan, G. R. Krieger, Eds. (Williams, Baltimore, Maryland, 1992), pp. 326-331.
10. P. S. Showalter, M. F. Myers, *Risk Analysis* **14**, 169 (1994).
11. K. V. Steinbrugge, H. J. Lagorio, J. R. Davis, J. H. Bennett, G. Borchardt, *Geology* **397**, 153 (1986).
12. J. W. Stratton, in *The Public Health Consequences of Disasters*, M. B. Gregg, Ed. (United States Department of Health and Human Services, Atlanta, 1989), chap. 4.
13. K. J. Tierney, *Urban Resources* **5**, 33 (1989).
14. K. White, *Environmental Health Perspectives* **101**, 584 (1993).

Figure 1. Type of natural incident associated with na-tech events

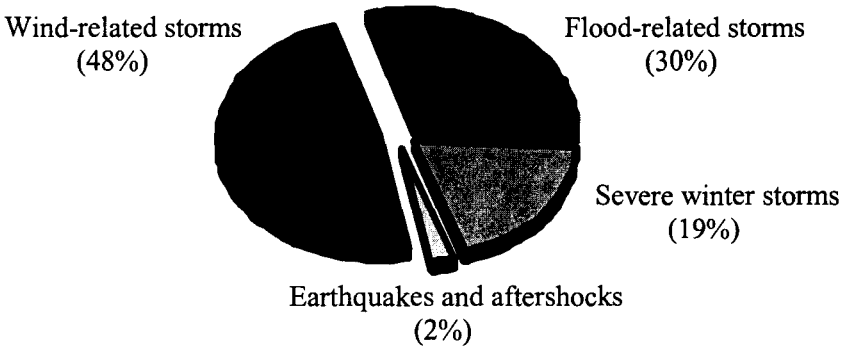

Figure 2. U.S. Environmental Protection Agency (EPA) regions

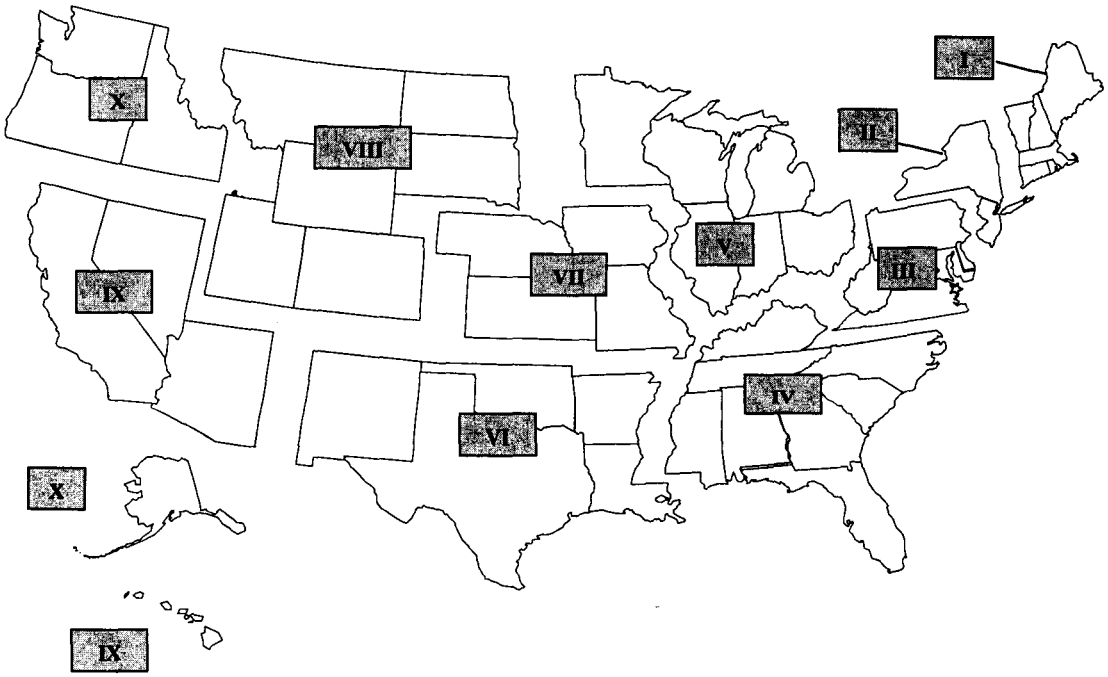

Figure 2. Two-year total NRC toxic releases and na-tech fraction of release per 1,000 NRC releases (95% CI)

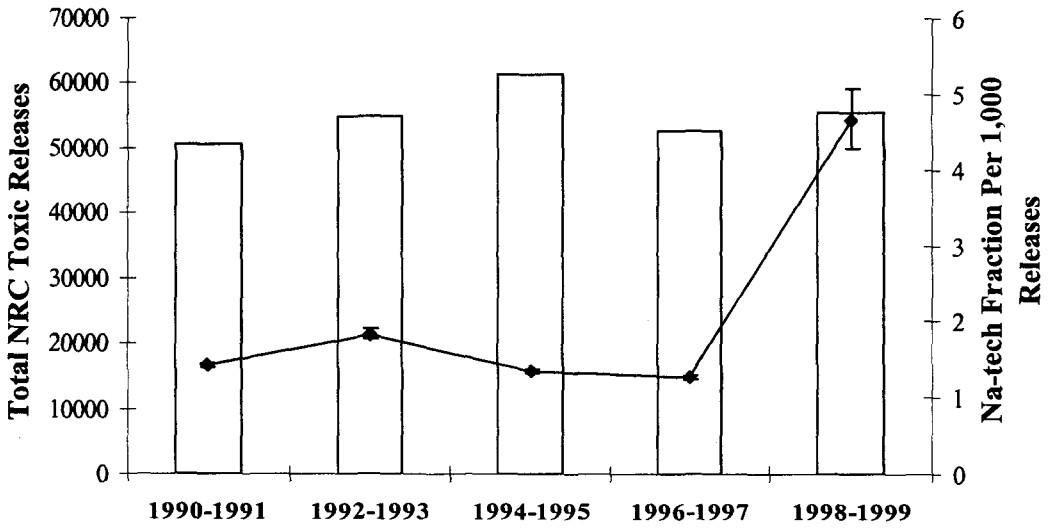

Disaster Information Systems and Seismic Countermeasures for Field Facilities in NTT

by

Kazuhiko Fujihashi[1]

ABSTRACT

NTT has experienced various disasters as a telecommunications operator, and has worked to develop a complete range of countermeasures. Particular emphasis has been placed on strengthening the early recovery systems when disasters occur in order to improve the reliability of telecommunications services. However, it was extremely difficult to understand and convey disaster conditions in the aftermath of the Hyogo-ken Nanbu Earthquake, and this delayed the start of disaster recovery activities. Drawing upon this experience, NTT is developing and introducing various disaster information distribution systems and services, and is also taking measures to improve the seismic performance of the field facilities. Of these efforts, this paper presents (1) support systems for distributing and sharing information within NTT and the NTT corporate group when a disaster occurs, (2) various systems for estimating and understanding the damage conditions of field facilities, and (3) technology for improving the seismic performance of field facilities.

KEYWORDS: Telecommunication Facilities, Disaster Information System, Hyogo-ken Nanbu Earthquake, Fiber Optic Sensing Technology

1. INTRODUCTION

The Hyogo-ken Nanbu Earthquake was a major earthquake with local severe tremors of degree VII (JMA seismic intensity scale), and produced large-scale liquefaction in coastal areas and reclaimed lands. For these reasons even NTT telecommunication facilities were unable to remain unscathed. In addition, understanding of disaster conditions and dissemination of this information was slow in the initial stages, and this delayed the start of disaster recovery activities. At the same time, calls flooded the circuits from all over the country to Kobe asking for information, creating congestion never before experienced and reaffirming once again the importance of information during disasters. Following the Hyogo-ken Nanbu Earthquake and in consideration of the importance of telecommunication services in an information society, NTT took the lessons of this earthquake to heart and established the Committee for Severe Metropolitan Disaster Countermeasures as an in-house committee for reviewing both hardware and software aspects in order to strengthen disaster countermeasures. This committee is further divided into 7 special committees that have conducted wide ranging investigations1) . This paper presents systems that have been investigated and introduced in this manner, or which are currently under development. Table 1 shows the relationship between the basic items investigated by these committees and the systems described in this paper.

---

[1] Senior Research Engineer, Supervisor, Disaster Prevention & Environmental Protection Group, Civil Engineering Project, Access Network Service Systems Laboratories, Nippon Telegraph and Telephone Corporation (NTT)

2. TELECOMMUNICATION SYSTEM CONFIGURATIONS AND DISASTER PREVENTION FEATURES[2)]

Fig. 1 shows an overview of the NTT telecommunication facility configuration. Telecommunication facilities are broadly divided into switchboard system equipment (node system) that process information and cable and wireless facilities (link system) that transfer information. Also, the telecommunication network is broadly divided into sections between telephone office where switchboards and transmission units are installed, and sections from user residences to telephone office, with the former called the trunk circuit network and the latter called the access system network.

2.1 Node System Facilities

Node system facilities are mainly installed in telephone office. In these cases the building itself has extremely high seismic performance, and the facilities are installed using methods that are both strong and offer superior anti-vibration performance. In addition, even should the facilities receive some damage, reserve systems are provided to minimize the effects. Furthermore, telephone calls and other traffic are monitored and controlled online, allowing automatic switching to the reserve system at the first sign of trouble. Storage batteries and emergency generators (some locations) are also installed as countermeasures against possible commercial power stoppages.

Although the Hyogo-ken Nanbu Earthquake caused some loosening and breakage of the switchboard foundation bolts and ceiling fixtures, there was no particular effect on service. However, commercial power stoppage, battery damage or discharge, and reserve engine damage all occurred at the same time, so the switchboards stopped and up to 285,000 lines were temporarily disabled and unable to make or receive calls.

The biggest problem for node system facilities is congestion so great that the number of inquiry calls exceeds the switchboard processing capacity, rendering it impossible to make or receive calls. In the aftermath of the Hyogo-ken Nanbu Earthquake, the number of calls reached a maximum of approximately 50 times the normal peak traffic, making it difficult to connect for five days. This congestion is a characteristic trouble for telecommunications facilities that does not exist for other lifelines. (Fig. 2)

2.2 Link System Facilities

2.2.1 Trunk circuit network

The trunk circuit network is comprised of wired and/or wireless sections, and has a multi-route and double-route configuration. Thus, should service be interrupted over a section, the system still allows traffic to flow by switching to the reserve system of a different route. For example, NTT maintains separate routes between Tokyo and Nagoya along the Tokaido and Chuo Route in both wired and wireless for a total of six routes. Tunnel networks have also been constructed in the central areas of Tokyo, Nagoya and Osaka to create a network with high reliability as underground facilities.

2.2.2 Access system network

The access system network is comprised mainly of metallic cables. Most of these are aerial cables, and only 21% of the total are underground cables installed in conduits and other underground facilities. In addition, portable phone systems are spreading rapidly in recent years, with most customers using a combination of wired and wireless communications. The access system network generally adopts a star (spoke) configuration, and alternate routes are not secured with the exception of certain regions or important users.

The access system network covers a wide area, and

includes vast amounts of facilities and diverse facility environments. Urban areas have high concentrations of older facilities, so localized damage occurs easily and it is not easy to estimate the damage conditions. Most disruption of service when an earthquake occurs is the result of damage to these access system facilities.

The Hyogo-ken Nanbu Earthquake caused building collapse and fires, which severed aerial and pull-in cables. In terms of conduits, manholes, underground cables and other underground facilities, underground cables suffered damage due to conduit breakage and disconnection and manhole duct sleeve damage, but damage leading to the disruption of service was much less than for aerial cables, thus confirming the high reliability of these facilities.

3. DISASTER INFORMATION SYSTEM CONCEPT

Possible disaster information system functions include detection of disaster occurrence, estimation and understanding of damage, support for recovery activities, and so on. As mentioned above, the greatest need in telecommunications is systems for understanding disaster conditions and assisting early recovery. Of these systems, online information systems in particular use the telecommunications network, and are differentiated from offline information systems that gather information directly from people at the disaster site through patrols, etc.

An overview of the online and offline information systems thought to be necessary for telecommunications is described below.

3.1 Online Information Systems

The ideal online information system should constantly monitor the network to make sure that telecommunications service is provided properly, and be able to understand trouble occurrence in real time and perform network control to minimize any drop in service. In addition, it is considered important and effective to construct a system that would allow centralized control and sharing of damage and recovery information in order to promote a smooth recovery when a large-scale disaster occurs. As mentioned above, access system facilities are vast in number and span a wide area, so a system that could gather disaster information remotely with as little human assistance as possible would also be extremely effective for promoting early recovery.

3.2 Offline Information Systems

When an earthquake occurs, it may be difficult to understand the damage conditions to telecommunications facilities using only the above-mentioned online information systems. In addition, online information systems are basically used to estimate and understand whether damage has occurred, and it is difficult to understand the degree of damage. Furthermore, the damage conditions of conduits, utility poles, buildings and other structures must essentially be surveyed directly on-site by patrols. Therefore, offline information systems that use this type of human intervention are also necessary for recovery. However, these activities should proceed after careful selection of survey methods and priorities based on the estimation results of the online information system. In addition, systems and tools are also necessary for obtaining plant records and other on-site information needed to gather disaster and recovery information, and for compiling information gathered on-site into databases, etc.

4. CURRENT STATE OF DISASTER INFORMATION SYSTEMS RELATED TO SERVICE, OPERATIONS AND NETWORKS

4.1 Network Monitoring and Control Systems

These systems were constructed by NTT prior to the Hyogo-ken Nanbu Earthquake. The systems were originally installed in prefectural units, but with the restructuring of NTT in January 1999 they were

integrated into wide-area groups, with ten network operation centers and two network control centers currently located around the country (Fig. 3). The network control centers monitor and control the trunk circuit network in real time 24 hours per day using the following systems. 1) Overall Traffic Monitoring System which monitors and analyzes communications conditions in full detail, 2) Traffic Control System which detects and controls switchboard volumes as necessary when tolerable limits are exceeded, 3) Common channel signaling Network Monitoring and Control System which monitors and analyzes the signal network between switchboards, and 4) New Synchronous Network Control System which performs remote control of transmission routes.

Furthermore, the network operation centers monitor and control the vast amount of telecommunications facilities including transmission facilities using the following systems. 1) Switchboard Maintenance Support System which monitors switchboard operating conditions and performs remote control and testing, 2) Control Measures Support System which monitors the overall communications facilities including switchboards, transmission units and wireless units, and 3) Transmission Monitoring Control System which monitors transmission unit operating conditions, determines breakdown locations, and switches to reserve transmission routes.

4.2 Disaster Information Transmission and Sharing Systems[3)]

4.2.1 Disaster information system

The disaster information system manages information such as the activity items of each NTT Disaster Countermeasures Headquarters team, damage conditions and recovery conditions using various databases when a disaster occurs. The system distributes this information and also displays it on a map. This client-server type system uses a LAN linking various corporate locations, and performs centralized management from the Disaster Countermeasures Headquarters server. The system uses commercially available Lotus Notes software that has been provided with group-ware functions.

When a disaster or accident occurs and disaster information is input from a client, the disaster location and area are displayed on a map. This disaster information can be easily referenced by simple point-and-click operations. Current facility conditions and other data can also be displayed during normal periods using the facility management database of this system.

The functions of this system are: 1) map display of disaster locations and areas, 2) display of disaster countermeasures system information, 3) display of various instruction and report information, 4) display of facility disaster recovery information, and 5) display of service call number "113" malfunction reception information. This information can be categorized and searched according to combinations of time, source/location, information type and other factors. In addition, various information required when disasters occur such as "Disaster Countermeasures Equipment List", "Disaster Countermeasures Goods List" and "Emergency Rations List" are compiled into databases.

4.2.2 Maintenance information network

The Maintenance Information NETwork (MI-NET) is an electronic bulletin board where information can be input and viewed in text format. This system can be accessed using web browser software from all PC terminals of the four NTT companies (NTT, NTT West, NTT East, NTT Communications) and specified PC terminals at each NTT Group company. This allows information sharing between all group organizations.

In April 1999 the entire NTT Group conducted a large-scale breakdown exercise that simulated a leased line accident with the aim of verifying the response during disasters. This system was used as an information linking tool during this exercise, and its practicality and effectiveness were confirmed. As

a result, while there was some need for enhancement of functions, the system was confirmed to be effective overall at speeding up information transfer and information sharing.

4.2.3 Disaster Emergency Message Dial[4)]

Disaster Emergency Message Dial is an information transmission system that makes full use of the nationwide telecommunication network to prevent the massive amount of communication following a disaster from causing congestion. This is a voice mail system for conveying personal safety and other information verbally using phone numbers within the disaster area as keys. To use this system, users dial "171" and follow voice guidance to register and playback messages. Unlike conventional voice mail, message registration and playback are dispersed throughout the country by distinguishing the telephone numbers for registering messages using the last three digits within the NTT network (Fig. 4). The main uses are: 1) to contact people who cannot answer calls due to evacuations, etc. and 2) to allow contact when residential phones cannot be used due to power failure or disasters. This system is expected to prevent congestion and reduce the effects on communication for disaster relief and recovery activities.

Disaster Emergency Message Dial was operated during the heavy rains and flooding that occurred in Tochigi and Fukushima Prefectures in August 1998 and also during the Iwate-ken Shizukuishi Earthquake that occurred one week thereafter, and the system was accessed approximately 69,000 times including both registrations and playback. The system has also been used a number of times since, and is also operated on a trail basis during the annual Disaster Prevention Week. Through these operations, the service has been confirmed to be an effective tool for transmitting information and solving the problem of congestion when disasters occur. Recently, the service was accessed 200,000 times during the Tottori-ken Seibu Earthquake (October 6, 2000) and 87,000 times during the Geiyo Earthquake (March 24, 2001).

4.2.4 Shared Map Database System[5)]

This system consists of a shared map information system for compiling map information databases and various map utilization systems that use this map information. The client-server system configuration has two dispersed databases: a map information management database and an attribute information management database. NTT had previously developed information systems that utilize map data, but these databases generally could be used only with the system in question. This system resolves this issue, allowing databases to be used by various systems. Map information position coordinate data can be supplied from figure data or attribute data, and figure data can be supplied in various formats.

Examples of applying the Shared Map Database System to disaster information systems include: 1) linking mobile technology with map information, 2) understanding damage conditions and searching damaged facility drawings, 3) searching damaged buildings and disaster prevention facilities, 4) arranging recovery work. 5) supporting on-site surveys, and 6) providing information on the web, etc. The ability to search and display these and other various types of information on maps is effective for sharing information.

5. CURRENT STATE OF DISASTER INFORMATION SYSTEMS RELATED TO FIELD SYSTEM FACILITIES

5.1 Application for Evaluating the Seismic Performance of Access System Underground Routes[6)]

5.1.1 Overview of the Seismic Performance Evaluation AP

Damage to underground communications facilities

caused by the Hyogo-ken Nanbu Earthquake was relatively minor. However, underground communications facilities span vast areas, and visual confirmation of damage conditions is difficult, so facility inspections take much time which posed a significant obstacle to recovery work. Drawing on this experience, NTT developed the Application for Evaluating the Seismic Performance of Access System Underground Routes (hereafter "Seismic Performance Evaluation AP"). This tool evaluates the seismic performance of underground conduit facilities based on earthquake, ground and facility information, and is used to estimate macro damage after earthquakes.

Fig. 5 shows an image of the AP. Advance evaluations conducted during normal periods are used to formulate overall plans and renewal plans, and macro damage estimations after earthquakes are used to calculate recovery costs and formulate emergency inspection plans, etc. The databases required by this AP are the various in-house shared databases, which greatly reduces the database compilation and maintenance costs.

5.1.2 General evaluation flow

Fig. 6 shows the general AP evaluation flow.

Analysis results of the emergency inspections of underground conduit facilities conducted immediately following the Hyogo-ken Nanbu Earthquake showed that underground conduit facility damage factors were broadly classified into liquefaction occurrence, the degree of seismic motion, the conduit type, and the year of construction. The AP can be broadly divided into a ground evaluation block and a facility evaluation block. The features of this AP evaluation flow are: 1) comprehensive liquefaction judgment using the micro-topography classification, boring data, and liquefaction risk factor maps issued by each municipality, and 2) ground evaluation in fixed distribution (FD) sections which are the unit sections used by NTT when managing the communications network. At the initial settings, topographical data and boring data are input and modified to evaluate the ground quality. Next, earthquake information is input and the seismic motion is estimated using a distance attenuation formula. Then, the AP makes an overall liquefaction judgment based on this seismic motion and ground information.

Facility evaluations target the six facility types of manholes, hand holes, building lead-in conduits, facilities attached to bridge girders, main line conduits, and distribution line conduits. Each facility is divided into a number of categories according to the structure type and year of construction, and the damage probability is estimated and evaluated according to the combination of liquefaction occurrence and the maximum ground surface acceleration (PGA).

The estimation and evaluation results are displayed on a map by colors corresponding to the FD unit liquefaction judgment results and the damage probability for each facility. Selecting a FD section with the mouse opens a window displaying the FD number, liquefaction judgment results, measured seismic intensity and other data. Also, selecting a span with the mouse opens a window displaying the facility name, facility section, average, maximum and minimum damage probabilities, number of conduits and other information. Selecting the [Detailed Conduit Information] button in this window opens a window displaying detailed information such as the damage probability and type of cables housed for each conduit. Fig. 7 shows an image of the evaluation results window display.

5.2 System for understanding Access System Damage Conditions

In contrast to the AP described above which is a tool for evaluating the seismic performance and predicting damage to underground conduit facilities that house cables, this system is a tool for testing cables to predict and understand the effects on service. This system is used for: 1) estimation of macro damage conditions in about half a day immediately after a disaster occurs, and 2)

understanding damage conditions in the recovery period. Fig. 8 shows an overview of the system.

5.2.1 Estimation of macro damage conditions by order line tests

Communication cables include order lines for each fixed distribution section that are lines used for contact during work. When estimating macro damage conditions immediately after a disaster, first an order line G/NG judgment is made using order line testing units, and these results are sent to and registered in a database. Next, a macro estimation of damage conditions is made using the off-site facility management system (MARIOS), and these results are indicated on maps and in ledgers.

5.2.2 Understanding damage conditions by all-line tests

Disaster conditions in the recovery period are understood by testing all lines from the MDF (main distribution board) inside the facility center buildings using automatic line switching and monitoring units. The test results are sent to and registered on a server, and the damage conditions are indicated on maps and in ledgers.

5.2.3 Other functions and features

In addition to macro estimation immediately after a disaster and understanding damage conditions in the recovery period, transmission technology that supports multiple communication means such as public network, leased lines and portable phones has also been established to enable reliable data transfer even under disaster conditions.

5.3 System for Monitoring Structure Degradation Using Fiber Optic Sensing Technology

NTT has researched and developed B-OTDR (optical pulse tester using Brillouin scattered light) based strain measurement technology as original fiber optic sensing technology.[7, 8] NTT has applied this technology to develop a system for monitoring cracking and other degradation caused by earthquakes, superannuation, adjacent construction, etc., and has begun introduction to communications tunnels in metropolitan areas.

5.3.1 Measurement principle

Fig. 9 shows the principle of fiber optic strain measurement using the B-OTDR method. When pulsed light is input to an optical fiber, Brillouin scattered light having the frequency shifted in proportion to the strain generated in the optical fiber can be observed. The position at which the strain is occurring can be determined by measuring the time for the scattered light to return. Therefore, integrating structures and optical fiber makes it possible to continuously measure the strain generated in structures.

5.3.2 Overview of tunnel monitoring system[9]

NTT has developed and started introduction of a system for constant remote monitoring of the strain produced in each section when cracking or other degradation occurs. This system uses optic fiber cables fixed at set intervals to the inner walls of communication tunnels as strain sensors. Fig.10 shows the system configuration, and Table 2 gives the performance. Tunnels within a radius of approximately 10 km can be monitored by a single B-OTDR using optical switches, and cracking on the concrete surface can be detected in 0.1 mm units for a fiber fixing interval of 2 m. This system makes it possible to quickly determine the presence of degraded locations after a major earthquake, and also monitors concrete cracking and peeling due to superannuation and other factors during normal periods. This is thought to help reduce maintenance costs by enabling quick detection and repair.

5.3.3 Development of Optical Fiber Sensing Technology to a Wide-area Disaster Monitoring

System

In addition to monitoring tunnel degradation, NTT is also working to apply fiber optic sensing technology to other R&D projects such as monitoring road escarpment collapse and river embankment collapse. B-OTDR fiber optic sensing features the ability to continuously measure the longitudinal direction for long distances, and development to applications such as monitoring changes in large structures that cover a wide area and ground conditions can be expected in the future.

6. SEISMIC COUNTERMEASURES FOR FIELD FACILITIES

The Hyogo-ken Nanbu Earthquake also caused great damage to telecommunications facilities. Comparing communication cable damage conditions for underground and aerial facilities shows a damage ratio of 1 to 9 at the service level and 1 to 30 at the facility level. These figures confirmed once again that burying communication cables is an effective means of ensuring communications reliability.
However, weak points were also confirmed such as the connections between different structural systems, so technology was developed and introduced to improve the seismic performance of these portions.[10] Fig.11 shows an overview of these technologies. Priority issues were the three locations of expandable joints for open-cut tunnels, manhole ducts, and building lead-in portions. In addition, cracking and protrusion also occurred at the connections between shield tunnels and pits due to the lack of reinforcing bars, so expandable joints with superior waterproof performance were recently developed.

6.1 Flexible Tunnel Joints

The Hyogo-ken Nanbu Earthquake caused no damage whatsoever to cables housed in tunnels, indicating that the tunnels fulfilled their intended function to protect the cables. However, of the expandable joints of open-cut tunnels installed in the liquefied ground, grade differences of up to 18 cm in both the vertical and horizontal planes occurred at the connections between the tunnels and buildings or pits, resulting in leakage and flooding. Therefore, flexible joints were developed as seismic countermeasures for the joints of open-cut tunnels in ground subject to liquefaction. Workability was improved to allow execution with as little movement of cables as possible, and these flexible joints have been installed in 130 locations thus far. In addition, cracking and leakage were also found in three locations where shield tunnels connect to pits, so joints capable of withstanding water pressure up to 0.7 MPa and having expandable performance of ±10 cm in the direction of the tunnel axis were also developed.[11] (Photo. 1)

6.2 SFRC Manhole Ducts

Manhole ducts are the connection points between the different structural systems of manholes and conduits, so ground deformation and other factors during earthquakes cause relative displacement between the two, applying large force to these portions. In areas with significant damage, there were cases where the damage did not stop at cracking, and concrete lumps also peeled away and damaged the communication cables. Therefore, steel fiber reinforced concrete (SFRC) was adopted as a method of providing the duct concrete with sufficient load bearing strength after cracking occurs.

6.3 Flexible Building Access Conduits

When ground subsidence and other factors during earthquakes caused comparatively large relative displacement between hand holes and customer buildings, the building access conduits were unable to absorb this variation and suffered damage such as conduit separation and breakage. As a countermeasure, a flexible joint structure capable of absorbing large displacement at the building end and joint portions was adopted.

7. CONCLUSION

Based on the experience of the Hyogo-ken Nanbu Earthquake and in addition to the various countermeasures for large-scale disasters that have been adopted thus far, NTT is pursuing new countermeasures aimed at realizing disaster-proof communications services. As the importance of data communications increases in the future, NTT intends to construct even more reliable networks and develop various systems in order to fulfill its social obligations in times of emergency.

REFERENCES:

1)Honda, et al.: Telecommunication Facilities, Damage and Restoration of Lifeline Facilities, Hanshin-Awaji Great Earthquake Disaster Investigation Report vol.9pp.467-505、1997(in Japanese)

2)Fujihashi , Komatsu,: Real-time Disaster Information Systems Related to Telecommunication, Proceedings of 2nd Real-time Earthquake Disaster Prevention Symposium, JSCE, pp.135-142,2000(in Japanese)

3)Fujihashi,Shigeta : Systems related to disaster countermeasure in NTT,UJNR Earthquake information system workshop,2000

4)Hashimoto, et al.: Disaster Emergency Message Dial Starts Operation, Journal of NTT Technology, 1999, Vol.10 No.3 (in Japanese)

5)Nakagawa et al.,: Disaster Measure Support Systems Using Common Map Information Database, Journal of NTT Technology,1999 ,Vol.11 No3(in Japanese)

6) Honda et al.: Development of Earthquake-proof Performance Evaluation Application for Underground Telecommunication Conduits、3rd China-Japan-U.S. Lifeline Earthquake Engineering Symposium、1998

7)Kurashima, *et al* :Optical fiber sensor for distributed strain measurement in concrete structures,19th Meeting on Lightwave Sensing Technology,1997

8) NTT News Release, Sep.2001,
URL:http://www.ntt.co.jp/news/news01e/0109/010920.html

9)Takatsuka, Fujihashi, :Telephone Tunnel Monitoring System Using Fiber Optic Sensing Technology,56th AnnualConerence,JSCE,2001(in Japanese)

10)Honda *et al.* :Aseismic Countermeasure Technologies for Outside Telecommunication Facilities Implemented Following the 1995 Hyogo-ken Nanbu Earthquake、Draft Proceedings of the 7th US-Japan Workshop on Earthquake Disaster Prevention for Lifeline Systems、1997

11)Okutsu,Fujihashi, :Study of Flexible Joints installed at the Connections between Shield tunnels and Pits, 57th Annual Conference,JSCE,2002(in Japanese)

Table 1 Contents Investigated by the Committee for Severe Metropolitan Disaster Countermeasures and Disaster Prevention Related Systems.

ITEM	CONTENT	SYSTEM
Securing and control of telecommunication resource	○Securing of communication resource by destruction prevention and up-grading the reliability of communication equipment. ○Reinforcement of network control function. ○Destruction prevention in network and reinforcement of control function	
Allotment and distribution of telecommunication resource	○Allotment, distribution and the operation of telecommunication resource when crowded or destructed.	◆ Disaster Emergency Message Dial
Disaster area Information network	○Construction of a new information circulation mechanism in disaster area, which uses the ISDN line, personal computer, LAN, etc..	
Crisis-management/ restoration formation	○Maintenance of crisis-management system. ○Quick ascertainment of damaged area within the access network.	◆ Disaster Information System ◆ Maintenance Information NW ◆ Access System Underground Routes Seismic Performance Evaluation AP ◆ Access System Damage Condition Understanding System ◆ Shared Map Information DB ◆ Fiber Optic Sensing Technology

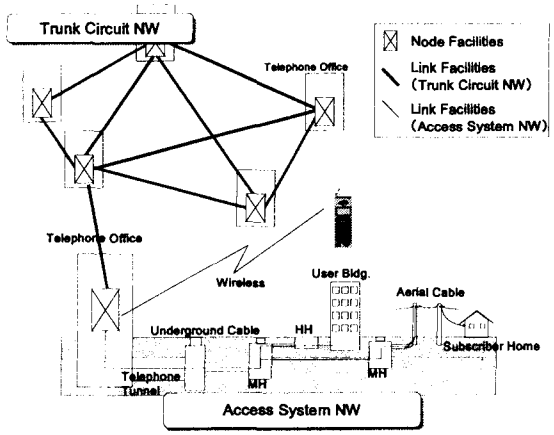

Fig. 1 Telecommunications Facility Configuration Overview

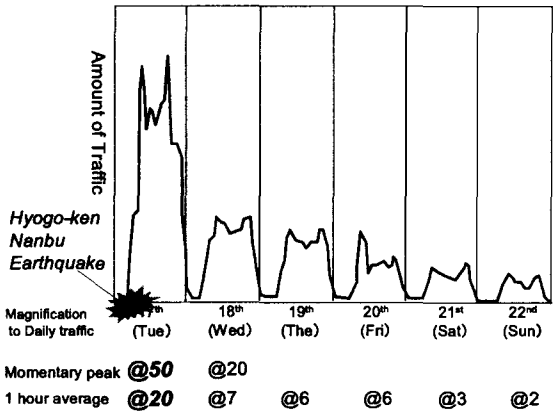

Fig. 2 Communications Congestion Immediately Following the Hyogo-ken Nanbu Earthquake

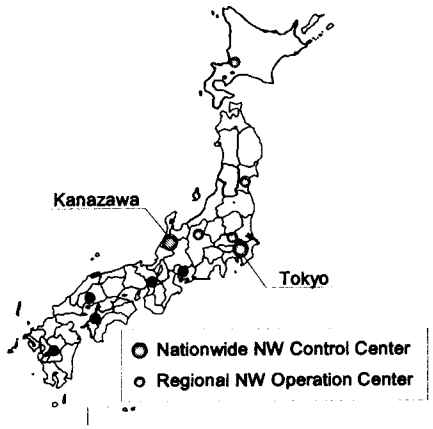

Fig. 3 NTT Network Monitoring and Operation System

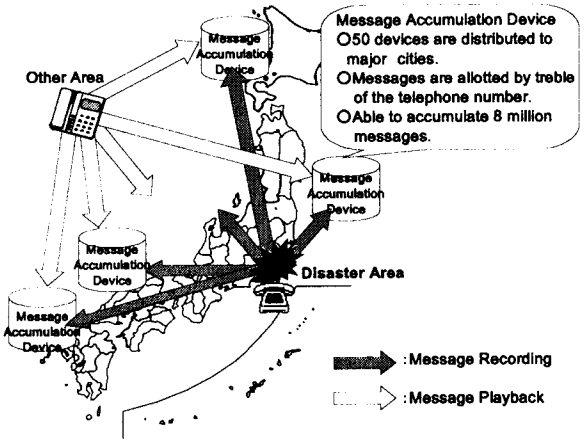

Fig. 4 Overview of Disaster Emergency Message Dial

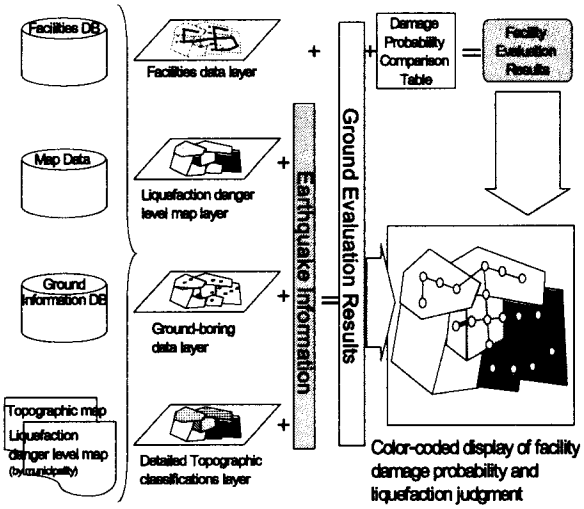

Fig. 5 Image of Application for Evaluating the Seismic Performance of Access System Underground Routes

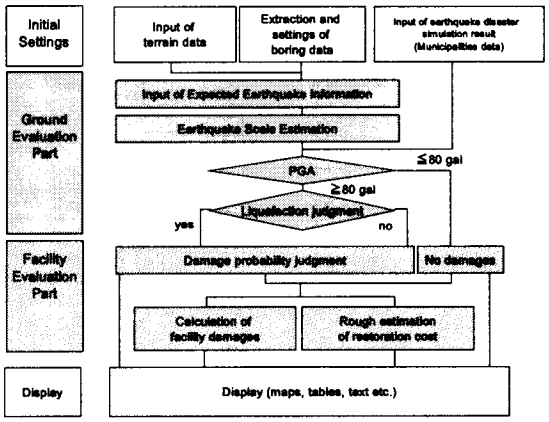

Fig. 6 General Evaluation Flow of Seismic Performance Evaluation AP

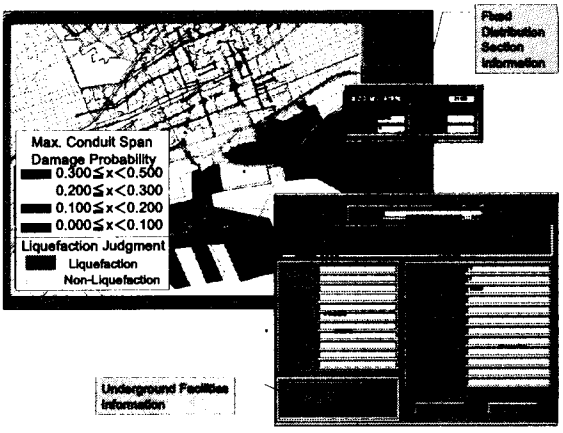

Fig. 7 Image of Evaluation Results Window Display

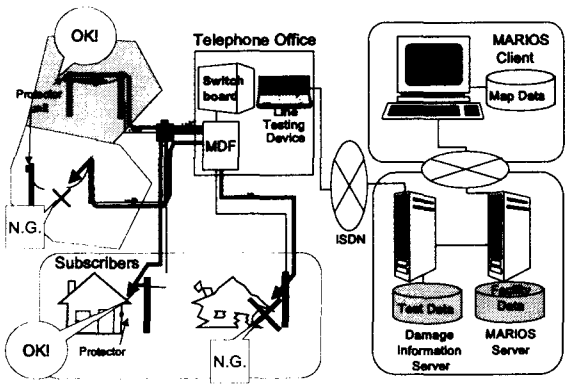

Fig. 8 Overview of System for Understanding Access System Damage Conditions

Table 2 Tunnel Monitoring System Performances

ITEM	System using B-OTDR	Present Systems using Electric Sensors
Measurement Object	Measurement of continuous section	Measurement at point
Measurement Distance	Up to 10km	Up to Several 100m
Strain Measurement Accuracy	50 μ Ability to detect crack of 0.1mm within 2m section	few μ
Electric Power Supply	Unnecessary. Thunder countermeasures are unnecessary.	Necessary for each sensor. Require thunder countermeasures.
Sensor Wiring/ Distribution	Single optical fiber. Regardless of measurement point.	Each sensor needs leading line. Becomes complex as measurement point increases.

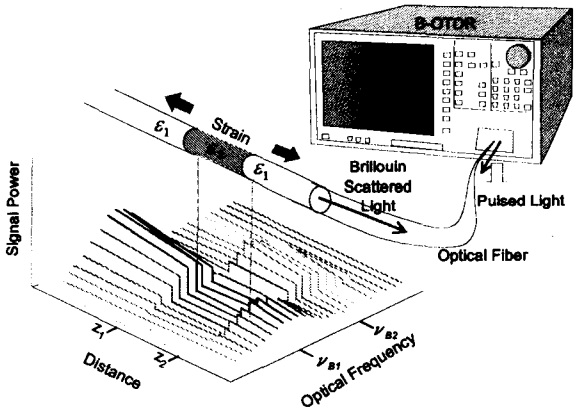

Fig. 9 Principle of Fiber Optic Strain Measurement Using the B-OTDR Method

Photo 1 Flexible Joints Installed at the Connections between Shield Tunnels and Pits

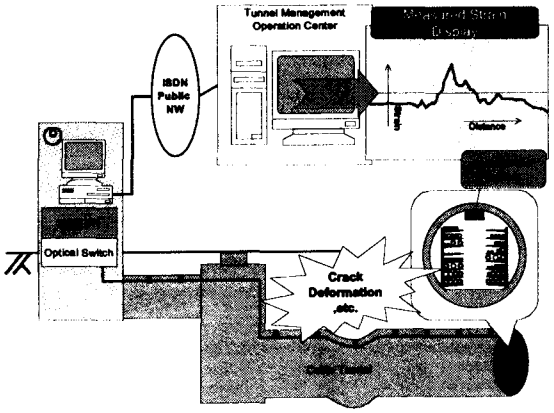

Fig.10 Tunnel Monitoring System Configuration

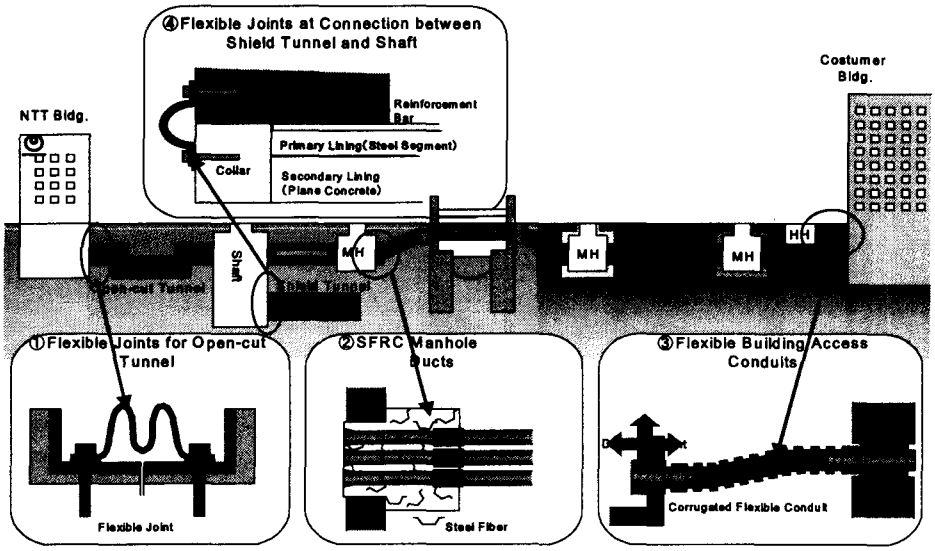

Fig.11 Overview of Seismic Countermeasures for Underground Structures Following the Hyogo-ken Nanbu Earthquake

SPECIAL THEME 3

MANAGEMENT OF INFRASTRUCTURE SYSTEMS

Management of Infrastructure Facilities as Disaster Protection

by

Tadayuki Tazaki[1],Takeo Nakajima[2], Kazuhiro Nishikawa[3]

ABSTRACT

NILIM was established in April, 2001 following the reform of the central government.
NILIM's organization and research policy was introduced. Its three comprehensive research centers characterize NILIM.
This paper concludes that discussing subjects, such as Management of infrastructure facilities to ensure the function as disaster protection, Disaster information technology and disaster mitigation, Application of ITS technologies as powerful tools for mitigating disaster, will be an important role for the UJNR joint panel meeting in the 21st century.

KEYWORDS : NILIM
Technological Policy
Management of infrastructure
Disaster Information
Application of ITS technology

1. INTRODUCTION OF NILIM

Japanese central government was restructured as of January 6, 2001. The number of ministries was drastically reduced to one cabinet office and 12 ministries. The Ministry of Land, Infrastructure and Transport, or "MLIT", was formed as a combination of the functions of these four ministries and agencies.

There were three research institutes relevant to construction in MLIT. These institutes were separated from the ministry and in principle transferred into Independent Administrative Institutions.
The functions of these three original institutes were taken over by these new institutions. Each of the three original institutes functioned to support the headquarters to make technological policies. NILIM has been established to take over half of researchers and this function.

When we are asked to explain the differences between NILIM and the three agencies. We reply that NILIM is for management, and considers the infrastructure requirements, whereas agencies are for technologies, and consider the performance of facilities.
For this purpose, NILIM was established in April, 2001 as the only national research institute in the field of infrastructure to support the headquarters of MLIT.

The figure shows the organization of NILIM. There are ten research departments and three comprehensive research centers. It could be said that these three comprehensive research centers characterize NILIM. They are organized based on demand-oriented subjects. They are engaged in cross sectional research activities.

They are the Research Center for Land and Construction Management, Research Center for Advanced Information Technology, and Research Center for Disaster Risk Management. The last one deals with the subjects closest to this joint panel, but the others also have relevant studies.

1) Director General, National Institute for Land and Infrastructure Management (NILIM), Ministry of Land, Infrastructure and Transport (MLIT)
2)Director of Planning and Research Administration Department, NILIM, MLIT
3)Research Coordinator for Evaluation, NILIM, MLIT

2. THE RESEARCH POLICY OF NILIM

The first four months was spent drafting the Research Policy of NILIM, because NILIM gathered researchers from three different institutes and had to show the direction in which to proceed together. This was a very important and basic process at the beginning of the new organization management.

The research policy was settled on July 30, 2001, and consists of Mission, Research Subjects and Research Activities.

The Mission says "We conduct research and development to contribute to technological policy-making that enhances the satisfaction of citizens as the end-users of infrastructures".
I would like to emphasize the necessity of taking into account the demand-side point of view in the research activities.

The goals are stated as:
- Conservation and creation of desirable national land
- Guarantee of safe and secure life
- Enhancement of quality of life
- Vitalization of civil society and economy

To achieve the goals, seven principal subjects are selected. The first four subjects are relevant to the goals of MLIT.

1. Creation of sustainable society with a beautiful national land
2. Building of a safe and reliable national land
3. Enhancement of quality of life
4. Vitalization of civil society and economy

We believe we can construct an image of Japan in the 21st century through research on these four subjects.

The last three subjects are relevant to the procedures for MLIT's activities.

5. Improvement of construction management for public works
6. Establishment of foundation for advanced information society
7. Contribution to international society

Under these seven principal subjects, sixteen technological research subjects are provided in the policy.

Here are some examples:
- Asset management
- Disaster information technology
- Intelligent transportation system
- Public involvement

The first three subjects will be mentioned later. The last one, study on public involvement, is now indispensable regarding public works procedures, of course, including disaster prevention and mitigation. Nowadays it is impossible to carry out public works without the participation of citizens.

3. ASSET MANAGEMENT

Introducing the research subjects along with the three research centers will help to understand the institute more deeply and what kind of subjects we propose dealing with at the joint panel meeting.

The first one is the Research center for land and construction management.
There are three subjects.
The first one is "Historical study on national land and infrastructure". It is important and useful to study the past to find out the future direction.

The second one is "Construction management for public works". Effective implementation of public works might be our permanent task.

The third one is "Asset management". We often use the term "Stock Management" instead.

Asset management is very important from various aspects. These include: dwindling availability of disposal sites and increasing CO2 emissions regarding the global environment, both of which are exacerbated by the renewal of infrastructure. Furthermore, massive demand for renewal will place a big burden on the decreasing younger generation. It is therefore essential to prolong the life of infrastructure with efficient management.

Aging and deterioration are inevitable for every infrastructure facility, but this also reduces the capacity against natural disasters.
To overcome this and to create a sustainable society, strategic management as a combination of inspection, diagnosis, rating, repair, strengthening and replacement technologies are necessary.

4. DISASTER INFORMATION TECHNOLOGY AND DISASTER MITIGATION

The next is the Research center for disaster risk management.
Its major subjects recently are Disaster information technology and disaster mitigation.
Research on disaster prevention is now spreading to include the use of information from satellites.

Hazard maps for various kinds of disaster and damage prediction technology provide valuable information.
Gathering damage information by mobile tools, integrating them with GIS, and distributing necessary information to people are extremely effective disaster mitigation methods.

5. APPLICATION OF ITS TECHNOLOGIES

The last one is the Research center for advanced information technology.

Its main research concerns ITS (Intelligent transport system), which seems to have little to do with disaster prevention or mitigation. But the application of developed technologies using new information technologies can be powerful tools for mitigating disaster.
For example, a car navigation system, already installed in over 10% of automobiles in Japan, can guide drivers along detour routes when they come across major damage caused by natural disaster. And ITS for pedestrians, developed originally for handicapped people, can inform strangers by cellular phone of where to evacuate in case of emergency.

6. CONCLUSIONS

UJNR has a tremendous track record from the 20th century. Many new technologies have been adapted in the design codes in both countries through the UJNR research-and-development programs in the field of earthquake disaster prevention and wind effect technology. The 21st century has just started, and we must create a sustainable society for future generations.

There are three subjects here that I have already mentioned. Discussing these kinds of subject will be an important role for the UJNR joint panel meeting in the 21st century. We are standing at the crossroads of the new millennium. We must define a suitable direction for UJNR activities and exchange the latest information each other.

Management of Infrastructure Facilities to Ensure the Function as Disaster Protection

Tadayuki TAZAKI, Takeo NAKAJIMA
Kazuhiro NISHIKAWA
National Institute for Land and Infrastructure Management

Central Government Reform

1 Office and **22** Ministries

Reformed ↓ *January 6, 2001*

1 Cabinet Office and **12** Ministries

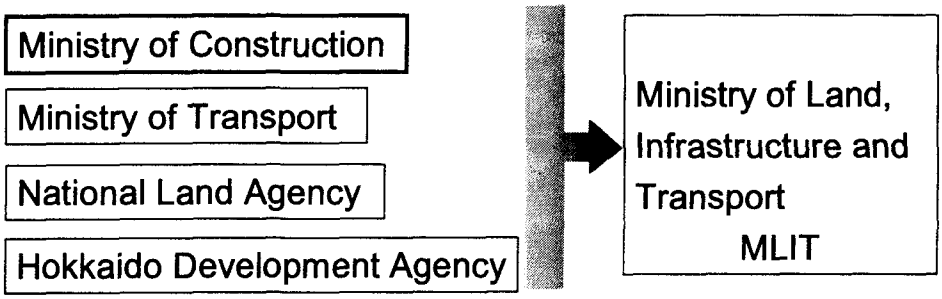

Independent Administrative Institution?

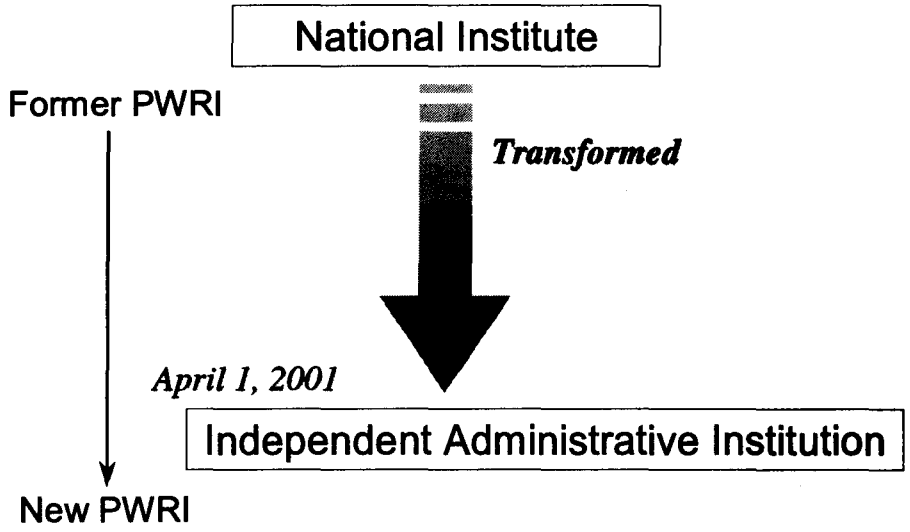

NILIM
&
Independent Administrative Institution

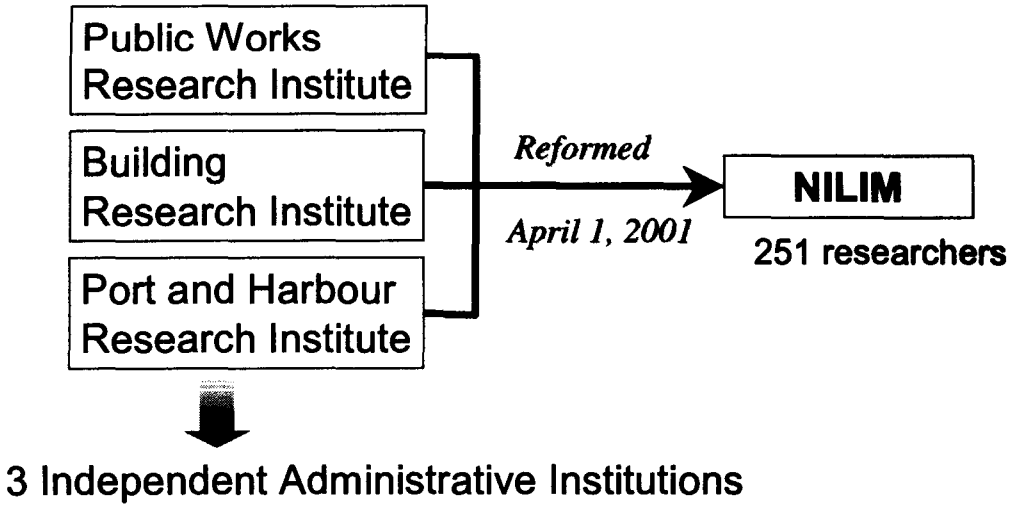

What's the difference?

NILIM	***vs.***	***IAIs***
Management		*Technology*
Infrastructure requirements		*Performance of facilities*

Establishment of NILIM

The only national institute in the field of Land and Infrastructure Management

April 1, 2001

Organization

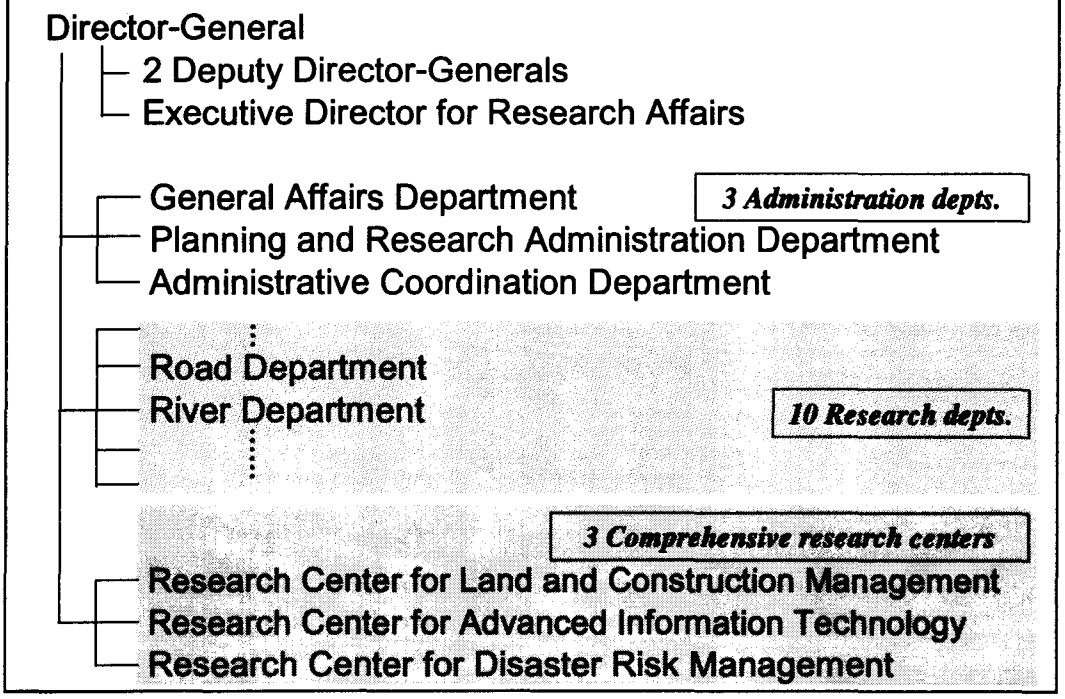

Three Research Centers

Research Center for
Land and Construction Management

Research Center for
Advanced Information Technology

Research Center for
Disaster Risk Management

Research Policy of NILIM

July 30, 2001

Mission

Research Subjects

Research Activities

Mission

"We conduct R&D to contribute to technological policy-making that enhances the satisfaction of citizens as the end-users of infrastructure."

Goals

- ✓*Conservation and creation of desirable national land*
- ✓*Guarantee of safe and secure life*
- ✓*Enhancement of quality of life*
- ✓*Vitalization of civil society and economy*

Seven principal subjects

1. *Creation of sustainable society with a beautiful national land*
2. *Building of a safe and reliable national land*
3. *Enhancement of quality of life*
4. *Vitalization of civil society and economy*

Seven principal subjects

(cont'd)

5. ***Improvement of construction management for public works***
6. ***Establishment of foundation for advanced information society***
7. ***Contribution to international society***

Research subjects

(examples)

- ✓***Asset (stock) management***
- ✓***Disaster information technology***
- ✓***Intelligent Transport System***
- ✓***Public involvement***

Research Center for Land and Construction Management

- ✓Historical study on national land and infrastructure
- ✓Construction management for public works
- ✓**Asset (stock) management**
  (from "scrap & build" to "stock & renovation")

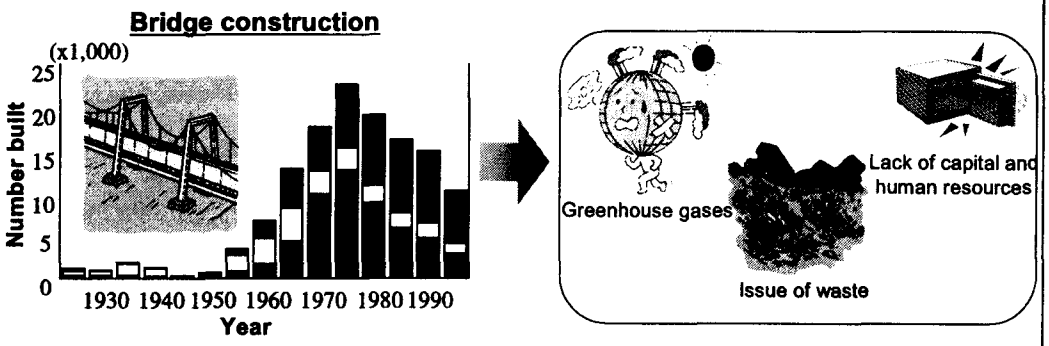

Stock Management to Ensure Disaster-Protection Function

Aging and Degradation
Inspection, Diagnosis, Repair, Rating
Strengthening, Replacement
of
Existing Facilities
Strategic Management Is Required !!

Research Center for Disaster Risk Management

✓Disaster information technology

✓Disaster mitigation

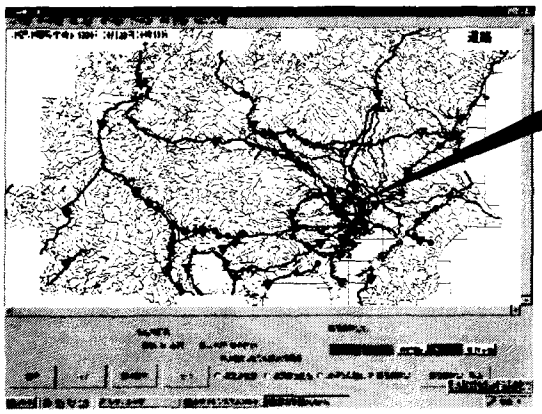

Earthquake damage prediction system

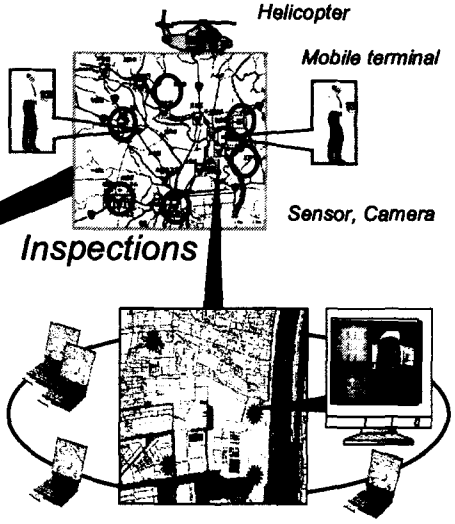

Disaster information technology and Disaster mitigation

- Hazard maps
- Damage prediction
- Information

  gathering by mobile tools

  integrating with GIS

  distributing to people

Research Center for Advanced Information Technology

✓*Promotion of intelligent technology in transportation*

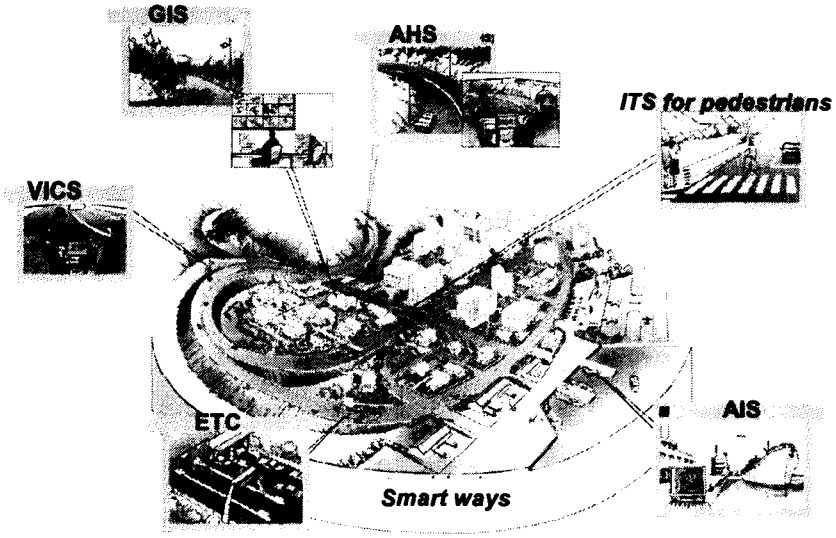

Application of ITS Technologies

Distribution of Disaster Information through

✓*Car Navigation Systems to guide along the detour route,*

✓*ITS for Pedestrians (cellular phone) for strangers to evacuate*

Conclusions

The roles of the Joint Meeting in the 21st century

- ✓*To renovate and make good use of existing infrastructures*
- ✓*To promote the disaster information system with IT such as GIS, GPS, mobile tools, etc.*
- ✓*To apply ITS technologies as disaster information tools*

Information Available

Please visit us at:

http://www.nilim.go.jp/

Information Systems for Infrastructure Management and Emergency Response

by

William E. Roper

ABSTRACT

Information systems and their application to infrastructure management for emergency response with particular focus on critical transportation infrastructure are addressed in this paper. The opportunities for information systems leveraging geospatial data sources are presented. Remote sensing imaging and non-imaging sources of information are explored. Coordination and sharing of in information is explored to improve the ability of multiple organizations to more effectively manage and respond to emergency situations. The use of geospatial information was only a part of the total recovery activity but did provide important assistance throughout the recovery operation. Samples of geospatial technologies used in the recovery are presented. These include 3-D visualization, thermal infrared imagery, LIDAR data systems, IKONOS one-meter panchromatic imagery, SPOT imagery and the use of digital aerial imagery. The general area of disaster response management is also addressed and the findings of various studies in this area are summarized. Recommendations for the use of information systems and geospatial sensors and products in the future for infrastructure management are presented.

KEYWORDS: Information systems, Critical transportation infrastructure protection, Geospatial information, IKONOS satellite data, Digital imagery, Data management, Disaster management, LIDAR, Infrared remote sensing, GIS mapping, Global Positioning System

[1]Professor and Chairman Civil and Environmental Engineering Department, Suite 643, Academic Center, George Washington University, Washington, DC, USA, 20052 wroper@seas.gwu.edu; phone 202 994-4901; fax 202 994-0127; http://www.seas.gwu.edu;

1.0 INTRODUCTION

Infrastructure managers at all levels face unprecedented challenges today. Increasing demands are being placed on agencies to preserve the existing infrastructure system and to take on new missions of improved system safety and security. A variety of advanced technologies are available to enhance planning, designing, managing, operating, and maintaining all aspects of the nations public and private facilities. The

national transportation system is one example of a major part of our infrastructure system and a critical asset for national growth and development. Aerial and satellite remote sensing represents one area of rapid development that can be leveraged to address these challenges. These technologies have significant and unique potential for application to a number of cross cutting transportation security issues. A summary of how some of these information systems were used in the recovery effort in New York City will be presented and assessed.

2. 0 INFORMATION MANAGEMENT CONSIDERATIONS FOR EMERGENCIES

It is clear that despite excellent efforts by many groups the approach to providing information for disaster management is not often effectively utilizing a wealth of data that resides, with various organizations. This existing information and technology could provide disaster mangers important information products that could save lives, reduce damage to property, and lessen the environmental impacts of disasters. The current situation is characterized by numerous shortcomings that inhibit optimal decision making for disaster management. The inability to access information and the lack of standardization, coordination, and communication are all obstacles that need to be overcome.

2.1 Information Management Goals

Considerable effort has been expended throughout the Disaster Management community to articulate issues and to characterize the dynamics and the inter-relationships that needs to be accommodated in a viable information management strategy. An important guide for this effort is found in the recommendations made by the Board On Natural Disasters (BOND) in their report to the National Research Council. The BOND's primary goals as articulated in its cha were to:

1. Improve decision making before, during, and after emergencies through better access to and quality of data and information
2. Identify users and their needs
3. Provide information products specifically designed to meet users' need
4. Promote efficiency and cost effectiveness
5. Stimulate and facilitate mitigation

These are important components in any workable framework for comprehensive disaster management. However, the focus here is directed towards derived products, procedure and protocol. It is important that the process develop baseline products and implement solutions that reflect the complex fabric of the disaster management community. This work is done at a lower, more formative level in the information management life cycle and in fact forms the basis for the production of the products referred to by the BOND. As noted above the assessment process will work to identify the constituent components associated with specific disaster events and scenarios. The constituent components will then become the basis for technology specifications and the delivery of capabilities that encompass the products identified by the BOND.[1]

2.2 Data Management Considerations

This section provides assumptions based on information and conclusions that have emerged from recent studies in disaster management community itself. These assumptions certainly do not constitute and exhaustive set of parameters. Rather, they provide a point of departure and a set of "operating hypotheses" that can be used to help frame discussion and consideration of needs and requirements. Available Information and capacity is not uniform, consistent and standardized for disaster managers. Large cities may have invested millions of dollars in their information systems, while smaller municipalities may be operating with one personal computer. Disasters will constantly crosscut established boundaries. A fundamental problem in dealing with disasters is that they do not respect boundaries that include organizational, political, geographic, professional, topical, or sociological consideration.[2]

Disasters will often overwhelm mechanisms for coordination and communication. In addition, the mechanisms to bring data and information to decision makers are uncoordinated. Information is often produced from disparate sources and transmitted in whatever format the provider prefers, requiring significant effort to compile it into a form that provides a coherent picture or even thwarting integration altogether. Data standards are often inconsistent, and, even more dangerous; users are sometimes unaware of the limitations and uncertainties in data or are presented with conflicting interpretations of data without the means to assess the reliability of the sources. All of these issues reduce the efficacy of the decision-making process. The problem is compounded because information delivery systems in many cases become overloaded during crises. For instance, in 1996 a moderate (magnitude 4.7) earthquake in San Jose, California, led to more than a million attempted hits in less than one day on the U.S. Geological Survey's World Wide Web earthquake information server.[3] Most of those attempts were

[1] NRC Report, Information Infrastructure for Managing Natural Disasters, Board on Natural Disasters, National Academies Press, 1998

[2] Tobin, Graham A., and Burrell E. Montz, *Natural Hazards: Explanation and Integration*, New York, NY: The Guilford Press, 1997

[3] Burton, Ian, Robert W. Kates, and Gilbert F. White, *The Environment as Hazard, 2d Edition*, New York, NY: The Guilford Press, 1993

unsuccessful, including those by emergency managers trying to access data and information to aid in the formulation of a response plan.

3.0 INFORMATION MANAGEMENT PROCESS ISSUES

Disaster management is an exercise in logistics and information processing and distribution. To effectively undertake these tasks requires a good understanding of disaster information requirements and the characteristics associated with disaster events knowing that each event is uniquely different. Disasters come in different sizes, have different behavior and can be categorized on the basis of their impact on natural resources, agriculture, communities etc. They can also be discriminated and classified along a number of dimensions including impact, severity, duration, geographic setting and advance warning (NAPA 1998). In order to develop the Information Technology architecture for case scenarios application it is essential to understand the disaster event from the perspective of those responsible for assimilating the data. The effective use of this information for producing operational plans to deal with the disaster event and its aftermath is critical.

3.1 Consideration of Infrastructure Information Phase Management

For instance, it is important to appreciate that the four basic phases of disaster management may actually manifest themselves in different ways depending on the nature of the disaster. The mitigation phase is essentially a continuous process of preparation, analysis of performance and subsequent modification and refinement. As a result it will likely exhibit the smallest amount of variance. However, the other phases (preparedness, response and recovery) will likely have significantly different attributes depending on the nature of the event. For example consider the difference in the preparedness phase that would be associated with major seasonal flooding along the Mississippi or the Missouri Rivers, the Chaparral fires along the Pacific Coast, a Tsunami that impacts much of the Pacific Rim and an earthquake such as Northridge or Loma Prieta. In each case the geographic coverage and the amount of time for planning and staging is very different. As a result, many of the other systemic aspects of the disaster management initiative will be different as well.

An event warning which impacts the manner in which the preparedness phase is managed also has implications and consequences for the recovery phase (e.g. In the case of the Loma Prieta earthquake the emergency response resources were directed to the bay area despite the fact that Santa Cruz and Watsonville had more significant damage). Partially as a result of this California is building the Tri-Net seismic sensing network to measure shake and model damage in order to make more informed decisions regarding staging recovery resources.

3.2 Infrastructure Disaster Management Communities

The disaster management is extremely heterogeneous. In order to develop effective systemic solutions to the needs of this community any framework must address the need to effectively and efficiently share information across institutional boundaries within and between the groups that make up this community. In essence an interface must be specified at each boundary that separates levels in an agency or at the juncture between different agencies or between different sectors. These interfaces each have at least three components: 1) technical, 2) institutional and 3) institutional administrative. The importance of these interfaces is also proportional to the difficulty of implementing them in an automated context. For instance, the lightest weight interfaces should be between levels within the same entity within a single sector. In contrast the heaviest interfaces would be those that attempt to span sectors.[4]

A number of these communities have made significant institutional investments in the construction of foundation data products that feed modeling, analysis and decision support in a range of contexts. Not surprisingly the situation

[4] NRC Report, Information Infrastructure for Managing Natural Disasters, Board on Natural Disasters, National Academies Press, 1998

in the disaster management community in regard to data parallels spatial data issues across the federal government and throughout state and local government and the private sector. The issue of data sharing by the disaster management community was also addressed by the BOND. Their findings recognized that despite the importance of significant databases, their utility is impaired by a host of problems deriving from incompatible formats, inconsistent geographic reference systems, conflicting standards, and other human-caused factors. Many of these problems could be resolved and the value and utility of the databases for disaster decision making greatly enhanced through improved organizational and technological coordination with only an incremental increase in cost.[5] This is clearly in the public interest to accomplish this.

Disaster management scales for international agencies and governments to the individual. However, a very significant level of responsibility is vested at the local level. For instance, it is the on the ground officials, many of whom are local, that ultimately play the role of first responders (e.g. police, fire, medical and public works) and who also manage many of the recovery operations. To be effective in this context protocols must define communications, database structure, data formatting, hardware and software requirements, networking, quality control, and other issues needed to assure the linkage will improve decision making before, during, and after emergencies through improved access to quality information. In addition, such a linkage will provide information products that are specifically designed to meet the needs of users

3.3 Common Characteristics of Disasters

Disaster management is not a linear process that can be documented easily in a flow chart with a readily apparent beginning and absolute end point. Rather, it is a cyclical process of approximation, response and re-calibration that involves many different actors whose roles in relation to one another are likely to change based on circumstances and the stage in the process. The one constant evident in the process is the chaos that drives the system. Another absolute is that the effective, efficient application of information technologies and products has the capacity to improve the system in a number of ways that will combine to save lives, mitigate overall damage, conserve resources and ameliorate human suffering.

To develop effective architectures and technologies that meet the needs of the disaster management community there must be a precise understanding of the disaster management life-cycle (Mitigation, Preparedness, Response and Recovery), the Information Communities that combine to define the disaster management community and the information processing requirements associated with the cycle of data development, dissemination, analysis and review. In addition, and perhaps more importantly, there must be a precise understanding of the dynamics between these components and the "interfaces" that these dynamics imply. Only with such an understanding can we effectively model the process and derive technology solutions that map well into the business model of disaster management.[6]

3.4 Data and Information Processing Requirements

Data needs, the characteristics of data and the ability of data to contribute to analysis, response and recovery is well understood. The basic attributes of information that are considered most important by this community include:

1. Timeliness: delivery of data and information in time to drive decision making
2. Consistency: delivery of data and information in a consistent, uniform manner
3. Understandability: delivery of data and information in a manner that is appropriate and understandable in the target community

[5] NAPA Report, *Geographic Information for the 21st Century: Building a Strategy for the Nation*, National Academy of Public Administration Press, 1998

[6] Disaster Information Task Force Report, Harnessing Information and Technology for Disaster Management, Global Disaster Information Network, 1997

4. Accuracy: precision in measurement and observation
5. Flexibility: adaptability to multiple situations

These information attributes have evolved over time within the disaster management community representing the viewpoint of a range of providers, users and consumers scaled from the local to national level. In this regard the communities involved transcend boundaries between recognized sectors at each of these levels (private, public, not-for-profit, NGO etc.).

4.0 TRANSPORTATION INFRASTRUCTURE INFORMATION SYSTEMS

The nation's transportation networks function as the lifelines of commerce, security, and recreation. They are also vulnerable to attack and severe disruption. As officials have discovered since September 11, protecting and preserving the extensive U.S. transportation networks against terrorist attacks remains a daunting task. Fortunately, today's powerful geospatial tools, especially remote sensing, positioning, navigation, and timing (PNT), and geographic information systems (GIS), can assist in this crucial effort.

4.1 Overview of America's Transportation Infrastructure

America's transportation infrastructure is a reflection of the nation's economic vitality, which in turn is predicated on maintaining stable economic, political, and social environments. Under most circumstances the nation's transportation system works smoothly and efficiently; but, as President Eisenhower recognized in authorizing the Interstate Highway system during the Cold War 1950s, it is vulnerable to attack from unexpected quarters. Although the U.S. public had become accustomed to peaceful stability within U.S. borders, the appalling events of September 11, 2001, require a shift in thinking. While the transportation system cannot be re-engineered in its entirety to cope with this new operational environment, a variety of coping strategies can aid in protecting its many modalities and components. Among these is a higher use of aerial and satellite imagery (and collateral sensor data from non-imaging systems), to obtain intelligence for situations that develop rapidly and which demand real-time decision-making.

The transportation system is extensive, complex and critical to maintaining the U.S. economy (table 1). The Administration's report, *Securing the Homeland, Strengthening the Nation*[7], underscores the urgency in strengthening transportation security. The proposed 2003 White House budget includes not only the establishment of a Transportation Security Administration within the Department of Transportation, but requests $4.8 billion "...to fulfill the mandates established by the [Aviation and Transportation Security Act of 2001]."

4.2 Potential of Image & Sensor Data for Improving Lifeline Security

Remote sensing technologies, together with other geospatial technologies such as GIS and PNT systems, have a significant role to play in the improvement of the Nation's transportation security and critical infrastructure protection. Remote sensing from space combines a broad synoptic view with the ability to detect changes in surface features quickly and routinely. Remote sensing from aircraft provides the ability to examine areas in great detail from below the clouds, and ground-based systems make possible the close-in observation of events in real time. Each of these spheres of remote sensing technology hold benefits and drawbacks for use in transportation, and in particular, for the security of the Nation's complex transportation networks.[8]

Examples of the use of remotely sensed data to support transportation security include the ability to:

[7] See http://www.whitehouse.gov/homeland/) or http://whitehouse.gov/homeland_security_book.html.

[8] Roper, William, *Geospatial Technology Support to the Nation's Navigation System*, Transportation Research Board, National Research Council, Washington, DC, January 1999

- Develop accurate digital terrain models and 3-D surface features as a means for modeling landforms along rights-of-way;
- Visualize terrain from different perspectives, with the potential for developing threat cones and viewsheds;
- Classify vegetation types along transportation lifelines as a possible deterrent to concealment ;
- Detect, classify, and analyze temporal and spatial changes in surface features;
- Identify facilities where topography or identifiable hazards (e.g., nuclear, chemical, fuel facilities), place communities at risk;
- Analyze environmental factors quickly and effectively;
- Merge real-time sensor output (video, bio-chemical sensors) with archived geospatial data;
- Identify, characterize, and analyze a wide variety of risks to transportation networks through a gradual program of gathering image intelligence along rights-of-way;
- Create detailed maps of an area that has suffered attack to assist in response.

The September 11 attacks have forced a reevaluation, not only of the security aspects of U.S. critical transportation infrastructure, but also of the nation's institutional policies toward access to and use of information. For example, current policies governing the collection, use, and sharing of critical geospatial information inhibit the most efficient use of these data in developing mitigation procedures and in responding to terrorist threats and actions. On the one hand, the potential for misuse of critical information has caused federal and state agencies to restrict access to information by removing it from the Internet and other public venues. On the other, combating the threat of terrorism and responding to future attacks will require more effective sharing and use of geospatial data and information. It will also necessitate within the geospatial community continued improvement of analytical geospatial methods and software directed at improving transportation security.

Accordingly, the nation needs new institutional policies to support coordinated efforts in support of improved transportation security and coordinated emergency response. The need for interoperability of communications systems is widely understood;[9] the need for interoperability of geospatial information is less well understood. Workshop participants recognized that meaningful progress toward preparing the nation to prevent and respond to attacks on elements of the nation's transportation networks required the coordinated effort of agencies across the federal government, among federal, state and local governments, as well as among government and private sector geospatial data providers and analysts. For example, it is little recognized by the general public that in addition to destroying two large buildings and killing nearly 3000 people, the attacks on the World Trade Center severely affected New York's transportation lifelines, making rapid response by emergency workers especially difficult. Throughout the cleanup process, transportation routings changed daily and even hourly, making timely map updates necessary. Although the agencies and individuals who responded to the challenges of saving lives and cleaning up after the attacks accomplished wonders despite having no advanced warning and working in extremely dangerous conditions, the lack of established coordination plans slowed their efforts. In effect the teams "made do" with what they could cobble together in terms of base data and imagery acquired by daily aircraft over flights, which commenced on September 14, three full days after the attacks.[10] Fortunately, thanks to the many individuals and organizations willing to help, they were eventually able to provide coordinated mapping, GPS, and imagery information in a rapid fashion.[11] This coordination was more a reflection of individuals committed to dealing with a massive problem,

---

[9] Statement of Bruce Baughman Office of National Preparedness, Federal Emergency Management Agency, before the Committee on Transportation and Infrastructure, Subcommittee on Economic Development, Public Buildings, and Emergency Management, U.S. House of Representatives, April 11, 2002.

[10] Jerry Dobson, "How Will GIS Help Fight the War on Terrorism?" *GEOWorld: http://www.geoplace.com, November2001.*

[11] Bruce Cahan and Matt Ball, "GIS Ground Zero: Spatial Technology Bolsters World Trade Center Response and Recovery," *GEOWorld: http://www.geoplace.com, January 2002.*

than the result of prior planning by the responsible local, state, or federal agencies. These organizations could have put teams in place and worked more quickly and effectively if institutional policies of their various agencies had encouraged the sharing of information and responsibility for response.

The geospatial data and information developed for other uses can also support improvements in transportation security. One of the strengths of a geospatial information systems approach is that one comprehensive database for a region can support many different applications. For example, as several workshop participants noted, much of the information developed by state and local communities to support infrastructure planning can be used to mitigate the threat of terrorist attacks or to enhance the speed and effectiveness of emergency response teams in case of attack or natural disaster. However, to be fully useful in combating potential terrorist threats, the structure and content of geospatial databases, including remotely sensed imagery, will have to be reviewed for their applicability in improving transportation security. In some cases, the existing framework and transportation databases will need to be enhanced.

The need to improve critical infrastructure protection has created new requirements for remote sensing and GIS analysis. In order to reap the benefits of data and information from non-transportation sources, it will be necessary to develop analytical software designed especially for the security mission. Such software and methods need to be widely available to provide comparable analytical capabilities across the United States. New analytical methods in RS/GIS specifically devoted to the support of critical infrastructure protection could greatly strengthen the nation's ability to improve transportation security. Particular attention should be given to a significant, but limited number of critical transportation assets (e.g., pipelines, bridges, ports, inter-modal facilities), rather than attempting to develop functionalities that encompass everything.

Some remote sensing methods that have been developed for military applications may be transferable to civilian security use. However, civilian measures must consider economic, social, and legal aspects that are be less relevant in a purely military situation. The measures must be designed for high reliability. Needs include:

- New methodologies and research to identify, assess and monitor high value, highly vulnerable transportation facilities across the United States;
- New methods of analysis and use of sensor and imagery assets to assess vulnerabilities, monitor assets, and aid in post-event recovery. For example, sensitive non-imaging sensors that can detect chemical, explosive, or radioactive plumes could help in monitoring container cargo ships from aircraft or bridges under which all ships in a port must pass.

Remote sensing technologies could be a major asset in identifying and mitigating transportation security weaknesses throughout the United States. In the past, security has not been a primary consideration in transportation planning. The U.S. transportation system as it now exists possesses many vulnerabilities that could have been avoided with careful advanced planning. For example, in some cases, critical infrastructure elements have by chance been co-located with high-value, vulnerable facilities, such as petroleum refineries or power plants. Such co-location has been a matter of convenience or of a previous lack of concern about terrorist attack. Remote sensing technologies can in time assist in reducing some of these vulnerabilities. Over the longer term, the need for instituting extensive security measures can be reduced by preemptive planning of lifeline facilities to minimize the criticality of individual facilities to the network. The planning process should emphasize decentralization of facilities and redundancy of the functions of those facilities. In this way individual facilities, be they pipeline corridors or roadway conurbations, are reduced in their critical role in the network and their attractiveness as targets. Future planning and implementation of transportation lifeline facilities must have security as a primary consideration.

The United States needs to develop an accessible geospatial infrastructure corresponding to, and compatible with, the nation's transportation infrastructure. The resulting geospatial

information should reflect all elements of the transportation infrastructure, and include detailed information on location, structure, condition, and other attributes. This information should be broadly accessible to transportation and security professionals. Improving the interoperability of transportation geospatial databases should be a high level priority in the attempt to enhance U.S. transportation security. Currently, in attempting to use transportation databases, users often experience limitations on availability, integration, and use of geospatial data and technologies for transportation security. Workshop participants pointed out that the information regarding the nation's information infrastructure is widely dispersed in a variety of databases, in a multiplicity of formats and software. Hence, many of these databases are not readily interoperable, making the task of using them especially difficult in times of crisis.

In particular, there is a lack of suitably interoperable technical standards, both for data sharing and for the operation of hardware and software. Although the Federal Geographic Data Committee (FGDC) has established federal standards for preparing and sharing geographic data, which have done much to improve interoperability of geospatial databases on the federal level, much more needs to be done on the state and local level to reap the benefits in times of crisis. State and local databases often lack sufficient interoperability in emergency situations, whether caused by natural disasters, human error, or deliberately by terrorists. Yet, most emergency situations involving transportation systems, either actively or passively, will involve state and local agencies and jurisdictions. The FGDC has recommended several actions that, if accomplished, would sharply improve the nation's security. [12] If extended to transportation, these recommendations would under gird the U.S. transportation security.

4.3 Value of Remote Sensing for Critical Infrastructure Protection

[12] "Homeland Security and Geographic Information Systems," http://www.fgdc.gov/publications/homeland.html.

4.3.1 Imaging Sensors

Scalability: Literally hundreds of civil applications make use of remotely sensed imagery in a variety of analytical products. A multiplicity of image types has evolved to address specific applications, and many can also be used for transportation lifeline protection, if ingested and integrated into shareable databases. Imagery can be acquired across many scales and corrected geospatially to fit agency-specific map projections. For incident management, planners already have tools available to them for integrating coarse with fine resolution satellite views, and with more detailed high, medium, and low altitude aerial data sets from LiDAR and RADAR systems. The large number of demonstrated applications meeting industry and government standards should be systematically reviewed for their use in transportation lifeline security.

Spatial Relationships, Vulnerability, and Up-Dating: Urban planners have traditionally recognized the importance of tone, texture, size, shape, and spatial arrangement in analyzing landscape features. For transportation lifelines, most applications focused on right-of-way planning, engineering cut and fill measurements, feature identification, and land use classifications for map-making purposes. The imagery was generally archived or even destroyed after its immediate use was achieved. Where these archives can be retrieved, they represent a resource for measuring the rates and directions of lifeline infrastructure growth. These images also show the changing spatial relationships among urban features that might not be considered by planners until the post-recovery phase of an incident (for example, obstructions like fences between buildings and roads that would prevent rapid evacuations, or road designs that have changed from two-lanes to four-lanes with a median). Most important, time series imagery is scalable from the local level for which it was acquired, to smaller scales for which it will be required for incident management. In short, lifeline vulnerabilities develop over time and can only be efficiently catalogued, referenced, and

assessed by examining the history of imagery of an area.

Data Mining & Visualization: For the more sophisticated needs of the 21st Century, transportation planners should recognize that time-series digital images represent a data archive that can be used to answer questions not yet posed. They are essential for responding quickly and efficiently to an emergency. Today's technology allows image archives (also called image pools) to be highly compressed for digital storage, and for them to be queried constantly for phenomena that are "out of the ordinary." Data mining algorithms can burrow through a set of chronologically arranged images (pixel-by-pixel if need be), and can be programmed to detect specific features, relationships, or trends that "trigger" an event or suggest locations where field personnel might visit. To take an example from the environmental realm, the ability to detect the future onset of El Niño episodes is enhanced by daily, seasonal, and annual data mining queries of sea surface temperatures in the equatorial Pacific. Future "episodes" of El Niño are being predicted on the basis of past occurrences melded with our growing understanding of the triggering mechanisms. Mathematical techniques such as. rule-based systems and fuzzy logic help the data mining algorithms to interpret the intelligence contained in the images. We are, in effect, "teasing" information out of data in much the same way an accountant can find aberrant numbers in a column of numbers.

Visualization: Exciting opportunities abound for visualizing aspects of transportation lifelines. Visualization usually involves integrating digital elevation models (derived from either stereo photographs, LiDAR, or Synthetic Aperture Radar) with imagery and other geospatial data. Airport glide path obstructions, inter-modal facilities, underpasses, overpasses, flyovers, bridges, pipelines, international border crossings, port facilities, and railroad crossings are all candidates for 3-D visualizations and virtual reality, once the proper data structure and environment have been established. For several years, military pilots have trained for missions in new settings by "flying over" an area virtually using imagery gathered by satellite, draped over a digital elevation model of the area. For lifeline security planning, this capability alone may help thwart or mitigate incidents involving shipments of hazardous materials, or interdict possible terrorist activities, by showing swat teams the entire incident area before deploying human resources (for example, height of roadside embankments, locations and sizes of culverts, view sheds, and related incident attributes. Visualizations can, of course, be created without image backdrops, and for some needs these may even be desirable; but for realistic, real-time, incident management, the actual ground area needs to be modeled.

Detecting Subtle Landscape Changes: Change detection over time is one of the major advantages of remote sensing technology. Two change detection applications that have widespread appeal for lifeline safety and proven adaptability for incident management are detection of thermal patterns and subsidence zones. The former represents mature technology in use for the last 30 years or more, particularly in fire mapping. Hot spots at WTC ground zero, were mapped in the days after September 11 and were used in recovery operations to direct ground crew operations. Figure 2b displays an image of these spots, collected by EarthData International. These hot spots are detectable in the 3-5μm spectrum because they are much hotter than their surroundings. For detecting specific phenomena in the ambient landscape a sensor operating in the 8-14μm spectrum would be used (for such phenomena as ship wakes, contrails, cool spots left by parked vehicles), all of which represent intelligence for counter terrorism or illegal activities.

Detecting subsidence patterns is a less mature technology, but one having proven transportation lifeline safety applications that should adapt well to incident management and planning. Subsidence occurs frequently in areas where ground water withdrawals exceed recharge on a seasonal or annual cycle. Subsidence is also a characteristic of active earthquake zones. Interferograms produced from time series of synthetic aperture radar phase data are capable of detecting subsidence on the order of centimeters;

enough to endanger pipelines, rail lines, and highways, and enough to damage bridges and make on- and off-ramp speeds unsafe. Figure 2a shows an area near Las Vegas, Nevada where seasonal subsidence occurs.

Monitoring Consequences of Incidents: Recovery from damaging incidents, natural or otherwise, is an ongoing element of security and public safety planning. Relief and health officials need to know where the transportation lifelines have been disrupted, which avenues are still available for evacuation, or where evacuees are beginning to congregate. Image analysis within a GIS architecture can assist to develop this information. In the case of a hypothetical airport incident the use of high resolution imagery could be used to provide overall situational awareness to supplement ground intelligence. Figure 3 illustrates the capability of the new quick bird II satellite system from Digital Earth that has a panchromatic resolution of 62 centimeters.

4.3.2 Non-Imaging Sensors

Detect Precise Object Locations at a Precise Time: The constellation of global positioning system (GPS) satellites is a well-known and widely used capability for pinpointing the locations of objects on Earth and for navigating between points. A
companion capability develops data from an inertial measurement unit (IMU) to translate platform location to precise object locations on the ground. In day-to-day office environments, object locations can be adequately derived from using imagery analyzed by soft-copy photogrammetric techniques and integrated with traditional GIS datasets; but incident management may require the determination of spot locations, or to the ability to follow objects moving along lifelines. These capabilities are possible and need to be incorporated into the stable of operational techniques employed at local and regional levels. Because the GPS satellites also broadcast precise time signals, they are also highly useful for recording the precise time of events, which may be critical in certain applications.

Detect Biological and Chemical Agents: Some remote sensors are designed to detect and ana/lyze the chemical constituents of gases emanating from objects. Recently developed technologies also include techniques capable of detecting trace amounts of gases (in the parts per million range, and finer). These are non-imaging multi-spectral sensors that can be "tuned" to find specific chemical compounds in a complex atmosphere of numerous gases. Sometimes called "sniffers," such devices could be deployed over multimodal transfer points and international border crossings to identify suspicious containers, railroad cars, or trucks. Harbor facilities might also monitor movements of ships and other watercraft by installing sniffers on uninhabited aerial vehicles (UAVs) that can stay aloft for anywhere from a few hours to several days or weeks. Within territorial waters, these devices might also be mounted on helicopters for monitoring ships well before they enter harbor areas.

4.4 Transportation Infrastructure Treat Reduction

Transportation organizations at all levels face unprecedented challenges today. Increasing demands are being placed on agencies to preserve the existing transportation system and to take on new missions of improved system safety and security. A variety of advanced technologies are available to enhance planning, designing, managing, operating, and maintaining all modes of transportation. Aerial and satellite remote sensing represents one area of rapid development that can be leveraged to address these challenges. These technologies have significant and unique potential for application to a number of cross cutting transportation security issues.

Advances in geospatial sensors, data analysis methods and communication technology present new opportunities for users to increase productivity, reduce costs, facilitate innovation and create virtual collaborative environments for addressing the challenges of security improvement for all modes of transportation. Sensor developments include a new generation of high-resolution commercial satellites that will provide unique levels of accuracy in spatial, spectral and temporal attributes. An example is shown in figure 3 using data from the Digital Earth's commercial Quick Bird satellite to image

a portion of Reagan National Airport at a spatial resolution of sixty-one centimeters. This provides a degree of detail not available previously to the civil transportation community from space based sources. In addition to the high resolution panchromatic imagery illustrated above there are a number of other commercial imagery products that are potentially applicable to transportation. They include air borne and satellite radar, LIDAR, multi-spectral, and hyper-spectral sensors. There is a range of spectral and spatial resolution capabilities for each of these sensor systems. Part of the challenge is matching the best sensor to the specific transportation related application.

Visualization and advanced data analysis methods are also important capabilities. Automated change detection within a defined sector is one example of analysis capability that will assist in detection of unauthorized intrusion events. A specific application of these techniques to transportation security is unauthorized right of way intrusion on pipeline systems. Pipelines often cover thousands of miles and are located in remote areas that are difficult and expensive to monitor. Figure 4 illustrates the use of satellite imagery and target identification analysis to detect unauthorized intrusion onto a pipeline right-of-way in a remote area of Canada.

These geospatial technologies and data analysis capabilities can also be applied to the evolution of other new methods and approaches for enhancing the safety and security of critical transportation systems and infrastructure. The geospatial area is a family of technologies that is in transition. The speed of geospatial product delivery will continue to get faster while the cost goes down. As the use of geospatial produces increases there will be an expansion in new software tool development. There will also be continued improvement in imagery resolution and the quality of derived products. There are a number of transportation related applications of geospatial technology. These include: site assessment and investigation, monitoring critical transportation corridors, designing security systems, monitoring critical infrastructure, rapid change detection over wide areas and security data and system integration.

There remain a number of challenges that may slow or impede the application of geospatial technologies to the transportation sector. These include the need for improved methods and authorities for better data sharing across institutional boundaries. The developed and user communities need to communicate better and overcome some significant disciplinary differences. There are also some very challenging technical issues in the multi-sensor data fusion area to be overcome. Finally, there is a need for a focused interdisciplinary effort for the development of geospatial transportation priorities and the identification of specific product requirements.

5.0 Geospatial Information Examples in New York

When terrorists attacked U.S. targets on September 11, America witnessed one of the worst days of its 225 year history. It also witnessed the best of the American spirit as people everywhere rushed to help. From giving blood to removing rubble to providing counseling and housing - we helped one another cope. And the geo-spatial community was no exception. Individuals and corporations lent their spatial expertise to those managing emergency situations in New York and Washington D.C. The form of this help was broad. Some staffed situation rooms. Others acquired aerial or satellite imagery or processed and interpreted data. For some, helping involved merging data from various agencies into coherent situational maps. Among the first spatial data providers into the breach were those providing satellite-based imagery.

Only three hours after the two jets crashed into the Twin Towers of New York's World Trade Center, SPOT Image's SPOT 4 satellite was over the East Coast. It used its middle-infrared capability to capture 20-meter resolution infrared images of the fires blazing in Manhattan. SPOT provided these images to government agencies and posted on its Web site free of charge. A government client then tasked SPOT with capturing imagery every day following the event.

SPOT accomplished this task using a combination of its satellites. It also posted samplings of these images on its Web site and distributed them free of charge. On September 12, Space Imaging's Ikonos satellite acquired 1-meter imagery of both the WTC area and the Pentagon (see Figure 5). That company donated its imagery to many state and federal agencies, including FEMA, U.S. Department of Transportation, the New York Governor's office, the New York/New Jersey Port Authority, and more. Also, like SPOT, Space Imaging offered imagery at no charge on the Internet, hoping to help the world understand the devastation. In just eight days, more than 720,000 of the 2 MB images were downloaded and more than 1 Terra Bytes of data was served. The imagery provided by these two firms were the only overhead views of the disaster area available for several days, as airplanes and helicopters were not allowed to fly.

On September 14, the New York State OFT in Albany asked EarthData to assist in recovery efforts at the WTC. The mission, jointly developed by OFT and EarthData, was to conduct a series of overflights above what had by then been dubbed Ground Zero. A combined suite of three sensors collected black-and-white digital imagery at 6-inch resolution, elevation data with a vertical accuracy of 6 inches, and thermal information that can detect changes in surface temperature of less than 1 degree centigrade.[13]

The combined geospatial information collected by these sensors was converted into a range of computer maps and application products that recovery effort personnel used to accurately define the position of underground gas and electric lines that were in close proximity to the disaster area, calculate movement and cubic volume of all rubble piles, monitor the development or retardation of the underground fires that burned for weeks, help develop structural audits of all damaged buildings in the vicinity, and develop debris removal plans. These capabilities and products helped the recovery plan move forward efficiently while ensuring the safety of personnel on the site. The data garnered by EarthData was rushed daily to command centers in Albany and lower Manhattan and distributed immediately to firefighters, engineers, city officials, and other rescue workers. Among the data collected were digital aerial imagery at 6-inch resolution acquired from 5,000 feet AGL (see Figure 6). Figure 7 is digital aerial imagery of similar resolution collected before the disaster occurred. EarthData converted the images to map form (horizontally accurate to 53 feet) through digital orthophotography. The resulting image showed all ground objects in their correct geographic position, enabling planners and rescue workers to obtain precise measurements of distances between objects as well as accurate computations of area. By showing current conditions at the site, these maps provided planners with tools to direct equipment and personnel.

Also flying at 5,000 feet AGL, EarthData acquired LIDAR (light detection and ranging system) elevation data for the WTC beginning on September 15 (see Figure 8). It acquired data daily for several weeks, then continued with weekly mapping thereafter. Among the products flowing from the LIDAR data were topographic maps created by a team at the Center for the Analysis and Research of Spatial Information at Hunter College. These topographic products revealed craters that dropped 30 feet below street level and rubble that rose more than 60 feet above. Rescue personnel consulted the maps to identify areas prone to shift or collapse when navigating the mounds of debris. A civil engineering unit from the New Jersey Institute of Technology (NJIT) helped position planes hovering above the site. Equipped with advanced LIDAR technology, working in concert with GPS, the planes provided data from which three-dimensional digital aerial images and maps were produced. Recovery crews on the ground used the maps to assess damage and assist in orchestrating the clean up. To monitor the fires that burned for weeks within the rubble, EarthData used a thermal sensor flown from 3,000 feet AGL. Figure 2b is a computer composite of an orthophoto map image (horizontally accurate to 53 feet) of the WTC site acquired on September 17, 2001 combined with a thermal image. EarthData generated the color composite overlay

[13] FEMA Press Release, *WTC Disaster Response Status Report*, FEMA-1391-DR-NY-PR-107, March 4, 2002

using a thermal sensor that is sensitive to infrared radiation rather than light.[14] Thus, it revealed the location of hot spots within the debris field, indicating a strong probability of lingering underground fires.

As with so many other activities in the wake of the attacks, the imaging mission was enabled by selfless teamwork and a volunteer spirit. ERDAS, Inc, for instance, donated software to produce maps. Hurley and Associates, Inc. of Maryland donated the thermal imaging system. The National Oceanic and Atmospheric Administration's National Geodetic Survey contributed staff and equipment to operate the GPS base station that was used to reference the aerial imagery. And the New York State OFT coordinated flight clearances and donated office space for personnel to produce maps based on the aerial information. But imagery was just one of many tools used to manage activities following the disaster. As with other geospatial challenges, imagery was only part of the information needed to respond to this disaster. It was used in conjunction with many other technologies and information sources, including, ground-based intelligence and GIS. Getting transportation moving again was also critical to response efforts. With subway tunnels destroyed, roads closed and normal transit routes disrupted, New York City was able to integrate data from several city departments into a single map (see figure 9). With these tools they were able to help people make better-informed decisions on how to restore and rebuild transportation routes. GIS provided the ability to create maps that helped rescue workers know where to look for subway entrances and water mains under all the rubble. The New York State Technology Office used GIS to provide other state officials with information on where every state office was located in Manhattan. State officials also deployed databases to track volunteers and to provide information to blood donors and those seeking to donate money or supplies.[15]

The New York response also illustrates how GIS can play a crucial role in infrastructure management of an emergency. Following the terrorist attacks, GIS companies were on site at or near ground zero to assist in damage assessment, development of evacuation plans and mapping of critical resources. One example of a 3D GIS product to characterize the site and allow for analysis and fly-through assessment is shown in figure 10. GIS helped get responders to specific sites and aided in identifying and locating areas of interest for rescue and recovery teams. An Emergency Command Center was set up at Pier 92 and personnel from various companies were consolidated at that location to handle requests from the field and provided rapid response data.

6.0 CONCLUSIONS

It is clear that despite excellent efforts by many groups the approach to providing information for infrastructure management in emergencies is not often effectively utilizing a wealth of data that resides, with various organizations. This existing information and technology could provide mangers important information products that could save lives, reduce damage to property, and lessen environmental impacts. The current situation is characterized by numerous shortcomings that inhibit optimal decision making for emergency management. The inability to access information and the lack of standardization, coordination, and communication are all obstacles that need to be overcome. In addition there are tools in the geospatial information area that could contribute immensely to infrastructure management in emergencies and in more routine operational situations. One of the ways to accomplish these aims is to make more effective and timely use of aerial and satellite surveillance and monitoring technologies. The challenge is how to adapt the

[14] Harwood, Susan, "*Creating a Disaster Management GIS on the Fly*", ESRI New York City Office, January 2002

[15] Page, Daniel, "*GIS played a critical role in the aftermath of September's attacks*", Mobile Government, Washington, DC, January, 2002

existing capabilities of image-derived intelligence in the short-term to fit new operating circumstances, and what new ways of doing business will we need in the long-term to develop an infrastructure that is resilient to various forms of attack.

Advances in Information systems, satellite imaging systems and improved software technologies have led to opportunities for a new level of information products from remote sensed wide situational awareness over a broad area could also be addressed using remote sensing data sources. In the area of spectral sensing new hyper-spectral sensing systems will allow detection and identification of specific surface materials, air and surface pollutants and ground vegetation types. All of these information products can be useful in the response, recovery, and rehabilitation phases of infrastructure management preparedness.

The strength of any paradigm shift is realized if new questions can be answered along with traditional ones. Using remote sensing technologies combined with information sharing will address many, if not most, traditional safety, hazards, and disaster issues facing infrastructure managers, as well as provide for those raised by data. The integration of these new products into existing disaster response systems can provide a wide range of analysis tools and information products that were not possible before. For example, with the higher resolution imagery change detection for building damage assessment can be conducted rapidly and accurately with these new data sources. Transportation infrastructure and system

deliberate acts of aggression. Despite technological advance, disaster risk continues to grow. Infrastructure emergency managers and others continue to be called on to make decisions during disaster events, as well as in the pre-and-post disaster phases, with incomplete information. In order to make optimal decisions to reduce the loss of life and property, stakeholders uniformly must be able to obtain the needed information in a format that is appropriate for their capabilities. There is also the need for parties at great distances from each other to be able to share information in a seamless fashion that also allows the shared information to be interactive with local data and be used to create new integrated products tailored to the situation.

Estimated Extent of America's Transportation System (Source: DOT/RSPA)		
System	Infrastructure	Use
210 million vehicles	4 million miles of road 000 bridges (1/3 of 127,000 urban ›ridges serve as major arterials	4 trillion passenger-miles 920 billion freight ton-miles
XX railroad cars 250 intercity Amtrak trains	150,000 track miles	20 million passenger miles 1.3 trillion ton-miles
175,000 aircraft	5,500 public use airports	403 million passenger miles
12 million watercraft	25,000 miles of waterways	600 billion ton-miles of oil
Pipelines	1.6 million miles	19 trillion cu.ft. of gas
:OMEX/TEU (Multimodal)	?reighters, trucks, railroad cars	5 million each year through major U.S. ports

Table 1: Summary of America's Transportation System

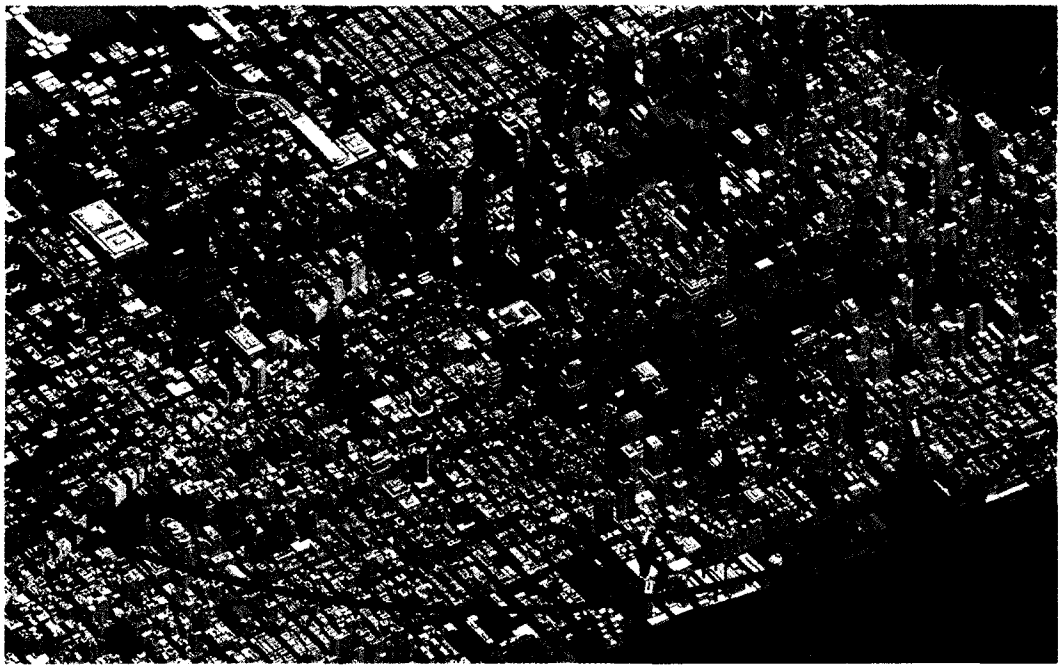

Figure 1. Sample LiDAR data set of the downtown New York area collected by EarthData. The vertical accuracy is about .8 feet on average across the data set.

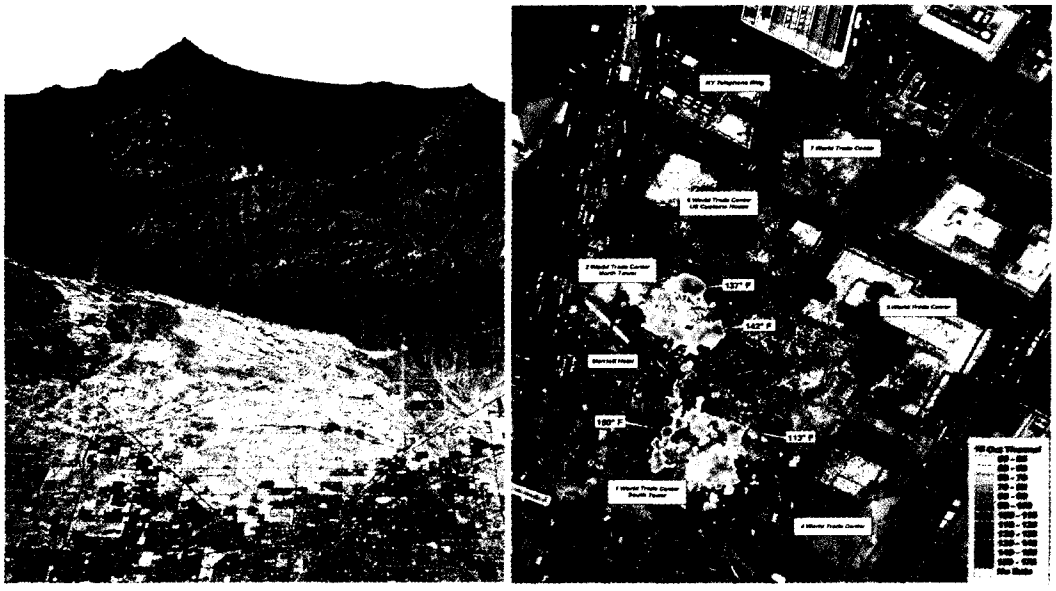

Figure 2a,b. Rainbow pattern at left shows land subsidence of a few centimeters near Las Vegas, NV. Such patterns can disrupt rail, pipelines, and road networks, and cause overpasses and bridges to be unsafe. The orange colors at right represent hot spots at the WTC "ground zero 5 weeks after the attack. Such patterns assist post-incident recovery.

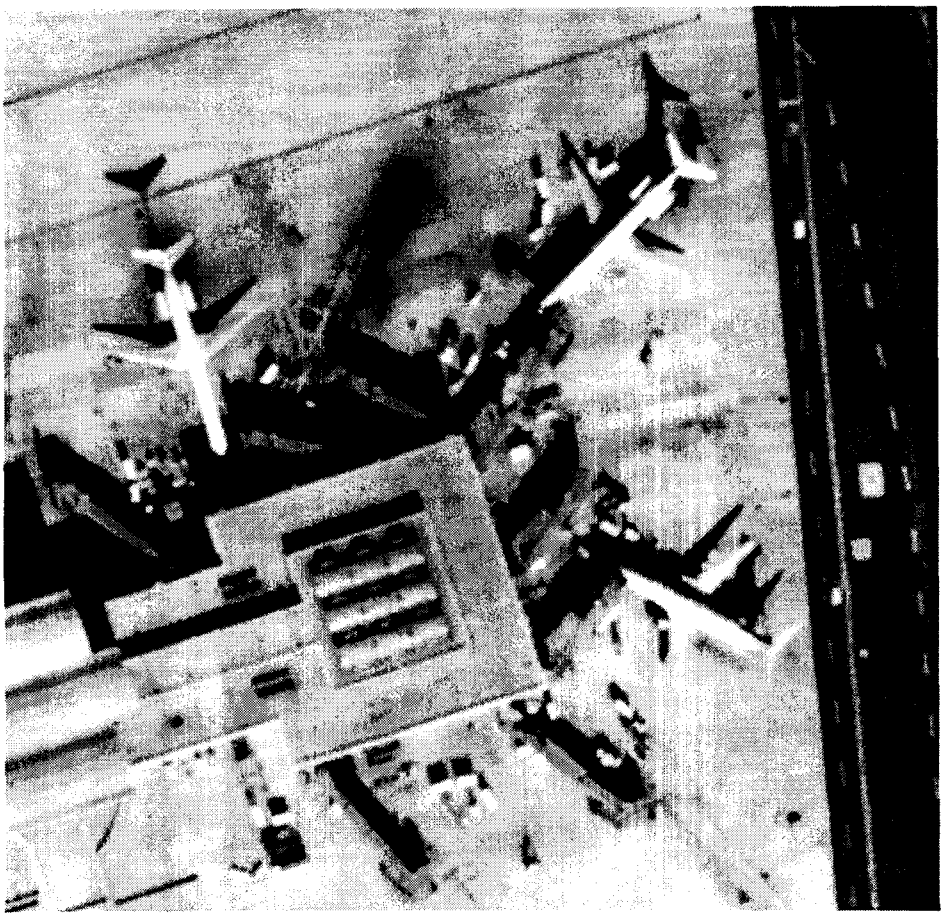

Figure 3: Digital Earth image of Regan National Airport at 62 cm spatial resolution

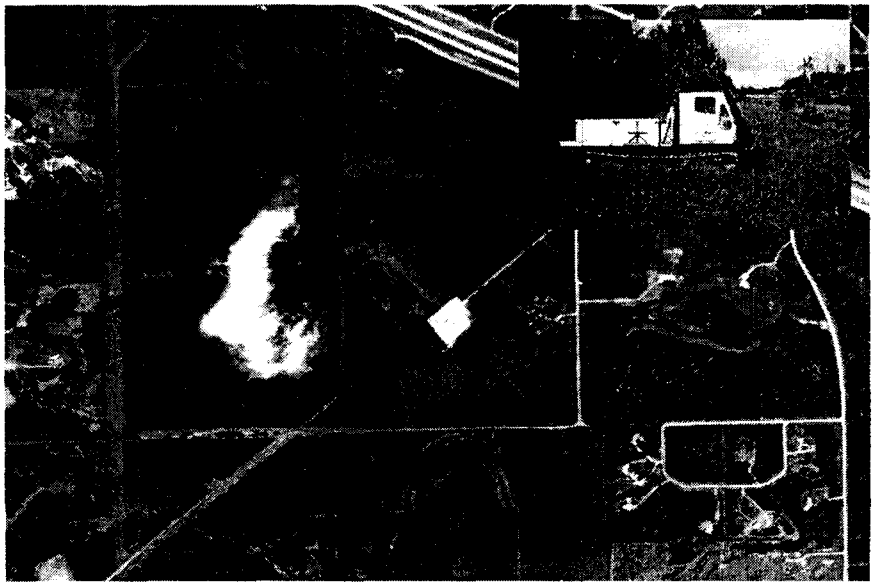

Figure 4: Unauthorized intrusion detection on Canadian pipeline using satellite imagery

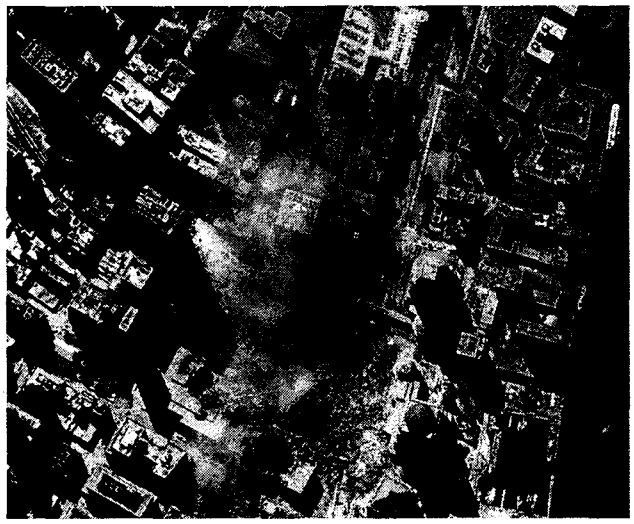

Figure 5: Space Imaging IKONOS pan-sharpened one meter spatial resolution image of the World Trade Center taken on September 15, 2001

Figure 6: Six-inch digital photograph near the disaster area

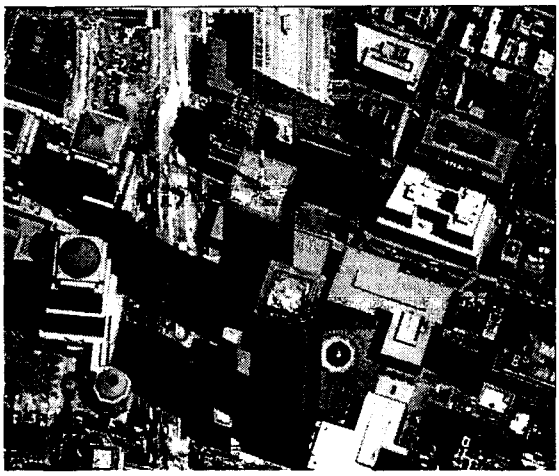

Figure 7: Digital photograph prior to disaster

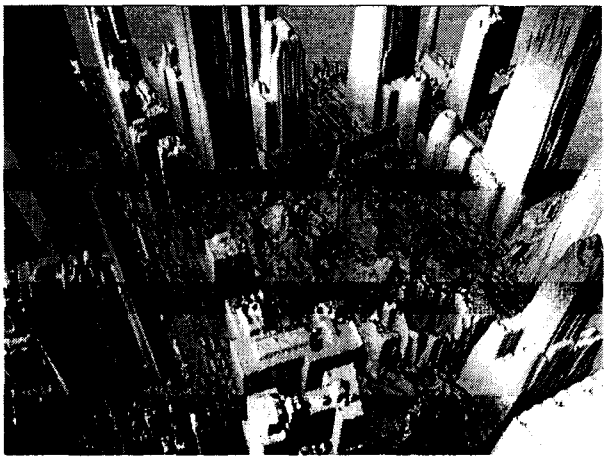

Figure 8: LIDAR data showing debris location

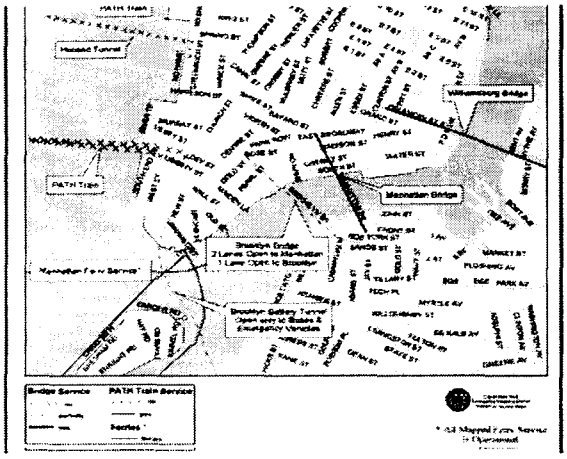

Figure 9: GIS map product of transportation routes

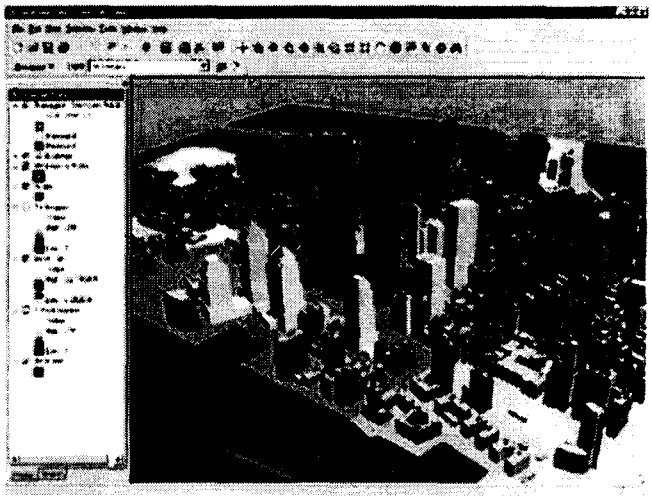

Figure 10: 3D GIS product showing color-coded buildings

Risk Assessment on Storm Surge Flood

by

Kenichi Torii[1], Fuminori Kato[2]

ABSTRACT

The method of risk assessment for hazard map on storm surge flood has not been established completely. For nationwide distribution of the hazard map, several research subjects in process of the risk assessment on storm surge flood will be investigated in this study. Probabilistic evaluation on tide level and wave overtopping rate, judgment on coastal dike break, and flood simulation are key elements in the risk assessment.

KEY WORDS: Flood, Risk Assessment, Storm Surges

1. INTRODUCTION

Typhoons have caused catastrophic damage by flooding due to storm surges in Japanese history. As shown in , large scale of storm surge disasters have occurred frequently until 1961. For example, about five thousands of people was dead with storm surge by a typhoon in 1959, which was called Ise Bay Typhoon. After 1970's, catastrophic flood disaster due to storm surges have been rare.

There are two main factors of small number of severe storm surge flood in recent 40 years. One is construction of coastal dike against storm surge, the other is improvement of weather forecast system. These factors made residents in coastal area feel as if their houses had been safe from storm surge flood.

Contemporary structure of great cities in coastal area is a complex including ground space and underground space. Storm surge larger than designed level in shore protection works may cause severe flood disaster of unexpected process in the great cities.

One of effective countermeasures against storm surge disaster is hazard maps on storm surge, however, the maps have not been distributed overall in Japan. The method of risk assessment for the map has not been established completely.

This study is to establish the method of risk assessment on storm surge flood.

2. FRAMEWORK OF RISK ASSESSMENT ON STORM SURGE FLOOD

There are some matters for making hazard maps on storm surge flood as shown in Figure 1.

One is how to set tide level and wave overtopping rate as boundary conditions of flood simulation. Return period of high tide level has not been evaluated accurately because of short period of tidal observation. Dependency of wave height on

[1] Head, Coast Division, River Research Department, National Institute for Land and Infrastructure Management, Ministry of Land, Infrastrucuture and Transport, Asahi 1, Tsukuba 305-0804, Japan
[2] Senior Researcher, ditto

tide level also makes it difficult to evaluate return period of wave overtopping rate.

Second one is how to judge coastal dike break. Most of coastal area in Japan is protected from storm surges and high waves by coastal dikes in designed level. Although most of coastal dike is armored with concrete or asphalt, tide level and wave higher than designed level may break coastal dike.

From the viewpoint of mitigating fatalities, risk assessment on storm surge flood can be conducted as shown in Figure 2.

(1) Probabilistic evaluation on tide level and wave overtopping rate
Tide levels and wave overtopping rates are necessary for flood simulation in coastal zones as boundary conditions. Return period of tide levels and wave overtopping rates can be evaluated on results of numerical simulation with a probabilistic generation model for parametric properties of typhoon.

(2) Judgment on coastal dike break
Break of coastal dike increases inflow rate of seawater awfully. The break can be judged based on wave overtopping rate and type of coastal dike.

(3) Flood simulation
Inundation depth, velocity of flood flow, and arrival time of flood in coastal zone can be estimated with a numerical model.

(4) Risk assessment
From the viewpoint of need and safety of evacuation and safety of houses, risk of storm surge flood can be assessed based on results of the flood simulation.

3. PROBABILISTIC EVALUATION ON TIDE LEVEL AND WAVE OVERTOPPING RATE

Probabilistic evaluation on tide level and wave overtopping rate can be conducted as shown in Figure 3. First is making a probabilistic generation model for parametric properties of typhoon based on recorded data. Second is evaluating return period of tide level and wave overtopping rate based on Monte Carlo method.

Probabilistic generation model for parametric properties of typhoon can be made in methods by Yamaguchi et al.(1994) and Hashimoto et al. (2001). In their method, probability of number, location and its variation, atmospheric pressure and its variation, and radius of typhoon are evaluated based on data of typhoon for the past fifty years.

In evaluating return period of tide level and wave overtopping rate, typhoons are supposed with the model for hundreds of years. After that, tide level and wave overtopping rate due to each supposed typhoon are calculated through numerical simulation. Finally, return period of tide level and wave overtopping rate are calculated.

Figures 4 to 9 show results of a typhoon simulation with the model. The simulation for past fifty years was conducted fifty times. It corresponds a simulation for 2,500 years. Although calculated standard deviations of atmospheric pressure at typhoon eye, typhoon speed and typhoon direction were smaller than observed ones, calculated average values of them were almost equivalent to observed ones.

4. PROBABILISTIC EVALUATION ON COASTAL DIKE BREAK

Although most of coastal dike is covered with concrete or asphalt in Japan, coastal dike might be broken due to excess waves and/or cavern in fill.

Table 2 shows an example of wave overtopping rate critical to destruction of dikes and revetments.
Probability of coastal dike break should be evaluated for each wave overtopping rate based on breach examples and results of physical model experiments.

5. RISK ASSESSMENT BASED ON FLOOD SIMULATION

If houses could be inundated due to a storm surge, the residents should evacuate to designated safe locations prior to any danger. Whether evacuation is required can be evaluated based on the maximum flood depth obtained from flood analysis using the worst scenario.

On the other hand, safety for evacuation depends on time for flood to reach each point as well as the maximum flood depth. In a low plain field, people in evacuation is safer at points far from the shoreline because it takes a long time for flood to reach there, although significant variation in the maximum flood depth is not observed throughout inundated area.

According to the criteria shown in Table 3, we ranked the relative hazards to human based on the maximum flood depth and the time for flood to reach obtained from flood analysis. The points where the maximum flood depth corresponds to the flood above floor level were assumed to be the evacuation-designated areas. Note that some of the houses that were not inundated completely or were not swept away even if flooded, might be ranked D indicating that evacuation is not required.

For the houses in the evacuation-designated areas, assuming that the residents began to escape when seawater overflowed the embankment, a comparison was made between the time required for evacuation and the time for flood to reach. If the time for flood to reach was longer, the houses were ranked C. Otherwise, the residents could escape when the flood depth was low by using the evacuation road, even if they began to escape at the onset of seawater invasion.

Further hazard ranking was made based on whether the residents could safely reach the walkable evacuation road even if they began to escape in case of a flood. The rank C houses were divided into subgroups based on whether residents could reach the safe evacuation road if they began to escape upon becoming aware of the flood on their houses.

This method allows us to evaluate the effects of improving evacuation locations and making the houses water-resistant inside the embankment. For example, if safe evacuation locations that are not inundated even during a flood, are improved into rank A or B locations, then the time required to escape is reduced and the houses in the vicinity of the locations are ranked C+ or C-.

Principal cities in Japan are in risk of riverine flood and flood due to drainage failure as well as storm surge flood. Flood risk should be assessed comprehensively for residents convenience.

We are now making a probabilistic generation model for parametric properties of typhoon. Evaluation on tide level and wave overtopping rate will be conducted for four coasts facing Tokyo Bay, Ise Bay, Osaka Bay and Tosa Bay, where severe storm surge has occurred.

REFERENCES:

Goda, Y.: Study on Wave Overtopping Rates at Seawalls, Report of Port and Harbor Research Institute, No.9, Vol.4, pp.3-42, 1970. (in Japanese)

Hashimoto, N., H. Satoh, K. Matsuura and M. Ichikawa: Modeling of Probable Typhoon and Its Statistic Properties, Proceedings of Coastal Engineering, Japan Society of Civil Engineers, pp.456-460, 2001. (in Japanese)

Torii, K. and F. Kato: Study on Storm Surge Disaster, Technical Memorandum of Public Works Research Institute, No.3803, 97p., 2001. (in Japanese)

Yamaguchi, M., Y. Hatada and Y. Nakamura: Probabilistic Typhoon Model and Its Application to Extreme Value Estimation of Storm Surges and Waves, Proceedings of Annual Conference of Japan Society for Natural Disaster Science, pp.135-138, 1994. (in Japanese)

Table 1 Storm surge disasters in Japan

Date	Major damaged area	Human casualties			Damage to houses			Typhoon
		Dead	Injured	Missing	Completely destroyed	Partially destroyed	Washed away	
1 Oct. 1917	Tokyo Bay	1,127	2,022	197	34,459	21,274	2,442	
13 Sep. 1934	Ariake Sea	373	181	66	1,420		791	
21 Sep. 1934	Osaka Bay	2,702	14,994	334	38,771	49,275	4,277	Muroto
27 Aug. 1942	Suo Sea	891	1,438	267	33,283	66,486	2,605	
17 Sep. 1945	Southern Kyushu	2,076	2,329	1,046	58,432	55,006	2,546	Makurazaki
3 Sep. 1950	Osaka Bay	393	26,062	141	17,062	101,792	2,069	Jane
14 Oct. 1951	Southern Kyushu	572	2,644	371	21,527	47,948	1,178	Ruth
7 Sep. 1959	Ise Bay	4,697	38,921	401	38,921	113,052	4,703	Ise Bay
16 Sep. 1961	Osaka Bay	185	3,897	15	13,292	40,954	536	Second Muroto
21 Aug. 1970	Tosa Bay	12	352	1	811	3,628	40	No.10
30 Aug. 1985	Ariake Sea	3	16	0	0	589	0	No.13

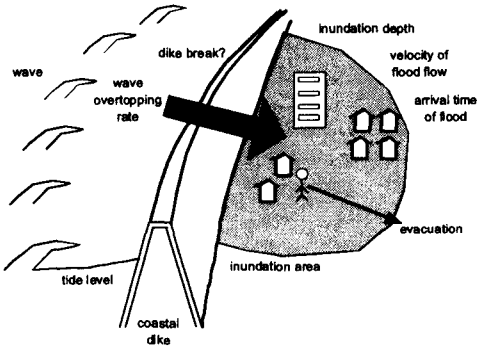

Figure 1 Schematic view of storm surge flood

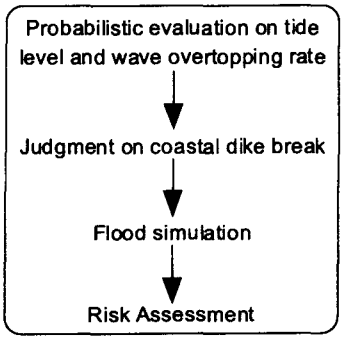

Figure 2 Flowchart of risk assessment on storm surge flood

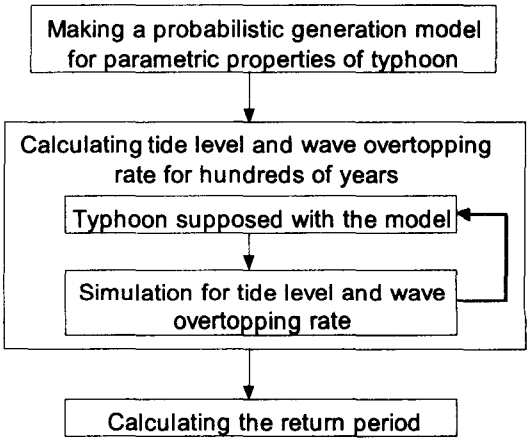

Figure 3 Flowchart of probabilistic evaluation on tide level and wave overtopping rate

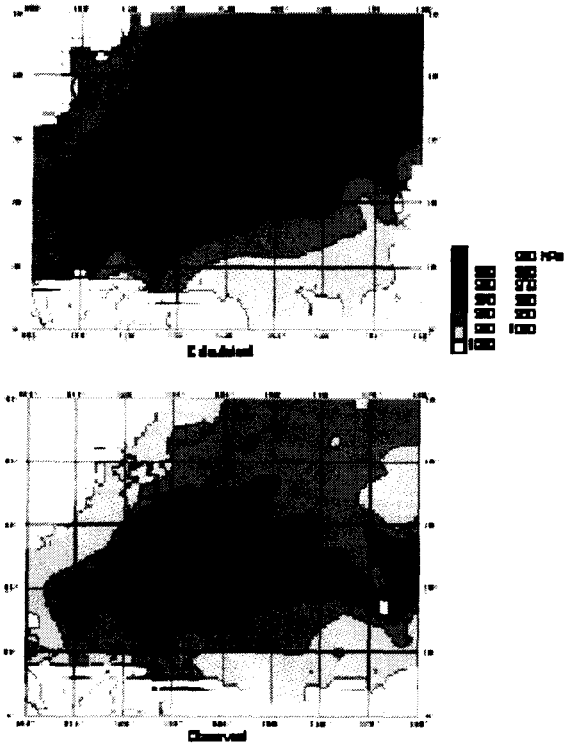

Figure 4 Average atmospheric pressure at typhoon eye

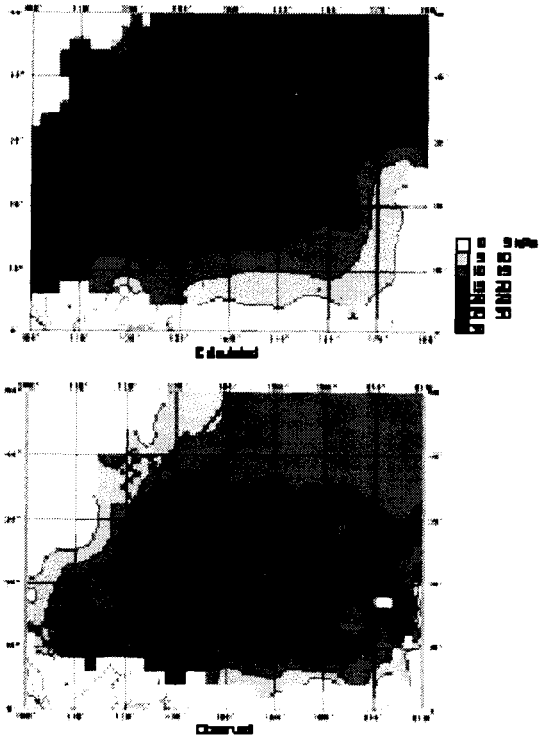

Figure 5 Standard deviation of atmospheric pressure at typhoon eye

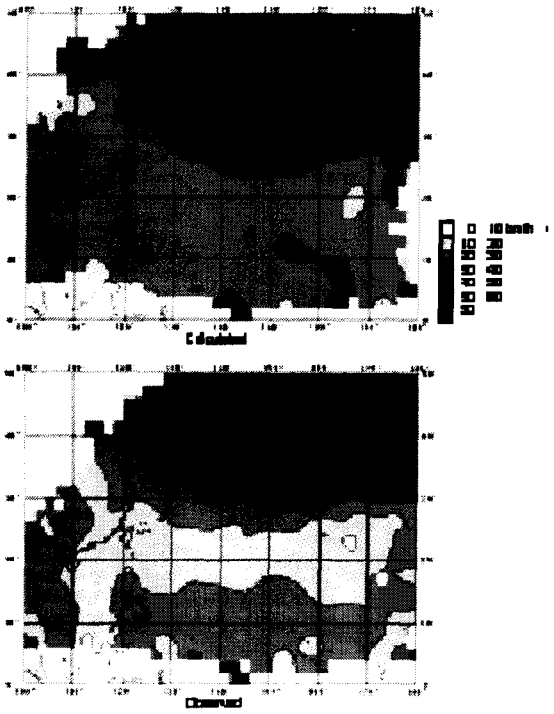

Figure 6 Average typhoon speed

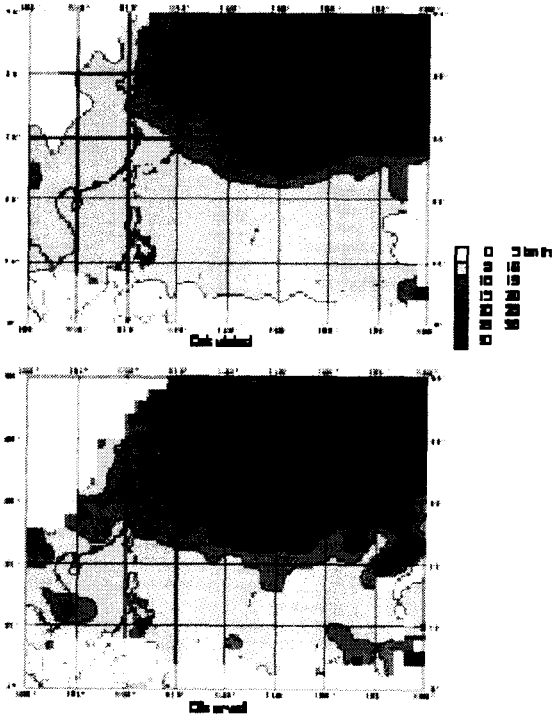

Figure 7 Standard deviation of typhoon speed

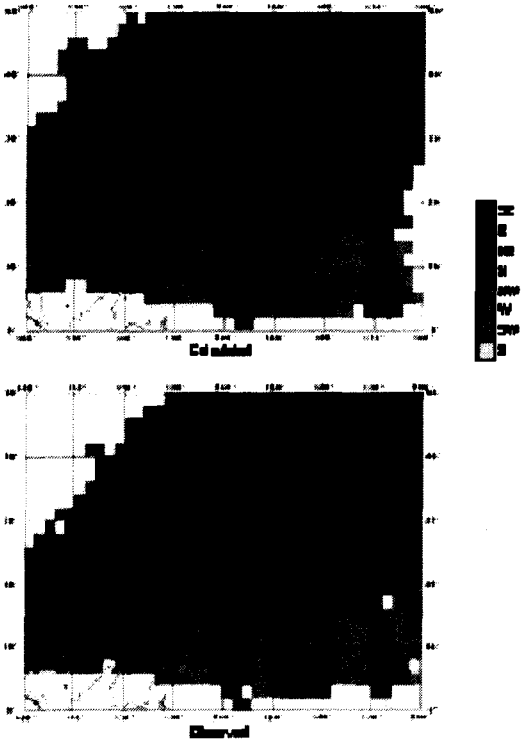

Figure 8 Average typhoon direction

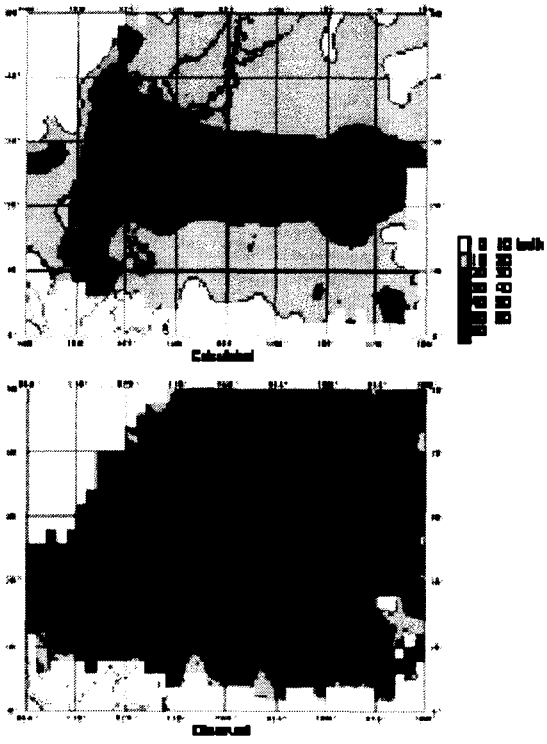

Figure 9 Standard deviation of typhoon direction

Table 2 Allowable wave overtopping rates (Goda, 1970)

type	crest of dike	landward slope of dike	wave overtopping rate (m^3/m/s)
1	not armored	not armored	<0.005
2	armored	not armored	0.02
3	armored	armored	0.05

Table 3 Hazard ranking criteria for storm surge flood (Torii and Kato, 2001)

Hazard rank	Expected maximum flood depth	Houses	Expected time for flood to reach	Safe evacuation if residents begin to escape on becoming aware of the flood on their houses	Expected condition	Desirable action
A	above floor level		shorter than Tl and Tr	impossible	evacuation is possible if residents begin to escape before the onset of seawater invasion	escape prior to the onset of seawater invasion
B	above floor level		shorter than Tl, but longer than Tr	impossible	evacuation is possible in flood if residents begin to escape at the onset of seawater invasion	
C+	above floor level		longer than Tl and Tr	impossible	evacuation is possible in dry condition if residents begin to escape at the onset of seawater invasion, but impossible if residents begin to escape upon becoming aware of the flood on their houses	
C-	above floor level		longer than Tl and Tr	possible	evacuation is possible even if residents begin to escape upon becoming aware of the flood on their houses	escape on self-judgment
D	above floor level	high-rising, water-resist			safe in their houses	stand by in their houses
E	below floor level				safe in their houses	
(none)	no inundation				safe in their houses	

Tl: Time for residents to reach an evacuation location
Tr: Time for residents to reach a walkable evacuation road

MANUSCRIPTS AUTHORED

FOR PANEL MEETING

BUT NOT PRESENTED ORALLY

Shaking Table Tests on Seismic Response Reduction Effects of Rocking Building Structural Systems

by

Tatsuya Azuhata[1], Mitsumasa Midorikawa[2], Tadashi Ishihara[3] and Akira Wada[4]

ABSTRACT

Shaking table tests are carried out to examine seismic responses of rocking structural systems with base plate yielding (base plate yielding systems) comparing with those of fixed-base systems and simple rocking systems. Furthermore a simple method using the equivalent one mass system to predict the base shear that base plate yielding systems suffer when they begin up-lifting response (critical base shear of up-lifting response) is proposed. It is concluded that the base plate yielding systems can reduce effectively the seismic response of structures and their critical base shear of up-lifting response can be predicted by the proposed method appropriately.

KEYWORDS: Shaking table test
Rocking system
Base plate
Earthquake response reduction
Smart structure

1. INTRODUCTION

It is pointed out that effects of rocking vibration (up-lifting response) can reduce the seismic damage of buildings subjected to strong earthquake ground motions [1][2]. Based on this knowledge, we are now developing the rocking systems that can cause rocking vibration under appropriate control during earthquakes [3].

The rocking system can be regarded as one of smart structural systems. Smart systems are defined as structural systems with a certain-level of autonomy relying on the embedded functions of sensors, actuators and processors that can automatically adjust structural characteristics, in response to the change in external disturbances and environments, toward structural safety and serviceability as well as the elongation of structural service life [4]. Although the rocking system has neither specific devices nor computer control systems, it satisfies this definition. It is thought the rocking system is one of the simplest smart structural systems.

One of the rocking systems we are developing has weak base plates at the bottom of each steel column of the first story. When the weak base plates yield by tension force of the column during a strong earthquake, the building causes rocking vibration.

In this paper, shaking table tests are carried out to examine seismic responses of this type of rocking systems (the base plate yielding systems) comparing with those of the fixed-base systems and the simple rocking systems which are fixed only in the horizontal direction under the footing beams.

[1] Senior Research Engineer, Building Research Institute, Tachihara 1, Tsukuba-shi, Ibaraki-ken, 305-0802, Japan

[2] Research director for International Codes and Standards, BRI

[3] Section Chief, Building Guidance Division, Housing Bureau, MLIT

[4] Professor, Tokyo Institute of Technology

Outlines of the base plate yielding system and the simple rocking system are illustrated in Fig.1.

When we apply the base plate yielding system to real structures, we must adjust the physical characteristics of the base plate such as those dimensions and yield point, so that the building structures cause rocking vibration before they yield. Therefore we need to grasp the relation between the physical characteristics of the base plate and the critical base shear of up-lifting response. In the following, a simple method to grasp this relation is proposed and the applicability of this method is verified using test results.

2. SPECIMENS AND TEST METHOD

Specimens for the tests are composed of a steel frame shown in Photo. 1 and some structural components such as weak base plates attached to bases of the frame. Each floor height of the steel frame is 1m and total height is 5m. In the oscillation direction, the frame span is 2m. Each floor mass is shown in Table 1. The cross sections of the members are shown in Table 2.

The base plate for the base plate yielding system is shown in Photo. 2 and Fig. 2. Thickness of the base plate is 6 mm or 9 mm. Material characteristics of steels used for base plates are shown in Table 3. In the following, the specimen with base plates whose thickness is 6 mm is referred to as BP6 model and the specimen with base plates whose thickness is 9mm is referred to as BP9 model respectively.

The structural component for the simple rocking system is shown in Photo. 3 and Fig. 3. In this component, shock absorbers can be installed between the upper and the lower part of it to weaken shock force which occurs when the structure lands after up-lifting.

However, it was cleared that the test results for this specimen were not affected by the existence of the absorbers and the kind of them after the tests. Thus only the results that we get when using rubbers as the shock absorbers are shown in this paper. The specimen for the simple rocking system is referred to as R model.

The specimens are oscillated only in one direction, that coincides with the strong axis direction of columns. And in this direction, the frame shown in Photo.1 has no brace. The input ground motion used for the tests is 1995 JMA Kobe NS, of which the time scale is shorten to $1/\sqrt{3}$.

3. TEST RESULTS

Fig. 3 shows the relation between maximum input acceleration and response values of each model. Up-lifting responses are small when the maximum input acceleration is nearly equal to 1.5m/sec2. These values of BP6 and BP9 models are almost 0.0. As the input acceleration becomes larger, the up-lifting responses increase monotonously. When the input acceleration becomes about 3.5 m/sec2, the up-lifting displacement of R model is 6.2 mm and that of BP6 model is 2.4 mm.

Base shears of all models are almost same each other when the input acceleration is smaller than 1.5 m/sec2. When the input acceleration becomes larger than 2.0 m/sec2, these values of R model are 40 kN to 50 kN and are constant approximately. And base shears of BP6 and BP9 models are also smaller than those of the fixed-base model (F model). In this study, base shears are evaluated as the summation of each story's horizontal force derived by multiplying each story's mass by each story's response

acceleration. Each story's mass is derived by multiplying the summation of the mass of structural members and weights by 1.05 in order to evaluate the mass of bolts and steel plates in the connection.

Roof displacements of all models are almost same when the input acceleration is smaller than 4.0 m/sec2. When the input acceleration is larger than 4.0 m/sec2, the displacement of R model is larger than those of the other models. It is thought the reason for this results are that the roof displacements of BP6 and BP9 model are smaller than those of R model and that hysteretic damping of base plates dissipates earthquake energy even when the specimens land.

Fig. 4 shows story shear forces of each model. These values are derived from the same method for the base shear. When the input acceleration is 1.5 m/sec2, the response values are almost same each other. When the input acceleration becomes 3.5 m/sec2, seismic response reduction effects of rocking structural systems can be observed clearly and all story shear forces of R and BP6 models are smaller than those of F model.

4. PREDICTION OF THE CRITICAL BASE SHEAR OF UP-LIFTING RESPONSE

To predict the critical base shear of up-lifting response, the moment balance of the equivalent one mass system shown in Fig. 6 is considered. The moment balance is expressed as Eq. (1).

$$M_u \cdot a \cdot H = M \cdot g \cdot (B/2) + n \cdot N_y \cdot B \qquad (1)$$

where,

Mu: the 1st effective mass in horizontal direction

a: horizontal response acceleration which occurs when the structure begin up-lifting response (critical acceleration of up-lifting response)

H: the 1st representative height

M: total mass

g: gravity acceleration

B: distance between columns

n: number of columns in the up-lifting side

Ny: tension yield strength of base plate

In the above equation, the first normal mode is needed to calculate the 1st effective mass *Mu* and the 1st representative height *H*. Now, we try to approximate this mode using horizontal story response acceleration distribution.

Fig. 7 shows this distribution is shaped like the reversed triangle before and after up-lifting (Input acceleration is 15 m/sec2 and is 3.5 m/sec2). Thus the 1st effective mass *Mu* and the 1st representative height *H* are calculated assuming the normal mode shape is the reversed triangle. The 1st effective mass *Mu* of BP6 and BP 9 models is calculated as follows.

$$M_u = \frac{\left(\sum_{i=1}^{N} m_i \cdot_1 u_i\right)^2}{\sum_{i=1}^{N} m_i \cdot_1 u_i^2} = 9.83 \quad \text{(t)} \qquad (2)$$

where,

m_i: mass of each story

The 1st representative height *H* of BP6 and BP9 models is calculated as follows.

$$H = \frac{\sum_{i=1}^{N} m_i \cdot_1 u_i \cdot h_i}{\sum_{i=1}^{N} m_i \cdot_1 u_i} = 3.66 \quad \text{(m)} \qquad (3)$$

where,

h_i: height of each story

The tension yield strengths of base plates of BP6 and BP9 models are calculated by Eq. (4) and Eq. (5) respectively.

[BP6 model]

$$N_y = \frac{n \cdot b \cdot t^2 \cdot \sigma_y}{2l} = 26.46 \quad \text{(kN)} \qquad (4)$$

where,

n: number of base plates

b: width of base plate

t: thickness of base plate

l: length of base plate

σy: yield point of steel used for base plate

[BP9 model]

$$N_y = 53.61 \quad \text{(kN)} \qquad (5)$$

By substituting Mu by Eq. (2) , H by Eq. (3) and Ny by Eq. (4) or Eq. (5) into Eq. (1), the critical acceleration of up-lifting response a is calculated as follows.

[BP6 model]

$a = 6.21$ (m/sec^2) (6)

[BP9 model]

$a = 9.23$ (m/sec^2) (7)

Furthermore the critical base shears of up-lifting response, which are approximated as the product between Mu and a are predicted by following equations.

[BP6 model]

$Q = Mu \cdot a = 61.10$ (kN) (8)

[BP9 model]

$Q = Mu \cdot a = 90.77$ (kN) (9)

In Fig. 8, the predicted values of the critical base shears of up-lifting response are compared with the corresponding test results. The figure shows the predicted values rather become underestimates to the test results, but they correspond each other with good agreements. When the input acceleration exceeds 5.0 m/sec2, the base shear of B6 model tends to ascend. It is thought the reason for these results is that tension displacements along the longitudinal direction become predominant under this input level. As for this point, we need to study furthermore by investigating the force deformation characteristics of base plates.

5. CONCLUSIONS

The earthquake responses of the rocking system with weak base plates (the base plate yielding systems) were examined comparing with those of the simple rocking system and the fixed-base system by shaking table tests. The results of this study are summarized as follows.

1) Base shears and story shear forces of BP6, BP9 and R models become smaller than those of F model, in the range of input acceleration where up-lifting response occur in these models.
2) Roof displacements of BP6 and BP9 models are not amplified extremely even in the range of input acceleration where those of R models become very large. And vertical acceleration around the frame base of BP6 and BP9 models is smaller than that of R models.
3) The simple method using the equivalent one mass system for prediction of the critical base shear of up-lifting response is proposed. And its applicability is ascertained using test results.

Acknowledgement

This work has been carried out under the US-Japan cooperative structural research project on Smart Structure Systems (Chairperson of Japanese side: Prof. S. Otani, University of Tokyo). The authors would like to acknowledge all project members for their useful advice and suggestions.

REFERENCES:

1) Hayashi, Y., Damage Reduction Effect due to Basement Uplift of Buildings, J. Struct. Constr. Eng., AIJ, No.485, 53-62, Jul., 1996 (In Japanese)
2) Rutenberg, A., Jennings, P. C. and Housner, G. W., The Response of Veterans Hospital Building 41 in the San Fernando Earthquake, EARTHQUAKE ENGINEERING AND STRUCTURAL DYNAMICS, vol. 10, 359-379, 1982
3) M. Midorikawa, T. Azuhata, T. Ishihara, Y. Matsuba, Y. Matsushima and A. Wada: Earthquake Response Reduction of Buildings by Rocking Structural Systems, SPIE's 9th Annual International Symposium on Smart Structures and Materials, 4696-33, 2002.3.
4) Otani, S., Hiraishi, H., Midorikawa, M. and Teshigawara, M., Research and Development of Smart Structural Systems, Proc. of 12WCEE, 2307, 2000

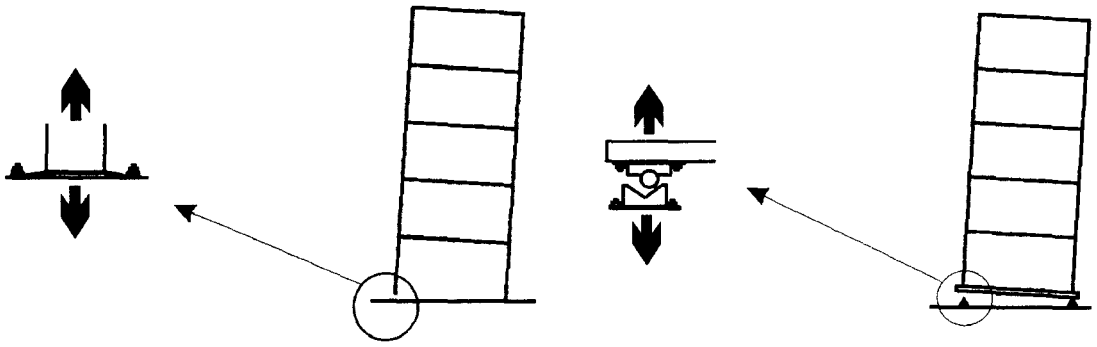

(a) Base plate yielding system (b) Simple rocking system

Fig. 1 Two types of rocking systems

Table 1 Mass of each story

Story	Mass (t)
RF	2.264
5F	2.292
4F	2.292
3F	2.292
2F	2.292
1F	1.456

Table 2 Cross sections of members

Column and beam	H148x100x6x9
Footing beam	H250x250x9x14

Table 3 Steels used for base plates

Model name	JIS	Yield point(N/mm^2)
BP6	SS400	334.18
BP9	SS400	300.86

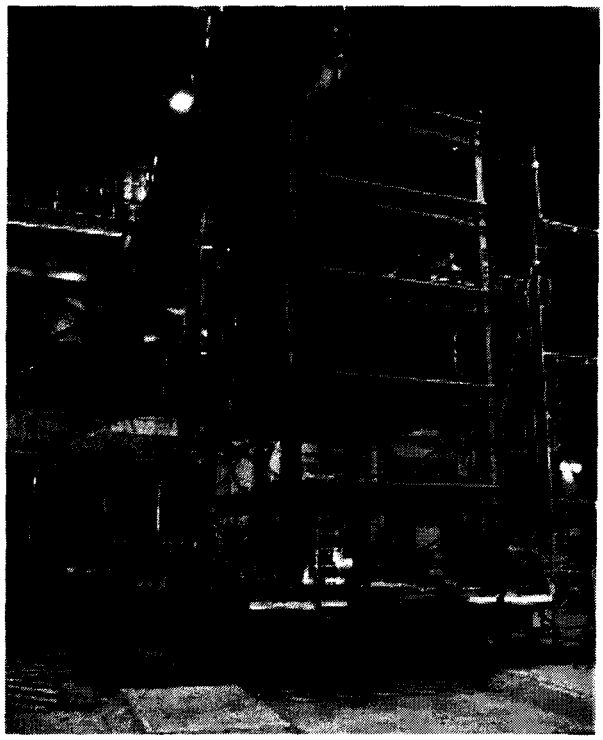

Photo. 1 Specimen frame

Photo. 2 Base plate for BP model (1)

Photo. 3 Structural component for R model (1)

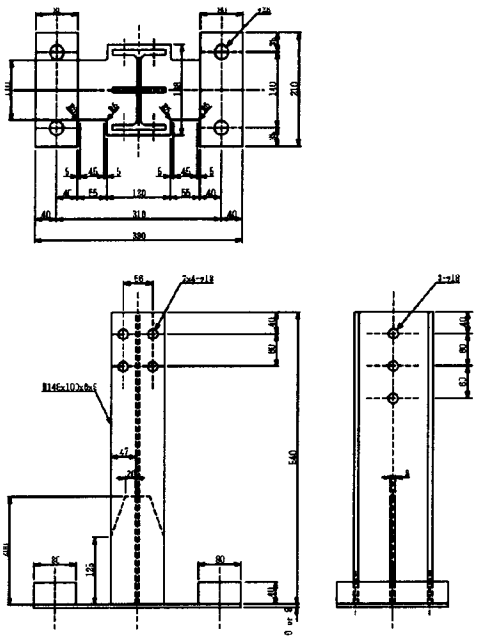

Fig. 2 Base plate for BP model (2)

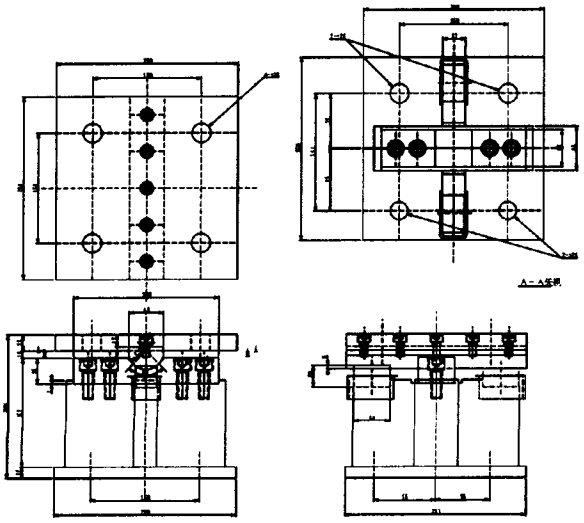

Fig. 3 Structural component for R model (2)

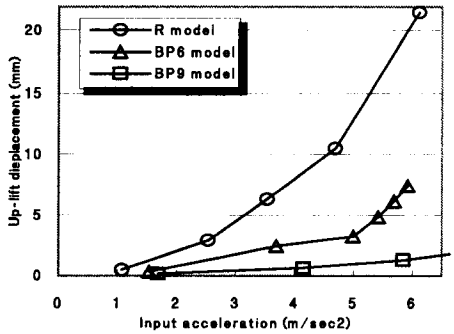

(a) Up-lifting

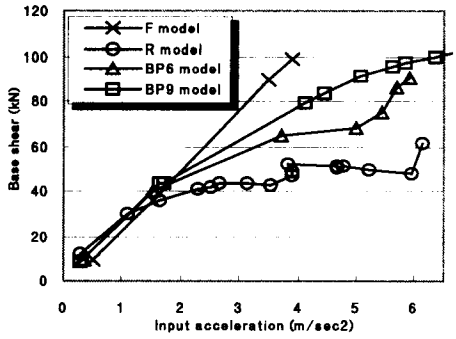

(b) Base shear

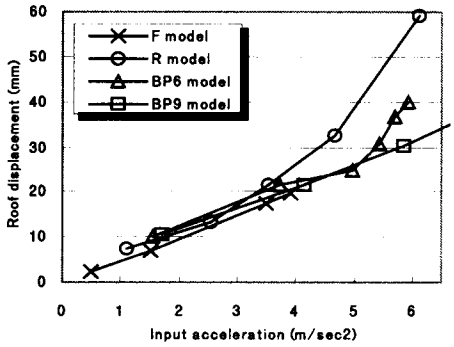

(c) Roof displacement

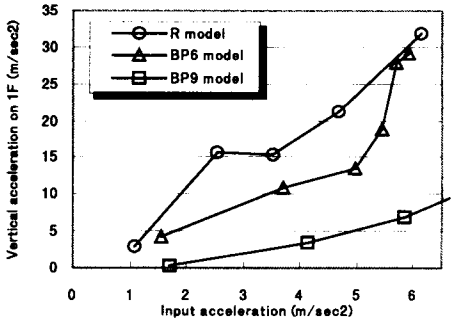

(d) Vertical acceleration around the base

Fig. 4 Maximum input acceleration vs. maximum response values

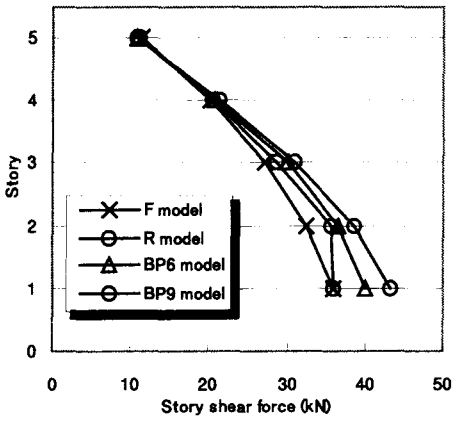

(a) Input acceleration: 1.5 m/sec2

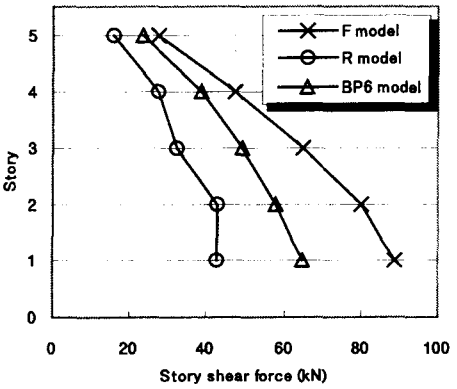

(b) Input acceleration: 3.5 m/sec2

Fig. 5 Story shear forces

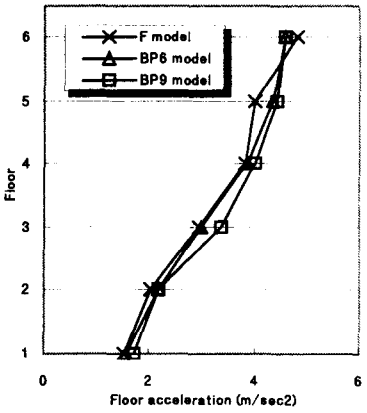

(a) Input acceleration: 1.5 m/sec2

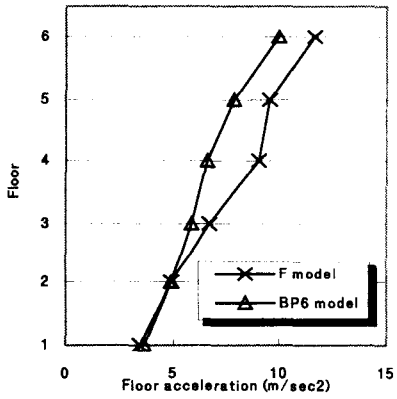

(b) Input acceleration: 3.5 m/sec2

Fig. 7 Each floor acceleration

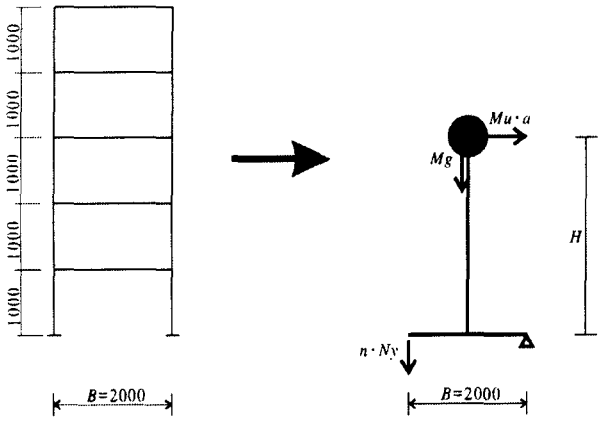

Fig. 6 Equivalent one mass system

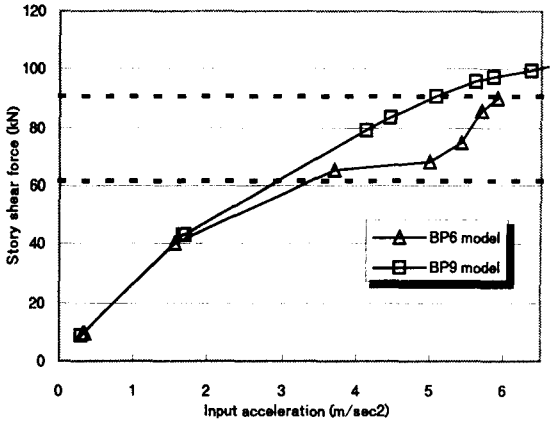

Fig. 8 Prediction of critical base shears of up-lifting response

Large-scale Tests for Performance Verification of Smart Structures

by

Mitsumasa Midorikawa[1], Masaomi Teshigawara[1], Masanori Iiba[1], Hideo Fujitani[1]
Koichi Morita[2], Tatsuya Azuhata[1], Akiyoshi Fukuda[3], Yoichi Shiozaki[3], Takeshi Hiwatashi[3]
and Chikahiro Minowa[4]

ABSTRACT

The objectives of these large-scale tests are to confirm the effectiveness of several proposed smart materials, members and structural systems. The tests were conducted on the shaking table of the test facility of the National Research Institute for Earth Science and Disaster Prevention (NIED), Tsukuba, Japan. It has a maximum displacement of 22 cm, a maximum velocity of 75 cm/s, and a maximum weight of 500 ton. The following test series was conducted: 1) semi-active control by MR dampers (base-isolation system and seismic control system), 2) damage detection system (identification of damaged members and evaluation of new sensors), 3) rocking energy dissipation system (lift-up system). This paper outlines the objectives of the large-scale tests, the design of the test frame for each objective, and the static and dynamic characteristics of the test frame.

KEYWORDS: Large Scale Test, Smart Structure, Performance Verification, Shaking Table, MR damper, Rocking System, Sensor Technology

1. INTRODUCTION

The Building Research Institute (BRI) of Japan and the U.S. National Science Foundation (NSF) initiated the U.S.-Japan Cooperative Research Program on Auto-adaptive Media (Smart Structural Systems) in 1998 [1], under the aegis of the U.S.-Japan Panel on Wind and Seismic Effects of the U.S.-Japan Cooperative Program in Natural Resources. At the Joint Technical Coordinating Committee (JTCC) meeting, research items and plans were discussed in detail for three research thrusts: (1) structural systems, (2) sensing and monitoring technology, and (3) effecter technology.

BRI planned a series of large-scale tests to verify some smart systems developed in this project. The effectiveness of "Semi-active control by MR dampers", "Damage detection system" and "Rocking energy dissipation system" will be also confirmed.

This paper outlines the objectives of the large-scale tests, the design of the test frame for each objective, and static and dynamic characteristics of the test frame.

[1] Building Research Institute, 1 Tachihara, Tsukuba-shi, Ibaraki-ken, 305-0802, JAPAN
[2] National Institute for Land and Infrastructure Management, Ministry of Land, Infrastructure and Transport, 1 Tachihara, Tsukuba-shi, Ibaraki-ken, 305-0802, JAPAN
[3] Visiting Researcher, Building Research Institute, 1 Tachihara, Tsukuba-shi, Ibaraki-ken, 305-0802, JAPAN
[4] National Research Institute for Earth Science and Disaster Prevention, 3-1 Tennodai, Tsukuba-shi, Ibaraki-ken, 305-0006, JAPAN

2. OBJECTIVES OF LARGE SCALE TESTS

The basic test frame used for this large-scale test is a 3-story steel frame. It is 3m (1 span) x 4m (2m x 2 span) in plan and 6m high, weighs a total of 20 ton (including the weight of the 1st floor), and has a natural period of about 0.5 sec. Some devices for the response control system with semi-active MR dampers and for damage detection are installed in the middle frame in the shaking direction. Devices for the rocking energy dissipation system are installed in each column foot of the 1st story.

The NIED's shaking table (Photo 1) was used. Figure 1 shows the performance of the shaking table. The shaking table has a maximum displacement of 22 cm, a maximum velocity of 75 cm/s, and a maximum weight of 500 ton.

The following subjects are discussed with regard to the large scale shaking table test.

2.1 Response Control by Magneto-Rheological (MR) Fluid

Magneto-rheological (MR) dampers have been expected to control the response of civil and building structures in recent years, because of their large force capacity and variable force characteristics. The passive control has a limitation of damping effect to a certain range with frequency and input level in general. Semi-active control reduces both response displacements and accelerations. MR damper generates damping force, which does not depend on the piston speed [2]. The target of this subject is to improve the safety and functionality and habitability by controlling the response displacements and accelerations by using MR dampers.

For this purpose, MR dampers and a control algorithm have been developed and their validity is discussed by an analytical study and shaking table tests.

2.2. Damage Detection by Sensors

Monitoring the structural soundness of a building effectively reduces its life cycle cost. A series of experimental tests for a monitoring system has been conducted by measuring the process in which a concrete device is broken. Devices are inserted in the central structural plane in each frame story (Fig. 3). The same device is installed in each story, and the purpose of the test is to detect damage. The table was shaken several times. White noise excitation and micro tremor measurement were carried out before and after shaking.

Two identification methods were carried out one using the data of before and after shaking and the other using the data during shaking. For the first, we used the flexibility method, the story stiffness method and the identification method using multiple natural frequency changes, etc., and for the second we used the ARX model and parallel processing identification method[3].

2.3 Rocking Energy Dissipation System

Rocking systems that cause rocking vibration under appropriate control during earthquakes are now under development[4]. Some researchers have pointed out that the effects of rocking vibration can reduce seismic damage to buildings subjected to strong earthquake ground motions. One of these systems has weak base plates at the bottom of each steel first-story column. When the weak base plates yield during a strong earthquake, rocking vibration is caused in the building, as illustrated in Fig. 4.

Fig. 5 shows the test frame for examining the earthquake response reduction effects of this rocking system with base plate yielding (base plate yielding system). In each story of each frame, braces made of PC steel bars are installed to adjust the fundamental period of the test. With these

braces, the first natural period of the test frame becomes 0.18 sec. In this shaking table test, 1940 El Centro NS is used with its time axis shortened by $1/\sqrt{2}$. Thus, the first natural period of the test frame is almost equal to the predominant period of the inputted wave motion.

3. CHARACTERISTICS OF TEST FRAME

Figure 6 shows the Fourier spectrum of response acceleration of each story of the superstructure excited by white noise. The roof's primary predominant (1st mode) frequency is 1.83Hz. This means that the first natural frequency is 0.546 sec. However, the 2nd spectrum value is smaller than the 3rd value on the 3rd floor and, the 2nd spectrum value is larger than the 3rd value on the 2nd floor. This means that the secondary mode vibration is being generated.

Tables 1-3 shows the characteristics of test frame.

4. CONCLUSIONS

This paper has described the characteristics of a large-scale test frame. One test frame was used for four series of experimental tests to verify each developing technology, such as semi-active control for base-isolation and seismic response control, damage detection and rocking energy dissipation. This large-scale experimental test verified the validity of application of those systems to smart structures, and useful experimental results were obtained for the settlement of future research.

Acknowlegement

This work has been carried out under the US-Japan cooperative structural research project on Smart Structure Systems (Chairperson of Japanese side: Prof. S. Otani, University of Tokyo, Chairperson of U.S. side: Prof. M. A. Sozen, Purdue University). We would like to acknowledge the hard work and contribution of all members of the project for their useful advice and suggestions.

REFERENCES:

[1] Otani S., Hiraishi H., Midorikawa M., Teshigawara M., Saito T. and Fujitani H.: Development of Smart Systems for Building Structures (Invited paper), Proc.of SPIE's 7th. International Symposium on Smart Structures and Materials, Paper No. 3988-01, 2000.3.

[2] Fujitani H., Sodeyama H., Hata K., Iwata N., Komatsu Y., Sunakoda K. and Soda S.: Dynamic Performance Evaluation of Magneto-Rheological Damper, Proceedings of Advances in Structural Dynamics 2000, Vol.1, 2000.12, pp.319-326.

[3] Morita K, Teshigawara M., Isoda H., Hamamoto T. and Mita A. (2001) Damage Detection Tests of Five-Story Steel Frame with Simulated Damages, Proc. of SPIE's 6th International Symposium on NDE for Health Monitoring and Diagnostics, Paper No. 4335-18, 2001.3.

[4] Midorikawa M., Azuhata T., Ishihara T., Matsuba Y., Mtsushima Y. and Wada A.: Earthquake response reduction of buildings by rocking structural systems, Proc.of SPIE's 9th. International Symposium on Smart Structures and Materials, Paper No. 4696-33, 2002.3.

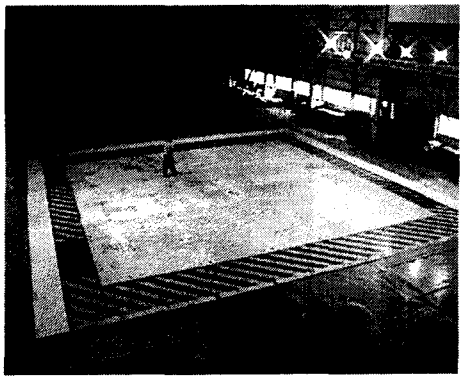

Photo.1 Shaking table of NIED

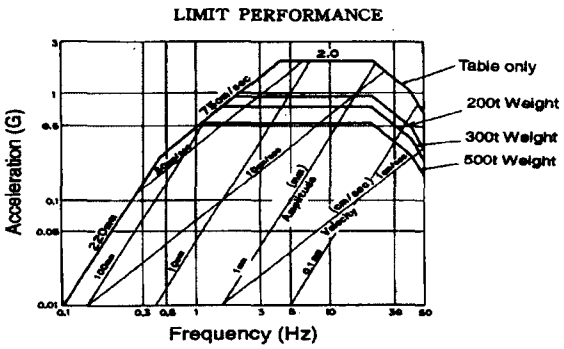

Fig.1 Performance of the shaking table

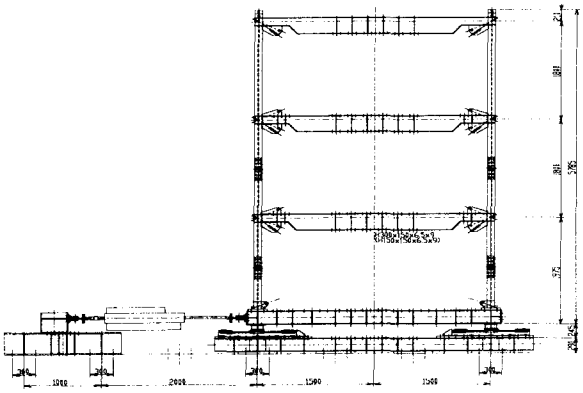

(a) Central frame of span direction for base isolation system

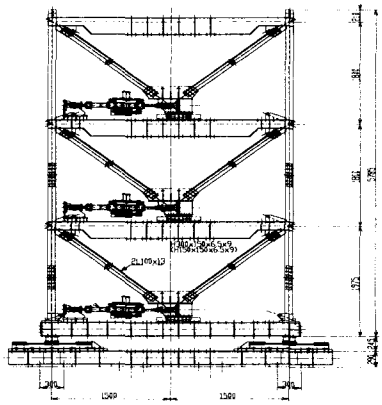

(b) Central frame of span direction for seismic response control

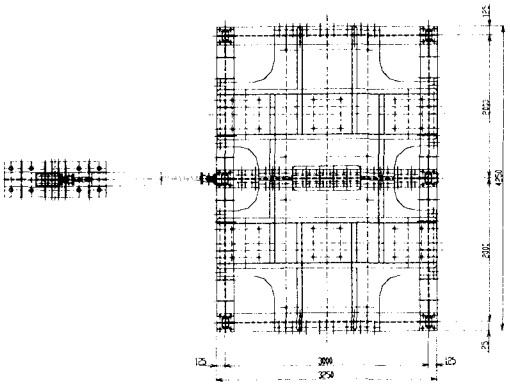

(c) First floor of base isolation system

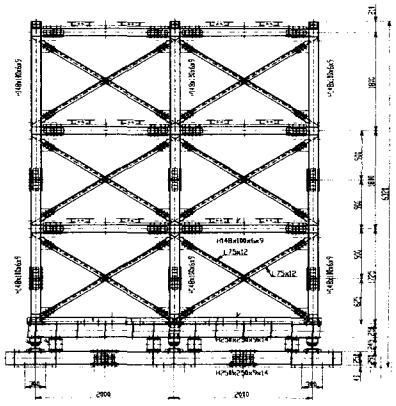

(d) Elevation of ridge direction for seismic response control

Fig. 2 Test frame for response control by MR dampers

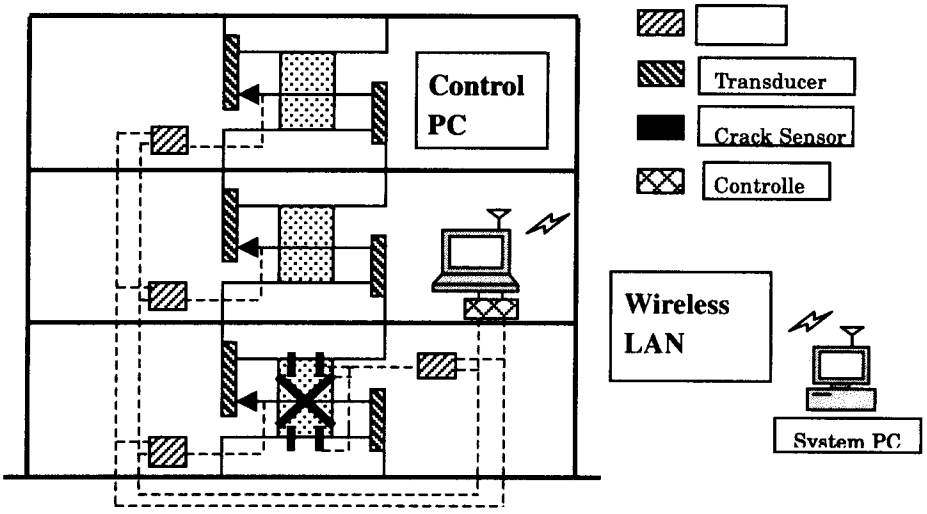

Fig.3 Central frame of span direction for damage detection and smart sensors

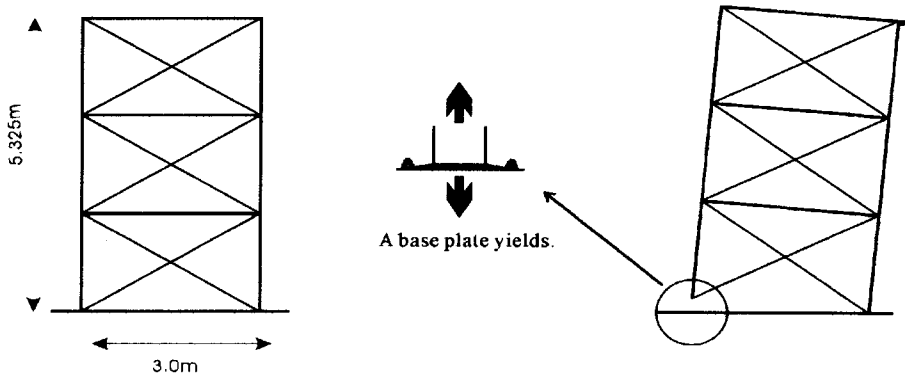

Fig.4 Outline of rocking system with base plate yielding

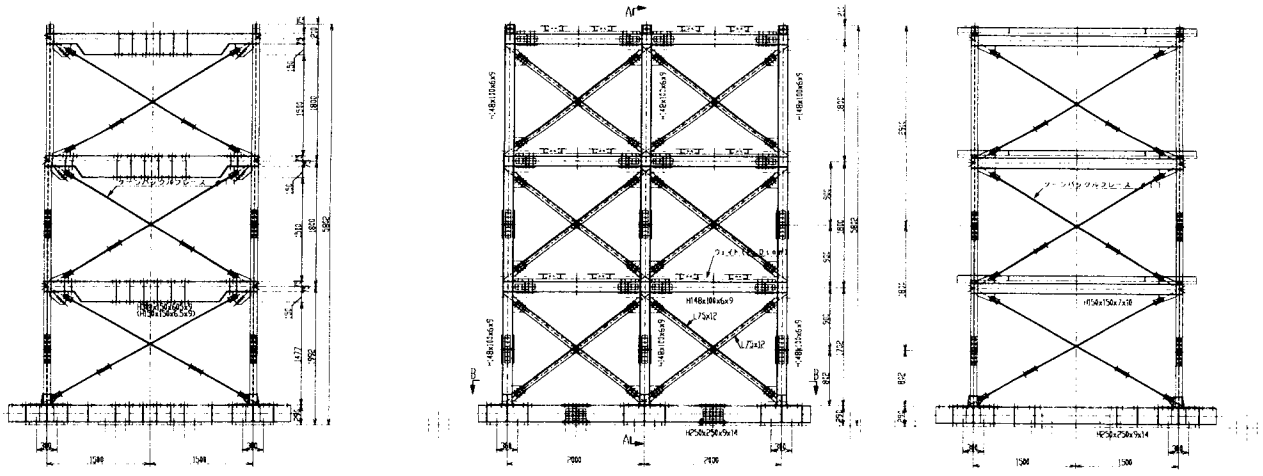

(a) Central frame in span direction

(b) Edge frame in ridge direction

(c) Edge frame in span direction

Fig.5 Test frame for Rocking Energy Dissipation System

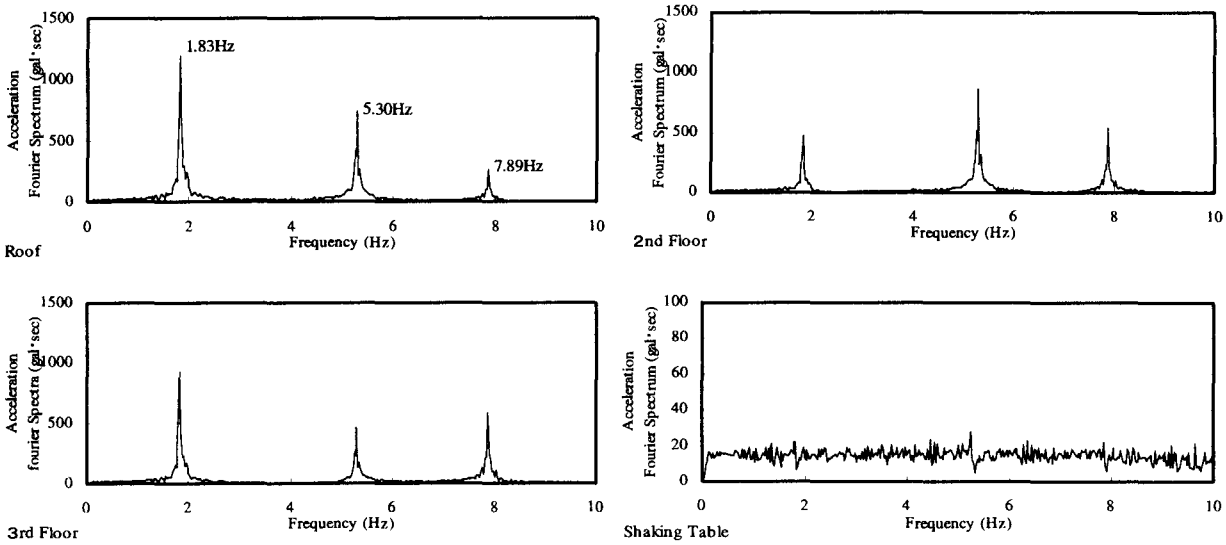

Fig.6 Fourier spectra of acceleration response of test frame

Table 1 Masses (ton)

Roof	4.67
3rd Floor	4.78
2nd Floor	4.78
1st Floor	6.00
Total	20.23

Table 2 Characteristics of Frame

	Stiffness(kN/cm)	Elastic Displacement(cm)
3F	27.6	1.74
2F	28.4	3.00
1F	35.4	2.27

Table 3 Characteristics of Base Isolation

Stiffness(kN/cm)	1.01
Friction Force(kN)	0.692
Damping Coefficient(kNs/cm)	0.0333
Damping Ratio	0.037
Natural Period(sec)	2.84

Earthquake Recording in Buildings as a Tool for the Comprehensive Structural Performance Evaluation

by

Izuru Okawa[1], Toshifumi Fukuta[2], Masanori Iiba[1], Masaomi Teshigawara[1], Toshihide Kashima[2], Kouichi Kusunoki[1], and Shin Koyama[3]

ABSTRACT

The Building Research Institute (BRI) has been in charge of the strong motion recordings in buildings since 1955. The BRI is currently maintaining totally 78 recording sites nationwide. After the 1995 Hyogo-ken Nambu earthquake, recognizing the importance of quick grasp of damage extent and setup of evacuation and restoration activity, nationwide strong motion observation networks such as Kyoshin net (K-net) maintained by the National Research Institute of Earth Science and Disaster Prevention, the Science and Technology Agency (STA) and the Seismic Intensity seismometers maintained by the JMA and most of local governments were established. Massive data are released open to the public, once big earthquake occurs. In October 6, 2000 and March 24, 2001, large earthquakes occurred in the western part of Japan. The previously mentioned networks collected the ground motion data for wide area surrounding the epicenters. Those data has actually brought great advances in the strong motion prediction methodology. However, when we focus on the *strong motion* property variations within the local area or even around one construction site, the aforementioned network does not necessarily give sufficient data for evaluating local site effect or effective input motions for specific building structures. The instrumentation density is still quite sparse except for large cities. Recently, the Building Standard Law of Japan has been revised in accordance with the performance-based-design oriented scheme. In the scheme, the structural designer is requested to quantitatively evaluate the structural performances for various types of external disturbances including earthquake motions. The developments of detailed evaluation techniques for structural performance will be one of the most important tasks of the BRI. This paper describes how we can develop and utilize our strong motion recording system for realizing the quantitative evaluation of structural performance against earthquake motions.

KEYWORDS: Earthquake Recording, Structural Performance, Nationwide Network, Effective Input Motion

1. INTRODUCTION

The Building Research Institute (BRI) published many epoch-making records such as the Kawagishi-cho apartment building, during 1964 Niigata earthquake, recording the tilting action of the apartment building due to soil liquefaction. We believe this was the first recording of liquefaction phenomenon in the world. After that, we had also obtained large earthquake record in the campus of Tohoku university, during 1978 Miyagiken-oki earthquake. The earthquake was recorded at the 1st and 9th floor of the building on the campus. The amplitude in the first floor was still large enough at the time. Attention was drawn from many researchers that the 9th floor accelerogram showed amplitude more than 1G. We had also large amplitude records during 1993 Kushiro-oki earthquake, and 1994 Hokkaido Toho-oki earthquake and 1994 Sanriku Haruka-oki earthquake from the recording system. The location of the recording sites maintained by BRI is shown in Figure 1 for nationwide recording sites. The BRI maintains totally 78 recording sites. There are four types of recording system, i.e.,

(1) Nationwide Strong Motion Recoding Sites
(2) Sendai Dense Instrumental Array in Ground
(3) Recording Network in Tokyo Metropolitan Area

[1] Structural Engineering Department, BRI
[2] IISEE, BRI
[3] National Institute for Land and Infrastructure Management

(4) Tsukuba Dense Instrumental Array in Building and Ground

The detail for each recording system is introduced in the references. The recording system (1) has the longest history among the BRI system and has been continued more than 40 years. The instrumentation is mostly made in the building. However, the newer sites has nearby free field seismometer, if it was made possible, to obtain the data on effective input motion. Three instrumentations in the newly built base-isolated buildings have recently been added.
The recording system (2) in Sendai area is conducted to clarify the soil amplification characteristics of the various surface soil conditions. This system does not include the instrumentation in buildings.
The systems (3) and (4) were completed quite recently. Therefore, the number of data is not so large until now. Most of the recording sites classified into (3) include the recording point nearby free field. The recording system (4) is deployed on the BRI campus in Tsukuba. It is equipped with 66 channels of sensors for detecting more detailed behavior of the building-soil system during earthquake.

2. ROLE OF THE NATIONWIDE STRONG MOTION OBSERAVATION SYSTEM

After the 1995 Hyogo-ken Nambu earthquake, recognizing the importance of quick grasp of damage extent and setup of evacuation and restoration activity, nationwide strong motion observation networks such as Kyoshin net (K-net) maintained by the National Research Institute of Earth Science and Disaster Prevention, the Science and Technology Agency (then STA) and the Seismic Intensity seismometers maintained by the JMA and most of local governments were established. Massive data are released open to the public, once big earthquake occurs.
The location of such nationwide recording sites is shown in Figure 2 for only Kanto area. The open circles indicate the K-net sites and the open triangles indicate the JMA sites. The solid circles indicate the BRI sites in the area. In addition to this, the small dots indicate the location of local governments in the area. It can be said that large proportion of the local governments installed seismometers in their main office. The installation was not, however, confirmed within the work of this paper.

In October 6, 2000 and March 24, 2001, large earthquakes occurred in the western part of Japan. The previously mentioned networks collected the ground motion data covering wide area surrounding each of the epicenters.
Figure 3 shows the location of the recording sites in the central part of Yonago city located in the western part of Japan facing to the Japan Sea. The BRI maintains a seismometer on the basement of Yonago city hall building. The K-net and JMA also keep the recording site near the BRI site. During the October 6, 2000 earthquake, three sites obtained large acceleration records. The velocity response spectra for those motions are shown in Figure 4. It is seen that there are big difference in spectral ordinates in spite that the sites locate closely. This is considered to be due to the difference of soil conditions and installation conditions. One should see the spatial distribution of ground motions to assign which motion represents the typical motion of the area. Therefore, it can be said that we should see the severity of ground motion by not only single recording point data but a scatter of motions within the area concerned.

3. IMPORTANCE OF EFFECTIVE INPUT MOTIONS FOR DESIGN PURPOSES

The BRI seismometers had generally been installed only inside of buildings with few exceptions since its beginning. Considering the larger amplitude recorded on the free field sites compared with the record in building, we came up to conclude that we need to identify the difference between the free field and in-building recorded motions. Recently we set up two series of earthquake recording systems previously identified as (3) and (4). One is a system with 2 to 4 three-component sensors in one site installing on first or basement floor, top floor and nearby free filed. We installed seismometers at 19 sites around greater Tokyo metropolitan area. The recording sites are also shown in Figure 2. It is not easy, however, to find places for free field, since there are few free grounds with negligible influence of buildings, especially in Tokyo. Here, we basically adopt the selection of the instrumentation locations in each building as shown in Figure 5.
The other is the dense instrumentation to building and surrounding ground including deep boreholes. We set up this system in newly constructed 8-story steel reinforced concrete (SRC) building

next to the main building on our campus. The deployment of instruments is shown in Figure 6. Totally 66 channels will record an event when the motion exceeds a preset amplitude level. We believe the recording system of this kind is necessary as a prototype for evaluating the near-actual behavior of building-soil system, although this is never a proposal for general recording system for buildings. The average spectral ratios of basement and 8th floor with respect to the ground surface are shown in Figure 7. Using the sway and rocking model, the interaction effect is evaluated for this building. (Kashima, 2001)

4. THE STRATEGIES OF THE EARTHQUAKE RECORDINGS IN BUILDINGS

Recently we set up the following items as our main target of the strong motion instrumentations.
(1) Evaluation of effective input motions
(2) Detailed database construction indicating Structural Performance
(3) Promoting the instrumentation in buildings
When we focus our attention on the strong motion property variations within the local area or even around one construction site, the aforementioned nationwide network does not necessarily give sufficient data for evaluating local site effect or effective input motions for specific building structures. The instrumentation density is still quite sparse except for specific large cities. However, it is not easy to increase the number of instrumentations only by appealing the necessity of the earthquake data for buildings. There should be incentives for promoting the instrumentations in buildings.
Meanwhile, the Building Standard Law of Japan has been recently revised in accordance with the performance-based-design oriented scheme. In the scheme, the structural designer is requested to quantitatively evaluate the structural performances for various types of external disturbances including earthquake motions. The developments of detailed evaluation techniques for structural performance should be done and it will become one of the most important tasks of the BRI. We need firstly identify that the earthquake recording gives a reliable tool for evaluating the seismic performance of buildings. The earthquake recording is generally still costly. If earthquake recording is to be utilized for detecting the vibratory characteristics of building as one of the crucial performance indices, a cost reduction of instrumentation will be secondly an important issue for wide use. When such situation is realized, more dense locations of instrumentation sites will be become possible. (See Figure 8)

5. CONCLUSIONS

The nationwide strong motion recording operated by NIED or JMA are mainly set up for ground behavior and does not assume some specific structures. The behavior of each structural system, such as building, bridge, dam, and port facilities is investigated by the organization as specific research objectives. A coordination may be necessary between such organizations with general and specific purposes for the efficient utilization of strong motion recording systems. In addition, the accumulation of the recorded motions with various classes of buildings including behavior not only for superstructure but also foundation and pile foundation as well as ground is our next issue to establish the advanced structural design schemes in the future. In addition, the possibility for the earthquake recording to be used for evaluating the structural performance should be considered. A low cost instrumentation and the performance evaluation utilizing the recorded motion in conjunction with development of the new design scheme will increase the database of earthquake response of buildings.

REFERENCES:

1) T. Kashima et al., "Strong-Motion Observation Program in the Metropolitan Area", (in Japanese) Proceedings of the AIJ Annual Meeting, Vol.B-2, pp.275-276, Kinki, 1997
2) T. Kashima et.al., "Earthquake Motion Observation in and around 8-Story SRC Building", (in Japanese) Proceedings of the AIJ Annual Meeting, Vol.B-2, pp.213-214, Kyushu, 1998
3) I.Okawa, et.al., "Dense Instrumentation in BRI Building and Surrounding Ground", Proceedings UJNR Workshop on Soil-Structure Interaction, Menlo Park, California, September 22-23, 1998
4) T. Kashima, "Earthquake Motion Observation and SSI Characteristics of an 8-story Building in BRI", The Proceedings of the 2nd U.S.-Japan Workshop on Soil-Structure Interaction, March 6-8, Tsukuba, Japan, 2001
5) I. Okawa, "Earthquake Recording for SSI Study by BRI", The Proceedings of the 2nd U.S.-Japan Workshop on Soil-Structure Interaction, March 6-8, Tsukuba, Japan, 2001

Table 1 The list of Recording Sites in Nationwide Strong Motion Observation Network by BRI

Code	Name	Instrument	Structure	SensorPlaces
KGC	Kushiro Government Collective	SMAC-MDU	RC(BI)/B1F+9F+P1F	GL, G10, G34, B1F, 01F, 09
HRO	Hiroo Town Office	SMAC-MD	RC/2F	01F
HKU	Hokkaido University	SMAC-MD		GL
HKD	Hakodate Development and Construction Department, Hokkaido Development Bureau	SMAC-MD		GL
HCN	Hachinohe City Hall	SMAC-MD	RC/B1F+6F+P1F	B1F, 06F
HCN2	Annex, Hachinohe City Hall	SMAC-MDU	SRC(BI)/B1F+10F+P1F	GL, G30, G105, 10F, 01F, P
ATG	Atago Junior High School, Miyako	SMAC-MD	RC/2F	01F
AKT	Akita Prefectural Office	SMAC-MD	RC/B1F+6F+P3F	08F, B1F
THU	Tohoku University	SMAC-MD	SRC/9F	01F, 09F
SND	Sendai Government Collective Office	SMAC-MD	S/B2F+15F+P2F	B2F, 15F, G40
IWK	Iwaki City Hall	SMAC-MD	SRC/B1F+8F+P1F	B1F, 09F
MNM	Minamisuna Apartment #3	SMAC-MD	SRC?/14F+P3F	15F, 01F
CGC	Central Government Collective	SMAC-MD	S/B3F+20F+P1F	01F, 20B, 19C
OTM	Otemachi Government Collective Office #3	SMAC-MD	SRC+S/B3F+15F+P2	16F, B3F
BRI	Building Research Institute	SMAC-MD	RC/1F	01F
NIG	Niigata City Hall	SMAC-MD	RC/B1F+6F+P2F	B1F, 07F
JET	Joetsu Social Education Office	SMAC-MD	RC/2F	01F
NGN	Nagano Prefectural Office	KSG	?/B1F+10F+P2F	B1F
ISK	Ishikawa Prefectural Office	SMAC-MD	RC?/B2F+4F+P1F	05F, B2F
KSO	Kiso Office, Nagano Prefecture	KSG	RC/B1F+5F+P2F	B1F
SMS	Shimoda Office, Shizuoka Prefecture	SMAC-MD		GL
SMK	Shimoda-kita High School	SMAC-MD	RC/4F	01F
HMO	Hamaoka Nuclear Power Plant	SMAC-MD		GL
MTS	Matsusaka Office, Mie Prefecture	SMAC-MD	RC/6F+P1F	07F, 01F
SNG	Shingu City Hall	KSG	RC/B1F+4F+P1F	B1F
MIZ	Maizuru City Hall	KSG	RC/4F+P2F	01F, 05F
OSK	Osaka Government Collective Office	SMAC-MD	S/B3F+15F+P3F	18F, B3F
YNG	Yonago City Hall	SMAC-MD	RC/B1F+5F+P1F	B1F
HRS	Hiroshima Government Collective Office #2	SMAC-MD	SRC/B1+11F+P2F	B1F, 11F
HMD	Hamada Office, Shimane Prefecture	SMAC-MD	RC/3F+B1F	01F
KCK	Kouchi Work Office, Shikoku Regional Construction Bureau	KSG	RC/4F	01F, 04F
MYZ	Miyazaki Prefectural Office	SMAC-MD	SRC/B1F+9F+P1F	01F, 09F
OIT	Oita City Hall	SMAC-MD	SRC?/B2F+9F+P1F	01F, 09F
NBO	Nobeoka Office, Miyazaki Prefecture	KSG	RC/3F+P1F	01F, 04F
MYK	Miyakonojo Office, Miyazaki	KSG	RC/B1F+3F+P2	B1F
YKH	Yokohama Government Collective Office #2	SMAC-MD	S/B3F+22F+P2F	23F, B2F
HRH	Hirosaki Legal Affairs Office	SMAC-MDU	RC/3F	01F
TRO	Tsuruoka Government Collective Offic	SMAC-MDU	RC/4F+B1F	01F, 04F
SMZ	Shimizu Government Collective Office	SMAC-MDU	SRC/6F	01F, 06F
NGY	Nagoya Government Collective Office	SMAC-MDU	SRC/11F+B2F	GL, B2F, 12F
TKM	Takamatsu Regional Taxation Bureau	SMAC-MDU	SRC/8F+B1F	GL, B1F, 09F
FKO	Fukuoka Government Collective Office	SMAC-MDU	SRC/10+B1	GL, B1F, 10F
NMW	National Museum of Western Art	SMAC-MDU	RC(BI)/B1F+3F	GL, PITE, PITW, 01FE, 01F
SGS	Sengen Shrine	SMAC-MDU		GL
KYM	Kiyomuzuyama Park	SMAC-MD2		01F
KSG	Koshigaya Branch, Urawa Legal Affairs Bureau	SMAC-MDU		1F, 1F[V]
ANX	Annex, Building Research Institute	AJE-8200	SRC/8F+B1F	A01, A14, A43, A89, N14, B C01, BFE, BFN, BFS, 1FE, 2FE, 2FW, 5FE, 5FW, 8FE, 8 8FS, MBC, M5C, M8C, M8E

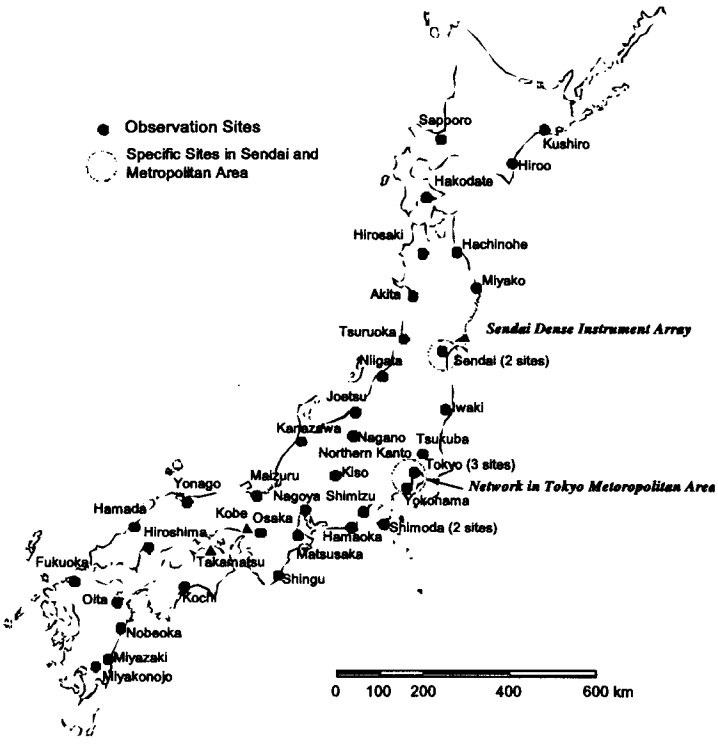

Strong Motion Observation Sites operated by Building Research Institute

Figure 1 Strong Motion Recording Sites by

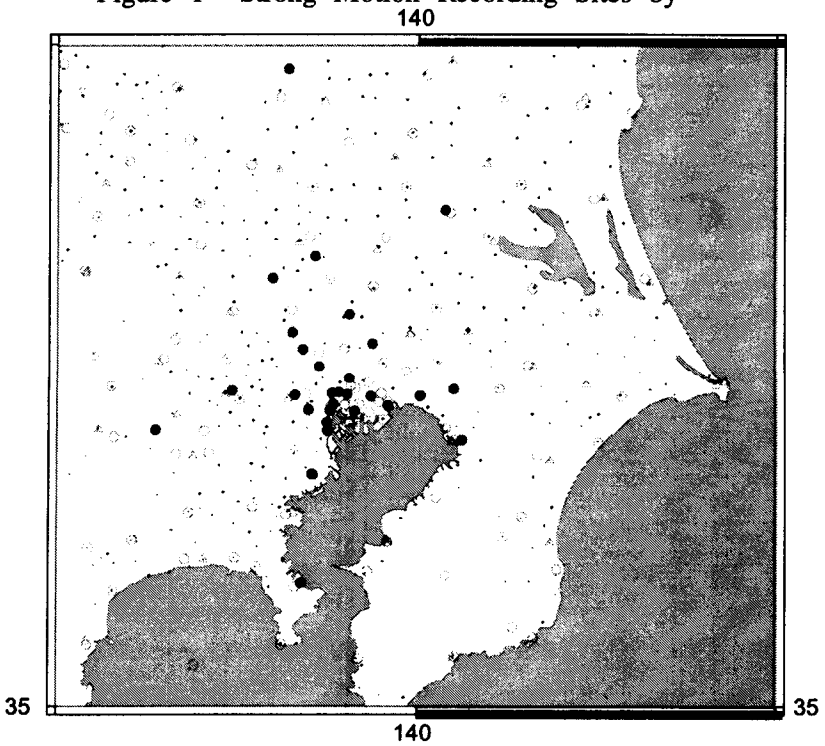

Figure 2 Strong Motion Recording Sites by BRI (Big solid circle), K-net (open circle), and JMA (open triangle). Other small dots indicate the locations of the main office buildings of local governments. The installation of seismometers thereupon are not confirmed

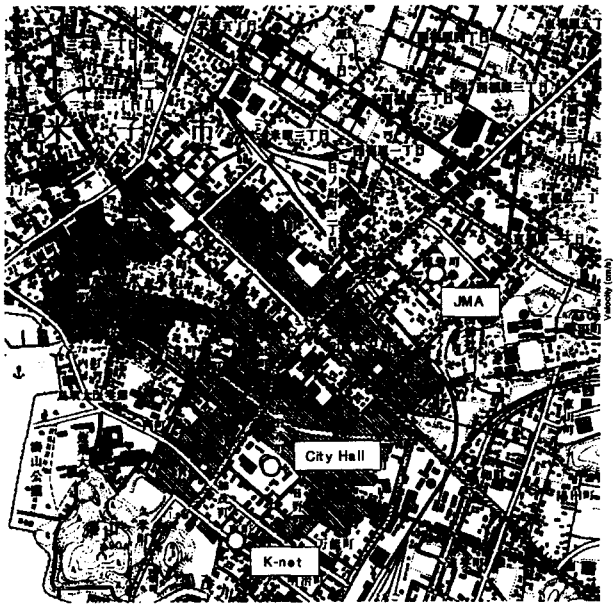

Figure 3 Strong Motion Recording Sites in Yonago city

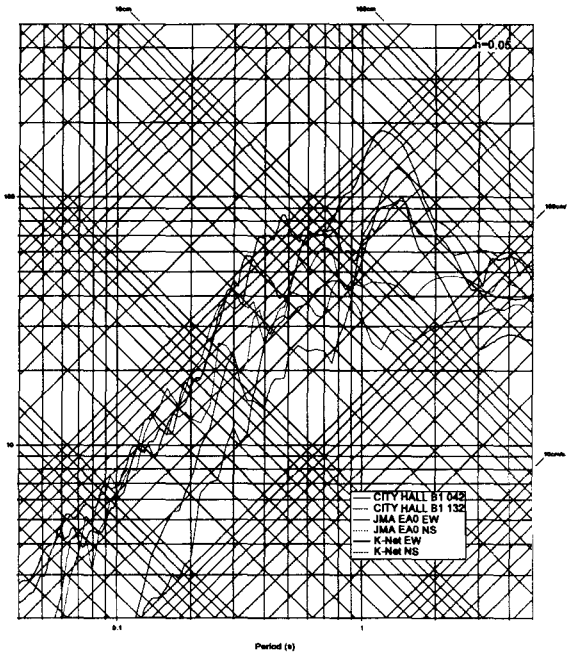

Figure 4 Comparison of velocity response spectra for BRI, K-net and JMA sites

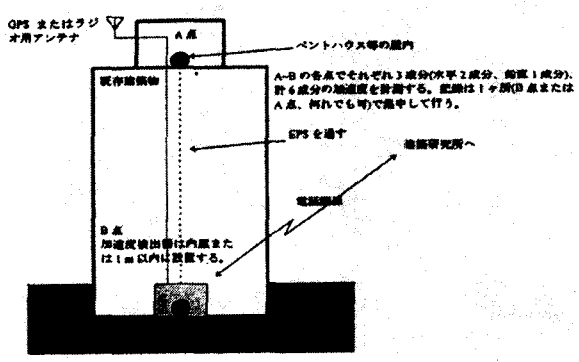

図1 6成分強震観測装置(①-③)

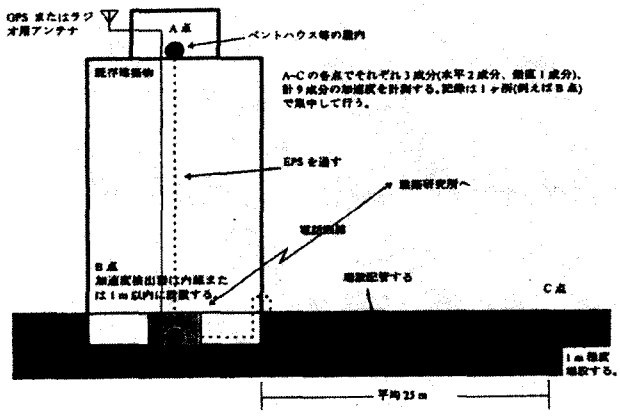

Figure 5 Installation of seismometers in buildings/
Upper: Basement and top floors
Lower: Basement, top floor and free field

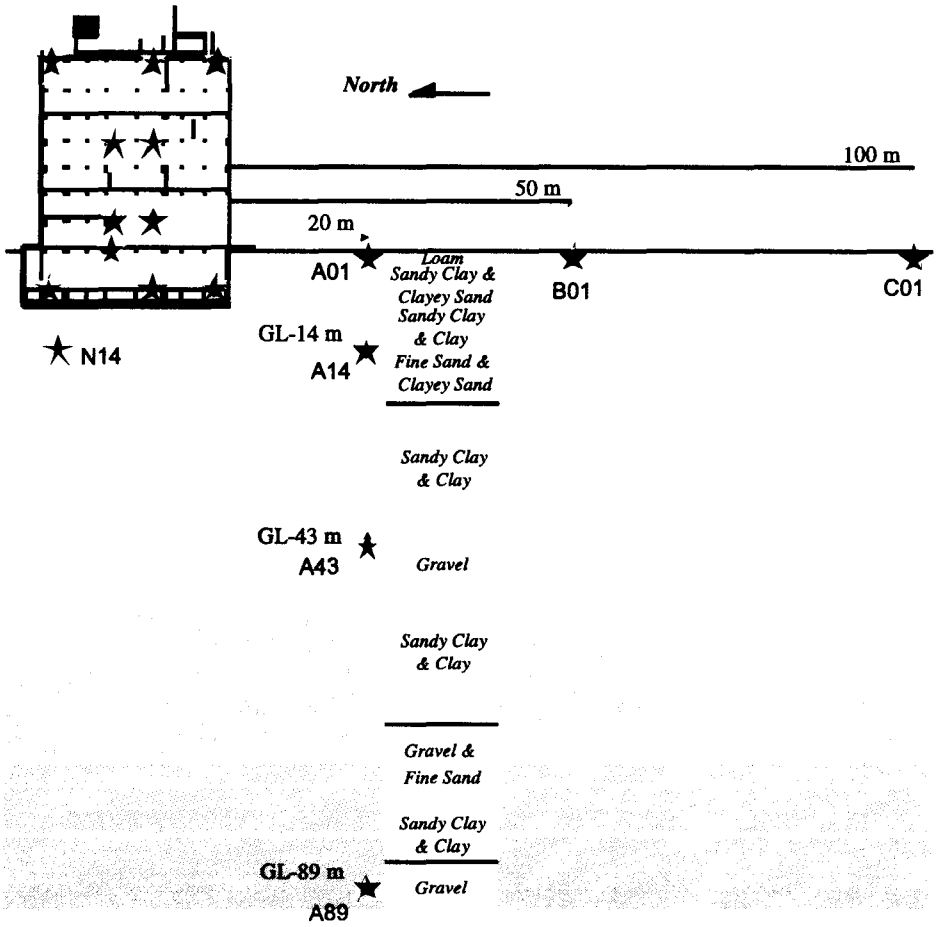

Figure 6 Dense instrumentation in and around the BRI annex building and surrounding ground

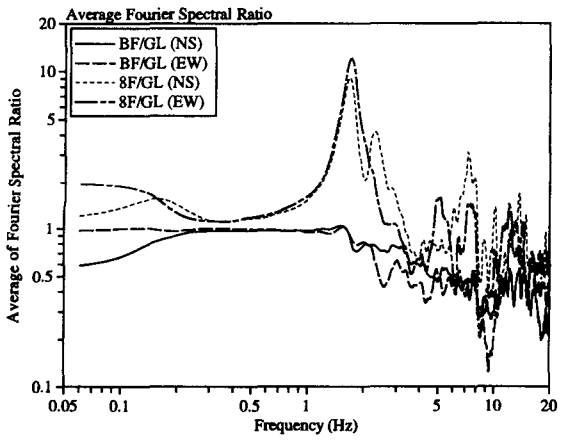

Figure 7. Average Fourier Spectral Ratio of records at BF and 8F to GL

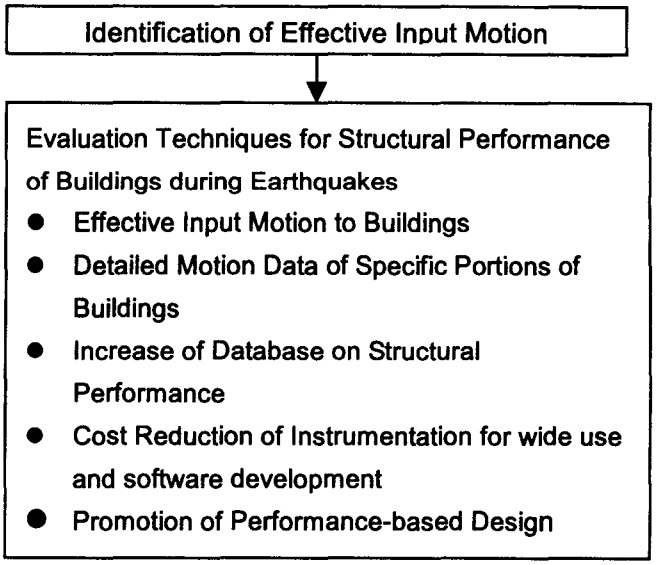

Figure 8. Objectives of Earthquake Recordings in Buildings

APPENDIX

Report of Task Committee A
GEOTECHNICAL ENGINEERING AND GROUND MOTION

Date: 13 May 2002

Place: National Institute of Standards and Technology, Gaithersburg, MD, USA

Attendees:			
	U.S. Side --	Mehmet Celebi (Co-Chairman)	USGS
		Michael Sharp (Co-Chairman)	CORPS
		Harish Chander	DOE
	Japan Side --	Osamu Matsuo (Co-Chairman)	NILIM
		Takahiro Sugano (Co-Chairman)	PARI
		Keiichi Tamura	PWRI
		Shojiro Kataoka	NILIM
		Shuji Tamura	Shinshu University

1. Objective and Scope of Work

The objectives of work include:
(1) To promote sharing of strong motion earthquake data among researchers and practicing engineers, and enhance the availability of technology for evaluating the destructive effects of earthquake motion, and
(2) To promote research on the dynamic behavior of soils, foundations and earth structures during earthquakes.

The scope of work includes:
(1) Exchange strong motion data regularly and identify significant issues.
(2) Exchange information on technological developments, state-of-the-art and practice related to strong motion recording, hazard mapping, soil-structure interaction, soil behavior and stability during earthquakes,
(3) Exchange field data related to geotechnical engineering, and
(4) Plan and conduct programs of cooperative research and/or workshops in coordination with the proposed or ongoing programs.

2. Accomplishments

(1) Task committee published and distributed (CD-ROM) the proceedings of the second U.S.-Japan Workshop on Dynamic Soil-Structure Interaction that was held in Tsukuba, Japan, March 6-8,2001.
(2) Through US side secretary general and through Japanese side experts, a new CD-ROM data set containing the main-shock and aftershock records of the 1999 Izmit and Duzce, Turkey earthquakes (USGS OFR 01-163) was provided to Japan side.
(3) The Task Committee members have been cooperating in the following research projects:
   a) Physical and Numerical Simulation of Structural Damages Due to Liquefaction and Development of Countermeasure Techniques, 1994-2004, by the National Research Institute for Earth Science and Disaster Prevention (NIED), Building Research Institute (BRI) and Wayne State University (WSU), and
   b) Application of the Nuclear Magnetic Resonance Imaging (NMRI) Method to the Study of Soil Behavior and Stability During Earthquakes, by Port and Airport Research Institute (PARI) and Colorado School of Mines and the Lovelace Institute.

3. Future Plans

The future plans include:

(1) Plan to hold the fifth workshop on geotechnical earthquake engineering in early 2003 in San Diego, in conjunction with the workshop on seismic performance of urban, reclaimed and port areas. The workshop will be coordinated by Dr. T. Sugano and Dr. Michael Sharp-co-chairmen of the Task Committee and Prof. Scott Ashford of U.C., San Diego.

(2) Plan the 3rd US-Japan Workshop on Soil-Structure Interaction for 2003 {Responsible members: Celebi & Okawa).

(3) Plan a workshop on Real-Time Instrumentation of Densely Urbanized Areas and Instrumentation of Civil Engineering Structure. [Temporary Committee: Fujiwara, Okawa, Kusakabe, Borcherdt, Wald, Celebi]

(4) Continue the cooperative research "Physical and Numerical Simulation of Structural Damages Due to Liquefaction and Development of Countermeasure Techniques, 1994-2004", by the National Research Institute for Earth Science and Disaster Prevention (NIED), Building Research Institute (BRI) and Wayne State University (WSU). [Responsible Members: Dr. Minowa and Professor Kagawa].

(5) Explore the possibility of joint research on site response issues (Responsible Members: Dr. Matsuo & Dr. Borcherdt).

Report of Task Committee B
NEXT-GENERATION BUILDING AND INFRASTRUCTURE SYSTEMS

Date: 13 May 2002

Place: National Institute of Standards and Technology, Gaithersburg, MD, USA

Attendees:			
	U.S. Side --	George Lee (Co-Chairman)	MCEER
		Peter Chang (Co-Chairman)	NSF
		H.S. Lew	NIST
		Adam Rose	Penn Sate
		William Roper	GWU
		Josephine Malilay	CDC
	Japan Side --	Masaomi Teshigawara (Co-Chairman)	BRI
		Keiichi Ohtani (Co-Chairman)	NIED
		Kazuhiko Fujihashi	NTT

1. Objectives and Scope of Work

1) Objective

The objective of the task committee is to enhance the development and implementation of innovative and new (i) materials; (ii) enabling technologies; (iii) evaluation, analysis, design, construction and maintenance methods; through cooperated individual and organized and networked analytical and experimental approaches for the next – generation building and infrastructure systems.

Opportunities during the next few years include experimental observations on the performance of model and near full – size structures using large scale testing facilities and networked earthquake engineering experimental facilities, and the development of innovative technologies and approaches to address the newly obtained analytical conclusions and observed experimental evidences and to formulate various performance based engineering guidelines for building and infrastructure systems.

2) Scope of work

(1) Enhancement of exchange of information and personnel
(2) Coordinate joint research including the utilizing experimental facilities.
(3) Coordinated development of database, test procedures, guidelines for test result interpretation and application.
(4) Development of new materials and technologies for condition assessment, retrofit of existing buildings and design of new buildings.
(5) Conduct joint workshops and joint meetings to identify research opportunities, new projects, and make recommendation for UJNR Panel.

2. Accomplishments

(1) The US-Japan grantees' meeting for Composite and Hybrid Structures, June 24 to 27, 2001 in Berkeley, CA. The committee will plan for the publication of CHS design guides and other research reports summarizing the experimental and analytical research activities.

(2) A workshop to identify and develop specific joint projects and cooperative activities within the general scope of Task Committee B was held at NSF attended by the four co-chairs together with Dr. S.C. Liu in August 13 of 2001.

(3) In February 27 of 2002, the two co-chairs of US and Japan together with Dr. S.C. Liu coordinated the session program of UJNR meeting.

3. Future Plans

(1) The 3rd U.S.-Japan Technical Coordinating Committee Meeting on Auto-Adaptive Media (Smart Structural Systems) will be held the end of October 2002, in Tsukuba, Japan.
(2) Task Committee B reviewed the status report of NEES (Network of Earthquake Engineering Simulation) provide by Dr. Joy Pauschke of NSF and expresses its desire for JTCC and/or other appropriate US and Japan groups to organize meetings to establish a US-Japan Coordinating research plan that will accelerate NEES program in US and performance-based design focusing on building functions, and health monitoring.
(3) Task Committee B plans to include societal and economic impact analysis in future activities, with initial emphases given to information technology, public health and security aspects of development of next generation building and infrastructure system. Alternatively, because information technology, infrastructure security, and disaster-related public health issues are important to activities of other task committees, it may be desirable to establish a separate panel-wide (task) committee to address such "trans-panel" or "trans-committee" activities as needs and opportunities arise.

4. Related Activity

(1) The 3rd grantee meeting, as part of the US-Japan cooperative research on urban earthquake disaster mitigation workshop was held on August 15-16, 2001, Seattle, Washington.
(2) JTCC for the discussion on next US/Japan cooperative research was held after the 3rd grantee meeting.
(3) The 4th grantee meeting, as part of the US-Japan cooperative research on urban earthquake disaster mitigation workshop will be held on October 21-22, 2002, Kyoto, Japan.
(4) The foundation work of the 3-D Full-scale Earthquake Testing Facility at Miki by NIED has been completed. Super structures are under construction. And whole facility will be completed by early 2005.

Report of Task Committee C
DAMS

Date: 13 May 2002

Place: National Institute of Standards and Technology, Gaithersburg, MD, USA

Attendees:	U.S. Side --	Dr. Robert L. Hall (Chairman)	USACE-ERDC
		Dr. Enrique E. Matheu	LSU
	Japan Side --	Dr. Yoshikazu Yamaguchi (Chairman)	PWRI
		Dr. Ken-ichi Torii	NILIM

1. Objectives and Scope of Work

To develop technical insights into better understanding of the response of dams to seismic effects, the T/C will plan, promote, and develop research initiatives to assist in assuring seismic safety and economical protective countermeasures against earthquake loading for these critical structures.

The scope of work includes:

(1) Develop methods of analysis for seismic design of dams including outlet works:

- Comparative analysis of design methods and evaluation criteria used by U.S. and Japan.
- Development of "Design Earthquake Ground Motions" for analysis and evaluation of dams.
- Assessment of models and numerical procedures used for seismic dynamic analysis.

(2) Perform research to better understand the dynamic characteristics of dam construction materials and site conditions.

- Strength and deformation characteristics of concrete, soil and rock materials during earthquakes.

(3) Evaluate observed performance of dams and outlet works during earthquakes.

- Develop a database that contains measured ground accelerations and dynamic response of dams and outlet works during earthquakes, and other related information necessary to evaluate their seismic behavior, such as experimental and/or analytical data with description of test and analysis procedures used.
- Investigation of damage mechanisms due to earthquake loading.
- Application of the analysis of the observed dynamic behavior to the improvement of design criteria.

2. Accomplishments

(1) The Task Committee developed a database that contains measured ground accelerations and dynamic response of dams and outlet works during earthquakes. The database has been expanded to include other relevant information necessary to evaluate their seismic behavior, such as experimental and/or analytical data with description of test and analysis procedures used.

(2) In investigating seismic design ground motions at dam sites in Japan, technical information from U.S. in this field was referred to.

(3) The U.S.- and Japan-side Task Committee members have actively planned, advertised, and organized the upcoming "***3rd U.S.-Japan Workshop on Advanced Research on Earthquake Engineering for Dams***", San Diego, USA, June 22-23, 2002:

- The Organizing Committee is chaired by Dr. Robert Hall (U.S. Army Corps of Engineers), and it also includes Dr. Yoshikazu Yamaguchi (PWRI), Dr. Enrique E. Matheu (Louisiana State University) and Dr. Ziyad H. Duron (Harvey Mudd College).
- The workshop is co-sponsored by the U.S. Army Engineer Research and Development Center (ERDC) and the U.S. Society on Dams (USSD). It will be part of the pre-conference activities of the ***22nd USSD Annual Meeting and Conference*** (to be held at the same location on June 24-28, 2002).

3. Future Plans

(1) The Task Committee will continue the current efforts focused on the development of improved mechanisms to facilitate the continuous exchange of results of research activities and general technical information related to dam earthquake engineering.

(2) The Task Committee will coordinate exchange visits of scientists and engineers from the U.S. and Japan. A series of technical problems of mutual interest will be identified and prioritized and they will serve as the focus for this exchange program.

(3) The Task Committee will promote the development of a research program to improve test and analysis procedures based on the comparative study of representative case studies that will be available in the jointly developed database

(4) The Task Committee will conduct the "***3rd U.S.-Japan Workshop on Advanced Research on Earthquake Engineering for Dams***" June 22-23, 2002. The Task Committee will compile the technical contributions in the corresponding Workshop Proceedings that will be published by ERDC later in the year.

- The workshop will focus on a variety of technical aspects covering concrete and embankment dams, and outlet works. The technical sessions will address seismic evaluation criteria, numerical techniques for seismic analysis, seismic design and evaluation of appurtenant structures, instrumentation, condition assessment, seismic upgrade and rehabilitation, foundation problems, case studies, as well as many other general topics.
- The program includes several keynote lectures and invited presentations from well-recognized participants from government agencies, academia, and private sector. The technical presentations include eight papers from Japan and 20 papers from the U.S. and other countries.

4. Task Committee Members:

U.S. Side --	Dr. Robert L. Hall (Chairman)	USACE-ERDC
	Dr. Enrique E. Matheu	LSU
	Ms. Anjuna Chudgar	USACE
	Mr. David Dollar	USACE
	Dr. Richard C. Dove	USACE-ERDC
	Dr. Richard Olsen	USACE-ERDC
	Mr. Rick Peoppelman	USACE
Japan Side --	Dr. Yoshikazu Yamaguchi (Chairman)	PWRI
	Dr. Osamu Matsuo	NILIM
	Mr. Kaoru Niwa	Japan Dam Eng. Ctr.

Dr. Choshiro Tamura	Nippon University
Dr. Tatsuo Omachi	Tokyo Inst. of Tech.
Dr. Yoshio One	Aichi Inst. of Tech.
Mr. Takashi Tokoro	Japan Inst. Civil Eng.
Mr. Shuju Takasu	PWRI
Dr. Yasuhiko Wakizaka	PWRI
Dr. Kei-ichi Tamura	PWRI
Mr. Takashi Sasaki	PWRI
Mr. Hideaki Kawasaki	NILIM
Dr. Ken-ichi Torii	NILIM
Mr. Fumio Yonezaki	Water Resources Dev. Public Corp.
Mr. Akira Hara	Water Resources Dev. Public Corp.

Report of Task Committee D
WIND ENGINEERING

Date: 13 May 2002

Place: National Institute of Standards and Technology, Gaithersburg, MD, USA

Attendees:	U.S. Side --	Dr. Peter Chang (Chairman)	NSF
		Dr. Partha Sarkar	Iowa State U.
		Dr. Emil Simiu	NIST
		Dr. Fahim Sadek	NIST
		Dr. Nicholas Jones	Johns Hopkins
		Dr. Harold Bosch	FHWA
	Japan Side --	Dr. Hisashi Okada (Co-Chairman)	BRI
		Mr. Jun Murakoshi (Co-Chairman)	PWRI
		Dr. Hiroshi Sato	PWRI
		Dr. Yasuo Okuda	BRI
		Mr. Koichiro Fumoto	PWRI

1.Objective and Scope of Work

To exchange technical information and to jointly plan, promote, and foster research and dissemination, to improve understanding of wind and its effects on structures, establish more rational wind resistant design methods for structures, and to contribute to wind hazard mitigation. Specific objectives include:

(1) Facilitate collaborative research and cooperation between U.S. and Japanese researchers in wind engineering.
(2) Identify nuggets of success in wind engineering.
(3) Identify research needs in the areas of hazards mitigation, new technology, basic and applied research and social and economic impacts of wind hazard.

The scope of work includes:

(1) To characterize strong wind, especially boundary layer extreme winds.
(2) To study wind effects including wind loading on and wind-induced response of structures.
(3) To perform experimental and analytical methods to predict wind and its effects.
(4) To perform damage, wind hazard, and risk assessments and develop technologies for wind hazard mitigation.

To facilitate the above scope of work, conduct annual or biannual workshops to evaluate current and future research agendas that may lead to synergistic research between U.S. and Japan. The workshops should be alternatively held in U.S. and Japan.

2. Accomplishments

(1) Following the Panel's Strategic Plan, approved at its 33rd Joint Meeting, the former Task Committee E, Design for Wind and Wind Hazard Mitigation was reactivated as Task Committee D, Wind Engineering. This decision was based on the Task Committee's past accomplishments and its solid approach as outlined in its Future Plans below that address its Objective.

3. Future Plans

(1) Plan a workshop on "Design for Wind and Wind Hazard Mitigation." This third U.S.-Japan Workshop will be held in Seattle, U.S. in September 2002. The theme of this Workshop is "Reducing Losses from Wind: Collaborative Opportunities for the 21st Century."

(2) Pursue collaborative research on the following topics
   a. Wind characteristics and wind hazards
      i. Wind effects due to complex terrain
      ii. Modeling and validation with full-scale data
      iii. Joint field studies
      iv. Cooperative quick-response post-storm damage assessments
   b. Wind effects on buildings
      i. Development of realistic aerodynamic loads for performance-based structural design
      ii. Comparison of wind tunnel data sets and CFD results to full-scale measurements
   c. Wind effects on bridges
      i. Improvement of methods for predicting wind-induced response of cable-suspended bridges with edge girders
      ii. Prediction and mitigation of rain/wind-induced vibration of stay cables
   d. Evolving Technologies
      i. Next generation wind tunnels: Improvement of methods to simulate non-stationary wind (straight-line, tornado and microburst)
      ii. Structural control

(3) Exchange technical information on the following topics
   a. Wind characteristics and wind hazards
   b. Wind pressures, loadings and dynamic characteristics of buildings
   c. Wind-induced response of cable-suspended bridges
   d. Prediction and mitigation techniques for wind effects

Report of Task Committee G
TRANSPORTATION SYSTEMS

Date: 13 May 2002

Place: National Institute of Standards and Technology, Gaithersburg, MD, USA

Attendees:	U.S. Side --	W. Phillip Yen (Chairman)	FHWA
		Hamid Ghasemi	FHWA
		Ray Zelinski	CALTRANS
	Japan Side --	Hiroshi Sato (Chairman)	PWRI
		Katsuhiko Kawashima	TIT
		Shigeki Unjoh	PWRI
		Keiichi Tamura	PWRI
		Katzuhiro Nishikawa	NILIM
		Ishida Masahiro	NILIM

1. Objective and Scope of Work

The objectives of work include:

(1) To plan, promote and foster research on the behavior of transportation facilities when subjected to wind and seismic forces, and

(2) To disseminate research results and provide specifications and guidelines based on the Task Committee's findings.

The scope of work includes:

(1) To investigate existing and new bridges design, the behavior of whole bridge systems and/or single component of a bridge without limitation on their size and function, and

(2) To investigate offshore, coastal and airport facilities' behavior during earthquake.

2. Accomplishments

(1) The 17th U.S. - Japan Bridge Engineering Workshop was held during 12 - 14 November 2001, at Tsukuba, Ibaraki, Japan. 16 U.S. and 73 Japanese participants attended the workshop. 47 technical papers were presented and discussed on the following main topics: a) Bridge Management Technology and b) Evaluation of Seismic Performance and Seismic strengthening.

(2) Dr. Phillip Yen (FHWA) was invited to the PWRI during November 18 – 22, 2001 to discuss the experimental evaluation methods for establishing a Guidelines for Seismic Performance Testing in Bridge Structures.

(3) Dr. Hiroshi Sato (PWRI) visited the Turner - Fairbank Highway Research Center on March 7, 2002, to discuss future plans of the Task Committee with Dr. Phillip Yen, and to exchange technical information on bridge management and bridge aerodynamics.

3. Future Plans

(1) The proceedings of the 17th U.S. - Japan Bridge Engineering Workshop will be published soon and distributed by the Japan-side. The 18th U.S. - Japan Bridge Engineering Workshop will be held in October 2002 in the U.S. Specific dates, location, themes, program, and itinerary will be proposed by the U.S.-side Task Committee G with the concurrence of the Japan-side Task Committee.

(2) Conduct the following cooperative researches:
   a) Seismic Performance Testing of Bridge Structures. This program is to establish a Guidelines for seismic performance testing of bridge structure. The objective of this program is to establish a Uniform National Guidelines for Testing Bridge Components, which will increase comparability of test results and reduce the duplications of similar testing. In 2002, FHWA and PWRI will meet to develop a draft common Guidelines for the experimental methods. The 1st US side Expert Panel Meeting will be held in August 2002.

(3) Following a devastated earthquake or hurricane (typhoon) in the US or Japan, the committee will form a joint reconnaissance team to investigate the performance of transportation system.

(4) Exchange technical information on the following topics:
   a) Seismic design and retrofit of highway bridges including the development of seismic response modification devices, smart materials such as SMA, seismic retrofit for long-span bridges, and the development of damage evaluation methods using sensor systems.
   b) Seismic and aerodynamic response of long span bridges including suspension and cable-stayed bridges, with emphasis on behavior of composite materials, cable inspection, vibration control, and corrosion protection.

(5) Encourage coordinated researches on the following topics:
   a) Bridge design methodologies that enhance performance based design concepts, limit state design concepts and life cycle cost analyses.
   b) Modeling of seismic isolator and the seismic isolation design methods.
   c) System identification techniques, non-destructive evaluation of bridge structures, use and performance of structural materials including new materials, and performance of jointless bridges.
   d) Bridge response due to near fault effects.
   e) Bridge foundation performance –based design methods.
   f) Post-earthquake damage evaluation methods for seismic retrofitted bridges.

4. Others

(1) The 3rd International Transportation Structure Workshop on Bridge Seismic Performance-Based Design will be held in July 9-11 at Tokyo Institute of Technology, Tokyo, Japan, Task committee members are encouraged to participate.